1127-21
1521

# JOURNAL OF COLLOID SCIENCE

**EDITOR-IN-CHIEF**

Victor K. La Mer
*Columbia University, New York*

**ADVISORY BOARD**

A. E. Alexander
Stephen Brunauer
J. A. Christiansen
P. J. W. Debye
B. Derjaguin
D. G. Dervichian
John T. Edsall
I. Fankuchen
John D. Ferry
J. J. Hermans
John G. Kirkwood
L. G. Longsworth
S. G. Mason
Karol J. Mysels
J. Th. G. Overbeek
J. H. Schulman
Leo Shedlovsky
Theodore Shedlovsky
Robert Simha
R. H. Smellie
Harry Sobotka
Jacinto Steinhardt
Torsten Teorell
A. C. Zettlemoyer
Bruno H. Zimm
W. A. Zisman

Volume 14
1959

ACADEMIC PRESS
*New York and London*

JOURNAL OF COLLOID SCIENCE **14**, 1–12 (1959)

# VISCOSITY-TEMPERATURE RELATIONSHIPS FOR DILUTE SOLUTIONS OF CELLULOSE DERIVATIVES

## I. TEMPERATURE DEPENDENCE OF SOLUTION VISCOSITIES OF ETHYL CELLULOSE

**W. R. Moore and A. M. Brown**[1]

*Physical Chemistry Research Laboratories, Department of Chemistry and Dyeing, Bradford Institute of Technology, Bradford, Yorkshire, England*

*Received June 25, 1958*

### Abstract

Viscosities of dilute solutions of six fractions of ethyl cellulose, molecular weight range 40,000–140,000, in six solvents have been determined at different temperatures between 25° and 60°C. Log $\eta$ is very approximately a linear function of the reciprocal of the absolute temperature $T$. Values of $Q$ and $A$ in the expression $\eta = Ae^{Q/RT}$ are obtained. The apparent activation energy of viscous flow, $Q$, is linearly related to concentration $c$ and molecular weight $M$ by

$$Q = Q_0 + K_eMc$$

and

$$A = A_0e^{-K_aM^{\alpha}c}$$

where $Q_0$ and $A_0$ are values for the pure solvents and $K_e$, $K_a$, and $\alpha$ are constants for a particular ethyl cellulose-solvent system. The values of $K_a$ and $\alpha$ may vary slightly with $M$. An expression is derived giving the intrinsic viscosity in terms of $K_e$, $K_a$, $\alpha$, $M$, and $T$.

### Introduction

The effects of temperature changes on the viscosities of dilute solutions of cellulose derivatives have not been very extensively studied. Large negative temperature coefficients have been noted (1–3). Mandelkern and Flory (1) have considered the temperature dependence of intrinsic viscosities of cellulose tributyrate and tricaprylate and, Flory and co-workers (4) that of intrinsic viscosities of cellulose acetates and cellulose trinitrate in terms of current hydrodynamic and thermodynamic theories of polymer solutions which relate viscosity and chain configuration (5). The large negative temperature coefficients observed were ascribed to increases in chain flexibility. Other approaches to the problem have been made. Manley (6) interpreted changes in intrinsic viscosities of ethyl hydroxyethyl cellulose fractions with temperature in terms of varying degree of hydration. Howlett *et al.* (7) reported a linear relationship between the logarithm of the relative viscosity and reciprocal of absolute temperature for dilute solutions of secondary cellulose acetate. Ferry and co-workers (8, 9) have discussed the effects of temperature changes on the viscosities of concentrated solutions of cellulose trinitrate and tributyrate. The apparent activation energy of viscous flow was found to be related to both concentration and molecular weight of polymer. This latter approach has been used in the present paper, in which we report viscosity measurements on dilute solutions of ethyl cellulose fractions in a number of representative solvents at temperatures from 25° to 60°C. The temperature dependence of intrinsic viscosities and related parameters will be discussed in terms of current hydrodynamic and thermodynamic theories in a further paper.

---

[1] Now at Department of Chemistry, Yale University, New Haven, Connecticut.

## Experimental Methods

Six ethyl cellulose fractions were obtained from samples kindly provided by the Hercules Powder Company. Characteristics of the fractions are given in Table I. Methods of fractionation and of characterisation have been described previously (10). Ethyl methyl ketone, ethyl acetate, butyl acetate, benzene, chloroform, and nitroethane were used as solvents. Their purification and reasons for their choice have also been given previously (10). Fractions A1 and A2 were not completely soluble in nitroethane.

Viscosities of the pure solvents and of solutions in the concentration range 0.1–0.4 g./dl. at 25°C. were determined using capillary viscometers of such dimensions that rate of shear effects were negligible. Kinetic energy corrections were made where applicable. Viscosities were determined over the temperature range 25°–60°C., in steps of 7°, except in the case of chloroform, where the highest temperature was 53°. Thermostats, at each temperature, were controlled to ±0.05°. Viscometers were fitted with small glass bulbs containing glass wool soaked with solvent to prevent evaporation at the higher temperatures. All solutions, after preparation with the aid

TABLE I

*Characteristics of Fractions*

| Fraction | Ethoxyl content (%) | Number-average molecular weight |
|---|---|---|
| A1 | 48.3 | 140,000 |
| A2 | 48.4 | 119,000 |
| B1 | 48.7 | 87,000 |
| A3 | 48.8 | 64,000 |
| B2 | 48.4 | 57,000 |
| B3 | 48.7 | 40,000 |

TABLE II

*Viscosities of Solutions of Fractions in Ethyl Methyl Ketone and Values of Q and A*

| Fraction | Conc. (g./dl.) | $\eta$ in millipoises at | | | | | | $Q$ (*kcal.*) | $A \times 10^5$ |
|---|---|---|---|---|---|---|---|---|---|
| | | 25° | 32° | 39° | 46° | 53° | 60° | | |
| A1 | 0.1 | 5.44 | 5.00 | 4.60 | 4.23 | 3.92 | 3.63 | 2.29 | 9.20 |
| | 0.2 | 7.75 | 7.01 | 6.33 | 5.72 | 5.19 | 4.71 | 2.84 | 6.46 |
| | 0.3 | 10.88 | 9.67 | 8.51 | 7.67 | 6.80 | 6.12 | 3.28 | 4.31 |
| A2 | 0.1 | 5.18 | 4.77 | 4.41 | 4.07 | 3.77 | 3.49 | 2.21 | 12.4 |
| | 0.2 | 7.08 | 6.46 | 5.87 | 5.33 | 4.90 | 4.46 | 2.64 | 8.28 |
| | 0.3 | 9.58 | 8.61 | 7.71 | 6.95 | 6.30 | 5.72 | 2.97 | 6.40 |
| | 0.4 | 13.00 | 11.60 | 10.21 | 9.08 | 8.14 | 7.26 | 3.41 | 4.22 |
| B1 | 0.1 | 4.87 | 4.50 | 4.16 | 3.85 | 3.59 | 3.33 | 2.15 | 13.0 |
| | 0.2 | 6.29 | 5.76 | 5.38 | 4.80 | 4.44 | 4.10 | 2.42 | 10.6 |
| | 0.3 | 8.23 | 7.20 | 6.60 | 5.98 | 5.46 | 4.99 | 2.80 | 7.83 |
| | 0.4 | 10.40 | 9.32 | 8.19 | 7.48 | 6.75 | 6.07 | 3.05 | 6.05 |
| A3 | 0.1 | 4.62 | 4.26 | 3.96 | 3.68 | 3.44 | 3.20 | 2.07 | 14.0 |
| | 0.2 | 5.64 | 5.29 | 4.77 | 4.41 | 4.09 | 3.80 | 2.27 | 12.3 |
| | 0.3 | 6.90 | 6.31 | 5.74 | 5.26 | 4.83 | 4.45 | 2.52 | 9.86 |
| | 0.4 | 8.45 | 7.66 | 6.93 | 6.25 | 5.74 | 5.22 | 2.76 | 8.05 |
| B2 | 0.1 | 4.50 | 4.17 | 3 87 | 3.60 | 3.35 | 3.14 | 2.01 | 15.1 |
| | 0.2 | 5.41 | 4.97 | 4.58 | 4.23 | 3.92 | 3.63 | 2.17 | 13.8 |
| | 0.3 | 6.47 | 5.92 | 5.40 | 4.96 | 4.57 | 4.20 | 2.44 | 10.5 |
| | 0.4 | 7.79 | 7.06 | 6.40 | 5.84 | 5.34 | 4.87 | 2.65 | 8.91 |
| B3 | 0.1 | 4.27 | 3.97 | 3.69 | 3.44 | 3.21 | 3.00 | 1.98 | 15.1 |
| | 0.2 | 4.85 | 4.49 | 4.15 | 3.85 | 3.59 | 3.33 | 2.15 | 13.9 |
| | 0.3 | 5.51 | 5.07 | 4.69 | 4.32 | 4.01 | 3.72 | 2.21 | 13.1 |
| | 0.4 | 6.27 | 5.75 | 5.30 | 4.85 | 4.49 | 4.15 | 2.35 | 11.9 |

of mechanical shaking, were stored in the dark for two weeks at room temperature and rapidly filtered immediately prior to use.

## RESULTS

Viscosities ($\eta$) of solutions of the fractions in ethyl methyl ketone and butyl acetate for different concentrations at 25°C. are given in Tables II and III. These may be regarded as typical of the results obtained with the other solvents. Typical examples of temperature dependence are shown in Fig. 1, where log $\eta$ is plotted against the reciprocal of the absolute temperature $T$. In most cases the lines are straight within experimental error but some slight curvature seems possible at the highest concentrations and molecular weights. Similar behavior was observed in all cases studied. Values of $\eta$ at temperatures above 25°C. were corrected to standard con-

## TABLE III

*Viscosities of Solutions of Fractions in Butyl Acetate and Values of $Q$ and $A$*

| Fraction | Conc. (g./dl.) | $\eta$ in millipoises at | | | | | | $Q$ (*kcal.*) | $A \times 10^5$ |
|---|---|---|---|---|---|---|---|---|---|
| | | 25° | 32° | 39° | 46° | 53° | 60° | | |
| A1 | 0.1 | 10.25 | 9.20 | 8.34 | 7.48 | 6.79 | 6.20 | 2.87 | 8.09 |
| | 0.2 | 15.05 | 13.39 | 11.72 | 10.38 | 9.28 | 8.33 | 3.37 | 5.12 |
| | 0.3 | 21.56 | 18.83 | 16.25 | 14.20 | 12.47 | 11.06 | 3.82 | 3.55 |
| | 0.4 | 31.49 | 27.17 | 22.80 | 19.70 | 17.15 | 15.00 | 4.17 | 2.75 |
| A2 | 0.1 | 9.66 | 8.73 | 7.88 | 7.13 | 6.51 | 5.96 | 2.75 | 11.1 |
| | 0.2 | 13.42 | 11.98 | 10.65 | 9.50 | 8.53 | 7.73 | 3.15 | 8.67 |
| | 0.3 | 18.32 | 16.12 | 14.08 | 12.41 | 11.09 | 9.94 | 3.45 | 6.76 |
| | 0.4 | 25.04 | 21.75 | 18.60 | 16.44 | 14.35 | 12.70 | 3.81 | 4.02 |
| B1 | 0.1 | 9.08 | 8.20 | 7.45 | 6.77 | 6.21 | 5.67 | 2.64 | 10.5 |
| | 0.2 | 11.99 | 10.74 | 9.60 | 8.64 | 7.80 | 7.03 | 2.98 | 7.85 |
| | 0.3 | 15.63 | 13.84 | 12.30 | 10.93 | 9.82 | 8.85 | 3.21 | 6.76 |
| | 0.4 | 20.49 | 17.93 | 15.62 | 13.83 | 12.20 | 10.83 | 3.62 | — |
| A3 | 0.1 | 8.44 | 7.67 | 6.97 | 6.36 | 5.83 | 5.37 | 2.55 | 11.4 |
| | 0.2 | 10.36 | 9.33 | 8.41 | 7.63 | 6.95 | 6.36 | 2.75 | 9.98 |
| | 0.3 | 12.62 | 11.24 | 10.09 | 9.09 | 8.25 | 7.50 | 2.94 | 8.81 |
| | 0.4 | 15.35 | 13.60 | 12.09 | 10.90 | 9.77 | 8.79 | 3.13 | 7.78 |
| B2 | 0.1 | 8.26 | 7.49 | 6.82 | 6.24 | 5.71 | 5.27 | 2.54 | 11.3 |
| | 0.3 | 11.88 | 10.62 | 9.54 | 8.63 | 7.83 | 7.16 | 2.86 | 9.48 |
| | 0.4 | 14.35 | 12.80 | 11.37 | 10.27 | 9.26 | 8.39 | 3.05 | 8.34 |
| B3 | 0.1 | 7.83 | 7.12 | 6.48 | 5.95 | 5.47 | 5.06 | 2.44 | — |
| | 0.2 | 8.93 | 8.09 | 7.31 | 6.70 | 6.13 | 5.63 | 2.57 | 11.6 |
| | 0.3 | 10.20 | 9.20 | 8.30 | 7.53 | 6.87 | 6.30 | 2.73 | 10.2 |
| | 0.4 | 11.65 | 10.43 | 9.38 | 8.49 | 7.70 | 7.06 | 2.82 | 9.93 |

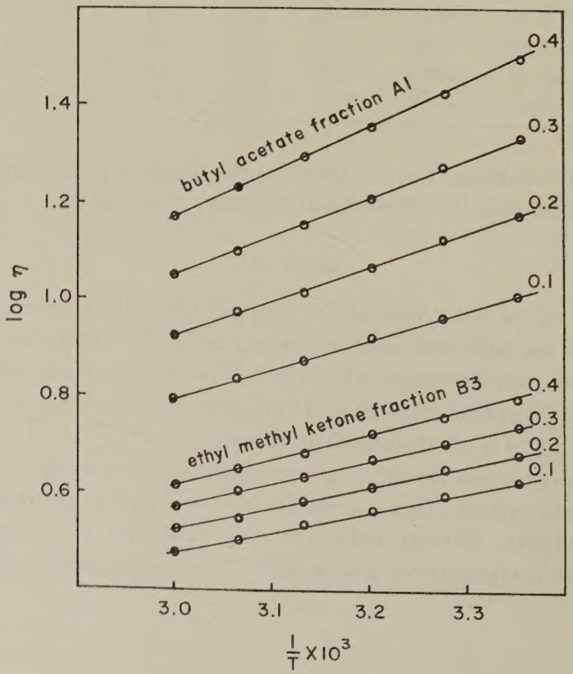

FIG. 1. Logarithm of viscosity plotted against reciprocal absolute temperature. Figures at right denote concentration in grams per deciliter.

centrations, 0.4, 0.3, 0.2, and 0.1 g./dl., by graphical interpolation from plots of $\eta$ against concentration.

## DISCUSSION

Assuming a linear relationship between log $\eta$ and $1/T$ we may write

$$\eta = Ae^{Q/RT}, \qquad [1]$$

where $Q$ is the apparent activation energy of viscous flow. The significance of $A$ is less clear. In Eyring's theory of rate processes (11) it is a term involving the entropy of activation. Values of $Q$ and $A$, for the mean temperature 42.5°C., were obtained from log $\eta$ vs. $1/T$ plots by the method of least squares. Those for the solutions involving ethyl methyl ketone and butyl acetate are included in Tables II and III, respectively, those for other solutions being collected in Table IV. For a given solvent, $Q$ depends on

TABLE IV

*Values of Q and A*

| Fraction | Conc. (g./dl.) | Ethyl acetate | | Benzene | | Chloroform | | Nitroethane | |
|---|---|---|---|---|---|---|---|---|---|
| | | $Q$ (*kcal.*) | $A \times 10^5$ | $Q$ (*kcal.*) | $A \times 10^5$ | $Q$ (*kcal.*) | $A \times 10^5$ | $Q$ (*kcal.*) | $A \times 10^5$ |
| A1 | 0.1 | 2.44 | 10.3 | 2.79 | 8.22 | 2.21 | 19.7 | | |
| | 0.2 | 2.96 | 6.27 | 3.20 | 6.17 | 2.68 | 13.5 | | |
| | 0.3 | 3.36 | 4.54 | 3.59 | 4.70 | 2.96 | 12.1 | | |
| | 0.4 | 3.74 | 3.4 | 4.03 | 3.27 | 3.25 | 10.6 | | |
| A2 | 0.1 | 2.36 | 11.1 | 2.75 | 8.46 | 2.19 | 19.5 | | |
| | 0.2 | 2.74 | 8.09 | 3.18 | 6.01 | 2.57 | 15.0 | | |
| | 0.3 | 3.05 | 6.52 | 3.56 | 4.56 | 2.89 | 12.6 | | |
| | 0.4 | 3.38 | 5.08 | 3.96 | 3.40 | 3.13 | 11.4 | | |
| B1 | 0.1 | 2.29 | 11.7 | 2.69 | 8.71 | 2.12 | 20.3 | 2.30 | 16.8 |
| | 0.2 | 2.55 | 9.86 | 3.02 | 6.79 | 2.38 | 17.5 | 2.71 | 10.8 |
| | 0.3 | 2.96 | 7.49 | 3.35 | 5.27 | 2.65 | 14.6 | 2.96 | 8.89 |
| | 0.4 | 3.08 | 6.76 | 3.66 | 4.19 | | | 3.29 | 6.50 |
| A3 | 0.1 | | | 2.66 | 8.55 | 2.13 | 18.5 | 2.18 | 19.2 |
| | 0.2 | | | 2.89 | 7.40 | 2.29 | 17.4 | 2.35 | 17.0 |
| | 0.3 | | | 3.12 | 6.34 | 2.48 | 15.6 | 2.54 | 14.5 |
| | 0.4 | | | 3.43 | 4.79 | 2.63 | 14.8 | 2.75 | 12.0 |
| B2 | 0.1 | 2.22 | 12.1 | 2.59 | 9.29 | | | 2.22 | 17.9 |
| | 0.2 | 2.41 | 10.6 | 2.76 | 8.63 | | | 2.38 | 16.0 |
| | 0.3 | 2.54 | 10.1 | 3.05 | 6.64 | | | 2.49 | 15.5 |
| | 0.4 | 2.71 | 9.1 | 3.31 | 5.37 | | | 2.68 | 13.1 |
| B3 | 0.1 | 2.13 | 13.3 | | | 1.99 | 21.5 | 2.14 | 19.6 |
| | 0.2 | 2.24 | 12.7 | | | 2.12 | 19.9 | 2.22 | 19.2 |
| | 0.3 | 2.38 | 11.5 | | | 2.27 | 17.7 | 2.33 | 17.9 |
| | 0.4 | 2.58 | 9.44 | | | 2.34 | 17.5 | 2.44 | 16.8 |

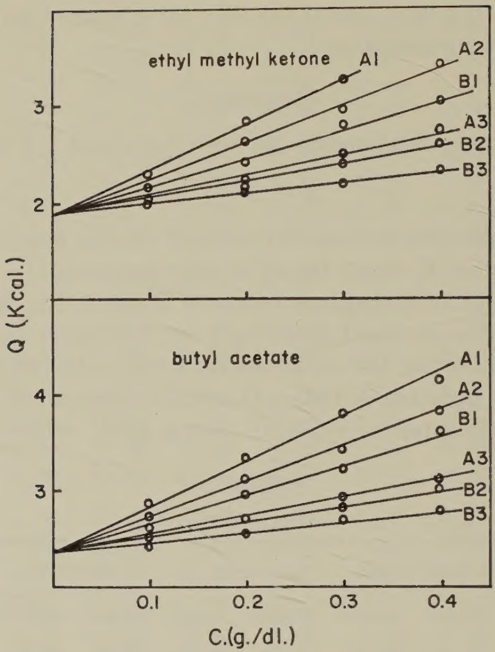

FIG. 2. Apparent activation energy of viscous flow plotted against concentration.

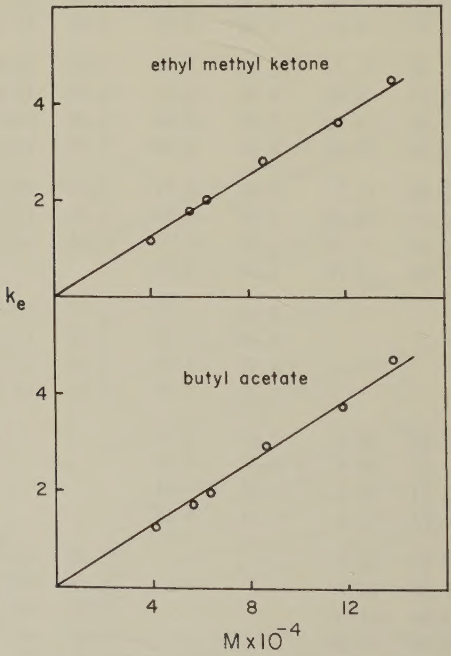

FIG. 3. The constant $k_e$ as a function of molecular weight of polymer.

TABLE V

*Values of $K_e$, $K_a$ and $\alpha$*

| Solvent | $K_e \times 10^2$ | $K_a$ | $\alpha$ |
|---|---|---|---|
| Ethyl methyl ketone | 3.20 | $2.42 \times 10^{-6}$ | 1.23 |
| Ethyl acetate | 3.07 | $1.62 \times 10^{-6}$ | 1.21 |
| Butyl acetate | 3.16 | $0.97 \times 10^{-7}$ | 1.48 |
| Benzene | 3.32 | $6.52 \times 10^{-5}$ | 0.93 |
| Chloroform | 2.92 | $1.50 \times 10^{-5}$ | 1.00 |
| Nitroethane | 3.20 | $2.48 \times 10^{-10}$ | 2.04 |

the concentration $c$ and molecular weight $M$ of the polymer. Figure 2, showing plots of $Q$ against $c$ for the fractions in ethyl methyl ketone and butyl acetate, suggests that $Q$ is a linear function of $c$. Similar plots were obtained with the other solvents. The intercepts, $Q_0$, representing the activation energies of viscous flow for the pure solvents, were in good agreement with published values (12). We may write,

$$Q = Q_0 + k_e c, \tag{2}$$

where the constant $k_e$ depends on the solvent and on $M$. As shown by typical examples in Fig. 3, plots of $k_e$ against $M$ are linear and pass through the origin, so that

$$k_e = K_e M, \tag{3}$$

where $K_e$ is a constant for a particular ethyl cellulose-solvent system. Values of $K_e$, obtained from such plots by the method of least squares, are given in Table V. Substituting in Eq. [2],

$$Q = Q_0 + K_e Mc. \tag{4}$$

Analysis of Manley's results (6) suggests a similar relationship. The results of Landel *et al.* (9) for low concentrations of cellulose tributyrate in 1,2,3-trichloropropane also seem to be in general agreement with Eq. [4].

The term $K_e Mc$ represents the contribution of the polymer to the apparent activation energy of viscous flow of a solution. Here $K_e$ may be regarded as the contribution per unit polymer molecular weight and concentration. The values of $K_e$ do not vary much with solvent. Flory and co-workers (4) found the temperature coefficients of the logarithms of intrinsic viscosities of cellulose derivatives to be similar for different derivatives and various solvents.

The $A$ term in Eq. [1] decreases with increasing concentration and molecular weight of polymer but not linearly. For a given molecular weight and solvent a plot of $-\log A$ against concentration does, however, appear to be linear and the values of $A_0$, obtained by extrapolation of such plots, are in good agreement with those obtained for the pure solvents and with

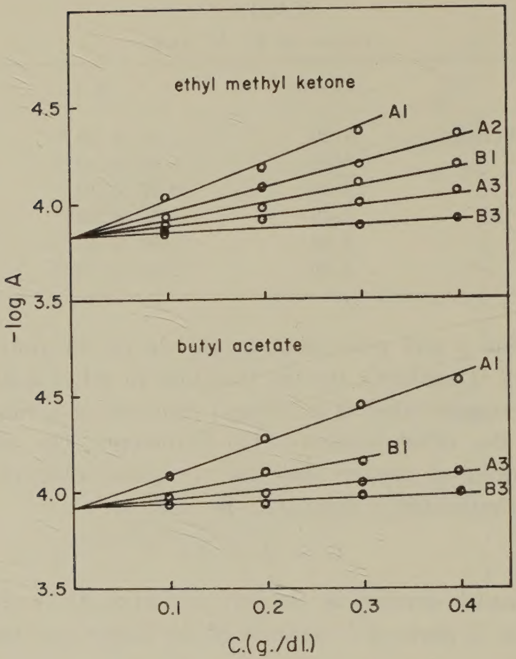

FIG. 4. Plot of −Log $A$ as a function of concentration.

published values (12). Some typical plots are shown in Fig. 4. The relationship between $A$ and $c$ may be expressed by

$$-\log A = -\log A_0 + k_a c, \qquad [5]$$

where $k_a$ depends on the molecular weight of the polymer and on the solvent. The variation of $k_a$ with $M$, for a given solvent, may be written

$$k_a = K_a M^\alpha, \qquad [6]$$

where the values of $K_a$ and $\alpha$ depend on the solvent and, possibly, to a lesser extent on $M$. Typical least-squares plots of log $k_a$ against log $M$ are shown in Fig. 5. A linear relationship has been assumed and may hold within experimental error, but there is a possibility of some curvature at the higher molecular weights. The values of $K_a$ and $\alpha$, obtained from such plots and included in Table V, may therefore vary somewhat with $M$. Assuming Eq. [6] to hold over the molecular weight range considered and substituting in Eq. [5],

$$-\log A = -\log A_0 + K_a M^\alpha c. \qquad [7]$$

The interpretation of this equation is not very clear. According to Eyring (11), −log $A$ should involve both a volume term and the entropy of ac-

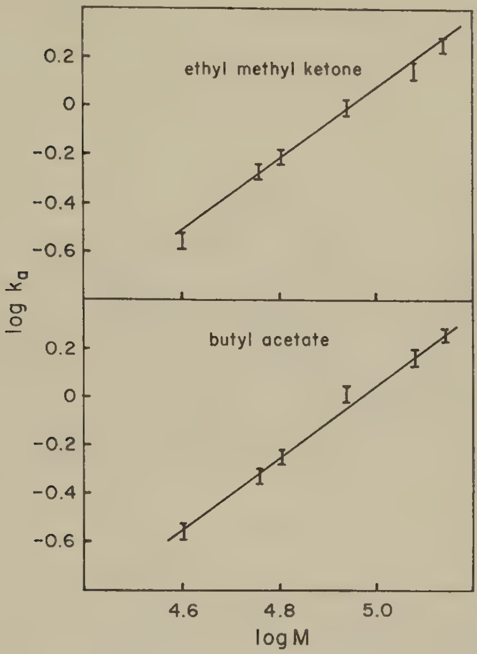

FIG. 5. Logarithm of $k_a$ plotted against logarithm of molecular weight.

tivation of viscous flow. According to Barrer (12), $-\log A$ is a function of the size of the activated zone.

Equations [4] and [7] are, of course, likely to hold only in the low concentration range considered and for low molecular weights. More complicated dependence of $Q$ on both $c$ and $M$ is to be expected at higher concentrations and molecular weights (8, 9). It is, however, possible to derive from Eqs. [1], [4], and [7] an expression relating intrinsic viscosity to the molecular weight of the polymer and the temperature. From Eq. [1], the specific viscosity, $(\eta - \eta_0)/\eta_0$, may be written

$$\eta_{sp} = \frac{Ae^{Q/RT} - A_0e^{Q_0/RT}}{A_0e^{Q_0/RT}}. \qquad [8]$$

Substituting from Eqs. [4] and [7] in [8] and simplifying gives

$$\eta_{sp} = [e^{-K_aM^\alpha c} \times e^{K_eMc/RT}] - 1, \qquad [9]$$

which, on expansion and neglect of terms beyond $c^2$, yields

$$\eta_{sp}/c = K + \tfrac{1}{2}K^2c, \qquad [10]$$

where

$$K = K_eM/RT - K_aM^\alpha.$$

The intrinsic viscosity, $[\eta]$, is given by

$$[\eta] = \eta_{sp}/c; \quad c \rightarrow 0$$

hence

$$[\eta] = K_e M/RT - K_a M^{\alpha}. \tag{11}$$

The values of $K_e$ are considerably greater than those of $K_a$ and the second term on the R.H.S. of Eq. [11] will become increasingly important as $M$ increases. At sufficiently low molecular weights, $[\eta]$ should be effectively a linear function of $M$. Experimental evidence for such dependence of $[\eta]$ on $M$ has recently been given for cellulose acetate (13) and ethyl cellulose (10). Badgley and Mark (14) have suggested an empirical expression for cellulose acetate in acetone at 26.5°C. which is similar in form to Eq. [11]. Their equation is

$$[\eta] = KM^a - K'M^{2a},$$

where $K$, $K'$, and $a$ are constants. In agreement with Eq. [11], the value of $a$ is unity.

Equation [11] and values of $K_e$, $K_a$, and $\alpha$ may be used to calculate $[\eta]$ for a given molecular weight, solvent, and temperature. Comparison of such values with those obtained by extrapolation of linear plots of log $(\eta_{sp}/c)$ against $c$ to zero $c$ shows that the calculated values differ from the experimental by less than 5% for the four fractions of lowest $M$. With the two highest molecular weights the calculated values become increasingly greater as $M$ increases, the difference being about 10% for the fraction of highest $M$. As previously indicated, it is possible that both $K_a$ and $\alpha$ may vary with $M$, $\alpha$ decreasing as $M$ increases. Equation [11] requires $[\eta]$ to be a linear function of $1/T$. The typical examples in Fig. 6 suggest that this is generally true. There is, however, some indication of slight curvature of the plots for the fraction of highest $M$.

Equation [10] implies that $k'$ in the Huggins

$$\eta_{sp}/c = [\eta] + k'[\eta]^2 c$$

has the value of 0.5 in every case. Values of $k'$ are known to vary with solvent, and in the present work such values varied from 0.35 to 0.71 and tended to decrease with increasing temperature. The value of 0.5 arises from the expansion of the exponentials in Eq. [9]. The possible curvature of the log $\eta$ vs. $1/T$ plots at the highest concentrations and molecular weights suggests that an exponential relationship between $\eta$ and $1/T$ may not hold strictly over the whole temperature range. Varying deviations from such a relationship with different solvents may account for the values

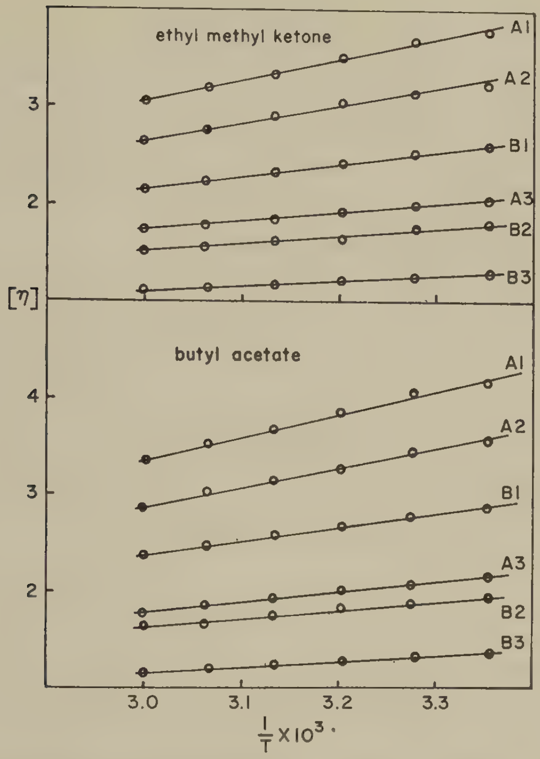

FIG. 6. Intrinsic viscosity plotted against reciprocal absolute temperature.

of $k'$. The temperature dependence of $k'$ and other viscosity parameters will be discussed in the further paper.

It must be emphasized that the relationships obtained may apply only to relatively stiff and polar polymers such as cellulose derivatives. The behavior of dilute solutions of flexible, less polar polymers may be quite different. The results of Bawn and Patel (15, 16) show that $[\eta]$ for polyisobutylene in cyclohexane and carbon tetrachloride varies little with temperature. More detailed analysis suggests that $Q$ is independent of both $M$ and $c$ up to molecular weights of $10^6$ and concentrations of 0.25 g./dl. Therefore $K_e$ is zero. Also $K_a$ is of opposite sign to the values obtained in the present work and hence $[\eta] = KM^{\alpha}$, the familiar Mark-Houwinck equation.

## ACKNOWLEDGMENTS

We are grateful to the Bradford City Council for the award of a research scholarship to A.M.B. and to Professor C. E. H. Bawn both for making detailed viscosity results available and for helpful discussion.

## REFERENCES

1. Mandelkern, L., and Flory, P. J., *J. Am. Chem. Soc.* **74**, 2517 (1952).
2. Kraemer, E. O., *in* "The Chemistry of Large Molecules," edited by R. E. Burk and O. Grummitt, p. 84. Interscience, New York-London, 1943.
3. Kraemer, E. O., and Sears, G. R., *J. Rheol.* **2**, 292 (1931).
4. Flory, P. J., Spurr, O. K., and Carpenter, D. K., *J. Polymer Sci.* **27**, 231 (1958).
5. Flory, P. J., "Principles of Polymer Chemistry," Chapter 14. Cornell University Press, Ithaca, New York, 1953.
6. Manley, R. St. J., *Arkiv Kemi* **9**, 519 (1956).
7. Howlett, F., Minshall, E., and Urquhart, A. R., *J. Textile Inst.* **35**, T133 (1944).
8. Plazek, D. J., and Ferry, J. D., *J. Phys. Chem.* **60**, 289 (1956).
9. Landel, R. F., Berge, J. W., and Ferry, J. D., *J. Colloid Sci.* **12**, 400 (1957).
10. Moore, W. R., and Brown, A. M., *J. Appl. Chem.* **8**, 363 (1958).
11. Eyring, H., *J. Chem. Phys.* **4**, 283 (1936).
12. Barrer, R. M., *Trans. Faraday Soc.* **39**, 48 (1943).
13. Moore, W. R., and Tidswell, B. M., *J. Appl. Chem.* **8**, 232 (1958).
14. Badgley, W. J., and Mark, H., *J. Phys. & Colloid. Chem.* **51**, 58 (1947).
15. Bawn, C. E. H., and Patel, R. D., *Trans. Faraday Soc.* **52**, 1669 (1956).
16. Patel, R. D., Ph.D. thesis, Liverpool, 1952.

JOURNAL OF COLLOID SCIENCE **14**, 13–26 (1959)

# PARTICLE MOTIONS IN SHEARED SUSPENSIONS

## VIII. SINGLETS AND DOUBLETS OF FLUID SPHERES[1]

**W. Bartok[2] and S. G. Mason**

*Pulp and Paper Research Institute of Canada and Department of Chemistry,*
*McGill University, Montreal, Canada*

*Received July 21, 1958*

### *List of Symbols*

$a, b$ = diameter and radius of spherical drop.
$B$ = breadth of ellipsoid.
$G$ = velocity gradient.
$k_2$ = internal streamline parameter.
$L$ = length of ellipsoid.
$p$ = viscosity ratio = $\eta'/\eta_0$.
$r_e$ = ellipsoidal axis ratio.
$r$ = radius vector.
$T, T_c$ = periods of (external) rotation and of internal circulation, respectively.
$u, v, w$ = velocity components along $X$-, $Y$-, and $Z$-axes.
$\gamma$ = interfacial tension.
$\eta', \eta_0$ = viscosity of disperse and continuous phases.
$\phi$ = polar coordinate, $Y$-axis as origin.

## INTRODUCTION

Previous communications in this series have dealt with the rotations and interactions of rigid particles (1–5) suspended in a laminar shear field. The experiments were performed in a field of flow defined by $u = Gy$, $v = 0$, $w = 0$, and observations were made both along the $Y$-axis (across the planes of shear) and the $Z$-axis (parallel to the planes of shear). In the present paper we describe a study of the shear-induced internal circulation, rotation, deformation and two-body interaction of liquid droplets.

In addition some preliminary experiments on the coalescence of colliding fluid spheres are discussed.

## EXPERIMENTAL METHODS

Observations and measurements were made in the two Couette double-cylinder devices which have been described previously (1, 5). The velocity gradient $G$ could be calculated accurately from the speeds of rotation of the cylinders (1), and the measurements could be made by using photomicrography and tape recording as in the study of rigid particles (5).

---

[1] Conducted with financial assistance from the Defence Research Board of Canada, DRB Grant 9510-05.

[2] Holder of a Studentship from the National Research Council of Canada.

As before, household corn syrup having a viscosity of 70 poises and a density of 1.38 gm./c.c. at room temperature was used as suspending medium for most of the experiments. Droplets of either cyclohexanol phthalate (subsequently designated CHP) or $CCl_4$ were dispersed in corn syrup. The viscosities and densities at room temperature were 155 poises and 1.08 gm./c.c. for CHP, and 0.0094 poise and 1.59 gm./c.c. for $CCl_4$. Falling ball viscosity measurements indicated Newtonian behavior by both the corn syrup and the CHP.

Attempts to produce coarse monodisperse emulsions of accurately known concentration in the viscous medium were unsuccessful. Instead, small numbers of drops of $CCl_4$ were injected from a finely drawn glass capillary tube placed beneath the surface of corn syrup in the annular gap of the apparatus. One of the cylinders, usually the outer one, was rotated to reduce the size of the drops by the viscous drag of the medium flowing past the capillary tube, which was adjusted so that its tip pointed along the streamlines. Droplets of about 50 to 200$\mu$ diameter could thus be dispersed in localized concentrations.

The highly viscous drops of CHP were injected beneath the corn syrup surface by means of a syringe, using a 0.5 mm. diameter hypodermic needle. The apparatus was at rest, but the end of the needle was moved concentrically with the cylinders in a roughly constant $XY$-plane, while a slight pressure was maintained on the piston of the syringe. The threads of liquid which were produced by shifting the hypodermic needle in corn syrup, broke up into nearly equal-sized drops of about 100$\mu$ in diameter aligned in "string-of-pearl" formations.

The rotations of single fluid particles and the pattern of internal circulation were followed by dispersing aluminum reference particles of 5$\mu$ to 10$\mu$ diameter in CHP and $CCl_4$ drops.

## Single Liquid Drops

### *Theoretical Considerations*

Starting with an equation derived in Taylor's theory of viscosity of dilute emulsions (6), the pattern of fluid motion outside and inside a fluid drop in a laminar shear field was calculated in the preceding paper in this series (7) for low values of $G$ when the drop remains spherical. The following relations were deduced from the theory:

*1.* The streamlines inside the drop are described by the polar equation

$$\left[\frac{r^2}{b^2}\cos 2\phi + (p+1)\right]^3\left[\frac{r^2}{b^2} - 1\right]^2 = k_2 . \qquad [1]$$

Here $(r, \phi)$ are the plane polar coordinates with the drop center as origin, $\phi = 0$ corresponds to the $Y$-axis (Fig. 1), $b$ is the drop radius, $p$ is the viscosity ratio of disperse to continuous phases, and $k_2$ is a constant which describes a particular streamline. It follows from Eq. [1] that for $p > \frac{1}{2}$ the streamlines are roughly elliptical in shape, while for $p < \frac{1}{2}$ two pockets of fluid circulation exist close to the center of the drop.

*2.* The period of rotation around the equatorial perimeter at the surface

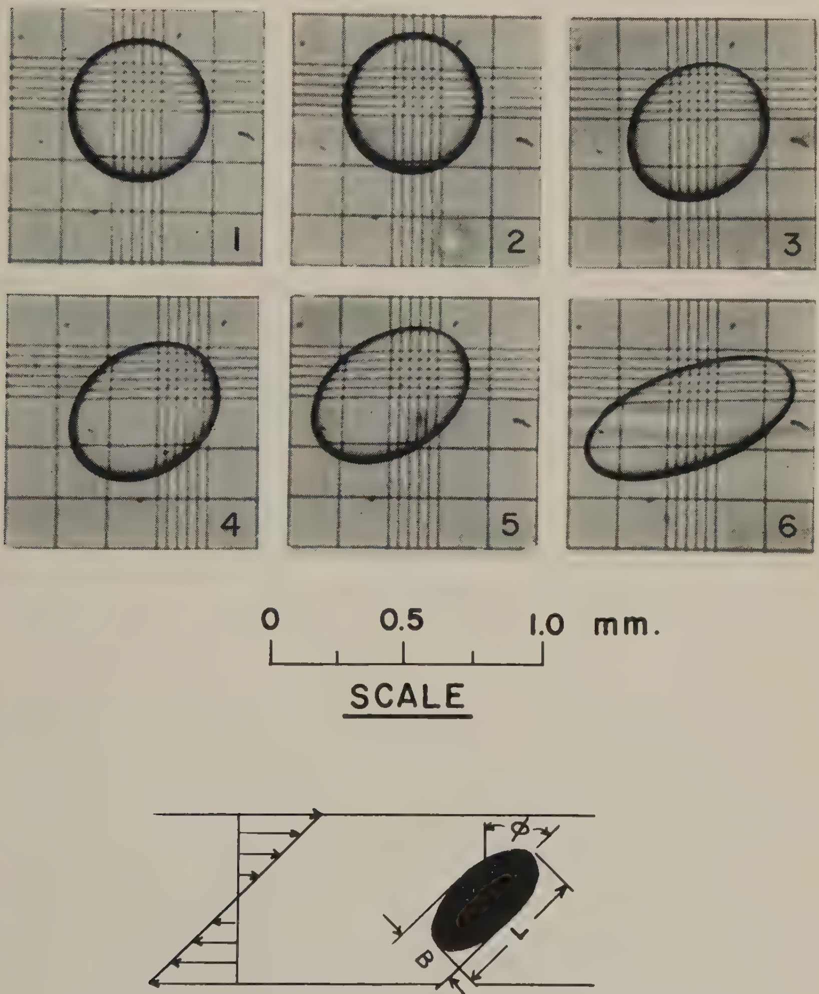

FIG. 1. Photomicrographs of the shear deformation of a cyclohexanol phthalate (CHP) drop in corn syrup as viewed along the $Z$-axis at increasing rates of shear. The deformations and orientations corresponding to the frames Nos. 1 to 6 are listed in Table II. Diameter of undistorted drop = 575 $\mu$.

of the sphere is

$$\frac{TG}{4\pi} = \frac{p+1}{\sqrt{p(p+2)}}. \qquad [2]$$

When $p \to \infty$, this reduces to

$$\frac{TG}{4\pi} = 1, \qquad [3]$$

which is identical with the value for a rigid sphere (1).

*3.* The period of circulation $T_c$ close to the center of the drop is

$$\frac{T_cG}{4\pi} = \frac{2(p+1)}{\sqrt{(2p+5)(2p-1)}} \qquad [4]$$

for $p > \frac{1}{2}$. It is readily shown that $T_c > T$, i.e., circulation inside the drop becomes slower towards the center. When $p \to \infty$, Eq. [4] reduces to Eq. [3].

As $G$ increases, the drop is distorted by the nonuniform pressure field created by the disturbed flow in the neighborhood of the drop. At low values of $G$ the particle is deformed into an ellipsoid of length $L$ and breadth $B$ with its major axis at an angle $\phi = 45°$ from the direction of the gradient. Taylor (8) derived and obtained a limited experimental confirmation of the following relationship for the eccentricity at small deformations

$$\frac{L-B}{L+B} = \frac{Gb\eta_0}{\gamma}\,\frac{19p+16}{16(p+1)}, \qquad [5]$$

where $\eta_0$ is the viscosity of the suspending medium and $\gamma$ is the interfacial tension of the drop. Some experiments on deformation are described later.

### *Spherical Drops*

Typical values of the period of rotation $T$ for a large number of observations of undeformed droplets of CHP and of $CCl_4$ are presented in Table I. Measurements were made over a range of values of $G$ and the locations of the reference particles were selected at random, i.e., on the surface of the drops, or inside the drops at various radial displacements from the centers. Although in some cases a drift was observed in their paths upon successive rotations, the reference particles appeared to move in circular orbits as the projection on the $XY$-plane of the field of motion was viewed. The drop size in these experiments varied from $100\mu$ to $150\mu$ in diameter.

The mean values of $TG/4\pi$ do not differ very significantly from unity, the theoretical value for a rigid sphere (Eq. [3]), and are much less than calculated from either Eq. [2] or [4] for both drop systems (Table I). This indicates that there was little, if any, internal circulation in these experi-

TABLE I

*Periods of Rotation of Spherical Drops*

Suspending medium—corn syrup.

| Drop No. | Type | Range of $G$ (sec.$^{-1}$) | $N$[a] | Mean $\frac{TG}{4\pi}$ | $p$ | $\frac{TG}{4\pi}$ Eq. [2] | $\frac{T_cG}{4\pi}$ Eq. [4] |
|---|---|---|---|---|---|---|---|
| 1 | CHP | 0.08–1.89 | 39 | 1.028<br>(.006)[b] | 2.2 | 1.05 | 1.13 |
| 2 | CHP | 0.06–0.49 | 8 | 0.997<br>(.008)[b] | | | |
| 3 | CHP | 0.13–1.87 | 42 | 0.999<br>(.006)[b] | | | |
| 4 | $CCl_4$ | 0.07–1.94 | 58 | 1.020<br>(.004)[b] | $1.3 \times 10^{-4}$ | 62 | — |
| 5 | $CCl_4$ | 0.09–1.86 | 71 | 1.020<br>(.004)[b] | | | |

[a] $N$ = number of periods of rotation measured.

[b] Bracketed quantities are estimated standard deviations of associated mean values.

ments. This was confirmed by observing that reference particles inside the sphere moved about the center in circular instead of elliptical paths and at the same angular velocity as the periphery.

### *Deformed Drops*

Internal circulation was, however, observed in larger drops ($>200\mu$ diameter) which became visibly deformed into prolate spheroids (Fig. 1) at gradients as low as 0.1 sec.$^{-1}$. Inside the drops the eccentricity of the paths of reference particles appeared to be higher than the outer contour of the deformed drops. Furthermore, particles inside the drop lagged behind those at the surface, i.e., the period of circulation was greater inside the drop. This effect became more marked when $G$ was increased.

The period of circulation of the outer surface was appreciably greater than that of a rigid sphere and appeared to increase with increase in $G$. This is illustrated in Fig. 2 for two drops of CHP. At sufficiently high values of $G$, $TG/4\pi$ exceeded the value of 1.05 calculated from Eq. [2].

A number of experiments on deformation of both CHP and $CCl_4$ drops were made as a function of $G$. The effect is illustrated by the photomicrographs of a CHP drop in Fig. 1 which show the increase in eccentricity and in the angle of orientation $\phi$ with increasing $G$. Table II summarizes the observations made on this drop. Figure 3 shows a plot of $(L - B)/(L + B)$ as a function of $aG$ for three $CCl_4$ drops of various diameters. Over the range of shear rates employed, the deformation data for the three drops fall on a single straight line passing through the origin as predicted

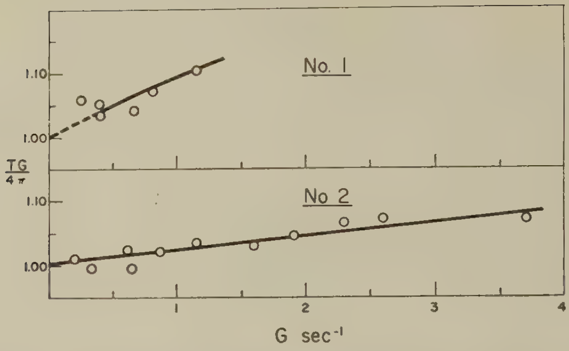

FIG. 2. Increase of $TG/4\pi$ with $G$ for two visibly deformed drops of CHP of diameter 300 $\mu$ approximately. Note that values of $TG/4\pi$ exceed unity except when $G \rightarrow 0$. The high scatter of points was due to experimental difficulties.

TABLE II

*Deformation of a CHP Drop by Fluid Shear*

Undeformed drop diameter = 575 $\mu$.

| $G$ (sec.$^{-1}$) | $\frac{L-B}{L+B}$ | $aG$ (mm. sec.$^{-1}$) | $\phi$ (degrees) | Frame no. in Fig. 1 |
|---|---|---|---|---|
| 0 | 0 | 0 | — | — |
| 0.0556 | 0 | 0.0319 | 45 | 1 |
| 0.1281 | 0.0066 | 0.0736 | 45 | 2 |
| 0.2191 | 0.0165 | 0.128 | 45 | — |
| 0.3247 | 0.0263 | 0.186 | 46 | — |
| 0.5141 | 0.0429 | 0.295 | 47 | — |
| 0.6984 | 0.0693 | 0.400 | 49 | — |
| 0.8286 | 0.0691 | 0.475 | 50 | 3 |
| 1.017 | 0.0951 | 0.584 | 53 | — |
| 1.394 | 0.123 | 0.800 | 55 | 4 |
| 1.844 | 0.179 | 1.059 | 57 | 5 |
| 2.719 | 0.264 | 1.562 | 64 | — |
| 3.931 | 0.375 | 2.255 | 68 | 6 |

by Eq. [5]. A similar straight line was obtained for four drops of CHP of diameters 130 to 600$\mu$ over a range of $G$'s from 0 to 4 sec.$^{-1}$. Unfortunately the interfacial tensions were not known so that the equation could not be tested completely.

The orientation angle $\phi$ increased with $G$ starting from the predicted value of 45° at $G = 0$. Silberberg and Kuhn (9) on the basis of indirect measurements postulated that for systems of $p \simeq 1$ the upper limit of $\phi = 60°$. The values shown in Table II are seen to exceed this.

As the shear rate was increased further the drops deviated markedly

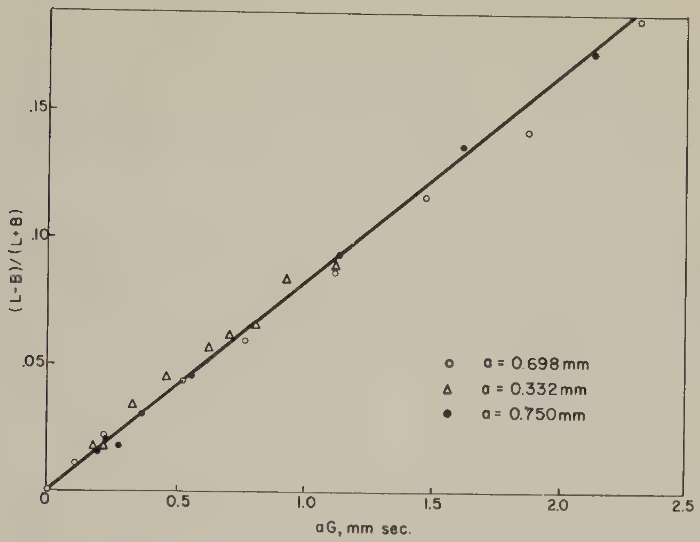

FIG. 3. Deformation of drops of carbon tetrachloride at various rates of shear Cf. Eq. [5].

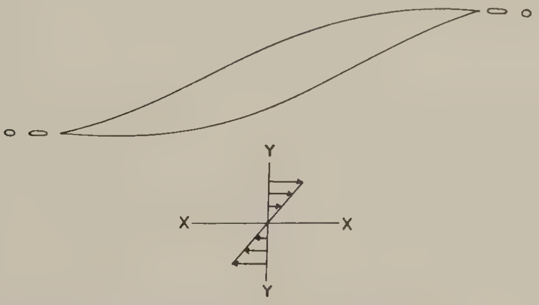

FIG. 4. Sketch of an unstable drop of $CCl_4$ deformed by shear. Fragments of liquid became detached from the parent drop at the pointed ends.

from the ellipsoidal shape. In agreement with Taylor's observations (8) on a system of comparable $p$, the $CCl_4$ drops assumed a sigmoidal shape as shown in Fig. 4 with thin streaks of liquid breaking off the pointed ends. As $G$ was increased further, however, the drop reverted to its stable ellipsoidal shape.

The CHP drops, however, showed a markedly different behavior. As $G$ was increased the elongation increased until a point was reached at which a neck was suddenly formed at the center (as shown in Fig. 5) which separated to form two drops. Similar behavior was noted by Taylor for a system in which $p = 0.9$ (8).

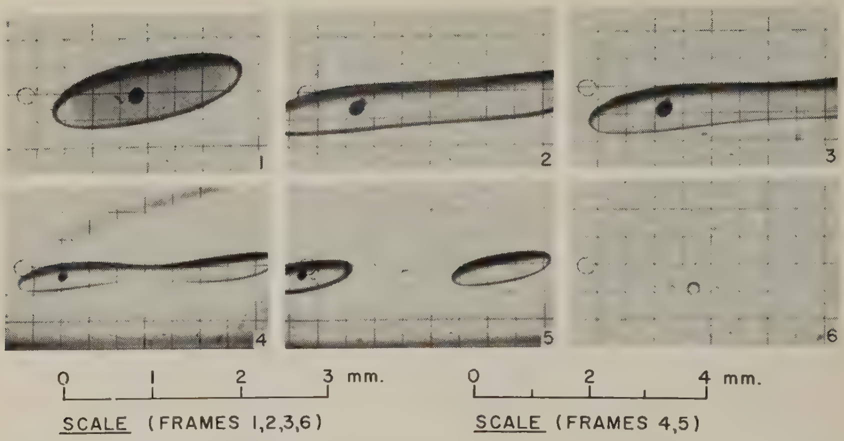

FIG. 5. Photomicrographs of the breakup of a CHP drop by shear. Frame 1 is at $G = 2.8$ sec.$^{-1}$ and Frames 2 to 6 are in chronological order at $G = 3.7$ sec.$^{-1}$. Note the formation of the neck which thins out until separation occurs (Frame 5) with the formation of three satellite drops midway between the two daughter drops. Frame 6 shows the three satellite drops. The broken circle on the left side of each frame is a reference mark on the microscope graticule.

## DOUBLETS

### *Standard Doublets*

Since monodisperse suspensions of liquid drops in corn syrup could not be produced, care was taken to select two interacting particles of equal size in these experiments and to employ low gradients so as to avoid particle deformation. The interaction mechanism was observed to be much the same as that of a rigid spherical particle (2, 5). The paths of approach and recession were curvilinear and mirror-images of one another, and during its life the doublet appeared to rotate as a rigid dumbbell. For clarity, these collisions are termed "standard" to distinguish them from the much less frequent "head-on" collisions discussed later. In aged suspensions, the two drops did not coalesce during a standard collision, but separated at the mirror-image of the initial position of contact about the plane $x = 0$, in exactly the same way as equal-sized rigid spheres (2, 5).

The doublet rotation was followed by measuring the orientation $\phi$ of the line joining the particle centers as a function of time. Figure 6 shows a plot of $\tan \phi$ against $\tan (2tG/5)$ for three different collision doublets of CHP. A similar plot was obtained for two doublets of $CCl_4$. Both systems show a slight deviation from the relation

$$\tan \phi = r_e \tan \frac{tG}{(r_e + 1/r_e)} \qquad [6]$$

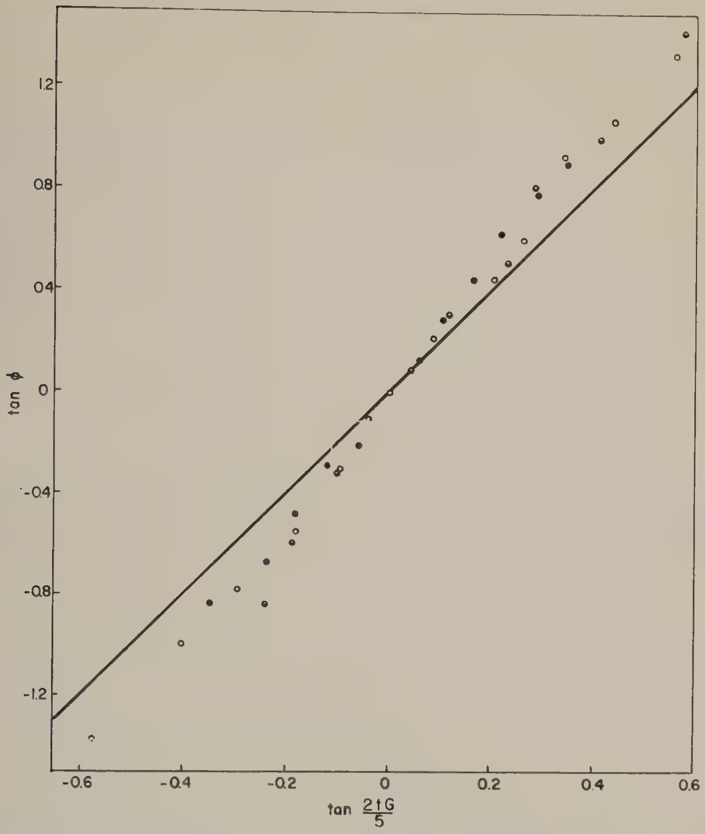

FIG. 6. The rotational behavior of these different collision doublets of CHP. The straight line is calculated from

$$\tan \phi = 2 \tan \frac{2tG}{5}$$

and corresponds to Eq. [6] for $r_e = 2$.

for the case where $r_e = 2$. Equation [6] is the theoretical relation for a prolate spheroid of axis ratio $r_e$ (10). It was previously shown (5) that standard collision doublets of rigid spheres conform very closely to Eq. [6] for $r_e = 2$.

The relationship for the fluid particles is nonlinear and, in each of the two liquid-drop systems, follows a steeper line than that corresponding to $r_e = 2$. While the drops appeared to remain spherical, it is estimated from Eq. [5], using the data of Table II, that in these experiments $L/B = 1.01$. It was therefore concluded that this small deformation was responsible for the slight deviation in doublet behavior from $r_e = 2$.

In these experiments, the $\Delta y$ between two colliding drop centers was

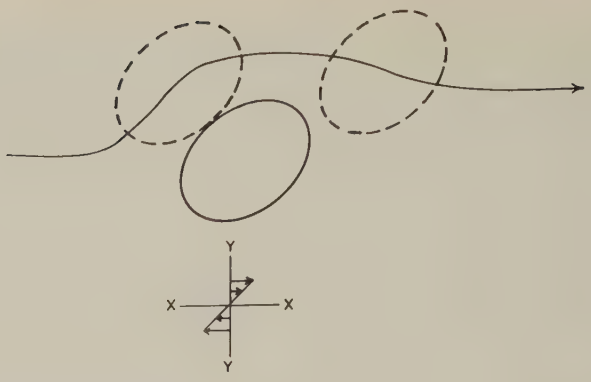

FIG. 7. Collision of two drops deformed by shear. Note the permanent increase in $\Delta y$ after separation (schematic).

restored, after separation, to the value prevailing before collision. When highly deformed drops interacted, however, it was found that $\Delta y$ was greater after separation. This is illustrated schematically in Fig. 7.

### *Head-On Doublets*

The behavior of head-on collision doublets of drops of both CHP and $CCl_4$ was the same as for rigid spheres (5). The relative velocity of the particle centers along the $X$-axis was small and $\Delta y$ remained small during the doublet rotations; $\Delta z$ changed appreciably and was nearly equal to one particle diameter at $\phi = 0$. Whereas the two spheres continued to rotate indefinitely without separating in the case of rigid spheres, head-on collision doublets of fluid spheres coalesced into single droplets after a number of doublet rotations; this number varied between wide limits depending upon the geometry of the collision doublets and, as will be seen later, the age of the corn syrup suspension.

Figure 8 shows the variation of $\phi$ with time for a complete rotation of a $CCl_4$ head-on collision doublet, which in this instance corresponded to $r_e = 3.86$.

It was noted in the course of these experiments that the $TG$ of a doublet appeared to decrease with progressive rotation. This is illustrated in Table III for a collision doublet (No. 1) in which the two CHP spheres appeared to the eye to be in continuous contact until coalescence occurred. It is interesting to note that during the last rotation, before coalescence, $TG/2\pi = 3.7$, which was very close to the value found for a similar doublet of rigid spheres (5) and for a touching doublet of air bubbles (3). Further evidence of the decrease of $TG$ is given in Table III for a doublet (No. 2) of CHP drops the centers of which were initially separated along the $X$-axis (when $\phi = \pm\pi/2$) by about two particle diameters. As the doublet

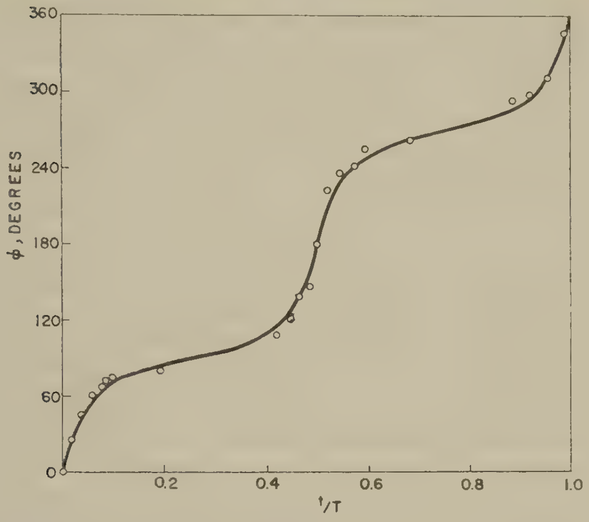

FIG. 8. Rotation of a head-on collision doublet of $CCl_4$ drops.
$G = 0.537$ sec.$^{-1}$; $TG/2\pi = 4.12$; $r_e = 3.86$.
The points are the experimental values, and the curve is that calculated from Eq. [6] using the measured value of $r_e$.

TABLE III

*Variation with Time of Period of Head-on Collision Doublets CHP in Corn Syrup*

| Rotation number prior to coalescence | Measured $TG/2\pi$ | |
|---|---|---|
| | Doublet No. 1 (Initially "touching") | Doublet No. 2 (Initially separated) |
| 5 | 4.2 | 13.7 |
| 4½ | 4.0 | 12.3 |
| 4 | 3.9 | 10.8 |
| 3½ | 3.8 | 9.3 |
| 3 | 3.8 | 7.9[a] |
| 2½ | 3.8 | 6.6 |
| 2 | 3.8 | 5.3 |
| 1½ | 3.7 | 4.5 |
| 1 | 3.7 | 4.0 |
| ½ | 3.7 | 4.0 |

[a] Drops appeared visually to be touching until coalescence occurred.

rotated the two spheres moved closer together until they appeared to be touching, and coalescence then occurred after three rotations.

In some instances, however, the droplets of collision doublets moved completely apart. This may have been due to a sudden adventitious disturbance of the local field of motion.

On a number of occasions it was observed that, when the motion of a standard collision doublet was arrested near the mid-point, i.e. near $\phi = 0$, and after an interval the motion was restored, it became a head-on doublet which eventually coalesced. The cause of this transformation is not known with certainty, but may have been due to rotation about a horizontal axis from sedimentation or convection.

### *Coalescence of Doublets*

The shear-induced coalescence of droplets of CHP undergoing standard collisions was studied using particles dispersed in "string-of-pearl" formations in corn syrup. At $G < 0.1$ sec. a considerable fraction of the collisions resulted in coalescence, *when freshly prepared systems were used.* At higher shear rates, the drops separated after collision in the same manner as rigid spheres. This suggested that sufficient time of contact was required to drain the intervening film of continuous medium to such a thickness that the interaction forces could cause coalescence. Further evidence for the need of contact time was provided by reversing the direction of the field of motion and thus re-forming a doublet whose individual spheres had previously separated, and then stopping the motion of the doublet. In every instance, the spheres of the doublet coalesced after a few seconds.

Because of the high localized concentration of droplets in these experiments, the formation of triplets and quadruplets was also observed; in many cases these coalesced into multiplets of lower order.

When the suspensions were aged, the tendency of doublets to coalesce decreased. Several hours after preparing the suspension, the drops of standard collision doublets invariably separated no matter how low the gradient. When brought to rest for as long as an hour, the doublet did not coalesce.

Since the corn syrup undoubtedly contained surface-active impurities which, when the suspensions were aged, would tend to accumulate at the interface, a pure liquid, glycerine, was used as the suspending medium. The fraction of collisions of CHP drops suspended in glycerine which resulted in coalescence was found to be independent of the age of the suspension. When the motion of a doublet was stopped, coalescence occurred after a few seconds in both freshly prepared and aged suspensions.

With 0.2% of a surface-active agent, polyoxyethylene sorbitan monolaurate dissolved in CHP before the drops were dispersed in glycerine, coalescence of the drops was completely inhibited even in freshly prepared suspensions.

In aged suspensions of $CCl_4$, CHP, and air in corn syrup, the continuous rotation of head-on collision doublets appeared to be the only means of coalescence. However, it was clearly evident that the number of rotations before coalescence occurred increased with age. The effect was very marked with $CCl_4$; here as many as 200 complete rotations of head-on collision doublets were described without coalescence in suspensions three days old.

## DISCUSSION

Both the inhibition of internal circulation and of coalescence in corn syrup suspensions suggested the formation of a semi-rigid or viscoelastic film around the droplets by surface-active impurities. Thus the transmission of tangential stresses from the medium to the disperse phase was inhibited, in contrast with the boundary condition which was assumed by Taylor (6, 8). Oldroyd (11) has extended Taylor's theory of emulsion viscosity to allow for the effect of viscoelastic interfacial films; this theory has been used to calculate the surface viscosity of the interfacial film in systems deviating from Taylor's theory (12).

The present results are in agreement with earlier observations on sedimenting fluid spheres. Internal circulation was inhibited by trace amounts of surface-active impurities (13–15) up to high sedimentation velocities. Nawab and Mason (12) obtained indirect evidence of internal circulation by careful measurements of the viscosity of dilute monodisperse emulsions, but concluded that the addition of surfactants tended to inhibit circulation with a resultant increase of the emulsion viscosity.

Since circulation inside deformed drops could be observed, it would appear that, as the rate of shear in the corn syrup suspensions was increased, the film surrounding the drops became progressively less resistant to the viscous forces exerted by the medium, so that tangential stresses were transmitted inside the drops although they were probably diminished in intensity.

It also appears from the experiments on coalescence that aging was required for the resistant film to develop in the corn syrup suspensions. Once the film became developed around the drops, only the continued rotation of head-on collision doublets could cause rupture of the film and coalescence. It should be noted that during the rotations of a head-on collision doublet the drops were kept together by stresses due to the nonuniform hydrodynamic pressure field, whereas in quiescent systems only long-range interaction forces of the London-Van der Waals type could act on the particles. The attraction between the drops due to such long-range molecular interaction forces in aged suspensions appeared to be insufficient to overcome the resistance of the film around the drops, so that two drops could remain indefinitely in apparent contact without coalescence.

The inhibition of coalescence by adding a surfactant to suspensions of glycerine is further evidence of the formation of films around the drops. In pure glycerine suspensions, as well as in freshly prepared corn syrup suspensions, coalescence did not occur instantaneously. Invariably some time had to elapse before coalescence took place between droplets of a head-on collision or in the absence of macroscopic fluid motion. Furthermore, since the number of collisions resulting in coalescence decreased as the shear rate was increased, it was evident that sufficient contact time was required before coalescence even in systems which were unaffected by aging.

The observations on coalescence described above are qualitative and preliminary in nature. Further experiments are planned.

## SUMMARY

The spin of single liquid spheres of carbon tetrachloride and of cyclohexanol phthalate suspended in corn syrup was measured over a range of laminar shear rates and was found to be practically identical with the value for rigid spheres. No fluid circulation inside the drops was evident until the gradient was increased sufficiently to deform the drops. The variation of drop deformation with initial diameter and velocity gradient agreed with Taylor's theory.

The standard and head-on collision doublets of equal-sized liquid spheres behaved similarly to those of rigid spheres. The angular velocity of standard doublets showed a slight deviation from the equation for rigid prolate spheroids of axis ratio 2, presumably because of slight deformation of each drop. Standard collisions resulted in coalescence only when sufficient contact time was allowed for film drainage and only in freshly prepared corn syrup suspensions. Head-on collisions almost always resulted in coalescence, although the time required increased with age of the suspension. When glycerine was used as the medium, there was no aging effect.

It is concluded that the inhibition of internal circulation and of coalescence in the corn syrup suspensions was due to the formation of a viscoelastic interfacial film.

## REFERENCES

1. TREVELYAN, B. J., AND MASON, S. G., *J. Colloid Sci.* **6,** 354 (1951).
2. MANLEY, R. ST. J., AND MASON, S. G., *J. Colloid Sci.* **7,** 354 (1952).
3. MANLEY, R. ST. J., AND MASON, S. G., *Can. J. Chem.* **33,** 763 (1955).
4. MASON, S. G., AND MANLEY, R. ST. J., *Proc. Roy. Soc.* (*London*) **A238,** 117 (1956).
5. BARTOK, W., AND MASON, S. G., *J. Colloid Sci.* **12,** 243 (1957).
6. TAYLOR, G. I., *Proc. Roy. Soc.* (*London*) **A138,** 41 (1932).
7. BARTOK, W., AND MASON, S. G., *J. Colloid Sci.* **13,** 293 (1958).
8. TAYLOR, G. I., *Proc. Roy. Soc.* (*London*) **A146,** 501 (1934).
9. SILBERBERG, A., AND KUHN, W., *J. Polymer Sci.* **13,** 21 (1954).
10. JEFFERY, G. B., *Proc. Roy. Soc.* (*London*) **A102,** 161 (1922).
11. OLDROYD, J. G., *Proc. Roy. Soc.* (*London*) **A232,** 567 (1955).
12. NAWAB, M. A., AND MASON, S. G., *Trans. Faraday Soc.* **54,** 1712 (1958).
13. GARNER, F. H., AND SKELLAND, A. H. P., *Chem. Eng. Sci.* **4,** 149 (1955).
14. HABERMAN, W. L., AND MORTON, R. K., Report 802, Navy Department, The David W. Taylor Model Basin, Washington, 1953.
15. SAVIC, P., Report No. MT-22, National Research Council of Canada, Division of Mechanical Engineering, Ottawa, 1953.

JOURNAL OF COLLOID SCIENCE **14**, 27–35 (1959)

# EFFECT OF ADSORBED SUBSTANCES OF HIGH MOLECULAR WEIGHT ON THE GROWTH OF SILVER HALIDE CRYSTALS[1]

**Ernest J. Perry**

*Research Laboratories, Eastman Kodak Company, Rochester, New York*

*Received August 18, 1958*

## Abstract

A study of the effect of adsorbed substances of high molecular weight on the crystal growth of silver bromide containing a minor amount of silver iodide has shown that, in addition to two factors previously postulated by other workers as contributing to coalescence during crystal growth, namely, the presence of trace quantities of "growth promoters" and the degradative destruction of the adsorbed protective colloid layer, another factor must also be considered, namely, the nature of the protective colloid layer. Depending on the type of protective layer formed, there may be wide variations in the relative contributions of coalescence ripening and of Ostwald ripening to crystal growth. The nature of the adsorbed protective layer has a profound effect not only on the ease of crystal growth but also on the morphology of the crystals obtained.

## Introduction

A mixture of crystals of moderately soluble salts will undergo changes in size distribution by dissolution of small and simultaneous growth of large particles, provided there is a difference in surface energy between the small and the large particles. This process is called "Ostwald ripening."

In addition to the specific surface area, the surface energy difference is related also to the crystal imperfections of the small and large crystals, modified by the presence of protective colloid or other adsorbed species. The presence of crystal imperfections at the surface also may greatly modify the rate of solution and reprecipitation but measurement of these effects is difficult and has not yet been accomplished except in certain etching experiments (1), in which crystals were shown to be preferentially attacked at sites containing crystal imperfections. In the simple case of silver halides in water at room temperature, the rate of Ostwald ripening is low because the amount of dissolved material available to produce supersaturation relative to large crystals is small. Crystal growth in these systems can be enhanced by elevated temperatures and by the presence of silver halide solvents, such as potassium bromide or ammonium hydroxide, which lead to the formation of such complex ions as $(AgBr_3)^=$ and $Ag(NH_3)_2^+$.

---

[1] Communication No. 1978 from the Kodak Research Laboratories.

It has long been a question of interest to determine what proportion of the crystal growth occurring in the presence of silver halide solvents and protective colloids, which is ordinarily referred to as "ripening" or "physical ripening," is due to processes other than Ostwald ripening. Sheppard and Lambert (2) believed that these alternative growth processes involved coalescence, followed by crystal orientation and recrystallization. Ammann-Brass (3) approached the same question in two ways. He studied the kinetics of particle growth by turbidimetric measurements and also examined the silver halide crystals obtained after ripening by electron micrography. He concluded that two different processes could indeed be distinguished, according to the shape of the ripening curve and the size distribution of the crystals obtained. He found that Ostwald ripening was characterized by a linear rate of increase of particle size with time, by the growth of *all* silver halide crystals discernibly present, and by a progressive inhibition of crystal growth with increasing protective colloid concentration. Coalescence ripening, on the other hand, was characterized by S-shaped growth curves, by an increase in the ease of ripening with increasing concentrations of protective colloid, and by the appearance of a limited number of large crystals as well as the clearly discernible survival of crystals of unchanged small size throughout the period of growth.

Ammann-Brass (3) found that coalescence ripening was associated with photographically "active" gelatins, i.e., gelatins containing trace quantities of certain low molecular weight materials. He found that these growth-promoting materials could be removed by procedures customarily used to convert "active" gelatins to inert ones. The explanation for this type of growth promotion may, quite likely, be the same as that offered (4) for the action of certain substances such as thiosulfate and substituted thioureas (5) which are believed to act as ripening-accelerators for silver halides stabilized by polyvinyl alcohol by displacing a small part of the adsorbed protective colloid from the silver halide surface.

The growth of silver bromide and of mixed silver bromide-silver iodide crystals in the presence of gelatin and of the silver halide solvent, ammonium hydroxide, has recently been studied by Malinowski (6, 7). After studying the change in crystal size with time and an examination of microphotographs of the crystals as well as of certain changes in surface and internal photographic sensitivity, Malinowski concluded that high concentrations of ammonium hydroxide, low concentrations of silver iodide, and a potassium bromide excess of 10% to 20% led to S-shaped growth curves, Ostwald ripening occurring initially and finally, while "coalescence ripening" took place during an intermediate time interval. The occurrence of coalescence ripening during the stated time interval confirmed pictorially as in the work of Ammann-Brass by the existence of two distinct maxima in the size-distribution curve, was ascribed by Malinowski to a destruction of the protective gelatin layer around the silver halide crystals by the ammonium hydroxide.

The studies of Sheppard and Lambert, of Ammann-Brass, and of Malinowski cited were all made in the presence of only one protective colloid, namely, gelatin. The present work represents an extension of these studies in a direction not heretofore covered, namely, an examination of the mechanism of growth during ripening in the presence of some protective colloids other than gelatin. The advantage of this approach is that growth-promoting substances which are known to occur in certain gelatins do not enter the picture, and it is also possible to determine the effect of changes in the nature of the protective colloid layer.

## Methods and Materials

The following materials were used:

Silver nitrate, ammonium hydroxide; Eastman Kodak Company, C. P. Grade.

Potassium bromide; Baker and Adams, Reagent Grade.

Gelatin, a relatively inert lime-processed gelatin.

Polyacrylamide "75," a product made by American Cyanamid Company.

Polyvinyl alcohol, Elvanol 70-05, made by E. I. du Pont de Nemours and Company, Inc.

Polyvinylamine; the sample used was prepared by the Organic Chemistry Department, of the Kodak Research Laboratories, according to the method of Reynolds and Kenyon (8).

Substituted polyvinyl acetal, substituted nylon (based on a polymer made by E. I. du Pont de Nemours and Company, Inc.).

Preparative details pertaining to these materials made by the Organic Chemistry Department, of the Kodak Research Laboratories, will be given elsewhere.

Three types of silver halide suspensions were prepared:

Type I suspensions were made by addition over a period of 95 seconds of a mixture of 7.1 ml. of 2 *M* silver nitrate, of ammonium hydroxide just sufficient to redissolve the silver oxide precipitated after initial addition of the ammonium hydroxide, and of 23 ml. of water to a mixture of 8.4 ml. of 2 *M* "mixed halide" (98.5 mole % potassium bromide; 1.5 mole % potassium iodide) and 18.6 ml. of water containing 0.8 g. of the protective colloid. The resultant suspension, which contained 2.66 g. of silver bromide and which was 0.052 *M* in potassium bromide and 0.57 *M* in ammonium hydroxide, was ripened at temperatures and during time intervals given below for each experiment. All suspensions were stirred continuously during mixing of the reagents as well as during ripening.

Type II suspensions differed from Type I in that the volume of the "mixed halide" solution was 7.3 ml. The resultant suspension was then 0.008 *M* in potassium bromide.

Type III suspensions were prepared by addition, over a period of 12 minutes, of a mixture of 1 ml. of 2 *M* silver nitrate and 3 ml. of water to a mixture (previously heated to the ripening temperature) of 8.4 ml. of 2 *M* "mixed halide" and 17.5 ml. of water containing 0.8 g. of the protective colloid. The resultant suspension was, therefore, 0.65 *M* with respect to potassium bromide before and 0.495 *M* after addition of the silver nitrate. Temperature and duration of ripening were again as indicated later in the paper.

The samples for making transmission electron micrographs were prepared by suitable dilution (by a factor of about 100) of the suspensions immediately after completion of a given ripening period in order to obtain single-layer coatings of the silver halide crystals. The resulting very low concentrations of silver halide solvents in these diluted solutions should minimize any changes of the crystals after coating. Visual observations under the optical microscope immediately after coating appear to indicate that no appreciable change of the silver halide crystals occurred during and after drying of the coatings used for electron micrography. The distance between the two parallel bars shown on each electron micrograph corresponds to 1 micron. All electron micrographs were obtained by C. F. Oster, Jr., of the Analytical Chemistry Department of the Kodak Research Laboratories The experimental work was carried out in a darkroom under Kodak Wratten Safelight, Series O.

## Results and Discussion

Very clear evidence of the occurrence of coalescence ripening may be obtained by inspection of Fig. 1, where a substituted nylon served as the protective colloid. The coexistence of two size classes of crystals is evident as well as the fact that, following coalescence, there is an appreciable amount of recrystallization, with the result that the recrystallized particles have distinctly octahedral features.

Inasmuch as the suspension contains no trace material known to act as a "physical-ripening accelerator" and as the polymer used is not attacked chemically by the ammonium hydroxide present, the type of ripening observed should most probably be ascribed to the nature of the "envelope" of polymer adsorbed to the silver halide surface. Coalescence between hydrophobic colloidal particles "protected" by a hydrophilic protective colloid is usually regarded as very improbable, because the adsorbed hydrophilic layer prevents the hydrophobic particles from approaching each other sufficiently for attractive Van der Waals-type forces to be effective (9). A "physical-ripening accelerator" apparently increases the probability of such

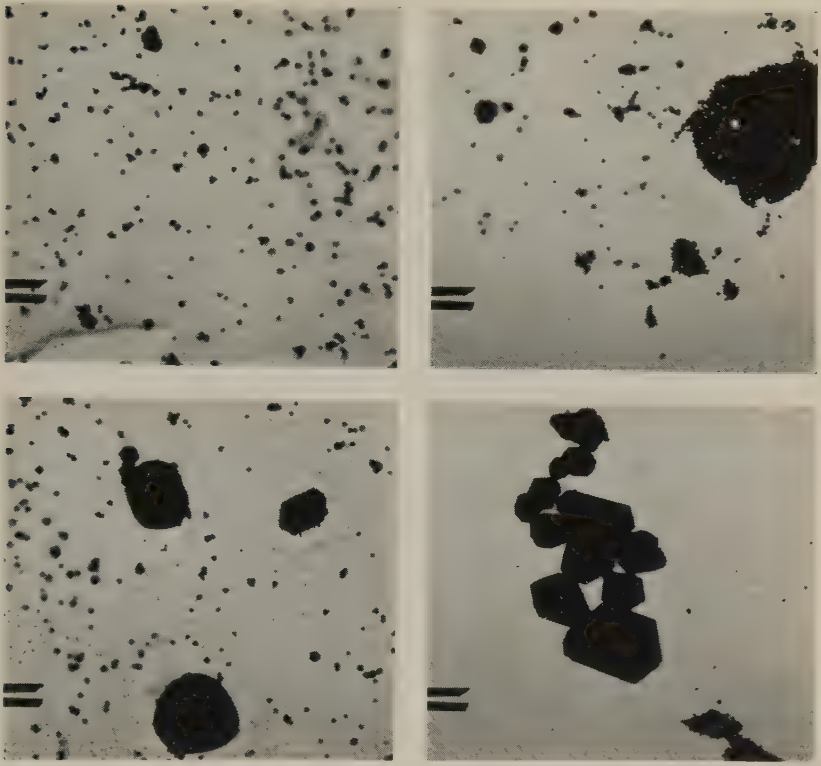

FIG. 1. Crystal species observed during 100 minutes' ripening at 54°C. of a Type I suspension containing a substituted nylon.

a close approach by creating small, nonprotected areas on the silver halide surface as the molecular bulk of the adsorbed accelerator is not sufficient to provide for "steric protection" (9). The processes illustrated in Fig. 1 show that the structure of certain protective colloid layers may be such as to provide for a low but finite probability of coalescence, perhaps because steric factors or the relative paucity of adsorbable groups causes the silver halide surface to be covered somewhat less efficiently than in the case of other protective colloids.

If ripening is carried out under the same conditions but with polyacrylamide as the protective colloid, then the results (Fig. 2) are quite different. The crystals obtained are quite similar to those resulting from the use of gelatin under the same experimental conditions. Instead of two there is now only one size class of crystals, the grains are more rounded, and there is no evidence of intermediate stages of coalescence processes.

The mechanism of crystal growth of silver halides in the presence of gelatin and of ammonia has never been fully explained, but it obviously

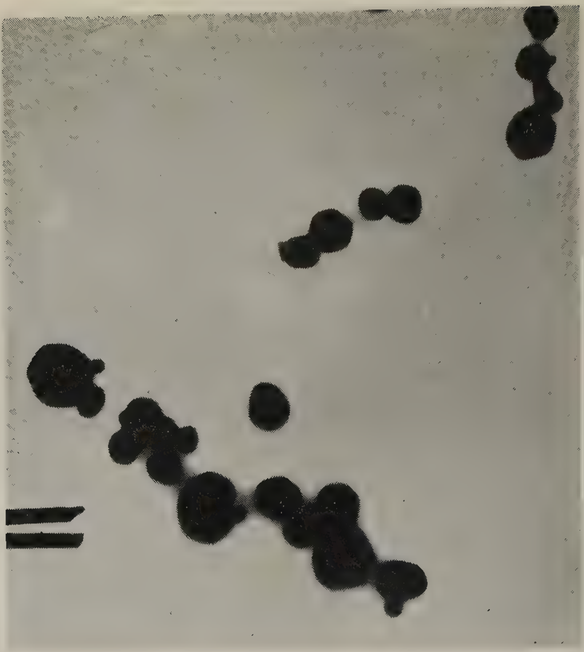

Fig. 2. Type I suspension containing polyacrylamide ripened for 50 minutes at 54°C.

differs considerably from crystal growth effected through the solvent action of excess soluble bromide. The suspensions obtained in the latter case are well known (10) to consist of crystals which are well-defined octahedra (triangles, hexagons, etc.) and which may fall within a very wide range of size distribution. It has been suggested (11) that during crystal growth of ammonia-containing silver halide suspensions there is a lowering of the negative potential around the growing silver halide crystals by adsorption of the ionic species, $Ag^+(NH_3)_2$, and that this factor promotes a more isotropic type of crystal growth (12). Ostwald ripening, modified by these effects rather than coalescence processes, may, therefore, be the dominating factor in obtaining crystals such as those shown in Fig. 2.

Polyvinyl alcohol is well known to have a strongly inhibiting effect on the growth of silver halide crystals. Thus, crystals stabilized by polyvinyl alcohol showed no appreciable growth at 77°C. in the presence of 0.57 $M$ ammonium hydroxide, irrespective of whether the bromide concentration was 0.052 $M$ or 0.008 $M$. Crystals stabilized by polyvinyl alcohol and ripened under these conditions attained a diameter of only 0.1 micron without any occurrence of coalescence ripening. However, the use of a highly substituted polyvinyl acetal in which a very large part of the hydroxyl groups had been replaced by other groups results in a suspension which shows clear

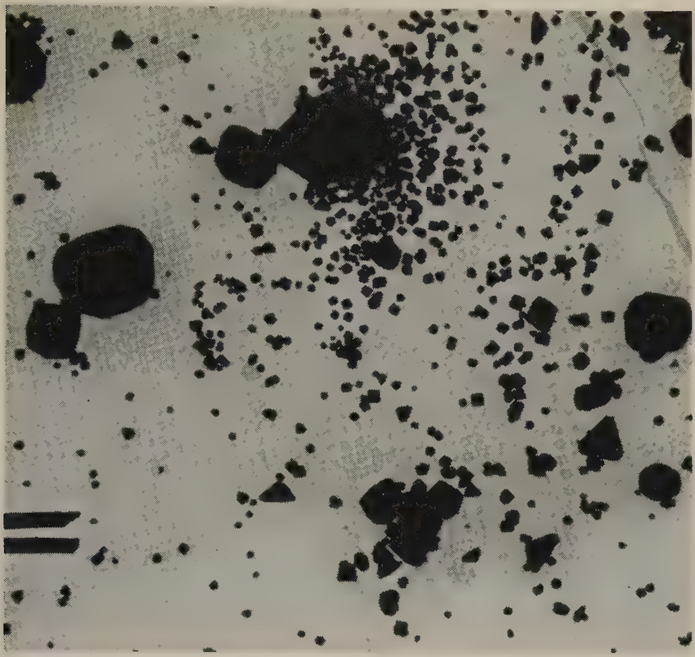

FIG. 3. Type II suspension containing a substituted polyvinyl acetal ripened at 77°C. for 135 minutes.

signs of coalescence ripening (Fig. 3), i.e., two size classes of crystals, with the large crystals evidently in various stages of crystal perfection. Substitution of part of the hydroxyl groups of polyvinyl alcohol has apparently altered the nature of the adsorbed protective colloid envelope sufficiently to render this type of crystal growth possible. Although experiments made with this polymer at constant ammonium hydroxide and different bromide concentrations have shown that a low bromide concentration favors this type of growth, a similar, although somewhat less pronounced, growth of the same type occurred also at the bromide concentrations used for the crystals stabilized by polyacrylamide and shown in Fig. 2. Experiments in which crystals stabilized by gelatin or polyacrylamide were ripened by ammonium hydroxide at the lower bromide concentration (0.008 $M$) gave results which did not differ visibly from experiments in which the higher bromide concentration of 0.052 $M$ had been used.

The fact that the crystal growth of silver halides in the presence of a protective colloid and of a silver halide solvent becomes more pronounced as increasing amounts of the hydroxyl groups of polyvinyl alcohol are substituted by polyvinyl acetal groups has been noted by Evva (13). In the light of the results reported here, it appears, therefore, that such substitu-

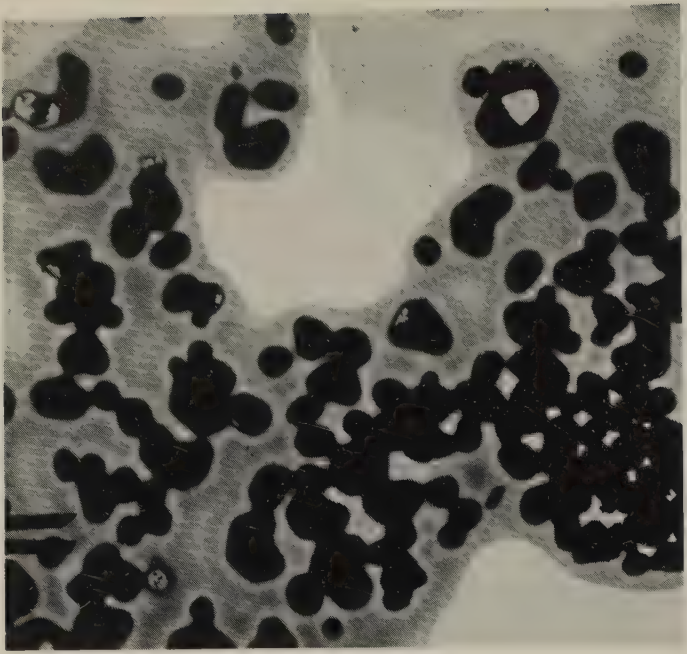

FIG. 4. Type III suspension containing polyvinylamine ripened at 70°C. for 90 minutes.

tion leads to coalescence ripening rather than to a significant increase in the ease of Ostwald ripening.

If a substituted polyvinyl acetal containing a greater number of residual hydroxyl groups was used as the protective colloid, then the occurrence of coalescence ripening was again evident. However, recrystallization and crystal perfection then occurred to a lesser extent than in the presence of the more highly substituted polyvinyl acetal.

The degree of crystal perfection usually observed with a given protective colloid was found to be related to the ease of crystal growth in the presence of the protective colloid, as determined by experimental methods described previously (14). However, the type of crystal obtained with protective colloids such as polyvinylamine (Fig. 4) is a clear indication that habit-modifying effects should also be attributed to certain adsorbed polymers. In this they resemble some adsorbed low molecular weight substances such as certain dyes or urea.

## REFERENCES

1. MITCHELL, J. W., *Z. Elektrochem.* **60**, 557 (1956).
2. SHEPPARD, S. E., AND LAMBERT, R. H., "Colloid Symposium Monograph," Vol. 6, p. 265. Chemical Catalog Co., New York, New York, 1928.

3. Ammann-Brass, H., *Z. Naturforsch.* **6a,** 372 (1951).
4. Oyama, Y., and Futaki, K., *Bull. Chem. Soc. Japan* **28,** 243 (1955).
5. Oyama, Y., and Futaki, K., *J. Soc. Sci. Phot. Japan* **16,** 39 (1953).
6. Malinowski, J., *Z. wiss. Phot.* **51,** 186 (1956).
7. Malinowski, J., *Z. wiss. Phot.* **51,** 200 (1956).
8. Reynolds, D. D., and Kenyon, W. O., *J. Am. Chem. Soc.* **69,** 911 (1947).
9. Heller, W., and Pugh, T. L., *J. Chem. Phys.* **22,** 1778 (1954).
10. Mees, C. E. K., "The Theory of the Photographic Process," 2nd (revised) ed., p. 4. The Macmillan Co., New York, 1954.
11. Abribat, M., "Chimie Physique des Couches Sensibles Photographiques," p. 81. Presses Universitaires de France, Paris, 1954.
12. Glafkidès, P., "Chimie Photographique," 2nd ed., p. 253. Publications Photo-Cinéma Paul Montel, Paris, 1957.
13. Evva, F., *Kolloid-Z.* **135,** 136 (1954).
14. Perry, E. J., *J. Phys. Chem.* **62,** 585 (1958).

JOURNAL OF COLLOID SCIENCE **14**, 36–48 (1959)

# SOME APPROXIMATE EQUATIONS USEFUL IN THE PHENOMENOLOGICAL TREATMENT OF LINEAR VISCOELASTIC DATA

**Kazuhiko Ninomiya and John D. Ferry**

*Department of Chemistry, University of Wisconsin, Madison, Wisconsin*

*Received August 19, 1958; revised October 10, 1958*

## Introduction

Several approximation methods (1–5) have been developed, all based on the theory of linear viscoelastic behavior (6), to calculate the relaxation spectrum, $H$, and/or the retardation spectrum, $L$, from dynamic mechanical data. Common to all of these is the use of derivatives from experimental curves of viscoelastic functions such as the real and imaginary parts of the complex modulus. As an alternative, an approximate method is presented here for calculating $H$ and $L$ without differentiation, using two or more measured values equally spaced on the logarithmic frequency scale.

Another important practical problem in the theory of linear viscoelastic behavior is the approximate calculation of one viscoelastic function from another. A useful approximation for obtaining the relaxation modulus from the storage modulus and $H$ has been given by Catsiff and Tobolsky (7), modified from a relation due to Marvin (8); and an analogous expression for compliances has been given by Smith (9). An alternative and somewhat simpler method is developed here for obtaining transient from dynamic functions.

## Approximation Formulas for the Relaxation and Retardation Spectra

### *H and L from the Imaginary Parts of the Complex Rigidity and Compliance*

The imaginary parts of the complex rigidity ($G''$) and compliance ($J''$) are related to $H$ and $L$ as follows:

$$G''(\omega) = \int_{-\infty}^{\infty} \frac{\omega\tau}{1 + \omega^2\tau^2} H \, d \ln \tau, \tag{1}$$

$$J''(\omega) = \int_{-\infty}^{\infty} \frac{\omega\tau}{1 + \omega^2\tau^2} L \, d \ln \tau + \frac{1}{\omega\eta}. \tag{2}$$

Here $\tau$ is the relaxation time in Eq. [1] and the retardation time in Eq. [2], $\omega$ is the angular frequency, and $\eta$ is the steady-flow viscosity. The kernel function $\omega\tau/(1 + \omega^2\tau^2)$, hereafter called the intensity function, gives a curve symmetrical about its maximum at $\omega\tau = 1$ and tends to zero on both sides when plotted against log $\omega\tau$. When it is approximated by a Dirac delta function, the zeroth approximations (1) for $H$ and $L$ are obtained, respectively, from Eqs. [1] and [2]. In the second approximation method of Schwarzl and Staverman (3) a linear combination of $G''$ and its second derivative with respect to log $\omega$ was used to obtain a sharper intensity function. Recently Fujita (4) has shown that higher approximations to $H$ can be obtained by linear combinations of higher derivatives of $G''$. However, it is hardly practical to determine precisely higher derivatives of experimental curves of $G''$. We shall show that a corresponding series of successive approximations to $H$ can be derived using experimental $G''$ values themselves. By combining Eq. [1] linearly, we may construct a relation such that

$$C\left\{\left(1+\frac{1}{a^2}\right)G''(\omega) - \frac{1}{a}\left[G''(a\omega) + G''\left(\frac{\omega}{a}\right)\right]\right\}$$
$$= C\int_{-\infty}^{\infty}\frac{(a^4-1)(a^2-1)}{a^4}\,\frac{\omega^3\tau^3}{a^{-2}+\omega^2\tau^2)(1+\omega^2\tau^2)(a^2+\omega^2\tau^2)}\,H\,d\ln\tau, \qquad [3]$$

where $C$ and $a$ are constants; the latter is assumed greater than unity without loss of generality. To simplify the discussion, the arbitrary constant, $C$, is chosen as the normalization constant for the kernel in Eq. [3], $(2/\pi)[a/(a-1)]^2$. Then we denote the normalized intensity function, $f''_1$, and the normalized combination function, $F''_1$ as follows:

$$f''_1 \equiv \frac{2}{\pi}\,\frac{(1+a^2)(1+a)^2}{a^2}\,\frac{\omega^3\tau^3}{(a^{-2}+\omega^2\tau^2)(1+\omega^2\tau^2)(a^2+\omega^2\tau^2)}, \qquad [4]$$

$$F''_1 \equiv \frac{2}{\pi}\left\{G''(\omega) - \frac{a}{(a-1)^2}\left[G''(a\omega) + G''\left(\frac{\omega}{a}\right) - 2G''(\omega)\right]\right\}. \qquad [5]$$

Figure 1 shows the curves of $f''_1$ vs. log $\omega\tau$ for several values of $a$; they are all symmetrical about their maxima located at $\omega\tau = 1$. It is seen from the figure that the shapes of $f''_1$ are sharper than that of the normalized intensity function in Eq. [1], $(2/\pi)[\omega\tau/(1+\omega^2\tau^2)]$, and that the closer the value of $a$ to unity, the sharper the curve of $f''_1$ becomes. In the limits $a \to 1$ and $a \to \infty$, we have

$$F''_1(a=1) = \frac{2}{\pi}\left[G''(\omega) - \frac{d^2G''(\omega)}{d\ln\omega^2}\right], \qquad [6]$$

$$F''_1(a=\infty) = \frac{2}{\pi}\,G''(\omega), \qquad [7]$$

$$f''_1(a=1) = \frac{2}{\pi}\,\frac{8\omega^3\tau^3}{(1+\omega^2\tau^2)^3}, \qquad [8]$$

$$f''_1(a=\infty) = \frac{2}{\pi}\,\frac{\omega\tau}{1+\omega^2\tau^2}. \qquad [9]$$

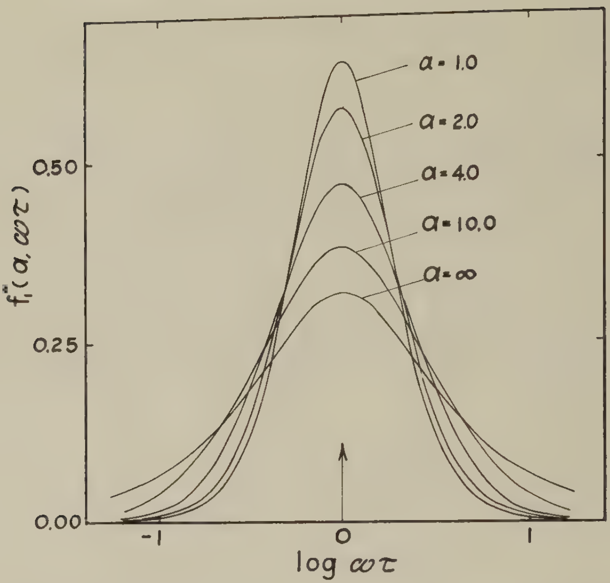

FIG. 1. The normalized intensity functions, $f''_1$, for different values of $a$.

When $f''_1$ is approximated to a Dirac delta function, $F''_1 |_{\omega=1/\tau}$ gives the approximation formula for $H$. It is seen that for $a = 1$ and $a = \infty$, the present method gives the second approximation of Schwarzl (3) and the zeroth approximation (1), respectively.

The same argument may be applied to the imaginary part of the complex compliance to obtain $L$ because the expressions for both $G''$ and $J''$ are formally the same except for the steady-flow term in the latter. Thus the corresponding approximation to the retardation spectrum is

$$L''_1 = \frac{2}{\pi}\left\{J''(\omega) - \frac{a}{(a-1)^2}\left[J''(a\omega) + J''\left(\frac{\omega}{a}\right) - 2J''(\omega)\right]\right\}\Bigg|_{\omega=1/\tau}. \quad [10]$$

It may be noted that the steady-flow term, $1/\omega\eta$, included in the expression of $J''$, does not appear in the final equation for $L''_1$.

It can be shown that the constants multiplied by $G''$'s in the linear combination of $G''$, such as $1 + 1/a^2$ and $1/a$, are chosen in such a way that the asymptotes of the intensity functions corresponding, respectively, to $(1 + 1/a^2)G''(\omega)$ and $(1/a)[G''(a\omega) + G''(\omega/a)]$ become coincident on both sides on the log $\omega\tau$ axis. Combining this and the fact that $f''_1$ has two asymptotes of slopes of $\pm 3$ on the log-log plot, we can obtain second approximations to $H$ and $L$.

The normalized intensity function, $f''_2$, and the normalized combination function, $F''_2$, for the second approximation to $H$ are, respectively,

$$f''_2 \equiv \frac{2}{\pi} \frac{(1+a)^3(1+a^2)^2(1+a^3)(1+a^4)}{a^6(1+a+a^2)} \times \frac{\omega^5\tau^5}{(a^{-4}+\omega^2\tau^2)(a^{-2}+\omega^2\tau^2)(1+\omega^2\tau^2)(a^2+\omega^2\tau^2)(a^4+\omega^2\tau^2)}, \qquad [11]$$

$$\begin{aligned} F''_2 \equiv{}& \frac{a^6+1}{(a^3-1)^2} F_1''(\omega) - \frac{a^3}{(a^3-1)^2}\left[F''_1(a\omega) + F''_1\left(\frac{\omega}{a}\right)\right] \\ ={}& \frac{2}{\pi}\left\{ G''(\omega) - \frac{a(a^2+1)(a^4+1)}{(a-1)^4(a^2+a+1)^2}\left[G''\left(\frac{\omega}{a}\right) + G''(a\omega) - 2G''(\omega)\right] + \frac{a^4}{(a-1)^4(a^2+a+1)^2}\left[G''\left(\frac{\omega}{a^2}\right) + G''(a^2\omega) - 2G''(\omega)\right]\right\}. \end{aligned} \qquad [12]$$

When $f''_2$ is approximated to a Dirac delta function, $F''_2|_{\omega=1/\tau}$ gives the second approximation to $H$. The second approximation to $L$ can be obtained by replacing $G''$ by $J''$ in Eq. [12] and substituting $1/\tau$ for $\omega$. For $a = 1$ and $a = \infty$, $f''_2$ and the second approximation to $H$, $H''_2$, reduce to

$$f''_1(a = 1) = \frac{2}{\pi}\frac{128}{3}\frac{\omega^5\tau^5}{(1+\omega^2\tau^2)^5}, \qquad [13]$$

$$f''_2(a = \infty) = \frac{2}{\pi}\frac{\omega\tau}{1+\omega^2\tau^2}, \qquad [14]$$

$$H''_2(a = 1) = \frac{2}{\pi}\left[G''(\omega) - \frac{10}{9}\frac{d^2G''(\omega)}{d\ln\omega^2} + \frac{1}{9}\frac{d^4G''(\omega)}{d\ln\omega^4}\right]\Bigg|_{\omega=1/\tau}, \qquad [15]$$

$$H''_2(a = \infty) = \frac{2}{\pi} G''(\omega)\Bigg|_{\omega=1/\tau}. \qquad [16]$$

Equation [15] is essentially the same as the fourth approximation to the relaxation spectrum derived recently by Fujita (4). Again Eqs. [14] and [16] show that for $a = \infty$ this method gives the zeroth approximation to the relaxation spectrum.

It is apparent that the third, fourth, and higher approximations to the relaxation spectrum and/or the retardation spectrum can be obtained successively by repeating the procedure described above.

### *H and L from the Real Parts of the Complex Rigidity and Compliance*

The real parts of the complex rigidity, $G'$, and the complex compliance, $J'$, are related to $H$ and $L$ as follows:

$$G'(\omega) = G_0 + \int_{-\infty}^{\infty} \frac{\omega^2\tau^2}{1 + \omega^2\tau^2} H \, d \ln \tau, \tag{17}$$

$$J'(\omega) = J_0 + \int_{-\infty}^{\infty} \frac{1}{1 + \omega^2\tau^2} L \, d \ln \tau. \tag{18}$$

Here $G_0$ and $J_0$ are the equilibrium modulus and the instantaneous compliance, respectively. Using Eq. [17] we may combine linearly $G'(a\omega)$ and $G'(\omega/a)$ such that

$$C\left[G'(a\omega) - G'\left(\frac{\omega}{a}\right)\right] = C \int_{-\infty}^{\infty} \frac{a^4 - 1}{a^2} \frac{\omega^2\tau^2}{(a^{-2} + \omega^2\tau^2)(a^2 + \omega^2\tau^2)} \cdot H \, d \ln \tau, \tag{19}$$

where $C$ and $a$ are constants which have the same meaning as before.

Also for $J'$

$$C\left[J'\left(\frac{\omega}{a}\right) - J'(a\omega)\right] = C \int_{-\infty}^{\infty} \frac{a^4 - 1}{a^2} \frac{\omega^2\tau^2}{(a^{-2} + \omega^2\tau^2)(a^2 + \omega^2\tau^2)} \cdot L \, d \ln \tau. \tag{20}$$

The intensity functions are the same for both Eqs. [19] and [20], and have symmetrical shapes about their maxima located at $\omega\tau = 1$ on the log $\omega\tau$ axis. The normalized linear combinations of $G'$ and $J'$, and the normalized intensity function for these combinations, are defined, respectively, by

$$F'_{G1} \equiv \frac{1}{2 \ln a}\left[G'(a\omega) - G'\left(\frac{\omega}{a}\right)\right], \tag{21}$$

$$F'_{J1} \equiv \frac{1}{2 \ln a}\left[J'\left(\frac{\omega}{a}\right) - J'(a\omega)\right], \tag{22}$$

$$f'_1 \equiv \frac{a^4 - 1}{2a^2 \ln a} \frac{\omega^2\tau^2}{(a^{-2} + \omega^2\tau^2)(a^2 + \omega^2\tau^2)}. \tag{23}$$

When $f'_1$ is approximated to a Dirac delta function as before, $F'_{G1}|_{\omega=1/\tau}(\equiv H'_1)$ and $F'_{J1}|_{\omega=1/\tau}(\equiv L'_1)$ give the first approximations to $H$ and $L$, respectively. In the limit $a = 1$, $f'_1(a = 1)$, $H'_1(a = 1)$, and $L'_1(a = 1)$ are

$$f'_1(a = 1) = \frac{2\omega^2\tau^2}{(1 + \omega^2\tau^2)^2}, \tag{24}$$

$$H'_1(a = 1) = \left.\frac{dG'(\omega)}{d \ln \omega}\right|_{\omega=1/\tau}, \tag{25}$$

$$L'_1(a = 1) = -\left.\frac{dJ'(\omega)}{d \ln \omega}\right|_{\omega=1/\tau} \tag{26}$$

equivalent to the first approximation of Andrews (1) to $H$ and $L$. On the other hand, when the value of $a$ approaches infinity, the shape of $f'_1$ becomes so broad on the log $\omega\tau$ axis that it is hardly practical to approximate it to a Dirac delta function.

Using the same procedure as before, we can obtain the second approximations to $H$ and $L$, since $f'_1$ has asymptotes of slopes of $\pm 2$ on the log-log plot. The normalized linear combinations of $F'_{G1}$ and $F'_{J1}$ in this case are

$$F'_{G2} \equiv \frac{a^4 + 1}{(a^2 - 1)^2} F'_{G1}(\omega) - \frac{a^2}{(a^2 - 1)^2}\left[F'_{G1}(a\omega) + F'_{G1}\left(\frac{\omega}{a}\right)\right], \qquad [27]$$

$$F'_{J2} \equiv \frac{a^4 + 1}{(a^2 - 1)^2} F'_{J1}(\omega) - \frac{a^2}{(a^2 - 1)^2}\left[F'_{J1}(a\omega) + F'_{J1}\left(\frac{\omega}{a}\right)\right]. \qquad [28]$$

The normalized intensity functions for $F'_{G2}$ and $F'_{J2}$ are the same, and they are

$$f'_2 \equiv \frac{(a^6 - 1)(a^4 + 1)(a^2 + 1)}{2a^6 \ln a} \cdot \frac{\omega^4\tau^4}{(a^{-4} + \omega^2\tau^2)(a^{-2} + \omega^2\tau^2)(a^2 + \omega^2\tau^2)(a^4 + \omega^2\tau^2)}. \qquad [29]$$

If $f'_2$ is approximated to a Dirac delta function, the approximation to $H$ is obtained as follows:

$$H'_2 \equiv F'_{G2}\Big|_{\omega=1/\tau} = \frac{G'(a\omega) - G'(\omega/a)}{2 \ln a} - \frac{a^2}{(a^2 - 1)^2} \cdot \frac{\left[G'(a^2\omega) - G'\left(\frac{\omega}{a^2}\right)\right] - 2\left[G'(a\omega) - G'\left(\frac{\omega}{a}\right)\right]}{2 \ln a}\Bigg|_{\omega=1/\tau}. \qquad [30]$$

The second approximation to $L$, $L'_2$, is obtained by replacing $G'(a\omega)$, $G'(\omega/a)$, $G'(a^2\omega)$, and $G'(\omega/a^2)$ in Eq. [30] by $J'(\omega/a)$, $J'(a\omega)$, $J'(\omega/a^2)$, and $J'(a^2\omega)$, respectively. In the limit $a = 1$, $J'_2$ and $H'_2$ are expressed by the following formulas:

$$f'_2(a = 1) = \frac{12\omega^4\tau^4}{(1 + \omega^2\tau^2)^4}, \qquad [31]$$

$$H''_2(a = 1) = \frac{dG'(\omega)}{d \ln \omega} - \frac{1}{4}\frac{d^3G'(\omega)}{d \ln \omega^3}\Bigg|_{\omega=1/\tau}. \qquad [32]$$

Equations [31] and [32] correspond to the normalized intensity function and the approximation formula of the third approximation of Schwarzl (3). When the value of $a$ approaches infinity, similar to the last step, no approximation can actually be derived therefrom.

By repeating those procedures, the higher approximations can be obtained for the relaxation and the retardation spectra using only experimental values of dynamic mechanical functions.

### *Evaluation of Accuracy*

In the methods above described, the intensity functions are all approximated to Dirac delta functions. Hence it is obvious that the sharper the intensity function, the higher the accuracy of approximation becomes. Schwarzl and Staverman (3) discussed the accuracy of their approximation formulas in terms of the concept of resolving power. In the case where the value of $a$ is close to unity, the normalized intensity functions, $f''_1$, $f''_2$, $f'_1$ and $f'_2$ can be expanded in powers of $\epsilon$ to give

$$f''_1(\omega\tau, \epsilon) = \frac{2}{\pi} \frac{8\omega^3\tau^3}{(1 + \omega^2\tau^2)^3} \left\{ 1 - \epsilon^2 \left[ \frac{4\omega^2\tau^2}{(1 + \omega^2\tau^2)^2} - \frac{3}{4} \right] + \cdots \right\}, \qquad [33]$$

$$f''_2(\omega\tau, \epsilon) = \frac{2}{\pi} \frac{128\omega^5\tau^5}{3(1 + \omega^2\tau^2)^5} \left\{ 1 - \epsilon^2 \left[ \frac{20\omega^2\tau^2}{(1 + \omega^2\tau^2)^2} - \frac{25}{6} \right] + \cdots \right\}, \qquad [34]$$

$$f'_1(\omega\tau, \epsilon) = \frac{2\omega^2\tau^2}{(1 + \omega^2\tau^2)^2} \left\{ 1 - \epsilon^2 \left[ \frac{4\omega^2\tau^2}{(1 + \omega^2\tau^2)^2} - \frac{2}{3} \right] + \cdots \right\}, \qquad [35]$$

$$f'_2(\omega\tau, \epsilon) = \frac{12\omega^4\tau^4}{(1 + \omega^2\tau^2)^4} \left\{ 1 - \epsilon^2 \left[ \frac{20\omega^2\tau^2}{(1 + \omega^2\tau^2)^2} - 4 \right] + \cdots \right\}, \qquad [36]$$

where $\epsilon = a - 1$. Since the factors multiplied by the braces in the above equations are the same as the intensity functions for the corresponding approximations of $a = 1$, it can be expected in this case that the present approximations are of almost the same accuracy as those of Schwarzl and Staverman (3). When the value of $a$ is fairly large as compared with unity, the intensity function clearly broadens. To illustrate qualitatively the dependence of its sharpness on $a$, the height of the maximum of the normalized intensity function is plotted in Fig. 2 for $f''_1$, $f''_2$, $f'_1$, and $f'_2$. When log $a$ is larger than 0.4, these approximations become less useful. On the other hand, when log $a$ is near zero, the errors involved in the experimental values of $G''$ and $G'$ (or $J''$ and $J'$) make the final results uncertain, as can be shown from Eqs. [5], [12], [21], and [30]. Thus for actual use, it is suggested that log $a$ should be in the range $0.2 \sim 0.4$ for these approximations.

### Approximations to Relaxation Modulus and Creep Compliance from Dynamic Mechanical Data

The difference between the relaxation modulus, $G(t)$, and the real part of the complex rigidity, $G'(\omega)$, can be expressed in terms of the relaxation spectrum, $H$, to give

$$G'(\omega) - G(t)\,|_{t=1/\omega} = \int_{-\infty}^{\infty} \left[ \frac{\omega^2\tau^2}{1 + \omega^2\tau^2} - e^{-(1/\omega\tau)} \right] H \, d \ln \tau. \qquad [37]$$

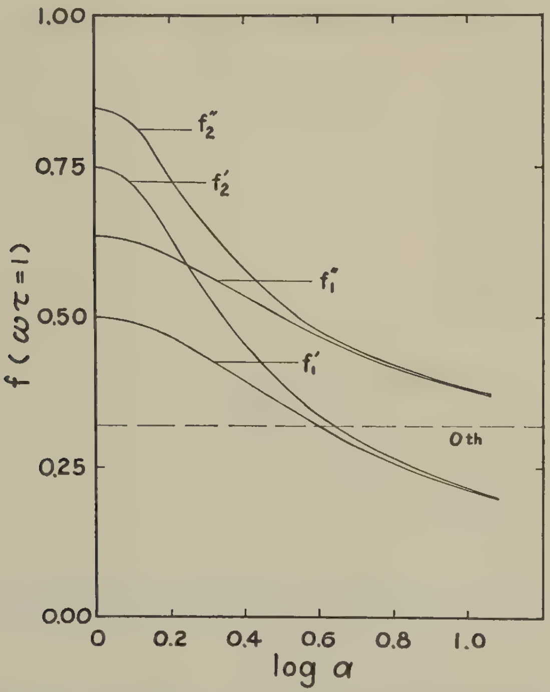

FIG. 2. The heights of maxima of the normalized intensity functions $f''_1$, $f''_2$, $f'_1$, $f'_2$ as functions of $a$.

Also the difference between the creep compliance, $J(t)$, and the real part of the complex compliance, $J'(\omega)$, can be written

$$-J'(\omega) + J(t)\,\big|_{t=1/\omega} = \int_{-\infty}^{\infty} \left[ \frac{\omega^2\tau^2}{1+\omega^2\tau^2} - e^{-(1/\omega\tau)} \right] L \, d\ln\tau + \frac{1}{\omega\eta}, \quad [38]$$

where $L$ is the retardation spectrum. The intensity functions, denoted by $K_D(\omega\tau)$, are the same in both Eqs. [37] and [38]. The maximum value of $K_D$ is 0.196 at $\omega\tau = 2.24$ and its area above the log $\omega\tau$ axis is equal to Euler's constant, 0.5772.

The intensity functions for the imaginary parts of the complex rigidity, $G''(\omega)$, and the compliance, $J''(\omega)$, are the same, giving

$$\frac{\omega\tau}{1+\omega^2\tau^2} \equiv K_I(\omega\tau).$$

$K_I$ has a maximum of 0.500 at $\omega\tau = 1.00$ and its area above the log $\omega\tau$ axis is equal to $\pi/2$. Figure 3, where $K_D$ and $K_I$ are plotted against log $\omega\tau$, suggests that it is possible to obtain a curve which is close in shape to the curve of $K_D$ by shifting $K_I$ properly along the vertical and the horizontal axes on the log-log plot. Thus

$$K_D(\omega\tau) \cong a_1 K_I(b_1\omega\tau), \quad [39]$$

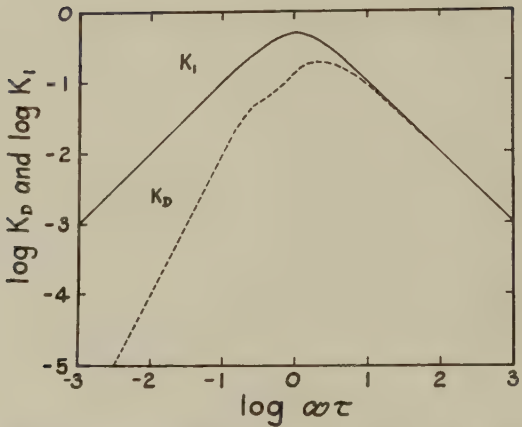

FIG. 3. Logarithmic plots of the intensity functions $K_D$, $K_I$ against log $\omega\tau$. Full and dotted lines show, respectively, $K_I$ and $K_D$.

where $a_1$ and $b_1$ are the constants which correspond, respectively, to the vertical and horizontal shifts. Since the ratio of the area under $K_D$ to that of $K_I$ on the log $\omega\tau$ axis is 0.367, the latter value is suggested for $a_1$. Also $b_1$ could have a value near 0.446 because the locations of the maximum for $K_D$ and $K_I$ are $\omega\tau = 2.24$ and $\omega\tau = 1.00$, respectively. However, it is desirable that the values of $a_1$ and $b_1$ are identical because of the following two reasons: (*1*) Both curves in Fig. 3 almost coincide and have unit slopes in the region of large values of $\omega\tau$. If $a_1$ and $b_1$ were identical, this coincidence could be kept also in the case of $a_1K_I(b_1\omega\tau)$. (*2*) $J(t)$ and $J''(\omega)$ have the same steady-flow term, $1/\omega\eta$ (or $t/\eta$). If $a_1$ and $b_1$ were identical, the steady-flow term of $J''(\omega)$ would be the same as that of $a_1J''(b_1\omega\tau)$. Considering those two reasons, Eq. [39] can be rewritten

$$K_D(\omega\tau) \cong a_1K_I(a_1\omega\tau),$$
$$0.367 < a_1 < 0.446. \qquad [40]$$

Then the approximation formulas for relaxation modulus and creep compliance from dynamic mechanical functions can be expressed thus:

$$G'(\omega) - G(t)\,|_{t=1/w} \cong a_1G''(a_1\omega), \qquad [41]$$

$$-J'(\omega) + J(t)\,|_{t=1/w} \cong a_1J''(a_1\omega). \qquad [42]$$

The accuracy of these approximations depends not only upon the value of $a_1$ but also upon the shape of $H$ (or $L$), which cannot be assumed *a priori*. Therefore it is hardly possible to determine uniquely the value of $a_1$ which minimizes the error of those approximations. However, it would be worth

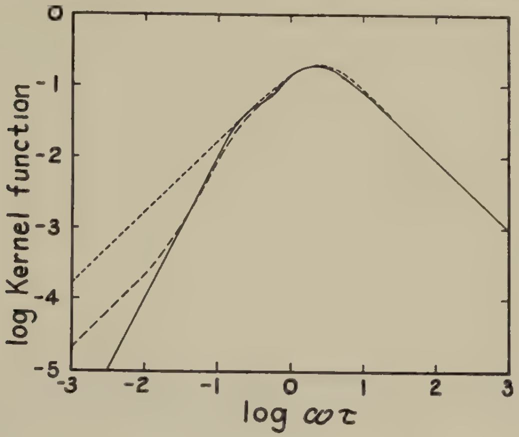

FIG. 4. Logarithmic plots of the intensity functions $K_D$, 0.40 $K_I(0.40\ \omega\tau)$, and 0.40 $K_I(0.40\ \omega\tau) - 0.014\ K_I(10\ \omega\tau)$ against log $\omega\tau$, represented by full, dotted, and dashed lines, respectively.

while to calculate the value of $a_1$ which minimizes the absolute value of the difference between $K_D(\omega\tau)$ and $a_1K_I(a_1\omega\tau)$. A value of 0.384 was obtained for $a_1$ from the minimization condition:

$$\frac{\partial}{\partial a_1}\left\{\int_{-\infty}^{\infty}[K_D(\omega\tau) - a_1K_I(a_1\omega\tau)]^2\,d\ln\tau\right\} = 0. \qquad [43]$$

For practical simplicity, 0.40 has been chosen as the value of $a_1$. Plots of $K_D(\omega\tau)$ and 0.40 $K_I(0.40\ \omega\tau)$ are shown in Fig. 4. In the range of log $\omega\tau$ from $+\infty$ to $-1$, both curves appear fairly close together; however, in the range log $\omega\tau < -1$, their separation increases. To reduce the divergence, additional terms, $-a_2b_2\omega\tau/[1 + (b_2\omega\tau)^2]$, $-a_2G''(b_2\omega)$, and $-a_2J''(b_2\omega)$ are introduced into the right-hand sides of Eqs. [40], [41], and [42], respectively. When $b_2$ was chosen arbitrarily as 10, the proper value for $a_2$ was found as 0.014. In this case, $a_2$ and $b_2$ are not identical, but it is easily seen that the contributions of these additional terms to the steady-flow term and also the divergence between $K_D$ and 0.40 $K_I$ (0.40 $\omega\tau$) for high values of log $\omega\tau$ are both negligibly small.

Thus the approximation formulas are finally obtained as follows:

$$K_D(\omega\tau) \cong 0.40\ K_I(0.40\ \omega\tau) - 0.014\ K_I(10\omega\tau), \qquad [44]$$

$$G'(\omega) - G(t)\,|_{t=1/w} \cong 0.40\ G''(0.40\omega) - 0.14G''(10\omega), \qquad [45]$$

$$-J'(\omega) + J(t)\,|_{t=1/w} \cong 0.40\ J''(0.40\omega) - 0.014J''(10\omega). \qquad [46]$$

The right-hand side of Eq. [44] is plotted in Fig. 4 also.

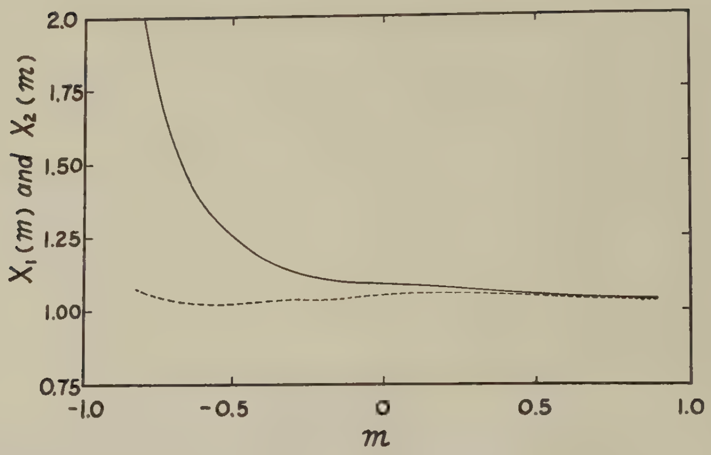

FIG. 5. Plots of $X_1(m)$ and $X_2(m)$ as functions of $m$, represented by full and dashed lines, respectively.

It may be worth while to show the results of these approximations in the case where $H$ (or $L$) can be expressed by a simple power function of $\tau$,

$$H \text{ (or } L) \equiv A\tau^m.$$

Here $A$ and $m$ are constants. The following quantities were calculated as functions of $m$ for the purpose of illustration:

$$\left.\frac{0.40\,G''(0.40\omega)}{G'(\omega) - G(t)}\right|_{t=1/\omega} \equiv X_1(m), \tag{47}$$

$$\left.\frac{0.40\,G''(0.40\omega) - 0.014\,G''(10\omega)}{G'(\omega) - G(t)}\right|_{t=1/\omega} \equiv X_2(m). \tag{48}$$

Mathematically $X_1(m)$ and $X_2(m)$ are the same as

$$\left.\left\{\left[0.40\,J''(0.40\omega) - \frac{1}{\omega\eta}\right] \Big/ \left[J(t) - J'(\omega) - \frac{t}{\eta}\right]\right\}\right|_{t=1/\omega}, \qquad \text{and}$$

$$\left.\left\{\left[0.40\,J''(0.40\omega) - 0.014\,J''(10\omega) - \frac{0.9986}{\omega\eta}\right] \Big/ \cdot \left[J(t) - J'(\omega) - \frac{t}{\eta}\right]\right\}\right|_{t=1/\omega},$$

respectively. $X_1(m)$ and $X_2(m)$ are plotted against $m$ in Fig. 5.

## ACKNOWLEDGMENTS

This work was supported in part by the Office of Naval Research under Contract N7onr-28509. The authors wish to express their sincere thanks to Professor H. Fujita for his helpful discussions in this work.

## SUMMARY

Two new approximation methods for treatment of viscoelastic data are introduced. In the first, the relaxation (or retardation) spectrum is obtained from several values of the real (or imaginary) component of the complex modulus (or compliance) without differentiation. In the second, the relaxation (or creep) function is obtained by a very simple calculation from the real and imaginary parts of the complex modulus (or compliance)

## REFERENCES

1. ANDREWS, R. D., *Ind. Eng. Chem.* **44,** 707 (1952).
2. FERRY, J. D., AND WILLIAMS, M. L., *J. Colloid Sci.* **7,** 347 (1952).
3. SCHWARZL, F., AND STAVERMAN, A. J., *Appl. Sci. Research* **A4,** 127 (1953).
4. FUJITA, H., *J. Appl. Phys.* **29,** 943 (1958).
5. LEADERMAN, H., *J. Appl. Phys.* **25,** 294 (1954).
6. GROSS, B., "Mathematical Structure of the Theories of Viscoelasticity." Hermann, Paris, 1953.
7. CATSIFF, E., AND TOBOLSKY, A. V., *J. Colloid Sci.* **10,** 375 (1955).
8. MARVIN, R. S., *Phys. Rev.* **86,** 644 (1952).
9. SMITH, T. L., *Trans. Soc. Rheology* **2,** in press.

## *Appendix*

Numerical calculations by the approximation formulas in this paper can be made with ease and speed if standard tables are combined with perforated guide cards as illustrated in Fig. 6. For example, if log $a$ is chosen as 0.20, the analog of Eq. [30] for calculating $L'_2$ from $J'$ becomes

$$L'_2 = 3.471[J'(\omega/1.585) - J'(1.585\omega)] - 1.193[J'(\omega/1.585^2) - J'(1.585^2\omega)] \big|_{\omega=1/\tau}$$

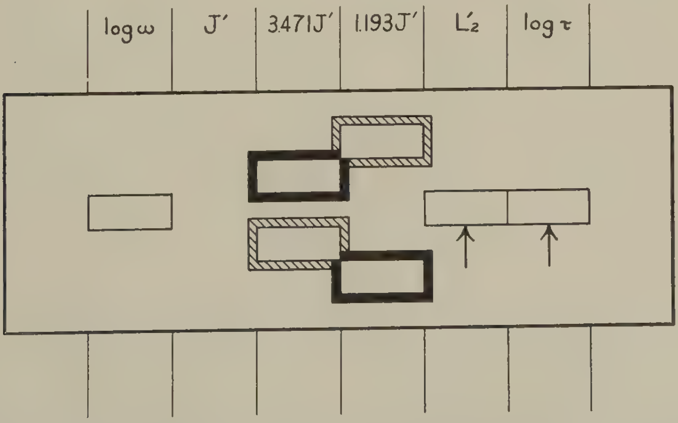

FIG. 6. Perforated guide card for calculating $L'_2$ from tables of $J'$ at log $\omega$ intervals of 0.2. Adding the numbers appearing in the black-bordered holes and subtracting those in the shaded-bordered holes gives $L'_2$, while log $\tau$ = $-$log $\omega$.

If parallel columns are set up for $\log \omega$, $J'$, $3.471\ J'$, and $1.193\ J'$, then the card shown in Fig. 6 can be used for filling in the columns for $L'_2$ and $\log \tau$ as explained below the figure. To calculate $H'_2$ from $G'$, the same card and corresponding columns are used but the signs of the terms are reversed. Similar tables and cards are readily arranged for obtaining $L''_1$ from $J''$, $H''_1$ from $G''$, $J(t)$ from $J'$ and $J''$, or $G(t)$ from $G'$ and $G''$.

JOURNAL OF COLLOID SCIENCE **14,** 49–58 (1959)

# EFFECTS OF BLENDING ON THE STRESS-RELAXATION BEHAVIOR OF POLYVINYL ACETATE IN THE RUBBERY REGION

**Kazuhiko Ninomiya**

*Physical Chemistry Laboratory, Department of Fisheries, Kyoto University, Maizuru, Japan, and Department of Chemistry, University of Wisconsin, Madison, Wisconsin*

*Received August 19, 1958*

## INTRODUCTION

The mechanical behavior of amorphous linear polymers in the rubbery region depends strongly on their molecular weights and molecular weight distributions. Fujita and Ninomiya (1–3) have recently investigated this problem and proposed a quantitative relation between the relaxation spectrum and the molecular-weight distribution (2). Their theory was essentially based on the following two phenomenological assumptions. (*1*) The shape of the relaxation spectrum of a monodisperse sample in the rubbery region is box-shaped when plotted against the logarithm of the relaxation time. (*2*) The relaxation spectrum of a blend can simply be represented by the linear superposition (i.e., additivity) of the relaxation spectra of the component fractions by volume. Any interaction effect on the mechanical properties which may occur on mixing of molecules of different sizes was neglected. In connection with the first assumption, it is worth while to note that Tobolsky and his collaborators (4) have recently shown that the relaxation spectrum in the rubbery region of an almost monodisperse polystyrene was very close to a box. The present paper is concerned with an experimental study of the interaction effects on the stress-relaxation behavior of polyvinyl acetate blends.

## MATERIALS AND METHODS

### *Samples*

Six polyvinyl acetate fractions were chosen as the starting materials for this study; they were taken from a series of fractions which had been prepared and used in the previous work (1). Their designations and molecular weights are given in Table I. The values of the number- and weight-average molecular weights, $\bar{M}_n$ and $\bar{M}_w$, in the table were estimated from the viscosity-average molecular weights of the subfractions of each fraction,

TABLE I

*Molecular Weights and Composition of Fractions and Blends*

| Fractions | $\bar{M}_n$ | $\bar{M}_w$ | $\bar{M}_w/\bar{M}_n$ |
|---|---|---|---|
| VI | $7.6 \times 10^4$ | $8.5 \times 10^4$ | 1.1 |
| VII | $7.2 \times 10^4$ | $7.9 \times 10^4$ | 1.1 |
| IX | $1.6 \times 10^5$ | $1.9 \times 10^5$ | 1.2 |
| X | $2.6 \times 10^5$ | $3.0 \times 10^5$ | 1.1 |
| XI | $4.0 \times 10^5$ | $4.1 \times 10^5$ | 1.1 |
| XIII | $7.2 \times 10^5$ | $7.6 \times 10^5$ | 1.1 |

| Blends | $\bar{M}_n$ | $\bar{M}_w$ | $\bar{M}_w/\bar{M}_n$ | Composition (weight) |
|---|---|---|---|---|
| A | $3.9 \times 10^5$ | $6.2 \times 10^5$ | 1.6 | IX (0.25) + XIII (0.75) |
| C | $1.4 \times 10^5$ | $4.2 \times 10^5$ | 3.0 | VI (0.50) + XIII (0.50) |
| D | $1.0 \times 10^5$ | $1.4 \times 10^5$ | 1.4 | VI (0.50) + IX (0.50) |
| F | $1.3 \times 10^5$ | $2.1 \times 10^5$ | 1.6 | VII (0.40) + X (0.60) |
| G | $1.0 \times 10^5$ | $1.7 \times 10^5$ | 1.7 | VII (0.60) + X (0.40) |
| H | $3.2 \times 10^5$ | $3.6 \times 10^5$ | 1.1 | X (0.50) + XI (0.50) |

assuming that each subfraction was monodisperse. This assumption is rather optimistic so that the values of the ratio $\bar{M}_w/\bar{M}_n$ indicated are only measures of the relative polydispersity of the samples. The detailed description of the preparation of the samples and the estimation of their molecular weights can be found in reference (1). Each blend was a mixture of two fractions; the calculated amounts of the two fractions were dissolved together in acetone, and then films of the blends were prepared in the same way as in the previous work (1). Taking different combinations and compositions of the six fractions, six blends were produced. Their $\bar{M}_n$ and $\bar{M}_w$ values were estimated from those of the component fractions using well-known formulas and are listed in Table I.

### *Methods*

The relaxometer used was essentially the same as that used before (1, 2); several minor improvements were made to increase the sensitivity and stability of the apparatus so that more precise measurements could be carried out. The details of the relaxometer have been described elsewhere (5).

Six fractions and six blends were studied over a temperature range 45°–160°C. Each relaxation run was made over a time interval of 1–100 min. For the measurements at temperatures above 90°C., the relaxometer chamber was filled with commercial nitrogen to keep the sample films from thermal degradation. The amounts of strain in tension applied ranged from 5% to 30%. Assuming the kinetic theory of rubberlike elasticity, all measured stresses at various temperatures and at various strains were converted to the relaxation moduli referred to infinitesimal strain and a temperature of 75.0°C. For each sample the converted relaxation moduli measured at various temperatures were shifted horizontally on a log-log graph towards the curve measured at 75°C. to form a composite curve. Slight vertical adjustments were sometimes needed to obtain the best superposition of the consecutive curves. However, they were of random nature, and may be attributed to the uncertainty in estimating the unstretched lengths of the sample films.

## RESULTS AND DISCUSSION

The horizontal shift factors, $a_T$, were independent of molecular weight. The curves of log $a_T$ vs. absolute temperature, $T$, fitted the WLF equation (6) with $c_1 = 8.86$ and $c_2 = 101.6$ over the entire range of temperature examined.

The composite curves for the six fractions, shown in Fig. 1, checked well with those obtained previously (1), except for slight differences in the region of rubber-liquid transition. Generally such differences appeared in the region of the relaxation modulus below $10^5$ dynes/cm$^2$. In the present study, these regions were more carefully measured than before so that the differences found may be due to less reliability of the earlier relaxometer.

Neglecting any interaction effect on the stress-relaxation behavior caused by mixing, a hypothetical composite curve can be calculated for each blend from those of its components in terms of the linear superposition assumption proposed previously. In actual calculations, weight fractions were used instead of volume fractions, since they are practically the same

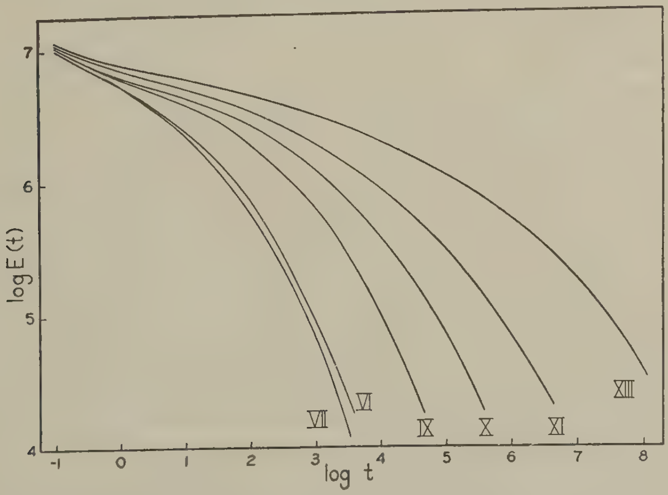

FIG. 1. Composite stress-relaxation curves for six fractions of polyvinyl acetate at 75.0°C.

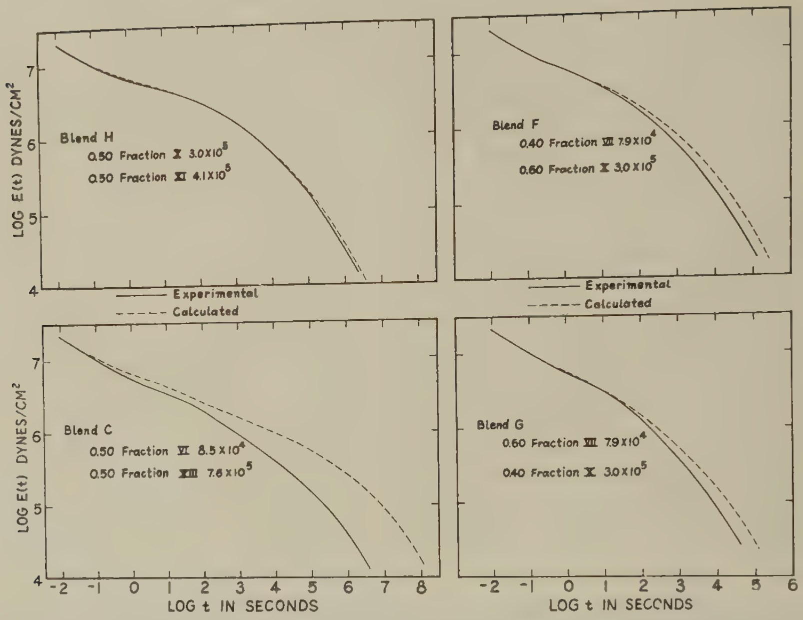

FIG. 2. Comparison of experimental composite stress-relaxation curves for four blends with those calculated for direct linear additivity of the contributions of the components.

in magnitude for the samples used here. Figure 2 compares the experimental composite curves with those so calculated for four blends, using doubly logarithmic plots. For a blend in which the difference in molecular size between the components is rather small (Blend H), both curves almost coincide with each other over the entire range indicated. On the other hand, the curves deviate from one another when the molecular sizes of the components are very different (Blend C). Both Blends F and G consist of the same components but with different weight compositions. It is apparent from this figure that the larger the difference in molecular size between the components, the less adequate the simple linear superposition assumption becomes. Common to all these examples is the fact that in the terminal region the two curves are almost the same in shape but different in location on the log *t* axis. This suggests that the smaller size component acts like a plasticizer to the larger size one so that the relaxation modulus curve of the latter is shifted towards the shorter time direction (7). To account for this phenomenon we shall assume that the linear additivity by volume (or by weight) is valid and that the apparent horizontal shifts of the component curves along the log *t* axis is due to interactions caused by mixing molecules of different sizes. Using these assumptions, it is found from the present work that a single shift factor for the time scale can be used for each component to fit the calculated curve to the experimental curve over the entire rubbery region. Thus the relaxation modulus of a blend, denoted by $E_{bl}(t)$, can be represented by

$$E_{bl}(t) = w_1 E_1(t/\lambda_1) + w_2 E_2(t/\lambda_2). \qquad [1]$$

Here $w_1$, $w_2$ are the weight fractions of the components; $E_1(t)$, $E_2(t)$ are the relaxation moduli of the components; $\lambda_1$, $\lambda_2$ are the constants which corresponded to the horizontal shifts. This treatment could be applicable only in the rubbery region; the transition region from glassy to rubberlike consistency will not be affected by blending of this kind. Hereafter the subscripts 1 and 2 will be used to denote the smaller and the larger molecular species, respectively. The process of determining the values of $\lambda_1$ and $\lambda_2$ is illustrated graphically in Fig. 3. The experimental curve is first compared with $w_2E_2$ at long times where no relaxation contributions from component 1 are to be expected, and the shift factor $\lambda_2$ is determined to make the two curves coincide in this region (upper figure). Then a plot of the experimental curve minus $w_2E_2(t/\lambda_2)$ is compared with one of $w_1E_1(t)$, and the shift factor $\lambda_1$ is determined to make these two curves coincide in the long time region (lower figure).

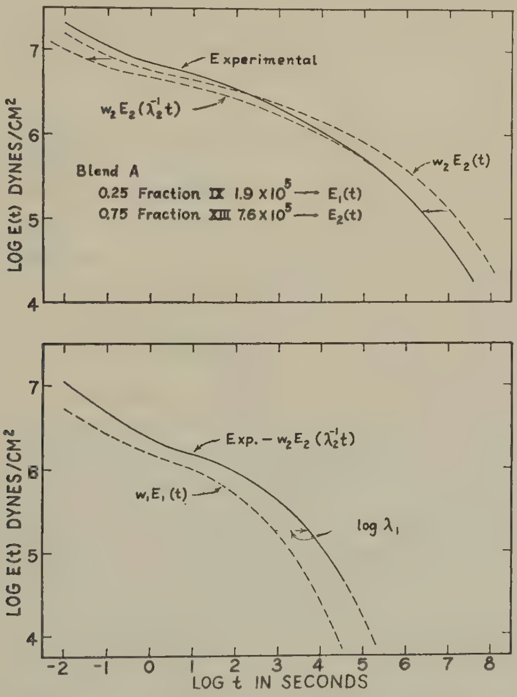

FIG. 3. Graphical illustration of the determinations of shift factors $\lambda_1$ and $\lambda_2$ for Blend A (see text for explanation).

The evaluated shift factors depend both on the combination and the weight fractions of the components; $\lambda_1$ is always greater than unity and $\lambda_2$ less than unity. The factor $\lambda$ may be regarded as the ratio of the average frictional resistance encountered by a molecule of given size in the blend to the resistance it would encounter surrounded only by other molecules of its own size.

It can be shown from Eq. [1] that the tensile steady-flow viscosity of a blend, denoted by $\eta_{bl}$, is written in terms of those of the components, $\eta_1$ and $\eta_2$, to give

$$\eta_{bl} = w_1\lambda_1\eta_1 + w_2\lambda_2\eta_2. \qquad [2]$$

In the Appendix of the earlier paper (2) it was shown that the approximate mathematical relationship,

$$\left[\int_0^\infty M^2F(M)\,dM \Big/ \int_0^\infty MF(M)\,dM\right]^{3.4} \fallingdotseq \left[\int_0^\infty M^{3.4}F(M)\,dM \Big/ \int_0^\infty F(M)\,dM\right], \qquad [3]$$

holds almost independent of the shape of $F(M)$ unless the shape of $F(M)$ is too far from a unimodal function (see Appendix). If the steady-flow viscosity is proportional to the 3.4 power of the *weight-average* molecular weight of the sample, it follows from Eq. [3] that

$$\eta_{bl} = w_1(\bar{M}_{nbl}/\bar{M}_{n1})\eta_1 + w_2(\bar{M}_{nbl}/\bar{M}_{n2})\eta_2. \qquad [4]$$

Comparison of Eq. [2] with Eq. [4] indicates that $\lambda_i$ should be equal to $\bar{M}_{nbl}/\bar{M}_{ni}$.

It was stated in the previous paper (1) that the viscosity of the polyvinyl acetate sample at 75.0°C. fits the equation,

$$\eta = 10^{-8.05}\bar{M}_v^{\,3.4}, \qquad (7 \times 10^4 < \bar{M}_v < 8 \times 10^5) \qquad [5]$$

where $\bar{M}_v$ is the viscosity-average molecular weight.

It has been mentioned that the $E(t)$ curves found from the present experiments differ slightly in their terminal regions from those reported previously. The details of the $E(t)$ curve in this region contribute greatly to the viscosity evaluated therefrom. Thus the steady-flow viscosities at 75.0°C. were re-evaluated using the data from the present measurements. The equation used, which can be derived from the well-known relations between the relaxation spectrum and $E(t)$ and $\eta$, as pointed out by Professor H. Fujita, was

$$\eta = \int_{-\infty}^{\infty} tE(t)\,d\ln t. \qquad [6]$$

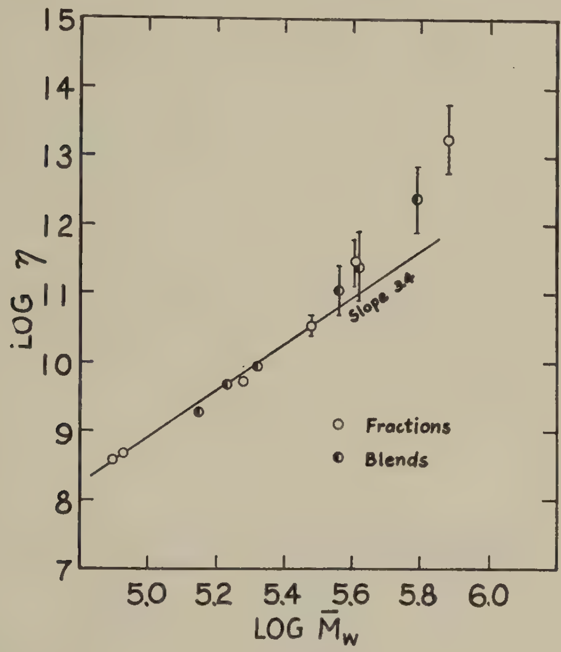

Fig. 4. Logarithmic plot of the tensile steady-flow viscosity vs. weight-average molecular weight.

In Fig. 4 the values obtained are plotted against $\bar{M}_w$ on a log-log graph. It should be noted that in practice the evaluation of $\eta$ in terms of Eq. [6] is not too reliable for the following reasons. The measurements of the relaxation curves could not be made with high accuracy in the terminal regions, and further, no actual data were available for $E(t)$ below $10^4$ dynes/cm.$^2$. Uncertainties due to these defects are indicated by vertical segments attached to the plotted points, estimated by plausible extrapolations of the observed $E(t)$ curves down to the lower regions. It appears from Fig. 4 that the viscosities vary with the 3.4 power of $\bar{M}_w$ in the range of $8 \times 10^4 < \bar{M}_w < 4 \times 10^5$. Thus we have $\eta = 10^{-8.10}\bar{M}_w^{\,3.4}$ for $8 \times 10^4 < \bar{M}_w < 4 \times 10^5$, in good agreement with Eq. [5] obtained previously. As seen in Fig. 4, the viscosities for samples of $\bar{M}_w > 4 \times 10^5$ deviate progressively from the 3.4 power line with increasing $\bar{M}_w$, in contrast with the previous study. Fox and Loshaek (8) have shown that the 3.4 power law of the steady-flow viscosity can be accepted over a wide range of molecular weight irrespective of both the heterogeneity and the species of the polymer. It is not as yet clear whether the marked deviation from this rule found here for the high molecular weight samples of polyvinyl acetate is real or not; this point could be clarified with direct viscosity measurements.

In Fig. 5, log $\lambda_i$ is plotted vs. log $(\bar{M}_{nbl}/\bar{M}_{ni})$ for all blends studied. The

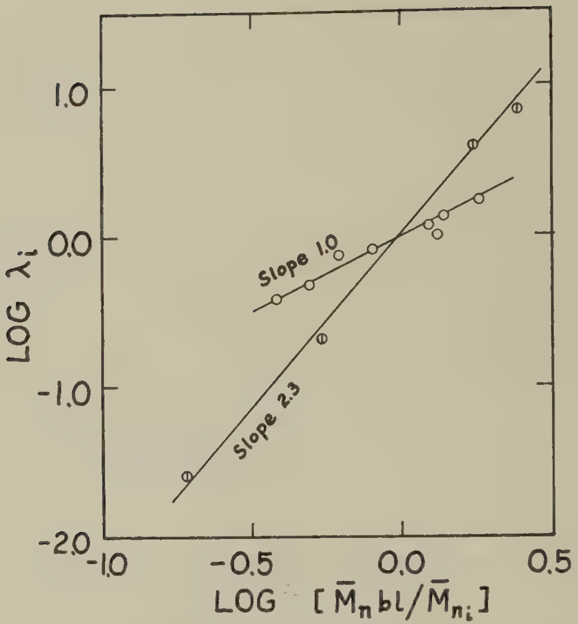

FIG. 5. Logarithmic plot of the shift factor, $\lambda_i$, vs. the ratio of the number-average molecular weight of the blend to that of the component, $\bar{M}_{nbl}/\bar{M}_{ni}$. Open circles, $\bar{M}_w < 4 \times 10^5$; slotted circles, $\bar{M}_w > 4 \times 10^5$.

points for the blends of $\bar{M}_w < 4 \times 10^5$ fall on a straight line of slope unity passing through the origin, in agreement with the prediction mentioned before. Those for the other blends fit a straight line with a slope of 2.3 passing through the origin, corresponding to the samples whose viscosities do not obey the 3.4 power law.

## ACKNOWLEDGMENTS

The author is greatly indebted to Professor H. Fujita of Kyoto University for many discussions, and is grateful for the continuous encouragement of Professor J. D. Ferry of University of Wisconsin. Analysis of the data was carried out with partial support from the Office of Naval Research under Contract N7onr28509.

## SUMMARY

Six blended polyvinyl acetate samples were prepared, each by mixing two fractionated samples selected from six fractions ranging in molecular weight from $8 \times 10^4$ to $8 \times 10^5$. Stress-relaxation curves in the rubbery region were measured in the range of temperature 45°–160°C. For each sample (blends and fractions) a composite curve, $E(t)$, was obtained by the method of reduced variables. Assuming that in a blend the contribution of the components to $E(t)$ are linearly additive by volume, $E(t)$ of each blend

was calculated from those of the component fractions. Comparison of the experimental and calculated composite curves showed that the larger the difference in molecular weight between the components, the less adequate becomes the assumption of linear additivity. But if we assume interaction effects which result in horizontal shifts of the component composite curves along the logarithmic time axis, the $E(t)$ curves of blends can then be satisfactorily represented by linear additivity. The horizontal shifts are always towards the right for the smaller molecular weight components and towards the left for the higher molecular weight components. The magnitudes of the horizontal shifts can be related to the ratio of the number-average molecular weight of the blend to those of the component fractions. For blends of molecular weights less than $4 \times 10^5$, the shift is simply equal to that ratio.

## REFERENCES

1. NINOMIYA, K., AND FUJITA, H., *J. Colloid Sci.* **12,** 204 (1957).
2. FUJITA, H., AND NINOMIYA, K., *J. Polymer Sci.* **24,** 233 (1957).
3. FUJITA, H., AND NINOMIYA, K., *J. Phys. Chem.* **61,** 814 (1957).
4. TOBOLSKY, A. V., MERCURIO, A., AND MURAKAMI, K., *J. Colloid Sci.* **13,** 196 (1958).
5. NINOMIYA, K., KISHIMOTO, A., AND FUJITA, H., *Chem. High Polymers (Japan)* **14,** 504 (1957).
6. WILLIAMS, M. L., LANDEL, R. F., AND FERRY, J. D., *J. Am. Chem. Soc.* **77,** 3701 (1955).
7. KISHIMOTO, A., AND FUJITA, H., *J. Polymer Sci.* **28,** 547 (1958).
8. FOX, T. G., AND LOSHAEK, S., *J. Appl. Phys.* **26,** 1080 (1955).

## *Appendix*

It was stated in the Appendix of the earlier paper (2) that the approximate mathematical relationship,

$$\left[\int_0^\infty M^2F(M)\,dM \Big/ \int_0^\infty MF(M)\,dM\right]^{3.4} \fallingdotseq \left[\int_0^\infty M^{3.4}F(M)\,dM \Big/ \int_0^\infty F(M)\,dM\right], \qquad [3]$$

holds almost independently of the shape of $F(M)$. Taking $MF(M)$ in this equation as a normalized weight distribution of molecular weight of a polymer ($\equiv\varphi(M)$), the following relation can be obtained:

$$\bar{M}_w^{\,3.4} = \bar{M}_n \int_0^\infty M^{2.4}\,\varphi(M)\,dM. \qquad [7]$$

Recently Dr. H. Leaderman of the National Bureau of Standards pointed out that these relations become less applicable when a polymer consists of

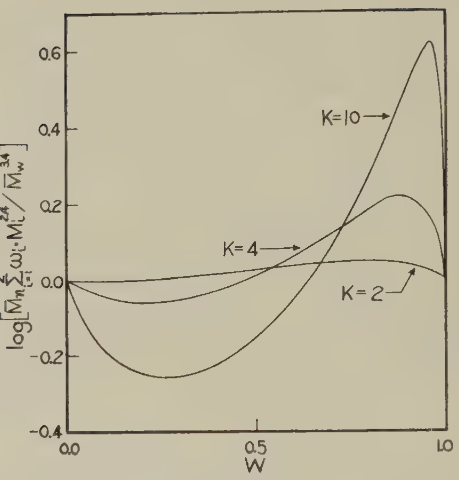

Fig. 6. Plots illustrating the degree of validity of Eq. [7] for binary blends of monodisperse fractions.

two monodisperse fractions the molecular weights of which differ from one another. This is illustrated numerically in the following. Consider a blend consisting of two monodisperse fractions of molecular weights $M$ and $KM$, where $K$ is an arbitrary constant greater than unity. Then it can be shown that the left- and the right-hand sides of Eq. [7] become $\bar{M}_w^{3.4}$ and $\bar{M}_n[wM^{2.4} + (1 - w)(KM)^{2.4}]$, respectively. Here $w$ represents the weight fraction of the small molecular size component. The ratio $\{\bar{M}_n[wM^{2.4} + (1 - w)(KM)^{2.4}]/\bar{M}_w^{3.4}\}$ was calculated as a function of $w$ for $K = 2$, 4, and 10 and plotted in Fig. 6. It is seen in this figure that when the molecular weight of the large-size component is tenfold of the other, Eq. [7] ceases to be practical. The author is grateful for the helpful advice of Dr. H. Leaderman.

JOURNAL OF COLLOID SCIENCE **14**, 59–73 (1959)

# THERMODYNAMIC BARRIER TO MICELLE FORMATION AND BREAKDOWN

## I. Cetyl Trimethyl Ammonium Salts

**T. Nash**

*Central Public Health Laboratory, Colindale Avenue, London N.W. 9, England*

*Received August 25, 1958*

## ABSTRACT

One possible condition under which simple micelle solutions might exist in nonequilibrium is that there should be a thermodynamic barrier to the formation of a micelle from the free molecules, or to its breakdown once it is formed, or to both. This would make it possible for micelle solutions to exist in which the average micelle size is either greater or smaller than at complete equilibrium. Relative to the latter, solutions having a smaller number of large micelles would be at a high chemical potential, whereas those having a greater number of small micelles would be at a low chemical potential. The rate at which such solutions attain equilibrium would depend on the difference between the rates of micelle generation and breakdown. The rate of equilibration would therefore be slow if either of the primary processes was slow or if the difference between their rates was sufficiently small.

Detailed experimental evidence is given by two independent methods for the existence of nonequilibrium states of solution for cetyl trimethyl ammonium bromide around the CMC. The time to complete equilibrium for 1 mM soap at 20°C. is about 30 hours when in 0.1 mM potassium sulfate and about 70 hours when in 1 mM sodium bromide. The way in which such nonequilibrium states can be prepared and the sign of their chemical potential are predicted by the hypothesis just formulated. Aggregates are also shown to be present down to less than half the CMC, and support is given to recent doubts expressed about the validity of the concept of constant micellar size.

## INTRODUCTION

In a preliminary paper (1) it was shown that dilute aqueous cetyl trimethyl ammonium bromide (CTAB) containing a little sodium bromide, could exist in distinct states which required 16 hours to equilibrate at 25°C. This result was contrary to current views on the rate of attainment of equilibrium in micelle solutions (2), and because of the indirect and unusual experimental method, and consequent difficulties of interpretation, a full discussion was postponed until more data should become available. Such data and discussion form the subject matter of the present paper.

The principal technique depends on the fact that the addition of naphthol to CTAB solution causes it to become viscoelastic to a degree depending not only on the composition of the original solution but also on the way it was prepared. This discriminating effect of naphthol is enhanced if a little salt is also present. Once naphthol has been added the properties of the solution change only very slowly with time (1, 3) so that the immediate measurement of some viscoelastic parameter can be properly related to the state of the original solution containing only CTAB and salt. The naphthol seems to act as a kind of amplifier for the hitherto imperceptible differences between the various possible states of a CTAB salt solution of any particular composition. This view is rendered the more plausible by the large random fluctuations found during studies of the naphthol complex in the Couette viscometer (3), indicative of a high "noise level" such as is commonly associated with a high degree of amplification. In fact the fluctuations were so great that conventional viscometry was abandoned in favor of an entirely different technique, developed from work done on the water-carrying capacity of the foam generated from such solutions (4).

Because of the novelty of this technique, and the fact that some new ideas on micelle solutions are to be presented, some of the experimental details would seem meaningless without prior knowledge of the writer's own views. It is therefore necessary at this stage to give the latter in some detail and to present the experimental section later.

### *Hypothesis Regarding the Generation of Nonequilibrium States in Simple Micelle Solutions around the CMC*

It is fundamental to the theory of aggregation colloids that there should be rapid diffusive equilibrium between any individual micelle and the neighboring solution of unaggregated material. It does not follow, however, that a homogenous solution of micelles must also attain equilibrium rapidly. Suppose, for example, that a solution contains fewer micelles than the equilibrium number. The rate at which such a solution approaches equilibrium will depend on the difference between the rates at which new micelles are generated and the rate at which old ones are broken down, which is essentially a problem of nucleation. At low concentrations of a compound with a correspondingly low CMC, both rates may be slow or the difference between them small. Of course if a micelle solution is suddenly diluted to well below the CMC, the micelles will break down rapidly since there are large numbers of molecules leaving each one, by diffusion, and very few coming in. Around and above the CMC, however, there are on the average about as many molecules entering each micelle as leaving, so that again something analogous to nucleation, but in reverse, is required to effect breakdown. Both formation and breakdown, under these conditions, come within the province of the theory of cooperative fluctuations (5).

### *Ways of Generating Nonequilibrium in Micelle Solutions*

If a strong micelle solution is simply diluted to some point at or above the CMC, the total number of micelles must decrease so as to supply free molecules in the larger volume between them. If this decrease in numbers is a slow process the freshly made dilution will not be in equilibrium, the number of micelles continuing to decrease over a period of time. Such a decrease could account for the observation of Debye and Anacker (6) that the light scattered from CTAB solution gradually decreased. They suggested various incidental causes, but there was no mention of such an effect with the myristyl (C-14 as compared to C-16) homolog. This is understandable on the nucleation hypothesis since the rate should depend very strongly on concentration, so that a measurable rate for C-16 soap (CMC 0.9 mM) might well mean an immeasurably fast rate for C-14 soap (CMC 3 mM).

If a little salt is introduced the system becomes more flexible, and in particular it allows of the preparation of solutions in which the number of micelles gradually increases, as well as those in which it decreases, with time. In considering how such solutions could be prepared, it is convenient to be specific and to deal with some of the actual mixtures used in the experiments. The stock solutions were typically 0.1 *M* CTAB and 0.1 *M* sodium bromide, the experimental ones being say 1 mM in each component, so that dilution is 100-fold for each. In the ordinary way no attention would be paid to the exact way in which the dilutions were made. With slow equilibration, however, the order of addition of the components could affect the final result, as follows:

*(C + S) 1 mM solution.* One milliliter of stock CTAB is added to 98 ml. of water and mixed. Since the CMC is 0.9 mM, many of the micelles belonging to the stock solution will be broken down by dilution into regions well below the CMC. After complete mixing, the solution will therefore contain the rather small number of micelles that have escaped this process. When 1 ml. of salt is added the CMC is suddenly decreased to 0.5 mM, so that much of the free soap should aggregate. By hypothesis, the number of micelles increases only slowly, so that the few already present are temporarily forced to accept all the surplus material. Initially, therefore, the solution contains a small number of oversize micelles; the mean aggregation number is higher than at equilibrium, and the chemical potential is higher.

*(S + C) 1 mM solution.* Stock salt is first added to 98 ml. water, and mixed. The CTAB is then run into approximately 1 mM salt, in which the CMC is only 0.5 mM. Breakdown of the micelles going in from the stock solution will therefore be arrested sooner than in the previous case, and the final number after mixing will be higher. It may well be higher than the equilibrium number, and if so the mean size will be smaller than at complete

equilibrium and the chemical potential lower. In any case it would be lower than for the (C + S) solution.

### *Different Kinds of Discriminating Agent*

Such differences as might actually be present between CTAB/salt solutions of the same composition but different histories cannot be obvious. For example, tests with a commercial conductivity meter showed that differences in conductivity, if any, were less than 2%. Two indirect methods by which such solutions can be readily distinguished are used in the present work. The first has already been indicated and consists of the addition of ethanolic naphthol solution and estimation of some parameter of the resulting viscoelasticity. The latter seems extraordinarily sensitive to any differences in the treatment of the original solution, and the method probably furnishes the most accurate simple way of discriminating closely aligned states of the same solution, as occurs in studies of the equilibration rate. It is, however, too indirect to afford any kind of test for the hypothesis, except in so far as the results are not inconsistent with it.

The second method is better in this respect since with it there is a 1:1 chance of disproving the hypothesis. The method is to add a very small amount of a fluorescent dye, of charge opposite to that of the soap, and to measure the fluorescence of the solution as a function of soap concentration. It is found that the fluorescence intensity depends somewhat on the history of the original solution, but the quantitative differences are not so large in relation to the probable error, compared to the first method.

### *Choice of Viscometric Discriminating Agent*

Many naphthalene derivatives form viscoelastic solutions with CTAB, around and even well below the CMC (7). Naphthalene itself and the less polar derivatives need a fairly high concentration of salt to show the effect. The carboxylic and sulfonic acids, on the other hand, behave more like dyes in causing aggregation below the CMC; the concentration of free soap molecules is thereby reduced so much that the particular technique found necessary would no longer be applicable. Either of the naphthols has the appropriate moderate degree of interaction, the 1-isomer being rejected as oxidizing too readily.

### *Choice of Fluorimetric Discriminating Agent*

The possibility of discriminating between C + S and S + C solutions by means of a dye lies in the observation of Mukerjee and Mysels (8) that a dye of charge opposite to that of the soap often forms an organic salt with it below the CMC, which gradually merges with true micelles as the soap concentration is increased. With some fluorescent dyes, the organic salt is not fluorescent, but the fluorescence is regained when the dye is adsorbed by the micelles, which can successfully compete with the organic salt for the dye. As the soap concentration is gradually increased from zero, the fluorescence of the dye (assumed to be present in very small amount) decreases to a minimum and is then gradually restored to its original value. In solutions represented by the rising part of the curve, the dye is distributed between the organic salt and the adsorbed state. In this region the system should be sensitive to changes in chemical potential, and the fluorescence/concentration curve for CTAB in C + S solutions should be different from that for CTAB in S + C solutions. This expectation was realized, as will be shown below. As organic salt formation is rather weak, a strongly acidic dye such as dichlorofluorescein was found suitable. The high quantum yield of the latter also meant that a very low concentration, approximately micromolar, was sufficient to give adequate readings, so that the dye would not of itself interfere very much with the course of micellization.

## Experimental

As previously mentioned the Couette viscometer was found unsuitable for accurate work with CTAB/naphthol solutions owing to large random fluctuations in the reading. The ordinary tube viscometer is also unsuitable, since the rate of flow of the solution is very little different from that of pure water (non-Newtonian behavior). It was, however, noticed that the foam produced by shaking some of the solution in a bottle was particularly dense, and a study was made of the rates of drainage of such foams (4). The time required for half of the liquid to drain out of the foam was found to be fairly reproducible, even with the rather crude technique of shaking the bottle a given number of times and then timing the rate of rise of the liquid level below the foam. The half-drainage time must have been related in some way to the various components of the non-Newtonian viscosity of the solutions. Accordingly an apparatus was constructed for generating foams by bubbling and collecting and weighing an accurately reproducible volume of foam under conditions which ensured a standard amount of drainage before collection. The viscoelastic parameter is then a weight, and the error was found to be only 0.3% to 0.4% at the 30-g. level (1). This weight is therefore an accurate index of the state of the solution before the addition of naphthol, although it is not at this early stage possible to relate any particular foam weight (or indeed any other viscoelastic parameter that can be imagined) to, for example, any particular micelle size or chemical potential.

The apparatus was very simple, and has been fully described (1). The same procedure was used as in the early experiments: 1.34 l. of foam was generated in 82 sec. and of this 1.06 l. was collected in a polythene bag and weighed, the drainage time at spill-over being 15 sec. The ambient temperature was set to 20°C. instead of 25°C. as in the early experiments so as to allow more time for some of the manipulations (much slower rate of equilibration) and also with a view to obtaining some information about the temperature coefficient of aging of the solutions. Stock solutions were 0.1 *M* aqueous CTAB, 0.1 *M* aqueous sodium bromide, 0.01 *M* aqueous potassium sulfate, and the discriminating agent, 0.1 *M* ethanolic 2-naphthol. Solutions of the same composition but different properties were made up and tested as follows:

*1.* Equilibration of all materials and apparatus in a room the temperature of which was thermostatically controlled to 20° ± 0.1°C.

*2.* Addition of water (approximately 98 ml.) to a beaker with a stirrer run by a synchronous motor, and starting to stir.

*3.* Preparation of the experimental solution in one of two ways, by adding the CTAB first and then the salt (C + S) or vice versa (S + C). The stock solutions were run in as uniformly as possible, intervals between additions being 30 sec. (stirring all the time) to ensure a homogenous solution before the addition of the second component.

*4.* Aging, if any, of the experimental solution, which so far is indistinguishable from its complementary state.

*5.* Addition of stock naphthol to bring the total volume to 100 ml. The solution now becomes viscoelastic to a degree depending not only on its composition but also, in general, on whether it was originally C + S or S + C.

*6.* Transfer of the viscoelastic mixture to the flask of the foam apparatus, and standing for 5 min.

*7.* Generation, collection, and weighing of the foam.

### *Discrimination by Fluorescence*

*5a.* In these experiments, instead of naphthol, 2 ml. of a 60 $\mu$M solution of dichlorofluorescein in 100 $\mu$M alkali was added to the experimental solution, to bring the total volume up to 100 ml.

*6a.* The fluorescence of 50 ml. of the latter was found in a simple fluorimeter with a light source (125W H.P.M.V. lamp with a Woods glass envelope) run from a well-stabilized power supply.

As the whole point of the work was to see how solutions of identical composition behaved differently according to their history, it is emphasized that pairs of solutions, C + S and S + C, were always treated identically with the discriminating agent. The naphthol concentration was chosen to be always equimolar with the CTAB, whether the latter was of constant or variable composition in any particular set of experiments. This was done because maximum viscoelasticity occurred when the two compounds were approximately stoichiometric.

### *Materials*

The salts were of ordinary reagent grade, and the CTAB and naphthol were purified as previously described (1). The question of homologous impurities in the CTAB is discussed below.

## RESULTS

Without naphthol, foam weights are low, and there was no perceptible difference between C + S and S + C solutions when measured at 25°C. in the earlier work (1). The term "foam weight," unless otherwise stated, is understood to mean the weight determined according to the complete experimental procedure just described, i.e., after the addition of naphthol, so that the solutions contained not only CTAB and salt but naphthol and alcohol as well. It is, however, convenient at this point to show that the salt is not necessary for demonstrating nonequilibrium in CTAB solution. When 1.1 ml. of stock naphthol was added to a freshly made dilution of CTAB (1.1 ml. stock to 98 ml. of water) the foam weight was 2.95 g. If the CTAB solution was allowed to stand overnight at the temperature of the experiment (25°C.) the foam weight after addition of the naphthol had increased to 4.62 g.—a change far outside the probable error. It will be seen from the results presented below that low concentrations of salt greatly increase the range of the weight differences, and also permit the observa-

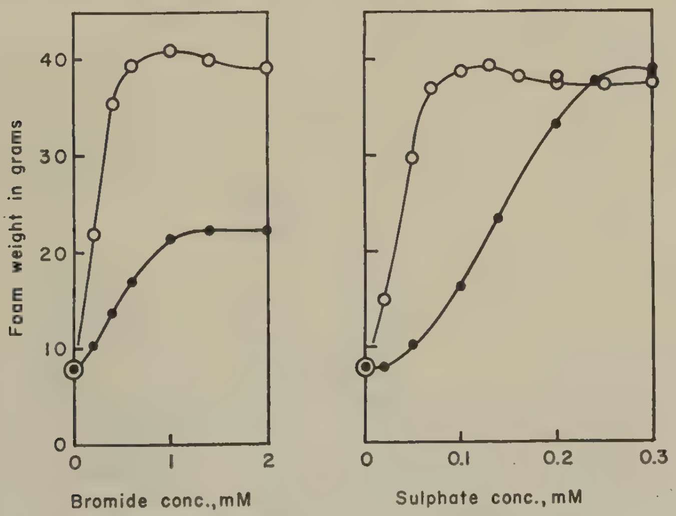

FIG. 1

FIG. 2

FIGS. 1 and 2. Foam weight naphthol complex derived from each state of 1 mM CTAB/bromide (Fig. 1) and each state of 1 mM CTAB/sulfate (Fig. 2) as a function of salt concentration, at 20°C. (C + S) state ··· ○ (S + C) state ··· ●

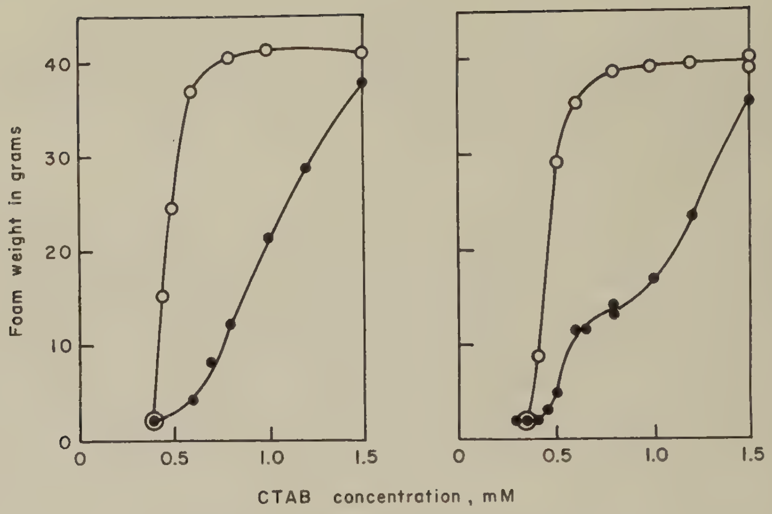

FIG. 3 FIG. 4

FIGS. 3 and 4. Foam weight from naphthol complex derived from each state of CTAB/mM bromide (Fig. 3) and each state of CTAB/0.1 mM sulfate (Fig. 4) as a function of CTAB concentration, at 20°C. (C + S) state ··· ○ (S + C) state ··· ●.

tion of approach to equilibrium from both sides by changing the time order of addition of the salt and CTAB as described above.

For uniformity in the diagrams, the foam weights from naphthol complexes derived from C + S solutions are plotted as circles, while the foam weights from naphthol complexes derived from S + C solutions are plotted as dots. The same convention is used with regard to the fluorimeter readings when the discriminating agent is a dye instead of naphthol (Fig. 9).

### *Concentration Effects*

The foam weight from 1 mM CTAB was 8.0 g. initially; as salt was added the weight increased, separation of the two states occurring at once with both sodium bromide (Fig. 1) and potassium sulfate (Fig. 2). It can be seen that the nature of the salt is important, and that good separation of states can be obtained using either 1 mM bromide or 0.1 mM sulfate. Keeping the salt concentration at these two values, the effect of varying the CTAB concentration was found (Figs. 3 and 4). The small maximum found at 0.1 mM CTAB has been omitted (1); so far below the CMC the solution could not be expected to exist in different states, and in fact no discrimination was ever observed.

### *Aging of Each State of a Typical Solution*

C + S and S + C solutions of 1 mM CTAB in either 1 mM bromide or 0.1 mM sulfate were made up and allowed to stand for different times be-

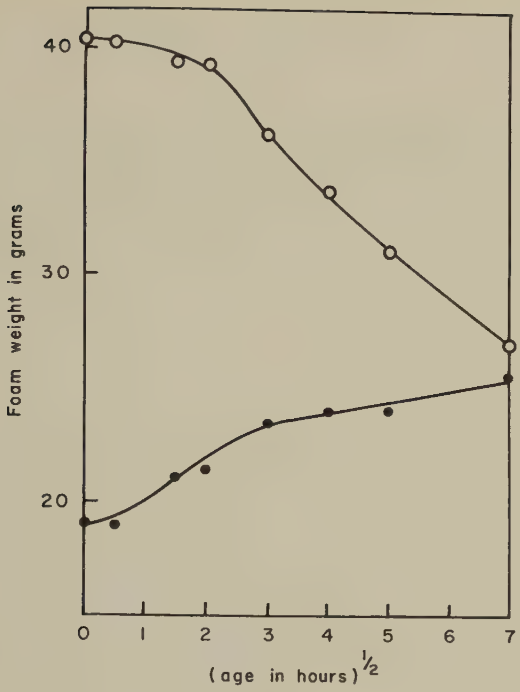

FIG. 5

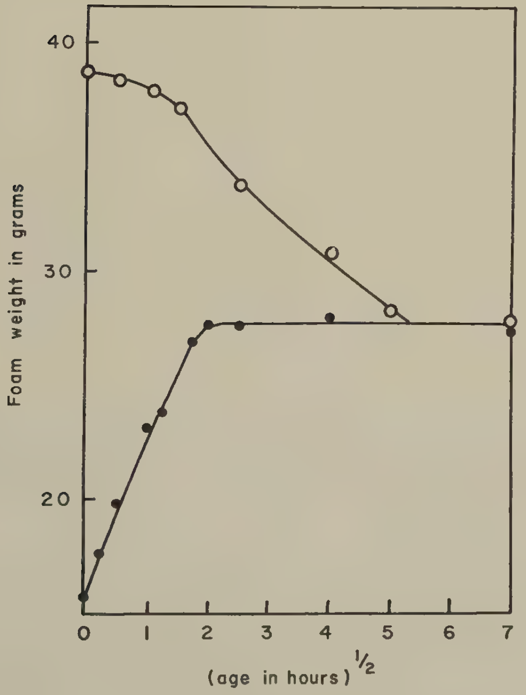

FIG. 6

FIGS. 5 and 6. Foam weight from naphthol complex derived from each aged state of mM CTAB/mM bromide (Fig. 5) and each aged state of mM CTAB/0.1 mM sulfate Fig. 6) as a function of age, at 20°C. (C + S) state ··· ○ (S + C) state ··· ●.

fore the addition of naphthol. The resulting foam weights were conveniently plotted against the square root of the time, as was done previously for bromide-containing solutions at 25°C., though the time scale had to be in hours rather than minutes (1). It can be seen (Figs. 5 and 6) that the initial and final foam weights are not very different for the solutions containing the two different salts, but that the aging of S + C (sulfate) seems to be faster than in the other three cases.

### *Mixtures of the Two States of One Solution*

C + S and S + C solutions of 0.01 mM CTAB bromide were made up, divided, and recombined so that the final volume was always 99 ml. One milliliter of stock naphthol was then added and the foam weight found. The latter is plotted against percentage composition in Fig. 7, the horizontal dotted line being at the expected equilibrium value, estimated from Fig. 5. The relation is clearly not linear; trial plots showed good proportionality between foam weight and the cube of (C + S) percentage. No such simple relation was found in the case of the sulfate-containing solutions, but the deviation was in the direction to be expected from the rather rapid apparent aging of (S + C) with sulfate while the solutions were being manipulated

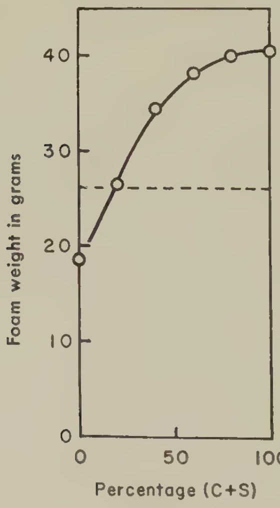

FIG. 7.

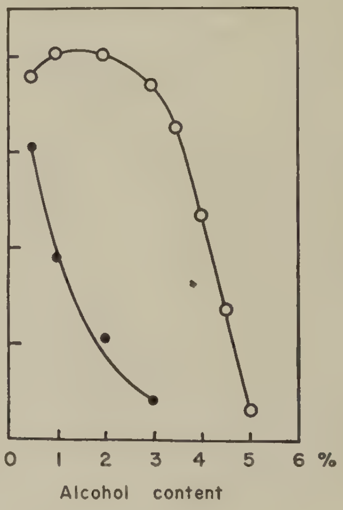

FIG. 8.

FIG. 7. Foam weight from naphthol complex derived from mixtures of each state of mM CTAB/mM bromide, as a function of composition of initial mixture, at 20°C. (C + S) state ··· ○ (S + C) state ··· ●

FIG. 8. Foam weight from naphthol complex derived from each state of mM CTAB/mM bromide, as a function of alcohol content of final solution, at 20°C. (C + S) state ··· ○ (S + C) state ··· ●

### *Effect of Alcohol*

Figure 8 shows how the foam weight from 1 mM CTAB varied with the strength of the alcoholic naphthol solution, such that the final concentration of naphthol was always 1 mM but had different amounts of alcohol. The foam weight falls off very rapidly with increasing alcohol concentration for the S + C solutions, but for the others it increases to a maximum at an alcohol concentration of 1.4% corresponding to a stock naphthol concentration of 0.07 *M*.

### *Effect of Agitation*

The obvious procedure in aging experiments was to take successive samples from a large volume of solution, adding the required amount of naphthol and finding the foam weight. Early work on these lines (not reported) gave irregular results, and it was eventually found that the errors arose through the progressively greater amount of agitation in the history of the samples. Experiments confirming the effect of gentle agitation were done by rotating flasks of solution for different times on a tilted turntable. It was found that agitation during aging always decreased the foam weight as compared to unrotated controls. No experiments were done in an apparatus capable of giving a controlled and known rate of shear.

### *Effect of Homologous Impurities*

CTAB is derived from natural cetyl alcohol and is not the pure C-16 compound; the conventional purification used would not be expected to remove close homologs. The material was from the same purified batch as was used in the earlier work at 25°C., and a new batch obtained about a year later was found to be somewhat different. For example, the S + C curve of Fig. 8 was shifted about 1% unit to the right, the C + S curve being altered to a lesser degree. The effect of aging was also rather different, but the general picture was not much altered.

## DISCUSSION

All the information about the simple CTAB/salt solutions was obtained by indirect means, and the results depend rather strongly on the experimental conditions. For example, the alcohol concentration experiment (Fig. 8) shows that the preceding figures would have been of a different shape had the stock naphthol solution been of a different strength. In general, therefore, it is not possible to make quantitative deductions from the results, and this discussion is mainly confined to showing in a qualitative manner that they are consistent with the ideas put forward in the Introduction. According to them a freshly made CTAB/salt solution has micelles of average aggregation number $N + n$, where $n$ is different for the two states, C + S and S + C, and $N$ is the aggregation number at complete equilibrium. The data of Figs. 5 and 6 also suggest that the sign of $n$ is different in the two cases, as equilibrium seems to be approached from either side.

### *Micelle Shape*

The sensitiveness of the CTAB/salt solutions to agitation could be taken as evidence for the presence of long thin fragile micelles, but this is unlikely since it would imply exposure of some of the hydrocarbon chain. The solutions are of the kind considered by Philippoff (10) as containing micelles that do not depart significantly from the spherical shape. Detailed calculations by Tartar, based on purely theoretical considerations, are in agreement, a small degree of oblateness being possible (11). Light scattering (6) showed that the micelles did not become appreciably dissymmetric (rod-like) until the salt concentration was over 100 times that used in the present work. It is of course easier to understand differences in chemical potential due to micelles of different size if they are approximately spherical.

### *Sign of Chemical Potential for Each State*

It is possible to fit the sign of $n$ to the appropriate solution, C + S or S + C, from the data of Fig. 9. When $n$ is positive the micelles have a posi-

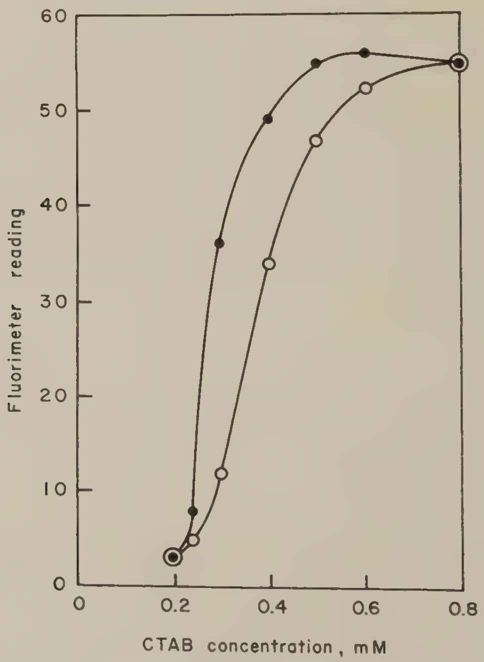

FIG. 9. Restoration of fluorescence of 1.2 $\mu$M dichlorofluorescein by each state of CTAB/mM bromide, as a function of CTAB concentration, at 20°C. (C + S) state ··· ○ (S + C) state ··· ●

tive chemical potential, so that the solution will have a somewhat higher concentration of free ions than at complete equilibrium. In reaction with dye ions, the formation of the organic salt will therefore be favored over the adsorption complex. As the latter is not fluorescent the solution should show less fluorescence than normal. Figure 9 indicates that this occurs for the C + S solution, so that $n$ is positive as predicted by the hypothesis. The reverse holds with regard to the S + C solution.

### *Relative Magnitude of Excess or Defect of Material in the Micelles for Each State*

It can be assumed (*a*) that a homogenous micelle solution contains only one kind of micelle, because the slightest energy difference would cause rapid diffusive exchange of material until the different kinds were identical; (*b*) that when CTAB/salt solutions of identical composition also give the same foam weight with naphthol, by the procedure described above, they are in fact identical in all respects. Any denial of the latter proposition would imply that CTAB solutions are of quite unbelievable complexity.

The data of Fig. 7 are then important because they enable one partially quantitative deduction to be made. The equilibrium state, with average micelle aggregation number $N$, can be seen to be identical with a mixture consisting of 20% C + S and 80% S + C. If the latter has micelles of average aggregation number $N - n$, it follows by intuition or simple calculation that the former must have micelles of average aggregation number $N + 4n$. This result depends on the reasonable assumption that mixing does not cause a sudden change in the total number of micelles present in the two solutions, but simply allows the oversize ones to shed material and the undersize ones to take it up. There is also a correction, of unknown magnitude, for the difference in the concentration of free ions which must exist between the two states.

### *Aggregation below the CMC*

The CMC of CTAB in 1 mM bromide is 0.5 mM (1). From Fig. 1 it may be seen that, using naphthol, discrimination between states begins rather below this, at 0.4 mM. With dichlorofluorescein discrimination begins at 0.2 mM (Fig. 9) but is lost above the CMC sooner than with naphthol, presumably because once the micelles are fully formed the proportion of organic salt is negligible. The two discriminating agents are therefore complementary, to some extent; the dye is valuable because it provides unequivocal evidence for the presence of aggregates down to less than half the CMC. It is suggested that the mass action relation (12) needs modification to allow for a considerable change in micelle size around the CMC.

### *Supersaturation*

The solutions made up with sodium bromide were probably supersaturated at 20°C., though not at 25°C., the temperature of the earlier work. However, there seems no reason why supersaturation with respect to the solid phase should in any way affect the results of measurements made on the liquid (micelle) phase. A separate investigation (13) showed in a formal manner that the phase relations between crystals, micelles, and solution were those to be expected if three phases, solid, liquid, and solution, were present, as has been surmised by many workers in the past (extension of Krafft point to low concentrations). It was also shown that sulfate-containing solutions are generally undersaturated, considerably so under the conditions of the present experiments.

### *The Temperature Coefficient*

Comparison with the results at 25°C. for bromide-containing solutions (1) showed that the temperature coefficient of the initial rate of loss of foam weight of the complex derived from the C + S solutions was 1.1, whereas for the S + C solutions it was much higher, 1.5 per degree. It is not possible to relate these figures in any quantitative manner to supposed rates of micelle generation and breakdown, but the large difference in the two coefficients supports the idea that the magnitudes of the actual rates are of the same order as the difference between them. The latter is known approximately from the results of the aging experiments (Figs. 5 and 6) so that it is possible to deduce a complete micelle turnover every few hours, very approximately.

## CONCLUSIONS

Much more work needs to be done on nonequilibrium states of micelle solutions, and now that there can be little doubt as to their existence it should be more profitable to apply direct physical methods, such as accurate measurements of conductivity, light scattering, or ultrasonic absorption. On the theoretical side, it would seem necessary to consider, apart from the statistical fluctuations of size in an assembly of micelles (14), the possibility of slow changes in the average size. It should be possible to derive some figure, however approximate, for the rate of nucleation at a given free molecule concentration and for the rate of breakdown for micelles of a given size. Until these matters have been considered, the theory of micelle solutions, as recently expounded, for example, by Hoeve and Benson (15) and by Matijevic and Pethica (16) remains essentially incomplete. This would still be true in the case of shorter chain compounds where the rate of equilibration is probably too fast for detection. The writer, however, fully agrees with the conclusion of the former authors (15) that "the assumption of one micellar size from the start is not a suitable basis for the development of a theory of micelle solutions."

## ACKNOWLEDGMENT

I am greatly indebted to Dr. J. A. Kitchener for much advice on the preparation of this paper, and in particular for suggesting the application of the ideas of nucleation and chemical potential.

## REFERENCES

1. NASH, T., *J. Appl. Chem.*, **8,** 440 (1958).
2. HARTLEY, G. S., *Quart. Revs.* (London) **2,** 152 (1948).
3. NASH, T., *Nature* **180,** 188 (1957).
4. NASH, T., *J. Appl. Chem.* **7,** 392 (1957).
5. UBBELOHDE, A. R., *Trans. Faraday Soc.* **33,** 1198 (1937).
6. DEBYE, P., AND ANACKER, E. W., *J. Phys. Chem.* **56,** 644 (1951).
7. NASH, T., *J. Colloid Sci.* **13,** 134 (1958).
8. MUKERJEE, P., AND MYSELS, K. J., *J. Am. Chem. Soc.* **77,** 2937 (1955).
9. NASH, T., *J. Appl. Chem.* **6,** 539 (1956).
10. PHILIPPOFF, W., *Discussions Faraday Soc.* **11,** 96 (1951).
11. TARTAR, H. V., *J. Phys. Chem.* **59,** 1195 (1955).
12. MURRAY, R. C., AND HARTLEY, G. S., *Trans. Faraday Soc.* **31,** 183 (1935).
13. NASH, T., *Chemistry & Industry* **1958,** 590.
14. STIGTER, D., AND OVERBEEK, J. T. G., *Proc. 2nd Intern. Congr. Surface Activity* **I,** 311 (1957).
15. HOEVE, C. A. J., AND BENSON, G. C., *J. Phys. Chem.* **61,** 1149 (1957).
16. MATIJEVIC, A. E., AND PETHICA, B. A., *Trans. Faraday Soc.* **54,** 587 (1958).

JOURNAL OF COLLOID SCIENCE **14**, 74–90 (1959)

# THE DETERMINATION OF THE PARTICLE SIZE DISTRIBUTION OF AEROSOLS BY PRECIPITATION OF CHARGED PARTICLES[1]

**Vadim G. Drozin[2] and Victor K. La Mer**

*Columbia University, New York, New York*

*Received June 11, 1958*

## Abstract

Previous methods for determining the particle size distribution of aerosols have involved counting the numbers and measuring the sizes, or some effects connected with size, of *individual* particles. This is a tedious and time-consuming procedure. When the size distribution changes with time, the processes cannot be investigated because of the relatively long times required for such determinations.

The method presented in this article is based on measuring macroscopic properties of a large number of particles. The electric current carried by a large number ($\sim 10^8$) of particles charged in a corona discharge and precipitated in an electric field, when measured as a function of precipitation time, is one such property. The number of charges acquired by particles is a single-valued function of particle size. From the knowledge of this function and measured values of current (or accumulated charges) versus time, the size distribution curve can be determined. The entire procedure, including the necessary calculation, takes about 20 minutes and requires relatively inexpensive equipment. All experiments were carried out with particles in the submicron range, the most difficult and at present the most important range.

The size distribution of particles smaller than 0.2 $\mu$ radius could not be determined by this method, since their charging follows another law. Theoretically it is possible to overcome this difficulty, but further investigation will be needed.

## Introduction

The determination of particle size distribution, especially in the submicron range, is of importance in meteorology, hygiene, medicine, colloid chemistry, and industrial processes, where particle size represents the parameter of greatest interest. Aerosols are important from the military point of view. Here artificial radioactive aerosols, created by the explosion of atomic and hydrogen bombs, become one of the most dangerous weapons of atomic warfare. The strongest radiation is often from particles in the submicron size range.

---

[1] This work was supported by the Atomic Energy Commission for which the authors express their appreciation.

[2] Present address: Bucknell University, Department of Physics, Lewisburg, Pennsylvania.

Every determination of size distribution in a given sample of an aerosol may be divided into two operations: one concerned with measuring the size of particles in a sample, the other with measuring the number of particles of every size present in that sample. In the Appendix are listed the principal methods used at present for the determination of the distribution of aerosol particles with such limitations as are related to the method. It is of interest to determine the absolute size distribution in the range from 0.2 to 1.0μ radius, i.e., the number of particles of every size in this range in 1 cm.$^3$ in a sample.

*1.* Particles electrified in a corona discharge acquire unipolar charges the number of which depends on their size. The dependence upon particle radius ($r$) of the number ($n$) of charges picked up by a particle can be determined experimentally by the procedures outlined in the next section and is valid for all particles having the same dielectric constant. The general form of this dependence is

$$n = kr^{\alpha}. \qquad [1]$$

Here $k$ is a constant and $\alpha$ is an exponent the value of which, determined experimentally, lies between 1 and 2.

*2.* The charged particles settle in the electrostatic[3] field of a precipitator with a velocity determined by the mass of the particles, their charge, and the field created in the precipitator. The curve, which represents the dependence between size and time of falling through a certain distance under given conditions, can be obtained from Stokes' law.

Stokes' equation for the fall of a particle under the combined action of gravitational and electrostatic forces is given by:

$$mg \pm neE = 6\pi\eta r \frac{S}{t}, \qquad [2]$$

where $m$ is the mass of a particle, $g$ is the gravitational constant, $e$ is the elementary charge, $\eta$ is the viscosity coefficient of the carrier gas, $t$ is the time during which a particle of radius $r$ carrying $n$ charges travels the distance $S$ under the influence of field $E$ and gravity in the precipitator. By applying a sufficiently strong field the gravitational force $mg$ becomes negligible in comparison with the electrostatical force $neE$. In this case (Fig. 1)

$$t = \frac{6\pi\eta S}{eE} \frac{r}{n}. \qquad [3]$$

---

[3] It is possible to apply a centrifugal or gravitational field instead of an electrostatic field in the precipitator. In these cases Stokes' law would give an even stronger dependence between time of falling and particle size. However, these two methods would be more difficult to handle experimentally.

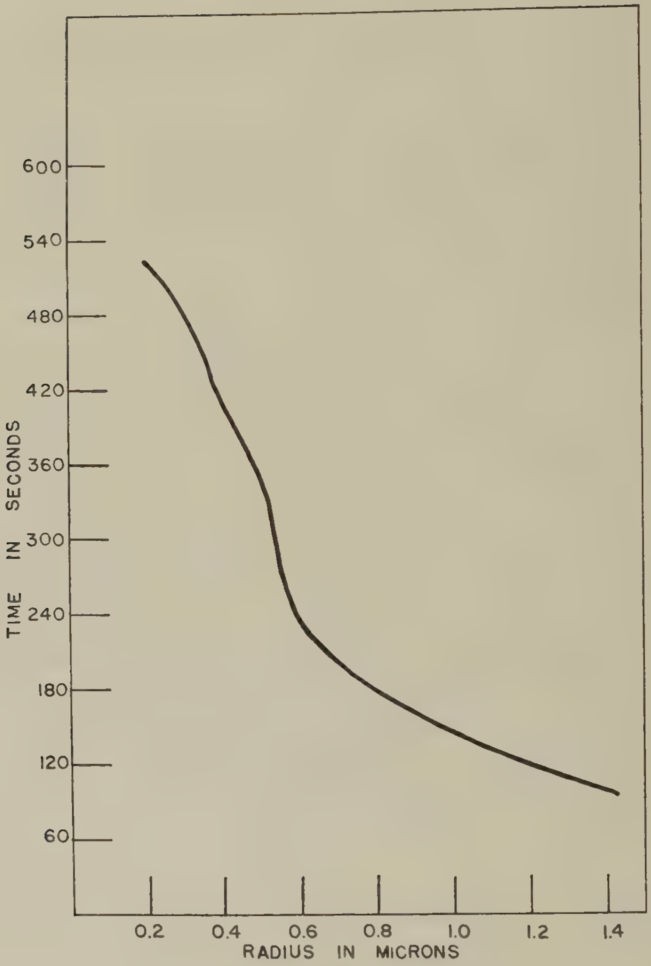

FIG. 1. Settling time (in seconds) of charged (at 120 μa. charging current) stearic acid aerosol particles versus particle radius in microns. Particles settle under the field $E = 0.0555$ c.g.s. in a precipitator through a height of 2.4 cm.

If $n$ is linearly dependent on $r$, all particles will precipitate with the same velocity independent of their size and, therefore, particle size cannot be determined by this method without further modification.[4]

*3*. When the particles reach the conducting bottom of a precipitator, they give up their charges. The current or charges accumulated during a certain time interval can be measured as a function of time. The area under this curve represents the total charges of all aerosol particles, which originally filled the precipitator.

---

[4] This limitation does not exist in the methods mentioned in footnote 3.

The analysis of this curve should be initiated from the last time interval before the current ceased. If this interval is short, it can be assumed that all particles precipitated during the last time interval are of the same size. They represent the fraction of particles of the smallest size present in the sample, which at the beginning of the experiment was at the top of the precipitator. From the time of falling to the bottom under given conditions we determine the radius of these particles using the curve illustrating radius as a function of time (i.e., from the graph of Eq. [3]). From the curve, representing the charging law (number of charges vs. radius) we determine the number of charges ($n$) carried by a particle of this size (i.e., from the graph of Eq. [1]). Equation [8] for accumulated charges ($\Delta Q$) shows that these three curves ($r$ vs. $t$, $n$ vs. $r$, $\Delta Q$ vs. $t$) supply all the data necessary for determining the number of particles in this fraction and, therefore, give the first experimental point on the size distribution curve. The fraction of particles precipitated during the preceding time interval consists of two parts: particles of the smallest size treated previously and of the next particle size determined by the time of precipitation. Subtracting the charges given by the smallest particles from the total accumulated charge during this time interval, the charges given by the fraction of particles of the next size will be obtained. The same procedure as for the particles of the smallest size will yield the second experimental point on the size distribution curve. Continuing these operations, we will obtain all experimental points, the number of which is equal to the number of the time intervals in which the curve $\Delta Q$ vs. $t$ was subdivided. Using a more sensitive recording micro-micro-ammeter than that available to us (Keithley Vacuum Tube Electrometer Model 200), one may obtain a practically continuous size distribution curve.

As far as we know, no one has determined size distribution by the method outlined above. In 1923 Rohman (1) determined the average size by precipitation of the particles moving as a jet perpendicular to an electric field and charged by corona from a point. His technique of jet production was improved in 1947 by Lipscomb, Rubin, and Sturdivant (2). They precipitated charged particles from a jet and determined by microscopic counting the size distribution of particles on the precipitator plate as a function of distance traveled by a charged particle in a given electric field. They could not achieve a sharp separation of particles of different sizes but obtained only a range of sizes of the particles precipitated at each given point. This result was due to the unsatisfactory charging devices used in their research (a heated filament, cotton cloth at high potential, and plate coated with rayon flock fibers) and to unfavorable flow conditions in the duct.

It may be possible to extend the method outlined above to the conifuge invented by Sawyer and Walton (3). Instead of counting individual particles, the current caused by charged particles can be measured. To do this the outer cone of the conifuge should be cut into circular rings which should be insulated from each other.

## Determination of Charging Law

The charging device should satisfy the following requirements:

*1.* The losses of particles in the device due to precipitation under the influence of the charging field should be as small as possible.

*2.* The particles may obey any charging law except one in which the number of acquired charges is linearly proportional to the radius of the particles.

*3.* All particles of the same size should pick up the same number of charges.

The device (BCI) which virtually satisfied these conditions was built in the form of a cylinder 13.85 cm. long, 2.45 cm. inside radius, with a wire of $25 \times 10^{-4}$ cm. radius stretched along the cylinder axis. A slit, 2.54 cm. long and 0.63 cm. wide, parallel to the wire, was cut through the cylinder wall. Half of a brass tube, cut along its axis, was placed on the slit so that aerosol particles traveled 2.54 cm. in the extended charging space of the cylinder.

The theory of charging in a unipolar corona discharge was developed by Pauthenier (4), Ladenburg (5), Arndt and Kallman (6), and Deutsch (7). Since the geometrical configuration of the charging space does not allow one to apply the theory directly, the charging law was determined experimentally.

Almost all experiments were performed with monodisperse stearic acid aerosols produced in a La Mer-Sinclair generator (8). The particles are in a spherical semisolid state, i.e., they are no longer liquid after leaving the cooling column of the aerosol generator. The dielectric constant of stearic acid is 2.2, density 0.94 g./cm.$^3$. The particle size was determined from the angular position of red bands in the Higher Order Tyndall Spectra (8) exhibited by monodisperse particles.

Another method tried was the electrical dispersion of liquids as aerosols. When one applies a high potential to certain liquids contained in a glass tube ending in a fine capillary, the liquid issues from the capillary as highly dispersed, relatively monodisperse, aerosol drops. It was found (9) that only polar liquids with relatively high dielectric constant could be finely dispersed. The particles are highly charged. Since the output obtained by this method was too small, and it was difficult to regulate the size of particles, the La Mer-Sinclair generator was preferred.

Two methods of measurements were used: one based on measuring the upward and downward velocity of charged particles in a known electric field in a Millikan chamber, and the other based on measuring the current caused by charged monodisperse aerosol particles of a known concentration precipitated in a given electric field.

The Millikan apparatus consisted of a brass chamber 3½ in. in diameter with windows which allow observation of the particles from the light scattered by them in the forward direction. The light source was a ribbon tungsten filament, which was focused at the center of the chamber by two lenses. A solution of copper sulfate, placed between the light source and the chamber, served as thermofilter. The particles were observed at the center of the chamber between two horizontal plates separated by 0.285 cm. with a telemicroscope of 2 in. focal length and a magnifying factor of approximately 40 to 60. The field between the plates was varied from 0 to 45 v. by a potentiometer. One division of the eyepiece scale was 0.019 cm.

If the size of individual aerosol particles could be determined optically, only one equation would be needed for determination of the number of charges ($n$) carried by a particle, that is, for the upward or downward motion:

$$neE \pm mg = 6\pi\eta r \frac{S}{t_{\text{up}}}. \tag{2'}$$

Here $E$ is the field strength in the Millikan chamber in c.g.s. units ($E = V/d$, where $V$ is the applied potential in c.g.s. and $d$ is the distance between plates), $\eta$ is the viscosity of the carrier gas, $r$ is the radius of a particle and $t_{\text{up}}$ ($t_{\text{down}}$) is the time during which a particle travels a given distance $S$ in an upward (downward) direction.

Aerosol particles, normally designated as monodisperse, show some size distribution. The size determined by the Higher Order Tyndall Spectra is an average size, optically weighted. Therefore the particle the velocity of which is actually measured in a Millikan chamber may not possess precisely the size determined optically. The procedure adopted for the determination of $n$ was: (*1*) the time was measured during which a particle travels a given distance $S$ in the one direction; (*2*) then the time was measured during which the same particle travels the same distance in the opposite direction (positive and negative potentials on the plates between which the particles move were reversed). By subtracting Eq. [2′] with + sign from Eq. [2′] with − sign and substituting $m = 4/3\pi r^3\rho$ where $\rho$ is the density of particle material, we will get

$$r = k\sqrt{\frac{1}{t_{\text{down}}} - \frac{1}{t_{\text{up}}}}, \tag{4}$$

where

$$k = \sqrt{\frac{9\eta S}{4\rho g}}.$$

From the known value of $r$ from Eq. [4] and Eq. [2′] with + or − sign we calculate $n$; $n$ can also be calculated from the sum of Eqs. [2′]. Then $n$ is plotted versus $r$, and the curve is drawn which best fits the experimental points. Different parts of the curve should then be approximated by analytical expressions.

The disadvantages of this method are the following: (*1*) the measurement of the velocity of small particles in the Millikan chamber is a very tedious operation; besides, the particles under $r = 0.3\mu$ are difficult to observe; (*2*) to establish a charging law, the velocities of a large number of particles of different sizes should be measured. This is a tedious operation. Therefore, we used this method only for preliminary experiments for the determination of the charging law, particularly for estimation of how uniformly the particles are charged in a given charging device under given charging conditions. Accordingly, we measured in most cases the velocities of not more than 20 particles.

If the aerosol particles are very monodisperse and are sufficiently uniformly charged, then instead of observing the motion of individual particles, it is better to determine the velocity of a moving "front" of the particles. Such a measurement is much easier to perform and represents the average over hundreds of particles. Figure 2 shows the charging law for stearic acid aerosol particles charged at 300 $\mu$a. in a charging device[5] (*CI*) under the rate of flow of 4 l./min.

The second method for the determination of the charging law follows the procedure:

*1.* Measurement of number concentration ($N$) of monodisperse aerosol particles of a given size. The determination of $N$ consists of three operations: Weighing a piece of zero-penetration filter, filtration of aerosol through this filter, and weighing the filter after about 15 to 20 minutes of filtration.

*2.* Measurement of penetration ($P$) through a charging device, i.e., determination of the ratio between the number of aerosol particles leaving and entering a charging device as a function of ionic current in the device.

*3.* Measurement of the current ($i_p$) caused by total precipitation of charged particles in a precipitator as a function of ionic current in the device.

Data obtained from operations (*1*) to (*3*) carried out on monodisperse aerosol particles give information sufficient to determine the number of charges ($n$) carried by a particle of given size.

$$i_p = NUPne, \qquad [5]$$

where $U$ is the rate of aerosol flow in cm.$^3$/sec., and $e$ is the charge of an electron ($e = 4.8 \times 10^{-10}$ c.g.s.). Therefore,

$$n = \frac{i_p}{NUPe}. \qquad [6]$$

---

[5] This charging device is very similar to one described above. It has a thicker wire ($r = 38 \times 10^{-4}$ cm.) stretched in the cylinder and the walls of this cylinder were four times thicker than that described above.

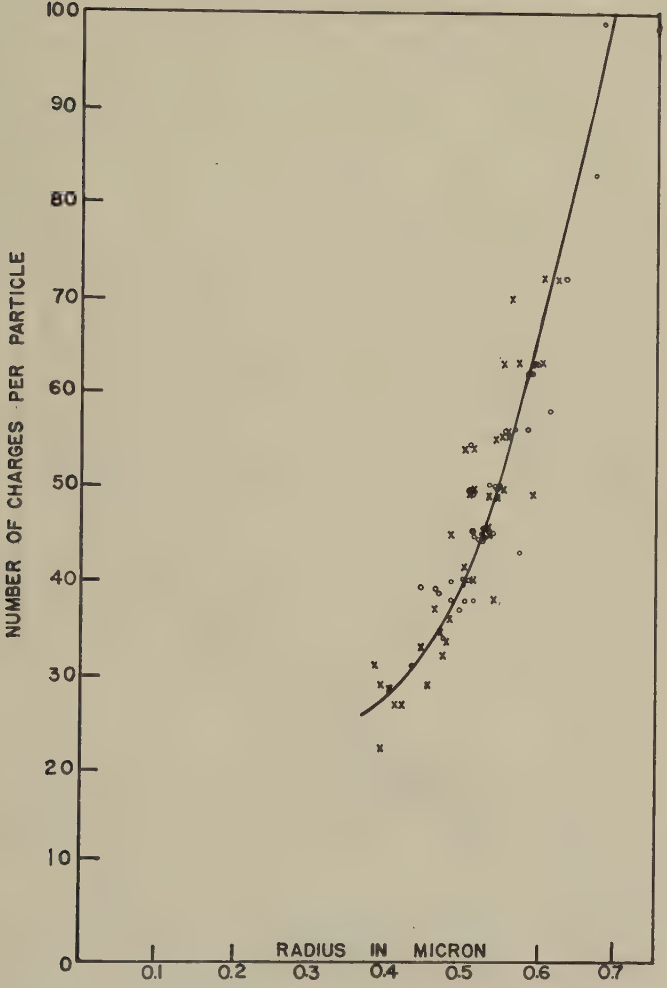

FIG. 2. Number of charges per particle measured in the Millikan chamber versus particle radius. The particles were charged in the device CI at 300 $\mu$a. charging current at a rate of flow of 4 l./min. The circles represent negatively charged particles; the crosses, positively charged particles.

To determine a charging law in a certain size range, operations (*1*) to (*3*) should be carried out on a number of monodisperse aerosols within this range.

The charging law for stearic acid aerosol particles has been determined using the precipitation method. The particles were charged in device BCI with an ionic current of 40 $\mu$a, 80 $\mu$a, and 120 $\mu$a (see Fig. 3, curves *A*, *B*, and *C*, respectively).

The length of rubber and glass tubing between the charging device and

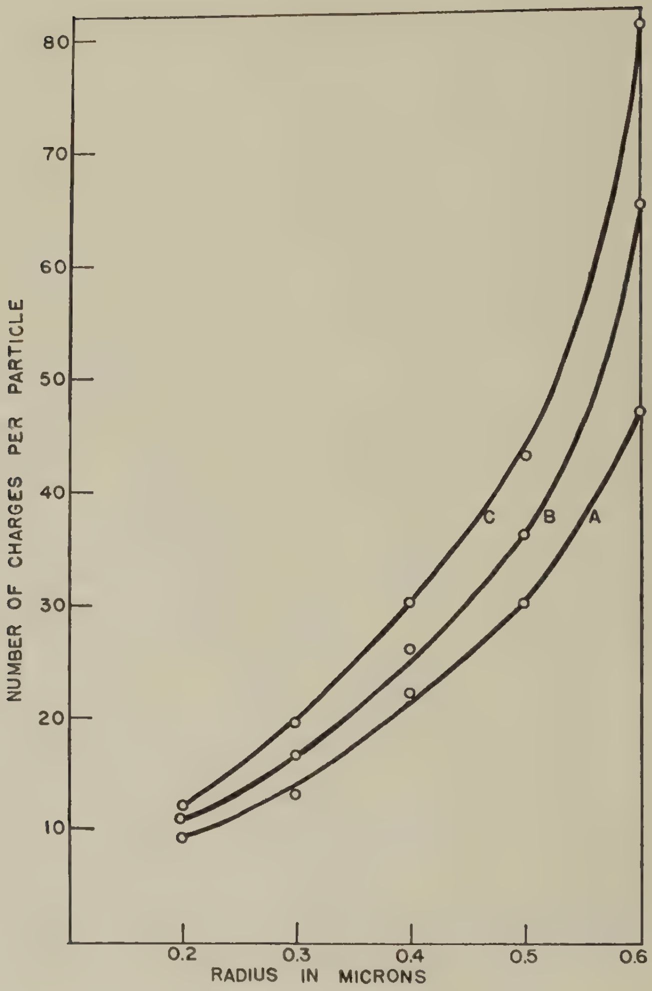

FIG. 3. Number of charges per particle versus particle radius. Stearic acid aerosol particles charged in the device BCI at a rate of air flow 2 l./min. by the charging current 40 μa. (Curve *A*); 80 μa. (Curve *B*); and 120 μa. (Curve *C*).

precipitator was about 15 cm. If the rate of air flow was under 4.5 l./min. no ions produced in the charging device reached the precipitator.

## DETERMINATION OF PARTICLE SIZE DISTRIBUTION BY METHOD OF ELECTROSTATIC PRECIPITATION

If charged monodisperse aerosols fill the precipitator, then the current is constant since all particles are falling with the same velocity. Particle size is determined by the time that particles, originally on the top of the cylinder, take to reach the bottom. This time equals the time when current starts and ceases ($t$) and is given by Eq. [3]. If we denote by $N$ the number of particles of size $r$ in 1 cm.$^3$ of the sample, and by $Q$ the total charge of all particles, then

$$N = \frac{Q}{neV}, \qquad [7]$$

where $n$ is the number of charges carried by a particle of radius $r$, $e$ is the value of a unit charge, and $V$ is the volume of the precipitator. If polydisperse charged aerosol particles fill the cylinder, then at the beginning of the experiment particles of all sizes present in the sample are distributed uniformly throughout the precipitator.

We measure and plot the charge accumulated during equal time intervals $\tau$ as a function of time and assume that during each of these intervals the charges are given up by particles of the same size corresponding to the middle of this interval. Let us consider two subsequent measurements of charges corresponding to $i^{\text{th}}$ and $(i+1)^{\text{st}}$ intervals. Their difference $\Delta Q_i = Q_i - Q_{(i+1)}$ can be attributed to particles of size $r_i$ which originally were on the top of the precipitator and in $t_i$ seconds reached the bottom. From the time $t_i$ we can calculate $r_i$ using Eq. [3].

In analogy to Eq. [7] we have:

$$N_i = \frac{\Delta Q_i t_i}{n_i eV}, \qquad [8]$$

where $\Delta Q_i/\tau$ is the charge accumulated during one second and $V/t_i$ is the volume of particles of size $r_i$ precipitated every second during interval $i$. This calculation repeated from the first to the last interval when all particles are precipitated gives $N_i$ as a function of $r_i$ or, in other words, the size distribution of aerosol particles in a given sample. By decreasing the interval of measurements more experimental points can be obtained, i.e., higher precision in the determination of particle size distribution can be achieved. In this equation: (*1*) $Q_i - Q_{(i+1)}$ and corresponding $t_i$ are known from the curve which represents the measured dependence between amount of accumulated charges during a certain time interval $\tau$ and time $t_i$ (see Fig. 4*b*); (*2*) $n_i$ can be determined from the curve representing charging law if the corresponding radius of the particles precipitated during this time interval is known (see Fig. 3); and (*3*) the average radius of these particles can be determined from Fig. 1, which shows the dependence between $t_i$ and corresponding $r_i$ was calculated from Stokes' law using a corresponding charging law (in this case charging current was 120 $\mu$a., the field was $E = 0.0555$ c.g.s., and the distance between the precipitator plates was 2.4 cm.). In other words, we have at our disposal three relations: (*1*) charging law (Fig. 3), (*2*) Stokes' law for electrostatic precipitation

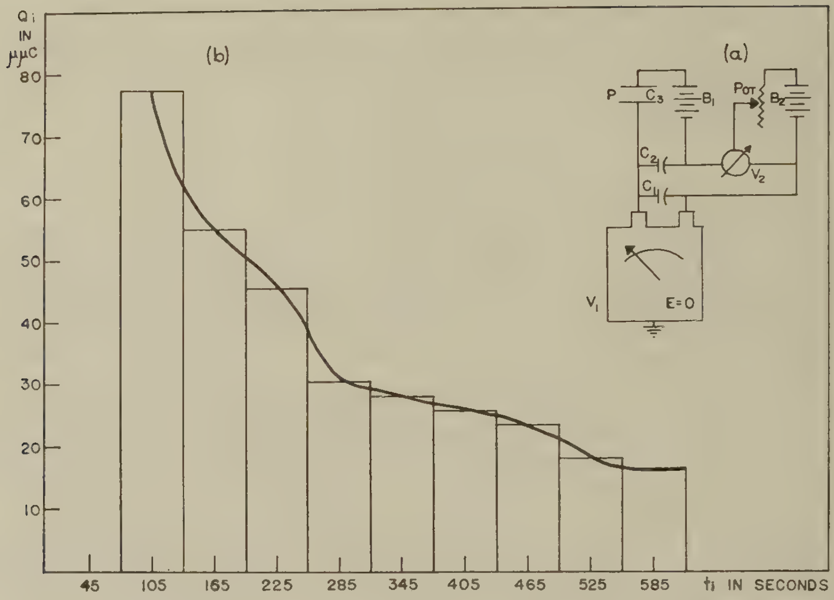

FIG. 4. (*a*) Circuit for measurement of the accumulated charges by the settling of charged aerosol particles in an electrostatic precipitator. (*b*) Charges in $C$ accumulated during a time interval of 1 minute versus time of settling under an electrostatic field of $E = 0.0555$ c.g.s.

(Fig. 1), and (*3*) accumulated charges versus time (Fig. 4*b*). From these three curves three unknowns $n_i$, $r_i$, and $N_i$ can be determined. The number of time intervals in which the curve expressed by Eq. [8] is subdivided, determines the number of experimental points on the size distribution curve.

We have not considered the slip effect on the values of radii of particles in all equations used. The reasons for this are the following: (*1*) there are different opinions as to the necessity of correcting the particle size determined from Stokes' law if particles are in the submicron range, e.g., Perrin (10) and Dallavalle (11) do not recommend any corrections for particles with radii larger than $0.1\mu$; Whytlaw-Gray (12) states that correction should be applied for values of $r$ less than $1\mu$; and Millikan (13) considered the size range from $0.2\mu$ to $2\mu$ radius as that which needs a correction (it should be pointed out that Millikan worked only with oil drops). (*2*) The previous work on dioctylphthalate and sulfur aerosol carried out in this laboratory (14) indicates that the radii of particles determined optically and from time of gravitational settling agree with each other much better if Stokes' law was used without any correction. The same observation was made by C. W. Hewitt (15) of Westinghouse Corporation, Pittsburgh, Pennsylvania, from his work on dioctylphthalate aerosol.

## EXPERIMENT

The dimensions of our precipitator were: length of a plate 33.1 cm., width 6.6 cm., distance between the plates 2.4 cm. Field strength in the precipitator was $E = 0.0555$ c.g.s.

The null method was used for measuring the charges given up by precipitated particles. See Fig. 4*a*, in which $P$ is the precipitator, $B_1$ and $B_2$ are batteries, 40 v. and 22.5 v., respectively, $C_1$ and $C_2$ are the internal and external capacitances (6$\mu\mu$f. and 7$\mu\mu$f., respectively) of the electrometer, $C_3$ is the capacitance of the precipitator (25$\mu\mu$f.) or a total of 38$\mu\mu$f., $V_1$ and $V_2$ are the voltmeters, and $P_0$ is the potentiometer. As voltmeter $V_1$, a vacuum tube electrometer Model 200 made by Keithley Instruments, Cleveland, Ohio, was used. The grid current of this instrument on the scale used for measurements was above 0.1$\mu$a. The voltmeter $V_2$ was a Weston instrument with three scales of which the smallest 0 to 3 v. was used.

The following procedure was adopted: the precipitator was filled with charged aerosol (charged at $i = 120\mu$a.) through a fish-tail taper for about one minute. Then the taper was removed and the precipitator was closed. The upper plate of the precipitator was connected to the positive pole of the 40 v. battery, and, at the same time, an electric timer was put in operation. The voltage on $V_2$, which compensated the charges accumulated on the condensors during 30 seconds, was read. Then 30 seconds were devoted to preparing for the next measurement. It was assumed that during the last 15 seconds preceding and the first 15 seconds following the actual measurement, the rate of accumulation of charges remained unchanged; that is, it was assumed that only particles of the size which correspond to

TABLE I

*Experimental Results Corresponding to Figure V*

| $t_i$ (*seconds*) | $V$ Compensating voltage for 1 min. (*v.*) | $Q_i = CV$ (*$\mu\mu$ C.*) | $Q_i - Q_{(i+1)}$ (*$\mu\mu$ C.*) | $r$ ($\mu$) | $n$ | $10^{-3}N$ |
|---|---|---|---|---|---|---|
| 45 | 4.50 | 171 | — | — | — | — |
| 105 | 2.04 | 77.5 | 22.8 | 1.34 | 400 | 1.2 |
| 165 | 1.44 | 54.7 | 9.1 | 0.86 | 164 | 1.8 |
| 225 | 1.20 | 45.6 | 15.2 | 0.62 | 85 | 8.0 |
| 285 | 0.80 | 30.4 | 2.3 | 0.55 | 55 | 2.4 |
| 345 | 0.74 | 28.1 | 2.3 | 0.51 | 47 | 3.4 |
| 405 | 0.68 | 25.8 | 2.2 | 0.41 | 31 | 5.7 |
| 465 | 0.62 | 23.6 | 5.4 | 0.33 | 23 | 21.8 |
| 525 | 0.48 | 18.2 | 1.5 | 0.20 | 12 | 13.1 |
| 585 | 0.44 | 16.7 | — | — | — | — |
| 1165 | 0.20 | 7.6 | — | — | — | — |

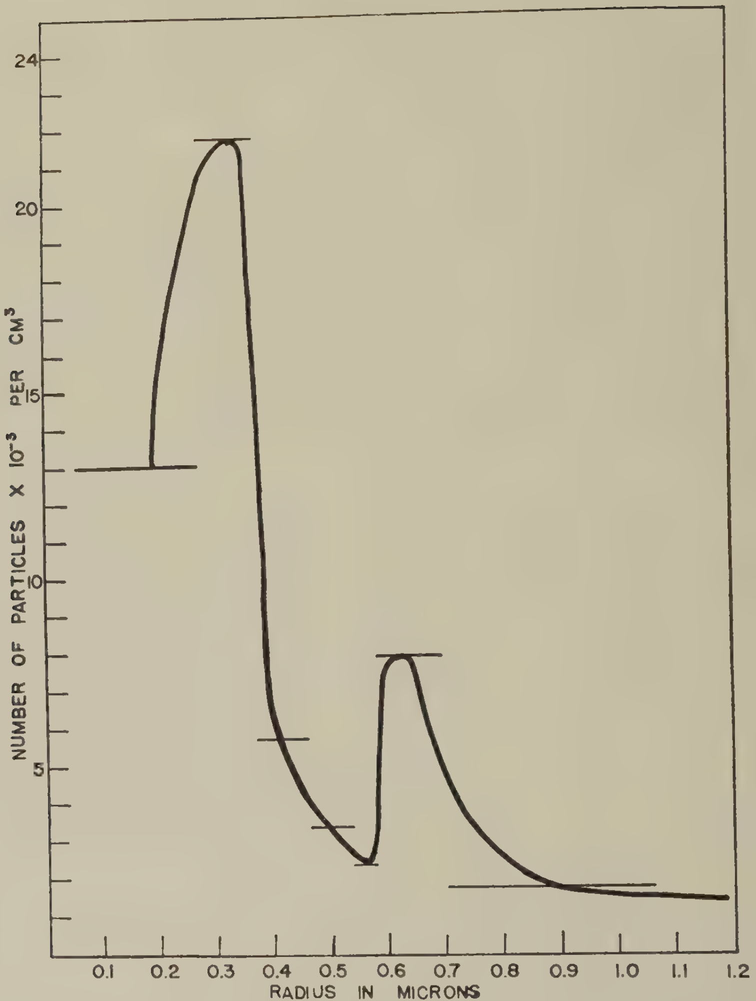

FIG. 5. Particle size distribution determined on a mixture prepared from two monodisperse stearic acid aerosols, produced in separate generators, each at a rate of 1 l./min., of $r = 0.30\ \mu$ and $r = 0.60\ \mu$, and charged in the device BCI at 120 $\mu$a.

the middle of the 60-second interval were precipitated during the 60 seconds. Such an assumption will be unnecessary if currents instead of accumulated charges are measured.

To test the method of electrostatic precipitation of charged aerosol particles we have mixed two aerosols produced in two generators: one of $r = 0.3\mu$ and another $r = 0.6\mu$, each of these at the rate of flow of one l./min. The experimental results and calculations are given in Table I.

Figure 4*b* represents $Q_i$ as a function of $t_i$. We omitted the first measurement since the very high $Q_i$ was apparently caused by aggregates of particles precipitated during the first 75 seconds. After 15 minutes, when all particles, even those which carry only one charge, should be precipitated, we could still measure some charges. This can be explained by small inhomogeneity of the field in the precipitator and small convection currents in it. However, the total amount of charges accumulated after about 10 minutes of precipitation was less than 1% of the total accumulated charges. This experiment was repeated three times, and the results were very similar to one another.

Figure 5 shows the particle size distribution (number concentration versus radius) in a mixture of two monodisperse stearic acid aerosols with $r = 0.3\mu$ and $r = 0.6\mu$. The horizontal lines represent a range of radii over which a given experimental point was averaged. The point where the curve touches this line corresponds to the radius calculated for the middle of the given time interval. The point corresponding to particles of $r = 0.2\mu$ comprises also all smaller particles as being charged by diffusion.

The maxima of the size distribution curve is close ($r = 0.33\mu$, $r = 0.62\mu$) to the corresponding radii of the aerosols used in the experiment, which were determined optically from Higher Order Tyndall Spectra.

## References

1. Rohman, H., *Z. Physik* **17**, 253 (1923).
2. Lipscomb, W. N., Rubin, T. R., and Sturdivant, T. N., *J. Appl. Phys.* **18**, 72 (1947).
3. Sawyer, K. F., and Walton, W. M., *Rev. Sci. Instr.* **27**, 272 (1950).
4. Pauthenier, M., and Moreau-Hanot, Mme., *J. phys. radium* **3**, 350 (1932).
5. Ladenburg, R., *Ann. Physik* **4**(5), 863 (1930); *ibid.* **14**(5), 510–520 (1932).
6. Arndt, P., and Kallman, H., *Z. Physik* **35**, 421 (1926).
7. Deutsch, W., *Z. tech. Phys.* **6**, 423 (1925); *ibid.* **7**, 623 (1926); *Physik. Z.* **34**, 448 (1933).
8. La Mer, V. K., and Sinclair, D., *Chem. Revs.* **44**, 245 (1949); also A.E.C. "Handbook on Aerosols." Washington, D. C., 1950.
9. Drozin, V. G., *J. Colloid Sci.* **10**, 158 (1955).
10. Perrin, Y., *Compt. rend.* **147**, 475 (1908).
11. Dallavalle, J. M., "Micrometrics," 2nd ed. New York and London, 1948.
12. Whytlaw-Gray, R., and Peterson, M. S., "Smoke." Arnold, London, 1932.
13. Millikan, R. A., *Phys. Rev.* **32**, 349 (1911).
14. La Mer, V. K., Drozin, V. G., Kruger, C., and Cotson, S., AEC. Rept. NYO 4526, 1953.
15. Private communication.

Appendix follows

# *Appendix*

## *Determination of Particle Size Distribution in an Aerosol Sample*

| | *Measurement of Particle Sizes* | *Measurement of Corresponding Concentrations* | *Limitations of Method* |
|---|---|---|---|
| I | Use of microscope or electron microscope to measure the diameter of particles precipitated on a slide by (*1*) gravitational sedimentation, (*2*) directed flow, (*3*) thermal precipitation, or (*4*) electrostatic precipitation. | Use of microscope or electron microscope to count number of particles of each size present in a given sample. | Tedious and time-consuming, since many particles should be measured and counted to find the relatively small statistical error. The assumption that *all* particles from a given vol. are caught on the slide is not always justified. |
| II | Sedimentation based on Stokes' law | Different Analytical Methods | |
| | *A*. Gravitational settling. Settling distance as a function of time. For small particles precautions against convection should be taken. | Aa)[1] Cumulative weight of particles precipitated on a sedimentation balance as a function of time. | Only relatively large particles (1–22$\mu$ radius) can be considered. |
| | | Ab)[2] Total intensity of transmitted or scattered light as a function of time. | Absolute size distribution of very heterogeneous aerosols cannot be determined. |
| | | Ac)[3] Electric current from precipitated charged particles as a function of time. | Ac1. Limitation is determined by the sensibility of the micro-micro-ammeter.<br>Ac2. The sedimentation time is very long for small particles. |
| | *B*. Centrifugal sedimentation. Settling distance as a function of time for a given set of parameters (angular velocity dimensions of apparatus, etc.). | Ba)[4] Weight of samples taken at different times or at different radii of rotation. Only suspensions in liquids are used. | Size distribution of the particles can be determined only if the particles are *suspended* in liquids. |
| | | Bb)[5] Microscopic counting of particles on a slide, or quantitative chemical analysis of particles placed on certain portions of a slide. | See limitations under I. A very low flow rate of aerosol is required. |

*Determination of Particle Size Distribution in an Aerosol Sample*

| | | |
|---|---|---|
| | Bc)[6] Electric current from charged particles precipitated on the conducting bottom as a function of time. | See limitations under IIAc, besides (*1*) Reynold's number should be less than 1. (*2*) $\omega^2 r$ must be much larger than g. |
| *C*. Electrostatic precipitation. Distance traveled by a charged particle as a function of time. | Ca[7] Electric current from the plate where particles of a given size are precipitated.<br>Cb[8] Electric current in a precipitator as a function of time. | See IIAc1. All particles charged by diffusion will precipitate in the same place. |
| III Cascade impactor. Particles in a given size range can be separated at a given velocity. | Weight of particles on successive slides, quantitative chemical analysis of these particles, or counting them on successive slides.[9] | Only a rough estimate of size distribution is possible. |
| IV Optical densities of particle images as a function of particle radii. | Counting the number of particle images of given optical densities on a photoplate.[10] | See I. Radii should be a single-valued function of intensity. The apparatus needs calibration with particles of given optical properties. |
| V A.[11] Electric pulses produced by charged particles hitting a wire connected to the grid of an amplifier as a function of particle size. | Counting pulses of given amplitudes. | Only relatively large particles can be measured (> 100) μ. |
| *B*.[12] Electric pulses produced in a photomultiplier by light scattered by individual particles as a function of particle size. | Counting pulses of given amplitudes. | The apparatus needs calibration with particles of given optical properties. The apparatus is very expensive. |

*Determination of Particle Size Distribution in an Aerosol Sample*

| | *Measurement of Particle Sizes* | *Measurement of Corresponding Concentrations* | *Limitations of Method* |
|---|---|---|---|
| VI | Angle-dependent scattering intensity as a function of particle size (Mie or diffraction theory).[13] | Total intensity of scattered light as a function of angle of observation. | Size distribution of a mixture consisting only of two monodisperse fractions of aerosol can be determined. |

1. S. Oden, "Colloid Chemistry," Vol. 1, ed. by J. Alexander, 1926.
2. (*a*) A. E. C., Handbook on Aerosols, Washington, D. C., 1950;
   (*b*) V. K. La Mer, J. Benedict, G. G. Goyer, and J. Kruger, Progress Reports on Contract AF-19(122)-164(1951).
   (*c*) M. Kerker, A. Lucile Cox, and M. D. Shoenberg, *J. Colloid. Sci.* **10,** 413 (1955).
3. See footnote 3 in this article.
4. C. Brown, *J. Phys. Chem.* **48,** 246 (1944); M. E. Robinson and S. W. Martin, *J. Phys. Chem.* **52,** 854 (1948); H. J. Kamak, *Anal. Chem.* **23,** 844 (1951).
5. K. F. Sawyer, and W. H. Walton, *Rev. Sci. Instr.* **27,** 272 (1950).
6. See footnote 3 in this article.
7. H. Rohman, *Z. Physik* **17,** 253 (1923); S. N. Fuchs, I. Petryanov, and B. Rotzeig, *Trans. Faraday Soc.* **32,** 1131 (1936); W. N. Lipscomb, T. R. Rubin, and T. N. Sturdivant, *J. Appl. Phys.*, **18,** 72 (1947); J. H. Daniel and I. S. Bracket, *J. Appl. Phys.* **22,** 542 (1951).
8. See this article.
9. K. R. May, *J. Sci. Instr.* **22,** 187 (1945); L. S. Sonkin, *J. Ind. Hyg. Toxicol.* **28,** 269 (1946); R. M. Ferry *et al.*, *Chem. Revs.* **44,** 389 (1949).
10. P. K. Lee and V. K. La Mer, *Rev. Sci. Instr.* **25,** 1004 (1954).
11. A. C. Guyton, *J. Ind. Hyg. Toxicol.* **28,** 133 (1946); F. T. Gucker, Jr., and C. T. O'Konski, *Chem. Revs.* **44,** 373 (1949); T. U. Geist, T. L. York, and G. G. Bard Brown, *Ind. Eng. Chem.* **43,** 1371 (1951).
12. C. T. O'Konski and G. J. Doyle, *Techn. Rept. No. 1*, Contract ONR 222 (1954).
13. M. Kerker and V. K. La Mer, *J. Am. Chem. Soc.* **72,** 3516 (1950).

JOURNAL OF COLLOID SCIENCE **14**, 91–100 (1959)

# AGGREGATION OF COLLOIDAL SUSPENSIONS BY FIBROUS SURFACES

## I. The Influence of the Fiber Surface

**G. T. Barnes[1] and A. E. Alexander[2]**

*School of Applied Chemistry, N.S.W. University of Technology,*
*Sydney, N.S.W., Australia*

*Received September 22, 1958*

### ABSTRACT

In an earlier paper (1) it was shown that the aggregation of a commercial D.D.T. formulation was accelerated by the addition of fibers, and that hydrophobic fiber surfaces were much more effective than hydrophilic ones. This investigation has now been repeated and extended using a simple D.D.T. suspension containing only pure materials.

The earlier assumption that the phenomenon is an aggregation process has been confirmed and the rate of aggregation has again been shown to depend on the wetting properties of the fiber surface. Some possible mechanisms are discussed.

### INTRODUCTION

During a study of the uptake by cattle hair of colloidal D.D.T. in aqueous suspension (1), it was observed that in the presence of the hair the normal aggregation process was greatly accelerated. A systematic examination showed that the phenomenon was associated in some way with the fiber surface, being shown in varying degrees by all fibrous materials (e.g., wool, hair, glass wool), and being particularly pronounced with the more hydrophobic surfaces. The conclusion was reached that aggregation occurred at the fiber surface, and some tentative mechanisms were advanced. However, since the D.D.T. formulation used was a commercial one, it was clearly desirable to repeat the investigation, using, as far as possible, materials of a chemically defined nature. This paper, and that following, present the results obtained with suspensions of pure D.D.T. alone and in the presence of soaps and simple salts.

The present investigations seem likely to be of considerable technological importance in connection with the widespread application of organic pesticides as aqueous dispersions, and are probably also relevant to the problem of the mechanical stability of polymer latices (2) and colloidal dispersions in general (3–5).

---

[1] Present address: Chemistry Department, Columbia University, New York, New York.

[2] Department of Physical Chemistry, University of Sydney, Sydney, N.S.W.

## EXPERIMENTAL

### *Materials*

*a. D.D.T.* (1,1,1,-trichlor-2,2-bis(*p*-chlorophenyl)-ethane). The pure *p*,*p*′ isomer was prepared by recrystallization from alcohol of the commercially pure material (Taubmans Pty. Ltd.).

*b. Potassium Chloride* (A. R. grade).

*c. Barium Chloride* ($BaCl_2 \cdot 2H_2O$, A. R. grade).

*d. Lanthanum Chloride.* Lanthanum chloride was prepared by dissolving $La_2O_3$ (A. R. grade) in the calculated amount of concentrated hydrochloric acid and desiccating over potassium hydroxide.

*e. Sodium Dodecyl Sulfate* (SDS). Pure SDS was prepared by Mr. D. K. O'Neill, according to the method of Dredger *et al.* (6) from dodecyl alcohol fractionated in a spinning hand column by the C.S.I.R.O.

*f. Cetyl Trimethyl Ammonium Bromide* (CTAB). The CTAB used had been purified by Mr. D. K. O'Neill by recrystallizing "Cetavlon" (I.C.I.) from acetone (twice) and methyl ethyl ketone (once).

*g. Triton X-100* (TX). The Triton X-100, an alkyl aryl polyether alcohol, was used as supplied. The manufacturers state that the product contains 100% active ingredient with less than 0.5% water (Rohm and Haas).

### *Fibers*

*a. Cattle Hair* (Surface area 490 cm.²/gm. (1)). This was part of a large sample which had been carefully teased, coned, and quartered. Clean hair was obtained by extracting the natural hair with light petroleum (40–60°C.) and then with water. The grease content of the natural hair was found to be about 2% by weight.

*b. Glass Wool* (Surface area 790 cm.²/gm. (1)). This was cleaned in a dichromate-sulfuric acid mixture and then boiled in several changes of distilled water for 4–5 hours.

Clean glass fibers were treated with CTAB by immersion in a solution (ca. 5% "Cetavlon") overnight, and the excess CTAB was removed by repeated washing with hot water.

The treatment of glass fibers with a methyl-chloro-silane solution was carried out by courtesy of Dr. R. J. Meakins, C.S.I.R.O.

### *Formulations*

*a. Commercial D.D.T. Formulation.* The D.D.T. concentrate was a sample of the commercial product (supplied by I.C.I.A.N.Z.) consisting of approximately 70% technical D.D.T. and 30% technical sulfated butyl oleate. Aqueous suspensions were prepared by melting a weighed amount in a boiling water bath and then pouring into cold water with vigorous mechanical stirring. The concentration of the $p,p'$ isomer of D.D.T. was always about 0.5%.

*b. Pure D.D.T. Suspension.* Pure $p,p'$ D.D.T. was dissolved in alcohol (95%) and the hot solution added through a coarse pipet tip to boiling water. The suspension was boiled for a further half-hour to remove all traces of alcohol, allowed to cool, and filtered (No. 1 grade paper).

## *Methods*

*a. Measurement of Precipitation Rate.* For work with the pure D.D.T. suspension the experimental procedure previously used for the commercial formulation (1) was modified considerably.

*1.* The "Microid" flask shaker was replaced by an apparatus driven by a synchronous electric motor, which provided a steady and reproducible back-and-forth motion to the flasks. The frequency was 24 cycles per minute, and the amplitude at the bottom of the flasks about 3.5 cm.

*2. Sampling.* A small portion of the suspension was poured through a sintered glass filter (No. 3 grade; maximum pore size 15–40$\mu$, according to B.S. 1752:1952) whenever a sample was required. An aliquot (0.4 ml.) of the filtrate was measured with a micrometer syringe into a volumetric flask (10 ml.) and diluted with alcohol. Only the one sintered glass filter was used within any one experimental series.

Some difficulty was experienced at first owing to clogging of the filter and syringe needle, but it was overcome by using larger bore syringe needles and by cleaning with hot alcohol between samples.

*3. D.D.T. analysis.* The D.D.T. was analyzed by measuring the absorption at 237 m$\mu$ with a Cary recording spectrophotometer (7). The various additives used do not interfere and no absorption other than that from D.D.T. could be detected. The molar extinction coefficient at 237 m$\mu$ was found to be $1.5 \times 10^4$.

*b. Adhesion to Fibers.* The amount of D.D.T. adhering to fibers (expressed as mg./g. fiber) was determined by extraction and analysis. The D.D.T. suspension was shaken with the fibers and small samples of fiber were removed at selected times. The samples were immersed in two changes of distilled water to remove losely adhering material, and then placed in small extraction tubes containing a perforated disk. The fibers were dried by a current of air and the D.D.T. was extracted by pouring cyclohexane (spectroscopically pure) slowly through the tubes into volumetric flasks, the extracts being analyzed as above. After drying, the weights of fibers in the samples were determined.

*c. Photomicrography.* For photographing D.D.T. particles on fibers the maximum depth of field was required. A Reichert Zetapan microscope with 11× objective, 12× Plan ocular, and Zeiss plate camera, was used. The illumination was vertical dark field. The Ilford Rapid Process Pan plates required an exposure of 15 sec.

## RESULTS

The influence of the various fiber surfaces on the rate of aggregation is shown in Figs. 1 and 2 and on the time of half-precipitation ($\tau_{1/2}$) in Table

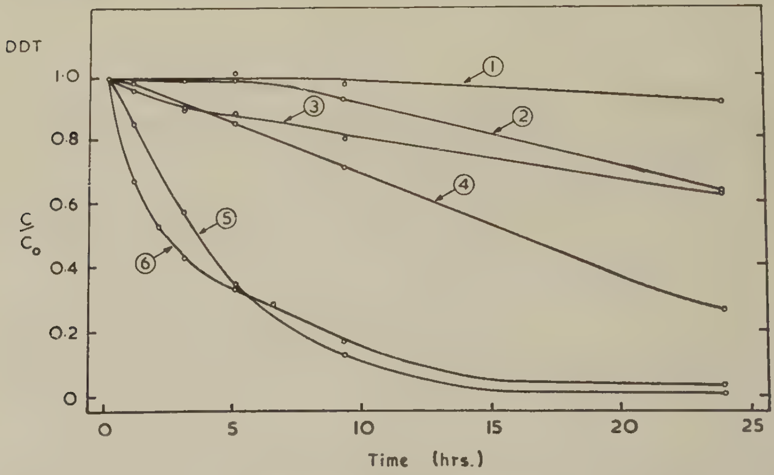

FIG. 1. Stability of D.D.T. suspension in the presence of: (*1*) no additive (blank); (*2*) glass; (*3*) glass, silane-coated; (*4*) hair; (*5*) glass, CTAB-satd.; (*6*) hair and $10^{-3}$ *M* KCl.

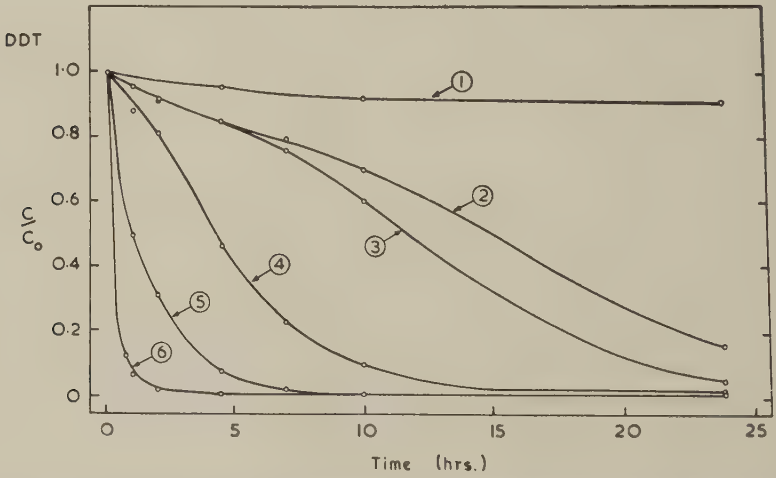

FIG. 2. Stability of D D.T. suspension in the presence of: (*1*) no additive (blank); (*2*) hair; (*3*) hair, SDS-satd.; (*4*) glass, CTAB-satd.; (*5*) hair, TX-satd.; (*6*) hair, CTAB-satd.

I. (The ordinate scale is plotted as $C/C_0$, i.e., the ratio of concentration at a particular time to the initial concentration.) The overall picture is as found with the commercial formulation (1), although there is less scatter in the experimental points and the change in the control (i.e., no added fibers) is much less.

In series 9 (Fig. 1) the silane-treated glass fibers floated on the surface of the liquid, giving poor contact with the suspension; this would probably account for the slow rate of aggregation observed.

With glass fibers, different CTAB treatments were found to vary in effectiveness, the first treatment (series 7) giving much slower aggregation than the second (series 9 and 10). This was probably due to a change in the method of removing excess CTAB, as the fibers in a third batch which was boiled for several hours reverted to their original hydrophilic nature.

The possibility that, in series 9 and 10, some of the soaps adsorbed on the fibers had come off and affected the aggregation rate, was checked by

TABLE I

*Effect of Various Fibers and Surface Treatments on the Rate of Aggregation of Pure D.D.T. Suspension*

| Fiber | Treatment | $\tau_{1/2}$ (*min.*) for series number: | | | |
|---|---|---|---|---|---|
| | | 7 | 8 | 9 | 10 |
| Blank | — | .. | .. | >5000 | .. |
| Hair | Clean | — | 880 | 945 | 900 |
| | CTAB-satd. | — | — | — | 10 |
| | TX-satd. | — | — | — | 55 |
| | SDS-satd. | — | — | — | 700 |
| | Natural | — | 940 | — | — |
| Glass | Clean | 1740 | >2000 | 1800 | — |
| | CTAB-satd. | 1030 | — | 215 | 250 |
| | Silane-coated[a] | — | — | 2000 | — |

[a] *Note.* Silane-coated fibers floated on the surface of the suspension.

TABLE II

*Surface Tensions of D.D.T. Suspensions at the Conclusion of Aggregation Experiments*

| Fiber | Treatment | Surface tension (*dynes/cm.*) |
|---|---|---|
| Blank | — | 66.7 |
| Hair | Clean | 67.1 |
| | CTAB-satd. | 66.7 |
| | TX-satd. | 64.0 |
| | SDS-satd. | 64.6 |
| Glass | CTAB-satd. | 67.3 |

TABLE III

*Effect of Mass of Hair (w) on the Aggregation of D.D.T. Suspension (50 ml.)*

| Series no. | $w$ (g.) | $\tau_{1/2}$ (min.) | $K^*$ ($10^4$/min.) | $K/w$ ($10^3$/min.g.) |
|---|---|---|---|---|
| 22, 23 | 0 | ∞ | — | — |
| 23 | 0.05 | 2440 | 2.9 | 5.7 |
| 23 | 0.1 | 1380 | 5.0 | 5.0 |
| 23 | 0.2 | 860 | 8.1 | 4.0 |
| 22 | 0.2 | 915 | 7.6 | 3.8 |
| 23 | 0.3 | 750 | 9.3 | 3.1 |
| 23 | 0.4 | 560 | 12.4 | 3.1 |
| 22 | 0.4 | 610(?) | 11.4 | 2.9 |
| 11 | 0.5 | 580 | 12.0 | 2.4 |
| 13 | 0.5 | 590 | 11.8 | 2.4 |
| 17 | 0.5 | 600 | 11.6 | 2.3 |
| 22 | 0.6 | 665(?) | 10.4 | 1.7(?) |
| 22 | 0.8 | 490 | 14.2 | 1.8 |

*Note:* The queried values refer to curves 3 and 4 of Fig. 3.

* Calculated from the relationship for a first-order process $K = (\ln 2)/\tau_{1/2}$

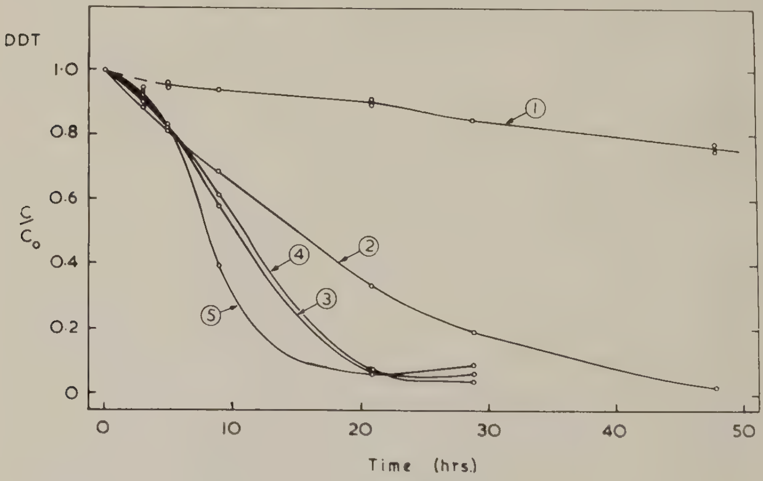

FIG. 3. Effect of mass of hair added on the stability of D.D.T. suspension: (*1*) no hair, (*2*) 0.2 g., (*3*) 0.4 g ; (*4*) 0.6 g.; (*5*) 0.8 g.

measuring the surface tension of the suspensions at the conclusion of the experiments. The results are in Table II. No significant lowering of surface tension was observed, indicating that the amount of soap removed from the fibers during the experiments was negligible.

The effect of the mass of hair on the aggregation rate is shown in Table III and Fig. 3 and the influence of the concentration of D.D.T. suspension in Fig. 4.

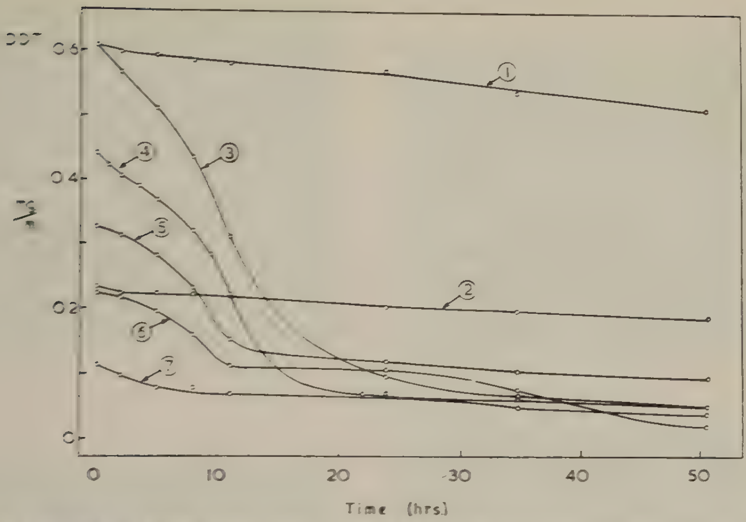

Fig. 4. Effect of initial concentration of D.D.T. suspension on the stability: (*1*) (*2*) no additive; (*3*)–(*7*) 0.5 g. hair in 50 ml.

TABLE IV

*Adhesion of D.D.T. to Fibers*

*a* ca. 0.1 g. fiber used; *b* 0.5 g. fiber used in conjunction with an aggregation experiment (series 9).

| Fiber | Treatment | Adhesion (*mg.DDT/g.fiber*) 1 hr. | 9.5 hr. | 24 hr. |
|---|---|---|---|---|
| (*a*) Hair | Clean | 6.1 | — | 17.2 |
| Glass | Clean | 0.3 | — | 0.5 |
| | CTAB-satd. | 3.2 | — | 12.3 |
| | Silane-coated | >5.5 | — | 26.1 |
| (*b*) Hair | Clean | 4.0 | 12.5 | 22.6 |
| Glass | Clean | 0.2 | 0.5 | 0.2 |
| | CTAB-satd. | 4.4 | 7.2 | 1.6 |
| | Silane-coated | 6.6 | 11.5 | 15.8 |
| Hair | KCl added ($10^{-3}$ *M*) | 31.7 | 30.1 | 33.3 |

The amounts of D.D.T. adhering to various fibers, treated and untreated, are shown in Table IV. The results are given in terms of fiber weight rather than surface area, as the surface areas are not accurately known, and because the fibers were measured out by weight in the aggregation experiments.

In Fig. 5 are photomicrographs of D.D.T. adhering to various fiber surfaces. Before examination the fibers were rinsed twice in distilled water to remove loosely adhering particles.

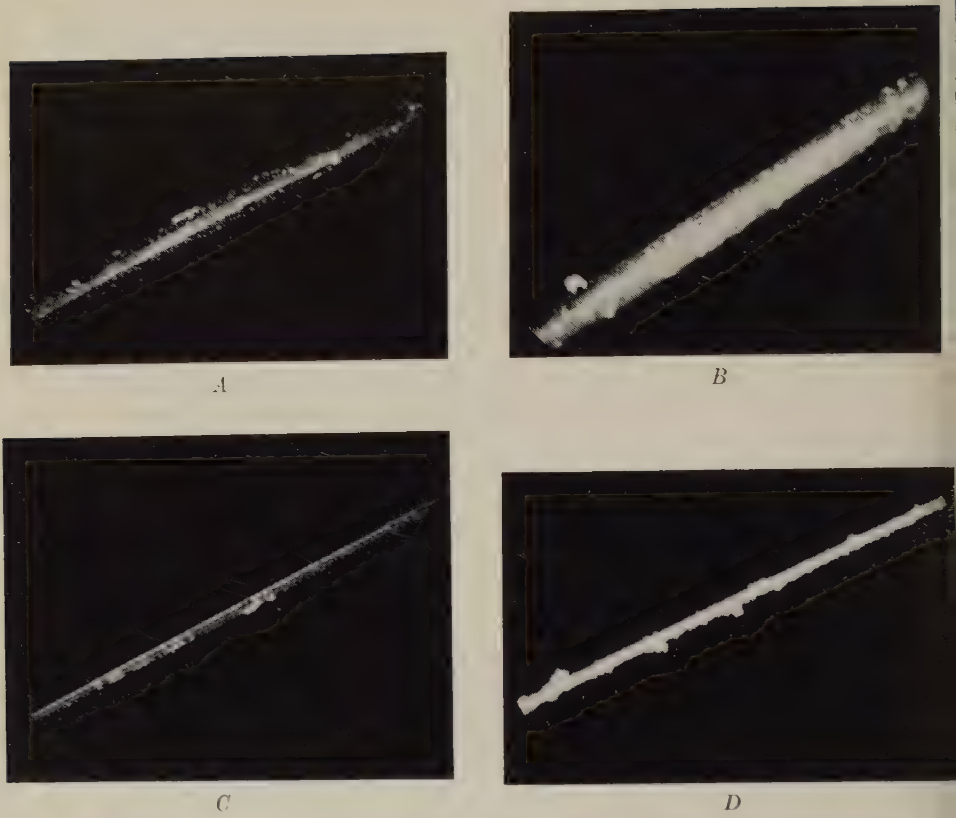

FIG. 5. Photomicrographs of D.D.T particles adhering to fibers after 30 hr. immersion in D.D.T. suspension: (*a*) hair; (*b*) hair with $10^{-3}$ *M* KCl; (*c*) glass; (*d*) silane-treated glass.

## DISCUSSION

With the pure suspension, as in the earlier experiments with the commercial formulation, the presence of hair fibers markedly increased the rate of precipitation of D.D.T. (Figs. 1–2). In the case of the commercial formulation this would conceivably have involved three processes: solidification of the supercooled melt, crystal growth, and aggregation, thus making difficult any detailed analysis of the phenomenon (1). However, since precipitation by fibers is observed with both suspensions, a common process is indicated.

Observations of the rate of crystallization of supercooled D.D.T. in bulk, in relation to the time scale of the present experiments, would seem to eliminate the first factor.

Examination of the deposits formed in both suspensions shows that whereas the D.D.T. from the commercial formulation is a mass of large crystals, the D.D.T. from the pure suspension consists of amorphous or microcrystalline particles, both in the presence and absence of fiber surfaces. Thus crystal growth does not appear to be important in the pure suspension.

Elimination of these two processes, solidification and crystal growth, would then indicate that the precipitation of D.D.T. from the pure suspension is an aggregation process and that the effect of fiber surfaces is to accelerate aggregation. The *nature* of the fiber surface clearly has a marked effect. Thus with the hydrophilic clean glass the rate is little faster than without fibers, but with the hydrophobic fibers, hair and CTAB-treated glass, the aggregation is greatly accelerated (Figs. 1–2). On the other hand, the electrokinetic ($\zeta$) potential, which might at first sight be thought to be important, does not seem to be so, the relevant values (all negative) being: clean glass—106 mv.; CTAB-treated glass—73 mv.; silane-treated glass—88 mv.; clean hair—81 mv. (1).

An earlier paper (1) made the suggestion that the D.D.T. particles, being hydrophobic in nature, tend to be adsorbed more strongly by hydrophobic surfaces and are thus brought into a higher local concentration which in turn would increase the rate of aggregation. This hypothesis is supported by the results given in Table IV which show quite clearly that much more D.D.T. adheres to hydrophobic surfaces than to hydrophilic ones.

Similar results have been obtained by Palmer and Rideal (8) from measurements of adhesion numbers by the method of von Buzagh (9, 10). They found that the adhesion number for hydrophobic particles on glass surfaces could be greatly increased by coating the glass to make it hydrophobic.

However, the expected correlation between the rate of aggregation and the adhesion on fibers in the present system is not very precise, as comparison of Tables I and IV will show. This may be due to the method of measuring adhesion, as such factors as the roughness of the fiber surface and the size of the particles could have appreciable effects. Nevertheless the adhering D.D.T. does seem to be involved in the formation of aggregates.

Two mechanisms for the aggregation of D.D.T. particles on surfaces can be suggested, namely, movement of particles over the surface, and collisions between particles in the suspension and particles adsorbed on the surface.

While measuring adhesion numbers von Buzagh (10) observed that particles adhering to glass surfaces could still exhibit Brownian movement. Examination of hair fibers in D.D.T. suspensions shows that some small particles very close to the fiber surface still have Brownian movement, but it is not possible to establish with certainty that these particles are actually adhering. Nevertheless it seems possible that loosely adhering D.D.T. particles can move over the fiber surface and form aggregates by colliding with other particles. In this scheme the function of the fiber surface would be simply to increase the local concentration of particles.

Alternatively, D.D.T. particles in the suspension may strike the particles adsorbed on the surface and form aggregates. These would grow by further collisions until they were large enough to be dislodged under the combined influence of agitation and gravity.

Probably aggregation takes place by both mechanisms. At first, movement over the surface may be the more important, but as the surface becomes covered with D.D.T. and large aggregates form the second mechanism would predominate.

The rate of aggregation of the D.D.T. suspension varied with the amount of added fiber, but not in a linear fashion, the changing values of $K/w$ in Table III showing that the effectiveness per unit mass decreases with the amount of added fiber. This can reasonably be ascribed to impeded movement of the liquid and to mutual screening of fibers as their volume, relative to the liquid, increases.

Owing to the complex nature of the aggregation process and the limited accuracy of the data a detailed kinetic analysis does not seem to be worth while. However, from a plot of log $(-dC/dt)$ against log $C$ (where $C$ is the concentration of unaggregated D.D.T. at time $t$) it would seem that the aggregation on fibers approximates to first-order kinetics.

## ACKNOWLEDGMENTS

Thanks are due to the C.S.I.R.O. for financial aid to one of us (G.T.B.) and to Dr. R. J. Meakins and Mr. D. K O'Neill for assistance in specific ways as indicated in the text.

## REFERENCES

1. BARNES, G. T., AND ALEXANDER, A. E., *Proc. 2nd Intern. Congr. Surface Activity* **IV,** 211 (1957).
2. ROE, C. P., AND BRASS, P. D., *J. Colloid Sci.* **10,** 194 (1955).
3. FREUNDLICH, H., AND BASU, S. K., *Z. physik. Chem.* **115,** 203 (1925); FREUNDLICH, H., AND KROCH, H., *ibid.* **124,** 155 (1926).
4. HELLER, W., AND ROEDER, H. F., *Trans. Faraday Soc.* **38,** 191 (1942).
5. STAMBERGER, P., *J. Phys. Chem.* **61,** 127 (1957).
6. DREDGER, E. E., *et al.*, *Ind. Eng. Chem.* **36,** 610 (1944).
7. NEAL, P. A., *et al.*, *U. S. Public Health Repts., Suppl. No.* **177** (1944).
8. PALMER, R. C., AND RIDEAL, E. K., *J. Chem. Soc.* **1939,** 573.
9. VON BUZAGH, A., *Kolloid-Z.* **51,** 105, 230 (1930); *ibid.* **52,** 46 (1930).
10. VON BUZAGH, A., "Colloid Systems." Technical, London, 1939.

JOURNAL OF COLLOID SCIENCE **14**, 101–110 (1959)

# AGGREGATION OF COLLOIDAL SUSPENSIONS BY FIBROUS SURFACES

## II. The Effects of Added Salts and Soaps

**G. T. Barnes[1] and A. E. Alexander[2]**

*School of Applied Chemistry, N.S.W. University of Technology,*
*Sydney, N.S.W., Australia*

*Received September 22, 1958*

### ABSTRACT

The addition of soaps or simple salts changes the stability of the D.D.T. suspension and also the rate of aggregation by fibrous surfaces. Low salt concentrations cause an immediate partial coagulation of the suspension, but further coagulation is generally very slow. The same salt concentrations produce very marked increases in the rate of aggregation of D.D.T. by hydrophobic fiber surfaces. This is attributed to decreases in the electrical repulsive forces around the fibers and the particles.

Added soaps usually lower the stability of the suspension (without added fibers), the lowering being much more marked at soap concentrations above the c.m.c. This observation and the formation of large D.D.T. crystals suggest a process of crystal growth by transport of D.D.T. in the soap micelles. When fibers are also present the soaps are shown to be adsorbed on the fibers, rendering them more hydrophobic, and hence increasing the rate of aggregation of the D.D.T. by the fiber surfaces.

### INTRODUCTION

The suspension studied in the preceding paper contained only pure D.D.T. and distilled water, and was prepared entirely without the aid of soaps. On the other hand, the commercial D.D.T. formulation used in our first studies (1) contained quite a high concentration of an impure soap[3] (0.32 % sulfated butyl oleate) and in normal usage is subject to the influence of salts in the water used. Therefore, in order to explain more fully the precipitation phenomena observed with the commercial formulation in practice it was necessary to investigate the effects of soaps and of simple salts on D.D.T. suspensions.

The problem could be conveniently studied by making appropriate additions to a pure D.D.T. suspension and measuring the stability, by the usual filtering technique, in the presence and absence of added fibers.

---

[1] Present address: Chemistry Department, Columbia University, New York, New York.

[2] Department of Physical Chemistry, University of Sydney, Sydney, N.S.W.

[3] The term "soap" is here used in the wider sense suggested by Alexander and Johnson (2).

## EXPERIMENTAL

The materials and methods used were fully described in the preceding paper.

Electrophoretic mobilities were determined by a simple U-tube apparatus, 2% sucrose being added to the suspension in order to keep the boundaries sharp.

## RESULTS

### *1. Aggregation in the Presence of Added Salts*

In the absence of fibers the addition of small amounts of salts produced an immediate partial aggregation, as shown by the results in Table I.

TABLE I

*Effects of Salts on the Stability of a Pure D.D.T. Suspension*

| Salt | Concn. (*M*) | D.D.T. (% of initial concn.) | |
|---|---|---|---|
| | | 0 hr. | 22 hr. |
| Blank | — | (100) | 89.0 |
| KCl | $10^{-3}$ | 94.0 | 75.4 |
| | $10^{-2}$ | 75.8 | 33.1 |
| $BaCl_2$ | $10^{-4}$ | 89.0 | 73.3 |
| | $10^{-3}$ | 65.6 | 29.0 |
| $LaCl_3$ | $10^{-5}$ | 86.5 | 67.2 |
| | $10^{-4}$ | 48.4 | 5.1 |

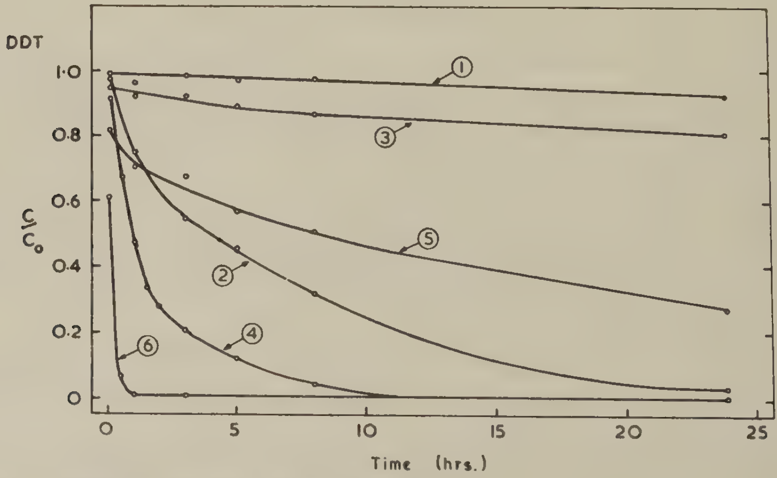

FIG. 1. Effect of KCl and hair on the stability of D.D.T. suspension: (*1*) blank; (*2*) hair; (*3*) $10^{-3}$ *M* KCl; (*4*) $10^{-3}$ *M* KCl and hair; (*5*) $10^{-2}$ *M* KCl; (*6*) $10^{-2}$ *M* KCl and hair. ($C_0$ = initial concentration of blank.)

With the lower salt concentrations used the suspensions then remained reasonably stable. The behavior was shown to be independent of the method of mixing the salt and suspension.

The addition of salts produced a marked increase in the rate of aggregation in the presence of hair fibers, but had comparatively little effect with clean glass fibers. The experimental curves (Figs. 1–3) have been plotted

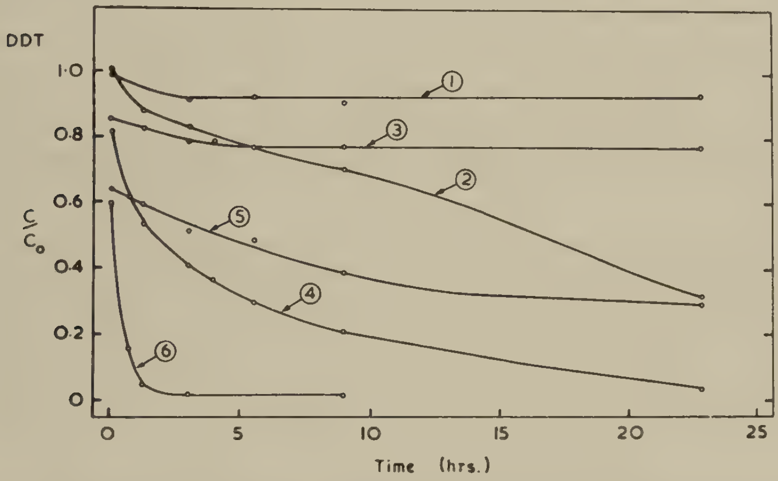

FIG. 2. Effect of $BaCl_2$ and hair on the stability of D.D.T. suspension; (*1*) blank; (*2*) hair; (*3*) $10^{-4}$ *M* $BaCl_2$ ; (*4*) $10^{-4}$ *M* $BaCl_2$ and hair; (*5*) $10^{-3}$ *M* $BaCl_2$ ; (*6*) $10^{-3}$ *M* $BaCl_2$ and hair. ($C_0$ = initial concentration of blank.)

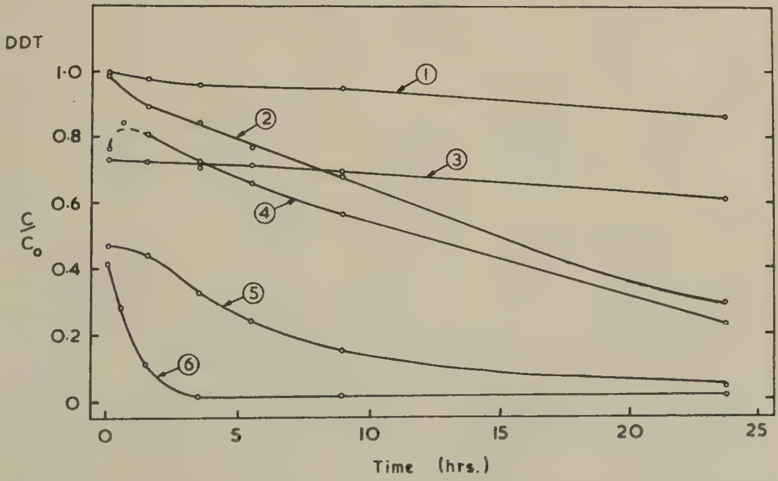

FIG. 3. Effect of $LaCl_3$ and hair on the stability of D.D.T. suspension: (*1*) blank; (*2*) hair; (*3*) $10^{-5}$ *M* $LaCl_3$ ; (*4*) $10^{-5}$ *M* $LaCl_3$ and hair; (*5*) $10^{-4}$ *M* $LaCl_3$; (*6*) $10^{-4}$ *M* $LaCl_3$ and hair. ($C_0$ = initial concentration of blank.)

against the initial concentration in the blank; the curves for glass fibers are shown in Fig. 8. Table II gives the values of $\tau_{1/2}$ calculated on the initial concentrations in each flask.

Although attempts were made to determine the particle size-frequency distributions before and after adding electrolytes, the results have little significance, as it is reasonably certain that many of the particles were too small or in too vigorous Brownian movement to be recorded by photomicrography and counted.

The results of the electrophoretic measurements are given in Table III.

### *2. Aggregation in the Presence of Added Soaps*

The effect of the soap concentration on the stability of the D.D.T. suspension in the absence of fibers is given in Table IV and illustrated in

TABLE II

*Effects of Added Salts and Fibers on the Aggregation of Pure D.D.T. Suspension*

| Fiber | Salt | Concn. ($M$) | $\tau_{1/2}$ (*min.*) for series number: | | | | |
|---|---|---|---|---|---|---|---|
| | | | 17 | 18 | 19 | 20 | 21 |
| Blank | — | — | ∞ | ∞ | ∞ | ∞ | ∞ |
| | KCl | $10^{-1}$ | 20 | — | — | — | — |
| | | $10^{-2}$ | 2000 | 810 | — | — | — |
| | | $10^{-3}$ | ∞ | ∞ | — | — | — |
| | $BaCl_2$ | $10^{-3}$ | — | — | 1100 | — | — |
| | | $10^{-4}$ | — | — | ∞ | — | ∞ |
| | $LaCl_3$ | $10^{-4}$ | — | — | — | 320 | — |
| | | $10^{-5}$ | — | — | — | ∞ | — |
| Hair | — | — | 600 | 250 | 990 | 920 | — |
| | KCl | $10^{-1}$ | 10 | — | — | — | — |
| | | $10^{-2}$ | 25 | 15 | — | — | — |
| | | $10^{-3}$ | — | 60 | — | — | — |
| | $BaCl_2$ | $10^{-3}$ | — | — | 25 | — | — |
| | | $10^{-4}$ | — | — | 170 | — | — |
| | $LaCl_3$ | $10^{-4}$ | — | — | — | 50 | — |
| | | $10^{-5}$ | — | — | — | 980 (?) | — |
| Glass | — | — | — | — | — | — | 1800 |
| | $BaCl_2$ | $10^{-4}$ | — | — | — | — | 1010 |

TABLE III

*Electrophoretic Measurements on Pure D.D.T. Suspension with Added Salts*

| Salt | Concn. ($M$) | Mobility ($\mu$/sec./volt/cm.) | $\zeta$ potential (*mv.*) |
|---|---|---|---|
| None | — | 1.76 | −22.9 |
| KCl | $10^{-3}$ | 1.19[a] | −16[a] |
| $BaCl_2$ | $10^{-4}$ | 1.62 | −21.1 |
| $LaCl_3$ | $10^{-5}$ | 1.52 | −19.7 |

[a] Appreciable gassing at electrodes.

Fig. 4 for the case of SDS. The soap concentrations are given relative to the critical micellar concentration (c.m.c.).

The addition of soaps sometimes produced a marked change in the appearance of the D.D.T. suspension. With soap concentrations above the

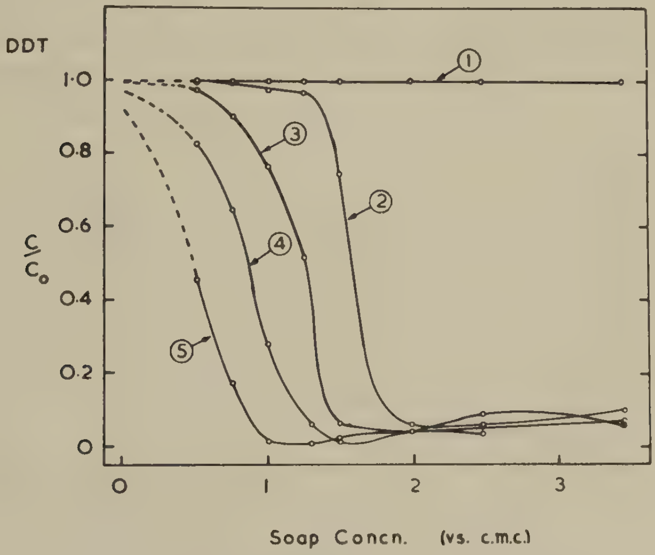

FIG. 4. Effect of SDS on the stability of D.D.T. suspension: (*1*) 0 hr.; (*2*) 1.5 hr.; (*3*) 5 hr.; (*4*) 10 hr.; (*5*) 24 hr.

TABLE IV

*Effect of Added Soaps on a D.D.T. Suspension*

| Fiber | Soap | Concn. c.m.c. | $\tau_{1/2}$ (*min.*) for series number: | | | |
|---|---|---|---|---|---|---|
| | | | 11 | 12 | 13 | 14 |
| Blank | — | — | — | 1800 | ∞ | ∞ |
| | SDS | 0.5 | 790 | — | — | 485 |
| | TX | 0.5 | — | 1530 | — | — |
| | | 2 | — | 870 | — | — |
| | CTAB | 0.5 | — | — | 270 | — |
| | | 2 | — | — | 35 | — |
| Hair | — | — | 580 | 480 | 590 | — |
| | SDS | 0.5 | 85 | — | — | — |
| | | 2 | 10 | — | — | — |
| | TX | 0.5 | — | 185 | — | — |
| | | 2 | — | 105 | — | — |
| | CTAB | 0.5 | — | — | 15 | — |
| | | 2 | — | — | 10 | — |
| Glass | — | — | — | — | — | 1740 |
| | SDS | 0.5 | — | — | — | 205 |

c.m.c. the suspension changed from mat white to pearly white, and schlieren effects could be seen on shaking. The change could be observed within an hour of adding the ionized soaps, SDS and CTAB, but was much slower with TX. At concentrations below the c.m.c. a similar but much less marked change could be observed after 10 to 20 hours. These effects were not found in the absence of soaps.

Microscopical examination showed that in the presence of soaps the D.D.T. deposits were invariably crystalline, whereas without additives the

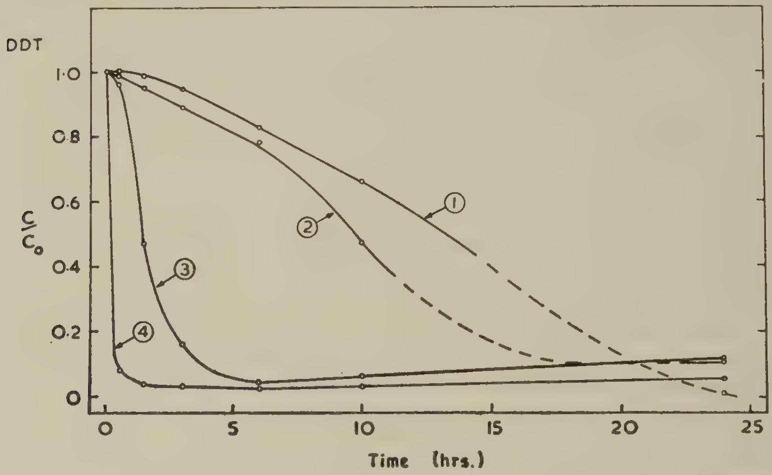

FIG. 5. Effect of SDS and hair on the stability of D.D.T. suspension: (*1*) SDS, 0.5 c.m.c.; (*2*) hair; (*3*) hair and SDS, 0.5 c.m.c.; (*4*) hair and SDS, 2 c.m.c.

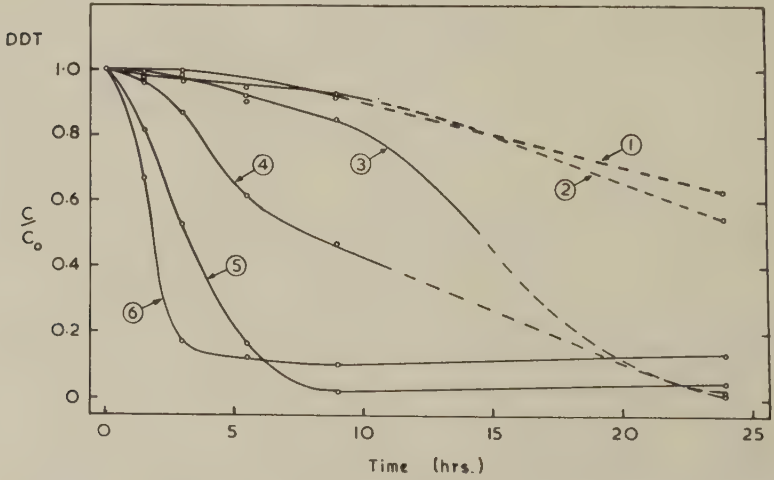

FIG. 6. Effect of TX and hair on the stability of D.D.T. suspension: (*1*) no additive (blank); (*2*) TX, 0.5 c.m.c.; (*3*) TX, 2 c.m.c.; (*4*) hair; (*5*) hair and TX, 0.5 c.m.c.; (*6*) hair and TX, 2 c.m.c.

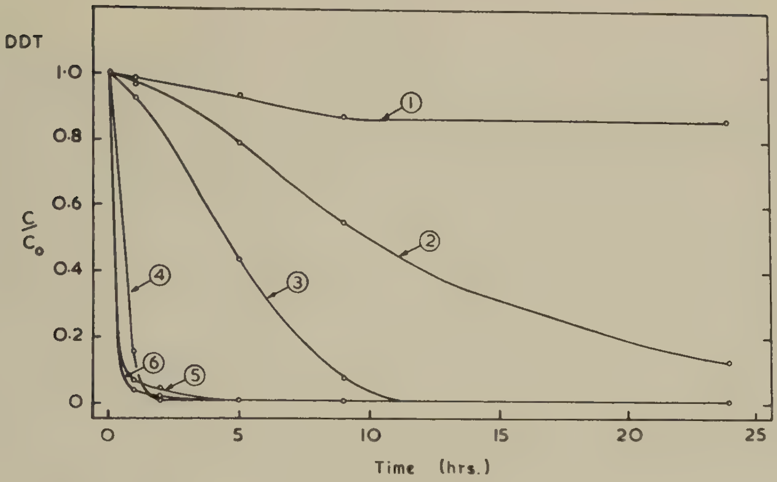

FIG. 7. Effect of CTAB and hair on the stability of D.D.T. suspension: (*1*) no additive (blank); (*2*) hair; (*3*) CTAB, 0.5 c.m.c.; (*4*) CTAB, 2 c.m.c.; (*5*) hair and CTAB, 0.5 c.m.c.; (*6*) hair and CTAB, 2 c.m.c.

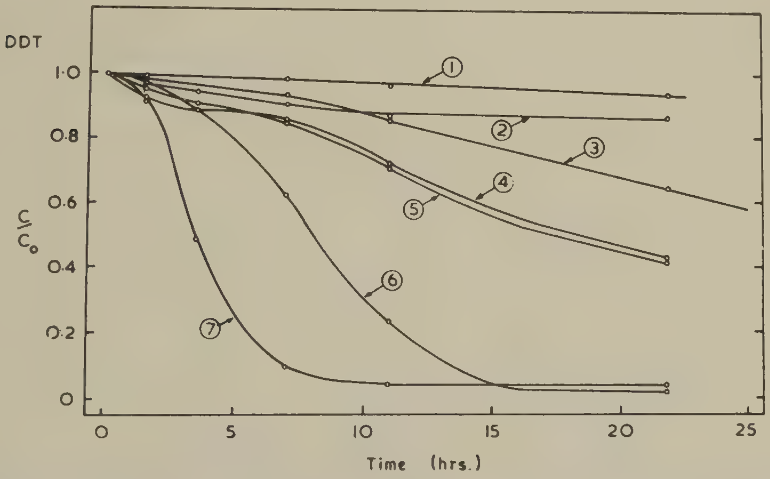

FIG. 8. Stability of D.D.T. suspension in the presence of: (*1*) no additive (blank); (*2*) $10^{-4}$ *M* $BaCl_2$; (*3*) glass; (*4*) glass, CTAB satd.; (*5*) glass and $10^{-4}$ *M* $BaCl_2$; (*6*) SDS, 0.5 c.m.c.; (*7*) glass and SDS, 0.5 c.m.c.

deposits contained no visible crystals (540×). The soaps appeared to modify the normal D.D.T. crystal habit, giving broader and flatter crystals. Such modification by dyes has been observed previously by a number of workers (e.g., 3, 4).

The combined effects of added soaps and fibers on the rate of aggregation are shown in Figs. 5–8 and in Table IV.

## Discussion

It has been shown here that the addition of salts markedly increases the rate of aggregation induced by hair fibers and with the series KCl, $BaCl_2$, and $LaCl_3$ the relative efficacy is seen from Table II to be in reasonable accord with the Schulze-Hardy rule. Also, the adhesion of D.D.T. particles to fibers was shown in the preceding paper (see Table IV) to be facilitated by the addition of salts.

Thus it seems likely that the marked increase in the rate of aggregation observed in the presence of both fibers and salts is due to a decrease in the electrical repulsive forces involved, in accord with modern theories of the stability of hydrophobic colloids (2).

The effect of added soaps, on the other hand, seems to be more complex. On general grounds based on earlier work it would be anticipated that soaps might influence the aggregation process in two principal ways: firstly, by adsorption on the surfaces of D.D.T. and fiber, and secondly, by assisting the crystal growth of D.D.T. through the medium of soap micelles.

The role of soap micelles in the transport and crystallization of sparingly soluble solids such as D.D.T. seems well established (5). With the D.D.T. suspension in the absence of added fibers it might be expected therefore that added soaps up to the c.m.c. would increase the stability (by adsorption) and would accelerate crystal growth only at higher concentrations.

Leaving aside the behavior of the cationic soap at *extremely* low concentrations (Fig. 7). which is readily explicable as due to charge reversal (the D.D.T. suspension being initially negatively charged), it is clear from the experimental data that at concentrations above the c.m.c. the D.D.T. particles are growing much faster than in water alone, and this can readily be ascribed to micellar transport. However, even at a soap concentration of 0.5 c.m.c. the rate is also faster. At first sight this is surprising, since at this concentration the monolayer of adsorbed soap should be largely complete and stabilization therefore close to its optimum.

Two possible explanations can be advanced. The first would postulate the presence of a small number of micelles at concentrations below the c.m.c. This is not unreasonable physically, particularly in view of the existence of dimers below the c.m.c. (6), but our attempts to show their presence by spectrophotometrical measurement of D.D.T. solubility have proved negative. The second involves surface transport of D.D.T. through the adsorbed soap monolayer leading to the originally amorphous particles becoming asymmetric needles which, being more readily filtered out by the experimental technique used, would show up as a reduction in colloidal D.D.T.

When both soap and fiber are present the two processes of aggregation and crystal growth could occur simultaneously. There is also the possibility of interactions between the two effects: the fibers could alter the rate of crystallization, or the soap could change the rate of aggregation on the fibers.

From the data on the separate effects of added soaps and of fibers alone it is possible to calculate the behavior to be expected when both soaps and fibers are present together (7), a typical result being shown for SDS in Fig. 9. From these comparisons it is clear that the interaction effects are quite considerable for all three soaps, the order being CTAB > SDS > TX. The most likely explanation seems to be that the soaps adsorb onto the hair fibers making them more hydrophobic—a likely possibility in view of the protein nature of the fibers concerned. In the case of wool fibers cationic soaps are generally more adsorbed than anionic soaps, while nonionic are only slightly adsorbed (8, 9).

This explanation is strengthened by the results obtained using hair fibers which had been allowed to stand in solutions of different soaps for several days and the excess soap removed by thorough washing. The aggregation of D.D.T. on these treated fibers was measured (Fig. 2 of preceding paper) and, after correction for the aggregation on untreated hair fibers, compared with the calculated interaction effects (7).

With CTAB and TX all the interaction effect could be ascribed to adsorption of soaps onto the fibers. With SDS the agreement was not nearly as good, but this may have been due to some loss of this soap during the thorough rinsing process.

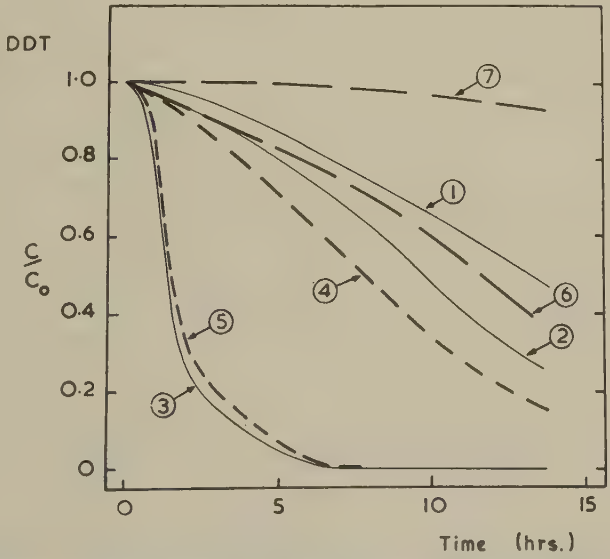

FIG. 9. Effect of SDS, 0.5 c.m.c. (*1*) SDS; (*2*) hair; (*3*) hair and SDS; (*4*) combined primary effects; (*5*) interaction; (*6*) hair, SDS satd.; (*7*) effect of SDS treatment in (*6*).

## ACKNOWLEDGMENT

Thanks are due to the C.S.I.R.O. for financial aid (G.T.B.).

## REFERENCES

1. BARNES, G. T., AND ALEXANDER, A. E., *Proc. 2nd Intern. Congr. Surface Activity* **IV,** 211 (1957).
2. ALEXANDER, A. E., AND JOHNSON, P., "Colloid Science." Oxford, 1949.
3. WHETSTONE, J., *Trans. Faraday Soc.* **51,** 973, 1142 (1955).
4. BUCKLEY, H. E., "Crystal Growth." Wiley, New York, 1952.
5. LAING-MCBAIN, M. E., AND HUTCHINSON, E., "Solubilization." Academic Press, New York, 1955. O'NEILL, D. K., AND ALEXANDER, A. E., *Proc. 2nd Intern. Congr. Surface Activity* **IV,** 218 (1957).
6. MCDOWELL, M. J., AND KRAUS, C. A., *J. Am. Chem. Soc.* **73,** 2173 (1951). MUKERJEE, P., DULIN, C. I., AND MYSELS, K. J., Abstr. of Papers, Am. Chem. Soc. Meeting, Miami, Florida, April. 1957, p. 14-I.
7. BARNES, G. T., Ph.D. dissertation, N.S.W. University of Technology, 1957.
8. LE COMPTE, G. C., AND CREELY, J. W., *Am. Dyestuff Reptr.* **31,** 121 (1942).
9. WEATHERBURN, A. S., AND BAYLEY, C. H., *Textile Research J.* **22,** 797 (1952).

JOURNAL OF COLLOID SCIENCE **14**, 111–112 (1959)

LETTERS TO THE EDITOR

# EQUATIONS OF STATE FOR IDEAL IONIZED MONOLAYERS

In a recent paper Haydon (1) has discussed the equations of state applicable to ionized monolayers at an oil-water interface. He has concluded that in the absence of added electrolyte the equation of Phillips and Rideal (2) holds, viz.,[1]

$$\pi = \frac{2kT}{A - A_0} + \Delta\pi, \qquad [1a]$$

where $\Delta\pi$ is the electrical term, whereas in the presence of excess electrolyte that of Davies (3) applies, viz.,

$$\pi = \frac{kT}{A - A_0} + \Delta\pi. \qquad [2a]$$

However, an examination of Haydon's paper reveals that this conclusion is unjustified, and that in fact, his arguments support the validity of equation [1*a*] irrespective of the presence or absence of added electrolyte.

The early part of the discussion in Haydon's paper is devoted to a derivation of the $2kT$ form of the equation of state corresponding to Eq. [1*a*] above. It is based on (*a*) the Gibbs adsorption isotherm; (*b*) the constancy of the chemical potential of an electrolyte in different phases at equilibrium; and (*c*) electroneutrality in the surface phase.

Since all these relationships are applicable in the presence or absence of added electrolyte, it would be inconsistent for any derived expression not to be similarly applicable. It would appear therefore that Eq. [1*a*] should apply irrespective of electrolyte concentration.

The derivation in Haydon's paper of the $2kT$ form is limited to the case of no added electrolyte, but it can be readily generalized by rewriting Eq. [8] of Haydon's paper, viz.,

$$\frac{C^s_{rx}}{C^b_{rx}} = K; \qquad [8]$$

in its more general form

$$\frac{C^s_{r^+} \cdot C^s_{x^-}}{C^b_{r^+} \cdot C^b_{x^-}} = K'. \qquad [3a]$$

---

[1] The symbols used throughout this letter will correspond to those in Haydon's paper.

Substituting for $C^b_{r^+}\cdot C^b_{x^-}$ from [3$a$] in the Gibbs equation [4$a$], i.e.,

$$d\pi = kT\tau'_{rx}\, d \ln C^b_{r^+}\cdot C^b_{x^-} \tag{4a}$$

leads to [5$a$]

$$d\pi = kT\tau'_{rx}\,\frac{d(C^s_{r^+}\, C^s_{x^-})}{C^s_{r^+}\, C^s_{x^-}}\,, \tag{5a}$$

which is identical with Eq. [10] of Haydon's paper, and from which the $2kT$ form of the equation of state follows. Such a derivation is independent of the presence or absence of added electrolyte.

No details are given in Haydon's paper as to the derivation of the $1kT$ form. The Gibbs approximation for excess electrolyte is given, and it is then stated that "following the reasoning outlined above [i.e., in the $2kT$ derivation] we find $\pi = \dfrac{kT}{A - A_0}$."

In the light of the above remarks it is difficult to see how the $1kT$ form could be obtained using the approximate form of the Gibbs equation when the complete Gibbs equation leads to the $2kT$ form. This suggests either that the Gibbs approximation is a poor one, which is not the case, or that the reasoning is unsound.

It would seem, therefore, that there is no justification for Haydon's conclusion that the form of the equation of state for ideal ionized monolayers is dependent on the presence or absence of added electrolyte. On the contrary, the paper supports the applicability of the $2kT$ form of the equation of state [1$a$] at all electrolyte concentrations.

## References

1. Haydon, D. A., *J. Colloid Sci.* **13**, 159 (1958).
2. Phillips, J. N., and Rideal, E. K., *Proc. Roy. Soc.* (*London*) **A232,** 159 (1955).
3. Davies, J. T., *Proc. Roy. Soc.* (*London*) **A208,** 227 (1951).

*Division of Plant Industry,*
*C.S.I.R.O.,*
*Canberra, Australia.*

J. N. Phillips

*Received October 23, 1958.*

JOURNAL OF COLLOID SCIENCE **14**, 113 (1959)

# BOOK REVIEW

**Progress in Stereochemistry,** Volume II. Edited by W. KLYNE and P. B. D. DE LA MARE. Academic Press Inc., New York, 1958. 323 pp. Price $8.80.

As does the volume to which this is a sequel, this book covers a rather broad range of topics. For example, there are chapters entitled Crystallography and Stereochemistry, Stereochemistry of the Group V Elements, Steric Factors in Immunochemistry, and Stereochemistry of Inorganic Molecules and Complex Ions as well as such organic chemical topics as The Stereochemistry of Homolytic Processes, The Stereochemistry of Displacements at Unsaturated Centres, Steric Effects on Mesomerism, and The Study of Optically Labile Compounds.

There is surprisingly little duplication of material in Volume I of the series or of that in the recently published volume, "Steric Effects in Organic Chemistry," edited by M. S. Newman, John Wiley and Sons, publishers. Where there is similarity in subject matter, the point of view in the two works is generally sufficiently different so that they complement each other.

DAVID Y. CURTIN, Urbana, Illinois

JOURNAL OF COLLOID SCIENCE 14, 115–122 (1959)

# ON THE MICELLAR MOLECULAR WEIGHTS OF NORMAL PARAFFIN CHAIN SALTS IN DILUTE AQUEOUS SOLUTIONS[1]

**H. V. Tartar**

*Department of Chemistry, University of Washington, Seattle, Washington*

*Received November 17, 1958*

## Abstract

The micellar molecular weights of four normal paraffin chain salts in dilute aqueous solution have been revised to give the values: dodecyltrimethylammonium bromide, 12200; sodium decyl sulfate, 9300; sodium dodecanesulfonate, 12300; sodium dodecyl sulfate, 11500.

A reference model of a spherical micelle has been proposed. The MMW's estimated with its use show substantial agreement with the experimental values, except for $C_{12}$ salts. The MMW's of spherical micelles of $C_{16}$ salts have been predicted and verified experimentally. The data on alkyl pyridinium bromides indicate that the radius of the sperical micelle is equal to the alkyl chain length.

## Introduction

In 1955 (1) we reported from this Laboratory on the micellar molecular weights of several normal paraffin chain salts (straight chain with polar group in 1-position) in dilute aqueous solutions. A theory (2) was proposed to account in part for the structure of these micelles. The present paper presents a continuation of this work and its purpose is chiefly threefold: (*a*) to report revisions of some of the micellar molecular weights; (*b*) to use the theory to predict the micellar molecular weights of spherical micelles of these salts; and (*c*) to revise the theory to cover solutions of salts with 12 carbon atoms in the chain.

Since our previous report was presented for publication, other papers (3–10) have appeared dealing with closely related material. These results will be referred to at appropriate points in the discussion.

## Revision of Micellar Molecular Weights

The micellar molecular weight (hereinafter designated, MMW) determinations were made with the same apparatus and by the same general procedure as in the previous work (1). Only some minor modifications were made in the calibration and handling of the apparatus. The salts were prepared with greater care to avoid contamination from extraneous sources and subjected to a larger number of recrystallizations. The chief difficulty was in obtaining sufficiently pure two-component systems, salt-water. The solutions should show inappreciable dissymmetric scattering. As is well known, salts with anionic chains are good detergents and have a greater tendency to hold small foreign particles in suspension than have the cationics. In the preparation of the anionics there is seemingly more opportunity for side reactions to contribute impurities. Efforts must be diligently directed toward obtaining the *minimum* turbidity for each solution.

---

[1] This paper was presented in large part at the "Symposium on the Structure of Micellar Solutions" sponsored by the Division of Colloid Chemistry, 131st National Meeting of the American Chemical Society, Miami, Florida, April, 1957.

Phillips and Mysels (4) have taken into account the various sources of error in the different steps of the measurements and estimate that the absolute accuracy of the MMW determination is ±10%. The author's experience tends to confirm this estimate. Closer agreement by workers in different laboratories may not be expected. Besides, there is the error due to the presence of extraneous turbidities in the solutions.

Four MMW's were determined, those most needed for the work in hand. The solvent was water alone and the runs were made at room temperature.

*a*). *Dodecyltrimethylammonium Bromide.* The revised value is 12200. This is 21% lower than that previously reported, 15400. Debye (11) first reported 15500; this was later lowered (12) to 13400.

*b*). *Sodium Dodecanesulfonate.* The revised value is 12300; that reported earlier 14700. In the preparation of the alkane sulfonates by the Strecker reaction (13) there appears to be a minor side reaction which yields small amounts of a substance which is difficult to remove satisfactorily in the recrystallizations. It tends to interfere with the turbidity determination at concentrations just above the CMC. The author has not had the opportunity to make a check MMW determination using a salt prepared by a different procedure (14, 15).

*c*). *Sodium Dodecyl Sulfate.* The turbidity determinations on solutions of this salt gave some widely fluctuating results. It was difficult to make sure that the selected turbidities were minimum values. When the solutions were refiltered the turbidities would occasionally increase instead of showing an expected decrease. Under the experimental conditions here employed some change may occur in these solutions which produces an increase in turbidity and hence an increase in MMW.

Consistent values for the turbidities were obtained in the concentration range $(1.20 \text{ to } 0.46)10^{-2}$ g./c.c. which gave a MMW of 11500. This happens to check very closely the value obtained by Kushner and Hubbard (5), 11400, closer than the experimental error involved.

The MMW previously reported (1) was very much greater, 20500. Phillips and Mysels (4) first obtained 23000. Very recently Princen and Mysels have reported a revised value, 18000 (10). They (16) have found that the ultrafine fritted-glass filter catalyzes the normally negligible hydrolysis of the ester linkage. The lauryl alcohol thus produced is solubilized in the micelles of the solution. This apparently accounts, at least in part, for the discrepancy in the reported values.

*d*). *Sodium Decyl Sulfate.* The same experimental difficulties obtained with these solutions as with those of the dodecyl compound. Our earlier report gave the MMW 13000. Later work has lowered this value to 10000. This appears to be still somewhat high. Prins and Hermans (9) found 9300; this is accepted as the better value.

## A Reference Model of a Spherical Micelle and its Use

The author wishes to propose a procedure, albeit a comparatively simple one, for estimating the approximate MMW's of uniunivalent normal paraffin chain salts in aqueous solution where the concentration of the ions (of the monomer) are essentially those required for the formation of a spherical micelle of the Hartley type (17). In most cases this is at or immediately above the CMC with no added electrolyte. For the estimations use will be made of a hypothetical reference model.

As previously (2), we will assume that the interior of the micelle consists of hydrocarbon chains and that the polar head groups with counter ions are spaced at the surface; also that the chains are in unordered ("liquid") arrangement except for any influence which might come from the spacing of the polar heads. This hydrocarbon interior is comparable in density and arrangement to that of the corresponding liquid hydrocarbon of like chain length. The radius of the spherical hydrocarbon interior is equal to the maximum length[2] of the hydrocarbon chain. Using this radius the volume, $V$, of this interior is obtained. From previous data (2) the volume, $v$, of a single chain is calculated; and $V/v$ is the number of chains, $n$, in the micelle. Then $n$ times the formula weight of the monomer salt, $M$, gives the MMW of the micelle (including the counter ions). The number of chains in the micelle has small variations and is here treated as being monodisperse.

The counter ions are in a "double layer" at the hydrocarbon-solution interface and are considered as being "bound" to the micelle. The fluctuating species for light scattering is deemed to be the micelle with its surrounding counter ions. The effect of electric charge on this type of micelle has been quite fully and extensively discussed (6–9, 11, 18–24) on theoretical grounds. Notwithstanding the able treatment which has been given, the findings are not sufficient to go beyond qualitative considerations. Estimates from light scattering (7) of the "degree of ionization" of micelles yield

---

[2] $CH_2$, 1.27 A.; $CH_3$, 2.00 A. Previously, an arbitrary allowance was made for the fraction of the bond distance connecting the $\alpha$ carbon atom to the polar group. Subsequent work indicates that more applicable data are obtained by omitting this allowance.

TABLE I

*Data on the Micellar Molecular Weights of Normal Paraffin Chain Salts*

| Solute | CMC (*moles/liter*) | Chain number | Micellar molec. weight | Deviation from mode micellar molec. wt. | Authors |
|---|---|---|---|---|---|
| *$C_8$ solutes; hydrocarbon chain length, 10.9 A.* | | | | | |
| Sodium octanesulfonate | — | 22.3* | 4800* | — | — |
| | 0.155 | 24 | 5500 | +14.1 | TandL[1] |
| Octyltrimethylammonium bromide | — | 22.3* | 5600* | — | — |
| | 0.224 | 23 | 5800 | +3.8 | TandH[6] |
| Octylpyridinium bromide | — | 22.3* | 6070* | — | — |
| | 0.193 | 24 | 6400 | +5.4 | TandH[6] |
| *$C_9$ solutes; hydrocarbon chain length, 12.2 A.* | | | | | |
| Sodium nonyl sulfate | — | 28* | 6900* | — | — |
| | 0.145 | 31 | 7730 | +12.0 | PandH[9] |
| Nonyltrimethylammonium bromide | — | 28* | 7500* | — | — |
| | 0.143 | 30 | 8000 | +6.7 | TandH[6] |
| *$C_{10}$ solutes; hydrocarbon chain length, 13.4 A.* | | | | | |
| Sodium decanesulfonate | — | 34.3* | 8880* | — | — |
| | 0.038 | 40.5 | 9900 | +11.5 | TandL[1] |
| Sodium decyl sulfate | — | 34.3* | 8900* | — | — |
| | 0.031 | 36 | 9370 | +5.3 | PandH[9] |
| | 0.031 | 42 | 11000 | | T |
| | 0.031 | 50 | 13000 | | TandL[1] |
| Decyltrimethylammonium bromide | — | 34.3* | 9600* | — | — |
| | 0.070 | 36 | 10200 | +6.2 | D[11] |
| | 0.063 | 44 | 12400 | | TandH[6] |
| *$C_{11}$ solute; hydrocarbon chain length, 14.7 A.* | | | | | |
| Undecylpyridinium bromide | — | 41* | 12900 | — | — |
| | 0.04 | 42 | 13200 | +2.3 | TandH[6] |
| *$C_{12}$ solutes; hydrocarbon chain length, 16.0 A.* | | | | | |
| Sodium dodecanesulfonate | — | 48.7* | 13270* | — | — |
| | 0.010 | 45 | 12300 | −7.3 | T |
| | 0.010 | 54 | 14700 | | TandL[1] |
| Sodium dodecyl sulfate | — | 48.7* | 14040* | — | — |
| | 0.008 | 40 | 11400 | −18.8 | KandH[5] |
| | 0.008 | 41 | 11800 | | T |
| | 0.008 | 62 | 18000 | | PandM[10] |
| | 0.008 | 70 | 20500 | | TandL[1] |
| Dodecyltrimethylammonium bromide | — | 49* | 15100* | — | — |
| | 0.0144 | 40 | 12200 | −19.2 | T |
| | 0.0144 | 43.5 | 13400 | | DandS[12] |
| | 0.0144 | 50 | 15500 | | D[11] |
| | 0.0144 | 50 | 15500 | | TandL[1] |
| | 0.0144 | 62 | 19200 | | TandH[6] |
| Dodecylamine hydrochloride | — | 49* | 10800* | — | — |
| | 0.0131 | 55.5 | 12300 | +13.9 | D[11] |
| *$C_{14}$ solutes; hydrocarbon chain length, 18.5 A.* | | | | | |
| Tetradecyltrimethylammonium bromide | — | 66* | 22100* | — | — |
| | 0.0034 | 75 | 25300 | +14.5 | D[11] |
| | 0.0036 | 92 | 30800 | | TandH[6] |
| Sodium tetradecanesulfonate | — | 66* | 19800* | — | — |
| | 0.0033 | 70 | 21400 | +7.47 | T |

| Solute | CMC (*moles/liter*) | Chain number | Micellar molec. weight | Deviation from mode micellar molec. wt. | Authors |
|---|---|---|---|---|---|
| Tetradecylpyridinium bromide | — | 66* | 23400* | — | — |
| | 0.002 | 79 | 28100 | +20.0 | TandH[6] |
| | $C_{16}$ *solutes; hydrocarbon chain length, 21 A.* | | | | |
| Hexadecyltrimethylammonium bromide | — | 84.7* | 31000* | — | — |
| | 0.00082 | 79.6 | 29000 | −6.45 | T |
| | [temp. 30°; $\Delta n/\Delta c$, 0.1560; $H$, $(6.577)10^{-6}$; $2B$, $(0.894)10^{-2}$] | | | | |
| Hexadecylpyridinium bromide | — | 84.7* | 32600* | | — |
| | 0.00034 | 87 | 33500 | +2.85 | T |
| | [temp. 40°; $\Delta n/\Delta c$, 0.1676; $H$, $(7.569)10^{-6}$; $2B$, $(1.029)10^{-2}$] | | | | |

comparatively small, widely varying, and uncertain values. The results hardly justify quantitative representation.

The area per polar head at the surface of the hydrocarbon interior is approximately 66 A. Hence there is considerable hydrocarbon-solution interface other than that with the ionic heads. The micelle is, of course, in dynamic equilibrium with the solution with chains, mostly curled up, entering and leaving with corresponding movements of counter ions. Consequently, the interface can hardly be regarded as being uniformly smooth.

At the CMC, we have the concentration of smaller ions at which an equilibrium is established between the short-range (van der Waals) forces and the long-range electrical forces of repulsion. It is assumed that the micelles formed under this condition are spherical, thus providing the minimum interfacial surface for the volume. The extrapolation from the plot of Debye (10) equation (hereafter designated Debye plot)

$$H\frac{C - C_0}{\tau} = \frac{1}{M} + 2BC$$

gives the MMW at zero concentration of micelles.

Using this proposed reference model micelle, computations have been made for the number of chains, $n$, and the MMW's of the micelles for a number of salts with chains ranging from 8 to 16 carbon atoms. The data are summarized in Table I and are marked with asterisks. For comparison the corresponding experimental results obtained in this Laboratory and elsewhere (from both older and more recent work) are given including the CMC values. In those instances where more than one MMW is available for a particular salt, the data are presented in the order of increasing MMW. The minimum value is judged to be the most trustworthy one. The percentage deviations of the minimum experimental value from the model values are also given. For convenient use the authors are designated by the initial letters of their names (column 6); the superscript numbers are the corresponding literature references.

During the progress of this work it was noted that a correlation appears to exist between the results with alkylpyridinium salts and normal paraffin chain salts of like alkyl chain length. Consequently data on alkylpyridinium salts are included in Table I and will be discussed in a later part of this paper.

## Discussion

*a. General Statement.* The agreement between the model and the experimental values (minima) is very striking considering the possible magnitude of the errors in the determinations. Phillips and Mysels (4) have estimated that the error in the MMW determination is ±10%. This does not include errors due to the turbidity of impurities in the systems. The variations in the MMW values obtained by different workers for the same salt indicate that these extraneous impurities may have large influence on the findings. Each determination truly presents a struggle to obtain a minimum value.

*b. Salts $C_8$–$C_{11}$.* The deviations from the model MMW's are all positive; the average is +7.4%. That these deviations are positive may be due (*1*) to the fact that the model is too great an oversimplification of the structure of the micelle and/or (*2*) to the effect of impurities which make the turbidities greater than they should be. The author believes that the latter has much the greater influence.

*c. $C_{12}$ Salts.* Except in the case of dodecylamine hydrochloride the MMW deviations from the model values are strongly negative. It appears that with these salts a relationship may obtain between the CMC and the length of the chain which permits the formation of a stable micelle (evidenced by a linear Debye plot) having radius less than the chain length and area per polar head greater than 66 A.$^2$ Here the nature of the polar head has a greater influence comparatively on micellar size than with other chain lengths. The addition of a small amount of electrolyte with common counter ion will reduce the thickness of the ionic atmosphere sufficiently to allow an increase in micellar size until the radius of the hydrocarbon interior is that of spherical micelle. The data by Kushner and Hubbard (5) indicate that sodium dodecyl sulfate in 0.01 *M* NaCl as the solvent would have a MMW equal to that of the model.

The experimental MMW reported for dodecylamine hydrochloride is quite out of line with those for the other $C_{12}$ salts. It should be redetermined. There is the possibility, too, that hydrolysis of sufficient magnitude may occur to vitiate the determination and give a higher value, quite analogous to the results obtained with sodium dodecyl sulfate solutions (10).

The data on the other $C_{12}$ salts appear to require a modification of our theory to allow for this characteristic behavior. Here the MMW's are lower than the model values. How much lower they should be we are unable to predict. Assuming spherical micelles, the radii are less than the hydrocarbon chain length.

*d. $C_{14}$ Salts.* Data are available for only three salts in water alone as the solvent. The CMC's are small and the MMW's were determined using very dilute solutions with the likelihood of large errors; note for example the great variation in the values found in two laboratories for tetradecyltrimethylammonium bromide. The MMW for sodium tetradecanesulfonate has been revised downward from that previously given (1); the data are as yet not sufficiently complete for thorough revision. Even with these limitations, the deviations (minima) from the model values are not unduly large considering the conditions under which they were obtained.

*e. $C_{16}$ Salts.* The solubility of these salts in water is too small at ordinary temperature to permit the formation of micelles. All available data on MMW's have been obtained with added electrolyte in sufficient concentration to give values too large for spherical micelles ($C_{16}$ radius).

Consequently MMW's were determined in this Laboratory for two salts under satisfactory conditions, hexadecyltrimethylammonium bromide and hexadecylpyridinium bromide; the values are presented in Table I. These salts were prepared by conventional methods (25, 26) and carefully purified by repeated recrystallizations. It was found by trial and error that 0.003 $M$ KBr is the lowest concentration (approximately) which is a satisfactory solvent for stable micelle formation at 30°C. Since these MMW determinations have not been reported previouly, the data on temperature, refractive index increment, $\Delta n/\Delta c$, optical constant $H$, and slope, $2B$, have also been included in Table I.

The agreement between the experimental and the predicted (model) MMW's is very satisfactory, even better than could be expected considering the errors involved.

*f. Alkyl Pyridinium Salts.* It was noted that the number of chains found by Trap and Hermans (6, 7) for the micelle of octylpyridinium bromide corresponds very closely to that found for *n*-octyl paraffin chain salts. This may be taken to indicate that here also the radius of the paraffin interior of the micelle is that of the alkyl chain length. Accordingly, calculations have been made on this basis for some alkyl pyridinium salts; the data are included in Table I.

The findings afford good support to the idea that the radii of the micelles are the respective chain lengths with the pyridinium group lying at the paraffin-solution interface. With an area of 66 A.$^2$ per polar head there is ample space for this to occur.

*g. Criterion for Validity of MMW.* No procedure is available for checking the validity of the MMW for a spherical micelle of a normal paraffin chain salt obtained by light scattering, such as the use of some colligative property. The data presented above indicate that the model values, except for $C_{12}$, afford minima to strive for in obtaining a valid experimental value. With $C_{12}$ the MMW should apparently be less than the value calculated for the model.

## ACKNOWLEDGMENT

The author is grateful to Professor E. C. Lingafelter, who has read the manuscript in preparation and has given helpful suggestions.

## REFERENCES

1. Tartar, H. V., and LeLong, A. L. M., *J. Phys. Chem.* **59,** 1185 (1955).
2. Tartar, H. V., *J. Phys. Chem.* **59,** 1195 (1955). [There is a misstatement in the illustrative calculation, p. 1196. The major semiaxis,

$$a = \sqrt{\frac{(5.588)\ 10^{-20}}{(4.189)(19.22)\ 10^{-8}}} = 26.34 \text{ A.}]$$

3. Stigter, D., and Mysels, K. J., *J. Phys. Chem.* **59,** 45 (1955).
4. Phillips, J. M., and Mysels, K. J., *J. Phys. Chem.* **59,** 325 (1955).
5. Kushner, L. M., and Hubbard, W. D., *J. Colloid Sci.* **10,** 429 (1955).
6. Trap, H. J. L., and Hermans, J. J., *Koninkl. Ned. Akad. Wetenschap., Ser. B*, **58,** 97 (1955).
7. Prins, W., Thesis, The University, Leiden, 1955.
8. Prins, W., and Hermans, J. J., *Koninkl. Ned. Akad. Wetenschap., Ser. B*, **59,** 162 (1956).
9. Prins, W., and Hermans, J. J., *Koninkl. Ned. Akad. Weterschap., Ser. B*, **59,** 298 (1956).
10. Princen, L. H., and Mysels, J., Eleventh Technical Report Project NR 356-254, Office of Naval Research, 1958.
11. Debye, P., *J. Phys. & Colloid Chem.* **53,** 1 (1947).
12. Debye, P., and Smudski, P. A., Tehcnical Report, Office of Rubber Reserve, 1951.
13. Reed, R. M., and Tartar, H. V., *J. Am. Chem. Soc.* **57,** 570 (1935).
14. Noller, C. R., and Gordon, J. J., *J. Am. Chem. Soc.* **55,** 1090 (1933).
15. Murray, R. C., *J. Chem. Soc.* **1933,** 739.
16. Princen, L. H., and Mysels, K. J., Division of Colloid Chemistry, 133rd Meeting of the American Chemical Society, San Francisco, April 13–18, 1958.
17. Hartley, G. S., "Paraffin Chain Salts." Hermann et Cie, Paris, 1936.
18. Edsall, J. T., Edelhoch, H., Lontie, R., and Morrison, P. R., *J. Am. Chem. Soc.* **72,** 4641 (1950).
19. Doscher, T. M., and Mysels, K. J., *J. Chem. Phys.* **19,** 254 (1951).
20. Mysels, K. J., *J. Phys. Chem.* **58,** 303 (1954).
21. Doty, P., and Steiner, R. F., *J. Chem. Phys.* **20,** 85 (1952).
22. Hutchinson, E. J., *J. Colloid Sci.* **9,** 191 (1954).
23. Hutchinson, E., and Melrose, J. C., *Z. physik. Chem.* [NF] **2,** 363 (1954).
24. Prins, W., and Hermans, J. J. *J. Phys. Chem.* **59,** 576 (1955).
25. Scott A. B., and Tartar H. V., *J. Am. Chem. Soc.* **65,** 693 (1943).
26. Adam, N. K., and Pankhurst, K. G. A., *Trans. Faraday Soc.* **42,** 523 (1946).

JOURNAL OF COLLOID SCIENCE **14**, 123–130 (1959)

# THE CAPILLARY RISE OF A LIQUID IN A VERTICAL STRIP OF FILTER PAPER

**Thomas Gillespie**

*Physical Research Laboratory, 2–280 Building, The Dow Chemical Company, Midland, Michigan*

*Received August 18, 1958*

## Abstract

A theory previously developed by the author to describe the horizontal spreading of liquids in paper has been applied to the case of a liquid rising by capillary action in a vertical strip of filter paper. The phenomenon is complicated by a surface roughness effect which had to be taken into account. The theory leads to simple expressions for the rate of rise and the distribution of liquid which are in agreement with experiment. When gravity can be neglected, the height of rise is proportional to the square root of the time. When gravity is important, the height of rise is a more complex function of time than the simple square root dependence. In addition, the liquid approaches a limiting height.

## I. Introduction

A satisfactory theoretical treatment of the rise of a liquid in a vertical piece of filter paper would be useful in current attempts to understand the process of paper chromatography and other phenomena associated with the entrance of liquids into porous materials.

The theories which have been developed (1–3) are all inadequate in one or more respects. In an oversimplified analysis, Peek and McLean (1) deduced an expression for the rate of rise in a filter paper, but did not consider the distribution of the liquid. As Wood and Strain (4) have pointed out, the equation of Müller and Clegg (2) for the height of rise as a function of time is obtained simply by integrating the differential equation of Peek and McLean. Müller and Clegg did not consider liquid distribution either. Fujita's (3) analysis seems to lead to an excellent description of the distribution of the liquid. The novel mechanism and assumptions that formed the basis of his analysis have, however, led him to the conclusion that the rate of rise is directly proportional to the atmospheric pressure and is independent of surface tension effects (see Equation 9, reference 3). This is very unlikely.

During a recent study of the stains produced by nonvolatile liquid drops on a horizontal sheet of filter paper (5), it was found that Fujita's analysis could not be modified to describe the experimental data. An alternative semiempirical analysis based on the concept that liquid tends to be concentrated in the smaller "pores" of the paper in regions where liquid concentration is below saturation level was found to lead to simple and satisfactory expressions for both the rate of spreading and the distribution of the liquid. This preference of the liquid for smaller pores is theoretically sound (6) and may, in fact, be observed when unsaturated paper is viewed under a low-power microscope.

It is the purpose of this article to outline an extension of this new analysis to include the case of a liquid ascending in a filter paper.

## II. THEORETICAL

When a strip of filter paper of uniform width is hung so that its bottom dips into a liquid, as indicated in Fig. 1, the liquid distributes itself in a characteristic fashion. At the base, there is an obvious meniscus which is usually of the order of 1 to 2 mm. high. Above this meniscus, there is a region where the paper holds an irregular film of liquid giving it a flooded appearance in some places. In other places, the fibers are visible. Above the somewhat indefinite boundary of this "oversaturated" region, the paper is definitely unsaturated and there is a concentration gradient.

In Fig. 1, $L$ denotes the length of the unsaturated region and $\lambda$ is the height at which the paper is just saturated. Owing to the rough nature of the paper surface, this saturation concentration is indefinite. Whatever value is taken, however, there will be a corresponding suction at that point in the paper. If $C_s$ is taken as the saturation concentration at $y = \lambda$, the capillary suction will be a constant at that point and may be denoted by $p_0$. Using this definition of $p_0$ and $C_s$, it is possible to calculate the change of the total height of the liquid, $h$, with time, $t$, and to obtain an expression for the distribution of the liquid.

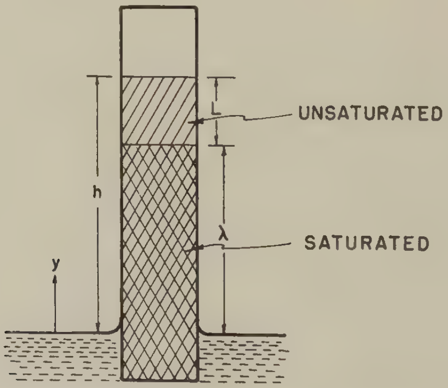

FIG. 1. Schematic diagram of liquid rising in a strip of filter paper.

### *Distribution of Liquid in the Unsaturated Region*

By combining d'Arcy's law with the equation of continuity, it has been shown (7) that, when a gas-liquid mixture flows through a porous medium, the liquid flow should satisfy the following equation:

$$\nabla \cdot (k_1 \cdot \nabla p) = \mu \frac{\partial C}{\partial t} \qquad [1]$$

Here $\nabla_p$ is the gradient of the pressure. The viscosity of the liquid is $\mu$ and $C$ is the liquid concentration measured in cubic centimeters of liquid per cubic centimeter of the porous medium. The permeability is called $k_1$ and is defined as the volume of liquid of unit viscosity passing through unit cross section of the medium under the action of a unit pressure gradient.

To solve Eq. [1], it is necessary to know both $k_1$ and grad $p$. In the horizontal spreading studies (5), it was assumed that

$$k_1 = k_0(C/C_s)^3, \qquad [2]$$

where $k_0$ is the permeability of saturated paper. Equation [2] was suggested by the permeability experiments of Wyckoff and Botset (5, 8). It was also assumed that $\nabla^2 p = 0$. This assumption combined with Eqs. [1] and [2] led to equations which describe the behavior of liquids spreading in paper both in one and two dimensions (5). The assumption that $\nabla^2 p = 0$ was suggested by measurements of the suction due to unsaturated paper using Haines' technique (5, 9).

Substituting $\nabla^2 p = 0$ and Eq. [2] in Eq. [1]

$$\frac{\partial C}{\partial t} = \frac{(\text{grad } p)}{\mu} \frac{k_0}{C_s^3} \frac{\partial C^3}{\partial y}. \qquad [3]$$

The distribution of the liquid in the unsaturated portion of the paper should be given by the solution of Eq. [3], with the following boundary conditions:

$$C = C_s \quad \text{at} \quad y = \lambda; \qquad [4]$$

$$C = 0 \quad \text{at} \quad y = h. \qquad [5]$$

The solution is

$$C = C_s \left\{ 1 - \frac{y - \lambda}{L} \right\}^{1/2}. \qquad [6]$$

### *Calculation of the Rate of Ascent*

The pressure gradient in the saturated region ($y \leq \lambda$) is given by

$$\text{grad } p = \frac{p_0}{\lambda} - \rho g. \qquad [7]$$

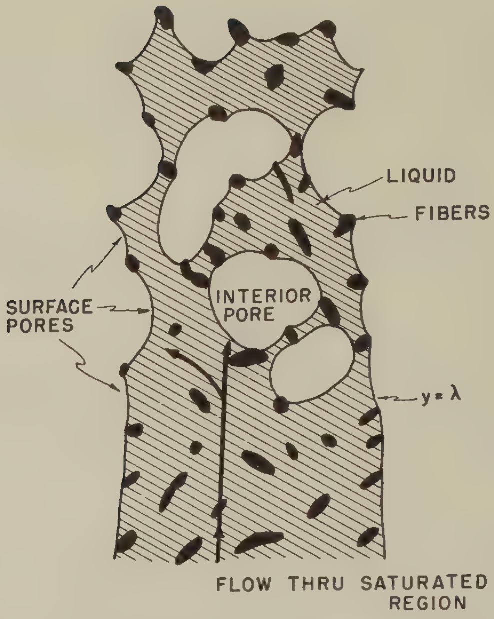

Fig. 2. Magnified cross-sectional diagram of paper showing liquid distribution in the vicinity of the saturated-unsaturated boundary.

Liquid being pulled up through the paper below $y = \lambda$ does two things eventually. It increases the height of the saturation level and it increases the total amount of liquid in the unsaturated region. Equating the flow to the increase in these

$$\left(\frac{p_0}{\lambda} - \rho g\right)\frac{k_0}{\mu} A = AC_s \frac{d\lambda}{dt} + \frac{dV}{dt}, \qquad [8]$$

where $V$ is the volume of liquid in the unsaturated region and $A$ is the cross-sectional area of the paper.

$$V = A \int_\lambda^h C\, dy = \frac{2}{3} AC_s L. \qquad [9]$$

Hence,

$$\frac{d\lambda}{dt} + \frac{2}{3}\frac{dL}{dt} = \left(\frac{p_0}{\lambda} - \rho g\right)\frac{k_0}{C_s \mu}. \qquad [10]$$

Knowing the relation between $\lambda$ and $L$, the total rate of ascent can be calculated. Experimentally, the present and previous work (3, 10) suggest that $\lambda$ is proportional to $L$. The reason for this can be seen by considering Fig. 2.

Figure 2 is an idealized side view of the paper strip showing the surface irregularities and the film clinging to the paper. As surface pores are filled up, $\lambda$ increases. As the liquid is pulled into interior pores (see Eq. [9]), $L$ increases. The number of surface pores and interior pores at the unsaturated-saturated boundary should be constant; hence

$$\frac{dL}{dt} = f\frac{d\lambda}{dt}, \qquad [11]$$

where $f$ is a constant.

Combining Eqs. [10] and [11]

$$p_0 \log\left(1 - \frac{\rho g\lambda}{p_0}\right) + \rho g\lambda = \frac{-3(\rho g)^2 k_0}{(3 + 2f)C_s\mu}\, t. \qquad [12]$$

Expanding the log term

$$\lambda^2 + \frac{2}{3}\frac{\rho g}{p_0}\lambda^3 + \frac{1}{2}\left(\frac{\rho g}{p_0}\right)^2 \lambda^4 + \cdots = \frac{6p_0 k_0}{(3 + 2f)C_s\mu}\, t. \qquad [13]$$

When gravity can be neglected

$$\lambda^2 = \frac{6p_0 k_0}{(3 + 2f)C_s\mu}\, t. \qquad [14]$$

As $h = (1 + f)\lambda$

$$h^2 = bt, \qquad [15]$$

where

$$b = \frac{6p_0 k_0(1 + f)^2}{C_s\mu(3 + 2f)}. \qquad [16]$$

Considering the surface pores to be cylindrical, an elementary calculation indicates that

$$p_0 = \frac{2\gamma}{r_{\text{max.}}} \cos\theta, \qquad [17]$$

where $\gamma$ is the surface tension of the liquid. The contact angle between the liquid and the fibers is $\theta$. The radius of the largest pores which must be filled for the paper to be considered saturated is $r_{\text{max}}$. Therefore,

$$b = \frac{12k_0(1 + f)^2\gamma\cos\theta}{C_s r_{\text{max.}}(3 + 2f)\mu}. \qquad [18]$$

Where gravity can be neglected, $b$ should be proportional to

$$\frac{\gamma\cos\theta}{\mu}.$$

## III. EXPERIMENTAL

The rate of rise of several liquids in vertical strips of Whatman No. 1 filter paper of uniform width was measured using a cathetometer. Only liquids of very low vapor pressure were examined. There was no radical departure from the procedure used by previous workers (4, 10).

In measuring the liquid distribution in the paper, the following procedure was adopted. The paper was first cut off at a point just above the obvious meniscus. Equal segments were then quickly cut off holding the paper vertically to prevent any drastic change in the distribution. The individual segments were then weighed to estimate the volume of liquid in them.

In a subsidiary set of experiments the effect of changing the amount of paper initially inserted into the liquid reservoir was assessed. There was no apparent effect when the length dipped into the reservoir varied from 3 mm. to 6 mm.

## IV. COMPARISON OF THEORY WITH EXPERIMENT

As $f = L/\lambda$ Eq. [6] can be put in the form

$$C = C_s\left(\frac{f+1}{f}\right)^{1/2}\left\{1 - \frac{y}{h}\right\}^{1/2} \qquad [19]$$

The liquid distribution in the unsaturated region should, therefore, be a function of the reduced variable $y/h$. Figure 3 illustrates experimental data for dibutyl phthalate rising in Whatman No. 1 filter paper. The full line was drawn from the help of Eq. [19] with $f = 0.38$. Apart from the obvious

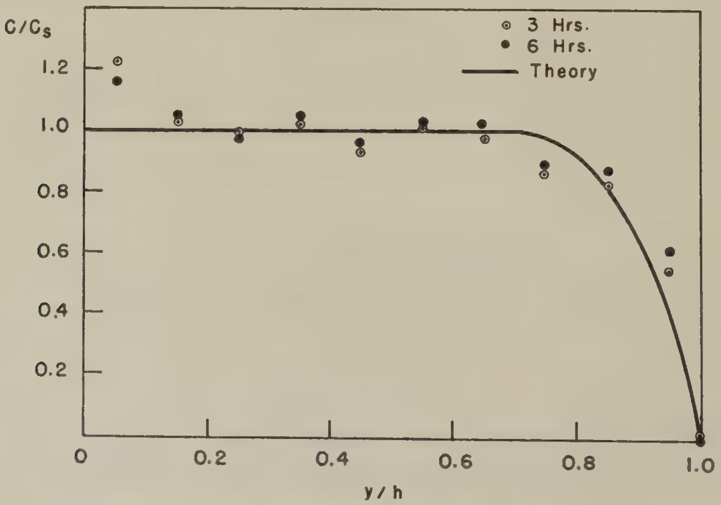

FIG. 3. Comparison of liquid distribution data with theory for dibutyl phthalate in Whatman No. 1 filter paper.

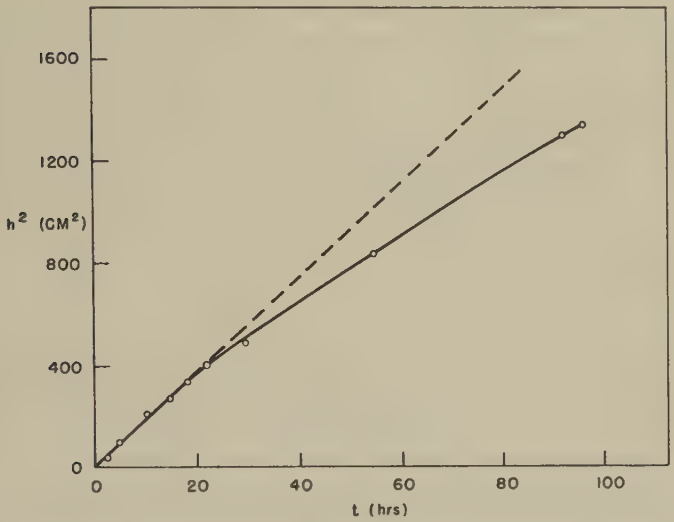

FIG. 4. Variation of $h^2$ with rise time in a long-term experiment (dibutyl phthalate in Whatman No. 1 filter paper).

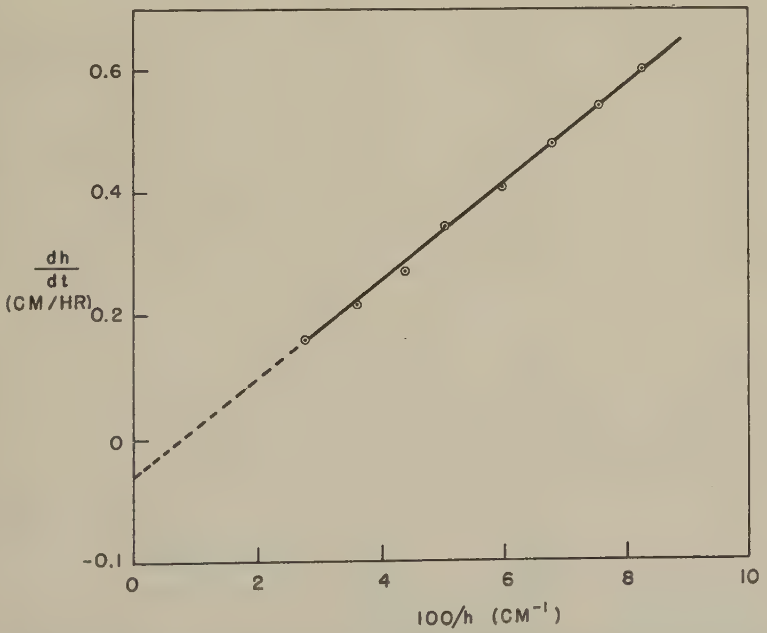

FIG. 5. Illustration of the linear relation between the rate of rise and the reciprocal of the height of rise (long-term experiment with dibutyl phthalate in Whatman No. 1 filter paper).

meniscus liquid which was not measured accurately and was not taken into account in the theory, there is agreement between experiment and theory.

For rise times up to 6 hours, $h^2$ was directly proportional to $t$ for several organic liquids, as suggested by Eq. [15]. Furthermore, $b$ was proportional to $\gamma/\mu$. These results are in agreement with data reported previously (1, 3, 10). They indicate that for the organic liquids tested (dibutyl phthalate, oleic acid, mineral oil), the contact angle with paper fibers is the same. In addition, the proportionality between $h^2$ and $t$ indicates that gravity effects were negligible.

## V. LONG-TERM CAPILLARY RISE

In a special experiment, the height of rise of a liquid was followed for a much longer period than usual. The data are plotted in Fig. 4. This figure indicates that $h^2$ is not proportional to $t$ after the liquid has risen sufficiently for gravity to become important. Using Eq. [10], it may be shown that

$$\frac{dh}{dt} = \frac{3k_0}{C_s\mu}\left(\frac{1+f}{3+2f}\right)\left[\frac{p_0(1+f)}{h} - \rho g\right]. \qquad [20]$$

A plot of $dh/dt$ against $1/h$ was linear (see Fig. 5).

The ratio of the slope to intercept should be $p_0(1+f)/\rho g$. For dibutyl phthalate rising in Whatman No. 1 filter paper, therefore, $p_0 = 83\rho g$. This large value of $p_0$ means that Eq. [15] would be a very good approximation for the heights of rise encountered in the main experiments. It also means that the radius of the largest pores which must be filled for saturation ($r_m$ in Eq. [17]) is of the order of $8\mu$. Finally, the dibutyl phthalate should approach a height at which $p_0(1+f) = \rho gh$. This condition corresponds to a height of rise of 114.5 cm. Calculations using Eq. [12] indicate that it would take a rise time of one year and 62 days for the liquid to reach a height within 0.5 cm. of the limiting height.

## REFERENCES

1. PEEK, R. L., JR., AND MCLEAN, D. A., *Ind. Eng. Chem., Anal. Ed.* **6,** 85 (1934).
2. MÜLLER, R. H., AND CLEGG, D. L., *Anal. Chem.* **23,** 403, 408 (1951).
3. FUJITA, H. J., *J. Phys. Chem.* **56,** 625 (1952).
4. WOOD, S. E., AND STRAIN, H. H., *Anal. Chem.* **26,** 260 (1954).
5. GILLESPIE, T., *J. Colloid Sci.* **13,** 32 (1958).
6. CHILDS, E. C., AND COLLIS-GEORGE, N., *Proc. Roy. Soc. (London)* **A201,** 392 (1950).
7. MUSKAT, M., AND MERES, M. W., *J. Appl. Phys.* **7,** 346 (1936).
8. WYCKOFF, R. D., AND BOTSET, H. G., *J. Appl. Phys.* **7,** 325 (1936).
9. HAINES, W. B., *J. Agr. Sci.* **20,** 97 (1930).
10. TAKAHASHI, A., *Kagaku* **20,** 41 (1950).

JOURNAL OF COLLOID SCIENCE **14**, 131–134 (1959)

# THE LINEARITY OF THE LOG SOLUBILIZATION-LOG CONCENTRATION FUNCTION IN MICELLAR SOLUBILIZATION

**A. M. Mankowich**

*Coating and Chemical Laboratory, Aberdeen Proving Ground, Maryland*

*Received August 25, 1958; revised October 8, 1958*

## Abstract

Slopes of linear log micellar solubilization-log concentration plots of three dyes in aqueous solutions of five types of surfactants were approximately parallel, and varied with the dye. No correlation of polarity of dye with the log-log slope or with the magnitude of micellar solubilization was found.

## Introduction

The object of this investigation was to study the log solubilization-log concentration function in the micellar solubilization of various water-insoluble dyestuffs by different types of surfactants. Lambert and Busse (1) observed that log-log plots of the solubilization-concentration data obtained by their method were linear. Examination of the equilibrium solubilization data of other investigators revealed that such linearity seemed to be characteristic of the concentration range between 0.1 *M* and the CMC (critical micellar concentration). Straight-line log-log relationships can be obtained from the Orange OT solubilization data of McBain, Wilder, and Merrill (2) in 0.0035–0.083 *M* nonaethylene glycol monolaurate and 0.0032–0.071 *M* hexanolamine oleate at 25°C. The data of Kolthoff and Johnson (3) for dimethylaminoazobenzene in 0.010–0.10 *M* sodium oleate at 50°C. form a linear log solubilization-log concentration plot. Linear log-log plots can also be prepared from the dimethylaminoazobenzene solubilization data of Kolthoff and Stricks (4) in 0.025–0.10 molal potassium palmitate at 50°C. and in 0.0125–0.10 molal sodium di-sec-butyl naphthalene sulfonate at 30°C.

This report covers the effects of polarity of the solubilized dye and type of surfactant on the slope of the linear log solubilization-log concentration function of micellar solubilization. Some workers (1) have noticed that the slope and position of the log-log plot indicated the class (i.e., detergent, as distinguished from wetting agent) of the surfactant. In this study all surfactants used were of the detergent class.

## MATERIALS

*Surfactants.* The following surfactants, all 100% active, commercial preparations, were used:

| *Name* | *Symbol* | *Molecular Weight* |
|---|---|---|
| isooctylphenyl nonaethylene glycol ether | IOPNG | 602 |
| *t*-dodecyl nonaethylene glycol thioether | TDNG | 598 |
| polyoxyethylene sorbitan monolaurate | PSML | 1226 |
| nonaethylene glycol monolaurate | NGML | 613 |
| sodium oleate, U.S.P. grade | $C_{17}H_{33}COONa$ | 304 |

*Dyes.* Three related phenylazonaphthol dyes were used. They were of different polarity because of the number and kinds of groups attached to the phenyl radical. The dyes, used in the as-received condition, were:

Orange OT—F. D. & C. Orange No. 2—1-*o*-tolylazo-2-naphthol.

Flaming Red—D. & C. Red No. 36—1-(*o*-chloro-*p*-nitrophenylazo)-2-naphthol.

Oil Red XO—Ext. D. & C. Red No. 14—1-xylylazo-2-naphthol.

## EXPERIMENTAL

Micellar solubilization was determined by the method of Lambert and Busse (1). Changes were made in some details previously reported (5) for added convenience and accuracy. The solubilizations were run in a constant

TABLE I

*Solubilization of Orange OT, Flaming Red, and Oil Red XO at 37.8°C.*

| Surfactant | | mg. dye solubilized per 100 ml. surfactant solution | | |
|---|---|---|---|---|
| Name | Molar conc. | Orange OT | Flaming Red | Oil Red XO |
| IOPNG | 0.0289 | 15.0 | 26.3 | 43.9 |
| | 0.0145 | 7.60 | 16.2 | 31.6 |
| | 0.00725 | 3.92 | 9.42 | 21.3 |
| NGML | 0.0289 | 23.6 | — | 38.7 |
| | 0.0212 | — | 32.5 | — |
| | 0.0145 | 12.1 | 24.8 | 23.4 |
| | 0.00725 | 6.57 | 14.8 | 14.3 |
| TDNG | 0.0289 | 9.45 | 19.7 | 40.0 |
| | 0.0145 | 5.03 | 12.5 | 27.1 |
| | 0.00725 | 2.84 | — | 18.0 |
| | 0.00686 | — | 7.3 | — |
| Sodium oleate | 0.0578 | 15.1 | — | 33.6 |
| | 0.0428 | 11.5 | 7.17 | — |
| | 0.0289 | 8.18 | 5.47 | 22.1 |
| | 0.0145 | 4.35 | 3.49 | 14.3 |
| PSML | 0.0145 | 9.00 | 11.7 | 29.6 |
| | 0.00725 | 4.60 | 6.42 | 18.0 |
| | 0.00363 | 2.25 | 3.71 | 10.8 |

TABLE II

*Log Solubilization-Log Concentration Slopes*

| Surfactant | Slope—$m$ | | |
|---|---|---|---|
| | Orange OT | Flaming Red | Oil Red XO |
| IOPNG | 0.970 | 0.742 | 0.523 |
| NGML | 0.925 | 0.733 | 0.720 |
| TDNG | 0.869 | 0.669 | 0.577 |
| Sodium oleate | 0.900 | 0.665 | 0.617 |
| PSML | 1.00 | 0.829 | 0.728 |
| *Averages* | 0.933 | 0.728 | 0.633 |

temperature water bath at 37.8 ± 0.1°C. with an interaction period of 25 minutes. Because of flocculation, Flaming Red and Oil Red XO tests were subjected to a repetition of the initial agitation at 8 and 16 minutes after the beginning of the interaction. The interaction period was followed by filtration in dry apparatus discarding the first few milliliters of filtrate, cooling to room temperature, dilution of an aliquot of the filtrate to a suitable volume with acetone (aliquots containing sodium oleate were diluted with a 70:30, acetone-water mixture to prevent precipitation of insoluble matter), and colorimetric analysis in terms of optical density at a wavelength of 425 millimicrons.

## Results and Discussion

Solubilization of Orange OT, Flaming Red, and Oil Red XO by five different types of surfactants in the 0.00363–0.0578 $M$ concentration range is given in Table I. The data indicate that for each dye the log-log lines of the five surfactants are approximately parallel. The actual values of the individual slopes, computed from Table I, are given in Table II. The computations reveal that the slopes for all five surfactants increase with the dye solubilized in the order of Oil Red XO, Flaming Red, and Orange OT. This order corresponds to decreasing solubilization by the surfactants.

Dipole moments of the dyes were estimated from known group moments (6) giving the following values:

| | |
|---|---|
| Oil Red XO | 1.6 Debyes |
| Orange OT | 2.0 Debyes |
| Flaming Red | 4.0 Debyes |

No correlation of polarity of dye with log-log slope or with magnitude of solubilization is indicated.

Table II also gives the average log-log slope for each dye. Using the average slopes, solubilizations may be computed and compared with experimental values. It is to be noted that the log-log slopes of other investigators agree with those obtained herein. Slopes of 0.996 and 1.067 may be calculated from the Orange OT solubilization data of McBain, Wilder, and Merrill (2) in solutions of nonaethylene glycol monolaurate, and hexanolamineoleate. These values are in good agreement with the Orange OT slope of 0.933 obtained in this investigation.

## Acknowledgment

Acknowledgement is made to Troy Nichols for help in obtaining many of these data.

## References

1. Lambert, J. M., and Busse, W. F., *J. Am. Oil Chemists' Soc.* **26,** 289 (1949).
2. McBain, J. W., Wilder, A. G., and Merrill, Jr., R. C., *J. Phys. & Colloid Chem.* **52,** 12 (1948).
3. Kolthoff, I. M., and Johnson, W. F., *J. Phys. Chem.* **50,** 440 (1946).
4. Kolthoff, I. M., and Stricks, W., *J. Phys. & Colloid Chem.* **52,** 915 (1948).
5. Mankowich, A. M., *Ind. Eng. Chem.* **44,** 1151 (1952).
6. Weissberger, A., ed., "Physical Methods of Organic Chemistry," Vol. 2, p. 991. Interscience Publishers, New York, 1946.

JOURNAL OF COLLOID SCIENCE **14**, 135–146 (1959)

# MECHANICAL PROPERTIES OF POLY-*n*-OCTYL METHACRYLATE AT LOW FREQUENCIES AND IN CREEP; ENTANGLEMENTS IN METHACRYLATE POLYMERS[1]

**John W. Berge, P. R. Saunders, and John D. Ferry**

*Department of Chemistry, University of Wisconsin, Madison, Wisconsin*

*Received September 10, 1958*

## INTRODUCTION

Poly-*n*-octyl methacrylate is among the methacrylate polymers whose dynamic mechanical properties we have studied in the audio-frequency range, encompassing the transition from rubberlike to glasslike consistency, in cooperation with the Feltman Research and Engineering Laboratories, Picatinny Arsenal (1). This polymer has now been investigated at much lower frequencies and in creep, delineating the plateau and terminal zones of the relaxation and retardation spectra. An anomaly in the application of reduced variables appears in the plateau region; this and similar anomalies in earlier data for the *n*-butyl (2) and *n*-hexyl (3) methacrylate polymers have been analyzed in terms of an apparent dissociation of entanglement coupling points with increasing temperature.

## MATERIALS AND METHODS

The polymer was the same fraction (weight-average molecular weight $3.62 \times 10^6$) used previously (1). The dynamic storage modulus, $G'$, and loss tangent, $\tan \delta$, were obtained over a frequency range from 0.06 to 1.6 cycles/sec. with the torsion pendulum of Plazek, Vrancken, and Berge (4), at eleven temperatures from 54.4° to 140.3°C. Torsional creep measurements were made with the same instrument at 120.3°C. A single sample, 1⅛ inch diameter by 5⁄32 inch thickness, was employed.

Where possible, the absolute values of $G'$ and $\tan \delta$ obtained from the torsion pendulum were compared with the same quantities calculated from earlier transducer measurements, using well-known relations to convert the components of the complex compliance, $J'$ and $J''$, to $G'$ and $\tan \delta$. To provide for overlapping of the frequency scales in this comparison, the data were reduced for the temperature dependence of the relaxation times by the factors $a_T$ taken from the earlier analysis of the transducer data (1), and also reduced for the temperature dependence of a new factor $f$ which will be explained below. The reduced values of tan $\delta$ agreed well for the two instruments, but the values of $G'$ measured in the torsion pendulum were lower by about 26 %, indicating an error in the sample coefficient. Although there may be some uncertainty in the absolute accuracy of the sample coefficient in the transducer measurements, that for the torsion pendulum depends very critically on the radial dimension; in this case it was assumed that the transducer results were correct, and the torsion pendulum values were adjusted by an arbitrary correction factor of 1.26.

---

[1] Part XXIX of a series on Mechanical Properties of Substances of High Molecular Weight.

## RESULTS

The data for $G'$ and tan $\delta$ from the dynamic torsion pendulum measurements are plotted in Figs. 1 and 2 together with those from the transducer data at the lowest frequencies. The moduli are in the neighborhood of $4 \times 10^5$ dynes/cm.$^2$, whereas the loss tangent at each temperature passes through a minimum of about 0.16. The creep function, $J(t)$, is plotted in Fig. 3. It does not extend to long enough times to ensure steady-state flow, but from its final slope the viscosity $\eta$ at 120° can be estimated to be at least $2.7 \times 10^7$ poises and the steady-state compliance $J_e$ to be at least $3.4 \times 10^{-5}$ cm.$^2$/dyne.

For reduction to a standard temperature, the dynamic data were converted to the components of the complex compliance, and $J'_p$ and $J''_p$ were calculated in the usual manner with $T_0 = 373.2$°C. as in the previous work (1). The same $a_T$ factors were used as before, since these had been well established over a wide range of temperatures. The resulting composite

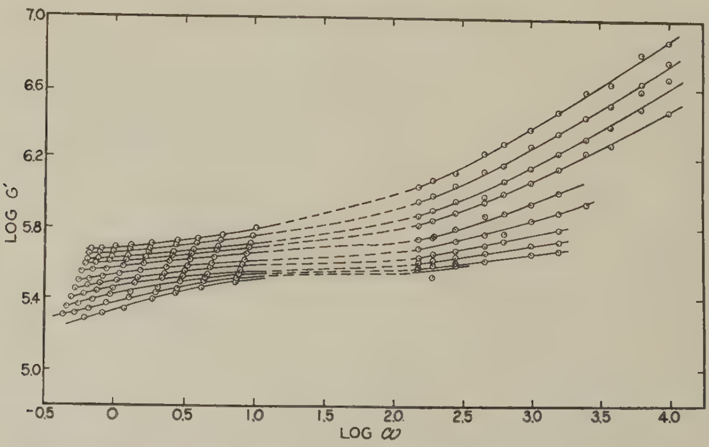

FIG. 1. Variation in the real part of the complex shear modulus with frequency for poly-$n$-octyl methacrylate at 11 temperatures; data at left from torsion pendulum, at right from transducer. Pip right (top curve), 54.4°C.; other curves successively downward, 59.8°, 65.8°, 70.9°, 80.2°, 89.5°, 99.8°, 109.4°, 120.3°, 129.5°, and 140.3°.

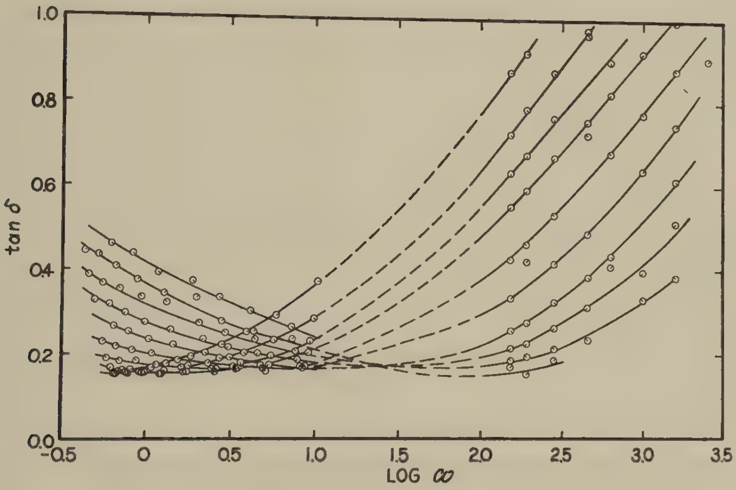

FIG. 2. Variation in the loss tangent with frequency at 11 temperatures, identified as in Fig. 1. Data at left from torsion pendulum, at right from transducer.

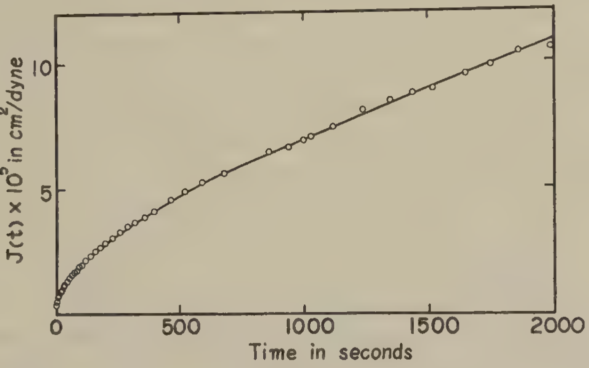

FIG. 3. Creep of poly-*n*-octyl methacrylate at 120.3°C. (linear plot).

plots showed a marked anomaly, which is represented for $J''_p$ in Fig. 4; the maximum in $J''_p$ shifts upward and to lower frequencies with increasing temperature. A very similar anomaly previously appeared in the data for poly-*n*-butyl (2) and poly-*n*-hexyl methacrylate (3); closer inspection of the high-frequency data for the octyl polymer (1) reveals its presence, though it is much more apparent in the low-frequency data which are added here. Before the present results are subjected to further derived calculations, therefore, this anomaly is subjected to closer scrutiny.

## ANALYSIS OF ENTANGLEMENT ANOMALY

The failure of the method of reduced variables in Fig. 4 and similarly near the maximum in $J''_p$ for the butyl and hexyl polymers shows that tem-

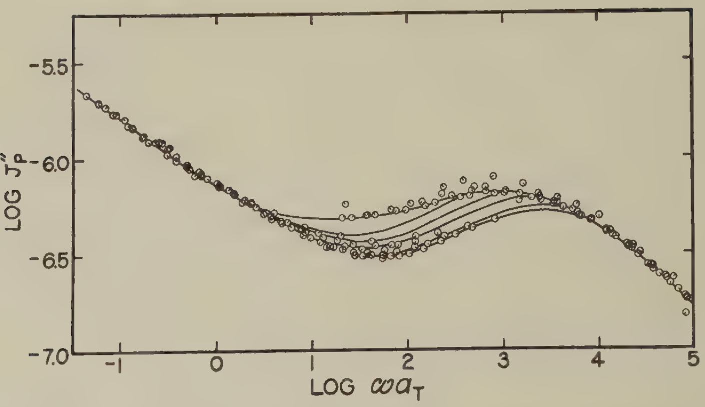

FIG. 4. Imaginary part of the complex compliance, reduced to 100°C. using $a_T$ factors given by WLF equation with constants specified in reference 1. Temperature key to pips same as in Fig. 1 (and as in reference 1).

perature has an added effect besides the change in magnitude of the relaxation times for backbone motions by the usual factor $a_T$ (which reflects the temperature dependence of the local friction coefficient (5)). In this region of the frequency scale, the mechanical properties are dominated by coupling between the motions of different macromolecules through certain widely spaced and only vaguely understood entanglement points. It is usually presumed that the maximum in the retardation spectrum, and hence in $J''_p$, in this region is determined by the number, distribution, and strength of the entanglement points. Evidently these features are being affected by changes in temperature.

If only the number of entanglements changes, leaving their strength and distribution constant, it is possible to predict the effect on the dynamic mechanical properties. In this frequency region, the entanglements will undergo very little slippage (which appears rather as a rise in $J''$ at considerably lower frequencies); in fact, the maxima in $J''$ for entangled and cross-linked polymers are somewhat similar in shape (6). We can, then, use theoretical expressions for cross-linked polymers to deduce the effect of a change in the number of linkage points on the mechanical dispersion.

In the theories of Blizard (7) and Bueche (8), the complex compliance for a cross-linked network is proportional to $(1/n_c)F(i\omega Z_c^2)$, where $n_c$ is the number of network strands (proportional to the number of linkage points), $\omega$ the circular frequency, and $Z_c$ the number of monomer units per strand. The function $F$ is continuous in Blizard's theory; in Bueche's, it is a series, but Gross and Fuoss have shown that the formulations are equivalent (9). If $n_c$ is increased by a factor $f$ (e.g., by lowering the temperature with a shift of some kind of association equilibrium), $Z_c$ will be decreased on the average by the same factor. Even if there is a distribution of strand lengths, each contribution will be affected in the same way if the form of the distribution remains constant. It follows, then, that with a temperature change from $T$ to $T_0$ the compliance will be altered over and above the usual effect of the factor $a_T$ so that $J^*(\omega)$ becomes

$$(1/f)J_p^*(\omega a_T/f^2).$$

Thus doubly logarithmic plots of $J'_p$ or $J''_p$ against $\omega a_T$, for which the ordinary temperature reduction has been applied, will shift to lower magnitudes and higher frequencies with decreasing temperature, along a direction with a slope of $-\frac{1}{2}$. This is in fact what is observed in Fig. 4 and similar plots of $J''_p$ for the butyl and hexyl polymers (2, 3). The shift is most noticeable where $J''_p$ has a positive slope, and is less apparent in $J'_p$, where the slope is always negative. Its effect disappears at higher frequencies where both $J''_p$ and $J'_p$ have approximately the same slope as the shift itself, *viz.*, $-\frac{1}{2}$ as prescribed by the Rouse (10) and Bueche theories. Indeed, at high frequencies where the cooperative motions are of a short-range character and oblivious of the distance between widely spaced linkage points, the dependence of $J^*$ on $n_c$ must vanish.

Values of $\Delta \log f$ between adjacent temperatures can be obtained by measuring separations on plots such as Fig. 4 in a direction of a slope of $-\frac{1}{2}$ (in this figure, 45° because of the difference in scales) and applying appropriate geometry. The curves are rather closely parallel with respect to this direction. After choosing 100°C. as the reference, $\log f$ can then be calculated for each temperature.

Application of this procedure to Fig. 4 provided values of $\log f$ which gave a good linear plot against $1/T$ with a slope corresponding to a heat of 1.6 kcal./mole. This could be formally interpreted as an apparent heat of dissociation, but the mechanism of the phenomenon need not be specified. The same treatment of the data for the butyl and hexyl polymers provided linear plots of $\log f$ against $1/T$ with an apparent heat of dissociation of 2.27 kcal./mole for both polymers.

A full reduction of $J'$ and $J''$ for both friction coefficient and entanglement spacing can now be accomplished by plotting (logarithmically) $J'_pf$ and $J''_pf$ against $\omega a_T/f^2$. The resulting composite curves are shown for the octyl polymer in Figs. 5 and 6 and for the butyl and hexyl polymers (transducer data only) in Fig. 7. Irrespective of the detailed interpretation of this treatment, it gives a quite satisfactory resolution of the anomaly.

## DISTRIBUTION FUNCTIONS

The retardation spectrum $L$ was calculated from $J'$ and $J''$, using the reduced data of Figs. 5–7; from the corresponding components of the complex shear modulus, the relaxation spectrum $H$ was calculated. For the

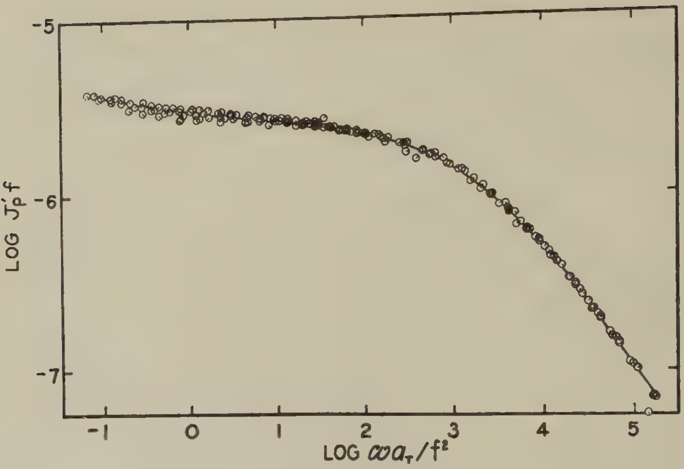

FIG. 5. Real part of the complex compliance reduced to 100°C. for temperature dependence of both $a_T$ and $f$. Temperature key to pips same as in Fig. 1.

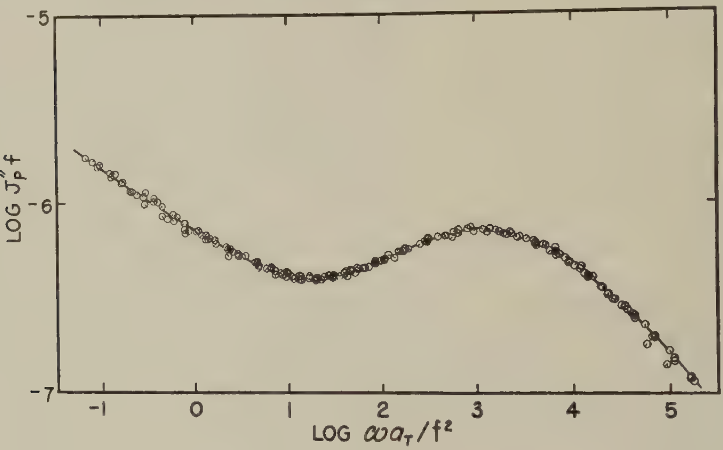

FIG. 6. Imaginary part of the complex compliance reduced to 100° for temperature dependence of both $a_T$ and $f$.

butyl and hexyl polymers, and for the octyl in the corresponding dispersion range, the usual approximation formulas of Williams and Ferry were employed (11), and the agreement between values derived from the real and imaginary components of $J^*$ or $G^*$ was as usual reasonably good. In the dispersion region of the octyl polymer where $J''$ and $G''$ pass through minima with rather strong curvature, however, the Williams-Ferry formulas failed to give agreement for the two components, as anticipated in their original presentation (12). Accordingly, in this region, different formulas

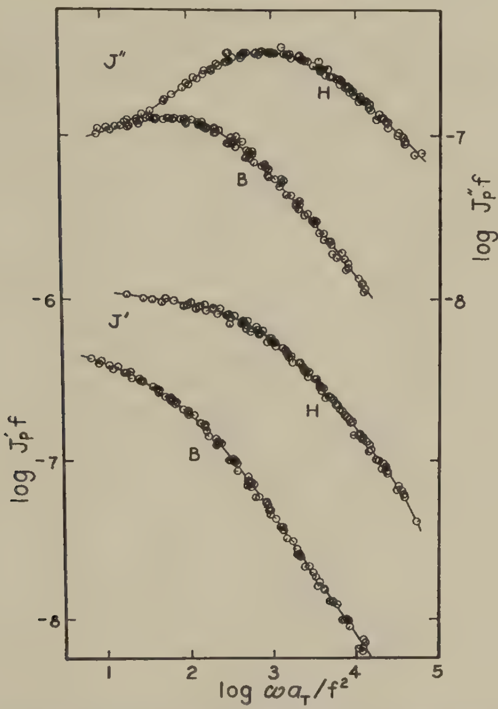

FIG. 7. Real and imaginary parts of the complex compliance for poly-$n$-butyl methacrylate (B) and poly-$n$-hexyl methacrylate (H) reduced to 100°C. for temperature dependence of both $a_T$ and $f$.

taking into account higher derivatives were employed. The spectra were obtained from the real components by an approximation of Schwarzl and Staverman (13):

$$H(1/\omega) = dG'/d\ln\omega - (\tfrac{1}{4})d^3G'/d\ln\omega^3 \qquad [1]$$

$$L(1/\omega) = -dJ'/d\ln\omega + (\tfrac{1}{4})d^3J'/d\ln\omega^3 \qquad [2]$$

and from the imaginary components by an approximation of Fujita (14), expressed here in a form convenient for numerical calculations:

$$H = (e^2/4\pi)G''\,\{1 - (d\ln G''/d\ln\omega)^2 - d^2\ln G''/d\ln\omega^2\}; \qquad [3]$$

$$L = (e^2/4\pi)J''\,\{1 - (d\ln J''/d\ln\omega)^2 - d^2\ln J''/d\ln\omega^2\}. \qquad [4]$$

In most cases reasonably good agreement was then obtained for the calculations from the two components.

To obtain $L$ from the creep measurements, it was necessary to employ an approximation in terms of the total compliance $J(t) = J_e\psi(t) + t/\eta$; the nstantaneous compliance $J_g$ could of course be neglected, but the magni-

TABLE I

*Retardation and Relaxation Spectra of Poly-n-Octyl Methacrylate Reduced to 100° C. Including Reduction for Change in Entanglement Density*

| $\log \tau_p$ (sec.) | $\log L_p$ (cm.$^2$/dyne) |  | $\log H_p$ (dynes/cm.$^2$) |  |
|---|---|---|---|---|
|  | From $J'$ | From $J''$ | From $G'$ | From $G''$ |
| −5.0 | −7.23 | −7.13 | 6.08 | — |
| −4.5 | −6.87 | −6.83 | 5.79 | — |
| −4.0 | −6.60 | −6.55 | 5.52 | 5.56 |
| −3.5 | −6.39 | −6.38 | 5.21 | 5.30 |
| −3.0 | −6.37 | −6.34 | 4.92 | 5.01 |
| −2.5 | −6.49 | −6.38 | 4.62 | 4.78 |
| −2.0 | −6.63 | −6.57 | 4.51 | 4.58 |
| −1.5 | −6.74 | −6.81 | 4.45 | 4.37 |
| −1.0 | −6.75 | −6.84 | 4.41 | 4.33 |
| −0.5 | −6.72 | −6.63 | 4.46 | 4.49 |
| 0 | — | −6.28 | 4.51 | 4.62 |
| 0.5 | — | −6.11 | 4.66 | 4.70 |

|  |  |  |  |  |  |  |
|---|---|---|---|---|---|---|
| $\log \tau_p$ (sec.) | 0.7 | 1.2 | 1.7 | 2.2 | 2.7 | 3.2 |
| $\log L_p$ from $J(t)$ | −6.16 | −5.87 | −5.70 | −5.43 | −5.17 | −4.85 |
| $\log \tau_p$ (sec.) | 1.0 | 1.5 | 2.0 | 2.5 | 3.0 | 3.5 |
| $\log H_p$ from $G(t)$ | 4.79 | 4.58 | 4.35 | 4.09 | 3.73 | 3.39 |

TABLE II

*Retardation and Relaxation Spectra of Poly-n-Butyl Methacrylate Reduced to 100°C. Including Reduction for Change in Entanglement Density*

| $\log \tau_p$ (sec.) | $\log L_p$ (cm.$^2$/dyne) |  | $\log H_p$ (dynes/cm.$^2$) |  |
|---|---|---|---|---|
|  | From $J'$ | From $J''$ | From $G'$ | From $G''$ |
| −4.0 | −8.33 | −8.33 | 7.18 | 7.23 |
| −3.5 | −8.06 | −7.96 | 6.79 | 6.80 |
| −3.0 | −7.55 | −7.60 | 6.50 | 6.51 |
| −2.5 | −7.21 | −7.29 | 6.20 | 6.18 |
| −2.0 | −7.09 | −7.01 | 5.95 | 5.91 |
| −1.5 | −7.04 | −7.12 | 5.65 | 5.61 |
| −1.0 | −7.15 | −7.09 | 5.42 | 5.40 |

tude of the $t/\eta$ term was large and undetermined. The second approximation of Schwarzl and Staverman (13)

$$L(t/2) = dJ_e\psi/d\ln t - d^2J_e\psi/d\ln t^2$$

can for this purpose be expressed in the form

$$L(t/2) = (d/d\ln t)\,[J(t) - dJ(t)/d\ln t] \qquad [5]$$

since the flow terms in $J(t)$ and its derivative cancel. Calculations made by Eq. [5], after reduction to 100°C. for the temperature dependence of both $a_T$ and $f$, were confirmed by converting $J(t)$ to $G(t)$ with an approximation

TABLE III

*Retardation and Relaxation Spectra of Poly-n-Hexyl Methacrylate Reduced to 100° C. Including Reduction for Change in Entanglement Density*

| Log $\tau_p$(sec.) | Log $L_p$(cm.$^2$/dyne) | | Log $H_p$ (dynes/cm.$^2$) | |
|---|---|---|---|---|
| | From $J'$ | From $J''$ | From $G'$ | From $G''$ |
| −4.5 | −7.30 | −7.31 | 6.31 | 6.26 |
| −4.0 | −7.00 | −7.05 | 5.99 | 6.01 |
| −3.5 | −6.78 | −6.77 | 5.69 | 5.74 |
| −3.0 | −6.64 | −6.70 | 5.43 | 5.47 |
| −2.5 | −6.86 | −6.72 | 5.17 | 5.21 |
| −2.0 | −7.02 | −6.95 | — | 4.97 |
| −1.5 | −7.08 | −7.11 | — | 4.83 |

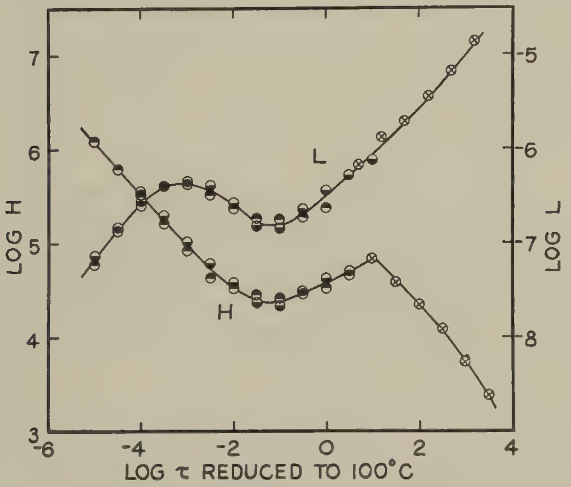

FIG. 8. Relaxation spectrum ($H$) and retardation spectrum ($L$) for poly-$n$-octyl methacrylate reduced to 100°C. for temperature dependence of both $a_T$ and $f$. Points top black, from $G'$ or $J'$; bottom black, from $G''$ or $J''$; crossed, from creep.

quoted by Smith (15), obtaining $H$ from $G(t)$ by the Ferry-Williams approximation (12), and finally showing that the relation of Gross and Pelzer (16) connecting $H$ and $L$, as approximated by Smith (15), was satisfied.

The calculated spectra are given in Table I–III for the three polymers. Those for the octyl are plotted in Fig. 8; the others, which differ only slightly from the values previously reported (2, 3), will be compared in a subsequent paper (17) with the spectra of all the methacrylate series through the $n$-dodecyl polymer. Figure 8 provides a detailed delineation of the plateau zone; both spectra pass through a well-defined minimum at almost the same point on the time scale. A similar coincidence in the location of minima for $H$ and $L$ has been noted in some other polymer systems (6).

## DISCUSSION

### *Temperature-Dependent Entanglement Anomaly*

If the heats calculated from the temperature dependence of $f$ are interpreted as heats of dissociation, it is implied that an equilibrium exists between entanglement points and potential entanglement sites, with the concentration of the latter in excess and essentially constant. The concept of entanglements is at present too vague, however, to take this picture literally. The values of 1.6 and 2.3 kcal. would certainly represent very mild interaction. A similar reduction anomaly near the maximum of $J''$ has appeared in a series of concentrated solutions of poly-*n*-butyl methacrylate (18), and it can be successfully treated in the same manner. The prominence of this phenomenon in methacrylate polymers may conceivably be related to the presence of short isotactic segments (19), although the polymers used in our investigations were not prepared at low temperatures (20). The linkage points are certainly not crystallites such as present in polymeric gels, since the latter do not undergo steady flow and have quite different mechanical properties at long times (6).

### *Time Dependence of the Plateau Zone*

From the minimal estimate of the viscosity, which reduced to 100°C. (including the temperature dependence of $f$) is $1.0 \times 10^8$ poises, one would calculate from the Rouse theory (21) that the terminal relaxation time is at least $10^4$ sec. Although the experiments do not extend that far, the width of the plateau can be estimated from the separation between the two regions of slope ½ (for $L$) and $-½$ (for $H$) on the doubly logarithmic plot in Fig. 8 (21). This is 3.85 and 3.75 decades, respectively, for the two spectra. If the average is equated (22) to 2.4 log $(M_w/2M_e)$, where $M_e$ is the average molecular weight between entanglement points, we obtain for the latter $4.8 \times 10^4$, corresponding to a degree of polymerization of 240. A rough confirmation can be obtained from the pseudo-equilibrium shear modulus in the plateau region, where $G' \cong 5 \times 10^5$ dynes/cm.$^2$, and the equation of equilibrium rubberlike elasticity, from which the degree of polymerization between junction points is calculated to be 300. These values are smaller than the estimates for nonpolar polymers (23), but larger than that for polymethyl methacrylate deduced by Bueche from viscosity measurements in concentrated solutions (24). Further interpretation must await additional information.

## ACKNOWLEDGMENTS

This work was supported in part by Picatinny Arsenal, Ordnance Corps, Department of the Army, and in part by the Research Committee of the Graduate School of the University of Wisconsin from funds supplied by the Wisconsin Alumni Research Foundation. We are much indebted to Dr. Donald J. Plazek for advice and help with the apparatus, to Mr. Kazuhiko Ninomiya for discussions of approximation calculations of spectra, and to Miss Rowena M. Green for help with the calculations.

## SUMMARY

The storage modulus and loss tangent have been measured between 0.06 and 1.6 cycles/sec. in the temperature range from 54° to 140°C. for a fractionated poly-$n$-octyl methacrylate with molecular weight $3.62 \times 10^6$. Creep was measured at 120°C. over a time interval up to 2000 sec. The usual method of reduced variables, using $a_T$ factors determined in an earlier study at higher frequencies, failed to give single composite curves for data at different temperatures; the residual anomaly appears most clearly in the loss compliance, the maximum of which shifts upward and to lower frequencies with increasing frequency, as previously observed in the $n$-butyl and $n$-hexyl methacrylate polymers. The data for all three polymers in this region can be brought into coincidence, however, by an additional reduction which is formally equivalent to assuming a dissociation of entanglement points with increasing temperature. The apparent heat of dissociation is 2.3 kcal./mole for the butyl and hexyl polymers and 1.6 for the octyl. In the plateau zone of the time scale, both the retardation and the relaxation spectra of poly-$n$-octyl methacrylate pass through minima at about the same point; the sharpness of curvature makes it necessary to use higher approximations than usual to calculate the spectra. From the width of the plateau zone, the average degree of polymerization between entanglement points at 100°C. is estimated to be 240.

## REFERENCES

1. DANNHAUSER, W., CHILD, W. C., JR., AND FERRY, J. D., *J. Colloid Sci.* **13,** 103 (1958).
2. CHILD, W. C., JR., AND FERRY, J. D., *J. Colloid Sci.* **12,** 327 (1957).
3. CHILD, W. C., JR., AND FERRY, J. D., *J Colloid Sci.* **12,** 389 (1957).
4. PLAZEK, D. J., VRANCKEN, M. N., AND BERGE, J. W., *Trans. Soc. Rheol.* **2** (in press).
5. FERRY, J. D., AND LANDEL, R. F., *Kolloid-Z.* **148,** 1 (1956).
6. FERRY, J. D., AND NINOMIYA, K., "Proceedings of Symposium on Phenomenological Aspects of Viscoelasticity." Academic Press, New York (in press).
7. BLIZARD, R. B., *J. Appl. Phys.* **22,** 730 (1951).
8. BUECHE, F., *J. Chem. Phys.* **22,** 603 (1954).
9. GROSS, B., AND FUOSS, R. M., *J. Polymer Sci.* **19,** 39 (1956).
0. ROUSE, P. E., JR., *J. Chem. Phys.* **21,** 1272 (1953).
1. WILLIAMS, M. L., AND FERRY, J. D., *J. Polymer Sci.* **11,** 169 (1953).
2. FERRY, J. D., AND WILLIAMS, M. L., *J. Colloid Sci.* **7,** 347 (1952).
3. SCHWARZL, S., AND STAVERMAN, A. J. in Stuart, H., "Die Physik der Hochpolymeren," Vol. 4, p. 44. Springer, Berlin, 1956.
4. FUJITA, H., *J. Appl. Phys.* **29,** 943 (1958).
5. SMITH, T. L., *Trans. Soc. Rheol.* **2** (in press).
6. GROSS, B., AND PELZER, H., *J. Appl. Phys.* **22,** 1035 (1951).

17. Kurath, S. F., Yin, T. P., Berge, J. W., and Ferry, J. D., *J. Colloid Sci.* **14**, 147 (1959).
18. Saunders, P. R., Stern, D. M., Kurath, S. F., and Ferry, J. D., *J. Colloid Sci.* (in press).
19. Fox, T. G., and others, *J. Am. Chem. Soc.* **80**, 1768 (1958).
20. Chinai, S. N., *J. Polymer Sci.* **25**, 413 (1957).
21. Ferry, J. D., in Stuart, H., "Die Physik der Hochpolymeren," Vol. 4, pp. 102, 399. Springer, Berlin, 1956.
22. Ferry, J. D., Landel, R. F., and Williams, M. L., *J. Appl. Phys.* **26**, 359 (1955).
23. Fox, T. G., Gratch, S., and Loshaek, S., in Eirich, F., "Rheology," Vol. 1, p. 446. Academic Press, New York, 1956.
24. Bueche, F., *J. Appl. Phys.* **26**, 738 (1955).

Note added in Proof. The applicability of Eq. [5] was pointed out by Dr. H. Leaderman, in Eirich, F., "Rheology", Vol. 2, p. 49, Academic Press, New York, 1958.

JOURNAL OF COLLOID SCIENCE 14, 147-160 (1959)

# DYNAMIC MECHANICAL PROPERTIES AND CREEP OF POLY-*n*-DODECYL METHACRYLATE[1]

**Sheldon F. Kurath[2], Theodore P. Yin, John W. Berge, and John D. Ferry**

*Department of Chemistry, University of Wisconsin, Madison, Wisconsin*

*Received October 16, 1958*

## INTRODUCTION

A series of methacrylate polymers with ester groups of varying length has been investigated in this laboratory in cooperation with the Feltman Research and Engineering Laboratories, Picatinny Arsenal. The time-dependent mechanical properties of the ethyl (1), butyl (2), hexyl (3), and octyl (4, 5) polymers have been reported previously. We now present data for poly-*n*-dodecyl methacrylate, in which the side groups are so long that they comprise by far the major part of the molecular volume. By combining measurements of dynamic mechanical properties and creep, a wide range of time scale is achieved.

## MATERIALS AND METHOD

The synthesis and fractionation of the polymer were carried out at Picatinny Arsenal (6), and the weight-average molecular weight was determined there to be $0.95 \times 10^6$. Although it had been dried from frozen benzene solution, there was a faint odor of solvent which was removed by heating *in vacuo* (spread in a thin film) at 60°C. for 36 hours.

Because of the extreme stickiness of this soft polymer, special methods for molding and handling were necessary. A portion of polymer was heated at 60°C. *in vacuo* in a miniature stainless steel scoop until the air bubbles introduced during its transfer had been removed; then, while maintaining vacuum, it was allowed to flow directly into the mold—a process requiring about 8 hours. The mold was pressed for several hours at 45°C., and then cooled by Dry Ice in a dry box and opened. The samples were removed, adhering to aluminum foil liners, and allowed to warm to room temperature for weighing. It was necessary to cool again with Dry Ice to remove the aluminum foil after each sample had been mounted with one face adhering

---

[1] Part XXX of a series on Mechanical Properties of Substances of High Molecular Weight.

[2] Present address: Institute of Paper Chemistry, Appleton, Wisconsin.

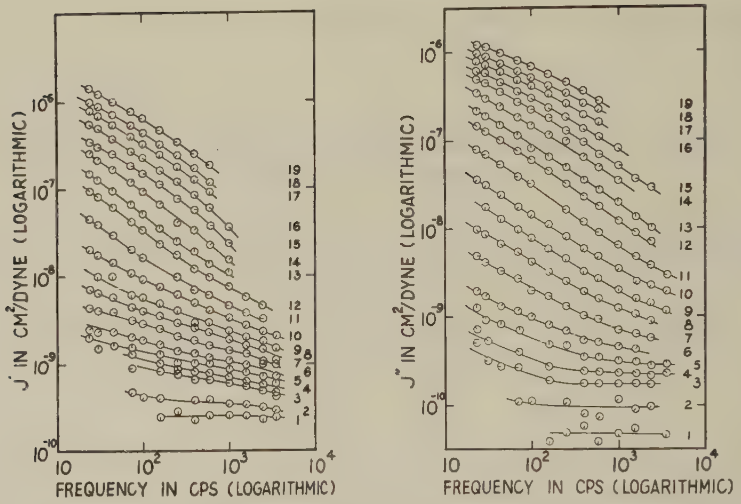

Fig. 1. Variation of the real part of the dynamic shear compliance, $J'$ (left) and the imaginary part, $J''$ (right) for poly-*n*-dodecyl methacrylate at 19 temperatures; numbers correspond to the sequence (with 45° successive clockwise rotations of pips) −40.4°, −35.0°, −30.0°, −27.8°, −23.8°, −19.7°, −14.6°, −9.6°, −5.4°, −0.3°, 5.1°, 10.9°, 14.8°, 20.6°, 25.2°, 30.0°, 34.7°, 39.7°, and 45.3°C.

in the apparatus. For calculating sample coefficients, the density and thermal expansion coefficient of the polymer were taken from the data of Rogers and Mandelkern (7).

Measurements of the complex shear compliance ($J^* = J' - iJ''$) were made between 24 and 3600 cycles/sec. with the Fitzgerald Apparatus (8). Three pairs of samples were used, detailed descriptions of which follow.

Samples 108, approximate dimensions $^{11}/_{16}$ in. diameter by $^{3}/_{32}$ in. thickness, had a sample coefficient of 18.3 cm. at 25°C. Measurements were made at approximately 0°, −10°, −15°, −20°, −5°, 5°, −25°, −30°, −35°, −28°, −32°, −12°, 10°, 15°, and 20°C., followed by a check run at 5° which agreed well with the first at this temperature. (The exact temperatures are given in the legend of Fig. 1.)

Samples 109, approximate dimensions $^{11}/_{16}$ in. by $^{1}/_{32}$ in., had a sample coefficient of 66.4 cm. Measurements were made at 25°, 15°, 20°, and then at 5° intervals up to 45° with periodic check runs at 25° to insure against sag of this very soft material. At overlapping temperatures, the values of $J'$ and $J''$ agreed well with those of Samples 108.

Samples 111, approximate dimensions $^{5}/_{16}$ in. by $^{1}/_{8}$ in., had a nominal sample coefficient of 4.23 cm. Measurements were made at approximately 5° intervals from −20° down to −40° and then from −20° up to 0°, followed by −25°. The check runs at −20° and −25° agreed well with the initial results. At temperatures of reliable overlapping data with Samples

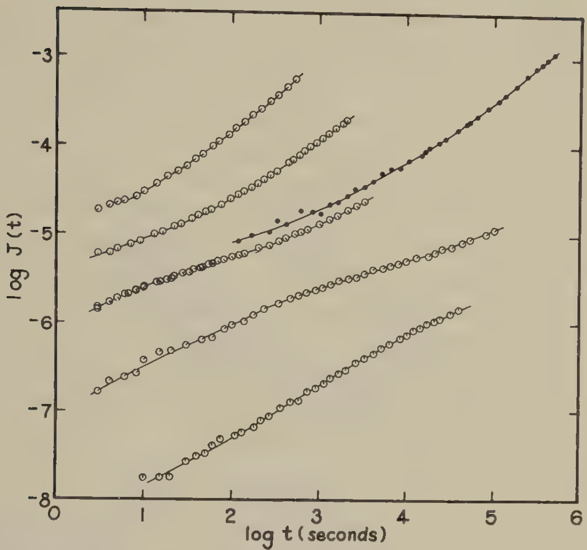

FIG. 2. Creep of poly-*n*-dodecyl methacrylate. Open circles, measured by torsion pendulum, temperatures successively from bottom curve −30.1°, −19.7°, −0.3° (at 2 different stresses), 20.6°, and 39.7°; filled circles, measured by parallel plate shear apparatus at −0.4°C.

108, the values of $J'$ and $J''$ from the latter were lower by 8% to 17%. This is the direction to be expected for an error in sample coefficient due to bulging of the thicker Samples 111, and the data from these were multiplied by an empirical correction factor of 0.88 to bring them to approximate agreement with those of Samples 108. This correction is not as satisfactory as usual, but the data at the lowest temperatures are complicated by crystallization in any case (as described below) and are not used for deduction of viscoelastic functions.

Measurements of shear creep were made in torsion with the torsion pendulum of Plazek, Vrancken, and Berge (9) at approximately −30°, −20°, 0°, 20°, and 30°C., followed by a check run at 0° with good agreement; and in simple shear with a parallel plate apparatus described elsewhere (10) at 0°. The exact temperatures are given in the legend of Fig. 2. At 0°, torsion pendulum measurements were made at two torques differing by a factor of 6, with results in excellent agreement. The parallel plate shear data at this temperature involved a stress approximately equivalent to the mean stress in the lower torque experiment in the torsion pendulum; the calculated values of the compliance were somewhat higher than those obtained from the torsion pendulum, but by the same factor throughout, indicating an uncertainty in the sample coefficient of one or both experiments.

To compare the absolute magnitudes of the creep and dynamic measurements, the latter were converted to the creep compliance $J(t)$ by an approximate relation of Ninomiya and Ferry (11) and reduced to a reference temperature by shift factors (to be described below) to provide an overlapping time scale. The torsion pendulum values were about 29% higher than those from dynamic measurements. In view of the extreme difficulty in handling the polymer, some sample distortion is possible and the absolute values remain in some doubt. Since the torsion pendulum sample coefficient is more critically dependent on sample shape, the Fitzgerald Apparatus data were assumed to be correct and the creep data were multiplied by an empirical correction factor of 0.775.

Since the creep experiments did not extend to long enough times to be sure that steady-state flow had been achieved, no attempt was made to calculate viscosity or steady-state compliance.

## RESULTS

The data for $J'$ and $J''$, measured at 19 temperatures from −40° to 45°, are shown plotted logarithmically in Fig. 1. Where data on different samples were taken at the same frequencies and temperatures, the values have been averaged (for Samples 111, after the empirical correction). The creep data for $J(t)$ at 5 temperatures are shown plotted logarithmically in Fig. 2.

For reduction to a standard temperature, 25°C. was chosen since the measurements did not extend to 100°, the choice made in previous studies of this series (1–5). Using the usual method, $J'_p$, $J''_p$, and $J_p(t)$ were calculated from the thermal expansion coefficient. Logarithmic plots of the reduced functions could be superposed quite well by the usual arbitrary shift factors $a_T$ except at the lowest temperatures. (In estimating $a_T$, the creep data were used before applying the empirical correction, which of course does not affect this treatment.) The empirical $a_T$ values fitted an equation of the WLF form (12):

$$\log a_T = -c_1^0(T - T_0)/(c_2^0 + T - T_0), \qquad [1]$$

with $c_1^0 = 8.52$ and $c_2^0 = 139.2$ for $T_0 = 298.2$°K. Values of $a_T$ calculated from this equation were actually used for the final logarithmic plots against reduced frequency ($\omega a_T$) and reduced time ($t/a_T$) shown in Figs. 3–5. The superposition with reduced variables is quite good except for an anomaly at low temperatures which will be discussed below.

Independently of the glass transition temperature $T_g$, the parameter $\alpha_f$ (interpreted as the thermal expansion coefficient of free volume relative to total volume) can be calculated (13) as $1/2.303\ c_1^0c_2^0$, or $3.7 \times 10^{-4}$ deg$^{-1}$. This is a reasonable value, though somewhat larger than those of

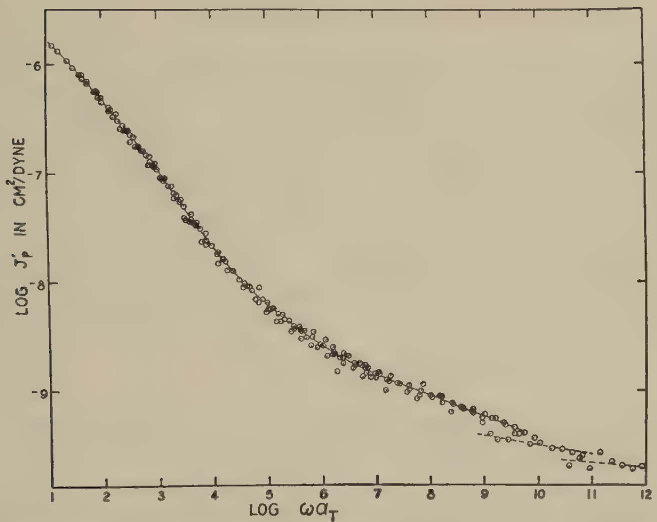

FIG. 3. Real part of the complex compliance, $J'$, reduced to 25°C. and plotted ogarithmically against reduced frequency with reduction factors calculated from Eq. [1]. Temperature key by pips same as in Fig. 1.

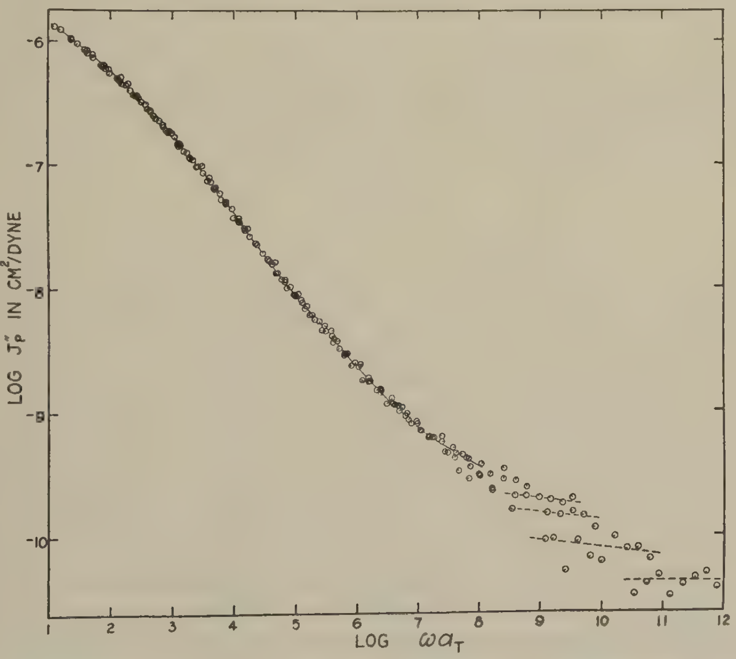

FIG. 4. Imaginary part of the complex compliance, $J''$, reduced and plotted as n Fig. 3.

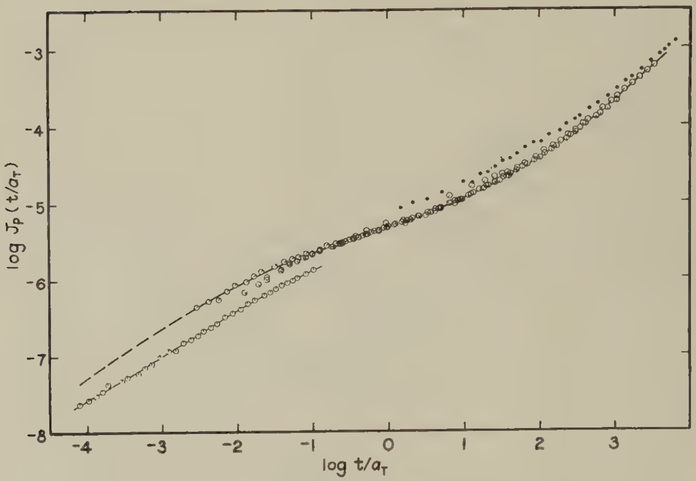

FIG. 5. Creep function reduced and plotted as in Fig. 3; temperature key by pips same as in Fig. 2.

other methacrylate polymers. For the parameter $f_g$ (interpreted as the relative free volume at $T_g$), knowledge of $T_g$ is necessary. Rogers and Mandelkern (7) report −65°, though the break in the volume-temperature curve is not very sharp; this gives $f_g = 0.018$, which is unusually small. Alternatively, if $f_g$ were the usual value of 0.025 found for other methacrylates as well as other polymers, $T_g$ would be −46°.

## DISCUSSION

### *Low-Temperature Reduction Anomaly*

At the lowest temperatures, $J'_p$, $J''_p$, and $J_p(t)$ fall progressively below their reduced curves. This deviation contrasts with the anomaly in polyethyl methacrylate (1), interpreted as a β-mechanism, in which the reduced compliance rises progressively with decreasing temperature. The behavior seen in Figs. 3–5 would be expected if the structure is altered at low temperatures by the onset of cross-linking through crystallization; in fact, a somewhat similar anomaly was seen in gels of cellulose tributyrate (14), where the chain backbones presumably enter crystallites. In the present case, no doubt the ester side groups crystallize. Evidence for crystallization at −34°C. has been reported by Greenberg and Alfrey from dilatometric measurements (15), although Rogers and Mandelkern (7) did not detect it. The anomaly in mechanical properties, which begins at −28°, is probably a more sensitive indication of crystallization than dilatometry.

### *Distribution Functions*

The retardation spectrum, $L$, was calculated by the second approximation formulas of Williams and Ferry (16) from the data of Figs. 3 and 4; and from the data of Fig. 5 by the modified Schwarzl-Staverman approximation, Eq. [5] of reference (5), which permits calculation from the creep compliance without knowledge of the steady-flow viscosity. The complex compliance data were converted to the real and imaginary components of the complex modulus, $G'$ and $G''$, by the usual reciprocal relation; also, the creep compliance was converted to the relaxation modulus $G(t)$ by an approximation quoted by Smith (17):

$$G(t) = \sin m\pi / m\pi J(t), \qquad [2]$$

where $m = d \log J(t)/d \log t$. Finally, the relaxation spectrum $H$ was calculated from $G'$, $G''$, and $G(t)$ by the Williams-Ferry approximations (16, 18). Both spectra are given in Tables I and II; the agreement between values from the real and imaginary dynamic data, and between dynamic and creep data where they overlap, is quite good.

The retardation spectrum is plotted in Fig. 6, together with those of the other polymers of the series; for the latter, individual points represent revised values recalculated since the original publications, after reduction for

TABLE I

*Retardation and Relaxation Spectra Reduced to 25°C. from Dynamic Data*

| Log $\tau_p$ | Log $L_p$(*cm.²/dyne*) | | Log $H_p$(*dynes/cm.²*) | |
|---|---|---|---|---|
| (*sec.*) | From $J'$ | From $J''$ | From $G'$ | From $G''$ |
| −9.5 | −10.07 | | | |
| −9.0 | −9.98 | | | |
| −8.5 | −9.89 | | | |
| −8.0 | −9.78 | −9.71 | 8.23 | 8.38 |
| −7.5 | −9.70 | −9.58 | 8.26 | 8.27 |
| −7.0 | −9.53 | −9.44 | 8.20 | 8.25 |
| −6.5 | −9.34 | −9.27 | 8.16 | 8.20 |
| −6.0 | −9.09 | −8.92 | 8.01 | 8.08 |
| −5.5 | −8.89 | −8.81 | 7.81 | 7.84 |
| −5.0 | −8.62 | −8.51 | 7.49 | 7.53 |
| −4.5 | −8.31 | −8.25 | 7.13 | 7.24 |
| −4.0 | −7.96 | −7.90 | 6.72 | 6.83 |
| −3.5 | −7.58 | −7.50 | 6.38 | 6.43 |
| −3.0 | −7.22 | −7.15 | 6.05 | 6.17 |
| −2.5 | −6.90 | −6.86 | 5.78 | 5.87 |
| −2.0 | −6.61 | −6.54 | 5.55 | 5.62 |
| −1.5 | −6.31 | −6.34 | 5.32 | 5.34 |
| −1.0 | −6.14 | −6.25 | 5.11 | 5.08 |

TABLE II

*Retardation and Relaxation Spectra Reduced to 25°C. from Creep Data*

| Log $\tau_p$ | Log $L_p$ | Log $\tau_p$ | Log $H_p$ |
|---|---|---|---|
| *(sec.)* | *(cm.²/dyne)* | *(sec.)* | *(dynes/cm.²)* |
| −2.8 | −6.90 | −2.5 | 5.75 |
| −2.3 | −6.66 | −2.0 | 5.47 |
| −1.8 | −6.43 | −1.5 | 5.22 |
| −1.3 | −6.20 | −1.0 | 4.98 |
| −0.8 | −6.10 | −0.5 | 4.83 |
| −0.3 | −5.98 | 0.0 | 4.77 |
| 0.2 | −5.89 | 0.5 | 4.64 |
| 0.7 | −5.74 | 1.0 | 4.51 |
| 1.2 | −5.51 | 1.5 | 4.29 |
| 1.7 | −5.34 | 2.0 | 4.03 |
| 2.2 | −5.11 | 2.5 | 3.55 |
| 2.7 | −4.72 | 3.0 | 3.00 |
| 3.2 | −4.39 | 3.5 | 2.44 |

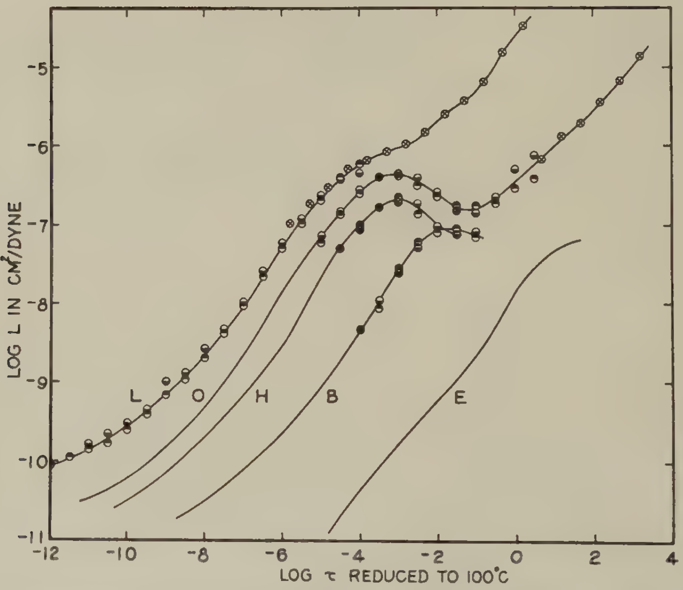

FIG. 6. Retardation spectrum of poly-*n*-dodecyl methacrylate (*L*), compared with those for the octyl (*O*), hexyl (*H*), butyl (*B*), and ethyl (*E*) polymers. Points plotted for *H* and *B* refer to revised calculations reduced for the temperature dependence of the density of entanglement points, as described in reference (5). Top black, from $J'$; bottom black, from $J''$; crossed, from creep.

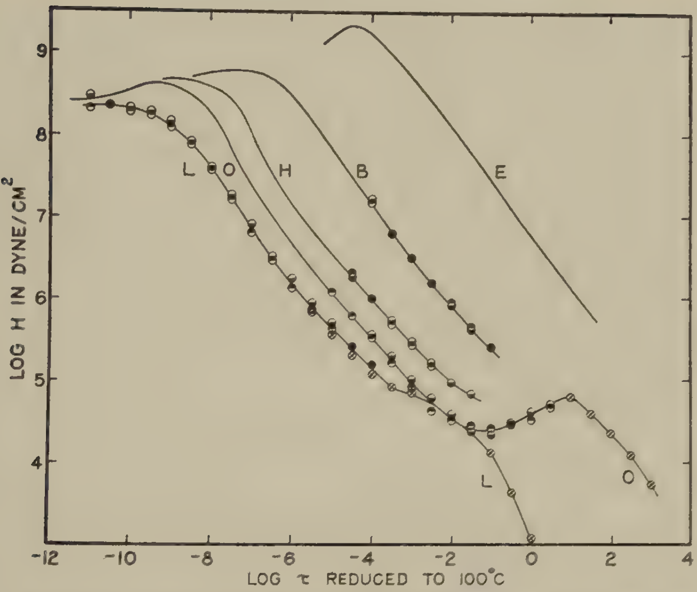

FIG. 7. Relaxation spectra of the five methacrylate polymers; identification of points same as in Fig. 6.

the entanglement anomaly as described in reference (5). Here for comparison with the other spectra $L$ has been shifted from 25° to 100° by the $a_T$ calculated from Eq. [1], viz., $-2.98$. This represents an extrapolation from the highest temperature of measurement (45°) which is reasonably dependable. The dodecyl spectrum shows no maximum nor minimum, but there is a point of inflection representing a slight entanglement effect. The relaxation spectra for all the polymers are similarly plotted in Fig. 7. Here again the dodecyl polymer shows only the suggestion of a short plateau, without the sharp minimum and maximum which characterize the octyl polymer. The maximum in $H$ at short times is lower ($\log H = 8.35$) than for the other members of the series, continuing the progressive decrease with increasing side group length.

### *Spacing between Entanglements*

The inflection points in $H$ and $L$ lie between two regions with the theoretical slope of $-\frac{1}{2}$ and $\frac{1}{2}$, respectively, separated by 1.1 units on the logarithmic time scale. Taking this as the width of the rudimentary plateau region, and equating it (19) to 2.4 log $(M_w/2M_e)$, where $M_e$ is the average molecular weight between entanglements, the latter is calculated to be $1.6 \times 10^5$, corresponding to a degree of polymerization of 650. The coupling points appear therefore to be much more widely spaced than in the octyl polymer, where the average separation is a degree of polymerization of 240.

The absence of a detectable temperature-dependent entanglement anomaly in the application of reduced variables, such as found in the butyl, hexyl, and octyl polymers (5), is understandable from the narrowness of the plateau region and the attendant shape of the retardation spectrum; $L$ does not pass through a region of negative slope (corresponding to a positive slope for $J''$) where the anomaly which has been attributed to an apparent dissociation of coupling points makes its most prominent appearance. Thus, it is impossible to determine whether this phenomenon occurs in poly-*n*-dodecyl methacrylate without studying a sample of much higher molecular weight.

### *Monomeric Friction Coefficient*

By fitting the relaxation spectrum to the left of the plateau inflection point to the theoretical slope of $-\frac{1}{2}$, the monomeric friction coefficient can be calculated. For this purpose, the root-mean-square end-to-end distance per square root of the number of monomer units, $a$, was taken as 8.75 A. (6). At 100°C., $\log \zeta_0 = -6.57$ (units dynes-sec./cm.), continuing the progressive decrease with increasing side chain length.

### *Relation of Friction Coefficient to Free Volume*

In a previous communication (4), the dependence of friction coefficient on side group length for the methacrylate series was related to the relative free volume at the reference temperature, 100°C., by postulating

$$\Delta \log a^2\zeta_0 = (1/2.303)(1/f_i - 1/f_B), \qquad [3]$$

where $\Delta$ refers to the difference between the values for a given polymer $i$ and another chosen as a reference for comparison—in this case the butyl; $f_i$ and $f_B$ are the relative free volumes in the two polymers. This equation, analogous to a similar one for the temperature dependence of $a^2\zeta_0$ (12, 20), was tested by comparing $f_i$ calculated from Eq. [3] with that calculated from the data of Rogers and Mandelkern (7) using their conclusion that 15% of the added specific volume associated with side chain length can be attributed to free volume. The comparison must now be revised slightly because of the new analysis of data for the butyl, hexyl, and octyl polymers taking into account the temperature-dependent entanglement anomaly. The revised figures, to which those for the dodecyl polymer have now been added, are given in Table III, and show again moderately good agreement.

Fujita and Kishimoto (21) have since given a more general treatment of the dependence of $\zeta_0$ on free volume, which starts also from Eq. [3] but

TABLE III

*Relation of $\zeta_0$ to Free Volume*

| Polymer | Ethyl | $n$-Butyl | $n$-Hexyl | $n$-Octyl | $n$-Dodecyl |
|---|---|---|---|---|---|
| Log $\zeta_0$ at 100°C. | −0.21 | −3.44 | −5.25 | −5.93 | −6.57 |
| $f$ at 100° from data of Ref. (6) | 0.033 | 0.042 | 0.047 | 0.050 | 0.055 |
| $f$ at 100° from Eq. [3] | 0.033 | (0.042) | 0.050 | 0.055 | 0.058 |
| Log $a^2\zeta_0$ at 62°C. | −8.19 | −15.03 | −17.60 | −18.71 | −19.45 |
| $\Delta T_g$ (from ethyl) | 0 | 35 | 67 | 82 | 108 |

employs specific volume data directly so that the 15% apportionment of Rogers and Mandelkern is unnecessary. When a given polymer $i$ of the methacrylate series is compared with a reference polymer 1, at the $T_g$ of the latter, the relation of Fujita and Kishimoto is in our notation

$$-1/\Delta \log a^2\zeta_0 = 2.303\, f_{g1} + 2.303\, f^2_{g1}/\Delta\alpha_i\Delta T_g, \qquad [4]$$

where $\Delta\alpha_i$ is the difference between the thermal expansion coefficients above and below $T_g$ for polymer $i$, and $\Delta T_g$ is the difference between the glass transition temperature of polymer 1 and polymer $i$. By plotting $1/\Delta \log a^2\zeta_0$ against $1/\Delta\alpha_i\Delta T_g$, the linear form of the equation can be tested and the value of $f_{g1}$ obtained independently of any other information.

Fujita and Kishimoto chose polymethyl methacrylate as polymer 1, using stress relaxation data of McLoughlin and Tobolsky (22), and made the comparison at 100°C. But because of the complications of the $\beta$-mechanism in the temperature reduction for the methyl polymer (23), and failure of data from various laboratories to agree, we prefer to base the comparison on polyethyl methacrylate at $T'_{g1} = 62°$C. Another slight difference from the Fujita-Kishimoto procedure is that we use actual values of $a^2\zeta_0$, instead of measuring horizontal displacements of the relaxation spectrum ignoring the differences in $\rho/M_0$ from one polymer to another. (Here $\rho$ is density and $M_0$ is monomeric molecular weight.) Also, we now can include the octyl and dodecyl polymers in the comparison. For this purpose, $\Delta\alpha_i$ was taken as $2.4 \times 10^{-4}$ deg.$^{-1}$ for all the polymers, and $T_g$ for the dodecyl polymer as −46°. The appropriate data for this treatment are also listed in Table III, and the test plot is shown in Fig. 8. The linearity is quite good, and the values of $f_g$ obtained are 0.026 from the intercept and 0.018 from the slope. Fujita and Kishimoto obtained 0.019 from both intercept and slope. The value from WLF analysis of the temperature dependence of relaxation times for polyethyl methacrylate is 0.025. The general agreement in magnitude lends confidence to the view that the free volume is the primary influence in determining the dependence of friction coefficient on side group length.

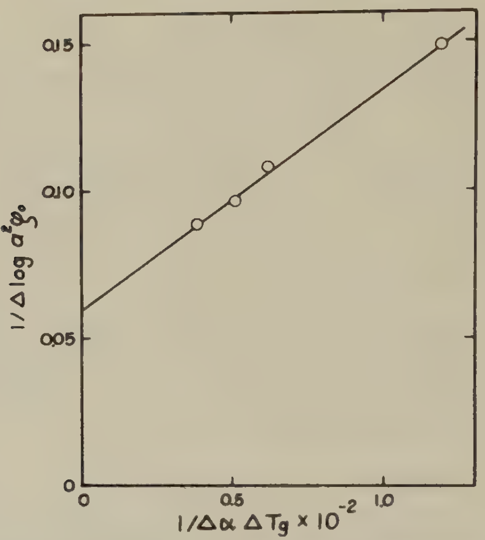

FIG. 8. Fujita-Kishimoto plot for four methacrylate polymers, based on polyethyl methacrylate at its $T_g$ as reference.

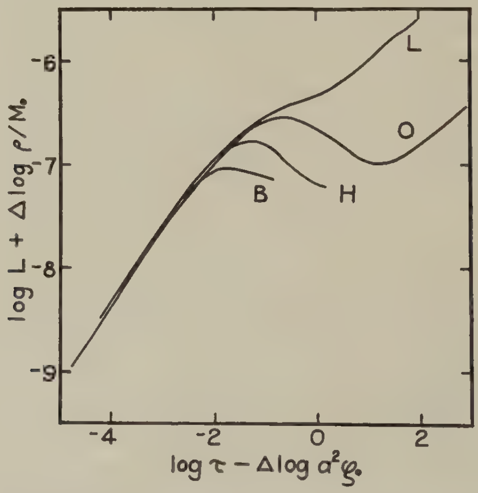

FIG. 9. Retardation spectra of four methacrylate polymers, identified as in Fig. 6, each reduced to the reference state of the $n$-butyl at 100°C. by the procedure described in the text.

### *Comparison of Retardation Spectra in Corresponding States*

In a preceding paper (4), it was shown that the retardation spectra for the methacrylate polymers from ethyl through octyl coincided rather closely in the transition zone when $\log L + \Delta \log \rho/M_0$ was plotted against log

$\tau - \Delta \log a^2\zeta_0$. Here $\Delta$, as in Eq. [3], refers to the difference between values for a given polymer and the butyl as reference; the term added to log $L$ takes into account the expected proportionality of the magnitude of spectral contributions to $\rho/M_0$. A new plot, embodying revisions due to the entanglement anomaly analysis (5), is shown in Fig. 9. The coincidence through the transition zone is very close; but the divergence near the maximum in $L$ which appeared previously is now accentuated. If the differences are interpreted in the same manner as the temperature dependence of the maximum in a single polymer, they imply that the average spacing between entanglements increases with increasing side group length. Shifts along a line with a slope ½ on the doubly logarithmic plot, with approximate matching of shapes, lead to the ratios 1:1.8:3.1 for the distance between entanglements in butyl:hexyl:octyl. Since the dodecyl does not have a well-defined maximum, it is not possible to obtain a ratio octyl:dodecyl in this manner to check the value 240:650 estimated above from plateau widths.

## ACKNOWLEDGMENTS

This work was supported in part by Picatinny Arsenal, Ordnance Corps, Department of the Army, and in part by the Research Committee of the Graduate School of the University of Wisconsin from funds supplied by the Wisconsin Alumni Research Foundation. We are much indebted to Dr. Donald J. Plazek for advice and help with the apparatus; to Mr. Kazuhiko Ninomiya for discussion of approximations for interconversion of viscoelastic data; and to Mrs. Garrett P. Droppers, Mrs. W. C. Frazier, and Miss Rowena M. Green for help with the calculations.

## SUMMARY

The real ($J'$) and imaginary ($J''$) components of the complex compliance have been measured between 24 and 3600 cycles/sec. in the temperature range from $-40°$ to $45°$ C. for a fractionated poly-$n$-dodecyl methacrylate with molecular weight $0.95 \times 10^6$. The creep compliance, $J(t)$, was measured from $-30°$ to 30°C. The method of reduced variables gave superposed curves for $J'$ and $J''$ against frequency and for $J(t)$ against time except for an anomaly at and below $-28°$, interpreted as due to crystallization of the side groups. The temperature dependence of relaxation times followed the WLF form with $\alpha_f$ (thermal expansion coefficient of free volume) = $3.7 \times 10^{-4}$ deg.$^{-1}$. The retardation and relaxation spectra, combining dynamic and creep data, show a rudimentary plateau region from which the average spacing between entanglement points is estimated to correspond to a degree of polymerization of 650. The logarithm of the monomeric friction coefficient (in dynes-sec./cm.) is $-6.57$ extrapolated to 100°C. The dependence of friction coefficient on side group length in the methacrylate series, using revised data including now those for the dodecyl polymer, can be rather satisfactorily attributed to differences in free volume

by either the treatment of Dannhauser, Child, and Ferry or that of Fujita and Kishimoto.

## REFERENCES

1. Ferry, J. D., Child, W. C., Jr., Zand, R., Stern, D. M., Williams, M. L., and Landel, R. F., *J. Colloid Sci.* **12,** 53 (1957).
2. Child, W. C., Jr., and Ferry, J. D., *J. Colloid Sci.* **12,** 327 (1957).
3. Child, W. C., Jr., and Ferry, J. D., *J. Colloid Sci.* **12,** 389 (1957).
4. Dannhauser, W., Child, W. C., Jr., and Ferry, J. D., *J. Colloid Sci.* **13,** 103 (1958).
5. Berge, J. W., Saunders, P. R., and Ferry, J. D., *J. Colloid Sci.* **14,** 135 (1959).
6. Chinai, S. N., to be published.
7. Rogers, S. S., and Mandelkern, L., *J. Phys. Chem.* **61,** 985 (1957).
8. Fitzgerald, E. R., *J. Chem. Phys.* **27,** 1180 (1957).
9. Plazek, D. J., Vrancken, M. N., and Berge, J. W., *Trans. Soc. Rheology* **2** (in press).
10. Berge, J. W., Ph.D. Thesis, University of Wisconsin, Madison, 1958.
11. Ninomiya, K., and Ferry, J. D., *J. Colloid Sci.* **14,** 36 (1959).
12. Williams, M. L., Landel, R. F., and Ferry, J. D., *J. Am. Chem. Soc.* **77,** 3701 (1955).
13. Stern, D. M., Ph.D. Thesis, University of Wisconsin, Madison, 1957.
14. Landel, R. F., and Ferry, J. D., *J. Phys. Chem.* **60,** 294 (1956).
15. Greenberg, S. A., and Alfrey, T., *J. Am. Chem. Soc.* **76,** 6280 (1954).
16. Williams, M. L., and Ferry, J. D., *J. Polymer Sci.* **11,** 169 (1953).
17. Smith, T. L., *Trans. Soc. Rheology* **2** (in press).
18. Ferry, J. D., and Williams, M. L., *J. Colloid Sci.* **7,** 347 (1952).
19. Ferry, J. D., Landel, R. F., and Williams, M. L., *J. Appl. Phys.* **26,** 359 (1955).
20. Ferry, J. D., and Landel, R. F., *Kolloid-Z.* **148,** 1 (1956).
21. Fujita, H., and Kishimoto, A., *J. Colloid Sci.* **13,** 418 (1958).
22. McLoughlin, J. R., and Tobolsky, A. V., *J. Colloid. Sci.* **7,** 355 (1952).
23. Iwayanagi, S., *J. Sci. Research Inst. (Tokyo)* **49,** 4 (1955).

JOURNAL OF COLLOID SCIENCE **14**, 161–167 (1959)

# SOLUBILITY OF SODIUM CHLORIDE IN ORGANIC SOLVENTS WITH AEROSOL OT IN THE PRESENCE OF MOISTURE[1]

**Claude M. Aebi[2] and Joseph R. Wiebush**

*National Institute of Drycleaning, Silver Spring, Maryland*

*Received October 22, 1958*

## ABSTRACT

Measurements were made of the solubility of NaCl in perchlorethylene and in dodecane solutions of dioctyl sodium sulfosuccinate (Aerosol OT), in the presence of various amounts of water. Part of this water was found to be bonded to the detergent and not available for the solution of NaCl. The addition of water to an anhydrous solution of Aerosol OT produced a progressive ionization of the detergent. The micelles of the studied systems were all saturated with detergent, which explains the constancy of the sodium chloride solubility for the studied range of water content.

## INTRODUCTION

Removal of water-soluble soils from fabrics is one of the main problems of the drycleaning process. Sodium chloride is a typical ingredient of perspiration and food stains. The physical chemistry of the drycleaning bath is not well understood. There have been no quantitative data to explain the solubility mechanism for such inorganic materials in the organic solvent system.

Most of the studies which have been made on nonaqueous systems up to now have been ternary systems composed of a solvent, detergent, and a solubilized substance which was usually an organic material such as a dyestuff, added to make the study of the micellar system possible (1, 2).

The study presented here concerns a quaternary system of solvent, detergent, water, and salt. The choice of such a system has not been arbitrary. It corresponds exactly to the working conditions encountered in the drycleaning bath.

## MATERIAL

Dioctyl sodium sulfosuccinate—more widely known as Aerosol OT (AOT)—was chosen as the surface-active agent because it has been studied in ternary systems and its properties are generally known. It is obtainable in a pure state and has been used in drycleaning formulations. Commercial detergents have been avoided for this study, because their precise composition is usually unknown. Aerosol OT 100 %, solid, was obtained from American Cyanamid Company (3).

---

[1] Presented during the Symposium on Micellization, Solubilization and Detergency in Solvents of Low Dielectric Constant, Division of Colloid Chemistry, 133rd Meeting of the American Chemical Society, April 13–18, 1958, San Francisco, California.

[2] Present Address: International Business Machines, Endicott, New York.

Perchlorethylene (Stauffer Chemical Company, New York), drycleaning grade, was twice redistilled. The fraction between 120° and 121°C. was used for the experiments. Theoretical boiling point: 121.02°C.

*n*-Dodecane, practical grade, was obtained from Eastman Organic Chemicals. It was twice redistilled under vacuum.

All other chemicals were certified reagents (Fisher Scientific Company).

## Experimental Procedure

### *A. Preparation of the Solutions*

AOT solutions in perchlorethylene and in dodecane were prepared a few hours before saturation with sodium chloride. The water was added to the solutions by a microburet. Samples with very small amounts of water were prepared by diluting systems of high water content with solvent solutions of the same detergent concentration.

After dispersing the water in the solvent—detergent system, 0.5 g. of NaCl were added to each sample formed of 30–50 ml. solution. Addition of water directly on the crystals of NaCl gave erroneous results.

### *B. Saturation*

The solutions were placed in 100 ml. volumetric flasks and treated at room temperature (72°–75°F.).

*1.* On the laboratory shaker used in the case of the perchlorethylene solutions, 20 hours of shaking was sufficient to obtain saturation. Control samples were shaken for 100 hours to be sure that the system had reached its equilibrium.

*2.* Ultrasonic agitation was used to saturate the solutions of *n*-dodecane, as reproducible results could not be obtained with the shaking method. The volumetric flasks were immersed in a water bath with a transducer in the bottom. The frequency used was 26 and 40 kilocycles per second. The saturation was obtained after 5 minutes of ultrasonic treatment. In order to check if complete saturation was reached for the perchlorethylene solutions, some of these samples were also saturated with the help of ultrasounds. The results correspond to those obtained by mechanical agitation.

The treatment with ultrasounds serves only the purpose of saturating a solution in minutes which would take days or weeks by simple shaking. This method can give solutions which seem to be oversaturated, the salt crystals being broken into ultrafine particles which, once in suspension, have great difficulty settling out again. Even centrifuging does not seem to be of much help in accelerating the settling. Ultrasonics may also generate heat although saturation was not carried out at an exact temperature. For these reasons, the samples were shaken for 24 to 48 hours following ultrasonic treatment so that equilibrium was assured.

The relative difficulty of saturating the perchlorethylene and *n*-dodecane solutions may be partially explained by the difference in viscosities of the two solvents, and by a possible difference of NaCl solubility in the pure solvents.

*Viscosity at 25°C.*

| | |
|---|---|
| *n*-Dodecane | 1.344 cp. |
| Perchlorethylene | 0.839 cp. |
| 0.1 *M* solution of AOT in *n*-dodecane | 1.529 cp. |
| 0.1 *M* solution of AOT in perchlorethylene | 0.946 cp. |

### *C. Titrations*

The amount of water in solution was determined by the Karl Fisher method as modified by Martin and Lloyd (4). The precision of moisture measurement was ±0.1 mg. $H_2O$.

Sodium chloride was determined by a modification of the method of F. E. Clarke (5), which permitted titration in an organic medium. The following procedure was used for *n*-dodecane solutions: To 10 ml. of acetone or propyl alcohol, 6 drops of approximately 0.05 *N* nitric acid, and 1 drop of diphenyl-carbazone—bromophenol blue indicator were added. The solution was neutralized to a blue color with a mercuric nitrate solution, approximately 0.05 *N*, pH 3.5 to 4.0. Then 5 ml. of the *n*-dodecane solution saturated with salt was added and titrated under good agitation with the $Hg(NO_3)_2$ solution.

For perchlorethylene solutions, alcoholic solution of mercuric nitrate is advantageous to prevent the formation of a white emulsion which makes the observation of the end point difficult. In both cases reproductivity of the results is good: using a semimicro buret, amounts of NaCl from 0.05 to 2.5 mg. can be measured with a precision of ±0.02 mg. or better.

## Results and Discussion

Figures 1 and 2 present the results obtained for perchlorethylene and *n*-dodecane solutions, 0.05 *M* and 0.1 *M* in detergent. It will be noticed that the four curves are nearly parallel. The extrapolation of each curve cuts the *X*-axis at almost identical values for the same detergent concentration. The ratio of $H_2O$ molecules to detergent molecules is $1.55 \pm 0.05$ for all four points. The phenomenon, then, is independent of the nature of the solvent but it depends upon the relative quantities of water and detergent present in the solution. Furthermore, there is a proportionality between the amount of NaCl and water which is independent of the detergent con-

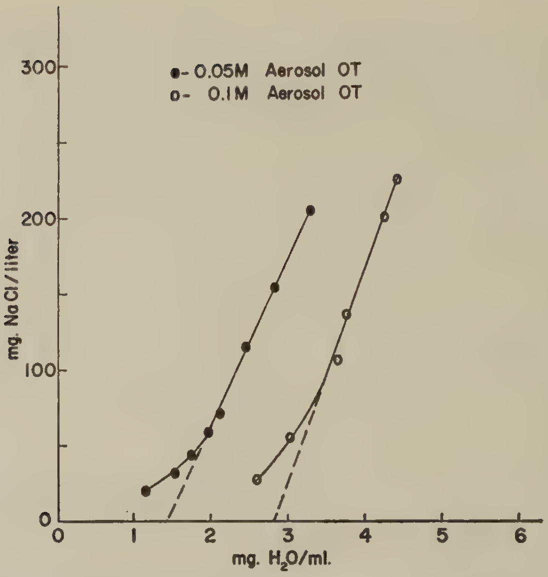

FIG. 1. Solubility of NaCl in *n*-dodecane solutions.

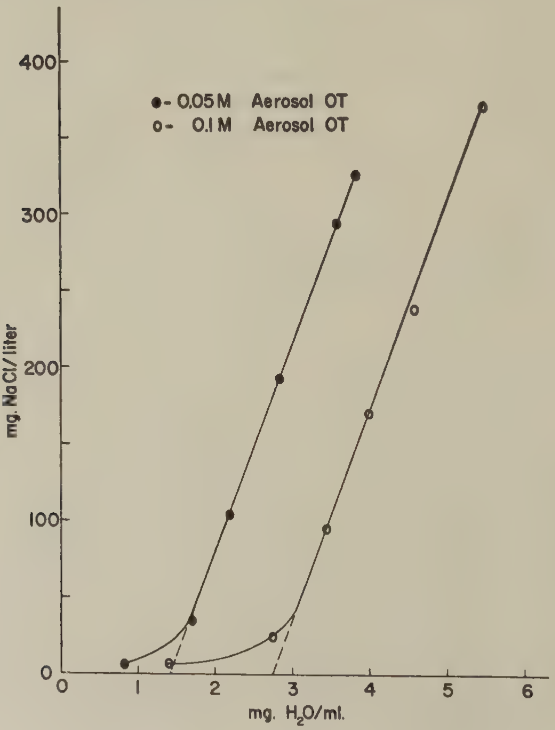

FIG. 2. Solubility of NaCl in perchlorethylene solutions.

centration in the system except near the origin of the curve. This leads to the first conclusion, that sodium chloride is dissolved in the water which is inside the micelles. The solubility is much below the expected solubility of sodium chloride in an equivalent amount of pure water:

140.5 g. NaCl/liter $H_2O$ in the micellar system.
370 g. NaCl/liter in bulk water.

Consider now the beginning of the curves. It is evident that a definite amount of water, proportional to the amount of detergent, must be added before the solution of salt begins. There are two possible explanations for this. First: there may be hydration water, or second, a definite amount of water inside of each micelle may be needed before the solution of NaCl can begin.

## INTERPRETATION OF THE RESULTS

The data can be discussed quantitatively if the following assumptions are made:

*1.* 1.55 moles of water per mole AOT are so associated with the detergent that they are not available for NaCl dissolution.

*2.* The constants for bulk solutions apply to the solution of NaCl in the water which is not bonded to the detergent.

*3a.* The activity coefficients of NaCl and AOT in the micellar system are approximately equal. All the sodium ions from AOT are available in the aqueous phase inside the micelles.

The solubility product for NaCl can then be written:

$$K_{sp} = \gamma_{\mathrm{NaCl}}[C_{\mathrm{Cl}} \cdot (\underset{\mathrm{NaCl}}{C_{\mathrm{Na}}} + \underset{\mathrm{AOT}}{C_{\mathrm{Na}}})],$$

where $C$ is the concentration that would result from complete dissociation of both salts and $\gamma$ is the mean activity coefficient for NaCl in the saturated solution.

The term in square brackets can readily be calculated for different water contents of the solution. AOT can be considered as dissolved in the total water. But the equation still contains two unknowns, $\gamma$ and $K_{sp}$. By means of the equation found by Harned and Nims (6), $\gamma$ can be calculated for a saturated sodium chloride solution. This paper gives values for solutions up to 4 $N$. The validity of this equation was extrapolated up to a normality of 6.14 (saturated solution) and gave a value of $\gamma_{\mathrm{NaCl}} = 0.97$ with a probable error of ±5%. Robinson and Stokes (7) found a value of 0.98 for a 6 $N$ NaCl solution. For convenience of calculation, a value of $\gamma = 1.0$ was chosen, making $K_{sp} = 37.7$ for a saturated sodium chloride solution. By putting these values in the equation, $\gamma$ then varies from 0.5 to 1.0. The results appear in Table I.

TABLE I

*Mean Activity Coefficient and AOT Dissociation Calculated from the Solubility Product Equation*

| Total $H_2O$/l. solution (g.) | Moles AOT/l. $H_2O$ | Grams NaCl/l. solution | Activity coefficient | Dissociated AOT/l. free $H_2O$ |
|---|---|---|---|---|
| | | | | *(moles)* |
| 1.7 | 29.42 | 0.035 | 0.495 | 13.4 |
| 1.8 | 27.78 | 0.051 | 0.510 | 13.0 |
| 2.0 | 25.00 | 0.080 | 0.590 | 12.5 |
| 2.2 | 22.75 | 0.105 | 0.625 | 13.4 |
| 2.5 | 20.00 | 0.146 | 0.714 | 14.2 |
| 2.9 | 17.23 | 0.200 | 0.815 | 13.6 |
| 3.3 | 15.14 | 0.253 | 0.933 | 13.8 |
| 3.66 | 13.67 | 0.300 | 1.01 | 14.2 |
| 3.84 | 13.02 | 0.326 | 1.05 | 15.8 |

*3b.* It now can be assumed that the activity coefficient of NaCl in a saturated solution is approximately 1, and that only sufficient AOT has dissolved in each case to satisfy $K_{sp}$ for NaCl in the system.

According to Table I, the solubility of AOT in the micellar system is extremely high. This solubility cannot be compared to what happens in bulk water; in the micelles, nothing else but the inorganic ends of the detergent molecules are dissolved in the water. But even so, the solubility of AOT is extremely high.

This leads to the hypothesis that the micellar water is "saturated" with the detergent: One part only of AOT is dissociated—that is, "dissolved"—in the water core of the micelles. The rest of it behaves like a solidus at the bottom of a saturated solution.

AOT is then coordinately bonded to the sodium until enough water is present to hydrate the sodium ions. The addition of water causes a progressive ionization of the detergent. These views are supported by the fact that the solubility of NaCl is constant for ratios of moles $H_2O$ per mole AOT between 2 and 4.1.

For ratios below 2 moles $H_2O$ per mole AOT, the solubility of NaCl falls sharply, indicating that most of the water is used for the hydration of the detergent. This has been postulated (8) to explain the diminution of the apparent specific volume of water when the micelles contain only small amounts of water. Singleterry (9) also indicates that water is coordinately bound to the metal ion of the detergent. This water is not available for NaCl dissolution.

Assuming the micellar water saturated with salt and detergent, the solubility product equation can still be written; the concentration of the dissociated AOT is then an unknown constant. By solving the expression with $\gamma_{NaCl} = 1.0$, $K_{sp} = 37.7$, and a solubility of 140.5 g. NaCl per liter of micellar water as determined by the slope of the solubility curve, the concentration of the dissociated AOT is found to be 13.3 moles per liter of micellar water. This apparent solubility in a saturated salt solution has been computed for each point referred to in Table I. An average value of 13.7 ± 0.6 moles AOT per liter of micellar water was found, that is 4.1 ± 0.2 moles $H_2O$ per mole AOT. If more water is added, the solution becomes unsaturated in detergent which, in turn, increases the solubility of NaCl.

Solutions with the highest water content which could be studied as clear solutions contained 4.2 moles $H_2O$ per mole AOT. The slightest addition of water to these solutions made them cloudy, and further addition of water gave a two-layer solution. But for now, no facts allow any connection between the appearance of the cloudy solution and the complete ionization of the detergent.

## Summary

In short, the system which was studied contained four components: an inert organic solvent, a detergent which dispersed in the solvent in the micellar form, water which was held by the detergent, and sodium chloride as a solute. The water is held by the detergent in two states: (*1*) bound water which is proportional to the concentration of the detergent and which is not available for the solution of NaCl; and (*2*) free water which is available for the solution of NaCl. The sodium chloride dissolves in any free water much as it would in ordinary bulk water.

Furthermore, for the studied range of moisture content, the micelles were found to be saturated with detergent and NaCl. AOT is soluble in the micellar water to the extent of 13.7 moles per liter. The addition of water to an anhydrous solution of AOT produces a progressive ionization of the detergent. Since all the solutions were saturated with AOT, this explains the constancy of the NaCl concentration in the available micellar water.

## Acknowledgment

The author wishes to express his thanks to Dr. Curtis R. Singleterry for his valuable suggestions and interest in this work.

## References

1. McBain, M. E. L., and Hutchinson, E., "Solubilization," pp. 47–50. Academic Press, New York, 1955.
2. Kaufman, S., and Singleterry, C. R., *J. Colloid Sci.* **10,** 139 (1955).
3. "Aerosol—Surface Active Agents". American Cyanamid Company (booklet).
4. Martin, A. R., and Lloyd, A. C., *J. Am. Oil Chemists' Soc.* **12,** 594–597 (1953).
5. Clarke, F. E., *Anal. Chem.* **22,** 533 (1950).
6. Harned, H. S., and Nims, L. F., *J. Am. Chem. Soc.* **54,** 423 (1932).
7. Robinson, R. A., and Stokes, R. H., "Electrolyte Solutions." Academic Press, New York, 1955.
8. Mathews, M. B., and Hirschhorn, E., *J. Colloid Sci.* **8,** 86–96 (1953).
9. Singleterry, C. R., Private communication.

JOURNAL OF COLLOID SCIENCE **14**, 168–174 (1959)

# A NUMERICAL APPROACH TO THE PROBLEM OF SEDIMENT VOLUME[1]

**Marjorie J. Vold**

*The Department of Chemistry, University of Southern California*
*University Park, Los Angeles, California*

*Received October 30, 1958*

## Abstract

The observed sediment volume of 3.5 c.c./gram for moist spheres in hydrocarbon solvents is shown to correspond exactly to a model in which each sphere coheres rigidly to the first sphere it contacts, but is inconsistent with strong forces operative over an appreciable range of distance. The mean number of neighbors for each sphere in this type of packing is 2.0. Sediment structure is more sensitive to the breadth of the size distribution than is sediment volume.

It seems to be an accepted principle that if a suspension dilute enough for each ultimate particle to be separated from every other is allowed to settle quietly, under gravity, the volume occupied by the sediment will gradually approach constancy, and will depend, among other factors, on the extent to which the particles cohere on first contact with each other to form loose voluminous aggregates in contrast with the compact packing that would ensue if each particle could slide freely over or around others to fill in interstices as efficiently as is consistent with random packing of particles of the given shape.

Careful work by a number of authors (for example, references 1, 2) has established that for glass spheres of fairly uniform size a minimum packing volume of 0.67 c.c./gram (close to 0.64 volume fraction) is established in polar solvents whereas moist spheres in nonpolar solvents run close to 3.5 c.c./gram or about 0.125 fraction.

Working with models, Chomse (3) gave objective results to support the reasonable presumption that anisometric particles settle to a looser packing than do spheres under the same conditions of interaction. Ross and Shaeffer's (4) finding that the sediment volume of graphite increases with increased surface area could be a manifestation of the same phenomenon,

---

[1] The initial stages of this work were supported by the Office of Scientific Research, contract No. AF 18-603-122 directed by H. L. Frisch and administered during the period by K. J. Mysels. It is being continued by the Office of Ordnance Research, contract No. DA-04-495-ORD-1296 directed by M. J. Vold.

the larger areas corresponding to relatively thinner plates compared to their mean width, although direct data are lacking. Vold (5) has reported volume fractions as low as 0.005 in suspensions of lithium stearate where the length-to-width ratio of the rod-shaped particles averages at least 10.

These results substantiate the argument that sediment volume depends on both particle shape and particle interaction.

The general object of the program the first results of which are reported here is to calculate numerically the sediment volume to be expected for various models of particle interaction, taking the readily determined shape factors into account, in order that this relatively straightforward measurement may become a tool for the direct study of interparticle forces.

The results here reported are confined to spherical particles. It is demonstrated that the packing fraction of 0.125 for moist glass spheres in hydrocarbon solvents is consistent with a model in which the particles cohere firmly on initial contact, but is inconsistent with the supposition that strong attractice forces exist which are influential over distances of the order of the particle radius. The calculations result also in a measure of the fraction of particles in the sediment which pack in contact with various numbers of neighbors, leading to the supposition that measurements of the yield value of such sediments may be able to measure the absolute value of the cohesive force per interparticle contact.

## Model and Method of Calculation

The physical process envisaged is that of distributing spherical particles randomly (but in macroscopically homogeneous fashion) throughout a very large volume, so that each one falls vertically under gravity. Each particle is presumed to cohere permanently to the first particle it encounters on the way down. Under these conditions the structure and final volume is not affected by the rate of fall of the particles and is identical with that which would obtain if each particle were dropped in individually.

The process of dropping $N$ spherical particles one by one into a container, allowing each one to stick at rest where it strikes either the bottom or a previously dropped particle, and of noting the number of neighbors each one eventually accumulates, together with the volume occupied by the particles at the end of the process, has been simulated with the aid of an electronic digital computer (NCR 102D, Engineering Center, U. S. C.). A slight modification, simulating longer range interparticle forces, allowed a particle to stick at rest against the first previously dropped particle which it approached within a prescribed distance $2\delta$.

To accomplish this process in the computer, $x$ and $y$ coordinates between 0 and 100 for the centers of the $N$ spheres were obtained from a table of random digits (6). For a given sphere $n$, the quantity

$$D_{ni}^2 = (x_n - x_i)^2 + (y_n - y_i)^2$$

was then computed for $i = 1, 2 \cdots (n - 1)$ (the previously dropped particles). For all cases in which

$$D_{ni}^2 \leq (r_n + r_i)^2 = R_{ni}^2 ,$$

where $r_n$ and $r_i$ are the radii of the particles, the further quantity

$$Z_n = Z_i + (R_{ni}^2 - D_{ni}^2)^{1/2}$$

was computed and the largest of these, together with the value of $i$ producing it, was recorded.

Provision was made for recalculating the $x$ and $y$ coordinates for a particle being attracted to another when it approached within the distance $2\delta$.

The result of the computation, then, is a table giving the final $x$, $y$, and $z$ coordinates of each particle, together with a table of digits which tells which particles came to rest in contact with each other. From these the volume fraction, tests for uniformity of packing, and contact numbers can be obtained by inspection.

The memory capacity of the available computer limited the number of particles that could be handled to 160. It was found that the packing of particles was invariably more dense for those near the bottom and edges of the container and much less dense for those near the top, where large holes remained that would have been filled in were $N$ larger. However, after the first 100, a substantial central core of the container had reached a density of particles which did not change appreciably when the last 60 were added, so that even without a proper analysis of the statistical significance of the results, it is felt that conclusions from them are entirely valid. Their acceptability is further substantiated by finding that very close agreement was obtained in "duplicate experiments" with a different selection of initial coordinates from the table of random digits.

## Results and Discussion

In all, nine separate runs were made. Three of these were with spheres of equal radius and varying tables of random numbers for the $x$ and $y$ coordinates of the spheres. The fourth varied the radius of the sphere in relation to the diameter of the container. The fifth and sixth were for the distribution of sphere sizes shown in Fig. 1. In each of these cases particles were allowed to come to rest only on direct contact. In runs 7, 8, and 9 the particles were made to stick in contact with the first particle which they approached within a distance $2\delta$($\delta$ being one fourth, one half, or one particle radius) moving into contact along the line of centers as shown in Fig. 2.

Results for volume fraction are shown in Table I, and in terms of sediment volume for glass spheres of density 2.3 in Fig. 3. In Fig. 4 the same data are presented in terms of volume fraction of solids in the sediment.

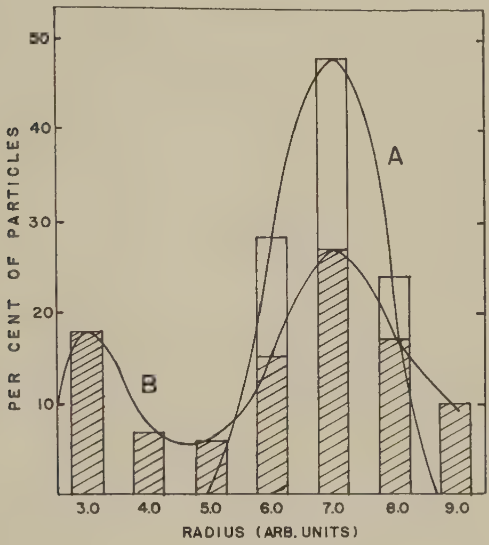

FIG. 1. Distributions of radii in model sedimenting suspensions. On the same scale the container is 100 units on edge.

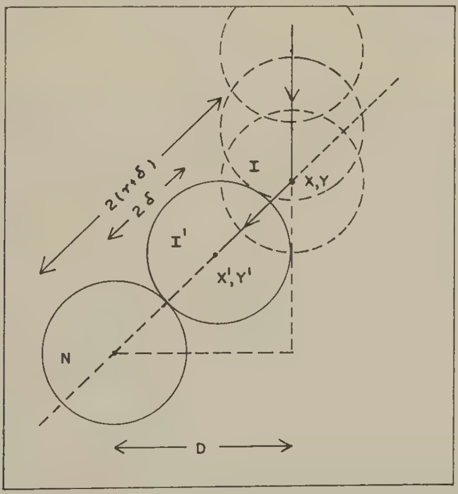

FIG. 2. Assumed path of particle $I$, attracted to particle $N$, beginning at separation $2\delta$.

Figure 4 is thus quite general, while Fig. 3 permits direct comparison with model systems, which are most frequently glass spheres.

The results for spheres of equal radius, which average 0.128, are in rather spectacular accord with the experimentally established value of 0.125. That the result is not very sensitive to size distribution is shown

TABLE I

*Sediment Volume of Spheres*

| Run | No. of particles | Particle radius[a] | Range of attraction | Vol. fraction |
|---|---|---|---|---|
| 1 | 108 | 10 | 0 | 0.132 |
| 2 | 155 | 10 | 0 | 0.127 |
| 3 | 155 | 10 | 0 | 0.128 |
| 4 | 155 | 7 | 0 | 0.126 |
| 5 | 150 | D1[b] | 0 | 0.122 |
| 6 | 150 | D2[b] | 0 | 0.124 |
| 7 | 140 | 7 | 0.25 r | 0.110 |
| 8 | 160 | 7 | 0.5 r | 0.095 |
| 9 | 142 | 7 | 1.0 r | 0.058 |

[a] Arbitrary units. On the same scale the container had a diameter of 100 units.

[b] See Fig. 1 for distribution of radii.

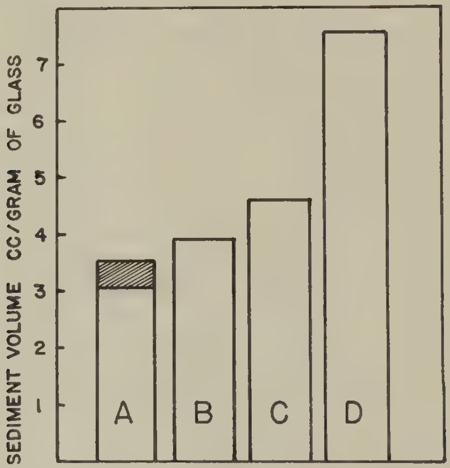

FIG. 3. Sediment volume of glass spheres. *A*, experimental result and model for surface forces. Shaded area shows variations for computations with varying conditions. *B*, *C*, *D*, range of forces 0.25 *r*, 0.50 *r*, and 1.00 *r*, respectively.

by runs 5 and 6. Presumably for a somewhat different model in which the spheres are able to slide past each other wide size distributions would pack more densely than narrow ones. In this case the very small difference, which is probably not significant, is actually in the opposite direction.

In contrast to its insensitivity to size distribution, the calculated packing volume is exceedingly sensitive to the presumption of long-range forces. This fact is shown most clearly in Fig. 4. The origin of the cohesion occurring with moist glass spheres in toluene is well recognized as lying in relative wetting powers of water and hydrocarbon for glass, which requires actual contact to be effective. The circumstance that a relatively small

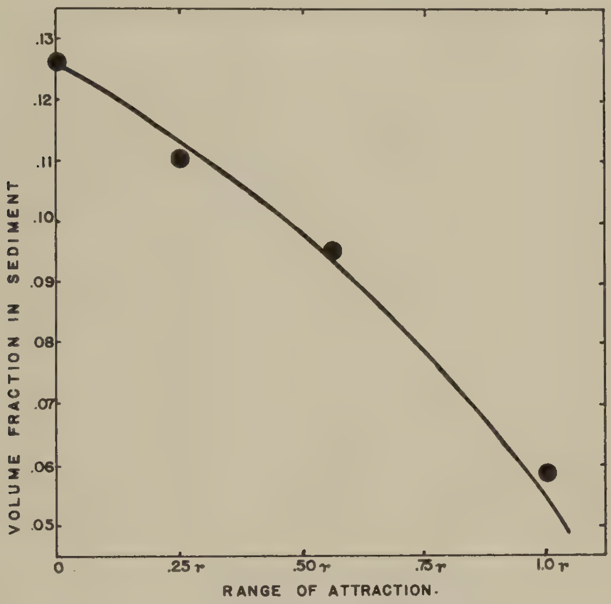

FIG. 4. Volume fraction in the packing of spheres attracting each other over an appreciable distance.

TABLE II

*Structure of the Sediment from Spherical Particles*

| Run | Per cent of particles making $n$ contacts | | | | Mean contact no. |
|---|---|---|---|---|---|
| | $n = 1$ | $n = 2$ | $n = 3$ | $n > 3$ | |
| 2 | 27 | 47 | 25 | 1 | 2.00 |
| 3 | 32 | 45 | 18 | 5 | 1.99 |
| 4 | 20 | 56 | 16 | 8 | 2.06 |
| 5 | 46 | 32 | 20 | 2 | 1.78 |
| 6 | 45 | 26 | 22 | 7 | 1.91 |
| 7 | 25 | 49 | 24 | 2 | 2.03 |
| 8 | 22 | 64 | 14 | — | 1.92 |
| 9 | 13 | 59 | 12 | — | 2.00 |

variation in the model produces a large change in the calculated volume, a very much larger change than the difference between theory and experiment for the reasonable model, leads to considerable hope for the utility of this approach to interpreting sedimentation data.

Results for the structure of the sediment are given in Table II. The mean number of contacts made by each sphere is in the vicinity of two in all cases. That is, on the average, each particle comes to rest first against some other and one more comes to rest against it. The mean contact number of spheres which can slide on each other is estimated by Eggleton and Puddington (2) to be about 9.

It is noteworthy that a substantial portion of the spheres in all cases make only one contact with another sphere. When the sediment is made to flow under shear such bonds do not need to be broken and hence contribute nothing to the observed yield value. These terminal particles are relatively much more numerous for the distributions of sphere sizes than for uniform spheres, and, as is to be expected on intuitive grounds, they are found to consist largely of the smaller particles. For example, for distribution 2, the number-average particle radius is 6.2, while the average radius of particles making only one contact is only 5.8 and the average of those making three or more contacts is 7.7.

The sediment structure is very much more sensitive, for these cases at least, to particle size distribution than to the model used for particle interaction. Accordingly no theory relating yield value or other flow properties to interparticle cohesion can be expected to give satisfactory results unless size distribution is taken into account.

## ACKNOWLEDGMENTS

The author wishes to thank Dr. K. J. Mysels for many valuable suggestions and Prof. E. Jagger for assistance in operating the computer.

## REFERENCES

1. BLOOMQUIST, C. R., AND SHUTT, R. S., *Ind. Eng. Chem.* **32,** 827 (1940).
2. EGGLETON, A. E. J., AND PUDDINGTON, I. E., *Can. J. Chem.* **32,** 86 (1954).
3. CHOMSE, H., *Mikrochemie Mikrochim. Acta,* **36/37,** 1026 (1951).
4. ROSS, S., AND SHAEFFER, H. L., *J. Phys. Chem.* **58,** 865 (1954).
5. VOLD, M. J., *J. Phys. Chem.*, **60,** 439 (1956).
6. "A Table of Random Digits," The Rand Corp., The Free Press, Glencoe, Ill. 1955.

JOURNAL OF COLLOID SCIENCE **14**, 175–189 (1959)

# REPLICA STUDIES OF HABIT-MODIFIED AMMONIUM DIHYDROGEN PHOSPHATE AND AMMONIUM DIHYDROGEN ARSENATE CRYSTALS[1]

**Joseph J. Comer**

*Mineral Constitution Laboratory, College of Mineral Industries, The Pennsylvania State University, University Park, Pennsylvania*

*Received November 25, 1958*

## ABSTRACT

Carbon replicas of fracture surfaces of ammonium dihydrogen phosphate and ammonium dihydrogen arsenate crystals grown from solutions containing chromic, ferric, or stannic ions reveal certain growth features not found in the pure crystals. In some areas a water-insoluble residue is found at the surface. It is believed that this residue is a metal phosphate or arsenate formed during growth of the crystal or occluded from suspension in the solution.

At high concentrations of foreign ions in solution a microstructure has been found, consisting of units tapered in a direction parallel to the $z$-axis of the crystal. Insoluble residues as amorphous films or discrete particles are found concentrated about these units. Similar tapered units visible to the eye are formed at the intersection of the prism and pyramid faces when growth is forced on seed crystals at concentrations of foreign ions sufficiently high to inhibit growth.

Other surface features found repeatedly include layer growth, dendrites, and polygonal boundaries outlined by small particles.

## INTRODUCTION

It has been shown by Kolb and Comer (1) that a habit modification results when crystals of $NH_4H_2PO_4$ are grown from solutions containing certain foreign metal ions. The crystals are tapered toward the $z$-axis, and the degree of tapering generally increases with decreasing solubility of the metal phosphate. Evidence showed that adsorption takes place mainly on the prism sides of the crystal where the phosphate reticular density is highest. It was proposed that tapering of the crystal was caused when the presence of the metal ion at the intersection of the (100) and (101) and (010) and (011) planes inhibited growth and caused successive layers to deposit at a slight distance in from the intersection of these planes. Those ions found to cause habit modification listed in decreasing order of effectiveness are: $Sn^{++++}$, $Cr^{+++}$, $Fe^{+++}$, $Ti^{++++}$, $Au^{+++}$, and $Be^{++}$.

---

[1] This paper was presented in part at the Fourteenth Annual Meeting of the Electron Microscope Society of America at the University of Wisconsin, Madison, Wisconsin, September 10, 1956. Contribution No. 57-103.

The purpose of this investigation was to explore the possibility of using combined electron microscope and electron diffraction techniques to study adsorption and crystal habit modification in crystals of $NH_4H_2PO_4$ and $NH_4H_2AsO_4$ grown from solution.

A recent attempt to study crystal growth and crystal habit modification by means of the replica technique was made by Ames, Cottrell, and Sampson (2), who examined the surface of several inorganic crystals grown from solutions with and without habit modifiers. Because they examined only the natural faces of the crystals they could not be completely certain whether some of the observed structures were introduced in drying the crystal. For this reason they concentrated on aspects of crystal growth already established by means of the optical microscope. More recently Truby (3) used a replica technique to study ice crystals grown from the melt and reported a microstructure of elongated hexagonal prisms varying greatly in size. Hibi (4) has shown by replica studies of natural and cleavage faces of alkali-halide crystals the effect of x-radiation on the development of crystallites. In the present study the surfaces examined were those of freshly fractured crystals. Comparisons between pure crystals and those modified by foreign ions made it possible to establish the existence of some characteristic surface structures for the crystals under examination. Water-insoluble material found on some of the replicas, and of special interest in this study, could have been deposited only during growth of the crystal.

## Experimental

### *a). Method of Growth*

With one exception all the crystals examined were grown from solutions by slow evaporation of the solvent. Saturated solutions of the salts containing added impurities were held at a temperature of 35.0° ± .1°C. Starting with seed crystals of 1–2 mm. in length it required up to 7 days to obtain crystals about 15 mm. in length, depending upon the amount of impurity added. Chromic ions were supplied by adding potassium chrome alum, and ferric ions were supplied by ferric chloride hexahydrate. The stannic ion was added as stannic chloride. Neither the sulfate nor the chloride ion caused any noticeable tapering of the two isomorphous crystals under study. The pH was lowered in some solutions by adding phosphoric acid in order to prevent precipitation of the metal phosphate.

The crystal of $NH_4H_2PO_4$ containing adsorbed chromic ions was grown from a solution initially saturated at 38°C. by keeping evaporation at a minimum and changing equilibrium conditions by lowering the temperature of the solution at a rate of 0.4°C. per day. Starting with seed crystals about 75 mm. in length, rotating in the solution at 60 r.p.m., growth was continued until about 30 mm. of new growth was added to the crystal.

### *b). Replica Techniques*

When enough growth had been obtained on a seed crystal to make it possible to obtain fracture surfaces, the crystal was removed from the solution and dried on filter paper. A fracture surface was obtained by holding the edge of a sharp knife blade on the crystal parallel to the direction of the desired plane and striking the top of the blade lightly with a hammer. It is probable that the fracture occurs along planes in the crystal where the bonding is weak because of strains introduced by the presence of impurity atoms or precipitates. Immediately after they were fractured the crystals were placed in a vacuum evaporating unit and coated with 100–200 A of carbon deposited at angles of incidence of from 20 to 30 degrees to obtain a shadow-casting effect (5). The use of metals for shadow casting was avoided because of their interference in electron diffraction identification of insoluble residue found on the replicas. Except when working with fractures parallel to the (001) plane it was possible to orient the crystal during the evaporation of carbon so that shadows in the replica are parallel to the $z$-axis. Replicas were removed by slowly lowering the crystals replica side up in distilled water. Frequently a water-insoluble residue at the surface of the fracture was transferred to the replica.

### *c). Analyses of Habit-Modified Crystals*

Crystals of $NH_4H_2PO_4$ containing $Cr^{+++}$ were dissolved in distilled water and the $Cr^{(III)}$ was oxidized to $Cr^{(VI)}$ by acidifying with $H_2SO_4$ and boiling with potassium persulfate in the presence of silver nitrate. The color developed by $Cr^{(VI)}$ with 1.5-diphenylcarbohydrazide was measured at 540 m$\mu$ on the G.E. recording spectrophotometer against a reagent blank. Standards were made up of $K_2Cr_2O_7$ with $NH_4H_2PO_4$ added.

Crystals of $NH_4H_2PO_4$ containing the ferric ion were dissolved in water and the ion was reduced to $Fe^{++}$ with hydroxylamine hydrochloride. The color was developed with *o*-phenanthroline and the solution was buffered with sodium citrate and diluted to volume. Measurements were made at 560 m$\mu$ on the G.E. recording spectrophotometer against a reagent blank. Standards were made up of $Fe(NH_4)_2(SO_4)_2 \cdot 6H_2O$ with $NH_4H_2PO_4$ added.

## RESULTS

### *a). Cation Adsorption*

Figure 1 is a graph showing per cent chromium adsorbed versus chromic ion concentration in solution. The adsorption curve starts leveling off at a concentration of $4 \times 10^{-3}$ mole $Cr^{+++}$/liter; crystals grown at this concentration contained 0.057% $Cr^{+++}$. Data published by Kolb and Comer show that tapering also reaches a maximum at this point. At higher con-

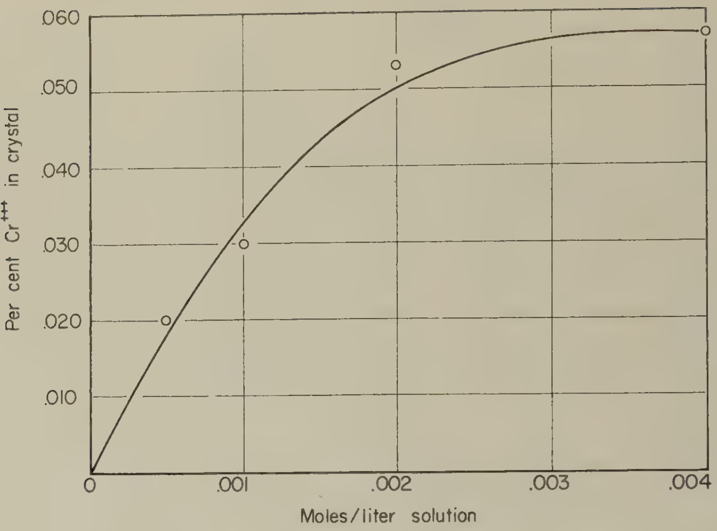

FIG. 1. Adsorption of Cr$^{+++}$ by $NH_4H_2PO_4$ during growth from solution.

centrations of chromic ion growth of the crystal is inhibited. The amount of iron found in crystals of $NH_4H_2PO_4$ grown from solutions containing from $0.5 \times 10^{-3}$ to $2 \times 10^{-3}$ mole Fe$^{+++}$/liter solution was essentially constant at about 0.006%. Kolb and Comer showed that at the same concentration of ferric and chromic ions in solution (approx. $2 \times 10^{-3}$ mole/liter) the tapering caused by the ferric ion is about 6.5 degrees as compared with about 16 degrees for the chromic ion.

### b). *Electron Microscope Studies*

Replicas of fracture surfaces of the pure salts showed, with few exceptions, no surface structure in the crystals. With increasing amounts of impurity certain features were found repeatedly; they consisted of the following types: growth layers, dendrites, precipitates, and mosaic structures. Water-insoluble residues were found adhering to the replicas in many areas.

Figures 2 and 3 show surfaces of $NH_4H_2PO_4$ crystals grown from solutions containing $4 \times 10^{-3}$ mole Cr$^{+++}$ per liter of solution. On only a few surfaces, representing fractures roughly parallel to the intersection of the prism faces, was enough water-insoluble residue found to give electron diffraction patterns by the selected area technique, and these could not be identified. One such area is seen in Fig. 2. The micrographs show growth lines in the area containing the residue running normal to the $z$-axis of the crystal. In addition to the large masses of residue there are many small particles. In areas adjacent to this structure the crystal appears

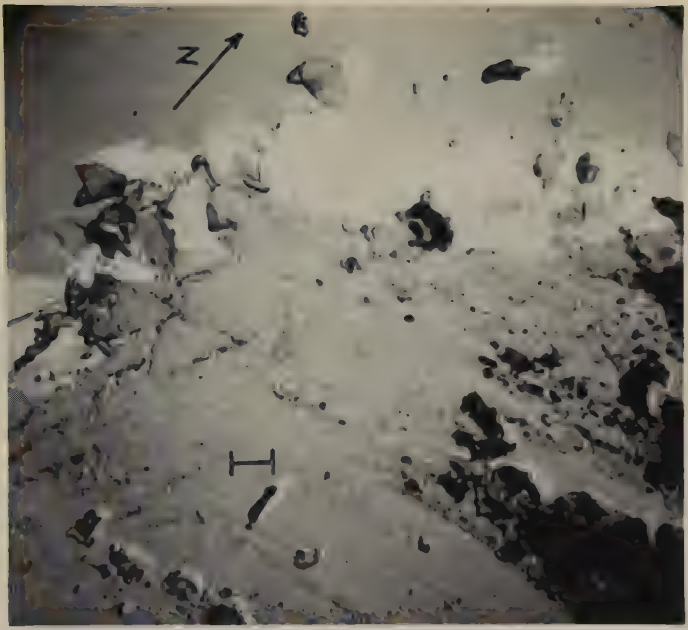

FIG. 2. $NH_4H_2PO_4$ grown from solution containing $4 \times 10^{-3}$ mole $Cr^{+++}$/liter. Fracture surface at intersection of (100) and (010) planes showing water insoluble residue (5000 ×).

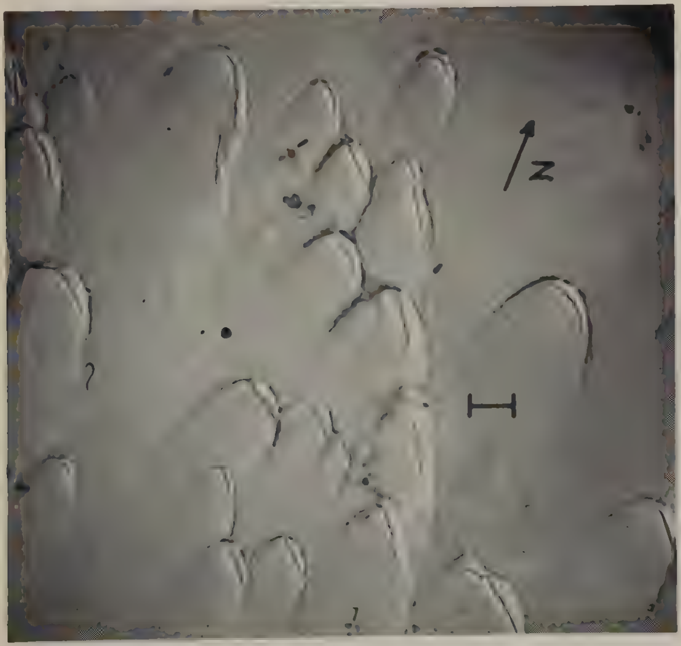

FIG. 3. $NH_4H_2PO_4$ grown from solution containing $4 \times 10^{-3}$ mole $Cr^{+++}$/liter. Fracture surface parallel (100) plane showing tapered microstructure and fine residue (5000 ×).

perfectly smooth, resembling the surfaces found on crystals grown from pure solutions.

In Fig. 3 the tendency is toward growth of microcrystals which are tapered toward the *z*-axis. These units, quite uniform in size, are distributed over a large area. Close observation of the micrograph will show that the area is completely covered with very small discrete particles about 300 to 400 A in size. Figure 4 is a micrograph of a crystal containing the ferric ion as an impurity. This shows a tapered microstructure with a greater variation in size. The opaque areas visible on the microcrystals are probably caused by the overlapping of a second layer of carbon film formed on the under surface of these particles. However, distributed around and on the particles is a very fine residue. Figure 5 shows the tapered structure on crystals of $NH_4H_2AsO_4$ containing ferric ions. Here the presence of shadows from the opaque material shows conclusively that this is not an overlapping carbon film but is a water-insoluble residue adhering to the replica. The arrows indicate particles having well-defined crystalline outlines. Figure 6 shows a different area with water-insoluble particles adhering to tapered microcrystals.

Under certain conditions sharply tapered units, visible under the light microscope and sometimes to the unaided eye, are formed at the inter-

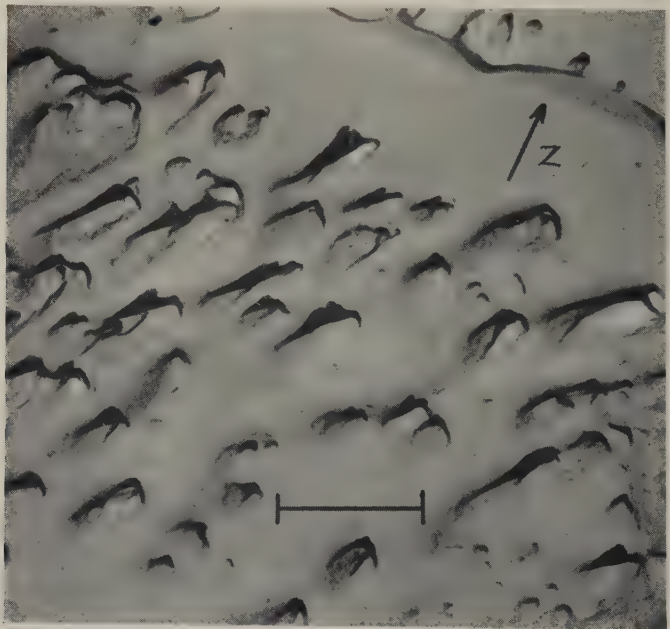

FIG. 4. $NH_4H_2PO_4$ grown from solution containing $1 \times 10^{-3}$ mole $Fe^{+++}$/liter. Fracture surface parallel (100) plane showing tapered microstructure and residue (18400 ×).

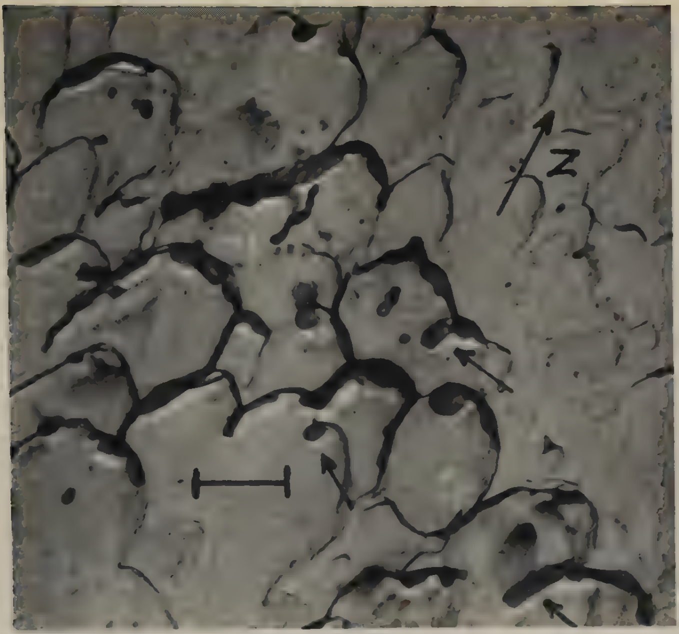

FIG. 5. $NH_4H_2AsO_4$ grown from solution containing $10 \times 10^{-3}$ mole $Fe^{+++}$/liter. Fracture surface parallel (100) plane showing tapered microstructure. Arrows indicate crystals of impurity compound (10800 ×).

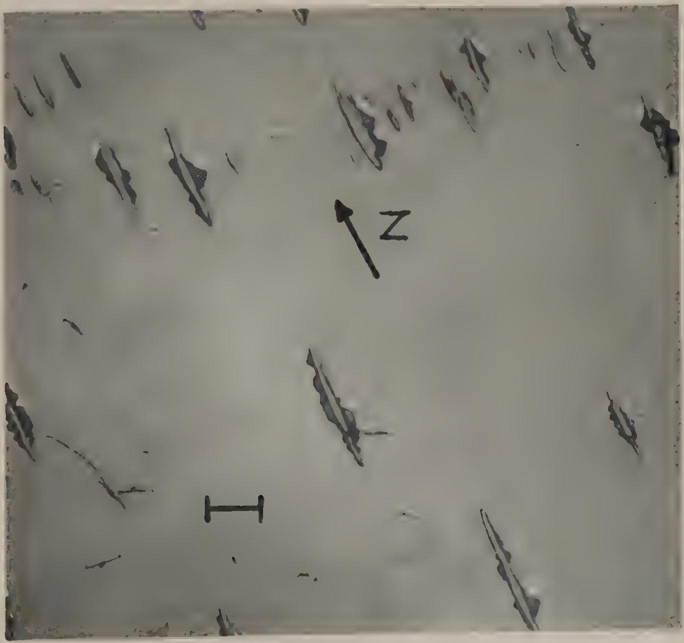

FIG. 6. $NH_4H_2AsO_4$ grown from solution containing $10 \times 10^{-3}$ mole $Fe^{+++}$/liter. Fracture surface parallel (100) plane (7200 ×).

section of the prism faces with the pyramid faces when pure seed crystals of $NH_4H_2PO_4$ are placed in solutions of the salt containing enough foreign ions to inhibit growth.

Surface features found on crystals of $NH_4H_2AsO_4$ were usually more pronounced than those found on the isomorphous phosphate, and greater concentrations of insoluble residue were found. Figure 7, a fracture surface parallel to the (001) plane, shows dendritic growth in the lower part of the image and a coarser, undercut structure with areas outlined by small particles with crystalline outlines. Figure 8 shows another field where crystallites, apparently euhedral octahedrons, are concentrated in parallel lines spaced about 2 microns apart. In a few areas on replicas of fractures parallel to the (001) plane a polygonal type structure seen in Fig. 9 was found. Residues from the small particles along the boundaries, which were transferred to the replica during the separation from the surface of the crystal, suggest the presence of an impurity formed preferentially at the surface of the growing crystal.

Many replicas of the arsenate contained large quantities of insoluble residue, often appearing as a fine amorphous layer and sometimes as discrete crystals like those in Fig. 10. Here the particles are relatively thick and rounded with some indication of crystalline outlines. In the upper right-

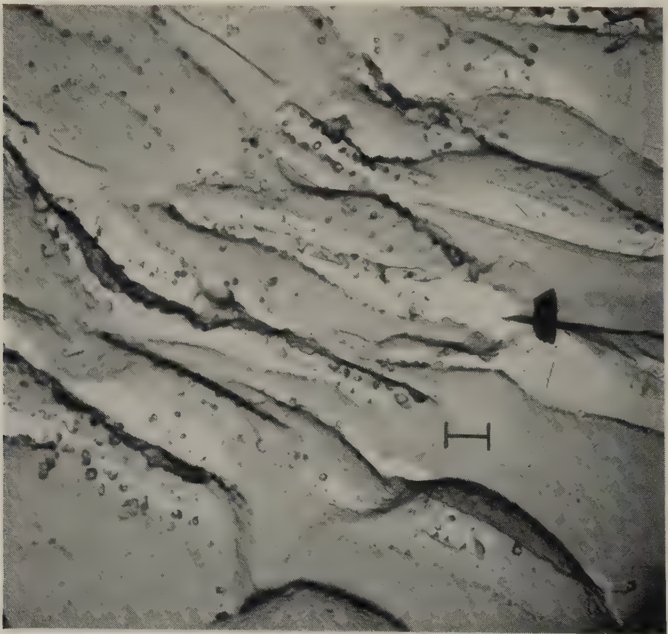

FIG. 7. $NH_4H_2AsO_4$ grown from solution containing $10 \times 10^{-3}$ mole $Fe^{+++}$/liter. Fracture surface parallel (001) plane (4800 ×).

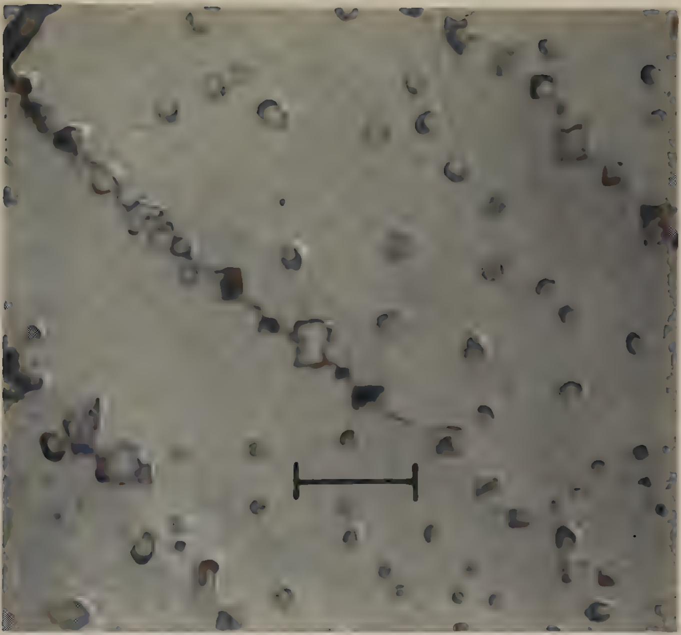

FIG. 8. $NH_4H_2AsO_4$ grown from solution containing $10 \times 10^{-3}$ mole $Fe^{+++}$/liter. Fracture surface parallel (001) plane (14800 ×).

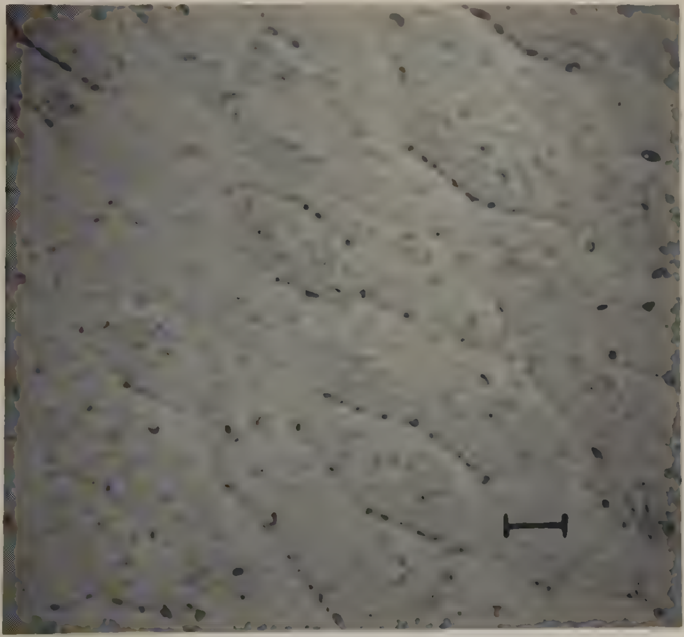

FIG. 9. $NH_4H_2AsO_4$ grown from solution containing $10 \times 10^{-3}$ mole $Fe^{+++}$/liter. Fracture surface parallel (001) plane showing polygonal units bounded by small particles (7200 ×).

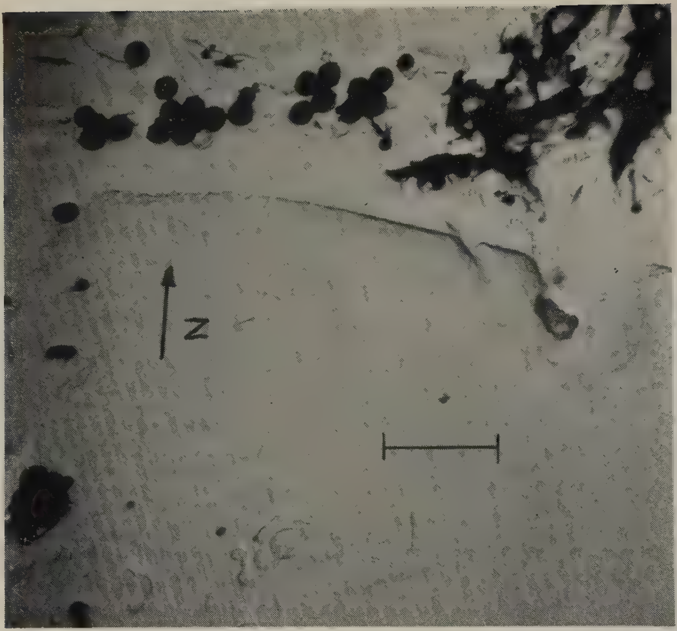

FIG. 10. $NH_4H_2AsO_4$ grown from solution containing 10 × $10^{-3}$ mole $Fe^{+++}$/liter. Fracture surface parallel (100) plane showing crystals of impurity compound adhering to the replica (14800 ×).

hand corner is a deposit of the more common "amorphous" material. In the lower part of the micrograph can be seen outlines of particles which were replicated but did not adhere entirely during separation of the replica from the crystal surface. Figure 11 shows a field containing very high concentrations of residue with slender tapered crystals visible also. Very few diffraction patterns were obtained from the residue and identification of these was not possible. Most of the residue appears to be amorphous.

At very high concentrations of stannic ions (20 × $10^{-3}$ mole per liter in solutions of $NH_4H_2PO_4$) no growth formed on the seed crystals. At extreme conditions of supersaturation crystal growth occurred on the sides of the beaker by creeping. Electron diffraction patterns of residue on the replicas could not be obtained. Figure 12 shows a typical field found on replicas of the material grown on the sides of the beaker. The particles are rounded and irregular in shape; most of the black, curved lines represent water-insoluble residue. Larger quantities of residue, concentrated by dialysis of the powdered crystals through a collodion membrane, were identified by electron diffraction as largely tetragonal $SnO_2$. Some lines present could not be identified. This material could have formed during the release of stannic ions from the phosphate crystals during dissolution, but the fact that it is formed under these conditions indicates the possibility of its

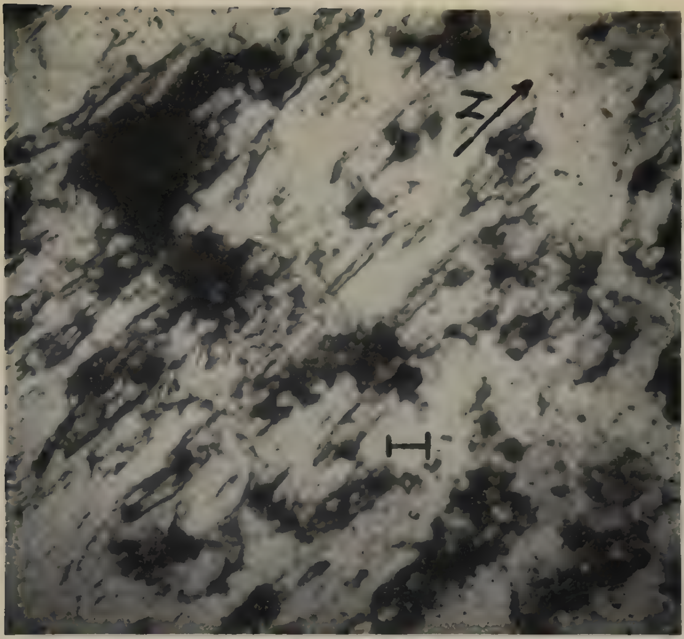

FIG. 11. $NH_4H_2AsO_4$ grown from solution containing $10 \times 10^{-3}$ mole $Fe^{+++}$/liter. Fracture surface parallel (100) plane showing impurity compound adhering to the replica (5000 ×).

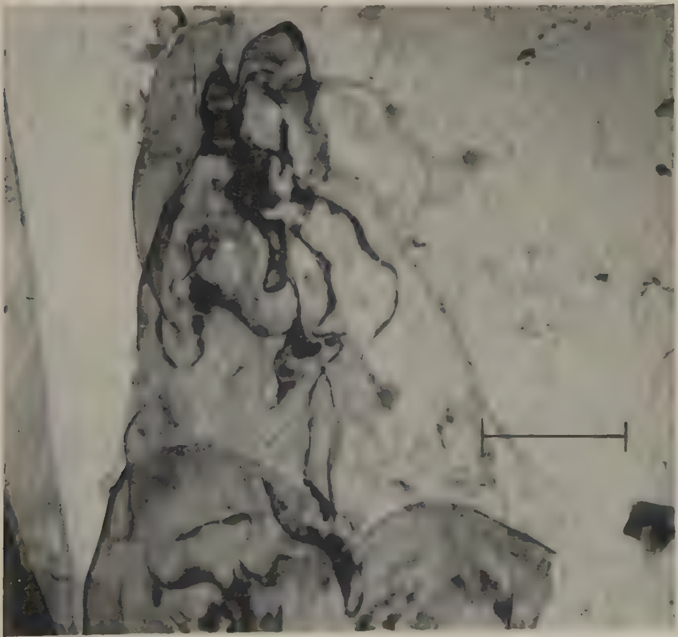

FIG. 12. $NH_4H_2PO_4$ grown from solution containing $20 \times 10^{-3}$ mole $Sn^{++++}$/liter. Growth by creep on side of beaker. Black lines represent water insoluble residue (18800 ×).

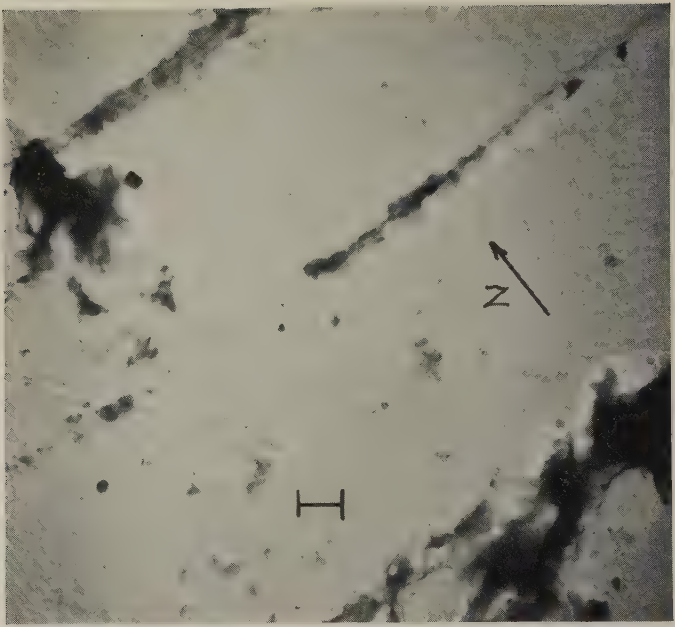

FIG. 13. $NH_4H_2PO_4$ grown from solution containing $8 \times 10^{-3}$ mole $Sn^{++++}$/liter. Natural (100) face showing water-insoluble residue at surface (5400 ×).

forming at the surface of the growing crystals. At lower concentrations of stannic ion ($8 \times 10^{-3}$ mole per liter) growth was obtained on seed crystals of $NH_4H_2PO_4$. Replicas of the natural (100) face, Fig. 13, show heavy concentrations of amorphous residue located in parallel lines running normal to the *z*-axis. The spacing is usually about 2 microns or multiples of this.

## DISCUSSION

There is general agreement with Ames *et al.* that pure crystals show essentially no surface features by the replica technique. Their work was done on natural surfaces, whereas in this study the surfaces examined were obtained by fracturing the crystals in directions roughly parallel to the (100), (010), or (001) planes. With increasing quantities of impurities in the solutions there is an increase in surface structure, even though crystals containing the highest amounts of impurities yielded some fracture surfaces which were structureless.

Several workers have proposed a relationship between the solubilities of the host crystal and the impurity responsible for habit modification (6–10).

Buckley (11) on the basis of his studies of the effect of the inorganic oxy-ions, $CrO_4^=$, $SO_4^=$, and $CO_3^=$, as impurities in crystals possessing the same type of anion, stated that "the impurity ions were distributed with some degree of statistical unevenness throughout those parts of the grown crystal which has passed into the interior via one of the affected faces, while in highly concentrated impurities several ions of the latter might get together with some cations and form localized crystals of impurity on the surface and get incorporated by subsequent deposition." However, he considered this to be merely incidental and inapplicable in cases where only minute traces of impurity were needed to cause a large habit change.

The idea of a metal phosphate or arsenate formation on the crystal surface during growth of $NH_4H_2PO_4$ and $NH_4H_2AsO_4$ from solutions containing the cations, $Cr^{+++}$ and $Fe^{+++}$, is given some support by the results of several workers in other fields of study. Sinha and Choudhury (12), in a study of the adsorption of phosphate by aluminum oxide, presented evidence to show that there is a chemical reaction between the oxide and phosphate to form an aluminum phosphate. Along similar lines is a study by O'Connor *et al.* (13) on electrokinetic properties and surface reactions of corundum, in which they show by the streaming potential method that $KH_2PO_4$ reacts with the surface of alumina by both anion adsorption and by anion exchange with the formation of $Al(H_2PO_4)$, $Al_2(HPO_4)_3$, and $AlPO_4$. Cole and Jackson (14) have shown that colloidal dihydrogen phosphates of aluminum and iron with crystalline character can be formed by reacting $AlCl_3$ or $FeCl_3$ with solutions of phosphate as $KH_2PO_4$ or $NaH_2PO_4$.

Although most of the insoluble residue on the crystals examined was concentrated in lines normal to the $z$-axis, in some unique areas containing the tapered microcrystals it was often distributed more uniformly throughout the field. In addition, water-insoluble crystals, well-defined morphologically, were found at the apices of the tapered units found on $NH_4H_2AsO_4$ containing the ferric ion. It has been known for some time that growth normal to the prism faces of the $NH_4H_2PO_4$ and $NH_4H_2AsO_4$ crystals is inhibited by strong adsorption of the cations, $Cr^{+++}$, $Fe^{+++}$, $Sn^{++++}$, and others; when one of these cations is present in sufficient concentration growth of the crystal occurs chiefly along the $z$-axis. There is a critical concentration for each cation at which growth of the crystal is completely inhibited. However, it has been found that when a high degree of supersaturation exists a limited amount of growth along the $z$-axis can take place on a seed crystal even when the foreign ion concentration is above the value where growth is normally stopped. Under these conditions growth occurs on a pure seed crystal until enough impurity is adsorbed on the surface to block further deposition of solute ions. When viewed along the prism faces the new growth consists of units of varying sizes tapered along the $z$-axis. The tapered micro units observed by the replica technique are probably formed in the same manner. Tapering is the result of the formation of micro steps; as the foreign ion concentration builds up on the surface growth is stopped and a precipitate of the metal phosphate may form at the surface. New micro units form at some distance in from the intersection of the prism and pyramid faces and as the process continues a gradual tapering of the crystal is observed.

Certain structures observed on $NH_4H_2AsO_4$ containing ferric ions are not yet understood. It is clear from this study that relatively large quantities of insoluble residue are present in these crystals. The polygonal type structure observed in a few areas is suggestive of the type of dislocation nets observed by Amelinckx (15) in rock salt, and by Hedges and Mitchell (16) in silver bromide. There is, however, no direct evidence to link these structures with networks of dislocations.

At present no explanation has been found for the presence of the residue in curved lines in the crystals which grew on the side of the beaker at very high concentrations of stannic ion. While residue from the crystalline material obtained by dialysis was identified as tetragonal $SnO_2$, it is not certain that this is the residue found on the replicas; it is possible that formation of the compound took place during the dialysis operation although the presence of $SnO_2$ in the crystal is entirely possible.

## Summary

Evidence has been presented to show that adsorption of the cations $Cr^{+++}$, $Fe^{+++}$, and $Sn^{++++}$ by crystals of $NH_4H_2PO_4$ and $NH_4H_2AsO_4$ during growth from solution is accompanied by the deposition of water-insoluble residues at the surface of the growing crystals. It is suggested that these are metal phosphates or arsenates formed at the surface or occluded from suspension. Those which form at the surface deposit preferentially at the prism faces and are partly responsible for a habit modification of the crystals. In the case of the stannic ion it is possible that some $SnO_2$ is present.

A microstructure observed on habit-modified crystals indicates a stepwise tapering of the crystal at the intersection of the (100) and (001) or the (010) and (011) planes. Other surface features include polygonal units bounded by small crystals.

The results suggest that under carefully controlled conditions the electron microscope may be a valuable tool in studying crystal growth in the presence of impurities.

## Acknowledgments

The author wishes to acknowledge the help of Mrs. Marilyn Grender for the chemical analyses. He is also indebted to Dr. Rustum Roy for encouragement and helpful criticism.

## REFERENCES

1. Kolb, H. J., and Comer, J. J., *J. Am. Chem. Soc.* **67**, 894 (1945).
2. Ames, J., Cottrell, T. L., and Sampson, A. M. D., *Trans. Faraday Soc.* **46**, 938 (1950).
3. Truby, F. K., *J. Appl. Phys.* **26**, 1416 (1955).
4. Hibi, T., and Ishikawa, K., *J. Phys. Soc. Japan* **13**, 709 (1958).
5. Bradley, D. E., *Brit. J. Appl. Phys.* **5**, 65 (1954).
6. Gaubert, P., *Rev. sci.* **48**, 74 (1910).
7. Gaubert, P., *Compt. rend.* **200**, 1120 (1935).
8. Walcott, A. J., *Am. Mineralogist* **2**, 259 (1926).
9. Bunn, C. W., *Proc. Roy. Soc.* (*London*) **A141**, 567 (1933).
10. Royer, L., *Bull. soc. franç. minéral.* **51**, 1 (1928).
11. Buckley, H. E., "Crystal Growth," pp. 351–352. Wiley, New York, 1951.
12. Sinha, P. R., and Choudhury, A. K., *J. Indian Chem. Soc.* **31**, 211 (1954).
13. O'Connor, D. J., Johansen, P. G., and Buchanan, A. S., *Trans. Faraday Soc.* **52**, 229 (1956).
14. Cole, C. V., and Jackson, M. L., *J. Phys. & Colloid Chem.* **54**, 128 (1950).
15. Amelinckx, S., *Phil. Mag.* **1**, 269 (1956).
16. Hedges, J. M., and Mitchell, J. W., *Phil. Mag.* **44**, 223 (1953).

JOURNAL OF COLLOID SCIENCE **14**, 190–205 (1959)

# SURFACE FILMS OF VINYL STEARATE, CETYL-VINYL ETHER, AND THEIR POLYMERS

**Tomlinson Fort, Jr.* and A. E. Alexander**

*Department of Physical Chemistry, The University of Sydney, N.S.W., Australia*

*Received August 19, 1958*

## INTRODUCTION

Studies of monomolecular films have provided a great deal of information concerning molecular structure and orientation at interfaces of organic molecules (1). In recent years, the techniques have been applied to polymers by Crisp (2, 3), Hotta (4), Schick (5), and many others, but no study has yet been made of vinyl monomers, probably because the common monomers are short-chain molecules which would not be stable at an interface. However, the attachment of a long hydrocarbon chain to a monomer molecule should not greatly alter the character of the vinyl double bond and the effects of neighboring functional groups should be identical. Thus, results obtained from monolayers of vinyl stearate should be very pertinent to vinyl acetate, and so on.

This paper reports a systematic study of vinyl stearate and cetyl-vinyl ether spread as monolayers at the air/water interface upon substrates of different acidity. The vinyl ester was chosen as representative of monomers whose double bond is adjacent to an electron-attracting group and which is subject to free radical polymerization while the ether, with its vinyl group adjacent to an electron-repelling oxygen atom, is representative of monomers subject to cationic, or Lewis acid, polymerization (6). In order to separate the effects of the double bonds from those of the adjacent polar groups the corresponding saturated compounds were also studied. Of the four compounds, only one, ethyl stearate, had been previously investigated (7). Results show that the vinyl groups affect the properties of the monolayers in a manner which can be related to the interaction of the adjacent polar groups with the double bonds.

Polymers of the two monomer species were also prepared and their properties as monolayers determined, the results being interpreted in terms of the structures of the polymer molecules.

---

* Present address: E. I. Du Pont de Nemours and Company, Kinston, North Carolina.

## EXPERIMENTAL

### *Materials*

A sample of cetyl-vinyl ether was kindly donated by Dr. S. A. Miller of the British Oxygen Company. It had a boiling point of 160°–165°/4 mm. and analyzed: C–80.85 %, H–13.57 %. A rough molecular weight determination (Rast method) indicated no polymerization, and the sample was used without additional purification.

Cetyl-ethyl ether was prepared by a Williamson synthesis in a manner similar to that described by Phillips and Mumford (8) and by Becker (9). It melted at 20°C. after three crystallizations from acetone and one from ethanol and drying for a week in a desiccator over anhydrous calcium sulfate.

Vinyl stearate was prepared as described by Adelman (10). The crude reaction product was not purified by distillation, however, but was washed twice with hot water and then dissolved in acetone and treated with an excess of 6 *N* NaOH. The soap which precipitated was removed by filtration and the filtrate cooled to 0°. The precipitated ester was then filtered, dissolved in ether, and extracted three times with water to remove any residual inorganic contaminant. The ether was evaporated and the product recrystallized from acetone. The white, waxlike crystals melted at 35°–36°C.

A sample of purified ethyl stearate was kindly donated by Mr. H. K. Welsh of the C.S.I.R.O. Laboratories, Sydney.

Polyvinyl stearate was prepared by bulk polymerization in a manner similar to that described by Port and co-workers (11). It had a melting point of 54°–59°C. and an intrinsic viscosity in benzene solution at 25°C. of 0.203 deciliter/gram, which, according to the data of Burlant and Adicoff (12), indicates a molecular weight of approximately 3600.

Cetyl-vinyl ether was polymerized by a method similar to those described for other poly alkyl-vinyl ethers by Chalmers (13) and by Eley (14). The polymer was dissolved in benzene and precipitated with cold acetone as described above for polyvinyl stearate. After three such precipitations the polymer was dried over calcium sulfate. The product was a white crystalline solid which melted at 53°C. It analyzed: C–79.75 %; H–13.65 %. A very approximate molecular weight determination (Rast method) indicated a low degree of polymerization.

Known quantities of these materials were dissolved in a 3 % solution of *n*-butanol in petrol ether (b.p. 60°–90°C.), both constituents of which had been redistilled, to make spreading solutions of approximate concentration 0.2 mg./ml. The various solutions used as spreading substrates were prepared by dilution of the reagent grade chemicals with distilled water. No attempt was made to keep these solutions at constant ionic strength.

### *Apparatus*

The film balance was a simple Wilhelmy plate type, sensitivity ca. 0.7 dyne/cm. per centimeter of scale deflection. The scale was read to the nearest 0.1 cm. Surface potentials were measured in the normal way, being read to the nearest millivolt.

Spreading was by means of an "Agla" micrometer syringe. All experiments were run at room temperature, which, however, was adjusted so that all measurements were made at 25° ± 0.5°C.

## RESULTS

All results are given graphically, each curve representing the average of at least two, and usually three or four, separate experimental determinations. In all cases, the solid curves represent force (Π)-area ($A$) measurements, the dashed curves surface potential ($\Delta V$)-area measurements, and the dotted curves surface moment ($\mu$)-area determinations calculated from the Helmholtz equation $\Delta V = 4\pi\mu/\mathrm{A}$. The letters adjacent to the curves refer to the substrates on which the film was spread which were, in all cases: (*a*) 0.005 $N$ HCl; (*b*) 0.010 $N$ HCl; (*c*) 0.050 $N$ HCl; (*d*) 0.100 $N$ HCl; (*e*) 0.500 $N$ HCl; (*f*) 1.00 $N$ HCl; (*g*) 5.00 $N$ HCl.

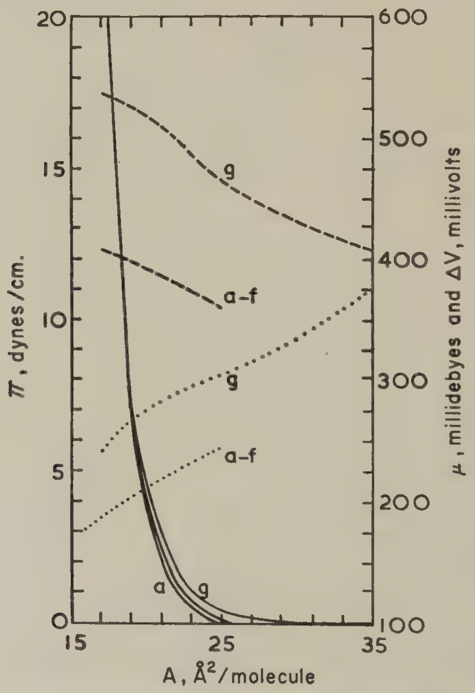

FIG. 1. Ethyl stearate. Surface pressure (Π), surface potential ($\Delta V$), and surface moment ($\mu$) as functions of area per molecule ($A$).

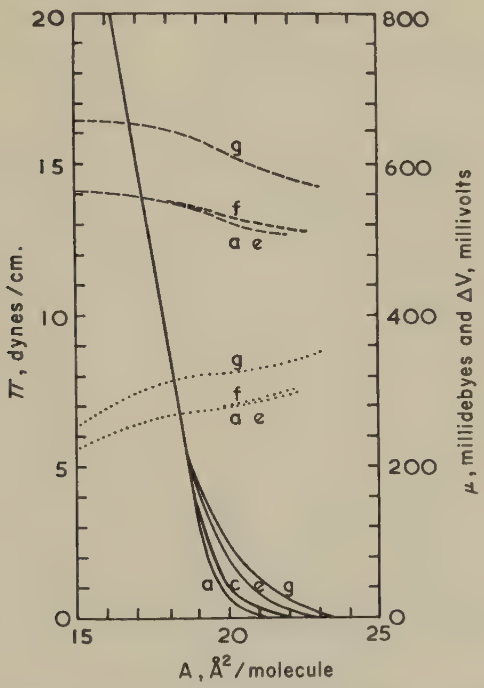

FIG. 2. Vinyl stearate. Surface pressure (Π), surface potential (Δ$V$) and surface moment ($\mu$), as functions of area per molecule ($A$).

*Ethyl and vinyl stearate* both yield condensed monolayers on all substrates as shown by the Π-$A$ curves of Figs. 1 and 2. The linear portions of these curves extrapolate to a limiting area of between 19.5 and 20.0 $A.^2$, in good agreement with that found for ethyl stearate by Alexander and Schulman (7). The departure from linearity observed at low surface pressures is greater with the saturated ester and appears to increase with the substrate acidity.

The Δ$V$ values of the two esters are quite different, the plateaux coming at ca. 410 mv. for ethyl stearate and 560 mv. for vinyl stearate. These values remain the same except on the most concentrated acid substrate (5 $N$ HCl), when an increase of the order of 100 mv. is noted for both compounds.

*Cetyl-ethyl ether* (Fig. 3) forms a liquid expanded film which on compression becomes condensed. The condensed portions of the Π-$A$ curves extrapolate to limiting areas of 19.0–19.5 A.$^2$, which agree with the value found for octadecyl-methyl ether by Marsden and Schulman (15). The films are not as stable as those of the esters. Surface pressures are first detected at areas of from 35–70 A.$^2$ depending on the acidity of the substrate. The Δ$V$–$A$ curves are reasonably constant except on 5 $N$ HCl, which shows a marked increase of over 100 mv.

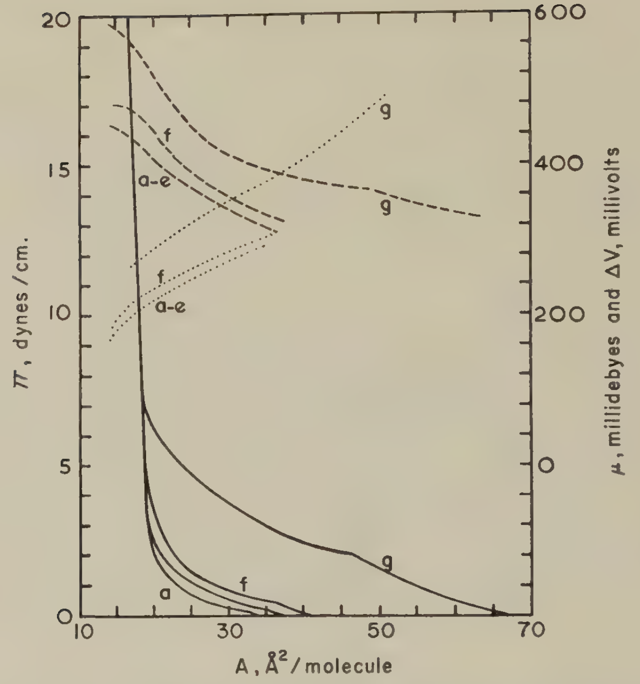

FIG. 3. Cetyl-ethyl ether. Surface pressure (Π), surface potential ($\Delta V$) and surface moment ($\mu$) as functions of area per molecule ($A$).

*Cetyl-vinyl ether* (Fig. 4) forms condensed films, the characteristics of which are strongly dependent on the acidity of the substrate, the compressibility decreasing with increasing substrate acidity. The linear portions of the Π-$A$ curves extrapolate to areas of about 19 A.$^2$ (on the more dilute acid substrates) up to 24 A.$^2$ (on 1 $N$ HCl). On 5 $N$ HCl the Π-$A$ curve is not linear at any surface pressure.

The $\Delta V$ results are unique among the compounds studied here in that the $\Delta V$-$A$ curves are linear and strongly dependent on the acidity (Fig. 5), with a variation of over 250 mv. from the most dilute to the most concentrated acid substrate.

*Poly-vinyl stearate* (Fig. 6) was spread on only one substrate, 0.05 $N$ HCl, giving a condensed film with a linear portion extrapolating to an area of *ca.* 26 A.$^2$ per monomer residue.

Surface potentials rose from their initial values of 220 mv. at 35 A.$^2$ per monomer residue to a reasonable plateau of *ca.* 340 mv. at 20 A.$^2$.

*Poly cetyl-vinyl ether* (Fig. 7) was also spread on only one substrate, 0.05 $N$ HCl, and also yielded a condensed film, with the linear portion extrapolating to *ca.* 21 A.$^2$ per monomer residue.

Surface potentials increased from about 380 mv. at 22 A.$^2$ per monomer residue to a maximum of 404 mv. when the film was compressed.

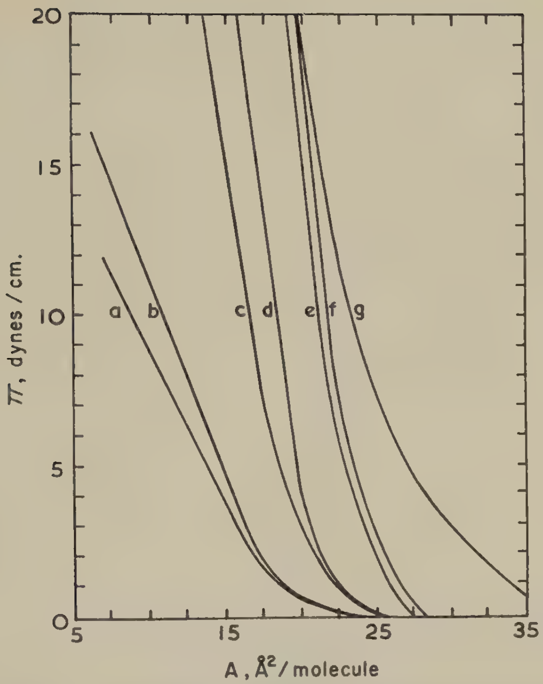

FIG. 4. Cetyl-vinyl ether. Surface pressure (Π) as a function of area per molecule ($A$).

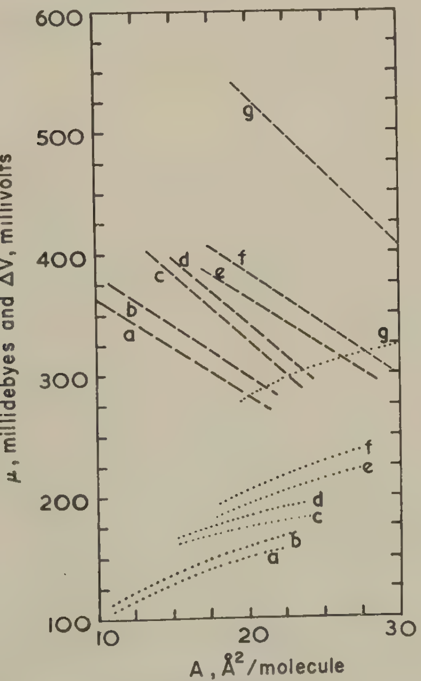

FIG. 5. Cetyl-vinyl ether. Surface potential ($\Delta V$) and surface moment ($\mu$) as functions of area per molecule ($A$).

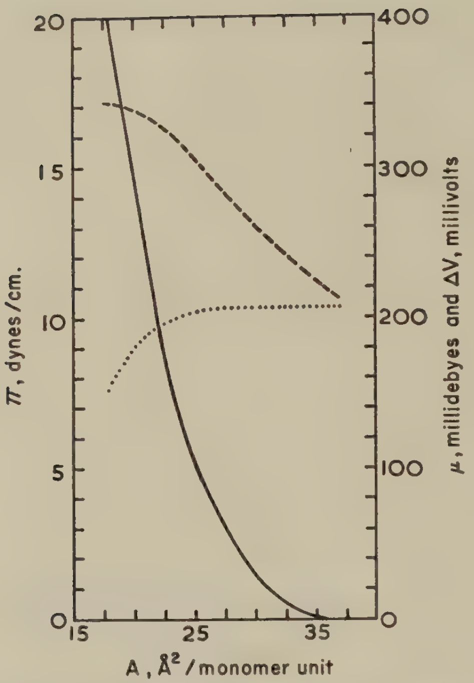

FIG. 6. Poly-vinyl stearate. Surface pressure (Π), surface potential ($\Delta V$), and surface moment ($\mu$) as functions of area per monomer unit.

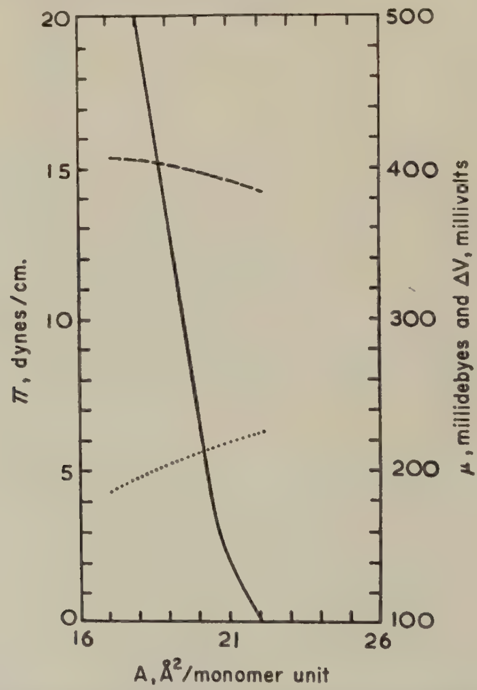

FIG. 7. Poly cetyl-vinyl ether. Surface pressure (Π), surface potential ($\Delta V$), and surface moment ($\mu$) as functions of area per monomer unit.

## DISCUSSION

Surface moments were first used as an aid in determining molecular orientation in monolayers by Alexander and Schulman (7). They were able to obtain good agreement between calculated and observed surface moments ($\mu$) for a variety of long-chain esters by considering the ester group to consist of three dipoles and ascribing to each of these surface moments as

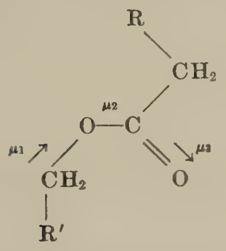

$\mu_1$ = 170 millidebyes (mD.)
$\mu_2$ = 0 mD.
$\mu_3$ = 360 mD.

indicated. The resultant surface moment ($\mu$) was then obtained by vector summation of $\mu_1$, $\mu_2$, and $\mu_3$. This treatment and the above numerical values have been used in the discussion which follows. Graphs of $\mu$ as a function of $A$ are shown by the dotted curves in Figs. 1, 2, 3, 5, 6, and 7.

First consider *ethyl stearate*. This compound forms a condensed film on all substrates, the linear portions of the $\Pi$-$A$ curves extrapolating to *ca.* 19.8 A.$^2$, at which area $\mu$ is *ca.* 205 mD. Both these figures agree with those of Alexander and Schulman (7). The configuration they suggest for the ester is given in Table I($A$).

Now, *vinyl stearate* also forms a condensed film with the same extrapolated area of *ca.* 19.5 A.$^2$ so that, from the $\Pi$-$A$ measurement, the vinyl ester is almost certainly in a similar configuration (Table I ($B$)). The linear portion is reached at lower surface pressures than with the saturated ester, but this is not surprising considering the more polar nature (and smaller size) of the vinyl group.

The surface moment of vinyl stearate is found to be considerably higher than that of ethyl stearate, being *ca.* 275 mD. at 19.5 A.$^2$. As the two compounds are identical except for the unsaturated ester group, this increase must be ascribed to the vinyl double bond. Now, the dominant dipole in the ester group is $\mu_3$, that associated with the carbonyl group. With the ester in the configuration shown in Table I($B$), the observed increase in surface moment of 70 mD. must then be due either to a strengthening of $\mu_3$ or to a weakening of $\mu_1$ by the vinyl double bond. The latter seems much the more likely, although some effect on $\mu_3$ cannot be excluded. The pi electrons of the double bond are polarizable and the vinyl group then acts as a source of electrons. These electrons are attracted by the carboxyl

TABLE I

*Orientation in Monolayers of Long-Chain Ethers and Esters*

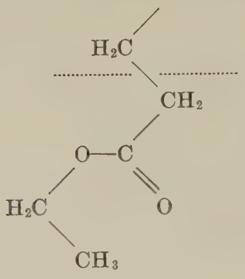

*A.* Ethyl Stearate
Area per molecule = 19.8 A.$^2$
$\mu$ (obs.) = 202 mD.
$\mu$ (calc.) = 198 mD.

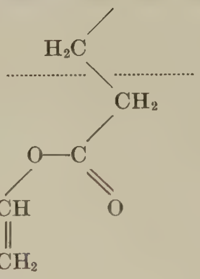

*B.* Vinyl Stearate
Area per molecule = 19.5 A.$^2$
$\mu$ (obs.) = 275 mD.

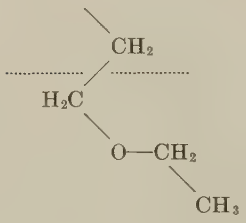

*C.* Cetyl-Ethyl Ether
Area per molecule = 19.8 A.$^2$
$\mu$ (obs.) = 208 mD.
$\mu$ (calc.) = 205 mD.

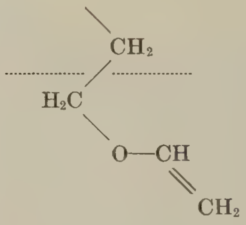

*D.* Cetyl-Vinyl Ether
Area per molecule = 20 A.$^2$
$\mu$ (obs.) = 150–205 mD.

*Note:* The orientation of the molecules with respect to the surface of the water *but not their depth of immersion* is given by the dotted horizontal lines.

group, partially neutralizing $\mu_1$.[1] The *resultant* surface moment is thus increased.

Some idea of the extent of the neutralization can perhaps be obtained by comparing the observed increase in surface moment, 70 mD., with that assuming complete neutralization, namely, 140 mD. This latter figure would represent the maximum possible effect of the vinyl double bond on the surface moment of the ester and may be compared with the increase of *ca.* 210 mD. observed by Hughes (16), for $\Delta$-$\alpha,\beta$, isooleic acid when compared with oleic acid. With the $\Delta$-$\alpha,\beta$, acid, polarization of the double bond which is conjugated with the carbonyl bond greatly reinforces dipole $\mu_3$, resulting in an increase in surface moment of almost 100%.

---

[1] This effect is well shown in bulk dipole moments. Thus vinyl chloride and chlorobenzene have lower moments than methyl chloride.

*Cetyl-ethyl ether* forms an expanded film at low pressures, which, on compression, changes to a condensed film of limiting area 19.5–20 A.$^2$, indicating close packing of the hydrocarbon chains in the condensed state.

The surface moment is 205 mD. at an area of 19.8 A.$^2$. This is a considerable moment for a symmetrical molecule like an ether but checks well with the data of Marsden and Schulman (15) for octadecyl-methyl ether.

Three orientations of the ether molecules at the interface would appear to be possible; they are given below. Of these (*1*) would appear to admit closest packing of the hydrocarbon chains. However, it is obvious that, in this configuration› the two C—O dipoles essentially cancel one another so far as moment normal to the interface is concerned and a surface moment of 200 mD. would be impossible. Configuration (*2*) is ruled out since it does not permit close packing of the hydrocarbon chains. Molecular models show, however, that reasonably close packing can be achieved in configuration (*3*). Further, considering the surface moment of the ether to be due only to the two C—O dipoles, and taking these to be the same as Alexander and Schulman's $\mu_1$ (170 mD.), vector addition yields a resultant surface moment of *ca.* 202 mD. This figure checks very well with the observed (205 mD.), confirming configuration (*3*) as correct and, incidentally, confirming the value for the C—O dipole determined by Alexander and Schulman from theoretical considerations.

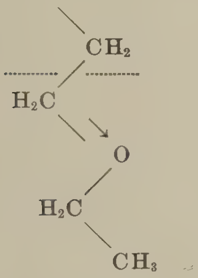

(1)

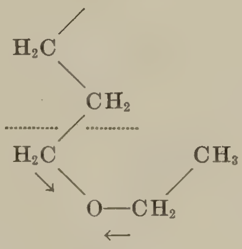

(2)

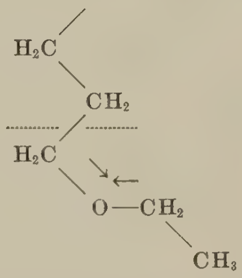

(3)

It is probable that when the film is under no compression the ethyl group has rotated so as to reduce its immersion in the water. This rotation would increase the area per molecule but would not affect the surface moment.

The behavior of *cetyl-vinyl ether* is the most interesting (and the most complex) of the compounds considered here.

Consider first the behavior on the most dilute acid substrate, 0.005 *N* HCl. The film is of the condensed type but highly compressible and not very stable. Compression to surface pressures greater than 11 or 12 dyne was impossible. The surface moment at 20 A.$^2$ is 160 mD., i.e., some 40 mD. less than the saturated homolog. If we consider again the configurations given above for cetyl-ethyl ether, then (*1*) can again be rejected because it would indicate little or no surface moment, and (*2*) because it would be inconsistent with the areas observed which indicate close packing of the hydrocarbon chains. Any model which is adopted for cetyl-vinyl ether must then have the molecules take configuration (*3*) at the interface.

Now, the behavior of alkyl-vinyl ethers is greatly influenced by the interaction of the vinyl double bond with the ether oxygen atom which allows the creation of the following structures:

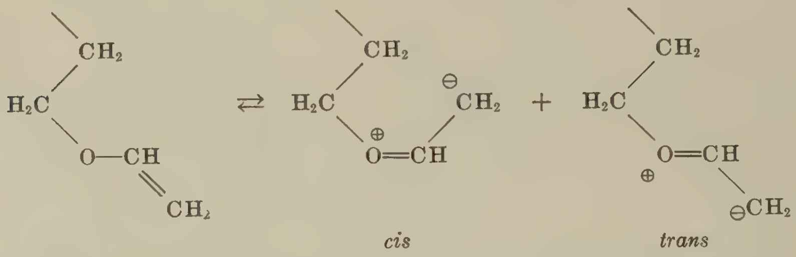

The stabilization of the ether molecule due to this electron shift has been studied by Kistiakowsky and co-workers (17), and spectral evidence for the existence of two (*cis-trans*)isomers has recently been presented by Brey and Tarrent (18).[2]

Now consider the effects of such an equilibrium on the properties of the monolayer in which the molecules are oriented as in configuration (*3*) above. The electronic shift will weaken the two C—O dipoles because in the process of the shift the negative oxygen atom becomes more positive. This weakening should decrease the surface moment, as this is a function of the strength of the C—O dipoles. From general reasoning one might also expect the weakening of these dipoles to weaken the anchorage of the ether molecules to the water, and so decrease the stability of the film, as observed.

The large increase in film stability and in surface moment on more acidic substrates remains to be explained. Possible explanations are:

*1*). Incomplete spreading on neutral and slightly acid substrates.

*2*). Appreciable solubility in water; the effect of acid would then be ascribed to "salting out."

*3*). The vinyl ether reacts with the acid producing a new compound which forms stable films.

*4*). The hydrogen ions coordinate with the vinyl ether and the resulting complex forms stable films.

These various possibilities were considered in turn.

---

[2] It has been stated above that the *cis* form is sterically impossible in the condensed monolayer.

Incomplete spreading was ruled out because the results were not affected by spreading from solutions containing varying proportions of petrol ether and butanol. The vinyl ether could also be spread successfully (but with difficulty) from benzene solution.

The acid substrate could not have been exerting a simple "salting out" effect as no expansion of the film was noted on 1 *N* KCl or on alkali.

The possibility of reaction in the monolayer was considered in some detail, as vinyl-alkyl ethers are known to be extremely reactive. Possible reactions considered included acid-catalyzed hydrolysis to acetaldehyde and cetyl alcohol (19), addition of hydrogen chloride across the double bond (20), and acid-catalyzed polymerization to form poly cetyl-vinyl ether (21).

Hydrolysis seems very unlikely as the shapes of the $\Pi$-$A$, $\Delta V$-$A$, and $\mu$-$A$ curves do not check with those of long-chain alcohols (1).

The same areas were observed when cetyl-vinyl ether was spread on HCl and $H_2SO_4$ substrates of similar acidity. This fact argues against addition across the double bond because the two acid anions are of quite different character, and this would be reflected in the properties of the films, had addition actually taken place.

A sample of poly cetyl-vinyl ether was prepared and spread as a monolayer, as part of this work. Results are discussed in detail below, but Fig. 7 shows its properties to be different from those observed for the ether monomer on any given substrate.

Finally, a strong argument against any reaction in the monolayer having taken place is the fact that the ether film results were reproducible. The films were all compressed soon after spreading but not after precisely the same time interval. If any reaction were responsible for the change in properties one would expect the results to be a function of the time between spreading and measurement. Such a dependence was never observed.

The simplest complex of a hydrated proton with a long-chain ether molecule at the interface would be one formed by the donation of a pair of electrons from the ether oxygen atom to the hydronium ion to form a coordinate link, as indicated below.

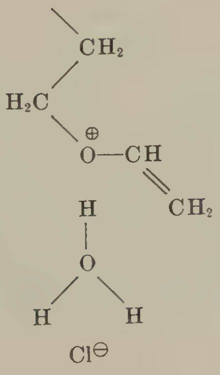

This structure would seem to be attractive as such a complex would be firmly anchored to the water by the strong attraction between the hydrated proton and its gegen ion. The charge separation between the two ions would also reinforce the surface dipole moment, and so an increase in moment with increasing substrate acidity would be expected. Such complexes were postulated long ago by Schulman and Hughes (22) to explain the behavior of monolayers on acid substrates. The difficulty is, however, that Schulman and Hughes noticed little or no effect at acidities less than 1 *N*, whereas the cetyl-vinyl ether shows marked changes at much lower acidities. Also, nothing similar was noted with films of cetyl-ethyl ether. If coordination were entirely due to the ether oxygen atom complex formation should have taken place more readily with the saturated ether with its more negative oxygen atom.

It appears, therefore, that coordination of the hydronium ion by vinyl ether, if it occurs, must involve the vinyl double bond. Thus, one could write:

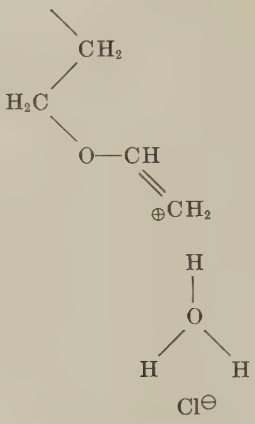

This complex is in accord with the generally accepted first step in the hydration of double bonds in acid solution (23), and it would result in an increase in film stability and surface moment for the same reasons as given above. Its stability would be expected to be a function of the availability of pi electrons at the terminal carbon atom; this would explain why no evidence of such a link was observed with vinyl stearate. No such complex is possible, of course, with cetyl-ethyl ether.

The picture is complicated, however, by the fact that there is evidence (24) that the initial step in hydrolysis of alkyl vinyl ethers is the coordination of the hydronium ion with *both* the double bond and the ether oxygen atom, in the fashion:

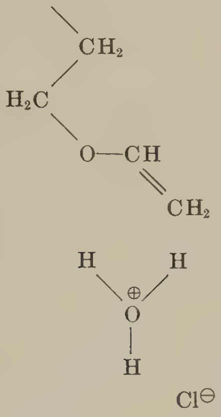

The increased stability of this complex over one requiring coordination to the ether oxygen atom only is shown by the fact that the rate of hydrolysis of vinyl-ethyl ether is thirteen orders of magnitude greater than the rate for diethyl ether, under similar conditions (19).

Probably, all three of the above complexes are involved, with the major contribution coming from the latter two.

There remain the questions of why cetyl-vinyl ether does not show an expanded film at low surface pressures as does cetyl-ethyl ether, and why its Π-$A$ curves on substrates of moderate acidity show linear portions extrapolating to areas greater than 19 A.$^2$.

The first is probably to be ascribed to the greater attraction of the double bond to the polar medium, reducing its tendency to be ejected at low pressures (*cf.* p. 199). As to the second question, examination of scale models shows that the difference in the O—C—C bond angle due to the unsaturated vinyl group (125° vs. 109°), plus the rigidity of the unsaturated structure, does not allow as close packing of the hydrocarbon chains as is possible with cetyl-ethyl ether. Thus, some increase in area is not surprising.

Finally, let us consider the behavior of all four compounds on the very concentrated acid solutions. With each, there is an increase in $\Delta V$ of *ca.* 100 mv. and in $\mu$ of *ca.* 60 mD. when values at similar areas on 1 $N$ and 5 $N$ HCl are compared. These increases are, certainly due to salt formation, as suggested by Schulman and Hughes and as indicated above. The presence or absence of vinyl double bonds seems to have little effect on this, the increase in $\mu$ being of approximately the same magnitude and occurring at approximately the same acidity for all four compounds.

The limiting area found for *poly vinyl stearate* on 0.05 $N$ HCl was found to be 26 A.$^2$ per monomer residue, which would indicate reasonably close packing of the polymer side chains. The maximum surface moment was found to be 207 mD., almost exactly that for ethyl stearate, indicating that the polar groups in the polymer molecule are similarly oriented at the interface.

Examination of scale models shows only one possible structure for the polymer molecule which allows vertically oriented side chains with reasonably close packing and the ester group in the configuration shown in Table I(*A*). This is with the polymer chain in vertical zigzag arrangement and the side chains all on one side. With the side chains as in Table I(*A*) the polymer chain would extend normal to the paper with the side chains attached to every other carbon atom (the "upper" one with the polymer chain in a vertical zigzag arrangement).

It is interesting to compare these results with those of Crisp (2) and Schick (5), who studied monolayers of polyvinyl acetate, and found this to take not the *trans* but the *cis* configuration (7) at the air/water interface. Examination of scale models shows that, with the polymer side chains in this latter configuration, the polar groups are more exposed to the water than they are in the *trans*. One would, therefore, expect that in a polymer with short side chains this configuration would prevail. However, the *cis* configuration does not allow close packing of the side chains and in poly vinyl stearate, where these are long, the attractive forces between these are sufficient to orientate the polar groups into the *trans* structure.

The Π-*A* curves for *poly cetyl-vinyl ether* show a limiting area of *ca.* 21 *A.*$^2$, indicating close packing of the side chains. The surface moment at 20 A.$^2$ is 211 mD., almost identically that found for cetyl-ethyl ether, again indicating that the C—O dipoles in the polymer are orientated as in the saturated ether. Referring again to molecular models it is seen that if the polymer side chains take a configuration as in Table I(*C*), and the polymer chain is put in a vertical zigzag arrangement normal to the paper with the side chains on one side of the main chain, a quite satisfactory polymer structure results in which the side chains are able to close pack and the ether linkages have an orientation relative to the water like that indicated in Table I(*C*).

## Summary

Monolayers of vinyl stearate and cetyl-vinyl ether, spread at an air/water interface on substrates of different acidity (0.005 *N*–5 *N* HCl), have been examined by the techniques of surface pressure, surface potential, and surface moment. The vinyl compounds were chosen as representative of monomers subject in the one case to free radical polymerization, and in the other to cationic polymerization. Parallel studies of the corresponding saturated compounds, ethyl stearate and cetyl-ethyl ether, permitted an analysis of the influence of the double bonds in the vinyl compounds.

All four compounds gave condensed films at 25°C. As compared with the corresponding saturated compound vinyl stearate was found to have a substantially *higher* and cetyl vinyl ether a substantially *lower*, surface moment. In the case of cetyl vinyl ether the surface moment was very sensitive to the acidity of the substrate. These results show that the vinyl groups affect the properties of the monolayers in a way which can be related to the interaction of the adjacent polar groups with the double bonds.

Polymers of the two monomer species were also prepared and examined as monolayers, the results being interpreted in terms of the structure and orientation of the monomer units.

## ACKNOWLEDGMENT

One of us (T. F.) is indebted to the University of Sydney for the E. A. and F. A. Q. Stephens Travelling Fellowship during the tenure of which this work was carried out.

## REFERENCES

1. e.g., HARKINS, W. D., "The Physical Chemistry of Surface Films." Reinhold, New York, 1952.
2. CRISP, D. J., *J. Colloid Sci.* **1,** 49 (1946).
3. CRISP, D. J., *J. Colloid Sci.* **1,** 161 (1946).
4. HOTTA, H., *J. Colloid Sci.* **9,** 504 (1954).
5. SCHICK, M. J., *J. Polymer Sci.* **251,** 465 (1957).
6. BILLMEYER, F. W., JR., "Textbook of Polymer Chemistry," p. 264. Interscience, New York, 1957.
7. ALEXANDER, A. E., AND SCHULMAN, J. H., *Proc. Roy. Soc.* (*London*) **A161,** 115 (1937).
8. PHILLIPS, J. W. C., AND MUMFORD, S. A., *J. Chem. Soc.* 1734 (1941).
9. BECKER, G., *Ann.* **102,** 220 (1857).
10. ADELMAN, R. L., *J. Org. Chem.* **14,** 1057 (1949).
11. PORT, W. S., HANSEN, J. E., JORDAN, E. F., DIETZ, T. J., AND SWERN, D., *J. Polymer Sci.* **7,** 207 (1951).
12. BURLANT, W., AND ADICOFF, A., *J. Polymer Sci.* **27,** 269 (1958).
13. CHALMERS, W., *Can. J. Research* **7,** 464, 472 (1932).
14. ELEY, D. D., AND RICHARDS, A. W., *Trans. Faraday Soc.* **45,** 425 (1949).
15. MARSDEN, J., AND SCHULMAN, J. H., *Trans. Faraday Soc.* **34,** 748 (1938).
16. HUGHES, A. H., *J. Chem. Soc.* 338 (1933).
17. KISTIAKOWSKY, G. B., RUHOFF, J. R., SMITH, H. A., AND VAUGHAN, W. E., *J. Am. Chem. Soc.* **58,** 137, 146 (1936).
18. BREY, M. L., AND TARRENT, P., *J. Am. Chem. Soc.* **79,** 6533 (1957).
19. SKRABAL, A., AND SKRABAL, R., *Z. Physik. Chem.* **181,** 449 (1938).
20. KUEHN, E., AND HOPFF, H., U. S. Patent, 2,061,946 (1936).
21. BLOUT, E. R., HOHENSTEIN, W. P., AND MARK, H., "Monomers." Interscience, New York, 1949.
22. SCHULMAN, J. H., AND HUGHES, A. H., *Proc. Roy. Soc.* (*London*) **A138,** 436 (1932).
23. INGOLD, C. K., "Structure and Mechanism in Organic Chemistry," p. 652. Cornell University Press, Ithaca, New York, 1953.
24. PRILEZHAEVA, E. N., SHAPIRO, E. S., AND SHOSTAKOVSKII, M. F., *Zhur. Obshchei Khim.* **18,** 1663 (1948); *Chem. Abstr.* **43,** 3272a.

JOURNAL OF COLLOID SCIENCE **14**, 206–221 (1959)

# SURFACE PROPERTIES OF POLYETHYLENE: EFFECT OF AN AMPHIPATHIC ADDITIVE

**A. J. G. Allan**[1]

*Polychemicals Department, E. I. du Pont de Nemours & Company, Inc., Du Pont Experimental Station, Wilmington, Delaware*

*Received November 3, 1958*

## Abstract

Previous studies have shown that small amounts of amphipathic (i.e., polar nonpolar) molecules, in particular oleamide, cause a marked lowering of the coefficient of friction between thin films of polyethylene. In this paper the surface chemical properties of the aging film and the nascent film (i.e., during the flat film extrusion process) have been studied. The wettability (contact angle) and friction of the aging film at room temperature show that the friction is reduced only when sufficient additive is present to form a weakly held monomolecular layer. This monolayer is formed by almost complete exudation of the additive from the bulk. Contact angle measurements show that the molecules become oriented on the surface such that the polar groups are in contact with the polyethylene and the hydrocarbon chains project into the air. The stability of the monolayer to water condensation is much improved by flame treatment of the film immediately on extrusion. On preparing film by extrusion through a water-quenching bath it has been found that water adheres more easily to films containing oleamide. By suitable adjustments, the water bath was modified to form a "dynamic" Langmuir trough. Contact angle measurements on the emerging film and studies on the effect of sweeping the water surface around the emerging film show that the surface tension of the water is lowered by the amphipathic molecule being quantitatively stripped off the film as it emerges through the water/air interface. From surface pressure area relationships, the surface concentrations of the spreading molecules are calculated. It is found that there is a surface concentration about one hundred times greater than would be expected from a uniform distribution of the additive throughout the polymer. This large surface excess is approximately proportional to the bulk concentration and implies a pronounced adsorption at the polymer melt/metal or polymer melt/air interface.

## Introduction

In the production of highly transparent films of polyethylene, undesirable increases in friction sometimes occur between contiguous surfaces. To reduce this friction, various empirical approaches have been tried, including the application of a solid size or addition of a surface-active agent to the quenching bath (1) used in flat film extrusion. Both these techniques separate the polymer surface: in the first case by a ball-bearing action, and in the second case by a lubricating action. A third and most successful approach made in these laboratories (2) has been to incorporate a variety of amphipathic molecules (i.e., polar nonpolar) into the raw polymer before fabrication of the film. These materials exude to the surface to form a thin layer, effectively preventing much direct polyethylene-to-polyethylene contact.

---

[1] Present address: European Office, E. I. du Pont de Nemours & Company, Inc., Bush House, Aldwych, London, W.C. 2.

In industrial application, we need to know how much additive is required to reduce friction to an acceptable level and what effect the additive has on the processes of heat sealing (3) and preprinting treatments (4, 5). Conversely, these processes affect the friction when additives are used. Again, when films containing additives are made by extruding the molten polymer into a water quenching bath (the flat film extrusion process), these films pick up drops of water more easily than films without additives.

To study these problems, various well-known techniques of surface chemistry have been adapted to the study of both nascent and aging films. In any particular instance, the information has not been sufficient to present a complete analysis, but a survey of the diverse experiments and observations shows that the processes can largely be understood and discussed in relation to well-accepted theories. In addition, there is evidence to suggest that the amphipathic molecules are surface-active at the molten polymer/air and/or molten polymer/metal interface.

## I. Experimental

### A. *Materials*

Film-grade polyethylene resin of density 0.923 was used throughout these experiments. Stearamide and oleamide were either milled into the polyethylene for friction and extrusion studies or made up into a 0.1% solution in a mixed solvent of petroleum ether (b.p. 60°–70°C.)/isopropyl alcohol for surface balance studies.

### B. *Apparatus and Methods*

*1. Extrusion.* A diagram of the apparatus is shown in Fig. 1. The film *A* emerges from the die *B* into the water in the bath *C* and under a roll *D* near the bottom. (When required, the edges of the film can be removed by razor blades fixed at *E*.) From this roll the film passes under a second roll *F* (the cut-off edges being deflected to the narrow section of the roll) and then upwards, vertically over a bar *G* fixed about 6 inches above the liquid surface, to the take-up rolls *H*. The peripheral speed of these rolls can be adjusted from 5 cm./sec. to 100 cm./sec. The quench tank is placed on three laboratory jacks (*J*) so that it can be leveled and the distance between the die and the water surface adjusted.

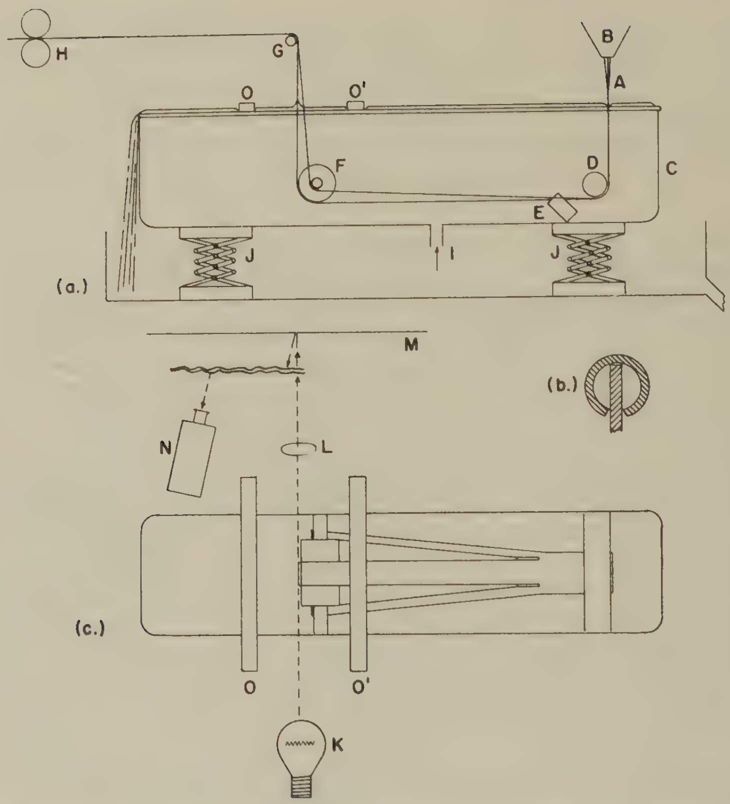

FIG. 1. Extrusion apparatus for measuring contact angles and spreading rates from moving film.

*2. Contact Angle of Moving Films.* To measure the receding contact angle between the film and the water, the water level is raised above the quench bath rim by making the latter hydrophobic. Polyethylene tubing, Fig. 1*b*, is split along its axis, pushed over the tank rim, and coated with paraffin wax. With a light source *K* and lens *L* (Fig. 1*c*), a magnified image of the meniscus is projected onto a screen *M*. By placing a moving picture camera at *N*, the receding contact angle can be recorded and later measured from individual frames of the film. In this way, the effect of vibration is reduced to a minimum.

Overflow at a desired place is achieved by cutting a notch in the polyethylene rim and regulating the liquid supply so that the level is maintained at a suitable height above the rim.

*3. Sweeping the Quench Liquid Surface.* To measure changes taking place when sections of the trough were isolated from the overflow or, alternatively, to make a new surface by sweeping, glass strips were coated with paraffin wax and placed across the trough rim ($O$, $O'$ Fig. 1). To sweep a section, the barriers were placed close together on either side of the film, lowered across the trough, and caused to slide apart on the rims until the desired area was swept, maintaining the slides parallel to each other and at right angles to the trough.

*4. Contact Angle of Stationary Films.* A simple projection technique previously described (6, 7) was used in these experiments.

*5. Film to Film Coefficient of Kinetic Friction.* The simple strain gauge technique has been described elsewhere (8), the films being supported on a table of polytetrafluoroethylene.

*6. Surface Tension Lowering: The Film Balance.* The surface pressure/area relation of spread monolayers at the air/aqueous interface was measured with a standard "Cenco Hydrophil" tray and torsion balance, but using Vaselined silk threads and the simplified float described by Allan and Alexander (9).

## II. The Aging Film

Additives which improve frictional properties are typical amphipathic molecules, e.g., stearamide, oleamide, palmitamide, and myristamide. Of these, oleamide has been found to be most effective in commercial practice. These molecules should orient themselves at the hydrocarbon film/air interface so that the polar group is in contact with the medium of higher dielectric constant—in this case polyethylene—and the free surface energy of the system is a minimum (10). It is well known that metallic friction is reduced most effectively when a close-packed monolayer of the amphipathic molecule is formed which has a high lateral adhesion between the hydrocarbon chains and firm anchorage to the metal by the formation of soaps (11). There is no such soap formation in the case of polyethylene, but it seems reasonable to suppose that friction will be reduced to a low value (ca. 0.1) only when a close-packed monolayer is formed. Assuming that the additive exudes to the surfaces with no losses in the preparation of the film, the minimum concentration of additive required in the original polymer, $C_B$, in parts per million by weight is given by

$$C_B = 2 \times 10^{10} \frac{M}{ptNA}, \qquad [1]$$

where $M$ = molecular weight of the additive, $g$;

$p$ = density of the polyethylene, g./c.c.;

$t$ = film thickness, cm.;

$N$ = Avogadro's number = $6.023 \times 10^{23}$; and

$A$ = minimum area in the close-packed monolayer from film balance studies (28 A.$^2$/molecule, Fig. 10).

For example, this relationship shows that, from a polymer containing 100 p.p.m. of oleamide, films of 50 μ thickness will have a close-packed monolayer present, whereas films of 25 μ thickness will not. To illustrate the importance of this, Fig. 2 shows the effect of concentration of oleamide on the coefficient of kinetic friction of films of 38 μ thickness prepared by the blown film extrusion process. By calculation, the monolayer is completed at *A* and higher concentrations show a marked reduction in friction. The various curves refer to increasing times after extrusion. For low concentrations of the additive, the friction is apparently erratic. With film extruded by the flat film process, a similar effect was observed. Figure 3 shows the variation of coefficient of kinetic friction with time for a polyethylene into which was milled 180 p.p.m. of oleamide. It is seen that the thin film (38 μ thickness) reaches a low friction after some 500 hours, whereas the thick film reaches its lowest value after only 3 hours.

These results are consistent and suggest that the monolayer requirement seems reasonable and, further, the rate of diffusion or exudation of the amphipathic molecule at room temperature is slow, since even with films of 100 μ thickness some hours elapse before a complete close-packed monolayer is formed on the surface.

It is interesting to speculate why the friction with incomplete monolayers is erratic and occasionally higher than the friction of the polymer with no additive (Figs. 2 and 3). It is possible that a certain proportion of the amphipathic molecules emerge polar head first, thereby increasing the surface energy and friction. (This would be analogous to the results of Zisman and his co-workers (12), who found marked increases in friction of high polymers when the concentration of polar groups on the high-polymer chain increased.)

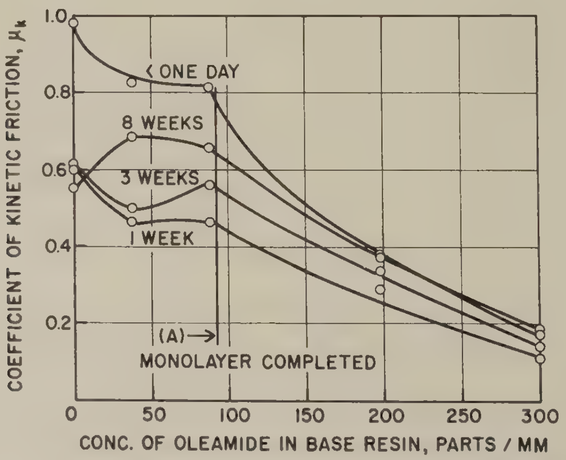

FIG. 2. Effect of oleamide concentration on the coefficient of kinetic friction.

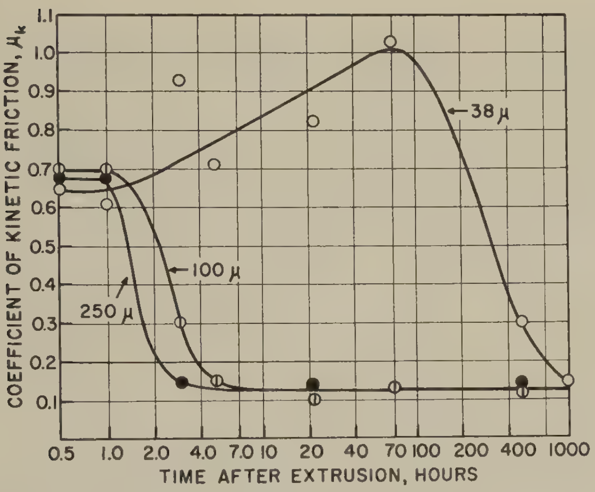

Fig. 3. Effect of time on the coefficient of kinetic friction for various film thicknesses of a polyethylene containing 180 p.p.m. of oleamide.

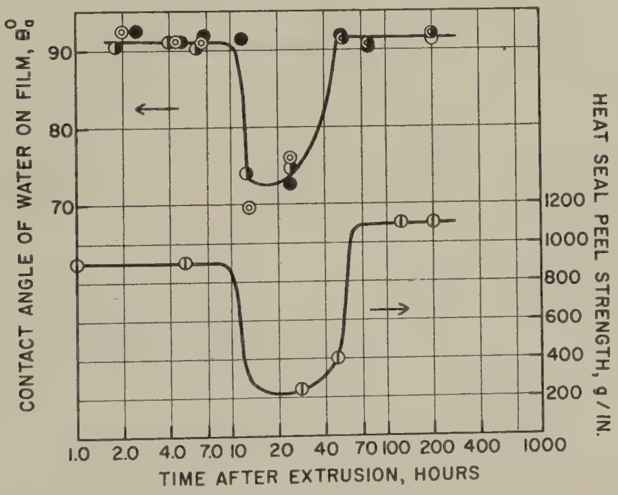

Fig. 4. Effect of time on (*a*) contact angle, (*b*) heat seal peel strength for a polyethylene containing 180 p.p.m. of oleamide and of 50 μ thickness. ◎ dry; ● 50% relative humidity; ◑ 90–100% relative humidity.

The work of Rideal and Tadayon (6) with stearic acid suggests that such a condition of high polarity is metastable and the molecules are capable of overturning into their configuration of lowest free surface energy (i.e., nonpolar end outwards toward the air). This should be detectable by contact angle studies.

Changes in contact angle with time after extrusion of polyethylene film containing 180 p.p.m. of oleamide are shown in Fig. 4*a*. There is seen to be no significant effect of relative humidity under these conditions where no liquid water condensed onto the film. The contact angle shows a marked reduction between 10 and 40 hours, being restored to a value greater than 90° after 40 hours. This change in the surface was confirmed by measurements on heat sealing (3) of two surfaces together. Figure 4*b* shows the heat seal peeling strength at a given temperature of sealing. There is seen to be a temporary reduction in strength of the heat seal (overcome by raising the sealing temperature) which can be attributed to the presence of polar heterogeneities which hinder the coalescence of the hydrocarbon.

The presence of an oriented monolayer is further suggested by the dramatic effect on the stability of the low friction surface when the polyethylene substrate has been flame treated to make it printable (7). Film containing oleamide and treated with a flame on one surface to make it printable was stored at 72°F. in an atmosphere of 50% relative humidity. On removing this film to an atmosphere of high humidity and high temperature (*ca.* 90°F.) the friction of the treated surface remained low but a high friction was produced on the untreated surface, typical of films not containing additives. This effect was reversible (13).

We can summarize what can be learned from these diverse experiments by reference to the diagram, Fig. 5. The additive in the bulk (*a*) exudes to the surface (*b*) and at equilibrium produces a weakly held oriented monolayer (*c*) which takes 1–500 hours to form, depending on the concentration of the additive and the surface-to-volume ratio of the film (i.e., film thickness). In the early stages of the extrusion, some of the polar heads are ex-

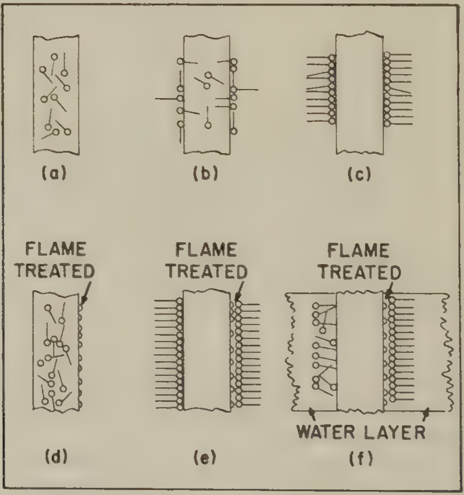

FIG. 5. The exudation of amphipathic molecules from polyethylene.

posed, causing higher friction and lower contact angles, and requiring slightly higher heat-sealing temperatures. The treatment of the surface to render the film printable results in the deposition of relatively firmly anchored polar groups (7, 14), as at (*d*), so that the monolayer of additive is more firmly held (*e*). Removing the film to a warmer atmosphere of high humidity, producing condensation on the cold film, easily disrupts the monolayer on the untreated side, whereas the monolayer on the treated side remains stable (*f*).

At the present time, this simple picture seems to explain all the diverse observations made on aging films.

## III. The Nascent Film

In the flat film extrusion process described above films prepared from polymers containing amphipathic additives pick up drops of water from the bath more easily than films without additives. Experiments on the moving film enable this phenomenon to be understood.

### *A. Contact Angles and Water Pickup with Overflow*

The receding dynamic contact angle ($\theta_r$) was measured for a variety of film thicknesses, speeds of withdrawal, and additive concentrations. A selection of the results is shown in Figs. 6*a* and 6*b*. For a constant film thickness (Fig. 6*a*) it can be seen that the plot of cosine $\theta_r$ versus film speed becomes progressively more convex to the abscissa at lower speeds as the bulk concentration of additive is increased. Since it can be shown (Appendix) that the speed at which water is picked up depends only on the static receding contact angle and the surface tension of the quench bath liquid, these results imply a reduction in surface tension of the liquid as speed is increased, this reduction at any given speed clearly depending on the concentration of oleamide in the polymer. Thus, appreciable quantities of the additive spread onto the water surface as the film emerges.

Figure 6*b* shows that, at any particular additive concentration and film speed, the contact angle decreases as the film thickness increases. Again, the speed at which water is picked up is critically dependent on film thickness when the additive is present, but independent of film thickness when the films are free from additive (Fig. 7). These are important and interesting results since they show that even prior to the film emerging from the quench bath, an excess of oleamide has emerged onto the surface; otherwise, film thickness would have no effect on the contact angle or on the speed at which water was picked up.

### *B. Sweeping Experiments*

It had been found that stopping the overflow resulted in rapid pickup of water on the film. With the sweeping technique described above, this

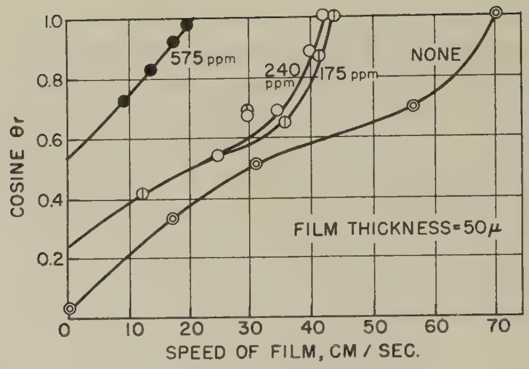

FIG. 6*a*

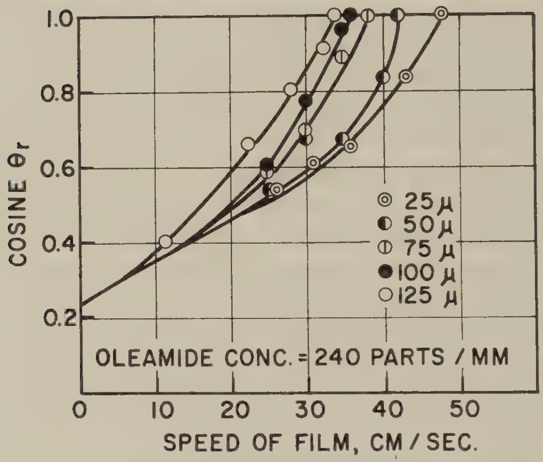

FIG. 6*b*

FIG. 6. The relation between speed and receding contact angle. (*a*) effect of oleamide concentration (in p.p.m.) (film thickness 50 μ) (*b*) effect of film thickness (oleamide concentration 240 p.p.m.).

could be examined quantitatively. The time taken from commencing the sweep to water pickup on the film was measured for several speeds, film thicknesses, and additive concentrations. It was found that in all cases the time taken for water pickup to commence was proportional to the area of water surface swept out and decreased as the speed increased. An example of the results is shown in Fig. 8. This suggests that the additive spreads on to water at a quantitative rate governed by the concentration of molecules on the film surface.

It was observed that even after water pickup commenced from a closed area, the oleamide continued to spread on the stagnant surface until crystals were formed. However, long before this point of crystal formation and

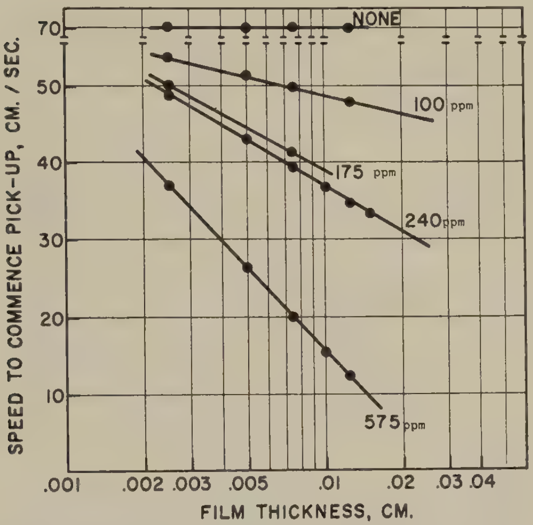

FIG. 7. Effect of film thickness on speed at which water pickup commences for films from polymers containing various concentrations of oleamide (in parts per million).

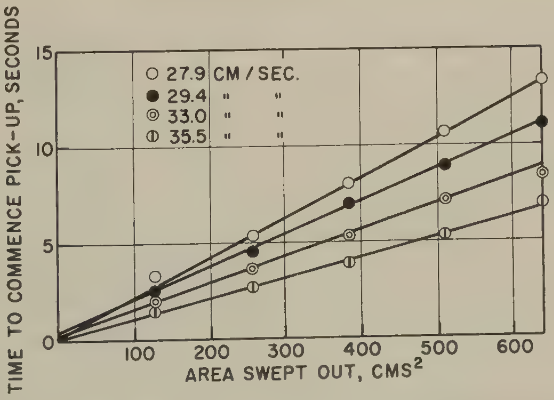

FIG. 8. Effect of trough area swept out on time to commence water pickup at constant film thickness.

long after water pickup commenced, a few talc particles sprinkled on the surface and gently blown about suddenly appeared to "freeze" showing that a solid invisible gel-like film was formed. With the sweeping technique, this surface gel point was measured for several speeds, film thicknesses, and swept areas. The time was again found to be reproducible, proportional to the area of clean surface originally swept out and decreasing as film speed or thickness increased (Fig. 9). This again suggests that the additive spreads quantitatively from the film onto the water surface. In fact, the reproduci-

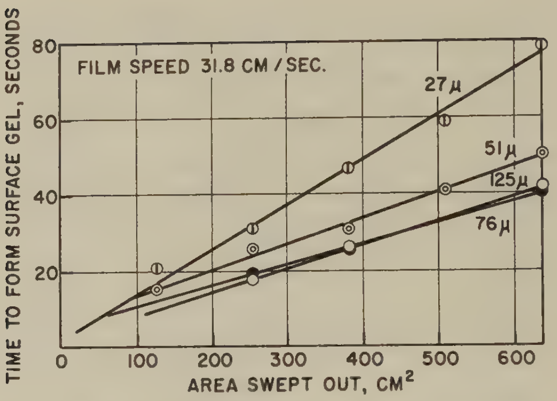

FIG. 9. Effect of area swept out on time to form a surface gel at constant speed.

bility of both the surface gel point and the time to start the water pickup from a clean surface over a wide range of conditions suggests that every molecule free on the polyethylene surface is stripped off onto the water surface as the film emerges.

### *C. Film Balance Studies*

To calculate the concentration of molecules on the water surface, and thus on the film surface, it is necessary to know the surface area/surface tension lowering characteristics of monolayers of this class of compounds spread on water. These curves are shown in Fig. 10. The results are in good agreement with earlier work by Adam (15, 16), who showed that the presence of a double bond in the hydrocarbon chain caused an expansion of the film. In the case of oleamide, the area at collapse is 28 A.$^2$/molecule. At this point, however, the film remains a two-dimensional liquid and only at about 9 A.$^2$/molecule does the film become solid ($A_g$ in Fig. 10). Further, the area of solidification is quite reproducible and implies a uniform collapsed layer three molecules thick. A reproducible gel point in collapsed monolayers does not seem to have been observed before, and should be studied further with more carefully controlled conditions of pH and a simultaneous study of surface potential and surface viscosity. (It is interesting to note that the gel point was observed in the extrusion studies discussed above before the surface balance studies were made.)

### *D. Concentration of Oleamide on the Emerging Film Surface*

From the various types of data above, the concentration of oleamide on the film surface can be calculated, provided the conditions for water pickup are specified. In general, it is suggested that the surface concentration is frequently lowest at the film periphery, since there is an effective mechani-

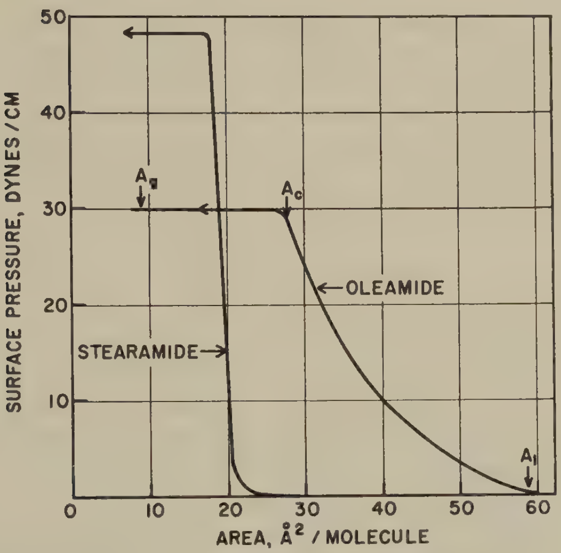

FIG. 10. Surface pressure/area relationship for amides.

cal pumping action of water moving down the meniscus which pushes the spreading molecules to the edge of the trough where they either go over the weir or are compressed into a monolayer of appreciable surface pressure. In all cases, the contact angle and thus the approach to water pickup will be affected by the surface tension at the film periphery.

*1. Time to Start Pickup from a Closed, Initially Clean Surface.* Assuming that pickup occurs when the surface tension at the film periphery is lowered from that of pure water and that this commences at an average area on the water surface of 59 A.²/molecule ($A_1$ in Fig. 10), we can determine the time taken to fill a unit area of surface from the slopes of the plots of time to pick up water ($t_p$) vs. area of surface swept ($A_w$). If every molecule is stripped from the film the concentration on the film surface $C_1^f$ is related to the concentration on the water surface $C^W$ as follows:

$$C^W \times \frac{A_w}{t_p} = C_1^f \times 2lS, \qquad [2]$$

where $l$ is the film width and $S$ is the speed.

It is more reasonable to suppose that the surface tension at which water is picked up varies with the speed. By determining the speeds at which water is picked up ($S_p$) from a clean flowing surface and from a saturated stagnant surface and assuming that these conditions refer to surface tensions of 72 dynes/cm. and 42 dynes/cm., respectively, we can determine the surface tension at pickup for any intermediate speed from a simple equation, $\gamma_p = aS_p + b$, $a$ and $b$ being estimated from the limiting conditions. We can then determine approximate values of $C^W$ from the surface-pressure vs. area curves and hence from Eq. [2] a second set of values of $C_1^f$.

*2. Time to Form a Surface Gel.* Since the gelation occurs only when there is a trimolecular layer present (Fig. 10), the area per molecule on the water surface is now 9 A.$^2$ or $C^W = 1 \times 10^{15}$ molecules/cm.$^2$, and hence, as in Eq. [2], we have

$$C^W \frac{A_w}{t_g} = C_2^f \cdot 2lS, \qquad [3]$$

where $t_g$ is the time to form a surface gel over the area $A_w$ (see Fig. 9).

*3. Time to Pickup with a Weir Overflow.* The rate of draining away of the compressed monolayer will have a marked effect on the lowering of surface tension close to the film. In these experiments, the velocity over the weir was sufficient to cope with the spreading monolayer so that the limiting rate of spreading (i.e., when pickup occurs) of the oleamide from the polyethylene film is given by the speed of spreading of a monolayer at some relatively stationary point midway between the film and the weir. Accumulation of the monolayer will result in surface tension lowering close to the film. The speed of spreading of oleamide was approximately 10 cm./sec., similar to the value for oleic acid obtained by Cary and Rideal (17). If $C^W$ close to the film is again $1.7 \times 10^{14}$ molecules/cm.$^2$, we can obtain a value for $C_3^f$ from

$$C^W S_m = C_3^f \cdot S_p, \qquad [4]$$

where $S_m$ is the monolayer speed and $S_p$ is the film speed at pickup. It is important to note that this equation is true only when water pickup occurs.

In Table I are summarized the concentrations of molecules on the film surfaces when water pickup commences calculated from data similar to those shown in Figs. 7, 8, and 9 for films of 50 $\mu$ thickness, and compared with the values to be expected from a uniform distribution of additive, i.e., $C_B^{2/3}$.

We may note that (*a*) there is fair agreement between the surface concentrations calculated from the three types of experiment, (*b*) basing the calculation on uniform distribution of the additive we get a surface concentration one hundred times too low to account for the observed effects, and (*c*) approximately 10%–20% of the close-packed monomolecular film is present on the surface of the film and is completely stripped off on to the water surface as the film emerges.

From the experiments on film aging at room temperature, it seems unlikely that such a marked exudation could occur in so short a lifetime of the solid (i.e., < 5 sec.); and it is therefore suggested that most, if not all,

TABLE I

*Comparison of Calculations for the Concentration of Oleamide on the Film Surface at Water Pickup Speed (Film Thickness = 50μ)*

| Concentration of oleamide in bulk (p.p.m.) | Concentration on film surface molecules/cm² × 10⁻¹³ | | | | |
|---|---|---|---|---|---|
| | $C_1^f$ | | $C_2^f$ | $C_3^f$ | $C_B^{\frac{2}{3}}$ |
| | $\gamma_p$ = Const | $\gamma_p = aS_p + b$ | | | |
| 100 | 1.9 | 2.0 | — | 3.3 | 0.037 |
| 175 | 4.4 | 6.1 | — | 3.8 | 0.054 |
| 240 | 6.0 | 5.5 | 6.0 | 4.0 | 0.067 |
| 575 | 6.7 | 7.0 | — | 6.5 | 0.120 |

of the molecules stripped off the cold emerging film are present on the surface of the molten film as it enters the water. This necessarily implies a surface adsorption either at the molten polymer/metal or molten polymer/air interface.

Surface activity in molten polymers is a new concept and analogous to the studies of surface activity at the oil/air interface at room temperatures recently discussed by Ellison and Zisman (18). In this particular case, the relation between the surface tension lowering and the bulk concentration is not known, and there is also a complex surface aging phenomenon involved. However, if we assume that a gaseous monolayer is formed on the surface of the molten polymer and that equilibrium is reached before the film is stretched appreciably, then it can be shown that the surface excess is proportional to the bulk concentration (19). From Fig. 7 and Eq. [4], the surface concentration ($C_s^u$) for unstretched film (250 μ thickness) can be determined approximately by extrapolation and is found to be directly proportional to the bulk concentration ($C_s^u = 4 \times 10^{11} C_B$, where $C_s^u$ is in molecules/cm.² and $C_B$ is in parts per million of additive in the polymer).

From this calculation and Table I, it is evident that a marked surface excess has been demonstrated and related to the bulk concentration. In conclusion, it may be suggested that the rate of diffusion of solute molecules in this molten hydrocarbon polymer is not drastically lower than the diffusion in a liquid hydrocarbon of low molecular weight at room temperature.

## *Appendix*

Considering the polyethylene film/air/water junction, water pickup will occur as soon as it is necessary to do more work to remove the water from the film than to break the water surface. Two factors must be considered: the relation between the free surface energies of the components of the system and the relative motion of the two materials, polyethylene and liquid. When the film emerges from the liquid at some speed $S$, the forces

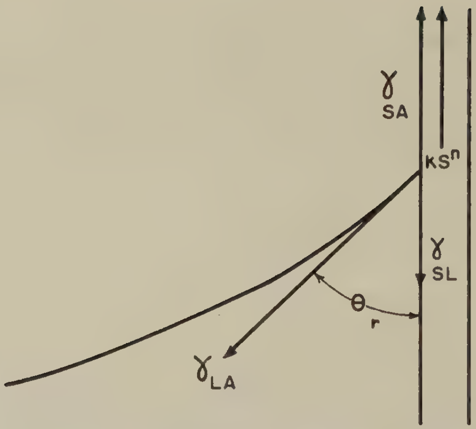

FIG. 11. The air/emerging film/water junction.

involved are those shown in the diagram Fig. 11. The surface free energies of the interfaces liquid/air, solid/air, solid/liquid are given by $\gamma_{LA}$, $\gamma_{SA}$, and $\gamma_{SL}$, respectively, and the receding contact angle between the solid and the liquid is $\theta_r$. The relative motion of the solid through the air/water interface imparts an acceleration to the liquid mass which results in an additional stretching force on the liquid. This will be some function of the speed of withdrawal, the liquid viscosity, and density. Let us assume that this force is $kS^n$, where $n$ is less than one. The well-known equation (reference 19, p. 41)

$$\gamma_{SA} = \gamma_{LA} \cos \theta_r^0 + \gamma_{SL} \qquad [5]$$

becomes

$$\gamma_{SA} + kS^n = \gamma_{SL} + \gamma_{LA} \cos \theta_r, \qquad [6]$$

where $\theta_r^0$ is the static receding contact angle and $\theta_r$ the receding contact angle when the film is moving at a speed $S$. Substituting for $\gamma_{SA}$ from [5] in [6], we have

$$kS^n = \gamma_{LA} (\cos \theta_r - \cos \theta_r^0), \qquad [7]$$

or

$$\cos \theta_r = \frac{kS^n}{\gamma_{LA}} + \cos \theta_r^0, \qquad [7a]$$

and if, when water is picked up on the film, $\theta_r = 0$, then

$$kS_p^n = \gamma_{LA}(1 - \cos \theta_r^0), \qquad [8]$$

where $S_p$ is the speed at which water is picked up on the film. Similarly, water is picked up on the film when

$$kS_p^n + W_{SL} = W_c , \tag{9}$$

where $W_c$ is the work of cohesion of the liquid $= 2\gamma_{LA}$ and $W_{SL}$, the work of adhesion, is given by the Dupré equation (19)

$$W_{SL} = \gamma_{SA} + \gamma_{LA} - \gamma_{SL} . \tag{10}$$

By substituting for $W_{SL}$ and $W_c$ in [9] and using Eq. [5], we again obtain Eq. [8], suggesting that at this point of pickup of water the receding contact angle is indeed zero, and that the speed at which water is picked up is determined solely by the static receding contact angle and the surface tension of the quench bath liquid.

## REFERENCES

1. HULL, D. R., U.S.P. 2,324,397.
2a. SYMONDS, A. E., U.S.P. 2,770,609.
 b. BARKER, H. C., LEWIS, E. E., AND HAPPOLDT, W. B., U.S.P. 2,770,608.
3. JENKINS, S. H., Paper presented at the National Meeting of the American Chemical Society, New York, 1957.
4. BLOYER, S. F., *Modern Plastics* **32** (July), 105 (1955).
5. KRICHEVER, V., U.S.P. 2,683,894.
6. RIDEAL, E. K., AND TADAYON, J., *Proc. Roy. Soc. (London)* **A225,** 346 (1954).
7. ALLAN, A. J. G., *J. Polymer Sci.* (in the press).
8. ALLAN, A. J. G., *J. Polymer Sci.* **24,** 461 (1957).
9. ALLAN, A. J. G., AND ALEXANDER, A. E., *Trans. Faraday Soc.* **50,** 863 (1954).
10. HARDY, W. B., *Proc. Roy. Soc. (London)* **A88,** 330 (1913).
11. BOWDEN, F. P., AND TABOR, D., "The Friction and Lubrication of Solids." Oxford University Press, Oxford, 1954.
12. BOWERS, R. C., CLINTON, W. C., AND ZISMAN, W. A., *Modern Plastics* **31** (Febr.), 131 (1954).
13. DARDEN, E. T., Private communication.
14. HINES, R. A., Paper presented at American Chemical Society meeting, New York, September, 1957.
15. ADAM, N. K., *Proc. Roy. Soc. (London)* **A101,** 516 (1922).
16. ADAM, N. K., *Proc. Roy. Soc. (London)* **A106,** 694 (1924).
17. CARY, R. F., AND RIDEAL, E. K., *Proc. Roy. Soc. (London)* **A109,** 310 (1925).
18. ELLISON, A. H., AND ZISMAN, W. A., *J. Phys. Chem.* **60,** 416 (1956).
19. ADAM, N. K., "Physics and Chemistry of Surfaces," 3rd ed., Oxford University Press, Oxford, 1941.

JOURNAL OF COLLOID SCIENCE **14**, 222–238 (1959)

# DYNAMIC MECHANICAL PROPERTIES OF CONCENTRATED SOLUTIONS OF POLY-*n*-BUTYL METHACRYLATE IN DIETHYL PHTHALATE[1]

**P. R. Saunders[2], Donald M. Stern[3], Sheldon F. Kurath[4], Charoen Sakoonkim, and John D. Ferry**

*Department of Chemistry, University of Wisconsin, Madison, Wisconsin*

*Received December 8, 1958*

## INTRODUCTION

Measurements of the dynamic mechanical properties of poly-*n*-butyl methacrylate over a wide range of frequencies have been reported previously (1), as part of a cooperative study of a series of methacrylate polymers undertaken with the Feltman Research and Engineering Laboratories, Picatinny Arsenal. We now present similar data on a series of four concentrated solutions of the butyl polymer, ranging in concentration from 30% to 60% by weight. Analysis of the frequency and temperature dependence reveals the effects of low molecular weight diluent on the monomeric friction coefficient, the entanglement spacing, and other features which determine viscoelastic behavior.

## MATERIALS AND METHODS

The polymer was Fraction FF-1 described previously (1), with a weight-average molecular weight of $3.05 \times 10^6$. The solvent was diethyl phthalate, obtained from Brothers Chemical Company, boiling point 127–128° at 3 mm. pressure. The solutions were made up by swelling the finely divided polymer (dried from the frozen state) in the solvent and then (depending on the consistency) homogenizing either by very slow stirring with a magnetic stirrer, by alternately molding under pressure and cutting into small pieces, or by extruding through grooves in a mold plunger. The temperature during these manipulations did not exceed 70°C.

The densities of the 40.3% and 60% solutions were determined by pycnometric measurements, and those of the others were calculated assuming a linear dependence of the specific volume on weight fraction. Refractive index measurements were made over a wide range of temperatures by the method of Jenckel and Heusch (2), using an Abbé refractometer placed in a room at −5° and further cooled by circulating trichloroethylene chilled with Dry Ice or liquid air. These measurements provided the glass transition temperatures ($T_g$) of two of the solutions, together with estimates of thermal expansion coefficients ($\alpha$) both above and below $T_g$, calculated from the Lorenz-Lorentz equation. The results are summarized in Table I.

---

[1] Part XXXI of a series on Mechanical Properties of Substances of High Molecular Weight.

[2] Present address: Chemstrand Corporation, Decatur, Alabama.

[3] Present address: Esso Research and Engineering Company, Linden, New Jersey.

[4] Present address: Institute of Paper Chemistry, Appleton, Wisconsin.

Measurements of the complex shear compliance ($\mathbf{J}^* = J' - J''$) were made between 10 and 2400 cycles/sec. with the Fitzgerald Apparatus (3). Two pairs of disc-shaped samples were used for each solution, molded at 40°C. (in some cases with brief heating to 70°C.). Detailed descriptions of the samples follow.

### *30% Solution*

Samples 118, approximate dimensions 1$\frac{1}{16}$ in. diam. by $\frac{1}{32}$ in. thickness, were compressed slightly in the apparatus and the nominal sample coefficient ($A_1/h_1 + A_2/h_2$, where $A$ and $h$ are the respective face areas and thicknesses) was 62.0 cm. at 25°C., calculated from the thicknesses *in situ* and the masses and density of the samples. Measurements were made at approximately 5° intervals from −30° up to 0°, followed by a check run at −10°. The exact temperatures are given in the legend of Fig. 2.

Samples 119, approximate dimensions 1$\frac{1}{16}$ in. by $\frac{1}{8}$. in., were compressed slightly, and the nominal sample coefficient was 22.7 cm. at 25°C. Measurements were made at approximately −30°, −40°, −50°, −45°, −35°, −25°, −15°, −20°, and −10°C. (Samples 118 experienced the same temperature sequence, but were not measured at the lower temperatures because of the high sample coefficient.) Values of $J'$ and $J''$ from Samples 119 were about 12% higher than those from 118 at corresponding temperatures; since the latter were considered less reliable because of the extreme thin-

TABLE I

*Density and Refractive Index Data*

| | | | | |
|---|---|---|---|---|
| Concentration, weight per cent | 30.0 | 40.3 | 50.0 | 60.0 |
| Density at 25° C., g./c.c. | (1.093) | 1.086 | (1.079) | 1.072 |
| Concentration, g./c.c. | 0.334 | 0.445 | 0.549 | 0.654 |
| Refractive index at 25° C., $n$ | 1.493 | 1.491 | 1.489 | 1.488 |
| $T_g$ | <−75° | <−75° | −67° | −46° |
| $dn/dT$ above $T_g$, × 10⁴ | −4.10 | −3.93 | −4.00 | −3.68 |
| $dn/dT$ below $T_g$, × 10⁴ | — | — | −1.99 | −2.98 |
| $\alpha$ above $T_g$, × 10⁴ | 6.5 | 6.2 | 6.5 | 6.1 |
| $\alpha$ below $T_g$, × 10⁴ | — | — | 3.1 | 4.8 |

ness and the difficulty of its measurement, they were multiplied by an empirical correction factor of 1.12.

### *40.3% Solution*

Samples 96, approximate dimensions $1\frac{1}{16}$ in. diam. by $\frac{1}{8}$ in. thickness, were compressed in the apparatus about 6% and the nominal sample coefficient was 16.0 cm. at 25°C. Measurements were made at approximately −25°, −30°, −35°, −40°, −49°, −45°, −20°, and −15°, followed by a check run at −25°. The values of $J'$ and $J''$ from the check run were about 13% higher than those from the initial run at −25°.

Samples 97, approximate dimensions $1\frac{1}{16}$ in. by $\frac{1}{16}$ in., were compressed about 6%, and the nominal sample coefficient was 28.7 cm. at 25°. Measurements were made at approximately −15°, −25°, −20°, −15° (check run), approximately 5° intervals from −5° to 25°, then −10°, and finally a check run at −15°. Both the check runs at −15° agreed with the initial results at that temperature. The data from Samples 97 at −25° agreed with those from the first run at that temperature on Samples 96. The data of the last three runs on Samples 96 were 13% higher than those at corresponding temperatures on samples 97. The discrepancies indicated that Samples 96 had changed in shape after the low-temperature measurements, and the data for the last three runs on those samples were discarded.

### *50% Solution*

Samples 115, approximate dimensions $1\frac{1}{16}$ in. by $\frac{1}{8}$ in., were compressed about 2% and the nominal sample coefficient was 16.7 cm. at 25°. Measurements were made at approximately 5° intervals from 15° down to −15°, followed by a check run at 15° which yielded values of $J'$ and $J''$ about 7% higher than the original results at that temperature. (The exact temperatures are given in the legend of Fig. 2).

Samples 116, approximate dimensions $1\frac{1}{16}$ in. by $\frac{1}{32}$ in., were compressed about 7%, and the nominal sample coefficient was 54.0 cm. at 25°C. They experienced the same temperature sequence as Samples 115; measurements were made at approximately 5° intervals from 15° down to −5°, and then at 20°, 25°, 35°, and 45°, followed by a check run at 15° which agreed within 2% with the original results at that temperature. The data from Samples 115 and 116 agreed closely at overlapping temperatures (except for the final run at 15° on Samples 115, which was rejected), and no empirical correction factor was applied.

### *60% Solution*

Samples 104, approximate dimensions $1\frac{1}{16}$ in. by $\frac{1}{8}$ in., were compressed slightly in the apparatus and the sample coefficient was 16.6 cm. Measurements were made at approximately 25°C., then at intervals of about 5°

from 0° down to −15°, and intervals of about 5° from 5° up to 40°, followed by check runs at 25° and −5° which agreed well with the initial results. (The exact temperatures are given in the legend of Fig. 1.)

Samples 105, approximate dimensions $\frac{5}{16}$ in. by $\frac{3}{16}$ in., were compressed about 6% and the nominal sample coefficient was 2.71 cm. They experienced the same temperature sequence as Samples 104; measurements were made at 5° intervals from 0° down to −45°, all completed before the higher temperature measurements on Samples 104, followed by check runs at 25° and −5°. The values of $J'$ and $J''$ were about 10% higher than those of Samples 104, and since this is in the expected direction for bulging of the thicker samples, the data for Samples 105 were corrected by an empirical factor of 0.90.

Sample coefficients at temperatures other than 25° were always calculated from the thermal expansion coefficients, assuming no change in sample thickness. In advance of the data of Table I, $\alpha$ was estimated by linear interpolation between the values for polymer and solvent, giving values near $7 \times 10^{-4}$ deg.$^{-1}$, in satisfactory agreement with Table I for the purposes of this calculation.

## RESULTS

For brevity, the original data are shown only for the 60% solution; $J'$ and $J''$ are plotted logarithmically in Fig. 1 for 18 temperatures ranging from −43.6° to 39.9°C. Here, the entire transition from glasslike to rubberlike consistency is encompassed. The data for the other solutions were

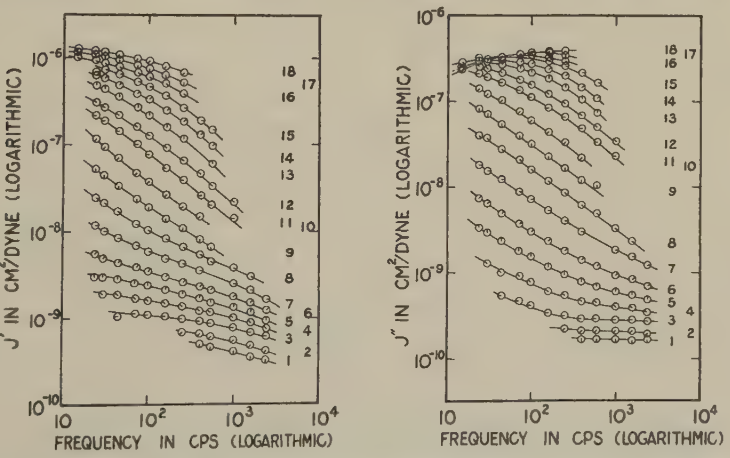

FIG. 1. Variation of the real part of the dynamic shear compliance, $J'$ (left) and the imaginary part, $J''$ (right) with frequency for 60% poly-$n$-butyl methacrylate in diethyl phthalate at 18 temperatures; numbers follow the temperature sequence −43.6°, −40.1°, −34.6°, −29.9°, −24.4°, −20.1°, −15.0°, −9.5°, −4.8°, 0.2°, 5.7°, 9.6°, 14.8°, 19.7°, 24.6°, 29.7°, 34.6°, and 39.9°C.

qualitatively similar except that they did not extend to low enough temperatures to reach the glassy end of the transition.

A standard temperature of 0°C. was chosen for reduction, since the standard of 100° which has been used for the series of undiluted methacrylate polymers (1) was inaccessible. With the usual formulas, $J'_p$ and $J''_p$ were calculated; logarithmic plots of these functions could be superposed very well by the usual shift factors $a_T$ except for two anomalies which are familiar in the undiluted polymethacrylates: one at very low temperatures in the 60% solution, and another near the maximum of $J''$ in all four solutions.

The empirical $a_T$ values followed closely equations of the WLF form (4):

$$\log a_T = -c_1^0(T - T_0)/(c_2^0 + T - T_0), \qquad [1]$$

and values of $a_T$ calculated therefrom were actually used for the final logarithmic plots of $J'_p$ and $J''_p$ against reduced frequency, $\omega a_T$, which are shown in Figs. 2 and 3. The coefficients $c_1^0$ and $c_2^0$ are given in Table II.

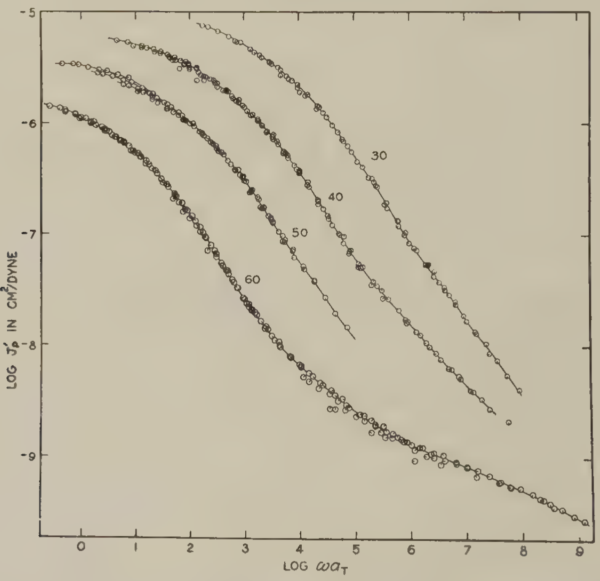

FIG. 2. Real part of the complex compliance, $J'$, for the 4 solutions with concentrations indicated, reduced to 0°C. and plotted logarithmically against reduced frequency with reduction factors calculated from the WLF equation with the coefficients in Table II. Successive counterclockwise rotations of pips (starting with pip down at highest reduced frequency) correspond to the following temperature sequences: 30%, −49.4°, −44.7°, −40.1°, −34.5°, −29.6°, −24.1°, −19.3°, −14.8°, −9.8°, and −0.1°; 40.3%, −48.9°, −44.3°, −40.2°, −35.0°, −30.0°, −24.9°, −20.0°, −15.0°, −9.8°, −5.3°, −0.4°, 4.9°, 9.4°, 15.0°, 19.8°, and 25.2°C.; 50%, −14.7°, −9.8°, −4.8°, −0.3°, 4.7°, 9.9°, 14.9°, 20.0°, 25.3°, 35.9°, and 47.1°; 60%, same as in Fig. 1.

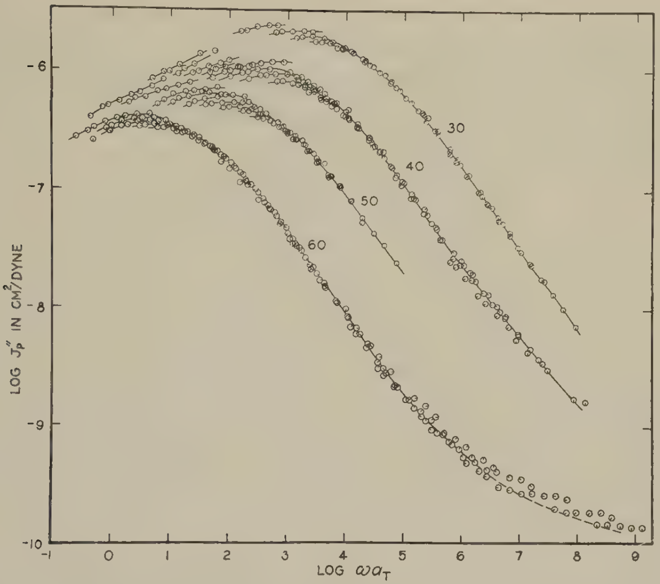

FIG. 3. Imaginary part of the complex compliance, $J''$, for the 4 solutions, reduced and plotted as in Fig. 2.

TABLE II

*Parameters for Temperature Dependence of Relaxation Mechanisms*

| Concentration, wt.% | 30.0 | 40.3 | 50.0 | 60.0 | 100[a] |
|---|---|---|---|---|---|
| $c_1^0$ ($T_0$ = 273° K.) | 9.58 | 9.95 | 9.98 | 12.80 | — |
| $c_2^0$ ($T_0$ = 273° K.) | 163.3 | 166.6 | 153.1 | 157.3 | — |
| $\alpha_f \times 10^4$, deg.$^{-1}$ | 2.8 | 2.6 | 2.8 | 2.2 | 2.6 |
| $f_g$ | — | — | 0.024 | 0.024 | 0.026 |

[a] From reference 1, for Fraction FF-2, considered to be the more reliable.

The parameter $\alpha_f$, interpreted as the thermal expansion coefficient of the relative free volume (4), may be calculated from $c_1^0$ and $c_2^0$, and is also given in Table II. The values fluctuate somewhat but are all of similar magnitude. For the two solutions whose glass transition temperatures are known, $f_g$, the fractional free volume at $T_g$, can also be calculated and is given in the table; it is gratifyingly close to the approximately universal value (4) of 0.025.

## REDUCTION ANOMALIES

### *Low-Temperature Anomaly*

The progressive drop in $J''_p$ at the lowest temperatures on the reduced plot is reminiscent of, though less marked than, the behavior of undiluted poly-*n*-dodecyl methacrylate (5), which was attributed to crystallization of the side groups; it resembles the latter more than the anomaly in polyethyl methacrylate (6), which was attributed to a $\beta$ mechanism. Conceivably, the plasticizer may be crystallizing out here, but no attempt has been made to clarify this anomaly since our major interest is in the behavior at the lower end of the frequency scale.

### *High-Temperature Anomaly*

The divergence in $J''_p$ near its maximum after reduction is an exaggerated form of the anomaly which has already been seen in the undiluted *n*-butyl, *n*-hexyl, and *n*-octyl polymers, and it can be analyzed in the same manner (7). If increasing the temperature from $T_0$ to $T$ increases the average degree of polymerization between entanglement coupling points, $Z_e$, by a factor $f$, then it follows from theories such as that of Bueche (8) that a reduced logarithmic plot like Fig. 3 will shift upward by log $f$ and to the left by 2 log $f$. Thus, values of the relative entanglement factor $f$ can be determined empirically from the divergences in Fig. 3. It turns out that, just as in the case of the undiluted polymers, log $f$ is a linear function of $1/T$, and the slope corresponds to an apparent heat of dissociation of entanglement points of 2.1 kcal./mole for all four solutions. This value is intermediate between those of 1.6 kcal. for undiluted poly-*n*-octyl methacrylate and 2.3 kcal. for the undiluted butyl and hexyl polymers (7).

Using 2.1 kcal./mole, calculated values of $f$ (based of course on 273°K. as reference temperature) were applied to complete the reduction of $J'$ and

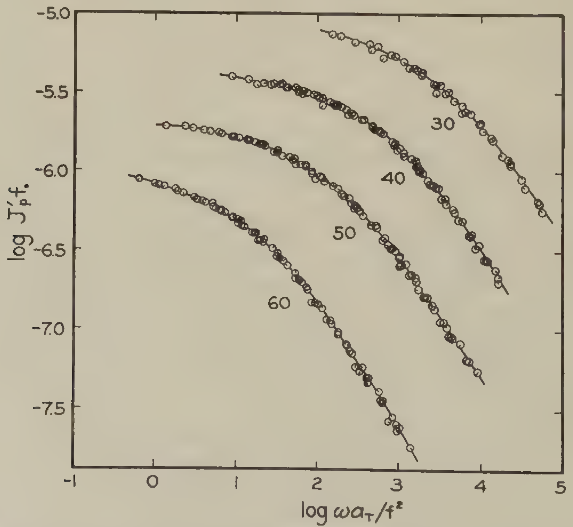

FIG. 4. Real part of the complex compliance for the 4 solutions in the low-frequency range, reduced to 0°C. for temperature dependence of both $a_T$ and $f$. Temperature key to pips same as in Figs. 1 and 2.

$J''$ for both $a_T$ and entanglement anomaly, plotting $J'_pf$ and $J''_pf$ against $\omega a_T/f^2$. The results are shown in Figs. 4 and 5, and manifest excellent superposition. The $f$-shift does not make so much difference to $J'$ because its direction is near the slope of the curve itself; at higher frequencies, both log $J'$ and log $J''$ acquire essentially the same slope as the direction of the shift, so that the effect of the latter vanishes as previously explained (7). The further success of this treatment lends confidence to its applicability, even though the significance of the apparent heat of dissociation is still not clear.

Such a dependence of entanglement point density on temperature would imply that the apparent activation energy for viscous flow must be higher than that for local frictional motion as revealed by mechanical behavior in the transition region—in this case, by about 7 kcal. Steady-flow viscosity measurements are yet not available for any of the methacrylate systems for which the entanglement anomaly has been observed. In polyisobutylene, by contrast, this anomaly is clearly absent as evidenced by the virtual identity (9) of the temperature dependences of steady-flow viscosity and segmental relaxation times (a very slight difference in the wrong direction was noted) as well as the success of reduced variables near the maximum in $J''$ (9, 10). Another consequence of the entanglement anomaly is that the break in a logarithmic plot of viscosity against molecular weight (11) should be temperature-dependent. The extensive data required to test this conclusion are not available, however.

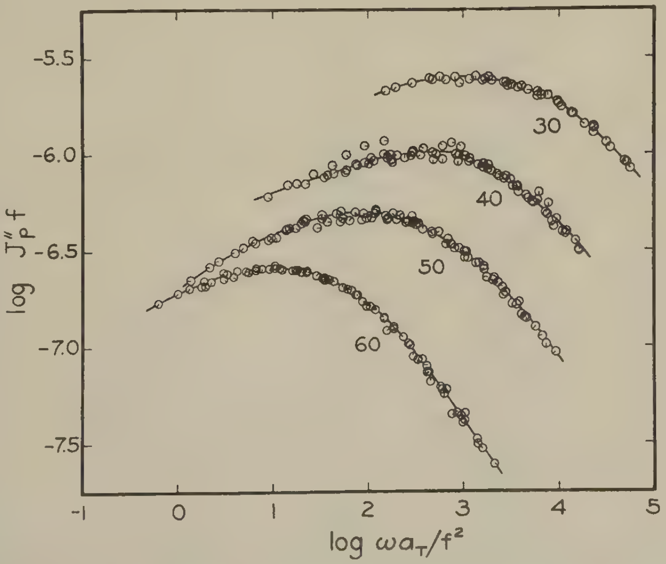

FIG. 5. Imaginary part of the complex compliance for the 4 solutions in the low-frequency range, reduced to 0°C. for temperature dependence of both $a_T$ and $f$.

TABLE III

*Retardation and Relaxation Spectra of Solutions Reduced to 0°C., Including Reduction for Change in Entanglement Density*

| Log $\tau_p$ (*sec.*) | Log $L_p$ (*cm.*$^2$/*dyne*) | | Log $H_p$ (*dyne*/*cm.*$^2$) | |
|---|---|---|---|---|
| | From $J'$ | From $J''$ | From $G'$ | From $G''$ |
| | | *30.0% Polymer* | | |
| −7.6 | — | −8.30 | — | 7.23 |
| −7.2 | −8.00 | −8.15 | 7.10 | 7.11 |
| −6.8 | −7.74 | −7.77 | 6.82 | 6.66 |
| −6.4 | −7.52 | −7.57 | 6.56 | 6.52 |
| −6.0 | −7.15 | −7.21 | 6.26 | 6.23 |
| −5.6 | −6.82 | −6.90 | 5.93 | 5.84 |
| −5.2 | −6.55 | −6.58 | 5.69 | 5.61 |
| −4.8 | — | −6.34 | — | 5.36 |
| −4.2 | — | −6.01 | — | 5.06 |
| −3.8 | −5.89 | −5.83 | 4.82 | 4.76 |
| −3.5[a] | −5.87 | −5.82 | 4.61 | 4.75 |
| −3.4 | −5.84 | −5.78 | 4.59 | 4.78 |
| −3.0 | −5.82 | −5.76 | 4.44 | 4.51 |
| −3.0[a] | −5.85 | −5.80 | 4.44 | 4.51 |
| −2.6 | — | −5.79 | — | 4.41 |
| −2.5[a] | −5.82 | −5.78 | — | 4.36 |
| | | *40.3% Polymer* | | |
| −7.6 | — | −9.00 | — | — |
| −7.2 | — | −8.70 | — | — |
| −6.8 | — | −8.52 | — | 7.67 |
| −6.4 | −8.25 | −8.22 | 7.33 | 7.27 |
| −6.0 | −8.05 | −8.05 | 7.12 | 7.11 |
| −5.6 | −7.80 | −7.82 | 6.87 | 6.84 |
| −5.2 | −7.48 | −7.55 | 6.58 | 6.56 |
| −4.8 | −7.15 | −7.22 | 6.28 | 6.20 |
| −4.4 | −6.85 | −6.88 | 6.00 | 5.88 |
| −4.0 | — | −6.54 | — | 5.65 |
| −4.0[a] | −6.64 | −6.67 | 5.59 | 5.54 |
| −3.6 | — | −6.45 | — | 5.35 |
| −3.5[a] | −6.36 | −6.34 | 5.32 | 5.27 |
| −3.2 | −6.23 | −6.20 | 5.30 | 5.02 |
| −3.0[a] | −6.15 | −6.18 | 5.01 | 5.03 |
| −2.8 | −6.18 | −6.07 | 4.90 | 5.14 |
| −2.5[a] | −6.17 | −6.21 | 4.85 | 4.82 |
| −2.4 | −6.13 | −6.25 | 4.79 | 4.68 |
| −2.0 | −6.25 | −6.22 | 4.63 | 4.62 |
| −2.0[a] | −6.27 | −6.16 | 4.64 | 4.66 |
| −1.6 | −6.46 | −6.36 | 4.29 | 4.89 |
| −1.5[a] | — | −6.32 | — | 4.50 |
| −1.2 | — | −6.31 | — | 4.94 |
| −1.0 | — | −6.41 | — | 4.36 |

TABLE III—*Continued*

| Log $\tau_p$ (*sec.*) | Log $L_p$ (*cm.²/dyne*) | | Log $H_p$ (*dyne/cm.²*) | |
|---|---|---|---|---|
| | From $J'$ | From $J''$ | From $G'$ | From $G''$ |
| | | *50.0% Polymer* | | |
| −4.4 | — | −7.72 | — | 6.70 |
| −4.0 | −7.39 | −7.39 | 6.49 | 6.46 |
| −3.6 | −7.06 | −7.28 | 6.23 | 6.16 |
| −3.5[a] | −7.15 | −7.09 | — | — |
| −3.2 | — | −6.73 | — | 5.81 |
| −3.0 | −6.73 | −6.75 | 5.72 | 5.70 |
| −3.0[a] | −6.76 | −6.78 | 5.71 | 5.79 |
| −2.6 | −6.55 | −6.52 | 5.60 | 5.66 |
| −2.5[a] | −6.56 | −6.53 | 5.42 | 5.48 |
| −2.2 | −6.45 | −6.47 | 5.33 | 5.26 |
| −2.0[a] | −6.48 | −6.46 | 5.21 | 5.21 |
| −1.8 | −6.48 | −6.47 | 5.15 | 5.16 |
| −1.5[a] | −6.47 | −6.55 | — | 5.00 |
| −1.4 | −6.52 | −6.49 | 4.97 | 5.01 |
| −1.0 | −6.64 | −6.62 | 4.75 | 4.76 |
| −1.0[a] | −6.60 | −6.63 | — | 4.80 |
| −0.6 | — | −6.70 | — | 4.69 |
| −0.5 | — | −6.76 | — | 4.62 |
| 0[a] | — | −6.95 | — | 4.48 |
| | | *60.0% Polymer* | | |
| −8.0 | — | −9.96 | — | 8.44 |
| −7.6 | −9.89 | −9.92 | 8.44 | 8.49 |
| −7.2 | −9.77 | −9.85 | 8.44 | 8.33 |
| −6.8 | −9.74 | −9.74 | 8.32 | 8.32 |
| −6.4 | −9.80 | −9.68 | 8.28 | 8.25 |
| −6.0 | −9.57 | −9.51 | 8.24 | 8.32 |
| −5.6 | −9.26 | −9.54 | 8.23 | 8.15 |
| −5.2 | −9.10 | −9.30 | 8.19 | 8.09 |
| −4.8 | −8.92 | −9.05 | 8.05 | 8.00 |
| −4.4 | −8.77 | −8.89 | 7.88 | 7.80 |
| −4.0 | −8.54 | −8.52 | 7.63 | 7.62 |
| −3.6 | −8.23 | −8.30 | 7.29 | 7.30 |
| −3.2 | −7.92 | −7.89 | 6.98 | 6.92 |
| −2.8 | −7.51 | −7.64 | 6.60 | 6.64 |
| −2.6 | — | −7.42 | — | 6.37 |
| −2.2 | −7.09 | −7.10 | 6.19 | 6.15 |
| −2.0[a] | −7.04 | −7.02 | 5.95 | 6.01 |
| −1.8 | −6.88 | −6.84 | 5.89 | 5.92 |
| −1.5[a] | −6.83 | −6.79 | 5.64 | 5.77 |
| −1.4 | −6.83 | −6.78 | 5.63 | 5.70 |
| −1.0 | −6.74 | −6.70 | 5.53 | 5.68 |
| −1.0[a] | −6.79 | −6.79 | 5.47 | 5.55 |
| −0.6 | −6.77 | −6.80 | 5.32 | 5.16 |
| −0.5[a] | −6.81 | −6.84 | 5.27 | 5.29 |
| −0.2 | — | −6.84 | — | 5.24 |
| 0[a] | −6.89 | −6.92 | — | 5.06 |

[a] Calculated by Williams-Ferry method.

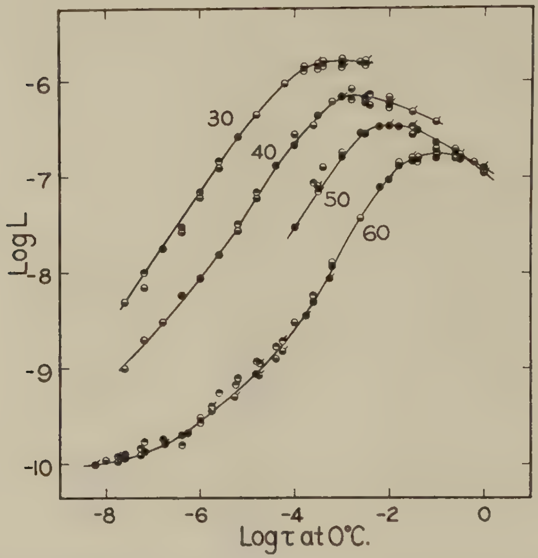

Fig. 6. Retardation spectra of the 4 solutions reduced to 0°C. Points top black, from $J'$; bottom black, from $J''$. Untagged points calculated by Ninomiya-Ferry method; tagged, by Williams-Ferry method.

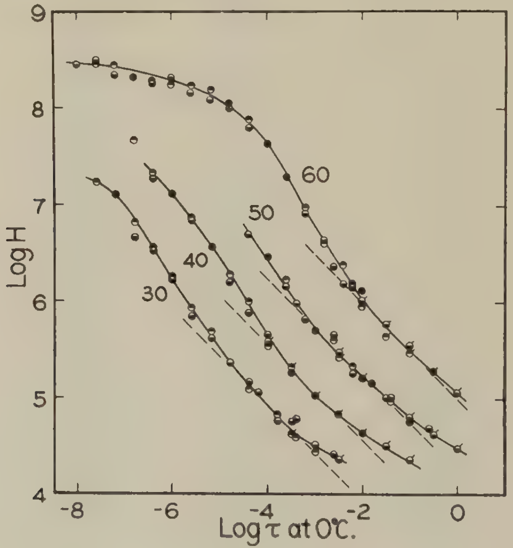

Fig. 7. Relaxation spectra of the 4 solutions reduced to 0°C. Points top black, from $G'$; bottom black, from $G''$. Tags have same significance as in Fig. 6. Dashed lines drawn with theoretical slope of $-\frac{1}{2}$.

## DISTRIBUTION FUNCTIONS

The retardation spectrum $L$ was calculated from $J'$ and $J''$, using the reduced data of Figs. 4 and 5 at low reduced frequencies and those of Figs. 2 and 3 at the high end of the frequency scale where the effects of the entanglement anomaly vanish. The calculation was made both by the approximation method of Williams and Ferry (12) and by that of Ninomiya and Ferry (13), using a differencing interval of 0.4 on the log $\omega$ scale with the second approximation for $J'$ and the first approximation for $J''$. Where the slope of $J'$ was small or there was irregular curvature, random fluctuations in the differencing made it necessary to reject some of the results of the second method. From the components of the complex shear modulus, $G' + iG''$ $(= 1/(J' - iJ''))$, calculations of the relaxation spectrum $H$ were also made by both approximation methods. The results are summarized in Table III and are plotted in Figs. 6 and 7. The shapes of the spectra are similar to those of the undiluted polymers; there is clearly a shift to longer times with increasing concentration, and also a diminution in the magnitudes of contributions to $L$ as indicated by the positions of the maximum in this function.

## DISCUSSION

### *Monomeric Friction Coefficient*

In Fig. 7, lines are drawn with the theoretical slope of $-\frac{1}{2}$ to fit the lower portions of the spectra. From the positions of these, the monomeric friction coefficient $\zeta_0$ can be calculated from the equation (14)

$$\log \zeta_0 = 2 \log H + \log \tau + \log 6/kT + 2 \log (2\pi M_0/acN_0), \qquad [2]$$

where $M_0$ is the monomer molecular weight, $N_0$ Avogadro's number, and $c$ the concentration in grams polymer per cubic centimeter; $a$, the root-mean-square end-to-end distance per square root of the number of monomer units, is taken as 6.4A. as in the undiluted polymer. Values of log $\zeta_0$ at 0°C. are listed in Table IV and plotted against $c$ in Fig. 8. The concentration dependence follows the equation $\zeta_0 = 5.8 \times 10^{-10}\, e^{24c}$. This extremely rapid increase reflects the diminishing proportion of mobile solvent molecules in the immediate neighborhood of a polymer segment, and (probably less importantly) differences in free volume due to altered packing efficiency. There appears to be no theoretical expectation for the form of the relation, although the concentration dependence of the diffusion coefficients of solvent molecules in very concentrated polymer solutions is also exponential (15) with a coefficient of the order of 20 to 25. This similarity reinforces the view (16) that the frictional resistance per monomer unit of a polymer segment, well above $T_g$, closely resembles that of a small foreign molecule of the same size.

TABLE IV

*Molecular Parameters from Viscoelastic Data*

| | | | | |
|---|---|---|---|---|
| Concentration, weight % | 30.0 | 40.3 | 50.0 | 60.0 |
| Log $\zeta_0$ at 0°C. | −6.28 | −5.30 | −4.05 | −2.90 |
| Log $\zeta_0$ at $T_g$ | — | — | 3.60 | 1.90 |
| $\Delta$ log $Z_e$ | 0 | −0.28 | −0.51 | −0.68 |

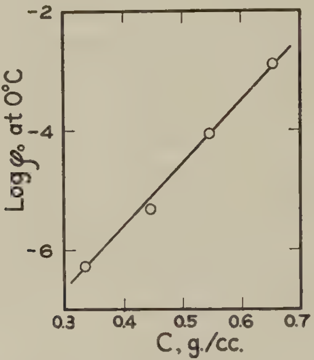

FIG. 8. Logarithm of monomeric friction coefficient at 0°C. (in dyn-sec./cm.) plotted against polymer concentration.

For the two more concentrated solutions, log $\zeta_0$ at the glass transition temperature is also listed in Table IV. It represents a rather long extrapolation, however. Since the value for the pure polymer (1) is 3.74, no significant trend is apparent.

### *Comparison of Spectral Shape and Magnitude*

In a comparison of the retardation spectra of several undiluted methacrylate polymers (17), it was pointed out that a plot of log $L + \Delta\log(\rho/M_0)$ against log $\tau - \Delta\log a^2\zeta_0$ should give coincidence of those regions of the spectrum where the contributions to compliance are proportional to the dilution (i.e., inversely proportional to polymer density in monomoles per cubic centimeter) and the relaxation rates are all governed by the monomeric friction coefficient. Here $\Delta$ represents the difference between a given polymer and one particular polymer chosen as reference. Failure of the curves for $L$ to coincide near their maxima when plotted in this manner was attributed to a change in entanglement coupling density with side group length.

The corresponding plot for a series of solutions of a single polymer, where $a^2$ is presumed constant throughout and the polymer density in monomoles per cubic centimeter is $c/M_0$, is log $L + \Delta\log(c/M_0)$ against log $\tau - \Delta\log \zeta_0$. This is shown in Fig. 9, based on the 30% solution as reference. The

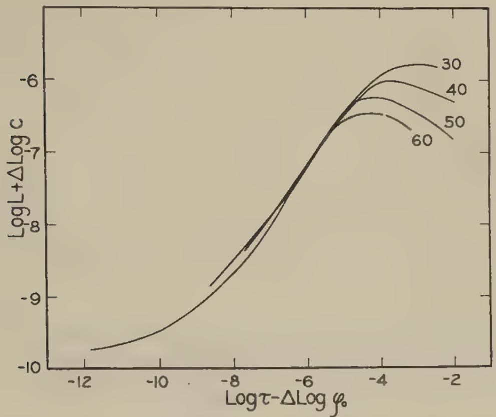

FIG. 9. Retardation spectra of the 4 solutions reduced to a reference state of the 30% solution by the procedure described in the text.

curves coincide rather closely through the transition region but diverge in the region of the maximum, whose height drops with increasing concentration.

If these divergences are indeed due to differences in the average degree of polymerization between entanglement points, $Z_c$, then a shift downward by $\Delta\log Z_c$ should be accompanied by a shift to shorter times of $2\ \Delta\log Z_c$ just as in the temperature-dependent entanglement anomaly. Measurements along a line of slope ½ on Fig. 9 show that this requirement is approximately fulfilled, and the values of $\Delta\log Z_c$ from the 30% solution are also listed in Table IV. They are plotted against the logarithm of concentration in Fig. 10, which shows that $Z_c$ is inversely proportional to the 2.3 power of the concentration.

The number of strands of the entanglement network per cubic centimeter, $n_c$, is given by $N_0c/M_0Z_c$ and hence is proportional to $c^{3.3}$. This contrasts with the $c^2$ which would be expected from a binary association equilibrium or simply from a constant probability of entanglement of two juxtaposed monomer units. The latter relation, equivalent to inverse proportionality between $Z_c$ and $c$, has usually been assumed (11, 18, 19), and it may in fact be valid for other polymers such as polyisobutylene, polystyrene, and cellulose derivatives. The exponent 3.3 is characteristic of methacrylate polymers, not only in solutions of a single polymer, but also in comparing undiluted polymers of different side chain lengths, as shown in the following paper (20).

In many previous studies of concentrated polymer solutions at frequencies corresponding to the plateau and terminal zones of the relaxation spectrum, successful reduction to a standard reference concentration (21) has shown that the contributions to compliance associated with very long

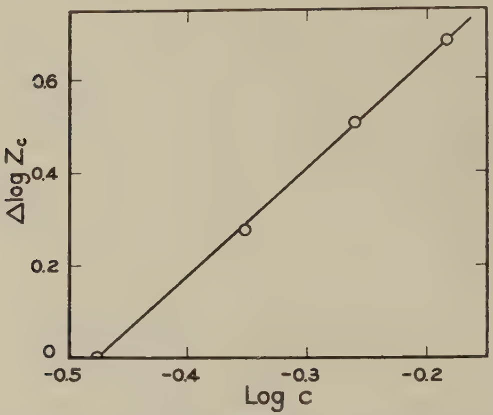

FIG. 10. Difference in the logarithm of degree of polymerization between entanglement points (from 30% solution as reference), plotted against logarithm of concentration.

times are simply inversely proportional to concentration; no complications involving a changing $Z_c$ appear. The most critical test is probably given by data on cellulose tributyrate solutions (22). This result is not inconsistent; it is a necessary consequence if the relaxation times dominating the behavior in this zone all depend identically on concentration, regardless of what that dependence may be. The longest times reflect entanglement slipping and presumably they all depend on concentration in the same manner as the steady-flow viscosity (23). In the zone near the maximum in $L$, on the other hand, there is practically no slipping, and the behavior approaches that of a cross-linked network, from which the divergences in Fig. 9 must follow.

From the concentration dependences of $\zeta_0$ and $Z_c$, it can be anticipated (19) that the increase of steady-flow viscosity with concentration in poly-*n*-butyl methacrylate solutions must be enormous. Measurements to test this conclusion are in progress.

## ACKNOWLEDGMENTS

This work was supported in part by Picatinny Arsenal, Ordnance Corps, Department of the Army, and in part by the Research Committee of the Graduate School of the University of Wisconsin from funds supplied by the Wisconsin Alumni Research Foundation. We are much indebted to Dr. Donald J. Plazek for advice and help with the apparatus, and to Mrs. W. C. Frazier and Miss Shirley Pomeroy for making most of the calculations.

## SUMMARY

The real ($J'$) and imaginary ($J''$) components of the complex compliance have been measured between 10 and 2400 cycles/sec. for four solutions of a

fraction of poly-*n*-butyl methacrylate with molecular weight $3.05 \times 10^6$. The solvent was diethyl phthalate. The temperature range for each polymer concentration was as follows: 30%, −49° to 0°; 40.3%, −49° to 25°; 50%, −15° to 47°; 60%, −44° to 40°C. The method of reduced variables gave superposed curves for $J'$ and $J''$ except for a low-temperature anomaly in the 60% solution and a high-temperature anomaly in each solution near the maximum in $J''$. The temperature dependence of relaxation times followed an equation of the WLF form in each case. The value of $\alpha_f$ (thermal expansion of free volume derived from the WLF equation) ranged from $2.2$ to $2.8 \times 10^{-4}$ deg.$^{-1}$. The glass transition temperatures, $T_g$, of the 50% and 60% solutions were determined refractometrically as −67° and −46°, respectively; $f_g$ (fractional free volume at $T_g$ from the WLF equation) was 0.024 for both. The high-temperature reduction anomaly was resolved by a treatment used earlier for several undiluted methacrylate polymers, formally equivalent to assuming a dissociation of entanglement points with increasing temperature; the apparent heat of dissociation was 2.1 kcal./mole for all four solutions. The relaxation and retardation spectra are similar in shape except for differences in time scale and in magnitude. The monomeric friction coefficient $\zeta_0$ at 0°C. ranges from $10^{-6.28}$ for the 30% to $10^{-2.90}$ for the 60% solution, and is closely represented by the equation $\zeta_0 = 5.8 \times 10^{-10} e^{24c}$, where $c$ is grams polymer per cubic centimeter solution. From the relative magnitudes and positions of the retardation spectra near their maxima, the average degree of polymerization between entanglement points is concluded to be proportional to $c^{2.3}$.

## REFERENCES

1. CHILD, W. C., JR., AND FERRY, J. D., *J. Colloid Sci.* **12,** 327 (1957).
2. JENCKEL, V. E., AND HEUSCH, R., *Kolloid-Z.* **130,** 89 (1953).
3. FITZGERALD, E. R., *J. Chem. Phys.* **27,** 1180 (1957).
4. WILLIAMS, M. L., LANDEL, R. F., AND FERRY, J. D., *J. Am. Chem. Soc.* **77,** 3701 (1955).
5. KURATH, S. F., YIN, T. P., BERGE, J. W., AND FERRY, J. D., *J. Colloid Sci.* **14,** 147 (1959).
6. FERRY, J. D., CHILD, W. C., JR., ZAND, R., STERN, D. M., WILLIAMS, M. L., AND LANDEL, R. F., *J. Colloid Sci.* **12,** 53 (1957).
7. BERGE, J. W., SAUNDERS, P. R., AND FERRY, J. D., *J. Colloid Sci.* **14,** 135 (1959).
8. BUECHE, F., *J. Chem. Phys.* **22,** 603 (1954).
9. FERRY, J. D., GRANDINE, L. D., JR., AND FITZGERALD, E. R., *J. Appl. Phys.* **24,** 911 (1953).
10. TOBOLSKY, A. V., AND CATSIFF, E., *J. Polymer Sci.* **19,** 111 (1956).
11. FOX, T. G., GRATCH, S., AND LOSHAEK, S., in F. R. Eirich, ed., "Rheology," Vol. 1, p. 431. Academic Press, New York, 1956.
12. WILLIAMS, M. L., AND FERRY, J. D., *J. Polymer Sci.* **11,** 169 (1953).
13. NINOMIYA, K., AND FERRY, J. D., *J. Colloid Sci.* **14,** 36 (1959).
14. FERRY, J. D., in STUART, H. A., "Die Physik der Hochpolymeren," Vol. 4, p. 103. Springer-Verlag, Berlin, 1956.

15. Prager, S., and Long, F. A., *J. Amer. Chem. Soc.* **73,** 4072 (1951).
16. Ferry, J. D., and Landel, R. F., *Kolloid-Z.* **148,** 1 (1956).
17. Dannhauser, W., Child, W. C., Jr., and Ferry, J. D., *J. Colloid Sci.* **13,** 103 (1958).
18. Bueche, F., *J. Appl. Phys.* **26,** 738 (1955).
19. Landel, R. F., Berge, J. W., and Ferry, J. D., *J. Colloid Sci.* **12,** 400 (1957).
20. Saunders, P. R., and Ferry, J. D., *J. Colloid Sci.* **14,** 239 (1959).
21. Ferry, J. D., *J. Am. Chem. Soc.* **72,** 3746 (1950).
22. Landel, R. F., and Ferry, J. D., *J. Phys. Chem.* **59,** 658 (1955).
23. Ferry, J. D., Williams, M. L., and Stern, D. M., *J. Phys. Chem.* **58,** 987 (1954).

JOURNAL OF COLLOID SCIENCE **14**, 239–243 (1959)

# DYNAMIC MECHANICAL PROPERTIES OF POLY-*n*-DOCOSYL METHACRYLATE[1]

**P. R. Saunders[2] and John D. Ferry**

*Department of Chemistry, University of Wisconsin, Madison, Wisconsin*

*Received December 11, 1958*

## Introduction

Measurements of time-dependent mechanical properties have previously been made in this laboratory on five *n*-alkyl methacrylate polymers, the ethyl, butyl, hexyl, octyl, and dodecyl (1), in a cooperative investigation with the Feltman Research and Engineering Laboratories, Picatinny Arsenal. Some data are now reported for poly-*n*-docosyl methacrylate, with $C_{22}$ ester side groups. Although the measurements were severely restricted by the properties of this unusual polymer, the results are of interest in comparison with those for the other members of the series.

## Materials, Method, and Results

The polymer was synthesized at Picatinny Arsenal (2). Though unfractionated, it was evidently of quite high molecular weight. Below 55°C. it was an opaque, very friable solid. From the work of Greenberg and Alfrey (3) there can be little doubt that the side groups crystallize; a melting point of 55°C. is a reasonable extrapolation from their series of methacrylates up to $C_{18}$. Above 55°C., the polymer was extremely soft and sticky. The density was 0.85 at 70°C., measured pycnometrically.

Measurements of the complex shear compliance ($\mathbf{J}^* = J' - iJ''$) were made between 24 and 100 cycles/sec. in the Fitzgerald Apparatus (4). The upper limit was set by the small mechanical impedance of the samples compared with that of the driving tube. The disc-shaped samples were inserted below the melting point; when the temperature was raised after closing the apparatus, the polymer melted, expanded, and adhered to the driving tube and floating mass. Samples 122, $^{11}\!/_{16}$ in. diam. by $^{1}\!/_{32}$ in. thickness, had a sample coefficient of 55.5; this is probably more reliable than for most very thin samples, since the thickness was checked with a micrometer before insertion. Measurements were made at 59.0°C. and

---

[1] Part XXXII of a series on Mechanical Properties of Substances of High Molecular Weight.

[2] Present address: Chemstrand Corporation, Decatur, Alabama.

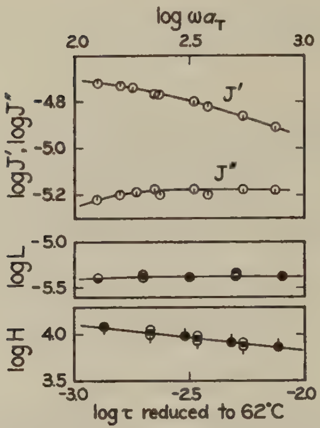

FIG. 1. Real ($J'$) and imaginary ($J''$) parts of the complex compliance, in cm.$^2$/dyne, plotted logarithmically against frequency after reduction to 62°C. Tags down, 59.0°C.; up, 65.2°C. Also, retardation spectrum ($L$) and relaxation spectrum ($H$); points top black, calculated from $J'$ or $G'$; bottom black, from $J''$ or $G''$. For $H$, tags denote individual temperatures for which calculations were made before reduction.

65.2°C. Samples 121, $1\frac{1}{16}$ in. by $\frac{1}{8}$ in., had a sample coefficient of 19.74, and were measured at 62.6°C. only. The results were consistent with the others within about 8%; no corrections were applied to these fragmentary data, however, and the subsequent analysis is based on Samples 122 alone.

The average spacing on the logarithmic frequency scale for the two temperatures, after multiplying $J'$ and $J''$ by the usual factor $T\rho/T_0\rho_0$, corresponded to $\log a_T = 0.15$. For reduction, 62°C. was selected as standard, with $\log a_T = 0.07$ at 59.0°C. and $-0.08$ at 65.2°C. (The corresponding apparent activation energy over this short interval is 12 kcal., which is reasonable; the WLF equation cannot be applied to such limited data.)

The components of the complex compliance are plotted against reduced frequency in Fig. 1, and show good superposition of the two temperatures. The data correspond to the region of the frequency scale where $J''$ passes through a maximum and $J'$ is entering the transition zone.

## DISCUSSION

The retardation spectrum $L$ was calculated from $J'$ and $J''$ by the approximation method of Williams and Ferry (5) and, the relaxation spectrum $H$ was similarly calculated from the components of the complex modulus $G'$ and $G''$. The spectra are also plotted logarithmically in Fig. 1.

Since the short segment of $H$ obtained does not include a region with the slope of $-\frac{1}{2}$ specified by the Rouse theory (6), the monomeric friction coefficient $\zeta_0$ cannot be calculated by the usual method employed for other members of the series (1). It can, however, be estimated by plotting $\log H - \Delta\log \rho/M_0$ against $\log \tau$ as described in a previous analysis (7), and determining the shift $\Delta\log a^2 \zeta_0$ which is necessary to bring the segment for poly-*n*-docosyl methacrylate into coincidence with the others. Here $\rho$ is the density, $M_0$ the monomer molecular weight, and $a$ the root-mean-square end-to-end distance per square root of the number of monomer units, taken for the docosyl polymer as 10 A. The segment of $H$ in Fig. 1 has a slope of about $-\frac{1}{3}$, and can be brought into coincidence with a similar segment for poly-*n*-octyl methacrylate by a shift from which (after reducing the octyl data to 62°C. from the original reference temperature of 100°C.) $\log \zeta_0$ (units dyne-sec./cm.) is estimated to be $-7.2$ for the docosyl polymer at 62°C.

The dependence of $\zeta_0$ on side group length at constant temperature for the methacrylate series has been correlated with differences in free volume by Dannhauser, Child, and Ferry (7) and by Fujita and Kishimoto (8). The latter treatment cannot be applied to poly-*n*-docosyl methacrylate because its glass transition temperature is not known. According to the former treatment, $\log \zeta_0 = 1/2.303f +$ constant, where $f$ is the relative free volume estimated from the conclusion of Rogers and Mandelkern (9) that 15% of the increase in specific volume with side group length is attributable to free specific volume. At 62°C., the values of $\log \zeta_0$ for the hexyl, octyl, and dodecyl polymers ($-3.35$, $-4.40$, and $-5.33$) follow this equation, and the extrapolation to the docosyl ($f = 0.055$ at 62°) gives $\log \zeta_0 = -7.0$, in reasonable agreement with the above estimate.

Of particular interest is the dependence of the height of the maximum in $L$, which reflects contributions to the compliance in a region of time scale dominated by entanglement coupling, on side group length. Fortunately, the fragmentary data on the docosyl polymer encompass this maximum, which in the dodecyl polymer could not be distinguished because of its lower degree of polymerization. The values of $L_{\text{max.}}$ of all those polymers for which well-defined maxima were obtained are given in Table I both at the original reference temperature and reduced to 62°C. In the latter reduction, the temperature-dependent entanglement anomaly (10) was taken into account.

In Fig. 2, $\log L_{\text{max.}}$ is plotted against the logarithm of polymer density expressed as monomoles per cubic centimeter, $\rho/M_0$. The excellent straight line with a slope of $-3.4$ corresponds to the conclusion that the number of strands per cubic centimeter in the entanglement network $n_c$, is inversely proportional to the 3.4 power of the concentration of polymer chains. A closely similar result was obtained for a series of solutions of a single polymer, the *n*-butyl methacrylate, in a diluent of low molecular weight, where the exponent was concluded to be 3.3, the same within experimental error (11). Even more striking is the fact that the proportionality constant is the same. In Table I, the heights of the $L$ maxima are also given for the butyl polymer solutions. After reduction of these to 62°C., taking into account the apparent temperature dissociation of entanglement points (10), they

TABLE I

*Maxima in Relaxation Spectra*

| Polymer | Original ref. temperature | Log $\rho/M_0$ at 62°C. | Log $L_{max}$ at orig. temp. | Log $L_{max}$ at 62°C. |
|---|---|---|---|---|
| *n*-Butyl | 100° | −2.15 | −7.04 | −7.19 |
| *n*-Hexyl | 100° | −2.25 | −6.67 | −6.82 |
| *n*-Octyl | 100° | −2.33 | −6.35 | −6.46 |
| *n*-Docosyl | 62° | −2.68 | −5.38 | −5.38 |
| 30% *n*-Butyl | 0° | −2.629[a] | −5.79 | −5.48 |
| 40% *n*-Butyl | 0° | −2.504[a] | −6.13 | −5.82 |
| 50% *n*-Butyl | 0° | −2.414[a] | −6.47 | −6.16 |
| 60% *n*-Butyl | 0° | −2.337[a] | −6.75 | −6.44 |

[a] log $c/M_0$ .

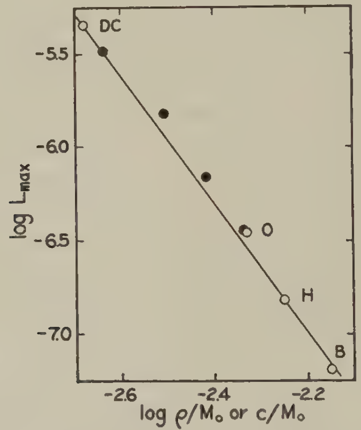

FIG. 2. Maximum in retardation spectrum, reduced to 62°C. including reduction for entanglement anomaly, plotted logarithmically against polymer concentration in monomoles per cubic centimeter. Open circles, undiluted polymers; black circles, solutions of poly-*n*-butyl methacrylate in diethyl phthalate.

are also plotted against monomoles polymer per cubic centimeter (in this case, $c/M_0$, where $c$ is grams polymer per cubic centimeter), and fall essentially on the same line as the values for the undiluted polymers; thus, $\log L_{max.} = 14.46 - 3.4 \log (c/M_0)$.

It may be concluded that the density of entanglement points in methacrylate polymers depends only on the concentration of chain backbones and not on whether they are diluted by solvent molecules or by side groups. This principle was postulated by Bueche (12), who did not, however, anticipate the exponent of 3.4. Although the nature of the entanglement coupling is still only vaguely understood, the present result is more easily reconciled with some aspect of the long-range molecular contour as proposed by Bueche (13) rather than a short-range kinking or knotting.

It should not be thought, of course, that all the viscoelastic properties are determined solely by the concentration of chain backbones. For example, the monomeric friction coefficients of undiluted poly-*n*-octyl and dodecyl methacrylates at 0°C. are larger by a factor of 200 than the corresponding values for solutions of poly-*n*-butyl methacrylate with the same concentration of monomoles polymer per cubic centimeter.

## ACKNOWLEDGMENTS

This work was supported by Picatinny Arsenal, Ordnance Corps, Department of the Army. We are indebted to Mrs. William C. Frazier for making most of the calculations.

## SUMMARY

The real ($J'$) and imaginary ($J''$) components of the complex compliance have been measured between 24 and 100 cycles/sec. at 59.0°C. and 65.2°C. for poly-*n*-docosyl methacrylate. The results, reduced to 62°C., provide the relaxation and retardation spectra over a short region which encompasses the maximum of the latter. The logarithm of the monomeric friction coefficient (units dyne-sec./cm.) is estimated to be $-7.2$. The maximum in the retardation spectrum for the butyl, hexyl, octyl, and docosyl methacrylate polymers is inversely proportional to the 3.4 power of the polymer density expressed in monomoles per cubic centimeter. The same relation is followed, with essentially the same proportionality constant, for solutions of poly-*n*-butyl methacrylate in diethyl phthalate. It is concluded that the number of strands per cubic centimeter in the entanglement network of a methacrylate polymer depends only on the concentration of chain backbones regardless of whether they are diluted by solvent molecules or by side groups.

## REFERENCES

1. KURATH, S. F., YIN, T. P., BERGE, J. W., AND FERRY, J. D., *J. Colloid Sci.* **14,** 147 (1959).
2. CHINAI, S. N., to be published.
3. GREENBERG, S. A., AND ALFREY, T., *J. Am. Chem. Soc.* **76,** 6280 (1954).
4. FITZGERALD, E. R., *J. Chem. Phys.* **27,** 1180 (1957).
5. WILLIAMS, M. L., AND FERRY, J. D., *J. Polymer Sci.* **11,** 169 (1953).
6. ROUSE, P. E., JR., *J. Chem. Phys.* **21,** 1272 (1953).
7. DANNHAUSER, W., CHILD, W. C., JR., AND FERRY, J. D., *J. Colloid Sci.* **13,** 103 (1958).
8. FUJITA, H., AND KISHIMOTO, A., *J. Colloid Sci.* **13,** 418 (1958).
9. ROGERS, S. S., AND MANDELKERN, L., *J. Phys. Chem.* **61,** 985 (1957).
10. BERGE, J. W., SAUNDERS, P. R., AND FERRY, J. D., *J. Colloid Sci.* **14,** 135 (1959).
11. SAUNDERS, P. R., STERN, D. M., KURATH, S. F., SAKOONKIM, C., AND FERRY, J. D., *J. Colloid Sci.* **14,** 222 (1959).
12. BUECHE, F., *J. Appl. Phys.* **26,** 738 (1955).
13. BUECHE, F., *J. Polymer Sci.* **25,** 243 (1957).

## Papers Accepted for Publication

B. S. Harrap. The Binding of Dyes by Soluble Wool Keratin Derivatives

A. J. Rutgers, M. de Smet and W. Rigole. Streaming Currents with Non-Aqueous Solutions

Raymond R. Myers, John C. Miller and A. C. Zettlemoyer. The Splitting of Thin Liquid Films. Kinematics

Satya Prakash and Ashim Kumar Ghosh. The Influence of Ultrasonic Waves on Silver Hydrosol

Jacques R. Hommelen. The Elimination of Errors due to Evaporation of the Solute in the Determination of Surface Tension

Kazuo Nagamatsu and Tatsuya Yoshitomi. On the Viscoelastic Properties of Crystalline Polymers. II. Polytrifluorochloroethylene

J. B. Bateman, E. J. Wenek and D. C. Eshler. Determination of Particle Size and Concentration from Spectrophotometric Transmission

H. H. G. Jellinek. Adhesive Properties of Ice

N. Rajalakshmi, R. S. Sivarajan and Robert D. Vold. The Viscosity of Sodium Humate Solutions from Coal

W. R. Moore and A. M. Brown. Viscosity-Temperature Relationships for Dilute Solutions of Cellulose Derivatives. II. Intrinsic Viscosities of Ethyl Cellulose

P. J. Napjus and J. J. Hermans. Electrophoresis, Conductance and Viscosity of Aqueous Solutions of Carboxymethylcellulose in the Presence of Sodium Chloride

Harry Sobotka, Margaret Demeny and Margarita Arnaki. Multimolecular Films of Triiodostearic Acid

J. Schurz. Interpretation of Flow Curves in Terms of Molecular Properties

Raymond Defay and Jacques R. Hommelen. II. Measurement of Dynamic Surface Tensions of Aqueous Solutions by the Falling Meniscus Method

Raymond Defay and Jacques R. Hommelen. III. The Importance of Diffusion in the Adsorption Process of Some Alcohols and Acids in Dilute Aqueous Solutions

Malcolm L. White and Arthur A. Frost. The Rate of Nucleation of Supersaturated Potassium Nitrate Solutions

O. L. Forgacs and S. G. Mason. Particle Motions in Sheared Suspensions IX. Spin and Deformation of Thread-Like Particles

O. L. Forgacs and S. G. Mason. Particle Motions in Sheared Suspensions X. Orbits of Flexible Thread-Like Particles

W. Albers and J. Th. G. Overbeek. Stability of Emulsions of Water in Oil I. The Correlation between Electrokinetic Potential and Stability

W. Albers and J. Th. G. Overbeek. Stability of Emulsions of Water in Oil II. Charge as a Factor of Stabilization against Flocculation

Letters to the Editor:

Herman E. Ries, Jr., Richard A. Ahlbeck and Joseph Gabor. Mixed Monolayers with Polyvinyl Acetate

Neil H. Farlow. Impingement of Aerosol Particles on Polyvinyl Alcohol Film

Book Review: G. T. Barnes. An Introduction to the Chemistry of Fats and Fatty Acids. John Wiley and Sons, Inc., 155 pp.

## Books Received for Review

Abstracts of Reports of the Fourth Soviet Conference on Electrochemistry. Consultants Bureau, Inc. 82 pp., $12.00.

Boyd, John (ed.), Lubrication Science and Technology. Vol. 1, No. 2. Pergamon Press. 346 pp., $10.00.

Chamot, Emile Monnin and Mason, C. W., Handbook of Chemical Microscopy. Vol. 1. John Wiley & Sons, Inc. 502 pp., $14.00.

Condon, E. U. and Odishaw, Hugh (eds.), Handbook of Physics. McGraw-Hill. 1504 pp., $25.00.

Danielli, J. F., Pankhurst, K. G. A., and Riddiford, A. C. (eds.), Surface Phenomena in Chemistry and Biology. Pergamon Press. 330 pp., $10.00.

Doremus, R. H., Roberts, B. W., and Turnbull, D., Growth and Perfection of Crystals. John Wiley & Sons, Inc. 609 pp., $12.50.

Eirich, Frederick R. (ed.), Rheology, Theory and Applications. Vol. 2. Academic Press Inc. 591 pp., $18.00.

Gordon, Louis, Salutsky, Murrell L., and Willard, Hobard H., Precipitation from Homogeneous Solution. John Wiley & Sons, Inc., $7.50.

Honigmann, B., Gleichgewichts- und Wachstumsformen von Kristallen (Fortschritte der physikalischen Chemie, Band 4). Verlag Dietrich Steinkopff.

Houstoun, R. A., Physical Optics. Interscience Publishers, Inc. 300 pp., $6.25.

Huggins, Maurice L., Physical Chemistry of High Polymers. John Wiley & Sons, Inc. 175 pp., $6.50.

Klaf, A. A., Calculus, Refresher for Technical Men. Dover Publications, Inc. 431 pp., $2.00.

Klaf, A. A., Trigonometry, Refresher for Technical Men, Dover Publications. Inc. 629 pp., $2.00.

Orr, Clyde, Jr., and DallaValle, J. M., Fine Particle Measurement. The MacMillan Company. 353 pp., $10.50.

Semenov, N. N., Some Problems of Chemical Kinetics and Reactivity. Vol. 1, revised and expanded; translated by J. E. S. Bradley. Pergamon Press. 305 pp., $12.50.

JOURNAL OF COLLOID SCIENCE **14**, 247–251 (1959)

# THE RATE OF NUCLEATION OF SUPERSATURATED POTASSIUM NITRATE SOLUTIONS[1]

**Malcolm L. White[2] and Arthur A. Frost**

*Department of Chemistry, Northwestern University, Evanston, Illinois*

*Received March 5, 1959*

## Abstract

A technique was developed for continuously producing small droplets of an aqueous solution in mineral oil. The rate of nucleation of supersaturated potassium nitrate solutions was studied by observing the fraction of a large number of these droplets crystallized after varying lengths of time. For ordinary solutions the nucleation appeared to be catalyzed by impurities. By the use of a partial recrystallization technique for removing the catalyzing material a very close approach to the theoretically predicted first-order nucleation rate was obtained.

## Introduction

One of the most promising methods for studying nucleation rates is that of observing a large number of small droplets of the system, dispersed so that they crystallize independently. The rate of nucleation can then be determined by measuring the fraction of droplets that have crystallized after varying times of supersaturation.

This method has been used by Vonnegut (1) and by Pound and LaMer (2) in studying the solidification of metals. These investigators dispersed molten metal into small droplets suspended in oil and followed the rate of solidification dilatometrically.

Since homogeneous nucleation is caused by the formation of critical size nuclei, the rate of nucleation should be proportional to the number of critical size nuclei present at any given time. Because the formation of these nuclei is governed by the random collisions of subcritical size particles, this process should be a first-order rate process. By means of the technique of following the crystallization of a large number of droplets of a supersaturated system, the rate, at a given temperature can be expressed by the equation:

$$\ln \frac{N}{N_0} = -At,$$

---

[1] This paper is based on a thesis presented by Malcolm L. White to Northwestern University in partial fulfillment of the requirements for the Ph.D. degree, August, 1953.

[2] Present address: American Cyanamid Company, Stamford, Connecticut.

where $N$ is the number of droplets uncrystallized out of a total of $N_0$ droplets observed; $A$ is the rate constant; and $t$ is time.

## EXPERIMENTAL

For the present study a method was devised for continuously producing small droplets of potassium nitrate solutions, supersaturating them by lowering their temperature, and following their crystallization as a function of time. Droplets of solution were formed at a temperature above the saturation temperature of the solution by use of the oil flow dropper shown in Fig. 1. A length of 1 mm. glass capillary tubing was drawn to a tip, around which was sealed a piece of 10 mm. glass tubing drawn down to about 4 mm. diameter around the capillary tip. The potassium nitrate solution flowed from a reservoir through the capillary tubing, and mineral oil was flowed through the outside tube and past the capillary tip.

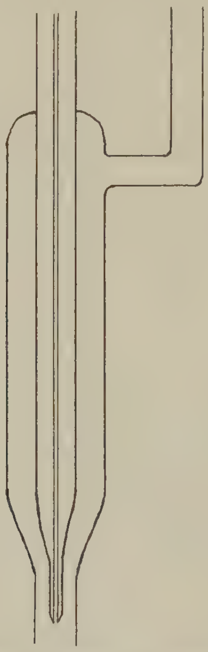

FIG. 1. Oil flow dropper.

With both the solution and oil flowing freely, droplets of solution continuously form on the capillary tip and are torn off by the flowing oil before they reach their maximum size, resulting in a continuous production of droplets of the solution suspended in oil. The size of the droplets can be regulated by the rate of flow of oil past the capillary tip and the rate of formation, by the rate of flow of the solution through the capillary.

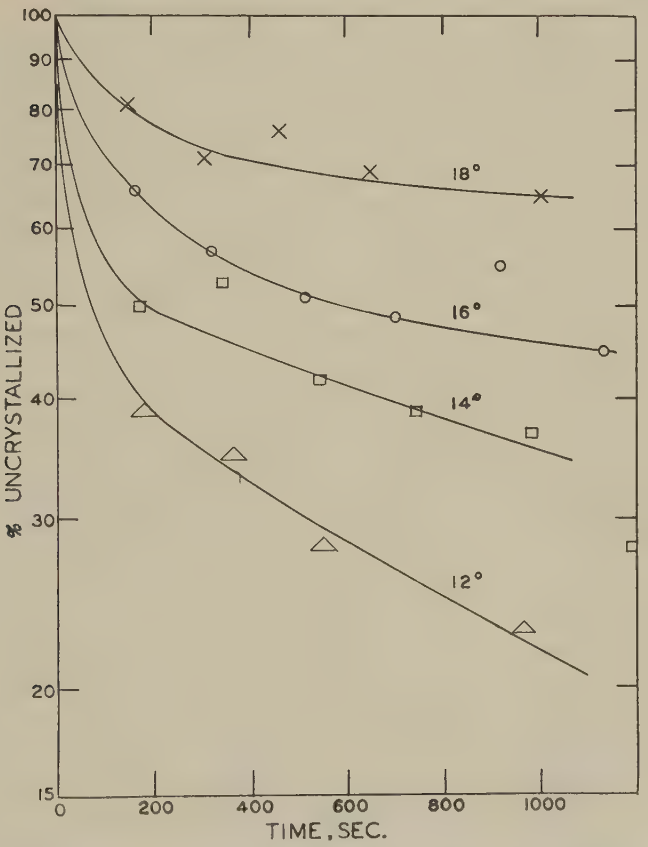

FIG. 2. Variation of per cent of droplets uncrystallized with time for unpurified solution. Concentration of solution: 80.44 g. $KNO_3$/100 g. $H_2O$. Saturation temperature: 47.7°C. Droplet diameter: 0.35 mm.

The oil flow dropper was immersed in a column of mineral oil at a temperature above the saturation temperature of the solution being studied so that the droplets formed a vertical row which traveled downward through the oil. Just below the tip of the dropper the temperature of the oil was changed to a lower, predetermined temperature below the saturation temperature of the solution by means of a thermostatted flowing water jacket. Although the droplets fell at a slower rate in the cooler oil, an evenly, but closer, spaced row was maintained. These droplets could be observed as they fell past any point along their path, each point corresponding to a definite time that they had been supersaturated. This time was determined by observing the rate of fall of one droplet in the row and assuming that the droplets became supersaturated when they passed into the top of the cooler oil. The droplets were observed with a microscope fitted with crossed

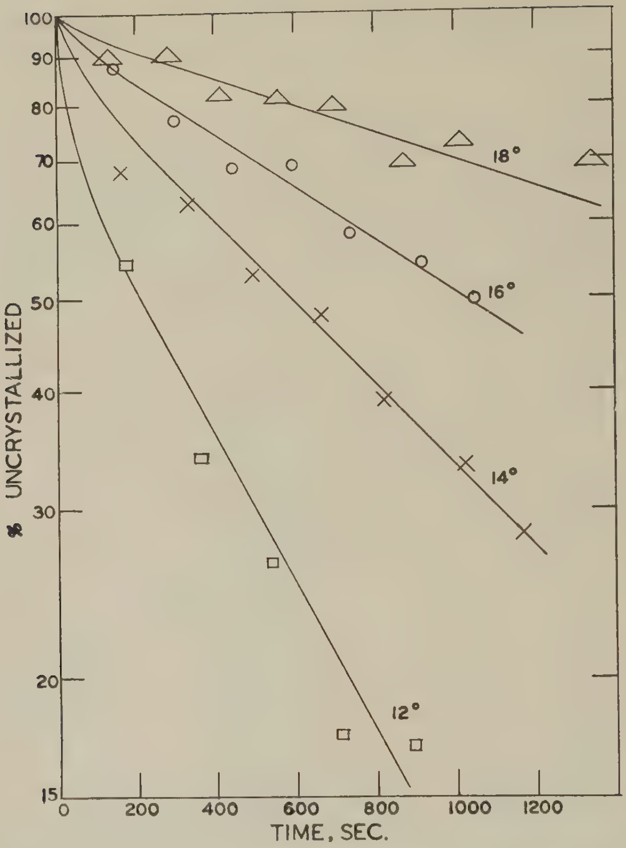

FIG. 3. Variation of per cent of droplets uncrystallized with time for purified solution. Concentration of solution: 83.41 g. $KNO_3$/100 g. $H_2O$. Saturation temperature: 49.0°C. Droplet diameter: 0.41 mm.

Nicol prisms so that crystallization in a droplet could be detected by the colored appearance of the anisotropic potassium nitrate crystals. The diameter of the droplets was measured with a calibrated eyepiece scale in the microscope.

In a typical run, 200 droplets were observed at each of five to ten positions along the row of droplets. The size of the droplets could be varied between a radius of about 0.2 mm. and 2 mm. The temperature of the oil column could be adjusted to give any desired supersaturation.

Two types of solutions were prepared and studied: (*1*) unpurified solutions, made by dissolving analytical grade potassium nitrate in distilled water without any further purification of the salt; and (*2*) purified solutions prepared in the following manner.

Analytical grade potassium nitrate was recrystallized three times from distilled water. The final recrystallization was carried out by adjusting the amounts of salt and water so the crystallization began about 10° above the final temperature to which the solution was cooled. This latter temperature was chosen so that the saturated solution at this temperature had the approximate concentration desired for a particular run. The supernatant solution was then decanted and kept above the saturation temperature to prevent any further crystallization. It was hoped that by using this technique any impurities catalyzing the nucleation would be used up in this first crystallization and remain with the crystals formed. The solution was then filtered through a Corning "Fine" grade fritted glass filter (maximum pore size of 5 microns), and transferred to the solution reservoir, which had been cleaned with sulfuric acid-sodium dichromate solution, rinsed thoroughly with distilled water and then with distilled water filtered through the fritted glass filter. A mineral oil seal was put on top of the solution to minimize evaporation. The solution was kept 10° to 20° above its saturation temperature. The exact concentration of the solution was determined by removing a small portion and weighing it before and after evaporation of the water. The saturation temperature was determined from the solubility data given by Seidel (3).

## Results

Figure 2 shows a plot of the per cent of droplets uncrystallized, on a logarithmic scale, versus time of supersaturation at four different temperatures of supersaturation, with a constant droplet size for a typical unpurified solution. If the nucleation of the solution was a simple, first-order process then the points should fall on straight lines. The original, curved portions of the lines indicate that the nucleation is being catalyzed by impurities (2).

Figure 3 shows the plot of the per cent of droplets uncrystallized against time of supersaturation for a typical solution purified by the procedure described above. It is apparent that the points fall much more closely on a straight line than in the plot for the unpurified solution. There is some slight curvature near the origin which is probably due to relatively small amounts of impurity which were not removed. Neglecting this small effect, the results indicate that homogeneous nucleation is occurring in these purified solutions.

## Acknowledgment

We wish to thank Dr. R. M. Garrels for his interest and many helpful suggestions during the course of this work.

## References

1. Vonnegut, B., *J. Colloid Sci.* **3,** 563 (1948).
2. Pound, G., and LaMer, V. K., *J. Am. Chem. Soc.* **74,** 2323 (1952).
3. Seidel, A., "Solubilities of Inorganic and Metal Organic Compounds," 3rd ed. Van Nostrand, New York, 1940.

JOURNAL OF COLLOID SCIENCE **14**, 252–267 (1959)

# ELECTROPHORESIS, CONDUCTANCE, AND VISCOSITY OF AQUEOUS SOLUTIONS OF CARBOXYMETHYLCELLULOSE IN THE PRESENCE OF SODIUM CHLORIDE

**P. J. Napjus and J. J. Hermans**[1]

*Laboratorium voor Anorganische en Fysische Chemie, Universiteit, Leiden*

*Received January 8, 1959*

## ABSTRACT

The electrophoretic mobilities of carboxymethylcellulose in several iso-ionic dilution series are measured in a Tiselius-Svensson apparatus and extrapolated to zero polymer content. The extrapolated values prove to be almost independent of the ionic strength. The electrophoretic mobility appears to be less than proportional to the degree of substitution. From a comparison with recent theories, a fairly reasonable value for the friction factor per glucose unit is derived. On the basis of the viscosity theories of Brinkman, Debye, and Bueche, this friction factor leads to acceptable values for the effective radius of the macromolecules.

There exists a discrepancy of the order of 15% between the experimental conductance and that calculated on the basis of the Debye-Hückel approximation in the absence of relaxation effects. It is pointed out that this result is of doubtful significance, because the effect of the viscosity on the data at finite polymer concentrations is unpredictable.

## INTRODUCTION

### *1. General*

Data on the conductivity of polyelectrolyte solutions are not abundant in the literature, and they usually deal with polyelectrolytes in the absence of extraneous salt. Interesting work on the transport numbers in these solutions was reported by Wall and co-workers (1), who came to the conclusion that the mobility of the low molecular weight counter ions is reduced considerably by the presence of the polymer ions. Direct measurements of the mobility of the polymer ion itself, i.e., its electrophoretic mobility, have been published by Alfrey, Fuoss, and co-workers (2), but their conclusions are of a general and rather qualitative nature. Fitzgerald and Fuoss (3) mention some data which they do not consider as conclusive, and a theoretical interpretation is not given. Reference is made, further, to Katchalsky, Shavit, and Eisenberg (4).

---

[1] Present address: Cellulose Research Institute, State University College of Forestry, Syracuse, New York.

Later results obtained by Goring (5), by Cook (6) for carrageenin, and by Nagasawa, Soda, and Kagawa (7) for polyvinyl alcohol sulfate have been compared with recent theories (7, 8). Finally, we mention the work of Van Geelen (9), who measured electrophoretic mobilities, transport numbers, and conductivities in solutions of polymethacrylic acid at various degrees of neutralization in the presence of sodium chloride.

### *2. Electrophoresis*

In their theoretical studies of the electrophoretic mobility, Hermans and Fujita (10), Hermans (11), and Overbeek and Stigter (12) make use of Debye's (13) spherical coil model with partial free draining: to each polymer segment with charge $e$ one attributes a friction factor $f$; the segments are supposed to be distributed uniformly over the volume of a sphere with radius $R$. It is assumed, further, that the electric potential is sufficiently small everywhere to apply the approximation introduced by Debye and Hückel, and all relaxation effects are ignored. The treatments of this model by the various authors mentioned differ considerably among each other, but it has been shown that the final formulas for the electrophoretic mobility $u$ lead to essentially the same result in all cases of practical interest (see also Fujita, reference 14). For this reason, we quote the simplest formula published (11):

$$u = (e/f)\{1 + (\sigma^2/3)(1 + e^{-2p})(3 + p^2)^{-1}\}. \qquad [1]$$

In this expression $\sigma$ is the shielding ratio introduced by Debye (13) and is determined by the radius $R$ of the sphere, the number $\nu$ of segments per unit of volume in the sphere, and the viscosity $\eta_0$ of the solvent:

$$\sigma^2 = \nu f R^2/\eta_0 . \qquad [2]$$

Further, $p$ is the ratio between $R$ and the characteristic length $1/\kappa$ of the Debye-Hückel theory:

$$p = \kappa R. \qquad [3]$$

In the absence of extraneous salt it is difficult to assign a value to $\kappa$ which has a useful physical meaning; compare, in this connection, Fujita and Hermans (15). In the presence of salt exp $(-2p)$ is almost always negligible compared with unity, and in many cases $p$ is so large that the second term in the braces of Eq. [1] (which will be called correction term) is small compared with unity. This reduces $u$ practically to $e/f$, which means that the particle is free-drained. The physical explanation of this result is given in the papers quoted (10–12).

Since the Debye-Hückel approximation will, as a rule, be a poor approximation, it is of interest to consider briefly a solution of the problem that does not suffer from this disadvantage. Kimball, Cutler, and Samelson

(16) replaced the Debye-Hückel approximation by the other extreme, in which the charge of the polymer molecule is completely compensated everywhere by the counter ions. Lifson (17) improved their result by a perturbation method and showed that his solution of the potential problem agreed very closely with that obtained by Wall and Berkowitz (18) by means of a computer. We have applied Lifson's solution for the electric potential to the problem of electrophoretic mobility, using the method of reference 11. It will not be necessary to give the details of the calculation, the final result of which is

$$u = e/f + (kTv\lambda^2 p/4\pi e\nu f)\, g(\kappa, \beta, R)\, H(p, \beta, \lambda, R).$$

$$\begin{aligned} g(\kappa, \beta, R) &= [1 + (\kappa/\beta) \tanh (\beta R)]^{-1} \\ H(p, \beta, \lambda, R) &= (1 + 1/p)(\beta^2 - \lambda^2)^{-1}[\beta^2 - \lambda^2 \Gamma(\beta R)/\Gamma(\lambda R)] - \Gamma(\beta R) \qquad [4] \\ \Gamma(x) &= 1 - (1/x) \tanh x \\ \lambda^2 &= 2\sigma^2/3R^2; \qquad \beta^2 = \kappa^2 \cosh v; \qquad \sinh v = \nu/c, \end{aligned}$$

$c$ being the number of small ions per unit of volume at a large distance from the polymer ion; the extraneous salt is assumed to be uni-uni-valent. An approximation for $\Gamma(x)$ which is quite sufficient for our purpose (11) is

$$\Gamma(x) \cong x^2(3 + x^2)^{-1}, \qquad [5]$$

which leads to the simple expression

$$u = (e/f)\,\{1 + \epsilon kTv\sigma^2\Gamma(\beta R)g/6\pi e^2\nu R^2\}, \qquad [6]$$

$\epsilon$ being the dielectric constant of the medium.

It can be shown that the "correction term" in Eq. [6] is always smaller than that in Eq. [1] and approaches it very closely when $\beta$ approaches $\kappa$ (i.e., small $v$, small electric potential). In some special cases, when $v$ is large, it will be of some interest to use Eq. [6] rather than Eq. [1]; however, we have not made a detailed numerical analysis, because in our own experiments $v$ was never large compared to unity and the correction term is small. Besides, when $v$ becomes large the theory is likely to become inadequate, because it neglects relaxation effects (see below).

As mentioned above, the fact that the "correction term" in Eq. [1] (or [6]) is usually small compared to unity means that in electrophoresis the molecule is almost free-drained, i.e., it behaves like a cloud of ions moving independently of each other. Under these circumstances, we must expect that $u$ is independent of the molecular weight and nearly independent of the ionic strength of the solution. These conclusions are confirmed by the data of Goring (see reference 8) and of Nagasawa, Soda, and Kagawa (7). It must be borne in mind, however, that $e/f$ will be independent of the ionic strength only when the friction factor $f$ remains constant. In reality $f$

will change with ionic strength, as a result of the well-known Debye-Onsager effects in the double layer surrounding each individual fixed ion, and because of the fact that at low ionic strengths the reciprocal characteristic length of the Debye-Hückel theory may become larger than the distance between adjacent charges on the chain. Under these circumstances, the mobility will become more nearly equal to $2e/f'$ instead of $e/f$, $f'$ being the friction factor for a dimer, which is almost always less than twice that for the monomer. This question is closely related to a remark made by Overbeek and Stigter (12), who point out that at high ionic strengths it may be better to replace the model of the porous sphere by that of a straight or curved cylinder or by an assembly of randomly oriented cylinders. Van Geelen (9) has worked this out in detail and comes to the conclusion that his data for polymethacrylic acid can be accounted for more satisfactorily by this model than by the porous sphere model. Nevertheless, it is of some interest to note that for Van Geelen's polymethacrylic acid, the friction factor $f$ calculated from the experimental $u$ on the basis of the Overbeek-Stigter formula, which is practically equivalent to Eq. [1], turns out to be independent of the ionic strength, although the mobility $u$ is not.

We encounter a similar uncertainty as regards the behavior of the friction factor $f$ when we consider changes in the charge density per unit chain length, for example, as a result of changes in the degree of neutralization. From the data of Nagasawa, Soda, and Kagawa (7), it follows that the electrophoretic mobility $u$ increases by about 15% when the degree of substitution and thus the charge density per unit chain length increases by 15%, but in Van Geelen's experiments the degree of neutralization, $\alpha$, was changed from 0.1 to 0.9 and the $u$-values increase much less than proportionally to $\alpha$. In part, this is doubtless due to the factor $f$ which relates to that part of the chain which carries, on the average, a charge $e$; if the average charge per unit chain length is doubled, we will become concerned with the friction factor for a chain segment which is half as long, and this will, as a rule, be larger than $\frac{1}{2}f$.

Our own results for two carboxymethyl celluloses, with different degrees of substitution, show the same trend: the ratio between the degrees of substitution is 1.5, whereas that between the electrophoretic mobilities is only 1.35 (see Table II).

### *3. Conductance*

The porous sphere model has been used by Fujita and Hermans (15) to estimate the specific conductance $\mu_s$ of the solution. On the assumption that the Debye-Hückel approximation is valid:

$$\mu_s = \mu_0 + (n/E) \int u_\tau s \, d\tau. \qquad [7[$$

Here $\mu_0$ is the specific conductivity that would be observed if it were possible to remove only the polymer ions, $n$ is the number of polymer ions per unit of volume, $s$ the charge density due to the small ions, $E$ the external electric field, and $u_r$ the velocity of the liquid relative to the polymer ion. The integration in Eq. [7] is to be performed over the entire volume of the polymer ion and its surrounding double layer.

The integration of $u_r s$ was carried out, using for $u_r$ the expression given in reference 11, for $s$ that of Hermans and Overbeek (19). The result will be used in the discussion of our data, and is written here as follows:

$$\mu_s = \mu_0 + Zen(e/f)\Delta, \qquad [8]$$

where $Ze$ is the total charge fixed on the polymer ion and $\Delta$ is a complicated function of the parameters $\sigma$ and $p$. In all those cases in which the "correction term" in Eq. [1] is small compared to unity, $\Delta$ is close to unity and

$$\mu_s \cong \mu_0 + Zenu. \qquad [9]$$

### *4. Relaxation*

An attempt to account for relaxation effects was made by Longworth and Hermans (20), who used the model of a porous sphere in which the charges fixed on the polymer are completely compensated everywhere by the counter ions. The result for the electrophoretic mobility is

$$u = (e/f)\, 3\mu_m(\mu_2 + 2\mu_m + e^2\nu/f)^{-1}, \qquad [10]$$

where $\mu_2$ is the contribution of the small ions to the specific conductivity inside the sphere and $\mu_m$ that outside the sphere.

The specific conductivity of the solution was found to be (see reference 8):

$$\mu_s = \mu_m + Zenu + 3(\mu_2 - \mu_m)\mu_s\varphi(\mu_2 + 2\mu_m + e^2\nu/f)^{-1}, \quad [11]$$

where $\varphi$ is the volume fraction of spheres. The results [10] and [11] are independent of whether the Debye-Hückel approximation is used or not. It must be borne in mind, however, that the model is crude and the calculation approximate. Moreover, a straightforward application is difficult because $\varphi$ is known only if one can assign a reliable effective radius to the polymer molecules, while $\mu_2$ and $\mu_m$ can be calculated only if an assumption is made regarding the distribution of the small ions over the inside and the outside of the sphere. The distribution chosen by us in the discussion of our data will be that which follows from a simple Donnan equilibrium between the inside and the outside, neglecting activity coefficients.

## MATERIALS USED

A commercial sample of the sodium salt of carboxymethyl cellulose, Na-CMC-72, which had been purified at the research laboratories of AKU in Arnhem, the Netherlands, was further purified and fractionated by repeated precipitation from an aqueous solution in the presence of NaCl,

TABLE I

*Data Used for the Samples Studied*

| | $10^3r$ | $10^{-3}M_n$ | $Z_n$ | $10^{-3}M_w$ | $Z_w$ |
|---|---|---|---|---|---|
| Na-CMC-72 | 1.81 | 64 | 115 | 86 | 155 |
| Na-CMC-73 | 2.70 | 150 | 405 | (200) | (540) |

using ethyl alcohol as precipitant. The product was washed with alcohol 80% and dried *in vacuo* at 40°C.

Another sample, Na-CMC-73, was purified in a similar manner, except that in this case the solution of the polymer, before precipitation with alcohol, was heated to about 80°C. to facilitate dissolution. Presumably this caused some degradation because we could confirm the results quoted by Ott and Spurlin (21), who state that a heat treatment of Na-CMC in solution leads to an irreversible decrease in the viscosity. From this experience, and from the fact that our purification procedure was slightly different from that described by Pals (22) and by Trap (23), it follows that the molecular weights found by these authors for similar preparations can be considered only as crude estimates of those pertaining to our own samples. Nevertheless, we will use the molecular weights found by Pals and Trap, because neither the electrophoresis nor the molecular radius derived from the viscosity is much affected by the molecular weight. Our own attempts to measure the light-scattering molecular weight were not successful: notwithstanding repeated filtration and centrifugation, the gel fraction could not be completely removed.

The equivalent weight of the polymer salt was determined by conductometric titration. The result is given in Table I, where $r$ is the number of equivalents per gram polymer salt and $Z$ the average number of elementary charges per molecule: $Z_n$ the number average and $Z_w$ the weight average. The weight-average molecular weight of Na-CMC-73 was unknown; it was estimated from $M_n$ by assuming that $M_w/M_n$ had the same value as for Na-CMC-72.

The water used to prepare the solutions was purified under nitrogen by means of Amberlite MB1 anion-cation exchange resin. If it is collected in a polyethylene flask, it is possible to obtain water with a specific conductivity of $1 \times 10^{-7}\ \Omega^{-1}$ cm.$^{-1}$. When exposed to glass, the specific conductivity increases to about $1 \times 10^{-6}\ \Omega^{-1}$ cm.$^{-1}$ within a few hours but afterwards remains constant for a very long time. We have always used the value $10^{-6}$ to correct for the conductance of the pure water.

The dilutions were made iso-ionically (22) using NaCl as extraneous salt. This means that if $c$ is the concentration of the polyelectrolyte in g./ml. and $x$ the concentration of NaCl in mole/l., the sum

$$x + 1000\,rc = x_0$$

is kept constant in each dilution series. Under these circumstances, the curves of $\eta_{sp}/c$ versus $c$ are straight lines (22). For series in which $x_0$ was less than $0.5 \times 10^{-3}$ mole/l., the dilutions were made under nitrogen. The pH of the solutions was always between 7 and 9.

## MEASUREMENTS

1. *The viscosities* were measured in a viscometer with suspended level (Ubbelohde), in which the correction for kinetic energy was very small. Possible effects of the shear rate were neglected; its influence on the viscosity of Na-CMC solutions has been discussed in previous work (22, 24).

2. *The electrophoretic velocities* were determined in a Tiselius-Svensson apparatus, LKB 3023, at 25° ± 0.005°C. Johnson and Shooter (25) have shown that at this temperature convection currents are not important provided that the energy dissipation as a result of the electric current remains below $2 \times 10^{-2}$ watt/ml.; in our own experiments, it was never more than $0.5 \times 10^{-2}$ watt/ml.

The theory of the moving boundary has been developed by Henry and Brittain (26) on the basis of Kohlrausch's (27) and Weber's (28) work. For a review, we refer to De Wael and Wegelin (29).

The solution brought into contact with the colloid solution of total ionic concentration $x_0$ was a sodium chloride solution of concentration $x_0$. Under these circumstances, the ascending boundary has the disadvantage that the specific conductivity which should be used to calculate the electric field strength is that of the solution through which the boundary has already moved, and is therefore unknown. It is customary to replace this by the specific conductivity of the original colloid solution below the ascending boundary at the beginning of the experiment, but this introduces an unknown error. This uncertainty does not exist at the descending boundary, but this boundary broadens rapidly as a result of diffusion because ions which lag behind find themselves in a region of lower potential gradient. It is then no longer permissible to identify the velocity of the peak in the Schlieren diagram with the electrophoretic velocity.

Both these errors are eliminated by extrapolating to zero polymer concentration; see reference 7. The extrapolated velocity of the ascending boundary is the same as that of the descending one; compare Fig. 1.

The Tiselius cell has a middle part which slides horizontally into position at the beginning of the experiment. As a result of this construction, a certain leaking current is unavoidable. In all series in which $x_0$ was not less than $3 \times 10^{-3}$ equiv./l., we have succeeded in keeping the leaking current below 0.5% by the following measures: (*1*) the glass plates which were to slide into position were treated with silicone oil of viscosity $10^5$ poises; (*2*) the horizontal shift needed to bring the middle part into position was always kept as small as possible, i.e., just sufficient to close the channels in the cell

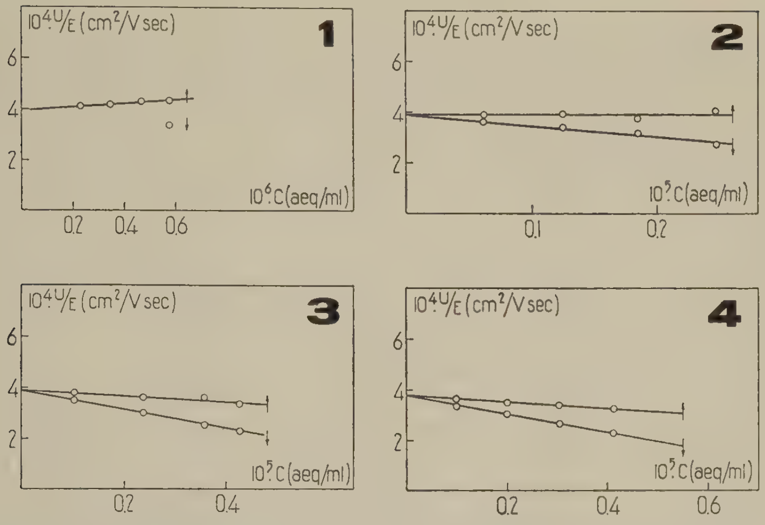

FIG. 1. Na-CMC-73; iso-ionic dilution series. Velocity of peak in Schlieren diagram, reduced to unit filed strength, as a function of polymer concentration *c*.

↑ ascending boundary, ↓ descending boundary

| Series: | 1 | 2 | 3 | 4 |
|---|---|---|---|---|
| 1000 $x_0$ = | 0.721 | 3.09 | 7.41 | 9.69 |

before the experiment was started. As a result, only a very small area of the glass plates had a chance to be wetted by the solutions.

Only one series was done at a total ionic concentration less than $3 \times 10^{-3}$ equiv./l. because in such series the polymer concentration must be low, so that the peak in the Schlieren diagram becomes small. Moreover, the specific resistance becomes so high that leaking currents become relatively too important. One series of measurements was done, however, with Na-CMC-73 at $x_0 = 0.7 \times 10^{-3}$ equiv./l. To this end, the leaking current was suppressed by removing the water from the temperature bath in which the Tiselius cell was immersed. Instead, air of 20°C. was circulated along the cell and the electric current was reduced to 0.1 ma. by the introduction of a shunt of 33,000 Ω over the electrodes. The result of this one series of experiments was in good agreement with that of the others; compare Table II.

3. *The conductances* of the solutions were measured under nitrogen in cells of the type described by Longworth (20), placed in a temperature bath filled with oil at 25° ± 0.005°C. Use was made of a Leeds and Northrup Wheatstone bridge described by Dike (30), the compensation resistances of which were calibrated with direct current. If the room temperature is kept constant at 20°C. and the relative humidity at about 55%, the accuracy of the measurements is 0.02%. The resistance at a frequency of 4500 cycles was always within 0.02% of that at 1500 cycles. To make sure that

TABLE II

*Intrinsic Viscosities* $[\eta]$ *in ml./g. and Electrophoretic Mobilities* $u_0$ *in cm.*$^2$*v.*$^{-1}$*sec.*$^{-1}$*, Both Obtained by Extrapolation to Zero Polymer Content*

The molecular radius $R$ (in cm.) and the friction factor $f$ (in g./sec.) for a segment carrying 1 electronic charge were calculated from Eqs. [1] and [12]; $x_0$ is the NaCl concentration in moles/liter.

| $10^3x_0$ | $[\eta]$ | $10^4u_0$ | $10^8R$ | $10^9f$ |
|---|---|---|---|---|
| Na-CMC-73 | | | | |
| 0.302 | 3200 | — | (765) | (4.6) |
| 0.721 | 2560 | 3.95 | 680 | 4.4 |
| 3.09 | 1820 | 3.90 | 590 | 4.2 |
| 7.41 | 1600 | 3.90 | 550 | 4.2 |
| 9.69 | 1550 | 3.80 | 545 | 4.2 |
| Na-CMC-72 | | | | |
| 0.1 | 2670 | — | (640) | (6.6) |
| 1.0 | 1730 | — | (540) | (5.7) |
| 10 | 900 | 2.90 | 420 | 5.5 |

a possible adsorption of polymer at the electrodes and at the glass walls had always reached equilibrium, the cells were emptied, and refilled with the same solution, until the resistance had reached a constant value to within 0.1%. The results given below are the specific conductances after subtraction of that of the water.

## Results and Discussion

As regards the viscosities, we restrict ourselves to giving the intrinsic viscosities $[\eta]$ listed in Table II. The experimental electrophoretic mobilities $u = U/E$, where $U$ is the velocity and $E$ the potential gradient, are shown as a function of polymer concentration for Na-CMC-73 in Fig. 1. The results for Na-CMC-72 are so similar that they are not reproduced. As explained in the section on Measurements, only the extrapolated values $u_0 = U_0/E$ (at $c = 0$) are significant; these are listed in Table II. Finally, the specific conductances are given in Tables III and IV.

A comparison of the intrinsic viscosities with those reported by Pals (22) reveals that for Na-CMC-73 there is excellent agreement at high ionic strengths, but that our values are about 30% lower at low ionic strengths. A possible explanation of this trend is the effect of the shear-rate: it is well known that this effect is more pronounced at low than at high ionic strengths (see, for instance, reference 24). Our $[\eta]$ values for Na-CMC-72 at all ionic strengths examined are about 30% lower than those found by Pals; this suggests that the molecular weight $M$ of our Na-CMC-72 was somewhat lower than that of Pals' sample. However, since the effect of $M$ on the calculated molecular dimensions and on the friction factor per segment is very small, we have not deemed it worth while to apply any corrections.

TABLE III

*Specific Conductance* $\mu(\Omega^{-1}cm.^{-1})$ *of Three Iso-ionic Dilution Series for Na-CMC-72*

Concentration $C$ (equiv./l.) in aqueous NaCl at 25°C.; $x_0$ is the NaCl concentration in moles/l. when $C = 0$.

| $x_0 = 0.0001$ | | $x_0 = 0.001$ | | $x_0 = 0.01$ | |
|---|---|---|---|---|---|
| $10^4C.$ | $10^5\ \mu$ | $10^3C.$ | $10^4\ \mu$ | $10^2C.$ | $10^3\ \mu$ |
| 0 | 1.255 | 0 | 1.240 | 0 | 1.183 |
| 0.099 | 1.245 | 0.098 | 1.185 | 0.098 | 1.136 |
| 0.248 | 1.228 | 0.234 | 1.120 | 0.234 | 1.070 |
| 0.351 | 1.210 | 0.469 | 1.025 | 0.469 | 0.970 |
| 0.500 | 1.181 | 0.704 | 0.930 | 0.704 | 0.868 |
| 0.750 | 1.103 | 0.940 | 0.842 | 0.940 | 0.763 |
| 1.000 | 1.037 | | | | |

TABLE IV

*Specific Conductance* $\mu$ $(\Omega^{-1}cm.^{-1})$ *of Five Iso-ionic Dilution Series for Na-CMC-73*

Concentration $C$ (equiv./l.) in aqueous NaCl at 25°C.; $x_0$ is the NaCl concentration in moles/l. when $C = 0$.

| $10^3x_0 = 0.302$ | | $10^3x_0 = 0.721$ | | $10^3x_0 = 3.09$ | | $10^3x_0 = 7.41$ | | $10^3x_0 = 9.69$ | |
|---|---|---|---|---|---|---|---|---|---|
| $10^4C$ | $10^4\ \mu$ | $10^4C$ | $10^4\mu$ | $10^4C$ | $10^4\mu$ | $10^3C$ | $10^4\mu$ | $10^3C$ | $10^4\mu$ |
| 0 | 0.3780 | 0 | 0.8911 | 0 | 3.751 | 0 | 8.813 | 0 | 11.460 |
| 0.323 | 0.3650 | 1.16 | 0.8327 | 0.621 | 3.413 | 1.05 | 8.282 | 0.995 | 10.848 |
| 0.584 | 0.3505 | 2.32 | 0.7923 | 1.24 | 3.046 | 2.37 | 7.486 | 2.02 | 10.200 |
| 1.010 | 0.3280 | 3.48 | 0.7259 | 1.85 | 2.711 | 3.56 | 6.900 | 3.03 | 9.609 |
| 1.510 | 0.3015 | 5.79 | 0.6203 | 2.48 | 2.428 | 4.28 | 6.740 | 4.15 | 9.936 |
| 2.010 | 0.2835 | 7.09 | 0.5673 | 3.09 | 2.177 | 5.94 | 5.933 | 5.09 | 8.424 |
| 3.020 | 0.2365 | | | | | | | | |

Table II shows that $u_0$ does not depend on the ionic strength. This is in keeping with Eq. [1] (or [6]), because the "correction term" is small compared with unity, so that $u$ is close to $e/f$. If, on this basis, we calculate the friction factor $f$ for a chain fragment carrying one electronic charge, we find about $4.2 \times 10^{-9}$ g./sec. for Na-CMC-73 and about $5.5 \times 10^{-9}$ for Na-CMC-72. On the basis of Stokes' law, this gives a radius of 2.0 A. for a segment in nr. 73 and 2.8 A. in nr. 72. In view of the fact that nr. 72 contains about 1 carboxyl group per 3 glucose units, whereas nr. 73 carries 1 elementary charge per 1.8 glucose units, we find a radius of roughly 1 A. per glucose unit. This is more realistic than the much smaller values derived for most polymer segments on the basis of the viscosity theories of Kirkwood and Riseman (31) or Debye and Bueche (13). It is, therefore, of some interest to calculate the molecular radius $R$ from the intrinsic viscosity, using the $f$-value derived from $u$. We have done this on the basis of the expression derived by Debye and Bueche (13):

$$[\eta] = (4\pi R^3/3)\ (N_0/M)\ \Phi(\sigma) \tag{12}$$

where $N_0$ is Avogadro's number, $M$ the molecular weight, and $\Phi(\sigma)$ a known function of the parameter $\sigma$ defined in Eq. [2], in which $\nu$ is (in our case) the density of fixed charges, i.e.,

$$\nu = 3Z/4\pi R^3. \tag{13}$$

Eliminating $R$ from Eqs. [2] and [12], we get

$$\Phi(\sigma)/\sigma^6 = (3[\eta]M/4\pi N_0)\ (4\pi\eta_0/3Zf)^3. \tag{14}$$

A graph was made of $\Phi/\sigma^6$ versus $\sigma^2$, so that $\sigma$ could be found for any given value of $f$. We inserted the weight-average $M$ and $Z$; the values found for $R$ on the basis of the number-average $M$ and $Z$ are only a few per cent higher. Our procedure was to insert in Eq. [14] the $f$-value which followed from the electrophoretic mobility according to the relation $u = e/f$. This gave a provisional value of $\sigma$ and thus of $R$. With this $R$-value, we calculated the "correction term" in Eq. [1], which thus led to a corrected value of $f$. This procedure leads very rapidly to those values of $R$ and $f$ that satisfy both Eq. [1] and Eq. [12]. The result is given in Table II; the figures in brackets refer to series for which $u_0$ could not be measured and were calculated on the assumption that $u_0$ had the same value as at the higher ionic strengths.

Direct measurements of $R$ for Na-CMC-73 are not available. A comparison with the light-scattering measurements of Trap (23) is possible only for Na-CMC-72 at $x_0 = 0.01$, where Trap found a radius of 500 A., which compares reasonably well with the figure 420 in Table II. However, Trap found a greater expansion at lower ionic strengths, suggesting that in reality the electrophoretic mobility increases somewhat with decreasing ionic strength—a conclusion which is supported by the experimental results of Nagasawa, Soda, and Kagawa (7).

It should be mentioned at this juncture that Ise, Hosono, and Sakurada (32) have interpreted the electrophoretic mobility of polyvinylalcohol, partially acetylized with glyoxylic acid, on the basis of Henry's equation for solid spheres. We believe that this model is inadequate, because it follows from a straightforward application of the Kirkwood-Riseman or Debye-Bueche concepts (references 8, 10, 11, 12) that in electrophoresis the molecule is almost free-drained when $\kappa R \gg 1$. At this limit, Henry's equation becomes

$$u = Ze/(4\pi\eta\kappa R^2).$$

The constancy of $u$ over a large range of $\kappa$-values (Na-CMC-73 in Table II) would, therefore, require that $\kappa R^2$ remain constant, which is not impossible but would be entirely fortuitous.

As regards the experimental specific conductances $\mu$, three examples are shown in Figs. 2, 3, and 4. These figures show, in addition, the contribution $\mu_0$ of the small ions as defined in connection with Eq. [7], the result $\mu_0 + Zen(e/f)\Delta$ predicted by Eq. [8], and the result $\mu_s$ according to Eq. [11]. The quantity $\mu_0$ was calculated from the mobilities and concentrations of the small ions. As has been explained at the end of the Introduction, the calculated values of $\mu_s$ are very uncertain: to estimate the volume fraction $\varphi$ of the spheres we used the radius $R$ of Table II; the polymer concentrations for which $\varphi$ turned out to exceed unity were not taken into consideration; $\mu_2$ and $\mu_m$ were estimated for any given $\varphi$ on the basis of a Donnan equilibrium between the inside and the outside of the sphere; the equations used in this procedure can be found in reference 20.

For Na-CMC-72, at total ionic concentrations of 0.01 and 0.001 equiv./l., the experimental specific conductance, $\mu$, is very close to $\mu_0 + Zen(e/f)\Delta$

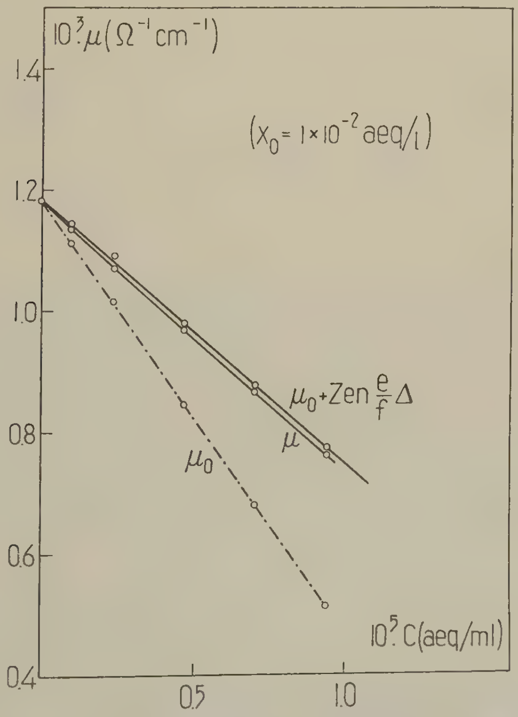

FIG. 2. Experimental specific conductance $\mu$ of an iso-ionic dilution series in which $x_0$ = 0.01 equiv./l.; $c$ = concentration of Na-CMC-72.

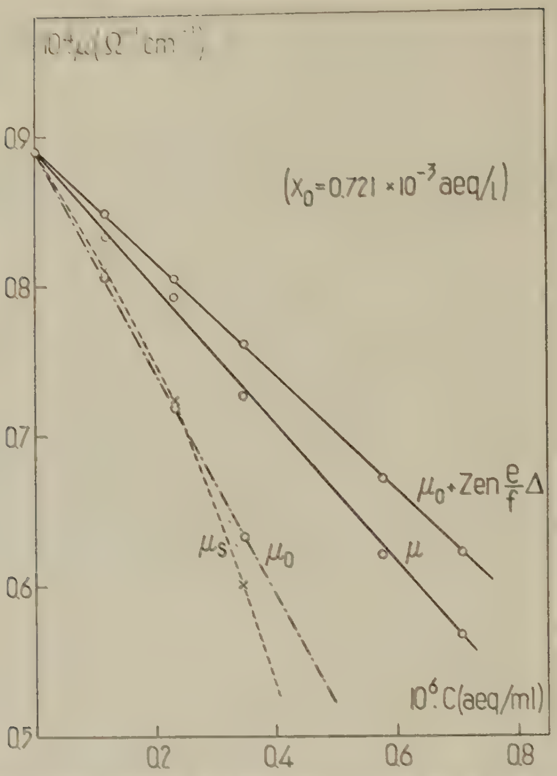

FIG. 3. Specific conductance of an iso-ionic dilution series for Na-CMC-73; $x_0 = 0.72 \times 10^{-3}$ equiv./l.

(compare Fig. 2); when $x_0 = 10^{-4}$, the value of $\mu$ was considerably larger than $\mu_0 + Zen(e/f)\Delta$. On the contrary, for Na-CMC-73, the quantity $\mu_0 + Zen(e/f)\Delta$ was always larger than $\mu$, the difference varying from about 5% to about 20% (compare Figs. 3 and 4). From a theoretical point of view, it is more satisfactory to compare the experimental value of $\mu - \mu_0$ with the theoretical one, but this does not change the magnitude of the discrepancy between theory and experiment, which remains of the order of 10% to 15%. Considering the highly simplifying assumptions which led to Eq. [8], the agreement between this equation and the experimental data must be considered as surprisingly good.

This result, in conjunction with the electrophoretic mobilities, suggests that relaxation effects did not play a very important role in either the electrophoresis or the conductance. If one remembers, in addition, that the application of the theory of relaxation must be based on uncertain data, it is not surprising that the application of Eq. [11] did not give very promising results. In the series of low ionic strengths, $\mu_s$ turned out to be lower than

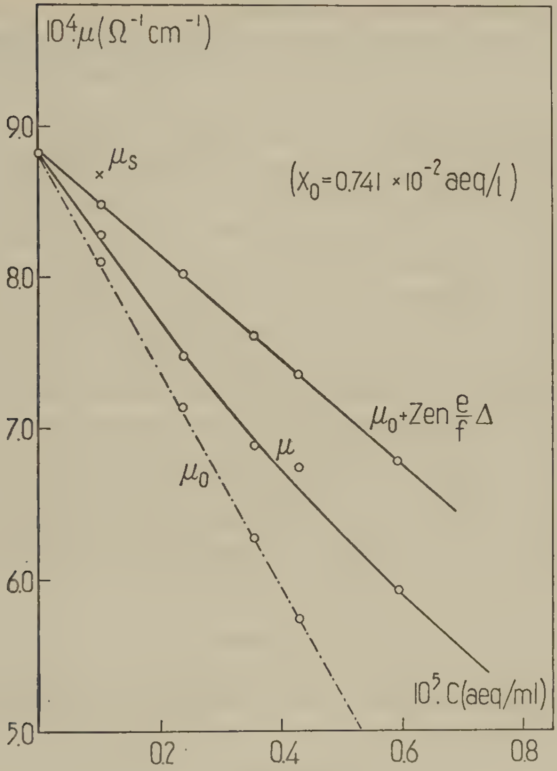

FIG. 4. Specific conductance of an iso-ionic dilution series, $x_0 = 7.4 \times 10^{-3}$ equiv./l.; Na-CMC-73.

$\mu$; at larger values of $x_0$ it was higher than $\mu$: see the examples in Figs. 3 and 4. In several cases, the value of $\mu_s$ could be calculated only for the lowest polymer concentration examined, because at higher polymer content the fraction $\varphi$ turned out to be larger than unity.

Van Geelen (9) estimates the mobility of the sodium ions from the total conductance of the mixture and the electrophoretic mobility of the polymethacrylate ion. To this end, he assumes that the contribution of NaCl to the conductance is independent of the polymer content. He then finds that the mobility of the remaining sodium always decreases with increasing degree of neutralization of the polymer and sometimes reaches negative values. We submitted our own data for Na-CMC to the same treatment and found almost constant (positive) values for the Na mobilities.

The assumption that the contribution of NaCl is not affected by the presence of the polymer ions, whereas that of the remaining ions is strongly dependent on polymer concentration is, of course, rather arbitrary. As an alternative, though equally arbitrary approach, one could assume that the contribution of the Cl ions is independent of the polymer content and then calculate an average mobility for *all* the Na ions in the mixture. If this is done for Na-CMC, one finds again that the mobility of the Na ions is almost constant.

Further attempts to analyze the conductance data have not been made, because we believe that the interpretation is complicated by a very serious factor which has not been mentioned so far: the viscosity of the solutions increases rapidly with polymer content. Many of the solutions investigated are several times as viscous as water.

It was shown by Stokes (33) that even in solutions of low molecular weight electrolytes, the product of ionic mobility and viscosity is not constant, so that it is impossible to introduce reliable corrections, the more so since we do not know whether the viscosity affects the mobility of the polymer ions to the same extent as it does that of the small ions. Under these circumstances, it is all the more surprising that Eq. [8] represents such a good approximation, and we cannot exclude the possibility that this is, to a large extent, fortuitous. The electrophoretic mobility is, of course, not affected by the viscosity because it is obtained by extrapolation to zero polymer concentration.

## Acknowledgment

This work was supported by the Foundation for pure scientific research (ZWO), the Netherlands, as part of the program of the Foundation for basic research on matter (FOM).

## References

1. Eisenberg, H., *J. Polymer Sci.* **30,** 47 (1958). Huizinga, J. R., Krieger, P. F., and Wall, F. T., *J. Am. Chem. Soc.* **72,** 2636 (1950). Wall, F. T., and Doremus, P. H., *J. Am. Chem. Soc.* **76,** 1557 (1954).
2. Alfrey, T., Morawetz, H., Fitzgerald, E. B., and Fuoss, R. M., *J. Am. Chem. Soc.* **72,** 1864 (1950). Alfrey, T., Fuoss, R. M., Fitzgerald, E. B., and Pinner, H., *J. Am. Chem Soc.* **74,** 438 (1952).
3. Fitzgerald, E. B., and Fuoss, R. M., *J. Polymer Sci.* **14,** 329 (1954).
4. Katchalsky, A., Shavit, N., and Eisenberg, H., *J. Polymer Sci.* **13,** 69 (1954).
5. Goring, D. A. I., and Young, E. Gordon, *Can. J. Chem.* **33,** 480 (1955).
6. Cook, W. H., Rose, R. C., and Colvin, J. R., *Biochim. et Biophys. Acta* **8,** 595 (1952).
7. Nagasawa, N., Soda, A., and Kagawa, I., *J. Polymer Sci.* **31,** 439 (1958).
8. Hermans, J. J., Structure of Electrolyte Solutions, Symposium Electrochemical Society, Washington 1957, Ch. 21. Wiley, New York, 1958.
9. Van Geelen, B., Thesis, Utrecht, 1958.
10. Hermans, J. J., and Fujita, H., *Koninkl. Ned. Akad. Wetenschap. Proc.* **B58,** 182 (1955).
11. Hermans, J. J., *J. Polymer Sci.* **18,** 527 (1955).
12. Overbeek, J. Th. G., and Stigter, D., *Rec. trav. chim.* **75,** 543 (1956).
13. Debye, P., and Bueche, A. M., *J. Chem. Phys.* **16,** 573 (1948).
14. Fujita, H., *Rec. trav. chim.* **76,** 798 (1957).

15. Fujita, H., and Hermans, J. J., *Koninkl. Ned. Akad. Wetenschap. Proc.* **B58**, 188 (1955).
16. Kimball, G. E., Cutler, M., and Samelson, H., *J. Phys. Chem.* **56**, 57 (1952).
17. Lifson, S., *J. Chem. Phys.* **27**, 700 (1957).
18. Wall, F. T., and Berkowitz, J., *J. Chem. Phys.* **26**, 114 (1957).
19. Hermans, J. J., and Overbeek, J. Th. G., *Rec. trav. chim.* **67**, 761 (1948).
20. Longworth, R., and Hermans, J. J., *J. Polymer Sci.* **26**, 47 (1957).
21. Ott, E., and Spurlin, H. M., "Cellulose and Cellulose Derivatives." Interscience, New York, 1956.
22. Pals, D. T. F., and Hermans, J. J., *Rec. trav. chim.* **71**, 433 (1952).
23. Trap, H. J. L., and Hermans, J. J., *J. Phys. Chem.* **58**, 957 (1954).
24. Akkerman, F., and Pals, D. T. F., *Rec. trav. chim.* **71**, 56 (1952).
25. Johnson, P., and Shooter, E. M., *J. Colloid Sci.* **3**, 539 (1948).
26. Henry, D. C., and Brittain, J., *Trans. Faraday Soc.* **29**, 807 (1933).
27. Kohlrausch, F., *Wied. Ann.* **62**, 209 (1897).
28. Weber, W. E., *Sitzber. preuss. Akad. Wiss. Physik.-math. Kl.* **1897**, 936.
29. De Wael, J., and Wegelin, E., *Rec. trav. chim.* **71**, 1035 (1952).
30. Dike, P. H., *Rev. Sci. Instr.* **2**, 379 (1931).
31. Kirkwood, J. G., and Riseman, J., *J. Chem. Phys.* **16**, 565 (1948).
32. Ise, N., Hosono, M., and Sakurada, I., *Mem. Fac. Eng. Kyoto Univ.* **19**, 417 1957).
33. Stokes, R. H., Structure of Electrolyte Solutions, Symposium Electrochemical Society, Washington, 1957, Ch. 20. Wiley, New York, 1958.

JOURNAL OF COLLOID SCIENCE 14, 268–280 (1959)

# ADHESIVE PROPERTIES OF ICE

**H. H. G. Jellinek**[1]

*U. S. Army Snow Ice and Permafrost Research Establishment, Corps of Engineers, Wilmette, Illinois*

*Received January 9, 1959*

## INTRODUCTION

The adhesive properties of ice have scarcely been studied experimentally from a fundamental point of view. There are numerous papers in the literature on ice-releasing substances, which have been investigated especially with regard to airplane de-icing, but all this work has been done from the applied point of view. Some fundamental experimental work on tensile properties of ice sandwiched between metal plugs and some theoretical work using heat of immersion and adsorption data have been carried out (1, 2). Attempts have also been made to calculate adhesive strength (3).

However, these approaches, though of intrinsic value, consider only some of the problems concerned with adhesion. It is generally true that substances with which water forms a large contact angle adhere less to ice than those which show a small contact angle. But the contact angle can be considered only as a guide. It is well known that ice and indeed all solid substances have imperfections statistically distributed throughout their mass. Thus, the actual cohesive strength of ice is many magnitudes smaller than the one expected from theory (1). The same is true for the adhesive strength. Moreover, the plastic-elastic properties of the substances involved will also play an important role for the adhesive strength. Another complication is caused by adsorption of gases at the interfaces. Unless extreme precautions are taken, adhesion between two substances does not take place between two clean surfaces but between surfaces which have gases adsorbed. Another complication arises owing to slight solubilities in each other of the substances involved. Last, the surface roughness down to molecular dimensions also plays a role. Thus, it is seen that adhesive studies deal with a complex situation. A realistic approach to adhesion will have to start with a systematic collection of experimental data, obtained under rigid experimental conditions.

In the present work, a beginning has been made in the study of the adhesive properties of ice with respect to stainless steel, polystyrene, and polymethylmethacrylate as a function of cross-sectional area and thickness of the ice specimen and also of temperature. Experiments were carried out by applying forces in shear and in tension.

---

[1] Presented at the 134th Meeting of the American Chemical Society, Chicago, September 8, 1958.

## EXPERIMENTAL

### *Materials*

Stainless steel was grade 304/A with polished surface; the finishing polish was obtained with Lapping Compound No. 38-900 A, U. S. Products Company. Cast polystyrene and polymethylmethacrylate (Lucite) sheets were selected such that no unevenness could be detected by visual inspection. Distilled water was passed through exchange resin and boiled out continuously; the procedure will be described subsequently. Snow-ice was prepared as described previously (4). All cleaning fluids such as methanol and benzene were of reagent grade.

### *Apparatus*

The tensile apparatus and the corresponding mounting device were the same as described in a previous paper (1).

The shear apparatus was similar to the tensile apparatus except that the mounting apparatus and the shear apparatus were combined. (For details see ref. 5.) The ice was sandwiched between two metal disks or between a metal disk and a plastic disk. One of the disks had a hook which was constructed in such a way that the force was acting in line with the disk-ice interface.

## PROCEDURE

### *Tensile Experiments*

The mounting, carried out at $-10°C.$, was critical and had to be standardized rigidly. The polystyrene, polymethylmethacrylate, and metal disks were cleaned carefully with methanol before each test. That this cleaning procedure is satisfactory was shown by contact angle measurements (6). Thus, polymethylmethacrylate and polystyrene gave—using similar cleaning procedures—initial contact angles of 87° and 90°, respectively. A metal disk was fixed into the steel rod of the vertical mounting device (see reference 1, Fig. 1) and the plastic disk was fixed into the lower part. A flask with water boiling on a hot plate was always ready next to the mounting apparatus and water was squeezed out directly (wash bottle fashion) on to the plastic disk, forming a large drop which covered the whole surface. The drop was left to cool for a standardized time, which had to be found by trial for each cross-sectional area. Then the water at the edge of the plastic surface was touched with a pointed ice crystal; if the conditions were right, the water froze so that the crystals traveled first across the plastic-water interface, driving residual air from the interface. As quickly as possible, the stainless steel rod carrying the metal disk was lowered to a predetermined distance; the whole assembly was left for at least 20 minutes and subsequently transferred to the tensile strength apparatus. It was noticed that the surface of the plastic disks became crazed and cloudy after a number of tests; thus, not more than three tests were carried out with each plastic disk.

### *Shear Experiments*

With stainless steel disks, only snow-ice was used. Cylinders were turned on a lathe at −10°C. and frozen to one of the steel disks. The snow-ice cylinder was then cut to the desired height and mounted (for details see reference 5).

In the case of a plastic disk, the seeding procedure as described in the previous section was used (see reference 5).

## EXPERIMENTAL RESULTS

### *Shear Experiments*

Shear experiments for snow-ice (density ca. 0.886 g./cm.$^3$) sandwiched between polished steel plates were carried out as a function of cross-sectional area at −5°C. (Table I) and as a function of temperature for constant cross section (Fig. 1, for details see reference 5).

As can be seen from Table I, the adhesive strength of ice/stainless steel is independent of the cross-sectional area of the specimens and of the thickness of the ice.

The adhesive strength of ice/stainless steel as a function of temperature rises linearly with decreasing temperature as is apparent from Fig. 1. It shows a very abrupt change from adhesive breaks to cohesive breaks in the

TABLE I

*Adhesive Strength of Snow Ice/Stainless Steel*

Obtained from shear experiments as a function of cross-sectional area at −5°C. All breaks were purely adhesive. Thickness of ice layer 0.2 to 0.4 cm.

| Cross section (*cm.*$^2$) | Adhesive strength (*kg./cm.*$^2$) | | | Time of load application (sec.) |
|---|---|---|---|---|
| | Mean | Standard deviation | Standard error of mean | |
| 1.54 | 5.44 | ± 0.40 | ±0.12 | 14 |
| 3.14 | 5.50 | ± 0.72 | ±0.19 | 23 |
| 4.91 | 5.32 | ± 1.14 | ±0.32 | 28 |
| 6.61 | 5.41 | ± 0.49 | ±0.15 | 41 |

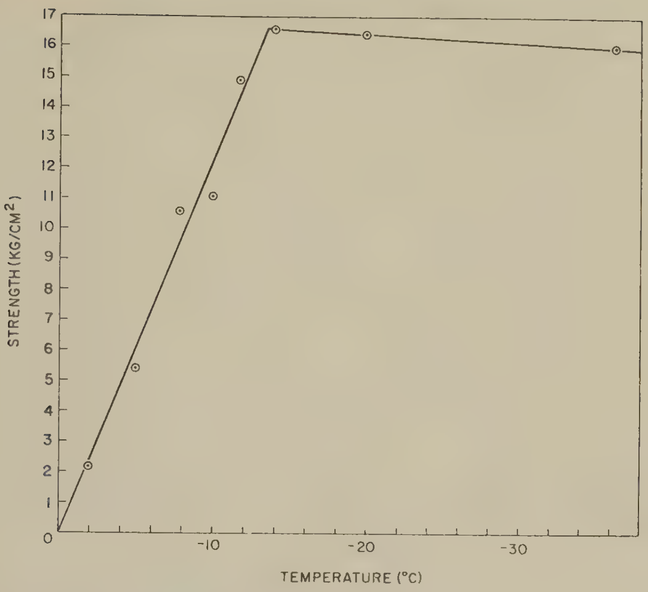

FIG. 1. Strength as a function of temperature for snow-ice, sandwiched between stainless steel disks, obtained by shear. Cross-sectional area 1.54 cm.$^2$, height 0.2 to 0.4 cm. Adhesive breaks only down to −13°C.; cohesive breaks only below −13°C. Each point represents the average of at least 12 tests.

neighborhood of −13°C. Below this temperature, practically all breaks are cohesive and show only a very slight decrease with temperature. The adhesive branch of the curve in Fig. 1 can be represented by the equation:

$$S_A = -1.24t - 0.18 \text{ kg./cm.}^2, \qquad [1]$$

where $S_A$ is the average adhesive strength and $t$ the temperature in degrees centigrade.

The magnitude of the cohesive strength is similar to that of the cohesive breaks by tension, reported in a previous paper (1). For instance, the tensile strength of snow-ice of height 0.5 cm. was found at −4.5°C. to be 15.5 kg./cm.$^2$ at a stress rate of 0.64 kg./cm.$^2$-sec., which is of slightly smaller magnitude than the cohesive strength values found by shear. The average stress rate for the shear experiments at −14, −20, and −34.3°C. was 0.52 kg./cm.$^2$-sec. The cohesive breaks are actually of similar shape to the most frequent type obtained previously under tension (see reference 1, Fig. 4*A*).

Shear experiments were also carried out with ice frozen to polystyrene disks (for detailed data, see reference 5). The cross-sectional areas in the range from 3.14 to 9.6 cm.$^2$ have no influence on the adhesive strength. The shear data on the adhesive strength of ice/polystyrene as a function

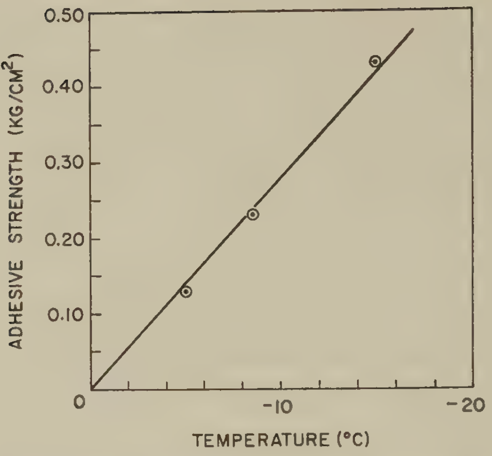

FIG. 2. Adhesive strength of ice/polystyrene as a function of temperature, obtained by shear. Cross-sectional area 9.61 cm.$^2$, height $7.6 \times 10^{-2}$ cm. Each point represents the average of at least 12 tests.

TABLE II

*Adhesive Strength of Ice/Polystyrene*

Obtained from tensile experiments, (*a*) at −5°C. for two cross-sectional areas; (*b*) as a function of rate of stress application at area 1.54 cm.$^2$ Thickness 0.1 cm.

| (*a*) Cross section (cm.$^2$) | Adhesive strength (kg./cm$^2$.) | | | | Type of break |
|---|---|---|---|---|---|
| | Mean, total | Mean, adhesive breaks only | Standard deviation | Standard error of mean | |
| 1.54 | — | 3.3 | ±2.4 | ±0.7 | All adhesive |
| 3.14 | — | 2.1 | ±0.16 | ±0.05 | |
| (*b*) Rate of Stress[a] application *kg/cm.$^2$ Sec.* | | | | | |
| 0.3 | — | 1.9 | ±0.34 | ±0.10 | All adhesive |
| 1.0 | 3.7 | 2.1 | ±0.50 | ±0.16 | 10 adhesive<br>2 cohesive |

[a] For rate 0.55 kg./cm.$^2$/sec., see under (*a*).

of temperature at constant cross section are plotted in Fig. 2 and can be expressed by the equation:

$$S_A = -2.8 \times 10^{-2} t \text{ kg./cm.}^2. \qquad [2]$$

These experiments also had an approximately constant rate of stress application (see reference 5).

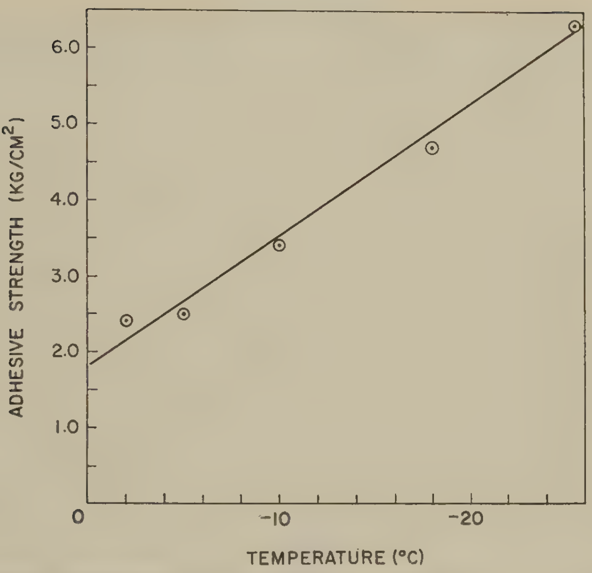

FIG. 3. Adhesive strength of ice/polystyrene as a function of temperature, obtained by tension. Cross-sectional area 1.54 cm.$^2$, height 0.1 cm. Each point represents the average of at least 12 tests. Atmospheric pressure should be subtracted from strength values.

### *Tensile Experiments*

Tensile experiments were carried out with ice frozen to polystyrene and polymethylmethacrylate (Lucite). The data for two different cross-sectional areas for polystyrene obtained at $-5$°C. are shown in Table II (*a*). Apparently, the cross-sectional areas have little influence in this range of areas.

The strength was also investigated as a function of temperature keeping the cross section constant. The mean adhesive values are plotted against temperature in Fig. 3 and can be represented by

$$S_A = -0.173t + 1.81 \text{ kg./cm.}^2. \qquad [3]$$

For the tensile experiments also, the rate of stress application was found to be approximately constant. (For details, see reference 5).

A number of experiments on the system ice/polystyrene were carried out at different rates of stress application (different speeds of motor). The results, listed in Table II (*b*), show that the rate of stress application in the range investigated has no effect on the adhesive strength.

A number of experiments were also carried out on adhesion of ice to polymethylmethacrylate (Lucite) at $-5$°C. For a cross-sectional area of 0.785 cm.$^2$, thickness 0.1 cm. and rate of stress application of ca. 1.1 kg./cm.$^2$/sec. a mean adhesive strength of 4.4 kg./cm.$^2$ was found (standard deviation ±2.9, standard error of mean ±0.7). There were 19 adhesive breaks and 4 borderline cases. These data indicate that the adhesive strength of ice/polymethylmethacrylate is larger than the adhesive strength of ice/polystyrene.

## DISCUSSION

The shear experiments where snow-ice was sandwiched between two stainless steel plates will be discussed first. These experiments bring out three remarkable characteristics: First, the adhesive strength is independent of cross-sectional area; second, the adhesive strength is independent of the thickness of the ice layer (only a small range has been investigated); and third, adhesive strength is a linear function of the temperature until it becomes larger than the cohesive strength of ice at about −13°C., where a very sharp transition from adhesive to cohesive breaks takes place.

The only experiments by other authors which are of interest in this connection are those by Hunsaker *et al.* (7). Their experiments on the adhesive strength of ice/brass as a function of temperature show a striking similarity to the results obtained here with stainless steel. The transition point from adhesive to cohesive breaks was found by these investigators to be about −12°C. whereas the one found in the present work lies at about −13°C.

Similarly, as in the case of tensile strength (cohesive strength) of ice (1), the experimental adhesive strength is several magnitudes smaller than expected from theory. Czyzak (3) has calculated the adhesive strength of water adhering to iron by a classical and a quantum-mechanical method. The classical adhesive strength at 300°K. was calculated as 13050 kg./cm.$^2$ and the quantum-mechanical one as 6770 kg./cm.$^2$. Moreover, this strength should be almost independent of temperature. The experimental adhesive strength at 268°K. was found in the present work to be about 6 kg./cm.$^2$. In a previous paper (1), the present author accounted for this discrepancy by the assumption of imperfections randomly distributed in the ice; these imperfections were assumed to have a definite strength distribution. It was found that the tensile strength increases very rapidly as the height of the ice disks decreases. Two theoretical cases can be distinguished. First: as soon as the strength of the weakest imperfection of the specimen is reached, rupture of the specimen takes place. For such a case, the average tensile strength should be a function of the volume of the specimens only. Second, when the strength of the weakest imperfection in the specimen is reached, a crack of definite average length is produced, then the next weakest imperfection opens up until in cascade fashion the specimen is ruptured. In this second case, the average tensile strength will depend not only on the volume but also on the cross-sectional area.

Similar assumptions can be made in the case of adhesion. If adhesive rupture takes place when the strength of the weakest imperfection is reached, the adhesive strength—using a Weibull distribution (1)—is given by

$$S_A = k_1 A^{-1/\beta} + C \qquad [4]$$

where $S_A$ is the average adhesive strength, $\beta$, $k_1$, and $C$ are constants, and $A$ is the cross-sectional area of the specimen. In the second case, where rupture takes place in cascade fashion (for derivations, see references 1 and 5), the adhesive strength is independent of cross-sectional area, in agreement with the experimental results.

Although the assumption of imperfections in or near the interface explains the low experimental adhesive strength as compared with the theoretically expected one, it fails completely to account for the marked difference found in the behavior of the ice disks in tension and in shear. If the ice is assumed to adhere directly to the stainless steel, there is no apparent reason at all why the adhesive bond should be so small in the case of shear and so large in tension. The adhesive strength at −5°C. was about 6 kg./cm.$^2$ in shear; in tension, if the ice disk was thin enough, 70 kg./cm.$^2$ could be applied without obtaining an adhesive break, and there is no reason why a larger stress could not be applied if the disk could be made still thinner. As a matter of fact, the bulk tensile strength of snow-ice is of similar magnitude as the bulk shear strength and also as that of the torsional shear strength (8), and they are only slightly dependent on the temperature. The large temperature dependence of the adhesive strength is indicative rather of a viscous process in a liquid than of shear strength of polycrystalline solids.

This contradictory behavior under shear and tension can, however, be reconciled if the assumption is made that a liquidlike layer, an amorphous layer, with properties somewhere intermediate between ice and water is situated in the interface.

The suggestion that a liquidlike layer exists on ice in the neighborhood of the melting point is not new. Faraday (9) suggested such a theory in 1859 to explain the phenomenon of regelation. Tyndall (10) supported Faraday's idea (see also Dorsey (11)), but J. Thomson (12) and W. Thomson (Lord Kelvin) (13) argued against it and put forward the idea of pressure melting. However, very large pressures are needed to depress the melting point of ice (e.g., under 590 atm. the melting point of ice is −5°C.), and this theory does not seem to be tenable. In this connection, Bowden's and Tabor's (14) discussion of a liquid layer on ice produced by friction is of interest (see also Bowden (15)). More recently, Weyl (16) assumed a liquidlike layer on ice for energetic reasons. Nakaya and Matsumoto (17) carried out experiments on the cohesion of ice spheres and found quite frequently that the spheres rotated before separating, which is a good indication of liquid layers on the ice spheres. Similar experiments in a more quantitative way were carried out by Jensen (18) supporting the conclusions of the Japanese workers. Hori (19) performed interesting experiments on the freezing and evaporation of thin water films. Observations indicated, though not with certainty, that very thin supercooled water films (ca. 1 $\mu$ thick) did not crystallize even when seeded.

On the basis of these observations, it is not unreasonable to assume that ice has a liquidlike layer on its surface not only when in contact with air but also when it is in contact with other substances, such as steel and polymers. The properties of such a film would be influenced by the nature of the solid surface. Thus, it is not to be expected that the liquidlike layer is of the same consistency and thickness when in contact with metal as when in contact with various polymers.

The consequence for shear and tensile experiments of assuming a liquidlike layer in the interface will now be considered. Such a discussion must be semiquantitative at best, as practically nothing is known quantitatively of the viscosity, thickness, and other properties of such films. In the case of shear, the liquidlike layer will be assumed to be a Newtonian liquid as a first approximation. For a film between two parallel plates of which one is stationary and the other moves with a velocity $v_t$ at time $t$, a relationship is valid as follows:

$$\sigma_t = \frac{\eta v_t}{L}, \qquad [5]$$

where $\sigma_t$ is the shear stress at time $t$; $\eta$ the effective viscosity coefficient and $L$ the thickness of the liquidlike layer; and $v_t$ the velocity of the metal plate at time $t$. As the adhesive strength was found to be independent of the cross-sectional area, boundary effects do not seem to be important. In Eq. [5] $\eta$, $L$, and $v_t$ are not known experimentally; only the breaking stress and total deformation velocity are known; the latter is given by the movement of the threaded steel rod. In the present instance, the total deformation rate was always $9 \times 10^{-3}$ cm./sec. However, this total deformation velocity is shared between the test sample and the chain connecting the sample to the load cell. It was shown in a previous paper (1) that practically all the deformation takes place in the chain. Thus, the system can be considered to be composed of a dashpot and spring in series (Maxwell unit), whose total rate of deformation is constant; hence

$$c = \frac{F_t L}{\eta \pi R^2} + \frac{l_2}{E} \frac{dF_t}{dt}, \qquad [6]$$

where $c$ is the constant total deformation rate; $F_t$ is the load at time $t$, $\eta$ the viscosity coefficient and $L$ the thickness of the liquidlike layer; $l_2$ the length and $E$ Young's modulus of the chain and $R$ the radius of the specimen. Equation [6] can be written as:

$$\frac{dF_t}{dt} = \frac{E}{l_2}\left(c - \frac{F_t L}{\eta \pi R^2}\right). \qquad [7]$$

Actually, the rate of stress application was found to be nearly constant. This means that the second term in the parentheses of Eq. [7] should be small compared with the first one. An upper limit of $L/\eta$ can thus be estimated. At $-5$°C., for instance, the adhesive strength for ice/steel was found to be 5.5 kg./cm.$^2$ = $5.5 \times 10^6$ dynes/cm.$^2$ and $c = 9 \times 10^{-3}$ cm./sec.; hence

$$\frac{F_t\, L}{\eta \pi R^2} = \frac{\sigma_t\, L}{\eta} = v_t \qquad [8]$$

should not be larger than about $1 \times 10^{-3}$ cm./sec. This gives:

$$L/\eta = 1.8 \times 10^{-10} \text{ cm.}^3/\text{dyne-sec.}$$

According to Weyl (16) the liquidlike layer should be several hundred molecules thick. If one puts $L = 10^{-6}$ cm., then $\eta = 5 \times 10^3$ poises. Such a viscosity coefficient can be considered an effective viscosity only over the whole layer and will be appreciably influenced by surface irregularities of the confining solids. It may be remarked that the viscosity of supercooled water at $-5$°C. is $2.1 \times 10^{-2}$ poise and that of crystalline ice is about $10^{14}$ poises (4).

The large difference in the adhesive strength for the tensile and shear experiments can now be accounted for readily by assuming a liquidlike layer between the ice and the stainless steel plates. Surface tension forces will be considered first. The situation is shown in Fig. 4. The two solid phases are bound together by surface tension forces. In the present case the contact angles between ice, steel, and the liquidlike layer are assumed to be zero[2] and the pressure difference $\Delta p$ is given by $\Delta p = 2\gamma/L$, where $\gamma$ is the surface tension of the liquid and $L$ the layer thickness. An upper estimate of the thickness of $L$ can be obtained easily. It was found previously (1), when the cohesive strength of ice was investigated as a function of ice thickness, that the thinnest ice specimen, $2.5 \times 10^{-2}$ cm. thick, showed a purely cohesive break with strength of 70 kg./cm.$^2$ at $-5$°C. Hence, the adhesive strength under tension must be at least 70 kg./cm.$^2$, probably appreciably higher. Taking $\Delta p = 7 \times 10^7$ dynes/cm.$^2$ and $\gamma = 76.4$ dynes/cm., which is the surface tension of water at $-5$°C., one obtains an upper estimate for $L$ of $2 \times 10^{-6}$ cm. Hence, an ice cylinder of several millimeters height as used in these experiments will break in cohesion long before the surface tension forces are overcome.

Even if the surface tension forces were small, the viscosity would play

---

[2] In a recent paper by L. E. Raraty and D. Tabor [*Proc. Roy. Soc.* (*London*) **A245**, 184 (1958)] it is stated that electrolytically degreased stainless steel has a zero contact angle, whereas stainless steel refluxed in benzene has an advancing contact angle of 55° and a receding angle of 30°, which would reduce $\Delta p$ by half if the ice/liquid and steel/liquid contact angles are both taken as 60° (cos 60° = ½).

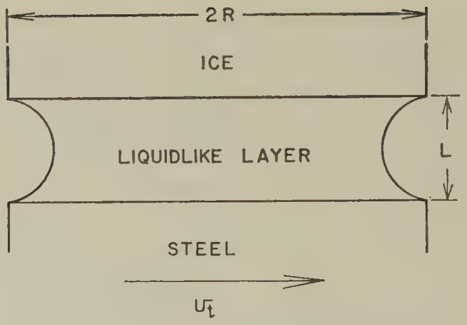

FIG. 4. Liquidlike layer between ice and solid material.

an important role when the two plates are pulled apart over time intervals of 10 to 20 seconds. The force $F_t$ holding the plates together, assuming the liquid to be Newtonian, is given by (20)

$$F_t = \frac{3\eta\pi R^4}{8tL^2}$$

where $\eta$ is the viscosity, $L$ the thickness of the liquidlike layer, $t$ the time of complete separation of the plates, and $R$ the initial radius of the liquid specimen. For $\eta = 5 \times 10^3$ poises, $L = 10^{-6}$ cm., $t = 10$ to 20 sec., the ice will break in cohesion long before the separation of the plates is effected.

The experimental results obtained with polystyrene and polymethylmethacrylate can also be accounted for on the basis of a liquidlike layer in the interface. In the case of the shear experiments with polystyrene, an adhesive strength of about 0.13 kg./cm.$^2$ was found at $-5$°C. Again using $v_t = 1 \times 10^{-3}$ cm./sec., the ratio $L/\eta$ becomes $7.7 \times 10^{-9}$ cm.$^3$/dyne-sec. Taking again $\eta = 5 \times 10^3$ poises, which is probably not permissible, $L$ becomes $3.9 \times 10^{-5}$ cm. The case of tension is more complicated because of the finite contact angle.

Though only a qualitative picture of the processes involved has been given here, it is believed that the assumption of a liquidlike layer is necessary for an understanding of the experimental results.

## ACKNOWLEDGMENTS

It is the author's pleasure to thank Mr. G. M. Walker and Mr. R. D. Setzer for the competent performance of the tensile and shear experiments, respectively. He also thanks Dr. J. K. Landauer for helpful discussions, Mr. B. L. Hansen for advice in the construction of the apparatus, and Dr. H. Bader and Mr. J. A. Bender for their interest in this work.

## SUMMARY

An apparatus has been constructed for the investigation of the adhesive strength of ice by shear experiments.

For the system snow-ice/stainless steel, shear experiments yielded pure adhesive breaks down to a temperature of about −13°C., where a sharp transition to cohesive breaks took place. The adhesive strength for this system is a linear function of the temperature, and is independent of the cross-sectional area and height of specimens in the ranges investigated.

The system ice/polystyrene gave pure adhesive breaks on shear. The adhesive strength was found to be a linear function of temperature down to a temperature of −15°C. and independent of cross-sectional area.

Tensile experiments on the system ice/polystyrene yielded a linear relationship between adhesive strength and temperature in a range from −2 to −25.5°C. Cross-sectional area and rate of stress application had no effect on the adhesive strength in the ranges investigated.

The system ice/polymethylmethacrylate showed a larger adhesive strength than the system ice/polystyrene.

The experimental results are explained by the assumption of a liquidlike layer between ice and the solid interface. The thickness and consistency of this liquidlike layer are a function of temperature and the nature of the solid interface. The surface tension forces and frictional forces operative in the liquidlike layer are discussed.

## REFERENCES

1. JELLINEK, H. H. G., U. S. Army Snow Ice and Permafrost Research Establishment, Corps of Engineers, Research Report 23; also JELLINEK, H. H. G., *Proc. Phys. Soc. (London)* **71,** 797 (1958).
2. BERGHAUSEN, P. E., GOOD, R. J., KRAUS, G., PODOLSKY, B., AND SOLLER, W., WADC Technical Report 53-461, (1953) and WADC Technical Report 55-44, (1955).
3. CZYSAK, S. J., *in* "Adhesion and Adhesives, Fundamentals and Practice, Society of Chemical Industry," p. 16. Wiley, New York, 1954.
4. JELLINEK, H. H. G., AND BRILL, R., *J. Appl. Phys.* **27,** 1198 (1956).
5. JELLINEK, H. H. G., U. S. Army Snow Ice and Permafrost Research Establishment, Corps of Engineers, Research Report 38 (1957).
6. JELLINEK, H. H. G., U. S. Army Snow Ice and Permafrost Research Establishment, Corps of Engineers, Research Report 36 (1957).
7. HUNSAKER, J. C., KEYES, F. G., HOUGHTON, H. G., JOHNSON, C. A., AND DOTSON, J. V., Progress Report to National Academy of Sciences, M.I.T., Report No. 1 (1940).
8. BUTKOVICH, T. R., U. S. Army Snow Ice and Permafrost Research Establishment, Corps of Engineers, Research Paper 11 (1954).
9. FARADAY, M., *Phil. Mag.* [4] **17,** 162 (1859); also *Proc. Roy. Soc. (London)* **10,** 440 (1860).
10. TYNDALL, J., *Proc. Roy. Soc. (London)* **A9,** 141 (1858).
11. DORSEY, N. E., Properties of Ordinary Water Substance, p. 412. Reinhold, New York, 1926.
12. THOMSON, J., *Proc. Roy. Soc. (London)* **A10,** 152 (1859); *ibid.* **A11,** 198, 473 (1861).
13. THOMSON, W., *Proc. Roy. Soc. (London)* **A9,** 761 (1858).
14. BOWDEN, F. P., AND TABOR, D., "The Friction and Lubrication of Solids," p. 65 and Chapter 15. Oxford University Press, New York, 1950.

15. Bowden, F. P., *Endeavour,* January, 1957, p. 5.
16. Weyl, W. A., *J. Colloid Sci.* **6,** 389 (1951).
17. Nakaya, U., and Matsumoto, U. S. Army Snow Ice and Permafrost Research Establishment, Corps of Engineers, Research Paper 4.
18. Jensen, D. C., On the Cohesion of Ice, M. S. thesis, Pennsylvania State University.
19. Hori, T., Teion Kazaku, Butsuri Hen (Low Temperature Science Laboratory), Ser. A, **15,** 34 (1956); SIPRE Translation 62.
20. DeBruyne, N. A., and Houwink, R., "Adhesion and Adhesives," p. 66. Elsevier, Amsterdam, 1951.

JOURNAL OF COLLOID SCIENCE 14, 281–286 (1959)

# MULTIMOLECULAR FILMS OF TRIIODOSTEARIC ACID[1]

**Harry Sobotka, Margaret Demeny, and Margarita Arnaki**

*Department of Chemistry, Mount Sinai Hospital, New York, New York*

*Received February 17, 1959*

## ABSTRACT

The study of thin films floating on a liquid hypophase ("H-layer") has emphasized the properties of unimolecular layers. The important force/area curves have been studied in detail at low lateral pressures in the so-called gaseous, highly compressible state and in the condensed state at higher pressures. Beyond this range collapse was observed and most investigators were satisfied with recording the visual observation of crumpling. During the years a few observations have been collected which suggest the formation of homogeneous polymolecular layers, "situated" in the upper left corner of the conventional force/area diagram.

The present report treats, as an example of this observation, the behavior of triiodostearic acid, which appears to change from the unimolecular to the trimolecular state. The analogy to a few other cases is discussed.

## INTRODUCTION

In previous studies we have compared the behavior of terminally branched stearic acids with that of the normal isomer (1). The shape of long-chain fatty acids that carry methyl groups in the middle of the chain and also of the addition products of chlorine to oleic acid (2) seems to prevent the formation of H-films or renders it at least precarious. On the other hand, a cyclopropene ring inserted in the middle of an aliphatic chain as found in sterculic acid (3) or a cyclopropane ring in an analogous acid from *Lactobacillus arabinosus* (4), in other words, an extra methylene bridge between $C_9$ and $C_{10}$ offers no obstacle to film formation.

In triiodostearic acid the iodine atoms certainly produce considerable bulges in the chain, but their arrangement is sufficiently symmetrical to permit the formation of films on an aqueous hypophase and even their building up on slides during alternating down and up trips. Combining the observations of force/area curves and thickness measurements on built-up films shows that triiodostearic acid may form "soft" condensed unimolecular films at lower pressure and multimolecular films of low compressibility under higher lateral pressure. The latter do not re-expand when the pressure

---

[1] Supported by U. S. Public Health Service Grants C-1791 and RG-4736. Part of the material of this paper has been reported to the Division of Colloid Chemistry at the 132nd Meeting of the American Chemical Society, September 1958, in Chicago.

is released, but they are of homogeneous structure and optically clear on building up.

## EXPERIMENTAL

*Preparation of 10,13,16-triiodostearic acid* (*5*). One part of freshly prepared linolenic acid (6) was dissolved in one part (by weight) of glacial acetic acid, mixed with a concentrated solution of HI (about 20% HI) in glacial acetic acid and stirred for 48 hours under a stream of nitrogen and occasional heating up to 60°–70°C. The hydriodic acid in glacial acetic acid was prepared by mixing carefully 78 g. of acetic anhydride with 29.7 g. of 57% aqueous HI for 2 hours and letting it stand over night until all the acetic anhydride had disappeared (7).

The triiodostearic acid was precipitated in form of its sodium salt by addition of cold petroleum ether (b.p. 66°–75°C.) and 10 *N* sodium hydroxide. From an alcoholic solution of this crude sodium triiodostearate the free acid was obtained by treatment with 60% of sulfuric acid and extraction with ether. Density = 1.5735; refractive index = 1.5455.

*Force/area diagrams.* Triiodostearic acid was dissolved to form a $10^{-3}$ *M* solution (66 mg./100 ml.) in benzene. This solution was used for spreading by placing about 0.3 ml. on the hypophase, which consisted of an aqueous solution of $8.10^{-4}$ *M* $KHCO_3$ and $1.10^{-4}$ barium acetate; the pH was 8.2. Figure 1 illustrates the force/area curves obtained at various temperatures on a Cenco Hydrophil balance; the measurements at 4°C. and 37°C. were carried out in constant-temperature rooms.

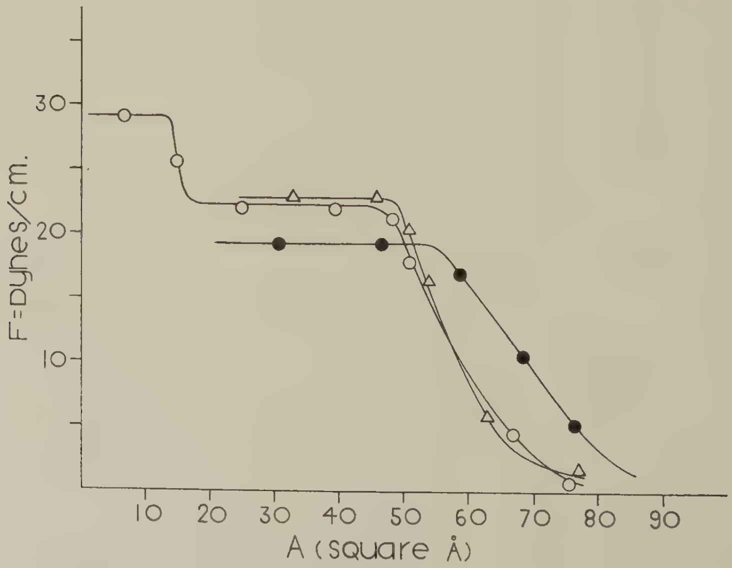

FIG. 1. Force/area curves of triiodostearic acid at 4°C., △; 22°C., ○; 37°C., ●.

Under pressures from 1 to 21 dynes/cm. at temperatures of 4° and 22°C. the molecular area decreases continuously from 80 to 50 sq. A. At 37°C. a parallel curve is found in the range up to 19 dynes/cm. At this limit the film becomes highly compressible and will contract to 20 A. without increase of pressure. Whereas this would indicate collapse, no crumpling occurs and the contracted film behaves quite stable in the building-up operation. The pressure may now be raised a few more dynes until collapse sets in between 29 and 30 dynes/cm.

*Built-up films.* Building up on metallized glass slides was carried out in a plastic tray of dimensions 21 by 45 cm. The thickness of the layers was measured with an ellipsometer of O. C. Rudolph, equipped with a photoelectric attachment. Building up at room temperature under 16 dynes/cm. (castor oil) or 19 dynes/cm. (neat's-foot oil) pressure gives a thickness of 30 A. for an AB-film, i.e., of 15 A. per molecular layer, from which the slant of the chain can be calculated to be 53°.

Under 29 dynes/cm. (oleic acid) the strongly contracted film builds up to form double films of about 150 A. thickness, a figure twice the threefold length of an upright 18-carbon chain. As a less likely alternative one may conjecture that the thickness of 75 A. per single layer results from a combination of, for example, 5 times 15 A. of slanted molecules instead of 3 times 25.

Transition pressure is not sharply defined. At 19 dynes/cm. pressure a fresh film will build up with a thickness of 15 A., whereas after about 15 minutes the film will have contracted and yield the higher figure of 75 A. A similar phenomenon of hysteresis may be observed under the pressure of oleic acid. Here the collapse point is approached and only freshly spread films may be built up.

## Discussion

The spreading of unimolecular layers and their behavior in the building-up operation forms a pattern which is fairly well understood. The factor, common to the great variety of compounds that undergo spreading, is the combination within a molecule of a hydrophobic and a hydrophilic portion, the latter usually comprising a positive or negative ionizable group. There are spreadable compounds of more involved structure, which carry several functional groups at various sites. In some instances such additional groups influence the arrangement of molecular films to a considerable degree.

In the simple case of monofunctional compounds it is known that compressibility is reduced to a minimum, but the pressure, capable of producing collapse, varies a great deal depending on the nature of the compound. In general, the larger the van der Waals' forces and their share in the force which holds the molecules together, the higher the collapse pressure. What happens when a film collapses? An interesting contribution to this topic is made by Ries and Kimball (8). They selected *n*-hexatriakontanoic acid because of the large van der Waals' forces and the correspondingly high collapse pressure, and also because of the fact that the thickness of its molecular layers is as high as 50 A., which lends itself to electron-microscopical observation. This acid was spread in doubly distilled benzene on deionized water on a modified Cenco film balance. The film was then deposited upon a collodium-covered standard 200-mesh screen, either by lifting through the monolayer or by building up as a B-film according to Blodgett and Langmuir, on the upward motion under constant lateral pressure. One had originally believed that monolayers were homogeneous at all stages of compression. Observations under the dark field ultra-microscope and surface potential measurements suggested heterogeneity at low pressures and again in the region of collapse. The electron microscope permits studies of such details on a minute scale. At medium pressures, about 15 dynes/cm., the expanded hexatriakontanoic acid film has begun to consolidate in crystalline islands; at higher pressures this phase becomes confluent and at 40 dynes/cm. the lacunas in the contiguous film have disappeared. Up to this point the thickness of the film, as measured by the shadow at its boundaries, is 50 A., corresponding to the length of the molecule. When the collapse pressure of *ca.* 57 dynes/cm. is reached, one observes the formation of tiny blisters or bulges, often in linear alignment. Eventually, ridges form and, by breaking and tumbling back on the monolayer, elongated folds are observed. These long flat structures, say 0.1 $\mu$ wide, are about 100 A. or two molecules thicker than the monolayer itself.

When an extremely dilute solution of hexatriakontanoic acid is brought directly on the screen in quantities smaller than needed for a closely packed monolayer, platelets of *ca.* 100 A., i.e., two molecules thickness, are obtained. This indicates the strong cohesion of the long aliphatic chains with strong attraction between the polar groups forming micellas polar face to polar face; these dimeric structures may be important for folding, previous to collapse, and also for the great facility with which alternating monolayers are built up by the Blodgett-Langmuir techniques.

Polyfunctional structure may be responsible for observations (Sobotka, 9) that porphyrins under 30 dynes/cm. on water form films 30–36 A. thick, which is twice the longest extension of the porphyrin molecules. The multipolar structure of the various porphyrin derivatives, so tested, makes it plausible that they form bimolecular sheets under high pressures with the molecules standing on edge. The building-up technique then leads to quadruple films.

Other observations (Sobotka and Rosenberg, 10), which call for the assumption of dimolecular films on water, have been made with the heptadecylsemicarbazone of cyclohexanone (11) with apparent molecular cross section of 11 A.$^2$ under 30 dynes/cm. This phenomenon was explained by twinning under the influence of hydrogen bonds; it is absent in the 4-heptadecyl-2-methylsemicarbazone of cyclohexanone (11).

Another analogous situation has been described by Ekwall and Ekholm (12) for lithocholic acid, a bile acid carrying polar groups, 1 carboxyl and 1 hydroxyl, at the extremities of its molecule. Its force/area curve reaches with increasing pressure a plateau at about 80 A.$^2$/molecule, which corresponds approximately to the smallest area compatible with dense packing of the molecules that would have both hydrophilic groups still in contact with the hypophase. From here on, instead of collapsing the film may be compressed. At an area of 29 A.$^2$/molecule, the pressure again begins to rise to reach a sharp break at 24 A.$^2$/molecule, resembling a collapse point. Since exchange with the saturated hypophase may be excluded, this value is little more than one-half of the smallest cross section of the molecule, *ca.* 44 A.$^2$, but it is in good agreement with the concept that the lithocholic acid molecules form a triple layer with the molecules in each of the monolayers being oriented in such a manner that they are standing on edge; the lowest layer dips its two hydrophilic groups into the hypophase, the upper two layers have their polar groups adjacent to one another, and the stability of this grouping is enforced by hydrogen bonds.

In the present case of triiodoacetic acid we believe that the formation of a triple film on water is favored by the strongly electronegative character of the iodine atoms in the upper part of the chain, sufficient to produce a macrohomogeneous film consisting of three monomolecular layers in the order ABA similar to the picture of the collapsed 36-carbon film. On building up, this would lead to a double film consisting of 6 monolayers, starting from the metal plate in the order ABA.BAB.

To sum up, molecules, in which the contribution of the main polar group to the cohesive forces is supplemented by strong van der Waals' forces or by competing electrostatic forces of functional groups such as halogen substituents or side chains in suitable positions, form monolayers more resistant to pressure; on higher pressure, where simpler films collapse, they form double or triple layers. These may be built up to what may be called "polymolecular films of the second order"; they collapse at much higher lateral pressures. Such essentially dimeric structures may pre-exist in solutions of nonpolar solvents and give rise to micellae formation; one may keep an eye on similar dimerizations in aqueous solution, e.g., the pH-dependent association of hemocyanin and of hemoglobin. Such phenomena may be of biological significance, when one considers hypotheses of growth, which postulate the formation of a protein molecule by duplication of an existing protein molecule as a template (*cf.* 13).

## REFERENCES

1. SOBOTKA, H., ROSENBERG, SH., AND BIRNBAUM, A., *J. Colloid Sci.* **5**, 567 (1950).
2. LANGMUIR, I., private communication.

3. Nunn, J. R., *J. Chem. Soc.* **1952,** 313.
4. Hoffmann, K., and Lucas, R. A., *J. Am. Chem. Soc.* **72,** 4329 (1950).
5. Erdmann, E., *Friedlaender's Fortsch. Teerfarbenfabrikation* **10,** 1128 (1911).
6. *Org. Syntheses* **22,** 82 (1942).
7. Pfister, K., private communication.
8. Ries, H. E., and Kimball, W. A., *Proc. 2nd. Intern. Congr. Surface Activity, London,* **I,** 75 (1957); *cf. Nature* **181,** 901 (1958).
9. Sobotka, H., *in* F. R. Moulton, ed., "Recent Advances in Surface Chemistry," p. 54. Science Press, 1939.
10. Sobotka, H., and Rosenberg, Sh., in H. Sobotka, ed., "Monomolecular Layers," p. 175, esp. 184. American Association for the Advancement of Science, Washington, 1954.
11. Chanley, J. D., Kalichstein, St., and Gindler, M. E., *J. Am. Chem. Soc.* **75,** 5113 (1953).
12. Ekwall, P., and Ekholm, R., *Proc. 2nd. Intern. Congr. Surface Activity, London,* **I,** 23 (1957).
13. Finean, J. B., *Experientia* **9,** 17 (1953).

JOURNAL OF COLLOID SCIENCE **14**, 287–299 (1959)

# THE SPLITTING OF THIN LIQUID FILMS. KINEMATICS[1]

**Raymond R. Myers, John C. Miller,[2] and A. C. Zettlemoyer**

*Lehigh University, Bethlehem, Pa.*

*Received November 5, 1958*

## ABSTRACT

The kinematics of film splitting have been explored inside a role nip using a disc and cone apparatus especially developed for the purpose. High-speed photographs and cinematographs have been made of the action in the nip.

Two regimes of flow have been discerned. At slow speeds, fluids have time to flow counter to the roll direction into the region of low pressure where separation begins. At high speeds, cavitation or bubble formation occurs in the low-pressure region. The number of bubbles formed has been counted as a function of speed, nip pressure, and film thickness: they increase with increases in the first and third of these variables, and decrease slightly with increase in the second. Pigmentation increases the number of bubbles formed. These cavitation studies have shed light on the mechanisms of film splitting and fluid transfer.

## INTRODUCTION

The splitting of liquid films is vitally important in lubrication, adhesion, and the application of coatings, paints, and printing inks. Nevertheless, little has been done to elucidate the exact mechanism of splitting. The first significant theoretical work was done by O. Reynolds (1) in 1886; yet the first high-speed pictures of splitting were just recently reported by Sjodahl (2) in 1949. These pictures of the filaments which form at the exit of a roller nip system in high-speed splitting showed the behavior only after most of the splitting action had taken place. Banks and Mill (3) had looked into the roll nip between glass rolls entirely immersed in liquid, but no previous examination has been made of behavior inside the nip when a thin film splits between separating surfaces.

The splitting of thin liquid films involves an elusive quality of stickiness or adhesiveness which may or may not be a unique physical property of the material being split. Tack, tackiness, and tacky adhesion are the terms usually used by craftsmen to describe this property. "Tack" is most commonly used and is adopted here to mean only the cohesive properties of the film as contrasted with its adhesive properties.

---

[1] Based on a portion of the Ph.D. dissertation of J. C. M. presented to Lehigh University, October 1956.

[2] Sinclair Fellow, Printing Ink Research Institute; present address, The Bakelite Company, Bound Brook, New Jersey.

Tack may be defined qualitatively as the resistance to rapid splitting of a thin liquid film (4), but a quantitative definition is considerably more complex and difficult to develop. Few attempts have been made toward this end (1, 5). The first step in arriving at a quantitative expression for the splitting of films is the development of a rheological equation of state. Therefore, the ultimate objective of the work is to establish a fundamental relation between tack and certain physical properties of the material. The complex flow pattern caused by shear normal to the confining surfaces must be defined before any attempts can be made to describe the forces; consequently, the present study is confined to the kinematic aspects of film splitting. The primary aim thus became one of obtaining a photographic record of the liquid at the instant of rupture.

In the separation of parallel plates, the beginning conditions of the experiment are static and are defined by the area of the plates and clearance between them. Although film splitting on a roller system is a simpler situation kinematically because of the controlled separating conditions, the incipient split is not static and, consequently, is more complex. This complexity is the result of the flow which occurs up to the rupture point which gives rise to shearing before splitting begins.

In the dynamic situation encountered in roller systems, the question arises as to whether true contact is attained during the time that the material is being compressed on its way through the nip (6). In this initial study, the reasonable assumption has been made that the force on the roller and its pre-wet condition are adequate to establish intimate contact.

Figure 1 is a description of the flow and pressure profiles under conditions which exist for a moving plate and rotating roller. The pressure peak is skewed toward the side at which the surfaces approach each other. Maximum pressure is reached at a plane of no shear (discussed later), to

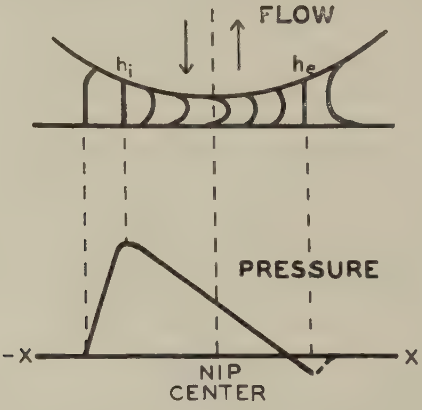

FIG. 1. Flow and pressure profile of rotating roller and plate.

the left of which is a liquid bank, and to the right of which the pressure profile is bowed into nearly parabolic envelopes the curvature of which rises to a maximum at the nip center, then drops to zero near the exit, indicating a second plane of no shear. The pressure also reaches a minimum at this point.

Cavitation occurs near the exit, that is, near the plane of no shear. Although usual hydrodynamic theory does not apply in the cavitation region, one can state that the pressure reaches some negative value in order for the liquid to fracture.

### *Photographic Studies of Splitting Films on Roller Systems*

Until the development of methods of time magnification by short-duration flashes and high-speed motion pictures, little photographic work had been done on the kinematics of rapidly splitting films. Sjodahl (2) obtained microsecond exposures of splitting films from outside a roller system, and established that filaments of liquid attached to both rollers were present and that rupture of the filaments of liquid attached to both rollers constituted final splitting. Later, high-speed motion pictures were obtained by the Interchemical Corporation Laboratories (7). Sjodahl (2) and Banks and Mill (3) suggested that cavitation occurred during the separation in air and that the cavitation provided an upper limit to the force or work required to separate the film.

In a remarkably accurate conjecture, Blockhuis (8) described the probable sequence of action of the film splitting as cavitation, bubble expansion, and finally elongation and rupture of the filaments. It was known that the patterns left by the rapid separation of parallel plates (9) are not smooth but have jagged valleys and peaks, with the peaks all connected like a range of mountains with small ridges branching off the main range.

The requirements of an instrument to investigate the origin of film splitting are simple. First, one of the surfaces must be transparent in order to observe the action when the split is just beginning; second, a method must be devised to observe the phenomenon; and finally, more fruitful results are to be expected from observation of the splitting in a steady-state condition. Although the parallel plate separation fits the first two requirements well, a roller system appears to be the only apparatus which will satisfy the third requirement. Furthermore, the pressure and flow pattern in a roll nip are quite different from those in parallel plate separation.

## METHODS AND MATERIALS

### *Discone Apparatus and Procedures*

The modified roller system designed from the requirements set forth above is shown schematically in Fig. 2. One of the "rollers" is a circular glass disc $A$; the other is a steel cone $B$ the largest diameter of which is

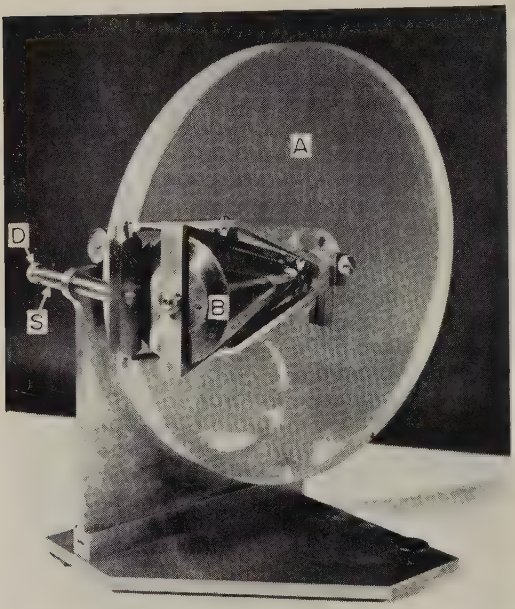

FIG. 2. Film splitting apparatus "the discone"

one-fourth the diameter of the disc. The disc rotates on its axis; the cone rotates with its apex at the center of rotation of the disc and with its lateral surface in contact with the disc to give an area of observation of the nip which is motionless with respect to an external observer. The interior of the nip is observed through an eight-to-twenty-power microscope.

To distribute a liquid film on the cone and disc, a volume of liquid from a pipet is spread on the plate, a portion on each of the quadrants. The drive to the plate is engaged and the roller system run until the film appears to be evenly spread over the cone and disc. After distribution of the film, the motor is halted and the microscope focused on the cone surface and adjusted so that the liquid film contact area in the roller nip is in the center of the photograph. The desired force was applied by tightening screw *D* on the spring *S* shown in Fig. 2.

Operation of the "discone" for the present studies consisted of matching the tangential velocities of the cone and disc at the desired velocity and then taking three or more photographs under each experimental condition. All photographs for a given film thickness were taken on the same area of the glass disc to minimize the effect of surface variations of the disc (as much as 0.005 in.). A mirror reflex 35 mm. Alpa Alnea Model 4 camera with a focal plane shutter was used.

To record the observations and to obtain a more detailed view of the splitting action, the low-power microscope was focused on the nip through the glass disc. The short exposures necessary to stop the motion were obtained by a 2-microsecond flash provided by discharging 40,000 volts across a gas-filled tube. The microflash unit was built by the Interchemical Corporation.

The camera, microscope, microflash, and discone were assembled so as to provide an intense beam reflected from the cone surface. The microflash was electrically connected to the camera shutter to synchronize the opening of the shutter and the flash. The film was Eastman Kodak Tri X with an ASA rating of 160 tungsten, 200 daylight. Most of the individual 35-mm. negatives were projected onto a screen at 40 to 60 magnification; some were enlarged and printed.

The high-speed motion pictures were taken with a Fastax high-speed camera at 2000 frames/sec. in the Bell Laboratories in New York.

### *Materials*

Two liquids were studied in the course of the experiments. Table I lists their molecular weight, the viscosity, and density.

Two dispersions were prepared to study the catalytic effect of a dispersed solid phase. Calcium carbonate, surface area of 16.2 m.$^2$/g. and particle size $0.13 + 0.08\ \mu$ (11), was coated with stearic acid from alcohol solution. After washing in benzene and drying, the surface was characterized as 90% hydrophobic by water adsorption at 79% relative humidity. The coated and uncoated calcium carbonate were dispersed in linseed oil and polybutene, respectively, at 2% by volume to produce two dispersions with widely different interfacial adhesions. Final mixing was done on a three-roll mill by passing the dispersion over the mill three times with a loose roller setting. The relative viscosity of both dispersions was 1.1.

## RESULTS OF OBSERVATIONS ON SIMPLE LIQUIDS

Two observations at tangential velocities low enough to permit visual observation through the microscope were found useful for interpretation at higher velocities where only the camera could stop the action. Three

TABLE I

*Physical Properties of the Liquids*

| | Molecular weight Avg. | Viscosity at 25°C. | Density at 25°C. |
|---|---|---|---|
| Indoil Polybutene H-100 | 780 | 220 | 0.88 |
| Superior varnish linseed oil | ca. 880 | 165 | 0.95 |

Viscosities were measured in a Sun Rotational Viscometer (10).

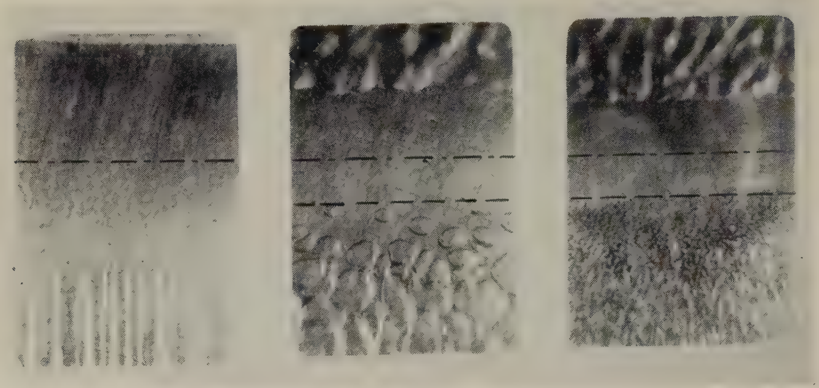

FIG. 3. Typical discone pattern.

typical patterns are shown in Fig. 3. In each of these exposures three regions are identifiable: the bank (top), the nip or contact area, and the cavitation and filamentation region. The scratches are the polishing marks left on the cone. The low shear velocity was 0.2 cm./sec.; moderate, 15 cm./sec.; and high, 31 cm./sec. What appear to be streamers at the edges of the arches at the bottom of the low-shear picture are webs of liquid perpendicular to the roller surface.

At the two higher velocities, a new phenomenon appears in the form of roughly circular discontinuities in the contact region which had been clear at lower tangential velocities. At moderate shear the discontinuities are elliptical and appear to touch one or both of the roller surfaces. At high shear a large increase in the number of discontinuities can be seen, and further, they appear as almost perfect circles. These discontinuities are the cavities postulated earlier (2, 3, 8). It can be seen that the cavities are rather large when first observed; therefore, their first growth is extremely rapid.

The interpretation of the photographs with respect to identifying the major features is best performed using the following picture of flow through a roller nip. As a model, an area of the liquid film perpendicular to the roller surface of length $l$ and width $2h$, equal to the film thickness on the roller system will be adopted, as shown in Fig. 4. An equivalent area (or plane of no shear) occurs on the downstream side of the nip.

The total thickness of the films from both rollers is equal to the clearance $2h$. At the plane corresponding to this clearance, pressure is built up to its highest value by the presence of a bank of liquid at clearances greater than $2h$. As the liquid moves through the nip, the clearance decreases and forces the liquid area of the model to bow forward at the center and assume a parabolic configuration, thereby producing a velocity gradient. The velocity

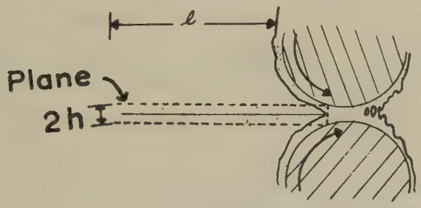

FIG. 4. Plane of no shear and maximum pressure.

gradient is a maximum at the minimum clearance and decreases as the surfaces begin to separate. At a plane as distant from the minimum clearance as the high-pressure plane on the other side, the velocity profile becomes flat again, indicating no shear. After passing this second plane of no shear, the fluid either cavitates or flows into the arches shown in Fig. 5. If the velocity is sufficiently high to produce cavitation, then the bubbles expand as they move toward the exit. Coalescence of the bubbles leaves attached to both rollers tiny filaments which are elongated by the increasing separation until the stresses become high enough to cause rupture. The film separation is then complete.

The high-speed motion pictures obtained at 2000 frames/sec. verified and amplified the sequence of action described above. The additional observation at velocities low enough to have well-defined arches coexisting with bubbles is that the arches penetrate explosively into the bubble as the bubble approaches the interface; this motion is opposite to the direction of roller movement. Since the pressure of the air on the external side of the interface is atmospheric, the push of the arch back onto the bubbles indicates that the bubble pressure is significantly lower than atmospheric.

At low velocities the flow between the separating members is purely viscous. The arches and streamers described previously are characteristic of this régime of separation. After the liquid has moved through the plane of no shear, most of the viscous flow is backwards into the nip. Figure 5 shows the probable streamlines of the webs of a roller system, viewed parallel to the axis of the rollers. The stagnation point at the leading edge may be noted.

Flow in the arches observed at low speeds in the discone system is more complex in that it is not as symmetrical as the pattern in Fig. 5.

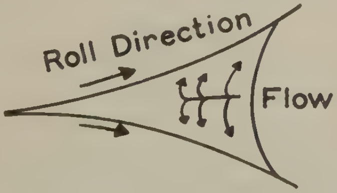

FIG. 5. Wet streamlines.

After the critical velocity for cavitation is reached, the kinematic picture changes. The arches and webs disappear and the bubbles and filaments take over the function of reducing the stress. The bubbles act as centers of dilation until they coalesce and leave an accumulation of filaments. The dilation of the bubbles gives rise to radial and tangential flow around the bubble by the interstitial liquid. In this second regime of flow the arches which characterize the first regime lose their identity, and the final split becomes more a coalescence of bubbles than arch penetration into the bubble.

The division into two regimes of flow is determined by the velocity of the roller system and the viscosity of the liquid. The higher the viscosity, the lower the velocity at which cavitation sets in. Between the two regimes of flow lies an ill-defined region similar to the region between laminar and turbulent flow well known in hydrodynamics. The arches of the first regime are present along with the cavitation bubbles of the second. In this region the bubbles enlarge in a direction transverse to the line of flow rather than isotropically (i.e., they squash out along the roller axis).

## DISCUSSION

### *Nucleation*

The pronounced increase in $\bar{B}$ with speed suggests an analogy with Von Weimarn's (12) concept that the degree of supersaturation during nucleation determines the number of nuclei. If the rate of cavity formation per unit area of liquid in the plane of observation is denoted by $\bar{B}$, then

$$\bar{B} = \frac{U - U_0}{U_0}, \qquad [1]$$

where $U$ is the instantaneous rim velocity and $U_0$ is the critical velocity at which Regime 1 (no cavitation) passes over into Regime 2.

Although nucleation theory has progressed far beyond this simple situation, the kinematic data obtained in this research obey Eq. [1] rather closely. The criterion of nucleation is not only $U$ but also the viscosity $\eta$, so that the $U\eta$ product controls the regime of flow and determines the number of nuclei in the second regime; i.e.,

$$\bar{B} = \frac{U\eta - U_0\eta}{U_0\eta}. \qquad [2]$$

The relation between $U\eta$ and $\bar{B}$ is called the *cavitation curve.* It is drawn as a linear function and does not include all the experimental points. Nevertheless, it reveals a number of significant experimental variables as discussed below.

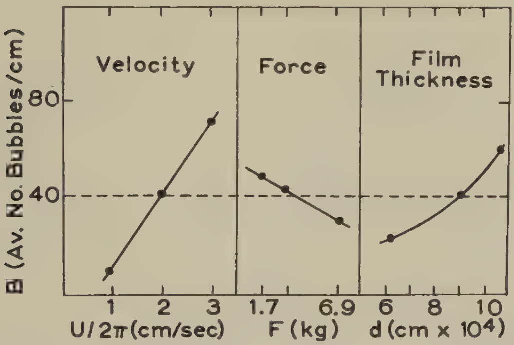

FIG. 6. Influence of operational variables on bubble formation.

### *Effect of Velocity, Force, and Film Thickness*

Three variables involving the instrument were considered to be important during the separation process: the clearance at the instant of separation (film thickness), the force applied to the cone, and the velocity of separation. The first experiments were concerned with establishing the relationship of these instrument variables with the average number of bubbles. Photographs at three speeds, three forces, and three film thicknesses were analyzed factorially. The results of the analysis of variance are shown in Fig. 6, where the average number of cavities per centimeter (transverse to the direction of flow) is plotted versus speed, force applied to the cone, and film thickness.

The small but significant effect of force is plotted in the middle section of Fig. 6, indicating that increasing force decreases the number of effective nuclei.

Likewise, film thickness does not influence greatly the number of bubbles. Figure 7 shows that as the film thickness increases, the dependence of $\bar{B}$ on $U$ increases. The critical velocity is unchanged. One explanation of the greater nucleation rate for thicker films is that the nucleation line has a finite thickness and consequently provides a larger volume for greater films; thus, the chance of finding nuclei in the zone becomes greater (13). The slope of the nucleation curve is then indicative of the probability of finding a nucleus. It should be pointed out that an increase in the clearance reduces the pressure or tension required to split the film according to theoretical concepts. Factorial experimentation also showed a large interaction between speed and film thickness. For these reasons, the effect of film thickness on bubble count $\bar{B}$ appears to be insignificant.

Since the equation of Banks and Mill (14) for the pressure in a liquid involves the separation velocity $U_s$ rather than the tangential velocity, and since the separation velocity is a linear function of the tangential velocity $U$, of the roller, the $U_s\eta$ product was used as the criterion of cavi-

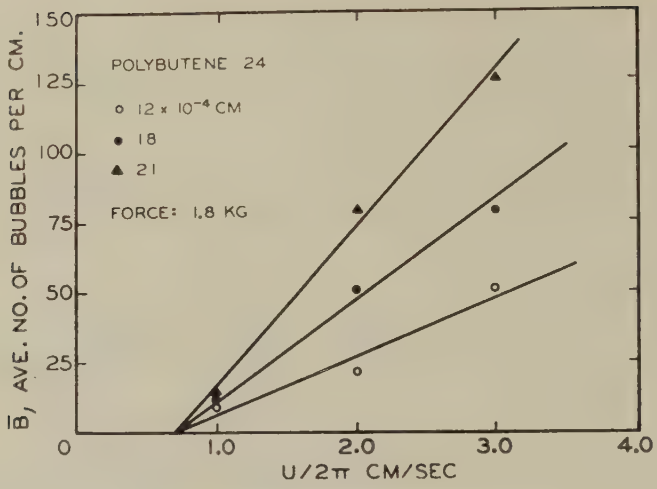

FIG. 7. Effect of film thickness on bubble count.

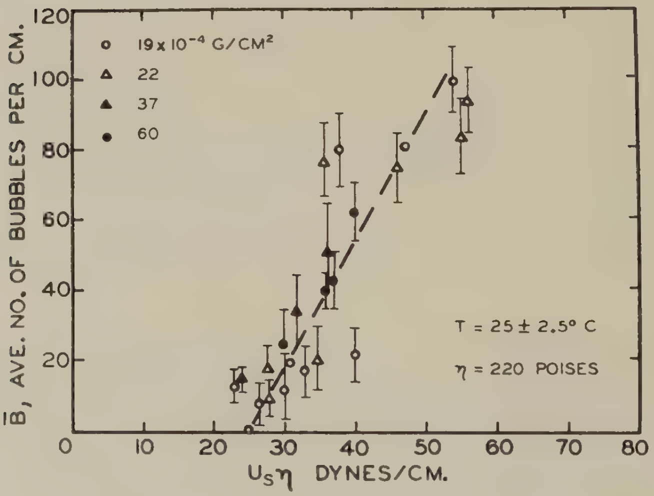

FIG. 8. Cavitation curve for polybutene.

tation. Figure 8 shows the relation between the $U_s\eta$ product and the number of bubbles for Polybutene H-100. The scatter greater than the standard deviation of the bubble counts reflects a number of influences: uncertainty in the $U_s\eta$ product, changes in the minimum clearance, and irregularities in the thickness of the film.

The viscosity used in the calculation of the $U_s\eta$ product was the viscosity at the room temperature of the run. The cavitation curve for Superior varnish linseed oil 165 is shown in Fig. 9. The slope and intercept of the

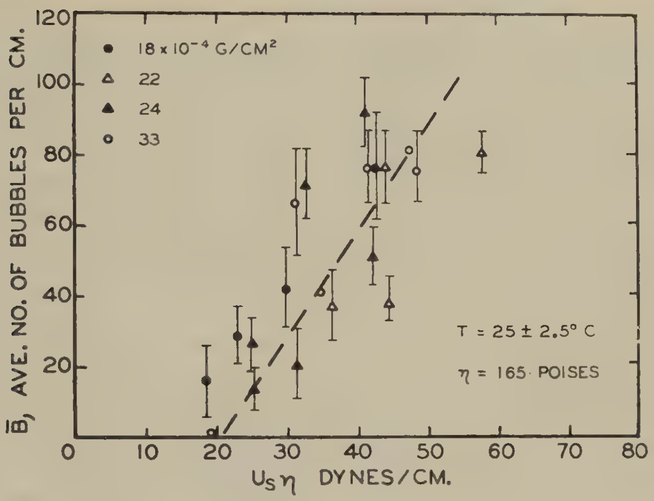

FIG. 9. Cavitation curve for linseed oil.

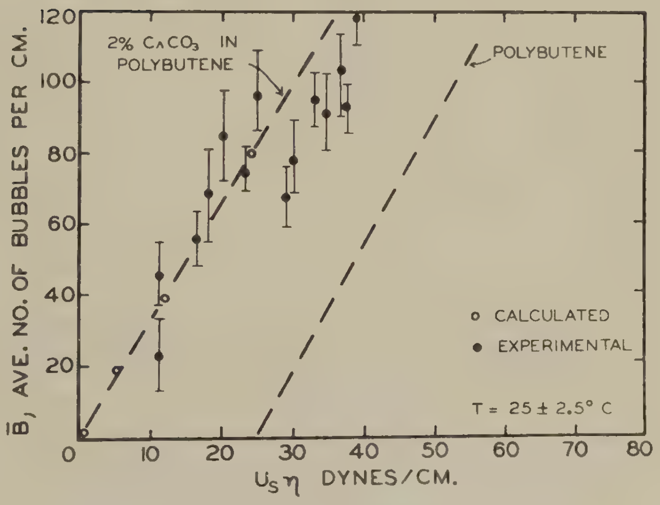

FIG. 10. Cavitation curve for pigmented polybutene.

Indoil Polybutene (Fig. 8) calculated by least squares are 0.28 and 25, respectively. For the linseed oil the slope is 0.34 and the intercept 21. It appears that the $U_s\eta$ product is the primary criterion for the average number of bubbles formed, since the composition of the vehicle had virtually no effect. This hypothesis is further strengthened by the fact discovered in connection with this work that the average number of bubbles is not affected by changes in ambient air pressure.

### *Effect of Nucleus (Pigments)*

To ascertain quantitatively the catalytic effect of solid foreign nuclei, two dispersions differing as widely as feasible in molecular attraction as the liquid-particle interface were prepared in order to provide dispersions of widely different cohesive strength. No precaution was taken to eliminate adsorbed air from the particle surface except to dry the solid to remove adsorbed water. The interfacial adhesion of the $CaCO_3$-linseed oil 165 dispersion is characterized by dispersion and polar forces while the stearic acid-coated $CaCO_3$ dispersed in Polybutene H-100 provides mostly dispersion forces for adhesion.

The cavitation curves for the two dispersions are plotted in Figs. 10 and 11. Both curves establish that the dispersed particles do catalyze bubble formation, apparently to the same extent. The slopes of both curves by the method of least squares are about the same as the slopes for the vehicles

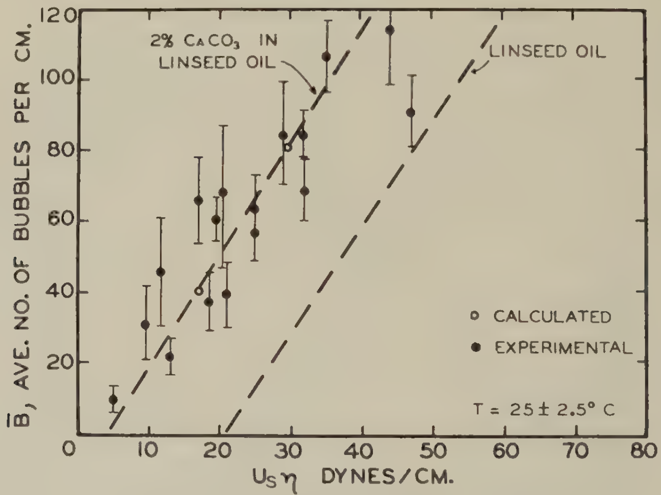

FIG. 11. Cavitation curve for pigmented linseed oil.

TABLE II

*Slopes and Intercepts of the Cavitation Curves*

| | Slope *m* | Intercept ($U_s\eta$) | Catalytic activity (*bubbles/cm.*) |
|---|---|---|---|
| Polybutene H-100 | 0.28 | 25 | — |
| Coated $CaCO_3$-Polybutene H-100 | 0.32 | −2.0 | 75 |
| Linseed oil 165 | 0.34 | 21 | — |
| $CaCO_3$-linseed oil 165 | 0.35 | 3.9 | 60 |

but the intercept on the $U_s\eta$ axis is much lower. Table II compares the intercepts and slopes of the dispersions with those of the vehicles. The difference in the intercepts of the two dispersions is too slight to be considered significant.

Interfacial adhesion between pigment and vehicle does not play a prominent role in the formation of bubbles in these dispersions. Air adsorbed on the particle surface is apparently the source of the catalysis and these nuclei overshadow the effect of interfacial adhesion. It appears likely that other systems might lead to different conclusions. The presence of volatile components such as water at the interface might have an important effect. Furthermore, pigments with other surface properties may behave quite differently.

The catalytic activity of the dispersions can be expressed as the difference between $\bar{B}$ of the dispersion and $\bar{B}$ of the vehicle for a $U_s\eta$ product above the $(U_s\eta)_0$ value for the vehicle. Since the slopes of the curves are equal or nearly equal, the catalytic activity is constant throughout the velocity range investigated. The catalytic effect of the 2% (by volume) dispersions increases the number of bubbles for any $U_s\eta$ by approximately 60 to 75 bubbles, as shown in the last column of Table II.

A description of the flow in the nip and a study of the factors involved were the objects of the present work. Chief requirement in future studies is to elucidate the forces resisting splitting. Finally, it should be stated that nucleation can be studied with this novel discone device under well-controlled conditions so that further light might be shed on this important physical phenomenon.

## REFERENCES

1. REYNOLDS, O., *Trans. Roy. Soc. (London)* **177,** 157 (1886).
2. SJODAHL, L., Paper presented at the First Annual Meeting of the Technical Association of the Lithographic Industry, April 15, 1949.
3. BANKS, W. H., AND MILL, C. C., *Proc. Roy. Soc. (London)* **A223,** 414 (1954).
4. ZETTLEMOYER, A. C., *Am. Ink Maker* **31** (No. 231), (1953).
5. BINGHAM, E. C., *J. Chem. Educ.* **6,** 1206 (1929).
6. HEIDEBROEK, E., AND PIETSCH, E., *Forsch. Gebiete Ingenieurw.* **12,** 74 (1941).
7. MORGAN, K., Private communication.
8. BLOKHUIS, G., *Intern. Bull. Printing and Allied Trades* **1956**(No. 73), 64.
9. ANONYMOUS, *Allgem. Papier-Rundschau* **1952**(No. 4), 154.
10. BUCHDAHL, R., CURADO, J. G., AND BRADDICKS, R., *Rev. Sci. Instr.* **18,** 168 (1947).
11. ZETTLEMOYER, A. C., AND LOWER, G., *J. Colloid Sci.* **10,** 29 (1955).
12. VON WEIMARN, P. P., "Die Allgemeinheit des kolloiden Zustandes." Th. Steinkopff, Dresden, 1925.
13. BIKERMAN, J. J., *J. Colloid Sci.* **2,** 163 (1947).
14. BANKS, W. H., AND MILL, C. C., *J. Colloid Sci.* **8,** 137 (1953).
15. Interchemical Corporation Laboratories, *Am. Ink Maker* **33**(No. 1), 51 (1951).

JOURNAL OF COLLOID SCIENCE **14**, 300–307 (1959)

# THE BINDING OF DYES BY SOLUBLE WOOL KERATIN DERIVATIVES

**B. S. Harrap**

*Biochemistry Unit, Wool Textile Research Laboratories, C.S.I.R.O.,*
*Parkville N.2, (Melbourne), Victoria, Australia*

*Received August 14, 1958; revised October 6, 1958*

## ABSTRACT

The binding of three acid dyes of slightly differing composition to a soluble wool keratin derivative has been measured by the dialysis-equilibrium method. The data satisfy the Klotz-Scatchard equation for the binding of small ions to proteins but the maximum amount of dye bound is much less than that equivalent to the number of basic side chains on the protein, given by amino acid analysis. It seems likely that the guanidino groups of the arginine residues are not able to bind dye anions, and it is suggested that this occurs because they are more firmly bound to other groups on the protein. Intermolecular bonding of this type would account for the high degree of aggregation shown by the soluble wool protein. The influence of pH and ionic strength on the binding of the three dyes is discussed in relation to their chemical structure.

## INTRODUCTION

A large body of data already exists on the interaction between acid dyes and the wool fiber (for recent summaries see 1, 2). However, interpretation of much of this data on a chemical basis is complicated by diffusion of the dye molecule through the complex structure of the wool fiber and by the uncertainty of the chemical nature of each of the various histological components taken individually. Similar difficulties are encountered with most chemical studies on the wool fiber, and attempts to overcome them have been made in these laboratories by preparing soluble derivatives of the wool (3–7) which can then be, at least partially, fractionated into several components. It is intended to compare the properties of the different soluble fractions in order to learn which play the major roles in dyeing and other chemical treatments of wool. Some results have recently been reported (8) on the interaction of the acid dye Orange II with one of these soluble fractions spread as a monolayer at the air-water interface. The present paper deals with the binding of some simple acid dyes to the same fraction in solution.

## MATERIALS AND METHODS

The soluble keratin fraction used was *S*-carboxymethyl kerateine 2 (SCMK2) prepared as described by Gillespie (3) by fractionally extracting

Merino 64's wool with alkaline thioglycolate and coupling the resultant —SH protein with sodium iodoacetate. Stock solutions ($\simeq$1 %) of protein were prepared by exhaustively dialyzing against several changes of distilled water at 2°C. The solutions were stored in the frozen state. A few experiments were also done with a derivative (SMeCMK2) which is similar in all respects to SCMK2 except that the coupling agent was the methyl ester of iodoacetic acid instead of the acid itself.

The three dyes used were Orange II (C.I. 15510), Orange 2G (C.I. 16230), and Crystal Ponceau 6R (C.I. 16250).

Orange II

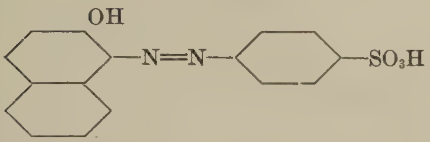

Orange 2G

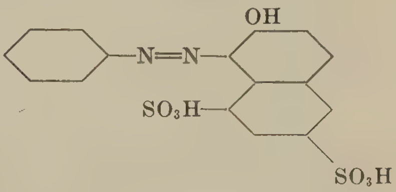

Crystal Ponceau 6R

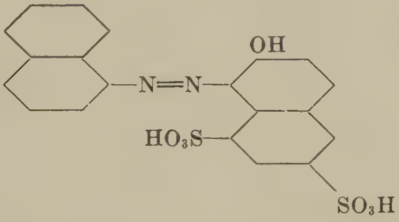

Commercial samples were deionized and converted to the free acids by passing through ion exchange columns as described by Kressman (9). The concentrations of stock dye solutions were determined by drying aliquots in an air oven at 110°C. to constant weight.

All solutions were buffered with 0.05 I acetate-HCl, KCl being added to give the required ionic strength. Buffer materials were of A.R. quantity and distilled water was used throughout. The Visking sausage casing dialysis tubing (24/32) was thoroughly boiled out using several changes of distilled water. The extent of binding of the dye to the protein derivative was determined by equilibrium dialysis, essentially as described by Klotz, Walker, and Pivan (10). Ten-milliliter aliquots of protein solution ($\simeq$0.1 %) were placed in bags of dialysis tubing and equilibrated against 20 ml. aliquots of dye solutions of different concentrations contained in glass-stoppered test tubes. The tubes were placed in a mechanical slow-rocking device and equilibrated for 18 hours at 2°C. The concentrations of unbound dye were determined using a Beckman DU spectrophotometer at the following wavelengths: for Orange II, 485 m$\mu$; Orange 2G, 474 m$\mu$; Crystal Ponceau 6R, 513 m$\mu$. The wavelength maxima and the adherence

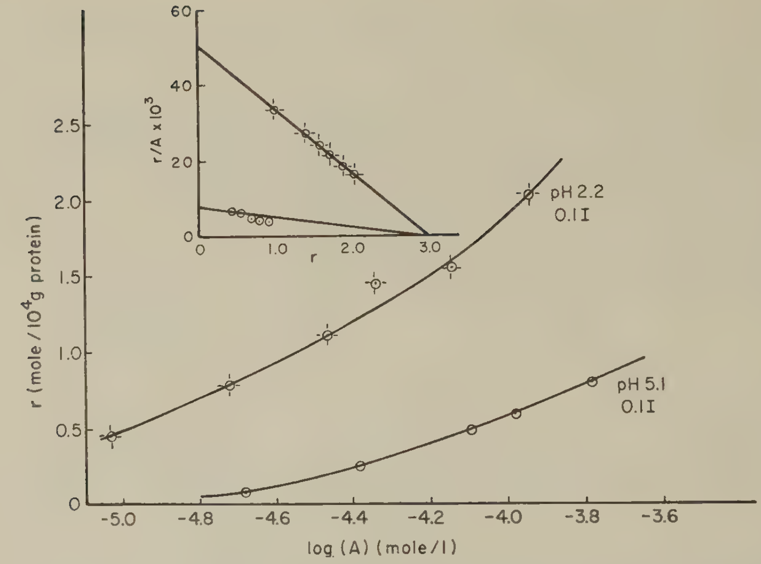

FIG. 1. Plots of $r$ vs. log $(A)$ and $r/A$ vs. $r$ for the binding of Orange II to SCMK2

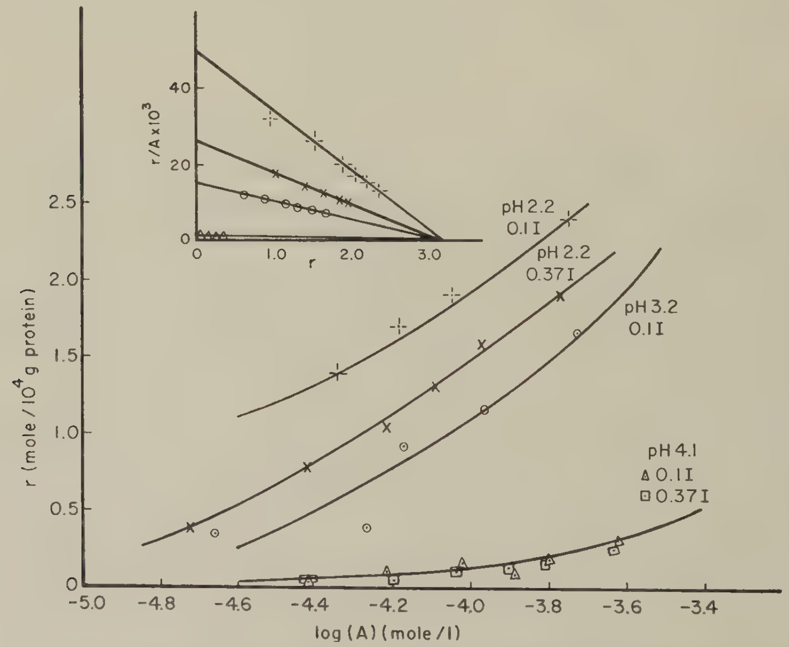

FIG. 2. Plots of $r$ vs. log $(A)$ and $r/A$ vs. $r$ for the binding of Orange 2G to SCMK2.

to Beer's law of the dyes were checked over the range of pH and ionic strength of the buffer solutions used.

## Results

The binding to SCMK2 of the three acid dyes of slightly different structure was measured at 2°C. as a function of pH and ionic strength, and the results are shown in Figs. 1–3, which give the isotherms of $r$ vs. log $(A)$,

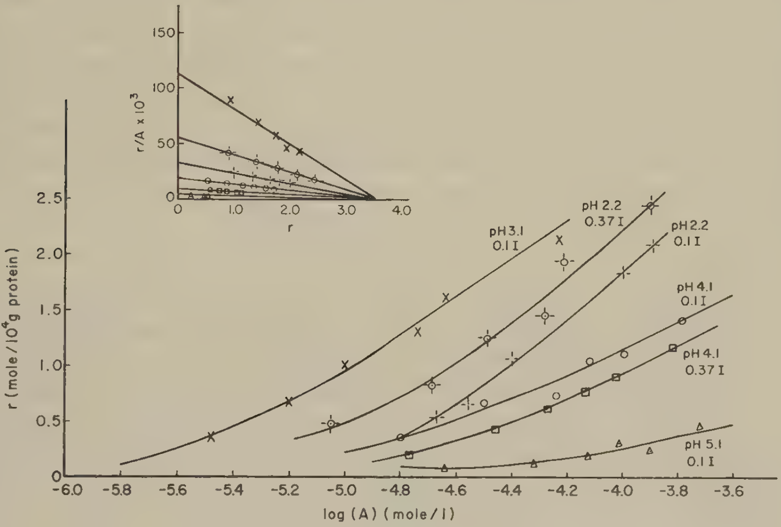

FIG. 3. Plots of $r$ vs. log $(A)$ and $r/A$ vs. $r$ for the binding of Crystal Ponceau 6R to SCMK2.

TABLE I

*Binding Constants for Dye-Protein Interactions as a Function of pH and Ionic Strength (I)*

| *pH* | *I* | Orange II | | Orange 2G | | Crystal Ponceau 6R | |
|---|---|---|---|---|---|---|---|
| | | *n* | *k* × 10³ | *n* | *k* × 10³ | *n* | *k* × 10³ |
| | | | | *SCMK2* | | | |
| 2.2 | 0.1 | 3.0 | 17.0 | 3.3 | 15.4 | 3.6 | 10.3 |
| 2.2 | 0.37 | | | 3.3 | 8.2 | 3.5 | 16.3 |
| 3.1 | 0.1 | | | 3.2 | 4.5 | 3.6 | 32.2 |
| 4.1 | 0.1 | | | 3.3 | 0.5 | 3.6 | 5.6 |
| 4.1 | 0.37 | | | 3.3 | 0.8 | 3.5 | 2.9 |
| 5.1 | 0.1 | 3.1 | 2.7 | | | 3.6 | 0.8 |
| | | | | *SMeCMK2* | | | |
| 3.2 | 0.1 | | | 3.3 | 1.5 | | |
| 4.1 | 0.1 | | | 3.3 | 0.5 | | |

where $r$ = moles bound dye/10,000 g. protein and $(A)$ = the equilibrium free dye concentration. Following Klotz (11) the data may also be plotted in the form $r/(A)$ vs. $r$. Straight-line relationships were obtained (insets Figs. 1–3), indicating that the results satisfied the equation $r/(A) = kn - kr$, at least over the experimental range of $r$ and $A$. This equation has been derived (11) for the binding of anion $A$ to $n$ independent binding sites on the protein, each with the same intrinsic association constant $k$. Assuming that the equation is satisfied at much smaller values of $r$, the values of $n$ and $k$ obtained by extrapolating the data in Figs. 1–3 are shown in Table I.

Since the coupling of the —SH keratin fraction with iodoacetic acid introduces a large additional number of ionizable carboxyl groups on to the protein, a few binding studies were made with a fraction which had been coupled with the methyl ester of iodoacetic acid. The derived values of $n$ and $k$ from these results are shown in Table I.

## Discussion

When dealing with solid wool fibers the number of equivalents[1] of dye bound is usually equal to the number of basic groups on the wool as determined from its titration curve (2). It is therefore somewhat surprising at first sight to note from Table I that the number of moles of dye bound per 10,000 g. protein is approximately the same for the three dyes studied, despite the fact that Orange II has only one —$SO_3^-$ group, whereas each of the other dyes has two such groups.

There seem to be two possible interpretations of this: either (*1*) the dibasic dye anions combine with twice the number of basic groups on the protein as do the monobasic dyes or (*2*) only one of the —$SO_3^-$ groups on the dibasic anions takes part in binding to the protein.

Furthermore, whichever of these alternatives is correct, the total number of equivalents of dye bound is considerably less than the total number of basic groups on the protein fraction as given by the amino acid analyses of Simmonds (12). If his results are converted to the number of residues per 10,000 g. protein, the figures are arginine 5.6, lysine 2.8, and histidine 0.5. Thus if we take the second of the above alternatives it is clear from Table I that the binding of each of the three dyes can be accounted for in terms of the lysine + histidine content of the protein, the arginine apparently not being involved in binding at all. There was the possibility that the large number of carboxyl groups in SCMK2 resulting from coupling the —SH groups with iodoacetic acid may have prevented the binding of dye anion up to the maximum expected from amino acid analysis. However,

---

[1] It is assumed that both sulfonic acid groups on the dibasic dyes are ionized over the pH range investigated since neither of them titrate at pH values greater than 2 (Harrap, unpublished data).

Table I shows that if methyl iodoacetate is used for coupling rather than the acid itself the maximum number of binding sites for the dye anions remains unchanged, the association constant $k$ becoming somewhat smaller. This indicates that the presence of additional carboxyl groups as such is not reducing the binding capacity. We might therefore consider reasons why the arginine side chains apparently do not bind dye anions.

The most obvious explanation is that the guanidino side chains of the arginine residues are firmly bound to some other groups on the protein. In this connection it is instructive to consider the earlier results of Harrap and Woods (13) and O'Donnell and Woods (7) on the physicochemical properties of SCMK2. At acid and slightly alkaline pH values this protein was found to be highly aggregated, the aggregation decreasing somewhat above pH 10 where the lysine groups are discharged. Above pH 12.5, where the arginine residues become unionized, there were marked changes in the sedimentation and viscosity properties of the protein which indicated a considerable degree of disaggregation in this pH range. These results are consistent with the idea that at pH values where the side chains of the arginine residues are ionized they may take part in strong intermolecular bonding leading to the observed aggregation. This bonding could be such that the binding of the dye anions to these side chains is prevented.

Klotz and Ayers (14) have suggested that hydrogen bonding may occur between the charged side chains of the arginine residues and the hydroxyl groups of serine and threonine residues. On this basis they have attributed the high affinity of bovine serum albumin for acid dyestuffs at neutral pH to the relatively low content of hydroxy amino acids in this protein. The possibilities for this type of hydrogen bonding are thereby limited and the basic residues are more freely available to combine with dye anion. In SCMK2 not only is the ratio (ser + thre)/arg high (12) but the large number of carboxymethyl groups introduced into the protein may also provide hydrogen bonding sites in the pH range in which they are unionized.

A possible reason why inhibition of binding should occur with the protein in solution while the native wool fiber binds dye anion equivalent to the total number of basic groups present is that in the wool fiber the polypeptide chains are probably held in a fairly rigid structure by the disulfide cross links of the cystine residues so that movement of the side chains of the arginine residues necessary for interaction is very limited. On the other hand, this freedom of movement is gained in solutions of SCMK2 where the rigid structure is broken down on reduction of the disulfide cross links.

It is clear from Table I that there is no significant variation in the maximum *number* of binding sites as the pH and ionic strength are changed but the association constants $k$ vary considerably with change of environment. In general, as the pH increases the binding constant decreases. This is to be expected since the extent of dye-binding to a large extent follows the titration curve of the protein, so that as the pH increases release of dye anions from the protein occurs together with the release of protons.

An increase in ionic strength normally leads to a lowering of the association constant *k*, indicating weaker binding of the dye anion. This is the reverse of previous results obtained (8) for the interaction of dye with monolayers of SCMK2 at the air-water interface, where with increase of ionic strength there was increased interaction. In solution the decrease in *k* with increase in ionic strength is probably due to competition of buffer anions and chloride ions for the positive binding sites on the protein. In the surface phase this would not be so since the surface activity of the small buffer ions is very low. On the other hand, their presence increases the surface activity of the dye anion, thus enhancing the possibility of its interaction with the monolayer.

There are exceptions to these generalizations in the case of Crystal Ponceau 6R in that *k* is less at pH 2.2 than at pH 3.1 and at the lower pH it also increases with increasing ionic strength. No explanation for this result can be offered. One might speculate whether one or both of the $—SO_3^-$ groups on the dye molecule is becoming unionized at the lower ionic strength at pH 2.2; this could account for the results but no data exist for the variation of ionization with pH and ionic strength for this dye.

Comparison of the three different dyes, Table I, shows that the values for *k* are about equal for Orange II and Orange 2G at pH 2.2; however, the value for Orange II is greater than for Orange 2G at higher pH values. This is probably due to the extra $—SO_3^-$ group on Orange 2G which leads to increased repulsion between dye anion and the carboxyl groups on the protein which are becoming ionized at higher pH values. On the other hand, the association constants for Crystal Ponceau 6R are generally higher than for Orange 2G. Here the nonpolar attractive forces due to the additional benzene ring in Crystal Ponceau 6R would tend to compensate for the increased repulsion due to the second $—SO_3^-$ group.

## ACKNOWLEDGMENTS

The author gratefully thanks Miss M. Cox and Mr. L. West for technical assistance.

## REFERENCES

1. "The Physical Chemistry of Dyeing and Tanning," *Discussions Faraday Soc.* **16,** (1954).
2. VICKERSTAFF, T., "The Physical Chemistry of Dyeing." Oliver and Boyd, London, 1954.
3. GILLESPIE, J. M., *Proc. Intern. Wool Textile Research Conf. Australia 1955*, **B,** 35 (1956).
4. GILLESPIE, J. M., AND LENNOX, F. G., *Australian J. Biol. Sci.* **8,** 97 (1955).

5. O'Donnell, I. J., and Woods, E. F., *Proc. Intern. Wool Textile Research Conf. Australia 1955*, **B**, 71 (1956).
6. O'Donnell, I. J., and Woods, E. F., *Australian J. Chem.* **9**, 212 (1956).
7. O'Donnell, I. J., and Woods, E. F., *J. Polymer Sci.* **21**, 397 (1956).
8. Harrap, B. S., *Proc. 2nd. Intern. Congr. Surface Activity* **4**, 295 (1957).
9. Kressman, T. R., *J. Phys. Chem.* **56**, 118 (1952).
10. Klotz, I. M., Walker, F. M., and Pivan, R. B., *J. Am. Chem. Soc.* **68**, 1486 (1946).
11. Klotz, I. M., "The Proteins," edited by H. Neurath and K. Bailey, p. 727. Academic Press, New York, 1953.
12. Simmonds, D. H., private communication.
13. Harrap, B. S., and Woods, E. F., *Australian J. Chem.* **11**, 581 (1958).
14. Klotz, I. M., and Ayers, J., *Discussions Faraday Soc.* **13**, 189 (1953).

JOURNAL OF COLLOID SCIENCE **14,** 308–329 (1959)

# DETERMINATION OF PARTICLE SIZE AND CONCENTRATION FROM SPECTROPHOTOMETRIC TRANSMISSION

**J. B. Bateman, E. J. Weneck, and D. C. Eshler**

*U. S. Army Chemical Corps, Fort Detrick, Frederick, Maryland*

*Received August 22, 1958; revised January 6, 1959*

## INTRODUCTION

The association of gross scattering of light with certain kinds of system has had significance in the emergence of colloid science, and may indeed be considered to constitute one of the earliest definitions of a colloid. Observations and measurements of light scattering in one form or another, although numerous, have not always kept pace with the development of the science, having until recently usually been semiempirical, despite the existence since 1908 of Mie's (1) rigorous theory. This was due to the labor needed to find numerical solutions for Mie's equations, to the scarcity of colloids which satisfied the restrictions adopted by Mie as to particle shape, homogeneity, and uniformity of size, and finally to the lack of satisfactory methods of characterizing these systems independently. These difficulties have been much reduced in the last few years: the first, by the development of high-speed computers, and the other two, by a number of advances in overlapping areas of polymer science, colloid science, and biochemistry. Although the Mie theory had already received some experimental verification, these new circumstances made possible studies much broader in scope, notably those of LaMer and colleagues (2–10), which confirmed in broad outline the scattering behavior of aerosols and hydrosols predicted by the theory. These and other studies, reviewed in several places (11, 12), with their illuminating discussions of experimental approaches, have led to renewed activity in the quantitative study of light scattering by colloids.

The present work was done in the preliminary stages of an attempt to use scattering measurements for characterizing certain biological hydrosols in the micron particle size range with respect to size, concentration, and index of refraction. It was recognized that pitfalls exist both in instrumentation and in valid use of the theory, and a study of the uniformly spherical monodisperse polystyrene particles which were available seemed to offer elementary safeguards. The limited objective with these latexes was the measurement of particle size and concentration by means of spectral extinction (turbidity) curves over the visible and long ultraviolet wavelength range, using principles which are far from new but which have seldom been applied with strict regard to the effect of dispersion of refractive index upon the theoretical extinction values. A second feature worth mentioning is the use of a conventional spectrophotometer, appropriately modified. The performance of this instrument meets most of the specifications laid down by Heller and Tabibian (13) in their study of errors in turbidity measurements, and the accuracy is comparable to that attained by Tabibian, Heller, and Epel (14) in measurements on suspensions of spheres at a single wavelength with a specially designed apparatus. Those measurements, in their opinion, constitute "a conclusive proof of the Mie theory." A subsidiary outcome of the present work is a further confirmation of the theory over a wider range of experimental conditions but to a rather less satisfactory degree of precision.

## METHODS OF CALCULATION

The procedure falls naturally into two parts, both very simple in principle. In the first, transmission data on aqueous suspensions of known concentration, $c$, of polystyrene spheres, of known radius $r$ and refractive index $n_p$, are converted to values of the total Mie scattering coefficient $K$ and compared with the appropriate theoretical values. Satisfactory agreement being obtained, the same experimental and theoretical data are then manipulated in such a way as to yield, first, values of apparent particle size, presuming the concentration to be known, and, second, particle size and concentration, presuming neither to be known.

### *1. Calculation of K or Particle Size from Transmission Data When Concentration Is Known*

The familiar definitions of the total Mie scattering coefficient $K$ and of the extinction $E$—see, for example, reference 12—lead to the equation

$$K = 2.303\, E/\pi r^2 N l, \qquad [1]$$

where $l$ is length of scattering cell and $N$ is the number of spheres per milliliter. If the mass concentration $c$ is known, then

$$K = 3.0707\, Erd/cl, \qquad [2]$$

where $d$ is particle density.

If it is desired to find particle radius from measured extinction and concentration, it is convenient to calculate the ratio $K/\alpha$ given by

$$\frac{K}{\alpha} = \frac{0.4887\, d}{(n/\lambda_0)} \cdot \frac{E}{cl}, \qquad [3]$$

$\alpha$ being the value of the size parameter $2\pi n r/\lambda_0$ for incident light of wavelength $\lambda_0$ in air, and to determine $r$ by interpolation on a theoretical curve

$K/\alpha$ against $r$. A similar procedure has been used by LaMer, Inn, and Wilson (10) in the special case where $r$ is to be determined by locating the first principal maximum. It is also equivalent to that used by Tabibian, Heller, and Epel (14), who compare experimental and theoretical values of $(\tau/c)_0$ where $\tau$, the turbidity, is 2.303 $E$.

### *2. Theoretical Values of K*

Computed values of $K$ are presented in several sets of tables in terms of the size parameter $\alpha$. These data are given for various values of the relative refractive index $m$, or $n_p/n$, spaced at intervals of 0.05. For polystyrene in water, $m$ is about 1.21 at 3700 A. and 1.18 at 10,000 A. Further, the particle radii of the polystyrene latexes used in this study fall within the range 0.05–0.6 $\mu$, giving values of $\alpha$ ranging from about 0.8 to 15.0. The tables covering these values are those of Pangonis, Heller, and Jacobson (15) which include $K(\alpha)$ for $m = 1.5$, 1.20, and 1.25 and $\alpha = 0.2, 0.4, 0.6 \cdots 7.0, 8.0, 9.0 \cdots 15.0$.

In order to obtain correct values of $K$ from these tables for all the wavelengths at which measurements were made, namely, 3500, 3600 ··· 6000, 6250, 6500 ··· 8000, 8500, 9000 ··· 10000 A. interpolations are necessary. These must be done rather accurately in order to match the accuracy of the transmission values (reproducible generally to 0.1 in per cent transmission over the range 12–80) and to make possible, in principle, a 1% accuracy in $r$. These considerations suggest that log $K$ should be interpolated with an accuracy of 0.004 or better.

Direct interpolation from plots of $[K(m)]_\alpha$ against $m$ can be at once rejected, since the intervals $\Delta m$ are large, the corresponding changes $\Delta \log K$ are also large, and the plots are in general strongly curved. We have found accurate interpolation to be possible by taking advantage of two facts noted by Van de Hulst (11, 12, 16): first, that the positions of the extrema of the damped oscillating functions representing $K(\alpha)$ for various values of $m$ coincide almost exactly if a normalized size parameter $\rho$ is used:

$$\rho = 2\alpha(m - 1), \qquad [4]$$

and further, that $K(\rho)$ when $m \rightarrow 1.0$ is given by:

$$K_1 = 2 - 4 (\sin \rho)/\rho + 4 (1 - \cos \rho)/\rho^2. \qquad [5]$$

A plot of log $K$ against log $\rho$ (Fig. 1) suggests that whereas the curves for the various values of $m$ do not coincide, interpolations at constant $\rho$ would be superior to interpolations at constant $\alpha$ since over the range of present interest it is usually true that

$$(\Delta \log K/\Delta m)_\rho \ll (\Delta \log K/\Delta m)_\alpha . \qquad [6]$$

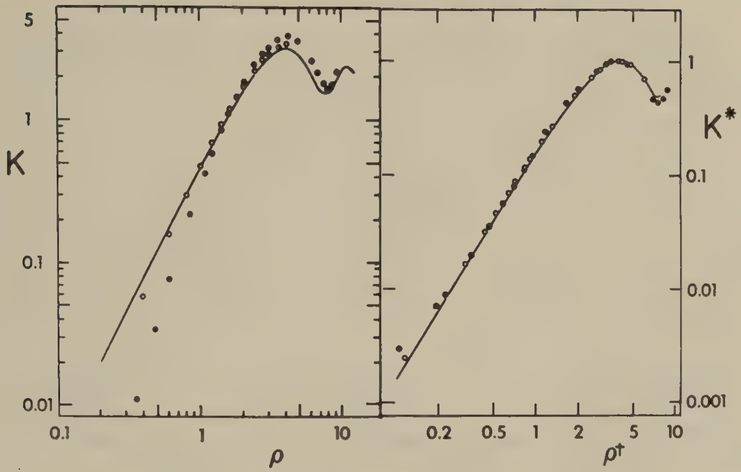

FIG. 1. *Left:* Variation of total Mie scattering coefficient $K$ with normalized size parameter $\rho$. *Right:* Variation of normalized total Mie scattering coefficient $K^*$ with modified normalized size parameter $\rho\dagger$. In both diagrams, continuous curve: $m = 1.0$; open circles, $m = 1.10$; closed circles, $m = 1.30$.

Thus the desired values of log $K$ can be represented by comparatively small corrections to log $K_1$, which is known precisely from Eq. [5].

The corrections can be made much smaller and less dependent upon $m$ by using the normalized size parameter in an empirically modified form:

$$\rho\dagger = 2\,(\alpha - 0.425)(m - 1) = \rho - 0.85\,(m - 1) \qquad [7]$$

and by plotting normalized values of $K$ defined by

$$K^* = K/K_y\,, \qquad [8]$$

where $K_y$ is the value of $K$ at the first principal maximum. The resulting improvement is illustrated in Fig. 1. The correction factor $\delta^*$ is now defined:

$$\delta^* = K^*/K_1^* \qquad [9]$$

and is calculated for all the values of $K(\alpha)$ at $m = 1.15$, 1.20, and 1.25 given in the tables (15), using Eq. [5], [7], [8], and [9]. These corrections are plotted in Fig. 2.

The procedure for calculating $K(\lambda_0)$ for polystyrene spheres of radius $r$ in water is now straightforward. Values of $\rho\dagger$ for the various wavelengths $\lambda_0$ are calculated (Eq. [7]), log $\delta^*$ is read from Fig. 2, $K_1^*$ is calculated or determined graphically from a large-scale plot, $K_y$ is interpolated from plots of the tabulated $[K(\alpha)]_m$ values, and then $K$ can be calculated from the same equations as before.

The calculations of $K$ required in the present work refer to seven particle

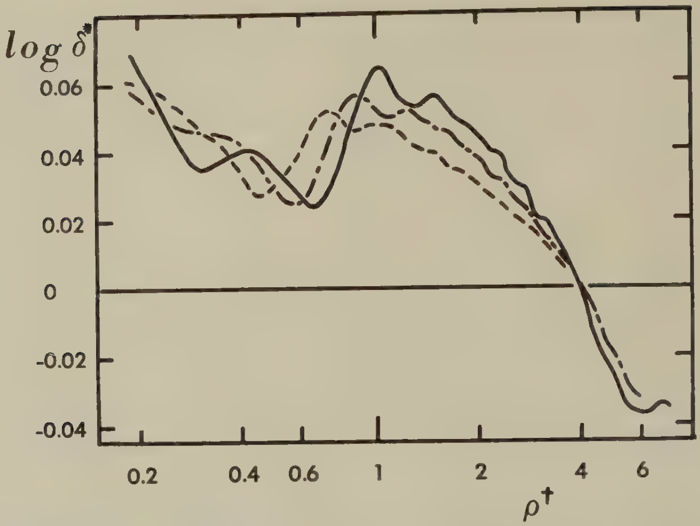

FIG. 2. Variation of correction factor $\delta^*$ (Eqs. [8]; [9]) with modified parameter $\rho\dagger$. Continuous line, $m = 1.25$; dash-dot line, $m = 1.20$; dashed line, $m = 1.15$.

radii from 800 to 7000 A., including the four values found by Bradford and Vanderhoff (17) for the four latexes used in this work, and to the wavelengths, already enumerated, at which experimental values were obtained. The values of $n(\lambda_0)$ and $m(\lambda_0)$ needed for the calculation of $\alpha$ and $\rho\dagger$ were obtained from the equation

$$n = a + b/\lambda_0^2. \qquad [10]$$

For water (18), $a = 1.324_0$, $b = 3.046 \times 10^{-11}$ if $\lambda_0$ is in centimeters. For polystyrene, the first detailed calculations were made using $a = 1.5613$, $b = 9.96 \times 10^{-11}$, derived from Starkie's (19) values: $n_{5893}^{20} = 1.5900$ and $(n_{5893} - 1)/(n_{4861} - n_{6563}) = 31.0$. Recent measurements by Heller and Pugh (20) give for polystyrene latex particles at 5461 A. $n_p = 1.602$, and the dispersion formula was therefore revised by changing $n_p$ at 5893 A. to 1.5974, retaining Starkie's value 31.0 for the dispersion ratio. The revised Cauchy constants are $a = 1.5683$, $b = 10.087 \times 10^{-11}$. The density of polystyrene, $d$ in Eqs. [2] and [3], has been taken as 1.057 (21).

The theoretical values of $K$ for polystyrene in water are given in Table I, and examples of the dependence of $K/\alpha$ upon particle size are shown in Fig. 3.

### 3. *Methods of Calculating Particle Size and Concentration*

*a. By Location of the First Principal Maximum.* This has been used previously in several forms (2, 3, 7, 11, 22, 23). When $m$ is 1.15–1.25, the first

TABLE I

*Total Mie Scattering Coefficients for Polystyrene Spheres in Water*

| $r$(A.) . . . . | 800 | 1320 | 1940 | 2555 | 3300 | 4070 | 5000 | 5855 | 7000 |
|---|---|---|---|---|---|---|---|---|---|
| $\lambda_0$ | $K$ | | | | | | | | |
| 3700 | 0.232 | 0.802 | 1.703 | 2.595 | 3.438 | 3.743 | 3.352 | 2.637 | 1.863 |
| 4300 | 0.144 | 0.526 | 1.185 | 1.945 | 2.792 | 3.450 | 3.723 | 3.458 | 2.710 |
| 5000 | 0.0891 | 0.333 | 0.809 | 1.387 | 2.147 | 2.864 | 3.466 | 3.698 | 3.474 |
| 5600 | 0.0614 | 0.232 | 0.611 | 1.084 | 1.730 | 2.400 | 3.084 | 3.500 | 3.691 |
| 6500 | 0.036 | 0.153 | 0.416 | 0.767 | 1.275 | 1.843 | 2.515 | 3.031 | 3.520 |
| 7500 | 0.0211 | 0.102 | 0.276 | 0.543 | 0.935 | 1.400 | 1.986 | 2.506 | 3.090 |
| 8500 | — | 0.0705 | 0.193 | 0.397 | 0.701 | 1.086 | 1.581 | 2.055 | 2.642 |
| 9500 | — | 0.0490 | 0.144 | 0.293 | 0.548 | 0.852 | 1.275 | 1.689 | 2.247 |

Dispersion equations assumed: for water, $n = 1.324_0 + 3.046 \times 10^{-11}/\lambda_0^2$; for polystyrene, $n_p = 1.5683 + 10.087 \times 10^{-11}/\lambda_0^2$.

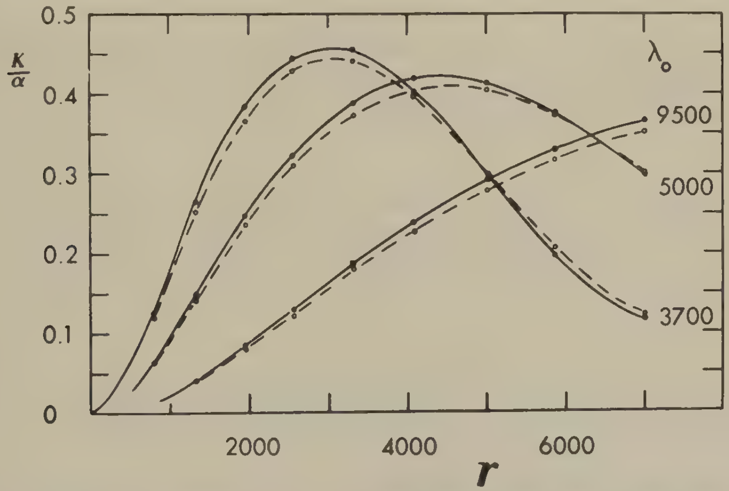

FIG. 3. Variation of theoretical $K/\alpha$ with radius of polystyrene spheres suspended in water. Parameter on chart: wavelength in air. Continuous curves calculated for polystyrene having dispersion constants $a = 1.5683$, $b = 10.087 \times 10^{-11}$; broken curves, $a = 1.5613$, $b = 9.96 \times 10^{-11}$ (Eq. [10]).

maximum occurs when $\rho(= \rho_y)$ is 4.05, so that if $m$ is known, $r$ can be calculated. The corresponding values $K_y$ are also known, so that $c$ can then be obtained from Eq. [2]. Since the method is not generally applicable it is not stressed in this paper, nor has the displacement of the maximum by use of functions $K/\alpha^x$ (10) been investigated.

*b. By Calculating Logarithmic Slopes.* Values of $K(\alpha)$ and $E(\lambda_0)$ can be represented as functions of $\alpha^a$ or $\lambda^{-b}$, where $a$ and $b$ are in general func-

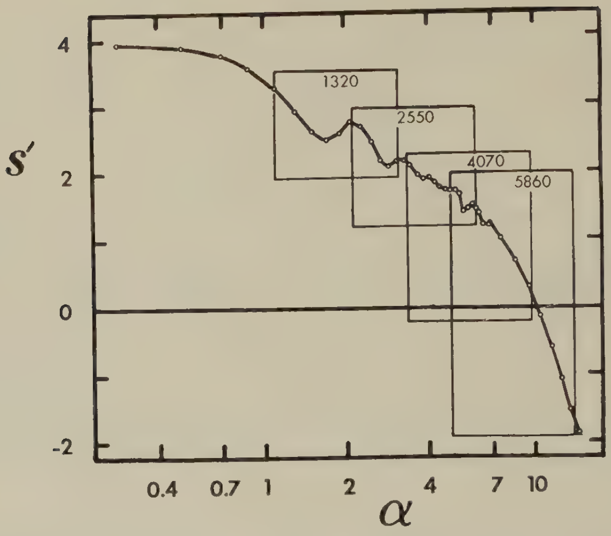

FIG. 4. Slope $s'$, with $m$ equal to 1.20, as a function of size parameter $\alpha$. Calculated from tabulated data for $K(\alpha, m)$, reference (15). Rectangles enclose portions of curve applicable to transmission measurements between 3500 and 10000 A. on suspensions of spheres of radii indicated.

tions of $\lambda$, the wavelength of the incident light in the continuous phase of the suspension. This type of expression has been much used, by LaMer (6) and Van de Hulst (12) *inter alia*. From Eq. [2], for particles of a given radius

$$d(\log K)/d(\log \alpha) = d(\log E)/d(\log n/\lambda_0) = s. \qquad [11]$$

Also $s = a = -b$; thus if $s$ is sufficiently dependent upon particle size, matching of experimental and theoretical slopes at one median wavelength should permit estimation of particle size.

In the polystyrene-water system with $\alpha = 0.8$–$15.0$, some idea of $s(r)$ can be gained by calculating the slopes from point to point, using the published values of $K(\alpha)$ at a chosen value of $m$: these slopes, designated $s'$, are shown in Fig. 4 for $m$ equal to 1.20. Two features are of special interest: the considerable dependence of $s'$ upon particle size and wavelength, and the existence of a fine structure resulting from slight ripples, when $m > 1.0$, superimposed on the smooth limiting curve $K_1(\rho)$.

The curve of Fig. 4 is not immediately applicable to spectrophotometric data since the values $s'$ approach the partial differential $(\partial \log K/\partial \log \alpha)_m$. The variation with wavelength, $s$, is given conveniently by

$$s = s' + \left[\frac{\partial \log K}{\partial \log (m-1)}\right]_\alpha \cdot \frac{d \log (m-1)}{d \log \alpha}. \qquad [12]$$

TABLE II

*Data Illustrating Importance of Second Term in Eq.* [*12*]

| $\alpha$ | 3 | | 10 | |
|---|---|---|---|---|
| $\lambda_0$ | 3700 | 9500 | 3700 | A. |
| $r$ | 1311 | 3420 | 4370 | A. |
| $s'$ | 2.15 | 2.15 | 0.10 | |
| $s$ | 2.8 | 2.4 | −0.2 | |

The second term, representing the effect of dispersion of refractive index of both phases, is dominated by the factor in $K$, which changes from positive to negative with increasing $\alpha$ in the vicinity of the first principal maximum. Since the second factor $d \log (m - 1)/d \log \alpha$ is always positive and varies comparatively slowly with wavelength, the net effect of the correction term is to make the curve $s(\alpha)$ generally steeper than $s'(\alpha)$ when $\alpha$ is varied by increasing $r$ at constant wavelength, and less steep when $\alpha$ is varied by decreasing $\lambda_0$ at constant $r$. The differences are quite large; examples given in Table II make it clear that any interpretations of transmission data which neglect dispersion will be erroneous.

The task of obtaining theoretical curves $s(r)$ for polystyrene spheres in water at various wavelengths is complicated by the fine structure, which is imperfectly resolved in the available theoretical values (15) and which tends to become further smeared in the course of calculating $K(\lambda_0)$ as already described. Since the experimental data are likewise imperfectly resolved, some compromise seemed justifiable in constructing the theoretical curves. It was decided to limit the calculations to eight selected wavelengths, 3700, 4300, 5000, 5600, 6500, 7500, 8500, and 9500 A. and in each case to define the average slope $\bar{s}$ at each of these points by the slope of the best straight line (method of least squares) through the point in question and one or two of its neighbors on either side—i.e., through 3 or 5 adjacent points with coordinates $(\log K)_i$, $(\log n/\lambda_0)_i$. The decision whether to take 3 or 5 points was made in each case after examining the data for uniformity of curvature or evidence of local distortion arising from fine structure.

Such calculations were made for the nine particle radii referred to in Table I and the eight selected wavelengths, and for each wavelength preliminary smooth curves $\bar{s}$ $(\log r)$ were drawn. Because of the wide spacing, the fine structure was very little in evidence, and this had to be filled in by trial and error using the following criteria: (*a*) the ten subsidiary extrema resolved in $s'(\alpha)$ (Fig. 3) were presumed present in all cases; (*b*) their relative positions along the abscissa were assumed to remain almost unchanged with change in wavelength; (*c*) the values of $s$ at the extrema were assumed to vary monotonically with $\lambda_0$. In this way the fine structure was inserted with insignificant distortion except at 7500 A., where some inconsistencies

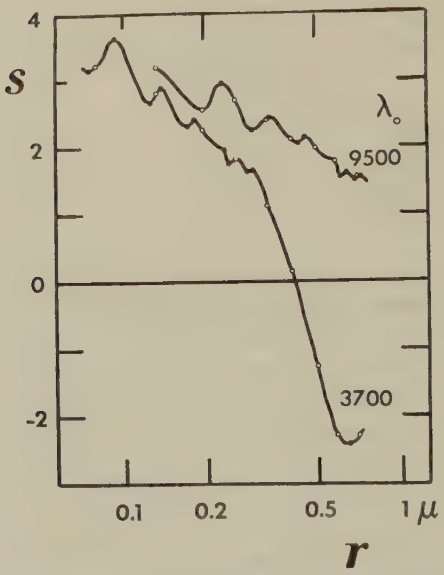

FIG. 5. Illustrating curves used for determination of particle radius from measured $s$. Abscissa: log $r$. Ordinate: $s$ (Eq. [11]). Parameter, wavelength in air. Open circles, calculated theoretical values. Closed circles, positions of secondary extrema obtained by analogy, as described in text.

appeared. Consequently some confidence is felt in the accuracy of the $\bar{s}$ (log $r$) curves, two examples of which are given in Fig. 5, and which served for the graphical determination of particle radius from experimental values of $\bar{s}$. In one instance ($r$ = 1320 A.) the values of $s$ were checked by combining in differential form Eqs. [4]–[9] and evaluating the individual terms graphically or arithmetically.

When particle radius had been obtained from experimental values of $s$ as just described, calculation of concentration by Eq. [3] could be made, the value of $K$ being obtained by interpolation on large-scale plots of log $K$(log $r$). Using $d = 1.057$, $l = 5.0$, Eq. [3] becomes

$$c = 0.649\ Er/K. \qquad [13]$$

## APPARATUS AND METHODS

### *1. Spectrophotometer*

Preliminary measurements with a Beckman model DU spectrophotometer showed that for particles in the 0.2–1.0 μ size range the mere introduction of small beam stops to limit the solid angle of the scattered light received by the photometer—as done successfully by Doty and Steiner (24) and Billmeyer (25) in the study of smaller particles—was not sufficient to reduce errors to an acceptable extent. The apparatus was further modi-

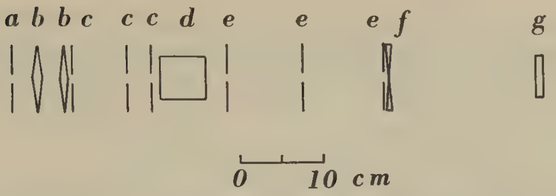

FIG. 6. Optical train of Beckman model DU spectrophotometer modified for transmission measurements. Light passes from left to right. Here *a* is monochromator slit; *b* are convex lenses; *c* are circular beam stops, diameter 3 mm.; *d* is 5 cm. cylindrical absorption cell; *e* are circular beam stops, diameter 2.5 mm.; *f* is a concave lens; and *g* is photoelectric cell or photomultiplier tube of the Beckman instrument.

fied at negligible cost as shown in Fig. 6, the essential changes being: (*1*) Remove crystal quartz entrance and exit windows (26). (*2*) Insert two convex lenses *b* in front of the exit slit of the monochromator. (*3*) Insert three 3-mm. circular beam stops *c* between the second lens and the entrance window of the scattering cell. (*4*) Remove phototube *g* to a distance of 39 cm. from the exit window of the 5-cm. scattering cell. (*5*) Insert three 2.5-mm. circular beam stops *e* and a biconcave lens *f* between scattering cell and phototube. (*6*) Blacken all interior surfaces of cell housing, all beam stops, and outer surfaces of cells containing suspension and solvent.

The two lenses *b* and beam stops *c* produce a beam of uniform intensity, whereas in the unmodified instrument the image of the filament is resolved. The beam diverges within the scattering cell by half angles of about 1.9° in the vertical plane and 0.4° in the horizontal plane. The three apertures *e* serve to exclude stray light while the third of these determines the angle of the cone of scattered light; the half angle, $\omega$(13), is 0.34°. The lens *f* forms a uniform circular image 2.5 cm. in diameter at the phototube which does not change in shape or uniformity when the monochromator slit width is altered.

The adequacy of this arrangement was judged by the absence of significant concentration dependence of specific extinction and by general agreement between experimental and theoretical results. The absence of stray light and corona (13) was shown by photographic examination of the light beam at several points in the system.

### *2. Spectrophotometric Measurements*

All measurements were done on three or four concentrations of latex. The concentrations were such as to provide at least one, and usually two, transmission values falling between 20% and 75% at each wavelength. Measurements on each filling of the 5-cm. scattering cell were done in triplicate, and were reproducible to better than 0.1 in per cent transmission; usually the three readings were identical. Readings at 6000, 6250, and 6350 were made with both red-sensitive phototube and photomultiplier attachment, and were identical. Occasional discrepancies were sometimes traced to deposition of a film of polystyrene on the scattering cell windows; this was removed with dioxane.

### *3. Polystyrene Concentration*

Weighed samples of stock latex, in triplicate, were dried to constant weight *in vacuo* at 65° C. The concentrations varied from 4 to 14 g./100 g., and the amounts dried were 0.5–1.4 g.—enough in each case to give about 60 mg. residue. The first dilution was made by weighing out 0.1 ml. and diluting volumetrically to 100 ml. Subsequent twofold dilutions were made volumetrically.

## RESULTS

### *1. Concentration Dependence*

In general, the specific extinctions ($E/c$) at the two lowest concentrations agreed to well within 0.5%, with occasional discrepancies—particularly with the smallest particles studied—as great as 2%. These were, however, apparently random in character, whereas systematic change became apparent at higher concentrations. An example is given in Table III.

### *2. Experimental Values of K*

The experimental results on four monodisperse polystyrene latexes are presented in Fig. 7 in the form of the total Mie scattering coefficient $K$ obtained from $E(\lambda)$ and $c$ by Eq. [2], using the values of $r$ determined in the electron microscope by Bradford and Vanderhoff (17). The theoretical values (Table I) are also plotted. The generally satisfactory agreement within the visible spectrum is apparent, except for latex LS-057-A, assumed radius 1320 A., where the experimental values are about 10% too small. In the long ultraviolet the measured extinctions tend to be a little too high.

TABLE III

*Concentration Dependence of Relative Specific Extinction*

Polystyrene spheres, batch LS-067; $r$ about 5855 A.

| $c$ (*μg./ml.*) | $(E/c)_{\text{rel.}}$ | | | | | |
|---|---|---|---|---|---|---|
| | $\lambda_0$ = 10000 | 7000 | 6000 | 5000 | 4000 | 3500 |
| 11.800 | 0.969 | 0.984 | 0.980 | — | — | — |
| 8.864 | 0.978 | 0.979 | 0.983 | 0.979 | 0.978 | 0.969 |
| 4.432 | 0.999 | 0.995 | 1.002 | 1.001 | 0.999 | 0.991 |
| 2.216 | 1.000 | 1.000 | 1.000 | 1.000 | 1.000 | 1.000 |

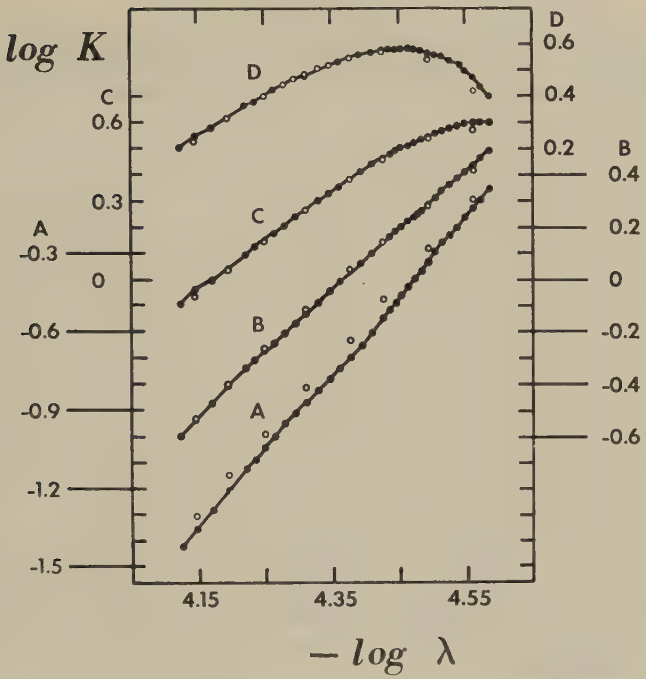

FIG. 7. Experimental and theoretical values of total Mie scattering coefficient compared for four polystyrene latexes. Theoretical values (open circles) calculated for particle radii obtained by electron microscopy (17): 1320, 2555, 4070, and 5855 A. for curves (*A*) to (*D*), respectively. Experimental values (solid circles) calculated from measured extinction and concentration by Eq. [2]. Abscissa: −log λ. Ordinate: log *K*. Scales of ordinates *A* to *D* are identified by letters on curves.

The latexes contain ultraviolet-absorbing soluble stabilizers but examination of the supernatant solutions after centrifuging suggested that their contribution to the extinction would be negligible. The particles themselves dissolved in dioxane showed only very slight absorption almost independent of wavelength between 3500 and 4500 A. Systematic discrepancies also appear at the other end of the spectrum in the case of the two largest particle sizes, the measured extinctions again being rather higher than those calculated. Since the best agreement is obtained close to the wavelength at which the particle refractive index is known with great accuracy, it is possible that the discrepancies at the extremes of the spectrum are due to use of incorrect values for the dispersion constants.

### *3. Particle Sizes Determined from $E/c$*

Values of $K/\alpha$ were calculated from $E/c$ by text Eq. [3] and particle radius was obtained by interpolation (Fig. 3). Table IV gives the results,

TABLE IV

*Latex Particle Size Determined from E/c*

| Latex batch no. | LS-057-A | 15N-8 | LS-066-A | LS-067 |
|---|---|---|---|---|
| Concentration (*μg./ml.*)........ | 10.77 | 4.224 | 3.301 | 2.216 |
| $\lambda_0$ | $r$ (interpolated, Fig. 3) in Angstroms | | | |
| 3700 | (1220) | (2690) | (3830) | (5670) |
| 4300 | 1215 | 2540 | 3730 | 5690 |
| 5000 | 1190 | 2520 | 3940 | 5670 |
| 5600 | 1200 | 2510 | 4100 | 5800 |
| 6500 | 1240 | 2480 | 4070 | 5940 |
| 7500 | 1250 | 2510 | 4210 | 5900 |
| 8500 | 1240 | 2520 | 4180 | 6220 |
| 9500 | 1260 | 2525 | (4380) | (6350) |
| $r$ | 1228 | 2515 | 4038 | 5870 |
| SD | 24 | 17 | 163 | 185 |
| CV% | 1.98 | 0.68 | 4.03 | 3.15 |
| $r$(em) | 1320 | 2555 | 4070 | 5855 |
| $\bar{r}/r$(em) | 0.930 | 0.984 | 0.992 | 1.003 |

$\bar{r}$ = average radius.
SD = standard deviation.
CV% = coefficient of variation, 100 SD/$\bar{r}$.
$r$(em) = radius measured by electron microscopy (17).

including averages obtained by omitting the bracketed values on the ground of the systematic errors just referred to. The coefficients of variation range from 2% to 4%. The averages are compared to those of Bradford and Vanderhoff (17) measured in the electron microscope. The agreement is excellent in three cases out of four, whereas for the latex of smallest particle size the value obtained by electron microscopy is 7% higher than that given by transmission measurements.

### *4. Particle Size and Concentration Determined by Locating First Mie Maximum*

Additional values of particle size and concentration can be obtained for two of the latexes examined because the data include the first maximum $E_y$ which for $m = 1.2$ occurs when $\rho = \rho_y = 4.05$. Thus $r$ and $c$ can be calculated from Eqs. [4] and [2] since $K(= K_y)$ is known. Alternatively, $r$ can be calculated from $E_y$ by Eq. [2] if $c$ is known. The values so obtained are included in the summarizing Table VI.

TABLE V

*Values of Polystyrene Sphere Radii and Concentrations Obtained from Slope s of Transmission Data*

| (1) Latex batch no. | LS-057-A | | 15N-8 | | LS-066-A | | LS-067 | |
|---|---|---|---|---|---|---|---|---|
| | *r* | *c* | *r* | *c* | *r* | *c* | *r* | *c* |
| (2) Electron microscopy, A | 1320 | | 2555 | | 4070 | | 5855 | |
| (3) Standard deviation | 30 | | 35 | | 55 | | ? | |
| (4) Dry weight, μg./ml | | 10.77 | | 4.224 | | 3.301 | | 2.216 |
| Values from transmission data<br>$\lambda_0$ | | | | | | | | |
| 3700 | (1380)[a] | (10.12)[a] | —[e] | —[e] | 4027 | 3.517 | 5754 | 2.260 |
| 4300 | —[b] | —[b] | —[e] | —[e] | 3981 | 3.417 | 5623 | 2.174 |
| 5000 | 1297 | 10.06 | 2483 | 4.456 | 4121 | 3.411 | 5794 | 2.257 |
| 5600 | 1265 | 10.46 | 2523 | 4.474 | 4121 | 3.411 | 5728 | 2.232 |
| 6500 | (1365)[a] | (9.46)[a] | 2523 | 4.410 | 4207 | 3.351 | 5916 | 2.246 |
| 7500 | 1259 | 11.03 | —[f] | —[f] | 4325 | 3.345 | 5754 | 2.299 |
| 8500 | 1334 | 9.92 | 2455 | 4.695 | —[g] | — | 5957 | 2.360 |
| 9500 | 1318 | 10.20 | 2547 | 4.285 | —[g] | — | 6095[h] | 2.356 |
| Average: | 1295[c] | 10.33[c] | 2506 | 4.464 | 4130 | 3.409 | 5828 | 2.273 |
| SD[d] | 29 | 0.49 | 33 | 0.133 | 113 | 0.055 | 141 | 0.059 |
| CV, % | 2.2 | 4.74 | 1.3 | 2.98 | 2.74 | 1.60 | 2.43 | 2.59 |
| Ratio to values in lines 2 & 4, % | 98.1 | 95.9 | 98.1 | 105.7 | 101.5 | 103.3 | 99.5 | 102.6 |

[a] Reasonable values of *r* can be obtained at these points only by assuming that they fall at one of the secondary minima; the experimental values of *s* are, however, less than the corresponding theoretical minimum values, although probably not by an amount exceeding the overall experimental error.

[b] No satisfactory value of *r*. In two concordant experiments *s* was about 3.5. Such a high value is incompatible with the theoretical curves as constructed in Fig. 5.

[c] Average omits values *a*.

[d] Standard deviation SD = $(\Sigma \bar{x}_i^2/N - \bar{x}^2)^{\frac{1}{2}}$, coefficient of variation CV = 100 SD/$\bar{x}$.

[e] Experimental curve departs systematically from theoretical at these points.

[f] Slight ripple of unexplained origin in extinction curve gives highly discrepant values of *s*, corresponding to particle size 3400–3800 A.

[g] These values unreliable. Anomalous concentration dependence.

[h] If the value 6095 is omitted, the average is 5789, 1.1% less than the electron microscope value.

TABLE VI

*Summary of Latex Radius and Concentration Values*

| Batch.... | LS-057-A | | 15N-8 | | LS-066-A | | LS-067 | |
|---|---|---|---|---|---|---|---|---|
| Method | $r$ | $c$ | $r$ | $c$ | $r$ | $c$ | $r$ | $c$ |
| EM$^a$ | 1320<br>±30 | | 2555<br>±35 | | 4070<br>±55 | | 5855<br>±? | |
| Phase contrast$^b$ | | | 2575<br>±16 | | 4050<br>±19 | | (5800<br>±24)$^c$ | |
| Dry wt. ($\mu$g./ml.) | | 10.77 | | 4.224 | | 3.301 | | 2.216 |
| $E/c$ (5600)$^d$ | 1200 | | 2510 | | 4100 | | 5800 | |
| $E/c$ (avg.)$^d$ | 1227<br>±23 | | 2537<br>±60 | | 4009<br>±167 | | 5841<br>±185 | |
| $s$ (5600)$^e$ | 1265 | 10.46 | 2523 | 4.474 | 4121 | 3.411 | 5728 | 2.232 |
| $s$ (avg.)$^e$ | 1295<br>±29 | 10.33<br>±0.49 | 2506<br>±33 | 4.464<br>±0.133 | 4130<br>±113 | 3.409<br>±0.005 | 5828<br>±141 | 2.273<br>±0.059 |
| $(\lambda_0)_y$(interp.) | | | | | 3803 | 3.275 | 5490 | 2.145 |
| $(\lambda_0)_y$, $s = 0$ | | | | | 3886 | 3.348 | 5627 | 2.191 |
| $E_y$ | | | | | 3850 | | 5703 | |

[a] Data of Bradford and Vanderhoff (17).

[b] Data of Kubitschek (33).

[c] Batch LS-067A.

[d] Table IV.

[e] Table V.

Figures following ± signs indicate standard deviations, except in case of phase contrast data, where they are standard errors.

### 5. *Experimental Slopes and Derived Values of Particle Size and Concentration*

The extinction data used in obtaining the results reported in Fig. 7 were also used in obtaining slopes $s$ (Eq. [11]) by the method of least squares, the procedure being the same as that described for the theoretical values of $s$. The results (Fig. 8) are compared with theoretical values for the particle sizes as determined by electron microscopy (17) and for particle refractive indices $m(\lambda)$ as calculated from the dispersion constants originally adopted prior to the work of Heller and Pugh (20) (see p. 312). Recalculation of a few isolated points with the revised values of $m(\lambda)$ showed that although the revision produced important changes in the values of $K(\lambda)$ and $[K/\alpha](\lambda)$ (*cf.* Fig. 3), the slopes $s$ were altered to the extent of only 0.02–0.07, an amount usually less than the uncertainty of the experimental values. The general agreement between experimental and theoretical values is very good, with occasional deviations such as the large one seen at 4300 A. for the latex of particle size 1320. This has been noted consistently in several experiments made with several modifications of the optical arrange-

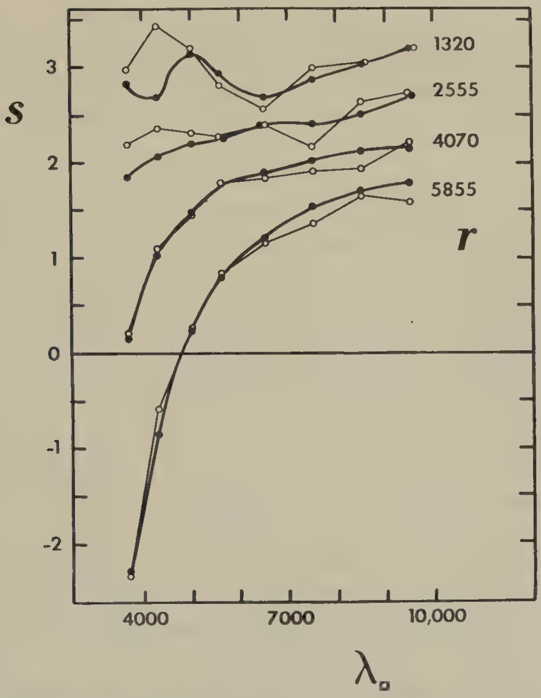

FIG. 8. Experimental and theoretical slopes, *s*, compared for four polystyrene latexes. Abscissa: wavelength in air. Ordinate: *s* (Eq. [11]). Parameter: particle radius by electron microscopy (17). Solid circles connected by heavy curve: theoretical. Open circles connected by thin straight lines: experimental.

ment. It will be noted that all the experimental values at this wavelength are higher than the theoretical, although to a diminishing extent as the particle size is increased.

The values of *s* reported in Fig. 8 were used to obtain particle size by interpolation on theoretical curves of the type shown in Fig. 5, followed by calculation of concentration by Eq. [13]. The results are given in Table V. With omission of certain values for reasons indicated in footnotes, the average radii agree with Bradford and Vanderhoff's values (17) to within 2%, and the concentrations agree with the dry weights to within $-4.1\%$ to $+5.7\%$.

## DISCUSSION

The foregoing is intended to show that with a simple adaptation of a commercial spectrophotometer and with adequate interpolation procedures for use with Mie theory tabulations, good agreement can be obtained between experimental and theoretical scattering parameters. With appropriate modifications in procedure the transmission method can thus be used for the determination of particle size and concentration, and it is shown how this can be accomplished by the extension of principles which have often been discussed but which have not hitherto been applied with the benefit of detailed theoretical data and strictly uniform test objects.

### *1. Instrumentation*

In their experimental examination of the validity of the Mie theory and of Lowan's calculations (27) based upon it, LaMer and colleagues (2, 3, 7) used both the Beckman and the Coleman spectrophotometers with success. Formal specifications for transmission instruments have been discussed elsewhere (13, 28–32). It only need be mentioned, therefore, that the inexpensive modification of the Beckman instrument described here seems adequate for suspensions with $m$ in the vicinity of 1.2 and particle diameters up to about 1 $\mu$. This conclusion refers to the uncorrected data; no calculation of correction factors—such as those derived by Sliepcevich *et al.* for the lens-pinhole optical transmission system (30–32)—has been attempted. Of the applicable sources of error discussed by Boll and Sliepcevich (32), it would seem that (*a*) the effect of divergence of the beam within the transmission cell has been minimized by use of a narrow pencil of light and several circular stops in the transmitted pencil; (*b*) the half angle of the cone of scattered light reaching the receiving lens, about 0.3°, is such as to lead to a maximum error of only about 0.02% in the extinction for a 1 $\mu$ particle at 3000 A.; (*c*) the effect of misalignment of the system may be significant for the larger particles and may be partly responsible for the fact that the values of $K_y$ calculated from extinction data for the 1.17 and 0.814 $\mu$ latexes were 2.7% and 6.0% higher, respectively, than the theoretical values. More reliable dispersion data are required, however, before these discrepancies can be finally judged to be instrumental in origin.

### *2. Experimental Values of Polystyrene Particle Size and Concentration*

For all four latexes examined it has been possible to derive values of particle radius from extinction measurements by calculating $E/c$, the ratio of extinction to particle concentration (Table IV). By making measurements from which the slope of log $E$ with respect to log $\lambda$ can be determined, both particle size and concentration can be found (Table V). When the values obtained by these two methods are assembled (Tables VI, VII) it becomes apparent that for three of the four latexes studied both methods give the same results whether applied at a single wavelength (5600 A.) or averaged over several wavelengths. Furthermore, these internally concordant values are also in agreement with those obtained by electron microscopy (17) to within 2%. In the exceptional case of the latex of smallest particle radius, 1320 A., the value obtained by the slope method agrees quite well with $r$(em) while the absolute extinctions are too small

TABLE VII

*Latex Particle Radii: Ratios of Results of Transmission and Electron Microscope Methods*

| Latex.... | LS-057-A | 15N-8 | LS-066-A | LS-067 |
|---|---|---|---|---|
| $r$(em).... | 1320 | 2555 | 4070 | 5855 |
| Method | $\bar{r}/r$(em) | | | |
| $E/c$ at 5600 A. | 0.909 | 0.982 | 1.007 | 0.991 |
| $E/c$ average | 0.930 | 0.984 | 0.992 | 1.003 |
| $s$ at 5600 A. | 0.958 | 0.987 | 1.013 | 0.978 |
| $s$ average | 0.981 | 0.981 | 1.015 | 0.995 |
| $(\lambda_0)_y$ interp. | | | 0.934 | 0.938 |
| $(\lambda_0)_y$, $s = 0$ | | | 0.955 | 0.961 |
| $E_y$ | | | 0.946 | 0.974 |

by some 8%—a discordance exceeding the limits of uncertainty of the concentration obtained from dry weights. Values of $r$ obtained from the position or height of the first principal maximum (Tables VI, VII) are less satisfactory, partly because both occur at wavelengths where some uncertainty of refractive index exists, partly because errors of alignment are possible, and perhaps partly because fine structure in the maximum renders it difficult to determine consistent theoretical values of $K_y$ and $\rho_y$ without resorting to dubious smoothing procedures (16).

The particle radii obtained by Tabibian, Heller, and Epel (14) at 5461 A. differ from $r$(em) by −7.2%–+7.0%. These authors include a value of $r$, 3825 A., for latex lot 066A, 6% smaller than Bradford and Vanderhoff's value 4070 A and 6%–8% smaller than ours (Tables VI, VII). In general it seems that the overall agreement between light transmission (this paper and reference 14) and electron microscopy is fairly satisfactory. Some justification for regarding the electron microscope values as definitive is provided by the agreement, to better than 1%, between these and the results of direct measurement of particle arrays by phase contrast microscopy; Kubitschek's values obtained in this way (33) are included in Table VI. The transmission values are probably about as reliable as those obtained by other indirect methods.

In the case of the well-known latex 580-9 lot 3584, which has received detailed study by several methods, unresolved discrepancies still exist, with the following percentage differences from the accepted electron microscope diameter of 2590 A. (34): sedimentation, −2.7% (35), light scattering, 5.0% (36), low-angle X-ray scattering 3.7% (37).

Concentrations determined simultaneously with $r$ from the slope $s$ and the corresponding values of $K$ appear to be reliable to within 3%–6% (Table V).

### *3. Verification of Mie Theory*

The general agreement between particle size obtained by direct measurement and from transmission data is not such as to permit us to subscribe without reservation to the contention already quoted (14) that the Mie theory is thereby conclusively proved, if by "proof" we mean the ability to predict any phenomena within the range of observation provided by available experimental methods. Proof in this sense, as far as the transmission method is concerned, would require quantitative agreement well within the amplitude of the "fine structure" ripples, as well as the demonstration that their observed positions and amplitudes are in agreement with theory. The present measurements go further than those of Tabibian, Heller, and Epel, in that they do cover a wide wavelength range and do show fine structure; however, these are imperfectly resolved in both the experimental and the theoretical data, and in at least one instance (Fig. 8) there are discrepancies as to their positions. At present the validity of the Mie theory rests upon the cumulative weight of many types of experimental data rather than upon any single example of extremely fine quantitative agreement.

### *4. Procedures for Characterizing Monodisperse Hydrosols*

The particle size can be determined by a single transmission measurement at a single wavelength provided particle concentration $c$ and relative refractive index $m$ are known. This case has been discussed by Tabibian, Heller and Epel (14), whose conclusions are fully confirmed in the present work. If particle size and concentration are both desired from transmission measurements, these can in principle be determined by measurements at two wavelengths at which values of $m$ are known accurately (38). This method has not been explored. An alternative, now shown to be feasible, consists in measuring transmission at a number of wavelengths, closely spaced on either side of a chosen median wavelength, sufficient to permit the precise determination of $s$ (equal to $-d \log E/d \log \lambda$), from which $r$ and $c$ can be found by the procedure already described. With perfect apparatus, a sufficiently accurate knowledge of $m(\lambda)$ and theoretical data sufficiently closely spaced to permit accurate interpolation, measurements in the vicinity of a single chosen wavelength are all that are needed. It is advisable in practice to obtain at least two values of $s$. One reason for this is presumably instrumental, manifested (Fig. 8) in occasional narrow regions of anomalous slope. These may, however, be partly due to imperfectly resolved subsidiary ripples in the theoretical $K(\lambda)$ curves. The fine structure shown in the calculated curves of Fig. 5 has been filled in partly by analogy and may be incomplete or locally erroneous. At cost of much labor the accuracy of these curves could probably be improved even when using the existing theoretical tabulations of $K(\alpha, m)$. However, data in which complete confidence might be placed could be obtained only if more extensive basic tabulations at smaller intervals of $m$ were available. Whether these would be justified in terms of their foreseeable practical usefulness is debatable. A further reason for obtaining values of $s$ at two or more wavelengths consists in the ambiguity of some values arising from the fine structure; for example, if $s$ were 3.2 at 3700 A., the particle radius (Fig. 3) might be 785 or 1072 A.

The transmission method is not, of course, necessarily the method of choice in all applications of light scattering to the characterization of colloids, nor is it always essential to have a detailed quantitative knowledge of the theoretical behavior. The work of LaMer and Plesner (39), for example, shows that the particle size of latex spheres can be determined quite accurately from the positions of the extrema of the Higher Order Tyndall Spectra provided specimens of known particle size are available for calibration. On the other hand, in the study of systems where the Mie theory is not strictly applicable by virtue of deviations from spherical shape, from uniformity of size, or from optical homogeneity, it may be necessary to combine some of the available procedures in order to obtain a consistent characterization of such systems in terms of "effective" values of the Mie theory parameters. Measurements of Higher Order Tyndall Spectra (3–5), polarization ratio (9, 40), phase angles (9), and angular dependence of scattered intensity (9, 36) have been made on several colloids and their mutual consistency has been demonstrated (3, 9).

Polydispersity has not been considered in the present work. One reason for believing, however, that greater resolution of fine structure will seldom be needed in practice is that most systems, even when the dispersed phase is homogeneous and unimodal, are likely to have size and shape distributions of much greater breadth than those of the remarkably uniform polystyrene latexes. Even a moderate broadening will smear out much of the fine structure and make possible the use of smoothed theoretical curves (41).

In some applications it will be desirable to consider particle refractive index as an additional unknown. Estimates of this can sometimes be obtained by varying the refractive index of the continuous phase, $n$, but this may be objectionable in biological hydrosols in which $n_p$ may be indirectly dependent upon $n$. The accuracy of estimates of $m$ obtained from pairs of values of $s$ at different wavelengths in conjunction with families of theoretical curves is now being studied and will be reported later.

## SUMMARY

Specific extinctions $E/c$ have been measured in the visible and long ultraviolet (3500–10000 A.) for four polystyrene latexes containing uniform spherical particles suspended in water, using a modified Beckman model

DU spectrophotometer. Methods were developed for making the interpolations required in calculating the Mie total scattering coefficients $K(\lambda)$ from published tabulations of $[K(\alpha)]_m$. The values so obtained were in good agreement with those calculated from extinction, dry weight, and particle radii determined in the electron microscope (17). In reversing the procedure, values of particle radius could be found from the experimental data which agreed very well (to $<1\%$ in 3 cases out of 4) with those determined by electron microscopy. In order to dispense with the need for independent concentration measurements, it was further shown that experimental slopes $s$, equal to $-(d \log E/d \log \lambda)$, agreed well with theoretical values equal to $d \log K/d \log \alpha$ (where $\alpha$ is the size parameter $2\pi r/\lambda$). Again reversing the procedure with the aid of suitable calibration curves $s(\log r)$ it was shown that particle size and concentration could both be determined from the experimental slope $s$, the former agreeing to better than 2% with the electron microscope values and the latter to better than 6% with the dry weights. Attention is drawn to the importance of the "fine structure" or presence of subsidiary extrema in the theoretical and experimental data $s(r)$ when characterizing highly uniform monodisperse suspensions of spheres by this method.

## ACKNOWLEDGMENTS

The authors are much indebted to Dr. Wilfried Heller of Wayne University for placing at their disposal, in advance of publication in any form, the pertinent tabulations since assembled in a volume by Pangonis, Heller, and Jacobson (15); and to Dr. H. E. Kubitschek of Argonne National Laboratory for permission to quote unpublished data. Acknowledgments are also extended to Dr. Rufus O. Howard for measurements preliminary to the present study. The polystyrene latexes were obtained through the courtesy of Dr. J. W. Vanderhoff, Dow Chemical Company.

## REFERENCES

1. MIE, G., *Ann. Physik* **25**, 377 (1908).
2. BARNES, M. D., AND LA MER, V. K., *J. Colloid Sci.* **1**, 79 (1946).
3. BARNES, M. D., KENYON, A. S., ZAISER, E. M., AND LA MER, V. K., *J. Colloid Sci.* **2**, 349 (1947).
4. KENYON, A. S., *Trans. N. Y. Acad. Sci.* **9**, 234 (1947).
5. JOHNSON, I., AND LA MER, V. K., *J. Am. Chem. Soc.* **69**, 1184 (1947).
6. LA MER, V. K., *J. Phys. & Colloid Chem.* **52**, 65 (1948).
7. ZAISER, E. M., AND LA MER, V. K., *J. Colloid Sci.* **3**, 571 (1948).
8. SINCLAIR, D., AND LA MER, V. K., *Chem. Revs.* **44**, 245 (1949).
9. KERKER, M., AND LA MER, V. K., *J. Am. Chem. Soc.* **72**, 3516 (1950).
10. LA MER, V. K., INN, E. C. Y., AND WILSON, I. B., *J. Colloid Sci.* **5**, 471 (1950).
11. HAWKSLEY, P. G. W., *Bull. Brit. Coal Utilisation Research Assoc.* **16**, 117, 181 (1952).
12. VAN DE HULST, H. C., "Light Scattering by Small Particles." Wiley, New York, 1957.
13. HELLER, W., AND TABIBIAN, R. M., *J. Colloid Sci.* **12**, 25 (1957).
14. TABIBIAN, R. M., HELLER, W., AND EPEL, J. N., *J. Colloid Sci.* **11**, 195 (1956).

15. Pangonis, W. J., Heller, W., and Jacobson, M., "Tables of Scattering Functions for Spherical Particles." Wayne State University Press, Detroit, Michigan, 1957.
16. Penndorf, R. B., "New Tables of Mie Scattering Functions for Spherical Particles, Part 6: Total Mie Scattering Coefficients for Real Refractive Indices." Geophysical Research Paper No. 45 Geophysics Research Directorate, Air Force Cambridge Research Center, Bedford, Massachusetts, March 1956.
17. Bradford, E. B., and Vanderhoff, J. W., *J. Appl. Phys.* **26**, 864 (1955).
18. Kaye, G. W. C., and Laby, T. H. "Physical and Chemical Constants," 11th ed. Longman's Green, London, 1956.
19. Starkie, D., *Brit. Plastics* **19**, 46 (1947).
20. Heller, W., and Pugh, T. L., *J. Colloid Sci.* **12**, 294 (1957).
21. Pugh, T. L., and Heller, W., *J. Colloid Sci.* **12**, 173 (1957).
22. Devore, J. R., and Pfund, A. H., *J. Opt. Soc. Amer.* **37**, 826 (1947).
23. Paul, W., and Jones, R. V., *Nature* **168**, 554 (1951).
24. Doty, P., and Steiner, R. F., *J. Chem. Phys.* **18**, 1211 (1950).
25. Billmeyer, F. W., *J. Am. Chem. Soc.* **76**, 4636 (1954).
26. Gibson, K. S., and Balcom, M. M., *J. Research Natl. Bur. Standards* **38**, 601 (1947).
27. Lowan, A. N., "Tables of Scattering Functions for Spherical Particles." Department of Commerce, National Bureau of Standards, Applied Mathematics Series 4 (1949).
28. Rose, H. E., "Measurement of Particle Size in Very Fine Powders." Chemical Publishing Co., New York, 1954.
29. Lewis, P. C., and Lothian, G. F., *Brit. J. Appl. Phys.* **5**, S71 (1954).
30. Gumprecht, R. O., and Sliepcevich, C. M., *J. Phys. Chem.* **57**, 90 (1953).
31. Gumprecht, R. O., and Sliepcevich, C. M., *J. Phys. Chem.* **57**, 95 (1953).
32. Boll, R. H., and Sliepcevich, C. M., *J. Opt. Soc. Amer.* **46**, 200 (1956).
33. Kubitschek, H. E., Private communication, February 28 and September 4, 1958.
34. Gerould, C. H., *J. Appl. Phys.* **21**, 183 (1950).
35. Sharp, D. G., *J. Appl. Phys.* **21**, 71 (1950).
36. Dandliker, W. B., *J. Am. Chem. Soc.* **72**, 5110 (1950).
37. Danielson, W. E., Shenfil, L., and Du Mond, J. W. M., *J. Appl. Phys.* **23**, 860 (1952).
38. Evva, F., *Kolloid-Z.* **133**, 79 (1953).
39. La Mer, V. K., and Plesner, I. W., *J. Polymer Sci.* **24**, 147 (1957).
40. Kerker, M., Jones, G. L. Jr., Reed, J. B., Yang, C. N. P., and Schoenberg, M. D., *J. Phys. Chem.* **58**, 1147 (1954).
41. Boll, R. H., Gumprecht, R. O., and Sliepcevich, C. M., *J. Opt. Soc. Amer.* **44**, 18 (1954).

JOURNAL OF COLLOID SCIENCE **14**, 330–337 (1959)

# STREAMING CURRENTS WITH NONAQUEOUS SOLUTIONS

**A. J. Rutgers, M. De Smet, and W. Rigole**

*Laboratory of Physical Chemistry, University Ghent, Belgium*

*Received October 17, 1958, revised March 2, 1959*

## ABSTRACT

Streaming currents have been measured in benzene solutions of tetraisoamyl ammonium picrate between $10^{-7}$ and $10^{-3}$ mole/l. in long capillaries of various widths and wide capillaries of various lengths. A considerable influence of width and length was found. High $\zeta$-values ($-280$ mv.) were obtained at low concentrations. The corresponding theory is developed; over the length of a glass capillary an electrostatic potential $V(x)$ develops, which shows resemblance to a catenary; measurements confirmed the theoretical expectation.

## INTRODUCTION

A few years ago we published (1) $\zeta$-values for solutions of (iso-$C_5H_{11})_4$N-picrate ("tiap") in dioxane, in mixtures of dioxane and water, in benzene, and in mixtures of benzene and acetone.

The experimental procedure consisted in the measurement of the electro-osmotic speed or the streaming current (S.C.) of the solution in a capillary system; this consisted essentially of a system of closely fitting glass rings, length 1 cm., width of the slits 0.005 cm. (50 $\mu$). The choice of this system was determined by the wish to have an apparatus of great sensitivity. The results obtained in benzene solution are shown in Fig. 1.

Recent work has indicated that the experimental method might have given wrong results for solutions of extremely low conductivity.

*a.* For very dilute solutions, the width of the slits was smaller than the thickness, $\delta$, of the double layer, which follows from our experiments in turbulent flow (2); in this case the S.C. becomes smaller than the value derived from Eq. [1].

*b.* For very dilute solutions, the length of the slits was shorter than the characteristic length $\bar{v}\tau$, where $\bar{v}$ is the average speed, and $\tau = D/4\pi\sigma$ the relaxation time of the liquid; in this case the S.C. becomes also smaller than the value given by Eq. [1], as has been pointed out by Schön (3) and by Klinkenberg and van der Minne (4).

## EXPERIMENTAL

We have measured streaming currents in benzene solutions of "tiap" at concentrations of 0, 0.1, 0.2, 0.5, 1, 5, 10, 50, 100, 500, and 1000 $\mu$moles/l.

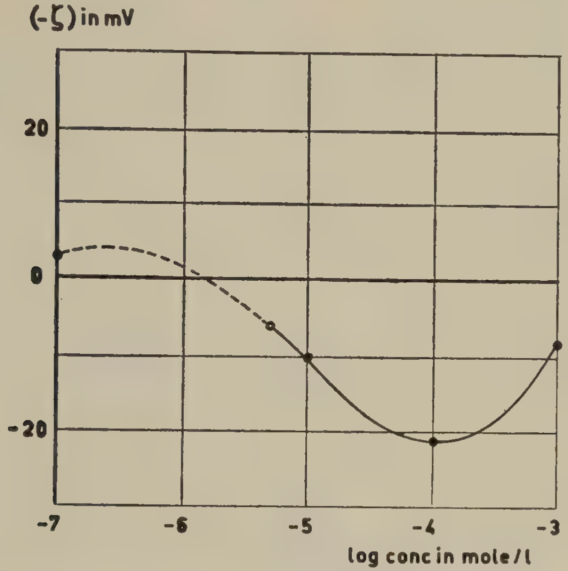

FIG. 1. The variation of ζ-potential with concentration for "tiap" in benzene.

*a.* in long capillaries (length = 100 cm.) of various radii: 0.188, 0.126, 0.0546, 0.0213 cm.;

*b.* in wide capillaries (radius = 0.126 cm.) of various lengths: 101.3, 24.8, 5.0 cm.;

*c.* also in a cylindric slit and in the old ring system.

Turbulence may occur; in this case, the S.C. increases with pressure in a nonlinear way.

In our experiments, two 5-liter vessels were connected by the capillary; the electrodes were placed very close to the ends of the capillary. We had some doubts as to whether they picked up the S.C. effectively; therefore the vessels were wrapped in tin foil and each foil was connected to its electrode. In another experiment a platinum tube was shoved inside the glass tube containing the electrode and connected to the electrode. All these measures had practically no influence upon the S.C.

The S.C., of the order of $10^{-13}$–$10^{-11}$ Amp., was measured by its potential drop over a known resistance, with a Lemouzy electronic voltmeter or with a Vibron electrometer.

## RESULTS

### *a. S.C. in Long Capillaries of Various Widths*

The S.C. were plotted as a function of pressure. About one hundred of such *I-p* curves were obtained; they are satisfactorily smooth, but at low

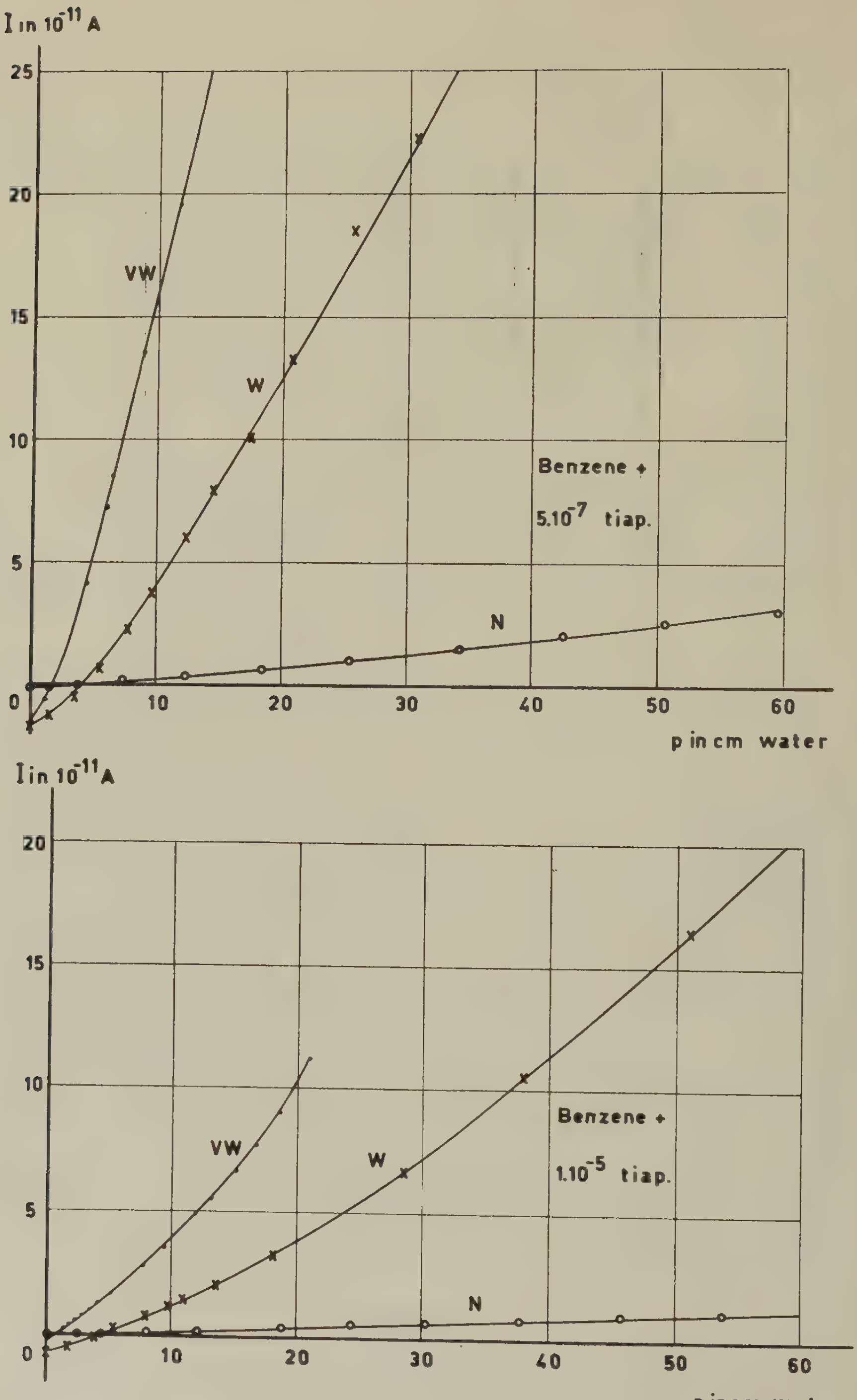

FIG. 2. Streaming current versus pressure for long capillaries (length 100 cm.).
VW, radius = 0.188 cm.
W, radius = 0.126 cm.
N, radius = 0.0546 cm.

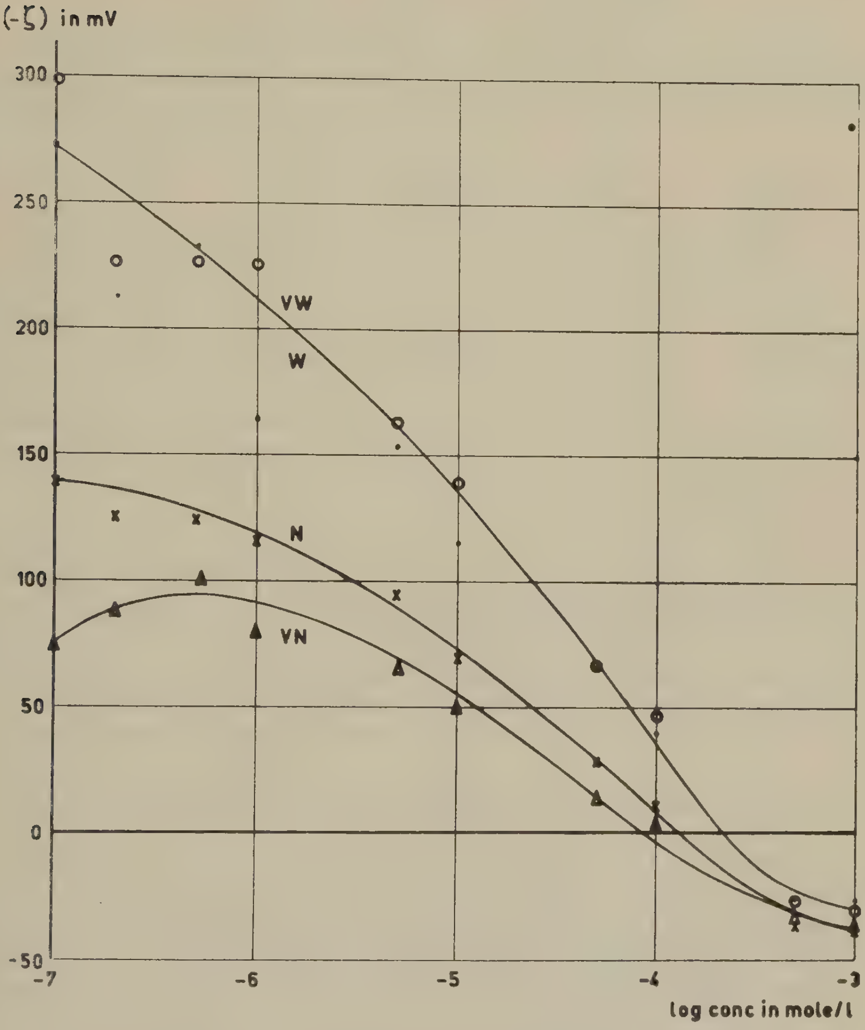

FIG. 3. Apparent ζ-values in long capillaries (length 100 cm.).
VW, radius = 0.188 cm.
W, radius = 0.126 cm.
N, radius = 0.0546 cm.
VN, radius = 0.0213 cm.

concentration they show a bend; at higher concentration this bend shifts to higher pressures (fig. 2). We attributed this behavior to the occurrence of turbulence; then the ζ-values must be derived from the low-pressure part of the curve. The ζ-values, thus obtained by means of the formula

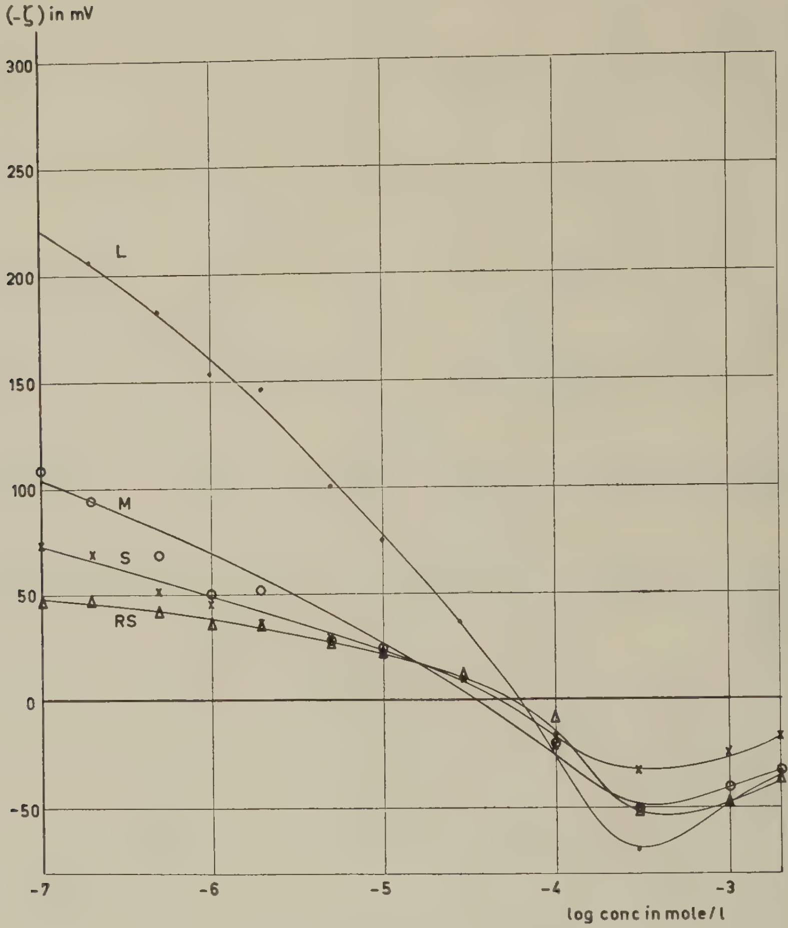

FIG. 4. Apparent ζ-values in wide capillaries (radius 0.126 cm.).
L, length = 101.3 cm.
M, length = 24.8 cm.
S, length = 5.0 cm.
RS, ring system used in previous work.

$$I_{\text{s.c.}} = D\zeta v_{\text{axis}} = 2D\zeta\bar{v}, \qquad [1]$$

are shown in Fig. 3. They agree mutually at higher concentrations; here they also agree with the old ring system measurements. At low concentrations the curves diverge; the narrow capillaries yield depressed ζ-values; this indicates that here $\delta > r$, and that Eq. [2] should be used. The high ζ-values (−280 mv.) obtained at low concentrations in wide capillaries are especially interesting.

### *b. S.C. in Wide Capillaries of Various Lengths*

The $\zeta$-values, obtained again with the aid of Eq. [1], are represented in Fig. 4; here again we have agreement at high concentrations, divergence at low concentrations (where $\bar{v}\tau > l$).

## THEORETICAL

### *a. Influence of the Thickness of the Double Layer*

If $\delta \gg r$, we have

$$I_{\text{S.C.}} = 2\pi r \frac{D\zeta}{4\pi\delta} \bar{v} = 2D\zeta\bar{v} \frac{r}{4\delta}. \qquad [2]$$

Here we have assumed that the surface charge/cm.$^2$ is the same in a wide and in a narrow capillary.

### *b. Influence of the Length of the Capillary (cf. 3, 4)*

The theory is presented in the following scheme; its left-hand side contains the theory given by Klinkenberg and van der Minne for a metal capillary; its right-hand side contains the theory for a glass capillary (of nonvanishing conductivity). In this scheme $q$ is the charge per centimeter of the liquid, $q_0$ is the value of $q$ when the liquid is at rest, $\bar{v}$ is the average speed of the charge particles, given by

$$q\bar{v} = \int_0^{r_1} 2\pi r\rho(r)v(r)\, dr,$$

$r_1$ being the inner, $r_2$ the outer capillary radius; $E_x$ is the axial component of the electric field, $E_r$ its radial component, $E_{0r}$ the radial component when the liquid is at rest; then the radial current/cm. is $2\pi r_1\sigma_l E_{0r}$ and the diffusion currents from the wall cancel out; therefore the net radial current/cm. is $2\pi r_1\sigma_l(E_r - E_{0r})$.

In the metal capillary, the liquid flows out freely at $x = l$; hence $I_w(l) = 0$. In the glass capillary measurements, the electrodes in the two vessels are connected by the measurement apparatus, and therefore at the same potential; hence

$$\int_0^l E_x\, dx = 0.$$

The field $E_x$ is assumed to be the same in the glass wall and in the liquid inside the glass capillary.

| | Metal Capillary | Glass Capillary |
|---|---|---|
| | 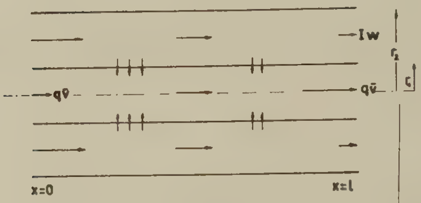 | 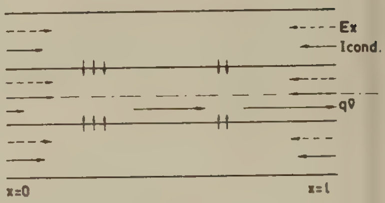 |
| $I$ | $I = q\bar{v} + I_w$ | $I = q\bar{v} + \beta E_x$<br>$\left[\beta = \pi r_1^2\sigma_l + \pi(r_2^2 - r_1^2)\,\sigma_{gl} = \frac{l}{R}\right]$ |
| Charge in liquid stat. (S) | $\bar{v}\,\frac{dq}{dx} + 2\pi r_1\,\sigma_l(E_r - E_{0,\,r}) = 0$ | $\bar{v}\,\frac{dq}{dx} + 2\pi r_1\,\sigma_l(E_r - E_{0,\,r})$<br>$+ \pi r_1^2\sigma_l\,\frac{dE_x}{dx} = 0$ |
| Poisson (P) | $2\pi r_1(E_r - E_{0,\,r}) = \frac{4\pi}{D}\,(q - q_0)$ | $2\pi r_1(E_r - E_{0,\,r}) + \pi r_1^2\,\frac{dE_x}{dx} = \frac{4\pi}{D}\,(q - q_0$ |
| From (S) and (P) (Q) | $\frac{dq}{dx} + \frac{1}{\bar{v}\tau}\,(q - q_0) = 0$ | |
| Integration, and $q = 0$ at $x = 0$ | $q = q_0(1 - e^{-x/\bar{v}\tau})$ | |
| Current $q_0\bar{v} = I_0$ | $I = I_0(1 - e^{-x/\bar{v}\tau}) + I_w$ | $I = I_0(1 - e^{-x/\bar{v}\tau}) + \beta E_x$ |
| Boundary Condition | $I_w(l) = 0$; hence $I = I_0(1 - e^{-l/\bar{v}\tau})$ | $\int_0^l E_x\,dx = 0$; hence<br>$I = I_0\left\{1 - \frac{\bar{v}\tau}{l}\,(1 - e^{-l/\bar{v}\tau})\right\}$ |
| $E_x$ | | $E_x = \frac{I_0}{\beta}\left\{e^{-x/\bar{v}\tau} - \frac{\bar{v}\tau}{l}\,(1 - e^{-l/\bar{v}\tau})\right\}$ |
| $V(x) = -\int_0^x E_x\,dx$ | | $V(x) = \frac{I_0\,\bar{v}\tau}{\beta}$<br>$\left\{\frac{x}{l}\,(1 - e^{-l/\bar{v}\tau}) - (1 - e^{-x/\bar{v}\tau})\right\}$ |

This function $V(x)$ resembles a catenary, with a minimum at $x = l/2$ if $l/\bar{v}\tau$ is small. For a glass capillary, filled with pure benzene, the value of $V$ at this minimum is calculated at a few hundred volts. Recent measurements carried out with an electrostatic voltmeter have given $V(x)$-curves of the expected shape.

## REFERENCES

1. RUTGERS, A. J., AND DE SMET, M., *Trans. Faraday Soc.* **48**, 635 (1952).
2. RUTGERS, A. J., DE SMET, M., AND DE MOYER, G., *Trans. Faraday Soc.* **53**, 393 (1957).
3. SCHÖN, G., in B. Hampel and H. Luther, *Chem.-Ing.-Tech.* **29** (No. 5), 323 (1957).
4. KLINKENBERG, A., AND VAN DER MINNE, J. L., "Electrostatics in the Petroleum Industry," Elsevier, Amsterdam, 1958.

JOURNAL OF COLLOID SCIENCE **14**, 338–342 (1959)

# THE INFLUENCE OF ULTRASONIC WAVES ON SILVER HYDROSOL

**Satya Prakash and Ashim Kumar Ghosh**

*Chemical Laboratories, University of Allahabad, India*

*Received October 20, 1958*

## Abstract

Silver hydrosol prepared by Voigt and Heumann's method was exposed to ultrasonic waves at a frequency of 1 megacycle per second and power of 225 watts per square centimeter. The original yellow color of the sol slowly disappeared leaving behind a colorless solution. It is concluded from the present investigation that a chemical reaction takes place when colloidal silver is exposed to ultrasonic waves. The particles of silver go into the solution state, forming silver ions; $Ag \rightarrow Ag^{+} + \ominus$. The change is of the first order.

## Introduction

The previous work on this subject is of Urazovskii and Polotskii (1), J. P. Causse (2), and the present authors (3, 4).

We are recording our results on the influence of the ultrasonic waves on silver hydrosol. The ultrasonic power was obtained from Mullard's high-frequency ultrasonic generator, type E. 7562.

## Experimental

The sol was prepared by the method suggested by Voigt and Heumann (5). Silver oxide was precipitated from a solution of silver nitrate by adding caustic soda solution. The precipitated oxide was washed thoroughly until free from all ions. It was treated with boiling water, when a small concentration of it went into the solution. This was filtered hot (100°C.) several times to ensure that no suspended particles of silver oxide were left behind. To 50 ml. of this solution were added a small quantity of 0.18 *N* sodium carbonate solution and 0.5 ml. of a formaldehyde solution containing 2 ml. of formaldehyde in 100 ml. of water. The mixture was heated rapidly to 50°–60°C. until a yellow sol was obtained. The heating was continued for an hour to obtain a stable sol. It was further evaporated to get a concentrated sol. The sol contained 0.0968 g. of silver per liter.

A constant volume of the sol was exposed each time to ultrasonic waves at a frequency of 1 Mc/s (megacycle per second) and power of 225 watts per square centimeter. The fading of color was very apparent. The con-

TABLE I

*Effect of Ultrasonic Waves on Silver Hydrosol*

Temperature = 25°C.

Viscosity of water = 1.00000

| Exposure (*minutes*) | Color (visual) | pH | Sp. cond. × $10^4$ ($ohm^{-1}$ $cm.^{-1}$) | Viscosity |
|---|---|---|---|---|
| 0 | Yellow | 6.9 | 0.67 | 1.00659 |
| 30 | Yellow | 6.8 | 0.79 | — |
| 60 | Yellow | 6.7 | 1.16 | 1.00439 |
| 90 | Faint yellow | 6.6 | 1.28 | — |
| 120 | Faint yellow | 6.5 | 1.47 | 1.00391 |
| 150 | Very faint yellow | 6.1 | 1.65 | — |
| 180 | Almost colorless | 4.5 | 2.20 | 1.00210 |
| 210 | Almost colorless | 4.0 | 3.06 | — |
| 240 | Colorless | 3.3 | 3.86 | 1.00191 |
| 270 | — | 3.2 | 4.65 | — |

ductivity and pH values were found to increase and the viscosity to decrease as the fading continued. The change in pH values slowed down as the sol became more and more colorless (Table I).

All the results recorded above showed that probably the silver was going into solution as silver ions. In principle any reaction which involves the transference of electrons is capable of providing an electrode. The electrode reaction will be represented by

$$\text{M} \rightleftharpoons \text{M}^{z+} + \text{Ze}$$

where $M$ is a pure metal of valence $Z+$ in contact with a solution of $M^{z+}$ ions.

The electrode potential will be given by

$$E_M = E_M + \frac{RT}{ZF} \log \frac{A_{M^{z+}}}{A_M}$$

where $A_{M^{z+}}$ and $A_M$ are the activities of $M^{z+}$ and $M$, respectively.

If this were the case it was very likely that the potential of the colloidal solution should increase as a result of the exposure's causing silver to change to silver ion. The following electrode was therefore set up:

$$\underset{\text{Anode}}{\overset{+}{\text{Hg}}} \;\Big|\; \text{Hg}_2\text{Cl}_2\ 0.1\ N\ \text{KCl} \;\vdots\vdots\; \begin{matrix}\text{Saturated}\\ \text{NH}_4\text{NO}_3\end{matrix} \;\vdots\vdots\; \begin{matrix}\text{Ag sol}\\ \text{containing}\\ \text{Ag}^+ \text{ ions}\end{matrix} \;\Big|\; \underset{\text{Cathode}}{\overset{-}{\text{Ag}}}$$

If $E$ be the potential difference between these electrodes and $E_1$ the po-

TABLE II

*Potential of Ag/Ag⁺ Half-Cell at 25°C.*

| Exposure (*minutes*) | 1st set potential (*volts*) | 2nd set potential (*volts*) |
|---|---|---|
| 0 | 0.2365 | 0.2360 |
| 30 | 0.2410 | 0.2400 |
| 60 | 0.2809 | 0.2421 |
| 90 | 0.2906 | 0.2752 |
| 120 | 0.3001 | 0.2911 |
| 150 | 0.3050 | 0.3054 |
| 180 | 0.3052 | 0.3056 |
| 210 | 0.3054 | 0.3057 |
| 240 | 0.3055 | 0.3059 |
| 270 | 0.3055 | 0.3059 |

tential of the calomel half-cell which is 0.336 volt at 25°C., then the potential $E_2$ of the Ag/Ag$^+$ half-cell will be

$$E_2 = E_1 - E.$$

As was expected the potential of the colloidal solution increased, showing a tenfold increase in silver ion activity with exposure, and became constant after a certain period, when the color of the sol entirely disappeared (Table II).

### *Kinetics of the Reaction*

The sol prepared by the method described was transparent to the transmitted light, and therefore the fading of color could easily be studied with a colorimeter and its kinetics determined. A green filter having a range be-

TABLE III

*Changes in Optical Density*

| Exposure (*minutes*) | Optical density | Concentration $(a - x)$ (*gm/l*) |
|---|---|---|
| 0 | 0.668 | 0.0968 $(= a)$ |
| 30 | 0.561 | 0.0812 |
| 60 | 0.490 | 0.0710 |
| 90 | 0.420 | 0.0608 |
| 120 | 0.300 | 0.0434 |
| 150 | 0.212 | 0.0307 |
| 180 | 0.123 | 0.0178 |
| 210 | 0.083 | 0.0120 |
| 240 | 0.049 | 0.0071 |
| 270 | 0.028 | 0.0040 |
| 300 | 0.012 | 0.0017 |

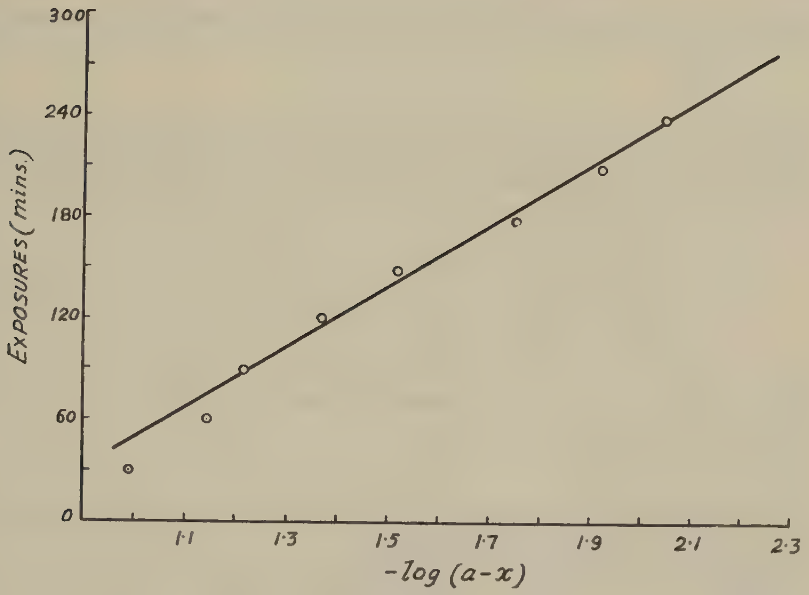

Fig. 1

tween 540 and 590 m$\mu$ was found to be suitable. The changes in optical densities are recorded in Table III. The measurements were made with a Klett-Summerson photoelectric colorimeter. The solution was taken in a tube of 1 cm. diameter. The concentration was taken proportional to optical density, and on this basis the values of $(a - x)$ in Table III were calculated. The value for $a$ has been determined gravimetrically. A plot of exposure time against log $(a\text{-}x)$ is shown in Fig. 1. The slope is found to be linear, showing that the reaction is of the first order.

## Discussion

From the foregoing results it appears that a chemical reaction takes place in which the metallic particles of silver are converted into silver ions, and the order of the change is unity.

$$Ag \rightarrow Ag^+ + \ominus.$$

This process is facilitated by the solvent action of hydrogen peroxide which is formed during the exposure. The quantity of hydrogen peroxide produced during the exposure is very small and most likely it is insufficient to account for the changes observed and also for the speed with which the reaction proceeds. This would suggest that the reaction is induced by the activation of oxygen. The preliminary step is the rupture of the water molecule by the absorption of 118 kcal. per gram mole of energy supplied by the waves.

$$HOH \rightarrow H^* + OH^*.$$

The H and OH radicals thus formed are in an activated state (as indicated by asterisks). The dissolved oxygen also gets activated by the cavitation process. The dissolution of silver may take place as follows:

$$\text{(i)}\ Ag + OH^* \rightarrow AgOH^* \rightarrow Ag^* + OH^-$$
$$\text{(ii)}\ O_2 \rightarrow 2O^*$$
$$\text{(iii)}\ O^* + H_2O + 2Ag \rightarrow 2AgOH^* \rightarrow 2Ag^+ + 2OH^-$$

## ACKNOWLEDGMENT

The authors are grateful to the Scientific Research Committee, Uttar Pradesh, for the award of a grant for this work.

## REFERENCES

1. URAZOVSKII, S. S., AND POLOTSKII, I. G., *Colloid J. (U.S.S.R.)* **6**, 779 (1940).
2. CAUSSE, J. P., *Compt. rend.* **230**, 826 (1950).
3. PRAKASH, S., AND GHOSH, A. K., *Kolloid-Z.* **151**, 72 (1957).
4. PRAKASH, S. AND GHOSH, A. K., *Kolloid-Z.* **158**, 33 (1958).
5. VOIGT, J., AND HEUMANN, J., *Z. anorg. u. allgem. Chem.* **169**, 140 (1928).

JOURNAL OF COLLOID SCIENCE **14**, 343–353 (1959)

# VISCOSITY-TEMPERATURE RELATIONSHIPS FOR DILUTE SOLUTIONS OF CELLULOSE DERIVATIVES

## II. Intrinsic Viscosities of Ethyl Cellulose

**W. R. Moore and A. M. Brown**

*Polymer Research Laboratories, Department of Chemical Technology,*
*Institute of Technology, Bradford, England.*

*Received December 29, 1958*

## ABSTRACT

Temperature variations of intrinsic viscosities and some other viscosity parameters for ethyl cellulose fractions in representative solvents are considered in terms of some current hydrodynamic and thermodynamic treatments of the viscosities of dilute polymer solutions. The value of $[\eta]$ decreases strongly with increasing temperature, the dependence being approximately linear. The temperature coefficient of $[\eta]$ appears to be linearly related to the molecular weight of the polymer. Except in the case of chloroform, in which aggregation of polymer may occur, values of the exponent $a$ in the expression $[\eta] = KM^a$ decrease slightly with increase of temperature suggesting decreasing chain extension. Values of the Porod-Kratky persistence length $q$, the Kirkwood-Riseman effective bond length $b$, and the angle between successive bond planes in the polymer chains suggest decreasing chain stiffness as the temperature increases. The Flory treatment is applied to obtain qualitative information regarding the contributions of different factors to the negative temperature coefficients of $[\eta]$, suggesting that these are primarily due to decreases in the value of $(\bar{r}_0^2M)$, where $\bar{r}_0^2$ is the mean-square unperturbed end-to-end distance of the chains and $M$ the molecular weight. The variations of $[\eta]$ and its temperature coefficient with solvent are briefly discussed.

## INTRODUCTION

In a previous communication (1) we discussed the temperature dependence of viscosities of dilute solutions of ethyl cellulose in terms of the variations of the quantities $Q$ and $A$, in the relationship $\eta = Ae^{Q/RT}$, with molecular weight $M$ and concentration $c$ of polymer. An alternative approach is the consideration of intrinsic viscosity, $[\eta]$, in terms of hydrodynamic theories applicable to dilute polymer solutions (2–5). These permit, at least in principle, the calculation from $[\eta]$ of parameters belonging to definite models of the polymer chains. Most theories assume considerable chain flexibility and coiling—assumptions unlikely to hold for cellulose derivatives, the chains of which are stiff and may assume the character of random coils only at high molecular weights. Porod (6) and Kratky (7) have suggested a "wormlike" chain, more generally applicable to stiff chains, which is characterized by a stiffness parameter, the "persistence length" $q$. This is defined as the mean value of the projection of an infinitely long chain along the direction of the first element in the chain. The Kirkwood-Riseman theory (5) may perhaps be more generally applicable to cellulose derivatives than other theories assuming relatively considerable coiling (8). This theory permits estimation of the effective bond length $b$, or mean length of the statistically independent units of the chain, from $[\eta]$ and a value of the exponent $a$ in the relationship $[\eta] = KM^a$. The angle between successive bond planes in the chain, $\psi$, may also be estimated. The quantities $q$, $b$, and $\psi$ are all measures of chain stiffness, and the exponent $a$ may be related, at least qualitatively, to chain configuration. The variations of these parameters with temperature should therefore provide information regarding the temperature dependence of chain configuration and stiffness.

Hydrodynamic theories, as Flory (9) has pointed out, do not consider interaction between remotely connected elements in the same chain as a result of which a certain volume is excluded from occupation by other parts of the chain and $\bar{r}^2$, the mean-square end-to-end distance of the chain, is increased. Chain configuration will also depend on polymer-solvent interaction, extended forms being favored in good solvents and contracted forms in poor solvents. In a sufficiently poor solvent attraction between distant chain elements may exactly compensate the effects of volume exclusion and the chains will adopt a so-called unperturbed configuration with mean-square end-to-end distance $\bar{r}_0^2$. Under all other conditions $\bar{r}_0^2$ will be increased by a factor $\alpha^3$ and the Flory treatment leads to

$$[\eta] = \Phi(\bar{r}^2)^{3/2}/M \qquad [1a]$$

or

$$[\eta] = \Phi(\bar{r}_0^2/M)^{3/2}M^{1/2}\alpha^3, \qquad [1b]$$

where $\Phi$ is a constant.

For this equation to hold the coiling of the chains should be such as to ensure approach to a spherically symmetrical form and the internal hydrodynamic resistance be large enough for $\Phi$ to attain its limiting value of *ca.* $2 \times 10^{21}$. These requirements are unlikely to be met by cellulose derivatives with $M$ less than several hundred thousand (10, 11). In spite of this, useful qualitative information has been obtained by application of the Flory treatment to cellulose derivatives (10–14). Flory, Spurr, and Carpenter (11) have used a modified form of Eq. [1$b$]:

$$[\eta] = \{\Phi\}\ (\bar{r}_0^2/M)^{3/2}M^{1/2}\alpha^3 \qquad [2]$$

to interpret temperature coefficients of intrinsic viscosities of cellulose acetates and trinitrate. Here $\{\Phi\}$ is less than the limiting value $\Phi$ and increases with both increasing temperature and $M$.

## EXPERIMENTAL

Characteristics of the six fractions used, covering the molecular weight range 40,000–140,000, have been given previously (1, 15). The solvents used were ethyl methyl ketone, ethyl acetate, butyl acetate, benzene, chloroform, and nitroethane. Their purification and the preparation and storage of solutions have also been previously described (1, 15). Viscosities of the solvents and of solutions in the concentration range 0.1–0.4 g./dl. were determined using capillary viscometers at temperatures from 25° to 60°C., in steps of 7°, except in the case of chloroform, where the highest temperature was 53°C. Temperatures were controlled to ±.05°. Kinetic energy corrections were made where applicable. Intrinsic viscosities were obtained by extrapolation of linear plots of log $(\eta_{sp}/c)$ against $c$ to zero $c$, using the method of least squares. Concentrations were appropriately corrected for thermal expansion. Only the four lowest fractions were soluble in nitroethane.

## RESULTS

Figures 1 and 2 show plots of $\eta_{sp}/c$ against $c$ for the fractions of highest and lowest molecular weight used in each solvent at the highest and lowest

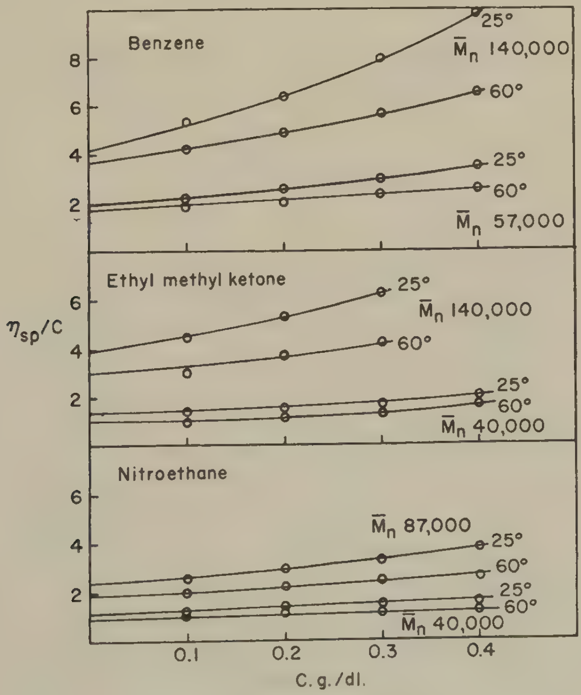

FIG. 1. Plots of $\eta_{sp}/c$ vs. $c$.

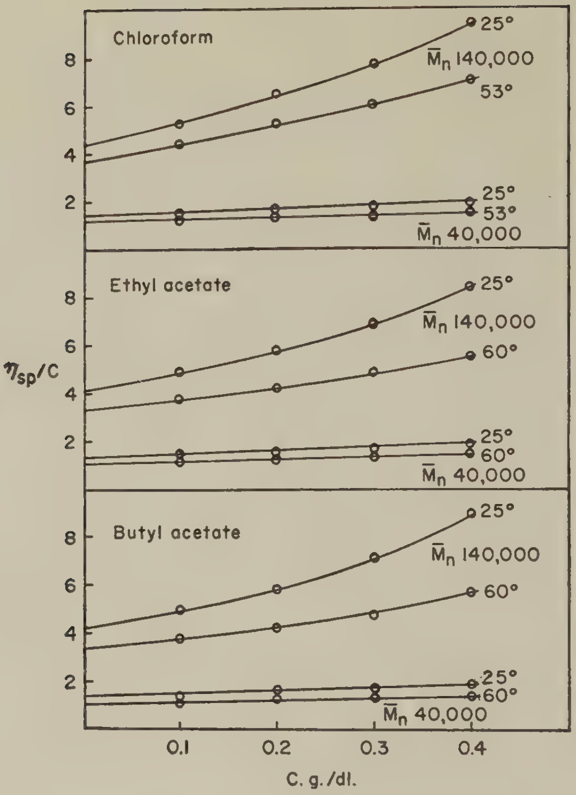

FIG. 2. Plots of $\eta_{sp}/c$ vs. $c$.

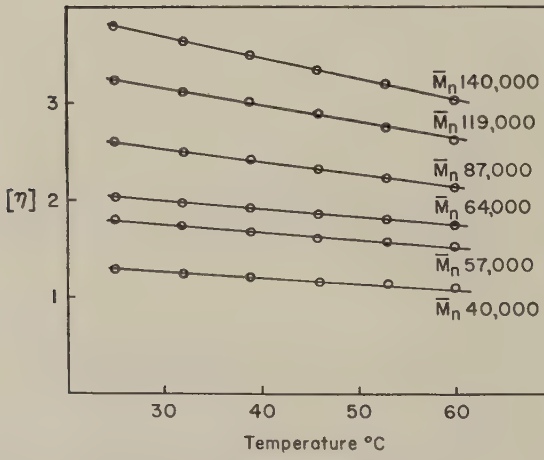

FIG. 3. Intrinsic viscosities in ethyl methyl ketone as a function of temperature.

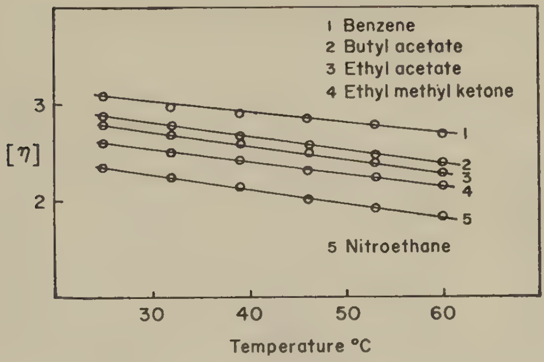

FIG. 4. Intrinsic viscosities for fraction of $\bar{M}_n$ 87,000 as functions of temperature.

TABLE I

*Temperature Coefficients of* [η]

| Solvent | $-d[\eta]/dT \times 10^2$ | | | | | |
|---|---|---|---|---|---|---|
| | $\bar{M}_n$ | | | | | |
| | 140,000 | 119,000 | 87,000 | 64,000 | 57,000 | 40,000 |
| Ethyl methyl ketone | 2.10 | 1.70 | 1.26 | 0.91 | 0.77 | 0.54 |
| Ethyl acetate | 2.23 | 1.71 | 1.37 | | 0.86 | 0.51 |
| Butyl acetate | 2.40 | 2.03 | 1.43 | 1.09 | 0.89 | 0.63 |
| Benzene | 1.69 | 1.37 | 1.09 | 0.94 | 0.69 | |
| Chloroform | 2.22 | 2.00 | 1.43 | 1.39 | 1.11 | 0.71 |
| Nitroethane | | | 1.49 | 0.71 | 0.60 | 0.45 |

temperatures. These are typical of results obtained with other fractions at other temperatures. The initial slopes and upward curvatures of the plots decrease with increasing temperature. Intrinsic viscosities of the fractions in ethyl methyl ketone are plotted against temperature in Fig. 3. An approximately linear dependence of [η] on temperature was obtained for the fractions in the other solvents and is further illustrated in Fig. 4, where [η] for the fraction of $\bar{M}_n$ 87,000 is plotted against temperature. The plot for chloroform is similar to that for benzene and is omitted for the sake of clarity. This dependence of [η] on temperature is not incompatible with the dependence on the reciprocal of absolute temperature previously reported (1), as the differences between the reciprocals do not differ greatly.

Temperature coefficients of [η] are collected in Table I. In common with those for other cellulose drivatives (11, 14, 16, 17) they are strongly negative and much larger than those observed with more flexible and less polar polymers. For a given fraction, excluding the highest, $-d[\eta]/dT$ tends to

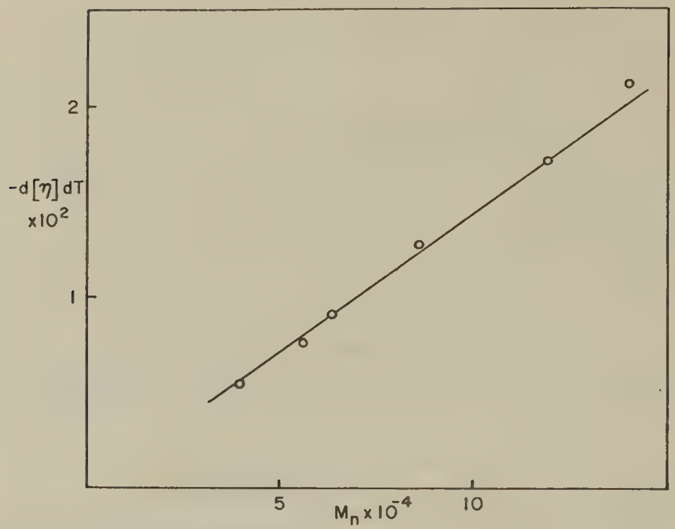

FIG. 5. Temperature coefficient of [η] in ethyl methyl ketone as a function of $\bar{M}_n$.

be greatest with chloroform and least with benzene. The value of [η] depends somewhat on the solvent. Figures 1–4 and Table I show that $-d[\eta]/dT$ depends on $M$. Figure 5, typical of results obtained with the other solvents, shows the dependence to be approximately linear. Similar results were obtained by Flory *et al.* (11) for cellulose trinitrate in ethyl acetate, but Manley (8), using aqueous solutions of ethyl hydroxyethylcellulose, found $d[\eta]/dT$ to vanish at a D.P. of approximately 200.

Values of the Huggins $k'$ in the relationship

$$\eta_{sp}/c = [\eta] + k'[\eta]^2c$$

decrease with increasing temperature. This is shown in Table II, where values for systems having the lowest and highest values are given. Values of $K$ and $a$ in the expression

$$[\eta] = KM^a$$

obtained from least-squares plots of log [η] against log $\bar{M}_n$, are given in

TABLE II

*Values of k′*

| Solvent | $\bar{M}_n$ | 25° | 32° | 39° | 46° | 53° | 63° |
|---|---|---|---|---|---|---|---|
| Chloroform | 87,000 | 0.39 | 0.37 | 0.37 | 0.36 | 0.35 | |
| Benzene | 40,000 | 0.71 | 0.69 | 0.68 | 0.64 | 0.63 | 0.60 |

TABLE III

*Values of K and a*

| Temp. (°C.) | Ethyl methyl ketone | Ethyl acetate | Butyl acetate | Benzene | Chloroform | Nitro-ethane |
|---|---|---|---|---|---|---|
| | | | $a$ (± 0.02) | | | |
| 25 | 0.84 | 0.89 | 0.87 | 0.81 | 0.89 | 0.96 |
| 32 | 0.84 | 0.87 | 0.87 | 0.80 | 0.88 | 0.93 |
| 39 | 0.82 | 0.86 | 0.86 | 0.81 | 0.89 | 0.90 |
| 46 | 0.82 | 0.86 | 0.84 | 0.79 | 0.90 | 0.87 |
| 53 | 0.81 | 0.85 | 0.84 | 0.78 | 0.90 | 0.81 |
| 60 | 0.79 | 0.85 | 0.83 | 0.78 | | 0.79 |
| | | | $K \times 10^4$ | | | |
| 25 | 1.82 | 1.07 | 1.40 | 2.92 | 1.18 | 0.42 |
| 32 | 1.76 | 1.30 | 1.36 | 3.20 | 1.27 | 0.56 |
| 39 | 2.12 | 1.40 | 1.46 | 2.80 | 1.09 | 0.75 |
| 46 | 1.82 | 1.35 | 1.75 | 3.42 | 0.93 | 1.01 |
| 53 | 2.21 | 1.45 | 1.69 | 3.71 | 0.90 | 1.88 |
| 60 | 2.67 | 1.40 | 1.81 | 3.58 | | 2.26 |

Table III. Except with chloroform, $a$ decreases slightly with increase of temperature and $K$ increases.

## DISCUSSION

The negative temperature coefficients of $[\eta]$ and the decreases in slope and curvature of the $\eta_{sp}/c$ vs. $c$ plots are indicative of decreasing chain extension as the temperature increases. This is also suggested by the corresponding decrease in the values of $a$ for all the solvents but chloroform. Osmotic studies on dilute solutions of the fraction of $\bar{M}_n$ 119,000 (18) show that with chloroform as solvent the extrapolated value of $\pi/c$ at zero $c$ decreases markedly with increase of temperature above 25°C. possibly because of desolvation and aggregation of polymer. Such aggregation may not greatly affect $[\eta]$ (19), but it makes any correlation of $a$ with chain configuration doubtful. The general decrease in the values of $k'$ is also rather difficult to interpret. With flexible polymers decreasing values reflect increasing solvent power with corresponding increases in chain extension. The latter is clearly unlikely in the present case and $k'$ is not generally a measure of solvent power for cellulose derivatives (20). The decreases in $k'$ may be simply a consequence of the decreasing values of $[\eta]$ and slopes of the $\eta_{sp}/c$ vs. $c$ plots.

The persistence length $q$ of the Porod-Kratky model may be obtained from (21):

$$\bar{r}^2 = 2Lq - 2q^2(1 - e^{-L/q}), \qquad [3]$$

TABLE IV

*Values of q for Fraction of $\bar{M}_n$ 140,000*

| Solvent | $q$ (cm. × $10^{-8}$) | |
|---|---|---|
| | 25°C. | 60°C. |
| Ethyl methyl ketone | 68 | 59 |
| Ethyl acetate | 72 | 62 |
| Butyl acetate | 73 | 63 |
| Benzene | 73 | 66 |

where $L$ is the fully extended length of the chains, in this case the degree of polymerization multiplied by the length of a substituted glucose unit (5.15 A.). For flexible polymers $\bar{r}^2$ can be obtained from Eq. [1$a$], giving $\Phi$ its limiting value, but this is not so in the present case. Values of $\{\Phi\}$ in Eq. [2] are not known. The difference between $\Phi$ and $\{\Phi\}$ should be least for the fraction of highest $\bar{M}_n$, and values of $\bar{r}^2$, obtained by use of [1$a$], have been used to calculate $q$ for this fraction in ethyl methyl ketone, butyl and ethyl acetates, and benzene at 25° and 60°C. The use of $\Phi$ in the calculation will lead to values of $q$ which are too small so that those given in Table IV are of only qualitative significance at best. The differences between the values of $\Phi$ and $\{\Phi\}$ should be least at 60° so that the variation of $q$ with temperature is likely to be greater than that suggested in the table. The values given may be compared with 111 A. (22) and 115 A. (23) for cellulose trinitrate in acetone and 200 A. (23) for the trinitrate in ethyl acetate at 25°C. They suggest that the ethyl cellulose chains are stiff but that stiffness decreases appreciably with increase of temperature.

Similar results are obtained from the Kirkwood-Riseman treatment. The effective bond length $b$ may be obtained from (24):

$$b^3 = 600M_0(6\pi^3)^{1/2}[\eta]/N_A\pi^3Z^{1/2}xF(x), \tag{4}$$

where $M_0$ is the molecular weight of a substituted glucose unit (232.25), $N_A$ the Avogadro number, and $[\eta]$ the intrinsic viscosity corresponding to the mean logarithmic degree of polymerization $Z$. Values of the function $xF(x)$ are tabulated by Kirkwood and Riseman (5) for various values of the viscosity-molecular weight exponent $a$. Values of $b$ are given in Table V. They are much larger than are obtained for flexible polymers and may be compared with 30–46 A. for cellulose trinitrate in acetone (25), 27.3 for cellulose acetate in the same solvent (25), and 37 for ethyl hydroxyethylcellulose in water (8).

The angle $\psi$ between successive bond planes can be obtained from (25)

$$b^2 = b_0^2\frac{(1 + \cos\theta)(1 + \cos\psi)}{(1 - \cos\theta)(1 - \cos\psi)} \tag{5}$$

TABLE V
*Values of b and ψ*

| Solvent | $b$ (cm. × $10^{-8}$) | | $\psi$ (degrees) | |
|---|---|---|---|---|
| | 25°C. | 60°C. | 25°C. | 60°C. |
| Ethyl methyl ketone | 31.5 | 26.8 | 26 | 30 |
| Ethyl acetate | 38.3 | 30.4 | 22 | 27 |
| Butyl acetate | 35.0 | 29.4 | 23 | 28 |
| Benzene | 31.5 | 28.3 | 26 | 29 |
| Nitroethane | 48.1 | 24.7 | 18 | 33 |

where cos $\psi$ represents a mean value, $\theta$ is the supplement of the valence angle, equal to 70° for cellulose derivatives, and $b_0$ is the length of a glucose unit (5.15 A.). Values of $\psi$, obtained from those of $b$, are included in Table V. Since cos $\psi$ is zero if there is free rotation about the bonds, the values of $\psi$, although qualitative, suggest considerable chain stiffness, even at the higher temperature. Manley (8) gives $\psi$ = 22.5°C. for ethyl hydroxyethyl cellulose in water.

Although the Flory treatment is not strictly applicable to cellulose derivatives in the molecular weight range considered, its use may give useful qualitative information regarding the contributions of different factors to the temperature coefficients of $[\eta]$. In Eq. [2], $\{\Phi\}$, $\alpha^3$, and $(\bar{r}_0^2/M)$ may all vary with temperature. In the cases of butyl acetate and benzene as solvents it is possible to make estimates of the contribution *ot* $d \ln \alpha^3/dT$ to $d \ln [\eta]/dT$. Osmotic studies of solutions of the fraction of $\bar{M}_n$ 119,000 have been made with these solvents at 25°, 35°, and 45°C. (18). From these values of the second virial coefficient $A_2$ can be obtained. With these and interpolated values of $[\eta]$ it is possible to estimate $\alpha^3$ at the three temperatures by means of an approximate relationship due to Orofino and Flory (26):

$$A_2 = (2^{5/2}\pi N_A/3^3\Phi)([\eta]/M) \ln [1 + (\pi^{1/2}/2)(\alpha^2 - 1)]. \qquad [6]$$

The data used and the results are given in Table VI. Here $\Phi$ was given the limiting value of 2 × $10^{21}$. Lower values which, strictly, should be used would reduce the value of $\alpha^3$.

The values of $d \ln \alpha^3/dT$ are similar in magnitude to those of $d \ln [\eta]/dT$ but of opposite sign. The negative temperature coefficients of $[\eta]$ would seem to be largely due to decreases in the value of $(\bar{r}_0^2/M)$ as the temperature increases. Similar conclusions were reached by Flory *et al.* (11), who point out that the temperature coefficient of $(\bar{r}_0^2/M)$ may be slightly modified by a change in the value of $\{\Phi\}$ with temperature. Since $\{\Phi\}$ will increase with increasing temperature the true value of the negative temperature coefficient of $(\bar{r}_0^2/M)^{3/2}$ may be somewhat greater than is suggested by the

TABLE VI

| Solvent | Temp. (°C.) | $A_2 \times 10^3$ (c.c./g.$^2$) | $\bar{M}_n \times 10^{-5}$ | $[\eta]$ | $\alpha^3$ | $d \ln [\eta]/dT \times 10^2$ | $d \ln \alpha^3/dT \times 10^2$ |
|---|---|---|---|---|---|---|---|
| Benzene | 25 | 1.56 | 1.19 | 3.74 | 1.52 | −0.40 | +0.79 |
| | 35 | 1.71 | 1.19 | 3.61 | 1.61 | | |
| | 45 | 1.98 | 1.19 | 3.45 | 1.78 | | |
| Butyl acetate | 25 | 0.99 | 1.19 | 3.56 | 1.32 | −0.61 | +0.50 |
| | 35 | 1.08 | 1.19 | 3.36 | 1.38 | | |
| | 45 | 1.19 | 1.19 | 3.15 | 1.46 | | |

magnitude of $d \ln [\eta]/dT - d \ln \alpha^3/dT$. Flory *et al.* also point out that the ratios $\{\Phi\}/\Phi$ and $(\bar{r}_0^2/M)^{3/2}/(\bar{r}_0^2/M)_\infty^{3/2}$, where $(\bar{r}_0^2/M)_\infty^{3/2}$ represents the limiting value for infinite $M$, should increase both with increasing temperature and molecular weight and contribute positive temperature coefficients tending to offset the negative ones of $(\bar{r}_0^2/M)_\infty^{3/2}$. These contributions will, however, decrease with increasing $M$. The increases in the values of $-d[\eta]/dT$ with increasing $M$ are in agreement with these suggestions.

It remains to consider the variations of $[\eta]$, $d[\eta]/dT$, and other parameters with solvent. At a given temperature and molecular weight $[\eta]$ is generally least in nitroethane and greatest in benzene and chloroform, although the solvent variations are not very large. Lower values in nitroethane might perhaps be expected since the polymer-solvent interaction parameter $\chi_1$, obtained with a rough fraction in this solvent at 25°C., is 0.45 (20). Values of $\chi_1$ for the fraction of $\bar{M}_n$ 119,000 in benzene and butyl acetate are 0.34 and 0.33, respectively (18). Chloroform at 25°C. gives 0.29 (18). Variations of $[\eta]$ with solvent are likely, at least in part, to reflect variations in $(\bar{r}_0^2/M)$. The rather larger values of $[\eta]$ for benzene compared with those for butyl acetate might be due to the larger values of $\alpha^3$ suggested for benzene and the smaller negative temperature coefficients of $[\eta]$ obtained with this solvent to the larger variation of $\alpha^3$ with temperature. The values of the exponent $a$ at all temperatures are least with benzene, and it is possible that the chains are less extended in this solvent. This is not in agreement with the values of $q$ and $b$, which are, however, only qualitative. Solvation, which is unlikely in benzene, may cause more extended configurations because of more extensive packing of solvent molecules around the chains. At lower temperatures solvation is likely to be greatest in chloroform (20), but here possible desolvation and aggregation at higher temperatures makes interpretation of the values of $[\eta]$ and $d[\eta]/dT$ doubtful. The large decreases in the values of $b$ and the exponent $a$ with increasing temperature observed with nitroethane may be partly due to the use of only the four lower fractions with this solvent. At low temperatures the chains may be relatively extended, increasing temperature leading to more contracted forms—an effect enhanced by the poor solvent power of nitroethane. In view of the qualitative nature of the treatment these suggestions can be only tentative.

## ACKNOWLEDGMENT

The authors wish to express their thanks for a Bradford City Research Scholarship to A. M. B.

## REFERENCES

1. MOORE, W. R., AND BROWN, A. M., *J. Colloid Sci.* **14,** 1 (1959).
2. SIMHA, R., *J. Phys. Chem.* **44,** 25 (1940).
3. KUHN, W., *Helv. Chim. Acta* **28,** 97 (1945).
4. DEBYE, P., AND BUECHE, A. M., *J. Chem. Phys.* **16,** 573 (1948).
5. KIRKWOOD, J. G., AND RISEMAN, J., *J. Chem. Phys.* **16,** 565 (1948).
6. POROD, G., *Monatsh.* **80,** 251 (1949).
7. KRATKY, O., AND POROD, G., *Rec. trav. chim.* **68,** 1106 (1949).
8. MANLEY, R. ST J., *Arkiv. Kemi.* **9,** 519 (1956).
9. FLORY, P. J., "Principles of Polymer Chemistry," Ch. 14. Cornell University Press, Ithaca, New York, 1953.
10. NEWMAN, S., AND FLORY, P. J., *J. Polymer Sci.* **10,** 123 (1953).
11. FLORY, P. J., SPURR, O. K., AND CARPENTER, D. K., *J. Polymer Sci.* **27,** 231 (1958).
12. HOLTZER, A. M., BENOIT, H., AND DOTY, P., *J. Phys. Chem.* **58,** 624 (1954).
13. HUNT, M. L., NEWMAN, S., SCHERAGA, H. A., AND FLORY, P. J., *J. Phys. Chem.* **60,** 1278 (1956).
14. MANDELKERN, L., AND FLORY, P. J., *J. Am. Chem. Soc.* **74,** 2517 (1952).
15. MOORE, W. R., AND BROWN, A. M., *J. Appl. Chem.* **8,** 363 (1958).
16. KRAEMER, E. O., in "The Chemistry of Large Molecules", edited by R. E. Burk and O. Grummitt, p. 84. Interscience, New York, 1943.
17. KRAEMER, E. O., AND SEARS, G. R., *J. Rheol.* **2,** 292 (1931).
18. MOORE, W. R., AND TIDSWELL, B. M., *J. Polymer Sci.* **29,** 37 (1958).
19. DOTY, P., WAGNER, H., AND SINGER, S., *J. Phys. Chem.* **51,** 32 (1947).
20. MOORE, W. R., EPSTEIN, J. A., TIDSWELL, B. M., AND BROWN, A. M., *J. Polymer Sci.* **23,** 23 (1957).
21. BENOIT, H., AND DOTY, P., *J. Phys. Chem.* **57,** 958 (1953).
22. KRIGBAUM, W. R., *J. Polymer Sci.* **28,** 213 (1958).
23. HUGUE, M. M., GORING, D. A. I., AND MASON, S. G., *Can. J. Chem.* **36,** 952, (1958).
24. BAWN, C. E. H., GRIMLEY, T. B., AND WAJID, M. A., *Trans. Faraday Soc.* **46,** 1112 (1950).
25. IMMERGUT, E. H., AND EIRICH, F. R., *Ind. Eng. Chem.* **45,** 2500 (1953).
26. OROFINO, T. A., AND FLORY, P. J., *J. Chem. Phys.* **26,** 1067 (1957).

JOURNAL OF COLLOID SCIENCE **14**, 354–361 (1959)

## LETTERS TO THE EDITOR

# MIXED MONOLAYERS WITH POLYVINYL ACETATE

Remarkable properties have been observed on the film balance for an equiweight mixture of polyvinyl acetate, which orients horizontally, and stearic acid, which orients vertically. The polyvinyl acetate (1) was of high purity; it had a weight-average molecular weight of about one million. The stearic acid (m.p. 69.61°C.) was specially prepared by the Research Division of Armour and Company. Apparatus and techniques for the study of mixed monolayers have been described (2). The volatile spreading solvent was twice-distilled benzene; films were studied at 25°C. In Fig. 1, pressure-area isotherms are plotted for the two individual components, duplicates of the mixture, and a calculated average based on simple additivity of areas.

The isotherm for the monolayer of stearic acid alone gives an extrapolated area of 0.43 square meters per milligram (m.$^2$/mg.) or 20 square Angstroms (A.$^2$) per molecule. The monolayer has a thickness of about 25 A., a compressibility of 0.0019, and a collapse pressure of 42 dynes per centimeter (2).

The isotherm for polyvinyl acetate gives an extrapolated area of 1.9 m.$^2$/mg. or about 27 A.$^2$ per monomer unit (3–7). This area corresponds to a film thickness of about 4.5 A. and establishes horizontal orientation for the polymer molecules. Compressibility is 0.0252. Collapse occurs gradually at about 23 dynes/cm.—a high pressure for a film of horizontally oriented molecules (8). The film shows no hysteresis on compression and expansion; moreover, the response to compression and expansion is *unusually rapid*. Complete compression and complete expansion can be performed within a few minutes, with all points falling on the equilibrium isotherm. After complete compression presumably little if any solvent remains; on release of pressure rapid spontaneous spreading without benefit of bulk solvent is thus indicated. No other film in our experience has shown such rapid response.

For the mixed film, extrapolated areas for the portions of the isotherm at low and high pressures are, respectively, 1.10 and 0.29 m.$^2$/mg.; compressibilities are 0.0195 and 0.0054. The low-pressure portion is slightly to the left of the calculated average curve; packing together is evidently tighter than packing alone. The inflection in the isotherm near 25 dynes/cm., which is close to the collapse pressure for the polymer, suggests that polymer is being squeezed out of the film. Area values at higher pressures closely approach those for stearic acid alone; probably little of the polymer remains

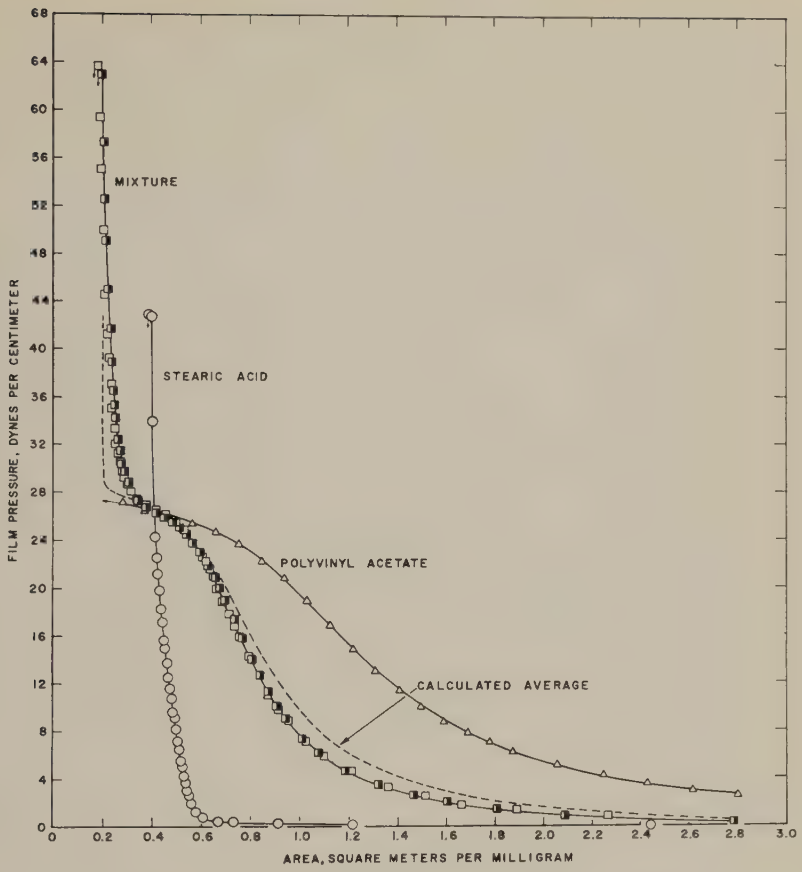

Fig. 1. Pressure-area isotherms for stearic acid, polyvinyl acetate, and an equiweight mixture.

in the monolayer. The steepness of the isotherm also indicates that stearic acid dominates in this region. Most striking, however, is the collapse pressure for the mixture: 63 dynes/cm. *This collapse pressure is far greater than that for either component and is about equal to the sum of the two.* Moreover, the film is unusually stable and shows little hysteresis in compression-expansion experiments. Evidently the polyvinyl acetate facilitates reversibility; stearic acid monolayers alone normally expand extremely slowly.

Additional preliminary experiments indicate that equiweight binary mixtures of polyvinyl acetate with *n*-hexacosanoic, *n*-hexatriacontanoic, and 2-hydroxystearic acids give somewhat similar results, including the high collapse pressures. However, binary mixtures of the polymer with octadecyl alcohol, methyl stearate, and cholesterol give collapse pressures close to those obtained without the polymer. Entirely different combinations, obtained principally by a penetration technique, may also give high film pressures (9, 10).

Although excess polymer may be squeezed out of the mixed monolayer on compression, enough may remain to maintain a polymer monolayer under or intimately mixed with the carboxyl groups of the fatty-acid films. Stability may result from hydrogen bonding between free carboxyl groups and acetate groups. Film structure may be tantamount to a fatty-acid monolayer on top of a polyvinyl acetate monolayer. Because the polymer is polar, bulky, and amorphous, it may interfere with the folding and structured collapse of the fatty-acid layer (11). Interaction of the acetate groups of the polymer with hydroxyl and other ester groups is evidently slight.

An understanding of the nature of the interaction between large and small molecules of various orientations in thin films should shed light on many areas of protein, polymer, and catalyst research.

## References

1. Prepared by R. A. Ahlbeck at the University of Michigan.
2. Ries, H. E., Jr., and Cook, H. D., *J. Colloid Sci.* **9**, 535 (1954).
3. Crisp, D. J., *J. Colloid Sci.* **1**, 49 (1946).
4. Benson, G. C., and McIntosh, R. L., *J. Colloid Sci.* **3**, 323 (1948).
5. Hotta, H., *J. Colloid Sci.* **9**, 504 (1954).
6. Llopis, J., and Rebollo, D. V., *J. Colloid Sci.* **11**, 543 (1956).
7. Schick, M. J., *J. Polymer Sci.* **25**, 465 (1957).
8. Harkins, W. D., Carman, E. F., and Ries, H. E., Jr., *J. Chem. Phys.* **3**, 692 (1935).
9. Schulman, J. H., and Rideal, E. K., *Proc. Roy. Soc.* (*London*) **B122**, 29 (1937).
10. Goddard, E. D., and Schulman, J. H., *J. Colloid Sci.* **8**, 309, 329 (1953).
11. Ries, H. E., Jr., and Kimball, W. A., *Proc. 2nd Intern. Congr. Surface Activity* **1**, 75 (1957); *Nature* **181**, 901 (1958).

*Research and Development Department,*
*Standard Oil Company* (*Indiana*),
*Whiting, Indiana*

Herman E. Ries, Jr.
Richard A. Ahlbeck
Joseph Gabor

*Received January 27, 1959; revised March 19, 1959*

## IMPINGEMENT OF AEROSOL PARTICLES ON POLYVINYL ALCOHOL FILM

A recent article by Drs. I. Gallily and V. K. LaMer (1) has prompted a reappraisal of some peculiar photomicrographs which were taken in 1956 while calibrating a polyvinyl alcohol-$AgNO_3$ film used to measure the size of water and salt water droplets (2).

The Gallily-LaMer article discussed the measurement of liquid droplet rebound from an hydrophobic plate during impingement of the aerosol. In

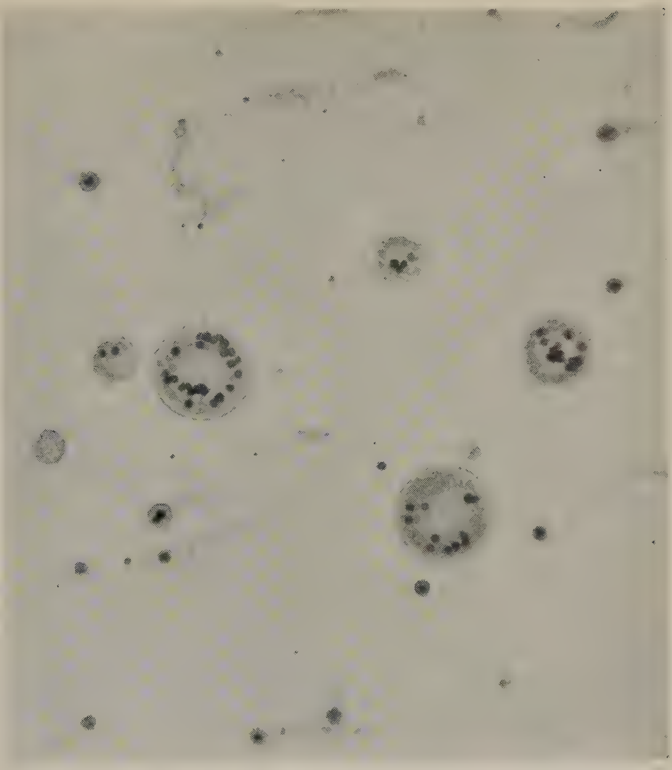

FIG. 1

one experiment they described how they coated a slide with very small droplets, then impinged much larger ones. The supposition was that if the droplets indeed rebounded and were redeposited without skid at another location, then no trails would appear through the small droplets. On the other hand, if the droplets skidded, the cleared paths would so indicate. No paths were observed and bounce rather than skidding was supported.

A search through old photomicrographs turned up a peculiar one[1] long forgotten in the files. This is a picture of the impressions left on the water-sensitive droplet measuring film by salt water droplets which were impinging at moderate speed (perhaps 10–30 m.p.h.). The larger droplets contained 8 $\mu$ diameter corn smut spores as a calibrating mechanism. A few small droplets contained a single spore, while many quite small droplets had no particulates. The impressions left by the large droplets were circular and quite normal for the technique, but in this particular calibration run, the reactions of the small droplets turned out to be quite unusual. Owing to some peculiarity of the run, the small droplets, upon striking the hydrophilic film, began to skid leaving behind a faint trail of salty moisture. This salt, upon reacting with the $AgNO_3$ in the film and after subsequent phenylhydrazine development, yielded a visible black trail. However, instead of a straight skid mark culminating in the final drop impression, the paths assumed a corkscrew pattern.

---

[1] The only remaining copy of the photomicrograph has been forwarded in personal correspondence to Dr. LaMer, who has suggested it may be reproduced if the *Journal* feels this note to be of sufficient general interest.

The interesting implications of this are, of course, that under the right circumstances of droplet properties, impinging speed and angle, and collecting surface condition, very small droplets may be more prone to skid than to bounce. But of more consequence is the observation that these droplets may be spinning very rapidly (as evidenced by the corkscrew path). If such a spin is a common phenomenon associated with small droplets in a moving air stream, then it might be one of the influential forces bringing about droplet rebound or skid. If it is an uncommon occurrence brought about by peculiar air stream conditions, then investigators might well be wary of sudden anomalies appearing in aerosol experiments where rebound, skid, or collection efficiency properties are of importance.

### References

1. Gallily, I., and LaMer, V. R., "On the behaviour of liquid droplets after impinging on solid surfaces," *J. Phys. Chem.* **62,** 1295–1299 (1958).
2. Farlow, N. H., and French, F. A., "Calibration of liquid aerosol collectors by droplets containing uniform size particles," *J. Colloid Sci.* **11,** 177–183 (1956).

*U. S. Naval Radiological Defense Laboratory,*
*San Francisco 24, California,*
Neil H. Farlow
*Received March 24, 1959*

## THE SOLUBILIZING PROPERTIES OF THE PROTEIN-DETERGENT COMPLEX

The physicochemical structure of protein-detergent complexes has long been the subject of speculation. It is generally accepted that the combination of detergent ions with proteins is principally electrostatic in nature (1). However, this simple picture becomes complicated by the fact that the combination is not stoichiometric, and in certain cases, there is apparently no limit to the binding (2). There are several points of view with regard to the disposition of the nonstoichiometrically bound detergent. Steinhardt (3) suggested that the extra detergent anions might be bound by a partially electrostatic mechanism which involved the prior combination of hydrogen ion to the weakly basic amide and peptide nitrogen atoms. The binding of hydrogen ion could occur at low hydrogen ion concentrations because the association of anions with the protein would decrease the net positive charge of the protein. The "extra" anionic detergent is then bound to the newly formed cationic sites. This view is also supported by the work of Pankhurst (4). Lundgren (5) suggested that additional detergent could be bound by nonpolar forces to detergent ions already electrostatically bound to cationic sites. Some time ago, it was pointed out (6) that the binding of one detergent ion at a site on the protein favored the binding of additional detergent in the immediate vicinity of that site owing to interaction of the paraffin chains of the detergent. This implies that detergent binding sites on the protein may act as nuclei for the formation of a kind of micelle, which, for want of a better name, could be called a micellar cluster. The solubilization of an oil-soluble dye in aqueous solutions of detergents is a standard technique for the determination of the critical micelle concentration of a colloidal electrolyte (7). The point at which a sharp break in the curve of dye solubility vs. detergent concentration occurs is defined as the critical micelle concentration as determined by this technique. This does not preclude the existence of associated detergent below that concentration; it merely indicates that the properties of the solution are such that the solubility of oil-soluble substances becomes greatly enhanced over a short concentration range of detergent, designated as the critical micelle concentration.

Since oil-soluble dyes are solubilized in aqueous detergent solutions only above the critical micelle concentration, solubilization of such dyes in detergent-protein solutions in which no micelles can be detected by the dye solubilization technique, might provide a useful approach to the characterization of the protein-detergent complex as a synthetic lipoprotein as suggested by the work of Ekwall (8) and Dervichian (9). The purpose of this report is to present the results of a preliminary investigation of the properties of the protein-detergent complex as a solubilizing agent in concentrations of alkyl sulfates in which no solubilization of oil-soluble dyes occurs, in the absence of protein.

The solubilizing power of certain alkyl sulfates below the critical micelle concentration in the presence of native bovine serum albumin [BSA] was investigated. An experiment designed to study the solubilizing power of a series of sodium alkyl sulfates from $C_{10}$ to $C_{16}$, toward *p*-amino azobenzene in the presence of BSA was carried out as follows. A series of tubes containing varying amount of alkyl sulfate was prepared which also contained a constant concentration of native BSA and some twice recrystallized solid *p*-amino azobenzene. The concentration of protein was also varied from 0.01% to 0.2% in other series. These tubes were securely sealed and allowed to rotate at constant temperature until equilibrium was reached. The results of the experiment involving tetradecyl sulfate may be seen in Fig. 1. There is apparently a linear increase in the amount

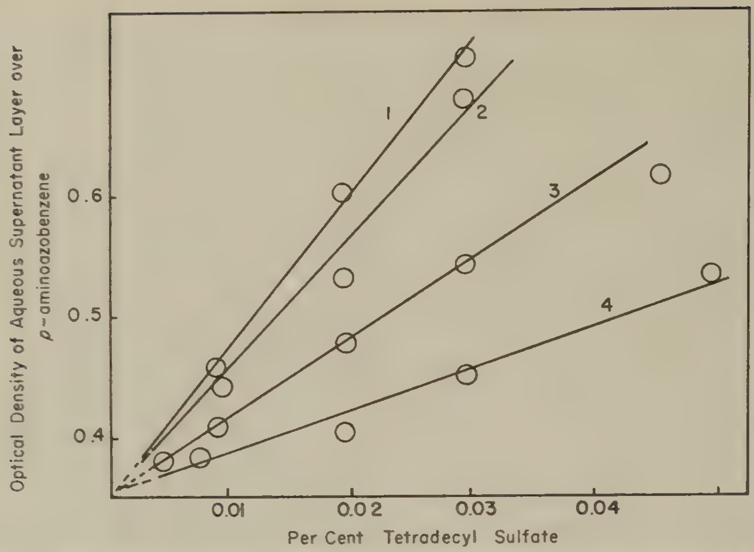

FIG. 1. The effect of bovine serum albumin on the solubilizing power of sodium tetradecyl sulfate below the critical micelle concentration. Curve 1—0.2% BSA; 2—0.1% BSA; 3—0.05% BSA; 4—0.01% BSA.

| Sodium Alkyl Sulfate | Moles Dye Solubilized per Mole of Detergent × $10^3$ |
|---|---|
| Decyl | 8.5 |
| Dodecyl | 37.0 |
| Tetradecyl | 102.2 |
| Hexadecyl | 152.7 |

of dye solubilized in the presence of the protein as the detergent concentration is increased below the CMC. This is in contrast to the fact that no solubilization of dye occurs in the pure detergent solutions until after the appearance of micelles. It was also found that over the range of protein concentrations used, there was little apparent solubilization of dye due to the protein. The slope of the line, corresponding to moles of dye solubilized per mole of detergent, is a function of protein concentration, and appears to reach a limit at about 0.2% protein. The solubilization of the dye by the protein-detergent complex was observed in experiments with decyl, dodecyl, tetradecyl, and hexadecyl sulfates. The slopes of the lines at one protein concentration, 0.05%, are presented in Table I. The results indicate that the solubilizing power increases markedly with carbon chain length just as is the case with detergents above the critical micelle concentration.

A thorough study of this phenomenon is in progress, and it is planned to describe the properties of the detergent-protein complex in these systems in greater detail at a later date.

## REFERENCES

1. PUTNAM, F., *Advances in Protein Chem.* **4,** 110 (1948).
2. YANG, J. T., AND FOSTER, J. F., *J. Am. Chem. Soc.* **75,** 5560 (1953).
3. STEINHARDT, J., AND FUGIT, C. H., *J. Research Natl. Bur. Standards* **29,** 315 (1942).
4. PANKHURST, K. G. A., *Discussions Faraday Soc.* **6,** 52 (1949).
5. LUNDGREN, H. P., *Textile Research J.* **15,** 335 (1945).
6. KARUSH, F., AND SONENBERG, M., *J. Am. Chem. Soc.* **71,** 1369 (1949).
7. McBAIN, M. E. L., AND HUTCHINSON, E., "Solubilization and Related Phenomena." Academic Press, New York, 1955.
8. EKWALL, P., *Acta Unio Intern. contra Cancrum* **10,** 44 (1954).
9. DERVICHIAN, D. G., *Discussions Faraday Soc.* **6,** 7 (1949).

*Lever Bros. Research Center* IRA BLEI
*Edgewater, New Jersey*
*Received December 5, 1958.*

JOURNAL OF COLLOID SCIENCE **14**, 362 (1959)

# BOOK REVIEWS

**Precipitation from Homogeneous Solution.** By Louis Gordon, Murrell L. Salutsky, and Hobart H. Willard. John Wiley & Sons, Inc., New York, 1959. 187 pp. Price $7.50.

A successful attempt is made to combine information from widely scattered sources into a small, well-organized volume which concerns itself exclusively with precipitation from homogeneous solution. The purpose of the book is to promote the widespread use of homogeneous precipitation methods, and in so doing, it continuously emphasizes the advantages of this method over those of ordinary mixing of solutions. The book does not discuss, nor does it claim to discuss, any homogeneous nucleation studies (although one brief reference is made to La Mer and Dinegar's preparation of monodisperse sulfur sols). It is a good book for quantitative separations of slightly soluble salts by the method of homogeneous precipitation. Enough experimental details are given so as to enable the reader to carry out many procedures without recourse to further reading. The discussions of results from the various procedures are good, and there are over 250 references to homogeneous precipitation work. However, as one might expect from the size and scope of the book, not all methods for generating the various anions are mentioned.

George R. Weiss, New York, New York

**An Introduction to the Chemistry of Fats and Fatty Acids.** By F. D. Gunstone with a foreword by Prof. T. P. Hilditch. Published by John Wiley and Sons, Inc., New York, 1958. 155 pp. Price: $6.00

Parts of this small book will have little to offer the physical chemist, but other sections on the preparation, purification, and chemical and physical properties of the fatty acids will give him much useful data in a concise form. The subjects discussed are: the fatty acids, the chemical nature of fats, the physical and chemical properties of fats and fatty acids, the synthesis and utilization of fats in living organisms, and the chief technical applications of fats. Within this range the coverage is quite thorough and includes some information not available in older texts. Numerous tables are given. The presentation is particularly clear although limitations of space occasionally make the treatment too general, and physical phenomena are discussed at a level suited to the nonphysical chemist. An objection must be made to the practice of giving many references by author and year only. A bibliography of the more important texts and reviews would be useful and also appropriate to an introductory text. The book is exceptionally well written and can be recommended to anyone interested in the fats or fatty acids.

G. T. Barnes

JOURNAL OF COLLOID SCIENCE **14**, 363–376 (1959)

# THE BALL-MILL HYDRATION OF TRICALCIUM SILICATE AT ROOM TEMPERATURE

**D. L. Kantro, Stephen Brunauer, and C. H. Weise**

*Portland Cement Association, Research and Development Laboratories,*
*Skokie, Illinois*

*Received April 20, 1959*

## ABSTRACT

The hydration of tricalcium silicate, $Ca_3SiO_5$, in a small steel ball mill at room temperature was investigated. The stoichiometry of the reaction is represented by

$$2Ca_3SiO_5 + 6H_2O = Ca_3Si_2O_7 \cdot 3H_2O + 3Ca(OH)_2$$

The initial products of the reaction are calcium hydroxide (both crystalline and amorphous) and a calcium silicate hydrate, designated as "hydrate III." The latter shows marked similarities to the calcium silicate hydrate, tobermorite, produced by other methods of hydration of $Ca_3SiO_5$. The similarities include $CaO/SiO_2$ ratio, specific surface area, water content, heat of solution, heat of hydration, and surface energy (enthalpy).

Hydrate III differs from tobermorite in that it is unstable; it slowly converts to another calcium silicate hydrate, afwillite. The chemical formula of afwillite is $Ca_3Si_2O_7 \cdot 3H_2O$, the same as that of hydrate III and tobermorite, but afwillite has a different crystal structure, and it is a well-crystallized substance. Hydrate III appears to be a form of tobermorite with a structure so disordered that it exhibits only a single X-ray diffraction line, that corresponding to the strongest line of tobermorite.

The kinetics of the hydration reaction and of the conversion of hydrate III to afwillite were examined. A possible mechanism for the former was proposed.

## INTRODUCTION

The hydration of tricalcium silicate, $Ca_3SiO_5$, under a variety of conditions has been studied extensively during the past few years. The interest in this compound is due mainly to its importance as a major constituent of portland cement.

When $Ca_3SiO_5$ is hydrated at room temperature with a limited amount of water in an undisturbed system, that is, as a "paste," it stiffens and hardens as does portland cement. The products of the hydration are calcium hydroxide and a calcium silicate hydrate which has been identified as a tobermorite (1, 2). When $Ca_3SiO_5$ is hydrated in an excess of water (9/1 liquid to solid ratio by weight) in an agitated system, the same products result. However, when a mixture of the same composition is subjected

TABLE I

*Composition of the Ball-Mill Preparations*

| 1 Batch | 2 Times in ball mill | 3 % $Ca_3SiO_5$ (X-ray) | 4 % Afwillite (X-ray) | 5 % Hydrate III (calculated) | 6 % $Ca(OH)_2$ (calculated) | 7 % $Ca(OH)_2$ (chemical) | 8 % $Ca(OH)_2$ (X-ray) |
|---|---|---|---|---|---|---|---|
| D-30 | 4h (C)(a) | 71.9 | 0.0 | 16.1 | 10.0 | 10.9 | |
| D-41 | 4h (C) | 57.2 | 0.0 | 25.1 | 16.1 | 16.0 | |
| D-38 | 8h (C) | 35.3 | 10.6 | 27.2 | 25.0 | | 22.1 |
| D-32 | 8h (C) | 25.5 | 22.2 | 21.6 | 28.4 | | 28.2 |
| D-29 | 16h (I)(a) | 28.6 | 17.0 | 26.0 | 26.4 | | |
| D-31 | 16h (C) | 6.0 | 26.8 | 29.2 | 35.7 | | 30.6 |
| D-33 | 48h (C) | 0.0 | 37.0 | 22.2 | 38.1 | | 33.9 |
| D-27 | 7d (I) | 0.0 | 43.7 | 16.2 | 37.3 | 37.1 | 31.4 |
| D-26 | 8d (I) | 0.0 | 39.6 | 20.5 | 37.6 | 38.0 | 32.3 |
| D-45 | 25d (I) | 0.0 | 51.8 | 7.9 | 37.7 | 37.7 | 34.3 |
| D-62 | 25d (I) | 0.0 | 59.4(b) | 0.0 | 37.7 | | 34.3 |
| D-57 | 44d (I) | 0.0 | 60.0 | 0.0 | 37.0 | | 33.2 |
| F-34 | 35d (I) | — | 80.9 | 0.0 | 16.7 | | 13.2 |

(a) (C) designates continuous, (I) intermittent grinding.

(b) Apparent complete conversion to afwillite. Figure given is the theoretical amount.

to grinding action in a small steel ball mill, the end products of the reaction are calcium hydroxide and a different calcium silicate hydrate, afwillite (3).

The stoichiometry of any of these reactions may be expressed by the equation

$$2Ca_3SiO_5 + 6H_2O = Ca_3Si_2O_7 \cdot 3H_2O + 3Ca(OH)_2 \qquad [1]$$

The chemical formulas of afwillite and of the tobermorite produced in the hydration of $Ca_3SiO_5$ are the same, but their crystal structures are different. It is interesting to note that the hydration of $\beta$-dicalcium silicate ($\beta$-$Ca_2SiO_4$, another important constituent of portland cement) produces calcium hydroxide and tobermorite, regardless of which of the three methods of hydration is used (2).

An earlier paper (3) dealt primarily with the stoichiometry of the hydration of $Ca_3SiO_5$ in the ball mill. The present paper describes an investigation of the energetics and kinetics of this system.

## EXPERIMENTAL

### *Preparation of Materials*

The $Ca_3SiO_5$ was from the same batch used by the present authors in a previous investigation (4). Hydration was carried out in a room kept at 24° ± 1°C. The $H_2O/Ca_3SiO_5$ weight ratio was 9.0. The same steel ball mills were used that were described in the earlier ball-mill hydration study (3). Some batches were prepared with continuous grinding (C), others were ground intermittently (I), as in the earlier work. Intermittent grinding was employed to avoid too much contamination by iron, rubbed off the steel balls. It is difficult to determine iron in its different stages of oxidation and, because of the very high heat of solution of free iron, a slight error in analysis leads to considerable error in the heat of solution.

The ball-milling times of the preparations (batches) are given in Table I, column 2. The intermittent grinding schedule consisted of continuous grinding for the first hour, then grinding for 15 min. of each subsequent hour. The only exception is Batch D-29, which was continuously ground for the first 30 min., then ground for 15 min. of each subsequent hour. Batch D-62, after the ball-milling period shown in the table, was subjected to further agitation in a polyethylene bottle for four weeks.

One preparation, designated as F-34, was made by the reaction of calcium hydroxide with Mallinckrodt's Standard Luminescent Grade Silicic Acid in the ball mill. The $Ca(OH)_2$ was prepared from freshly ignited CaO, which in turn was prepared from Fisher's Certified Reagent Grade Calcium Carbonate, low in alkali. The molar $CaO/SiO_2$ ratio of the preparation was 2.0.

At the end of the reaction period, the mills were placed in a controlled-atmosphere cabinet containing $CO_2$-free air, and their contents were transferred to plastic containers. The slurries were quickly frozen and then placed in the vacuum drying apparatus described by Copeland and Hayes (5). After removal of most of the water, each sample was thoroughly homogenized and then dried at a vapor pressure of $5 \times 10^{-4}$ mm. of Hg (the vapor pressure of ice at −78°C.). Batch D-32 thawed in the course of drying, probably because of a clogged dry ice trap. A comparison with D-38 showed that in the thawed batch further hydration had taken place.

### *Chemical and X-Ray Analyses*

Chemical analyses were performed and compositions calculated according to methods given in earlier papers (6, 7). The free calcium hydroxide was determined by two modifications of the Franke method: the multiple-extraction method (8), in which repeated extractions are performed on the same sample, and the solvent-variation method (9), in which equal weights of different samples are extracted with different amounts of solvent. In either method, an extrapolation is made to correct for the CaO extracted from the calcium silicate hydrate.

X-ray quantitative analyses were performed by the method of Copeland and Bragg (10), described earlier (2). The 2.38 A. line of $Mg(OH)_2$ was used as the internal standard; the amount of $Ca(OH)_2$ was determined by its 2.63 A. line, $Ca_3SiO_5$ by its 2.20 A. line, and afwillite by its 2.73, 2.83, and 3.18 A. lines. In the last case, the results obtained from the three lines were averaged.

### *Other Measurements*

Heats of solution were determined as described before (4, 11). Three sample weights were used: 0.7, 1.0, and 1.3 g. The calorimeter acid was a mixture of 8 ml. of 49.4% $H_2F_2$, with sufficient $2N$ $HNO_3$ added to make the total weight 420 g.

Surface areas were measured by the B.E.T. method, using water vapor and nitrogen as adsorbates. Water vapor adsorption was measured gravimetrically at 25°C. and nitrogen adsorption volumetrically at −195.8°C.

## RESULTS AND DISCUSSION

### *Compositions of the Preparations*

*1.* The compositions of the preparations are given in Table I. Only the amounts of the principal components are shown. Each preparation contained, in addition, some calcium carbonate, tricalcium aluminate hydrate, magnesium hydroxide, sodium sulfate, and iron in various stages of oxidation. The total amount of these impurities was about 2%. Each impurity in each preparation was determined quantitatively by methods reported before (7).

The amounts of $Ca_3SiO_5$, afwillite, and $Ca(OH)_2$, determined by X-ray quantitative analysis, are shown in columns 3, 4, and 8 of Table I, respectively. From the amount of $Ca_3SiO_5$, one can calculate the potential amounts of afwillite and calcium hydroxide in each preparation by means of Eq. [1]. In general, X-ray analysis gave lower than the calculated values for both compounds.

*2.* The shortest reaction period used was 4 hr. Two batches, D-30 and D-41, were hydrated for this period. Although in one case 25% and in the other 38% of the original $Ca_3SiO_5$ had disappeared, neither batch contained afwillite. A batch hydrated 8 hr. (D-38) did contain some afwillite, but much less than would be predicted from the amount of $Ca_3SiO_5$ that had reacted. After 48 hr. of hydration, all the $Ca_3SiO_5$ had reacted (D-33), but still the afwillite content was lower than that expected on the basis of $Ca_3SiO_5$ reaction. Batches of longer reaction periods contained progressively higher amounts of afwillite, tending toward the maximum amount predicted from the stoichiometry, but only after 25 days in the ball mill (D-62) did the afwillite content attain this value.

These results demonstrate that the hydration of $Ca_3SiO_5$ in the ball mill does not yield afwillite directly. An intermediate substance is formed first, which converts to afwillite relatively slowly. Since this intermediate calcium silicate hydrate has only one very broad X-ray diffraction line, at about 3 A., it is not like the tobermorite obtained by the other modes of hydration of $Ca_3SiO_5$. Hence, to distinguish it from both afwillite and tobermorite, it is called here "hydrate III."

*3.* In order to get quantitative values for the afwillite contents, it was first necessary to obtain a preparation in which all the hydrate III had converted to afwillite. Under these conditions, the afwillite content is calculable from the stoichiometry by Eq. [1]. Three such batches were prepared, the last three shown in Table I. It was assumed that D-62 contained the stoichiometric amount of afwillite, 59.4%, and the calibration constants for the three afwillite diffraction lines used in the X-ray analysis were calculated on the basis of this assumption. With the use of these calibration constants, the afwillite contents of D-57 and F-34 were found to be 60.0% and 80.9%, respectively, as compared with the stoichiometric values of 60.1% and 80.6%. The agreement is especially impressive if one considers the differences in the methods of preparation of the three batches, described before.

The broad diffraction line at 3 A., corresponding to hydrate III, did not appear in the X-ray diagrams of Batches D-57, D-62, and F-34. This in itself is not an adequate criterion because the line is so weak that a few per cent of hydrate III could be easily missed. However, the excellent internal consistency of the afwillite data leads to the clear conclusion that the three batches contained no hydrate III. The afwillite contents of all other batches were determined by using the calibration constants obtained for D-62. The values are given in Table I, column 4.

*4.* The hydrate III contents of the preparations were calculated as follows. All silica not in $Ca_3SiO_5$ and afwillite was taken to be in hydrate III. The $CaO/SiO_2$ ratio in hydrate III was 1.5, as will be shown. The water content of hydrate III was the difference between the total water content of the dried batch and the water contents of the other constituents of that batch. This point will also be discussed later. The calculated hydrate III percentages are given in Table I, column 5.

*5.* The $Ca(OH)_2$ contents of the preparations were calculated by subtracting the CaO contents of all the other constituents from the total CaO content of the preparation. These values are given in Table I, column 6. The $Ca(OH)_2$ values obtained by X-ray analysis are shown in column 8. It will be noted that the X-ray values are smaller than the calculated values for all preparations except one (D-32).

The difference between the calculated $Ca(OH)_2$ and that determined by X-rays is caused by the presence of some amorphous $Ca(OH)_2$ in the preparations. Amorphous $Ca(OH)_2$ was reported in an earlier paper (2) for preparations in which the calcium silicate hydrate was tobermorite. The evidence cited there was strong but not incontrovertible, for two reasons. In the first place, tobermorites have a variable $CaO/SiO_2$ ratio; consequently, the possibility existed that the missing $Ca(OH)_2$ was actually part of the tobermorite. In the second place, the tobermorite had a very large specific surface, of the order of 300 m.$^2$/g.; consequently, the possibility existed that the missing $Ca(OH)_2$ was adsorbed on its surface.

The evidence for the existence of amorphous $Ca(OH)_2$ in the present work, at least for three preparations, is incontrovertible. In D-62, D-57, and F-34 the calcium silicate hydrate is solely afwillite, which has a definite molar $CaO/SiO_2$ ratio of 1.5. The missing $Ca(OH)_2$, therefore, could not be a part of afwillite. In addition, afwillite has a surface of the order of 15 m.$^2$/g.; this is an order of magnitude smaller than that needed for the adsorption of the missing $Ca(OH)_2$. It appears, therefore, that in the above three preparations 10% to 20% of the $Ca(OH)_2$ was amorphous.

Batch D-32 had no amorphous $Ca(OH)_2$ within experimental error, as a comparison of columns 6 and 8 of Table I shows. It was pointed out in the experimental part that the drying of this batch was different from those of the others. In the earlier work (2), there was also one preparation, D-35, that had no amorphous $Ca(OH)_2$.

### *Hydrate III*

*1.* If the molar $CaO/SiO_2$ ratio in hydrate III is assumed to be 1.5, as in afwillite and tobermorite, the $Ca(OH)_2$ contents of the preparations can be calculated as previously described in this paper. Because of amorphous $Ca(OH)_2$, the X-ray values do not check the calculated values; however, chemical analysis gives very good agreement with the calculated values, as a comparison of columns 6 and 7 of Table I shows. The conclusion from this is that the molar $CaO/SiO_2$ ratio in hydrate III is 1.5.

*2.* The water content of hydrate III varied from batch to batch, as shown in Table II, column 2. In the calculation, allowance was made for excess water associated with $Ca(OH)_2$ and afwillite.

It was found in a previous investigation that calcium hydroxide, dried under the conditions used here, retained a monolayer of adsorbed water (12). It was assumed that this was also true of the calcium hydroxide produced by the ball-mill hydration of $Ca_3SiO_5$. The specific surface area of D-62, which contained no hydrate III, was 16 m.$^2$/g. X-ray line broadening experiments indicated that the specific surface areas of $Ca(OH)_2$ and afwillite were approximately equal in this preparation, as well as in several other preparations investigated. On this basis, the specific surface areas of $Ca(OH)_2$ and afwillite were taken to be 16 m.$^2$/g. in all preparations. A monolayer of water adsorbed on the surface of $Ca(OH)_2$ corresponds to 0.0047 g./g. when the area of the water molecules is taken to be 10.3 A.$^2$ (12).

The water contents of preparations D-62 and F-34 were such that when allowance for $Ca(OH)_2$ was made, there remained 0.0176 g. excess $H_2O$ per gram of afwillite. This amount is far in excess of that equivalent to a

TABLE II

*Water Contents, Surface Areas, and Heats of Solution of Hydrate III (H3)*

| 1 Batch | 2 Moles H O/ mole $SiO_2$ | 3 $w_j$ (g./g. H3) | 4 $A_j$ (m.$^2$/g. H3) | 5 $\bar{H}_{0.7}$ (cal./g. H3) | 6 $\bar{H}_{1.0}$ (cal./g. H3) | 7 $\bar{H}_{1.3}$ (cal./g. H3) |
|---|---|---|---|---|---|---|
| D-30 | 1.02 | 0.00237(2) | 288.3(2) | 486.8(2) | 478.8(4) | 487.8(4) |
| D-41 | 1.28 | 0.03067(3) | 421.5(2) | 481.9(3) | 483.6(3) | 486.8(3) |
| D-38 | 1.08 | 0.00852(4) | 300.1(2) | 469.6(4) | 465.6(5) | 474.7(4) |
| D-29 | 1.91 | 0.10122(4) | 379.0(2) | 449.2(3) | 446.6(2) | 447.8(2) |
| D-32 | 1.42 | 0.04624(4) | 339.9(2) | 454.1(4) | 462.2(5) | 465.1(4) |
| D-31 | 1.42 | 0.04603(4) | 271.7(4) | 460.2(4) | 451.4(5) | 457.0(4) |
| D-33 | 1.15 | 0.01665(4) | 289.8(4) | 481.8(4) | 475.7(6) | 481.1(4) |
| D-26 | 1.03 | 0.00357(2) | 326.0(4) | 491.5(3) | 487.8(2) | 491.8(4) |
| D-27 | 1.05 | 0.00552(4) | 248.6(4) | 482.4(2) | 475.7(2) | 478.3(2) |
| D-45 | 1.59 | 0.06566(6) | 134.3(4) | 452.8(5) | 433.5(6) | 429.7(6) |

single monolayer adsorbed on the afwillite surface. This indicates that at least part of the water is dissolved in the afwillite. The afwillite in every batch was considered to have the same excess water content.

None of the water contents shown in Table II, column 2, is less than 1.0 mole per mole of $SiO_2$, and in two cases only does the value exceed 1.5 moles. This behavior is similar to that of the tobermorite produced in the hydration of $Ca_3SiO_5$ and $\beta$-$Ca_2SiO_4$.

The water contents, $w_j$, of hydrate III in the different preparations, in excess of 2 moles/mole of $Ca_3Si_2O_7$, are given in Table II, column 3. The values given in this column, as well as those given in columns 4 to 7 of Table II, are averages, and the numbers in parentheses give the number of determinations averaged.

*3.* The surface area of hydrate III in each preparation was obtained as the difference between the surface area of the preparation determined by water vapor adsorption, and the surface area contributions of the $Ca(OH)_2$ and afwillite present. The area of a water molecule adsorbed on hydrate III was taken to be 11.4 A.$^2$, which is the value found for adsorption of water on tobermorite (2). The specific surface areas, $A_j$, thus obtained are shown in Table II, column 4. Eight of the ten values obtained for hydrate III are in the same range as those obtained for tobermorite, 250 to 380 m.$^2$/g. (2, 7).

The specific surface area of afwillite, as was pointed out before, is an order of magnitude smaller than that of tobermorite or hydrate III. For D-62 and F-34, batches containing no hydrate III, the specific surface areas obtained by nitrogen and water vapor adsorption were the same. (The molecular area of nitrogen was taken to be 16.2, water 11.4 A.$^2$.) For samples containing hydrate III, however, the nitrogen areas were always smaller than the water areas. The greater the hydrate III content, the greater was this difference. In this respect, too, hydrate III resembles tobermorite (2).

*4.* The heat of solution of hydrate III in a given preparation was obtained by subtracting the heats of solution of the other constituents from the heat of solution of the preparation, then applying a nonadditivity correction. The heats of solution of all other constituents, except afwillite, were given in an earlier paper (7). The heats of solution of afwillite were obtained from Batch D-62, which contained no hydrate III. They were 411.8, 414.8, and 414.7 cal./g. of afwillite for samples having weights of 0.7, 1.0, and 1.3 g., respectively.

The nature of the nonadditivity correction was discussed in an earlier paper (7). Because of the great similarity of the systems investigated in the earlier and the present work, in general, and because of the similarity of hydrate III to tobermorite, in particular, the same nonadditivity factor was adopted (X in Table VII, column 6, of earlier paper (7)).

The average heats of solution of hydrate III in 0.7, 1.0, and 1.3 g. samples of the different preparations are given in Table II, columns 5, 6, and 7, respectively.

*5.* All properties of hydrate III investigated show similarity to those of tobermorite. Hydrate III is a calcium silicate hydrate having a composition $Ca_3Si_2O_7 \cdot xH_2O$ where $x$ is not less than 2 and seldom greater than 3. It shows only one X-ray diffraction line, but that has the same $d$ spacing as the strongest line of tobermorite. Both hydrate III and tobermorite exist in the same state of subdivision, and both show smaller areas by nitrogen adsorption than by water adsorption.

In the following section other, and more quantitative, data are given to bring out further similarities. Thus it appears that hydrate III is a highly disordered form of tobermorite, so disordered that its entire X-ray diffraction pattern is a single line.

### *The Surface Energy and Heat of Hydration of Hydrate III*

*1.* The surface energy and other parameters were evaluated from the data by the same type of least squares analysis used in earlier work on silica (12) and on tobermorite (7). A system of equations was set up

$$\bar{H}_{jk} + w_j h - A_j \epsilon_s = H_k, \qquad [2]$$

where $\bar{H}_{jk}$ is the mean heat of solution, in cal./g. of $Ca_3Si_2O_7 \cdot 2H_2O$ of hydrate III in the $j$-th batch, having sample weight $k$;

$w_j$ is the water content of hydrate III in the $j$-th batch in excess of the composition $Ca_3Si_2O_7 \cdot 2H_2O$, in g./g. of $Ca_3Si_2O_7 \cdot 2H_2O$;

$h$ is the average heat evolved, in cal./g. of water, when $Ca_3Si_2O_7 \cdot 2H_2O$ reacts with water to form a hydrate III of higher water content;

$A_j$ is the average specific surface area of hydrate III in the $j$-th batch, in m.$^2$/g. of $Ca_3Si_2O_7 \cdot 2H_2O$;

$\epsilon_s$ is the average surface energy (or surface enthalpy) of hydrate III having composition $Ca_3Si_2O_7 \cdot 2H_2O$, in cal./m.$^2$;

and $H_k$ is the heat of solution, in cal./g. of $Ca_3Si_2O_7 \cdot 2H_2O$, of hydrate III having zero surface and zero water in excess of 2 moles per mole of hydrate III, for a sample of weight $k$.

The values of $w_j$, $A_j$, and $\bar{H}_{jk}$ used in the least squares treatment are given in Table II, columns 3 to 7. The evaluated parameters, $H_k$, $h$, and $\epsilon_s$, are given in Table III together with their standard errors. For comparison, the corresponding values are given also for tobermorite, obtained in earlier work (reference 7, Table VII, columns 6 and 7). In every case, the hydrate III value is higher than the corresponding tobermorite value. Thus, in spite of the fact that the standard errors are such as to indicate that the corresponding values could be the same, it seems more likely that the differences are real. However, the differences are small enough to indicate marked similarities in the two sets of values.

Even though hydrate III is quite similar to tobermorite, it differs significantly in at least two points: it is unstable, converting to afwillite, and it has only one X-ray line.

Natural tobermorite and some of its synthetic varieties, especially those produced by hydrothermal means, are relatively well crystallized, showing many X-ray reflections (13). Tobermorites, prepared in this laboratory by the room temperature reaction of calcium hydroxide and silica, show 7 to 10 X-ray lines, including the basal reflection (unpublished). Tobermorites, prepared by paste or "bottle" hydration of $Ca_3SiO_5$ or $\beta$-$Ca_2SiO_4$ at room temperature, show only 3 X-ray lines, and the basal reflection is absent (2).

The best crystallized tobermorites have two strong lines in the vicinity of 3 A. These lines fuse into one, which then becomes the strongest line in the 7- and 3-line tobermorites. Hydrate III, which can be looked upon as a 1-line tobermorite, has its only line at 3 A.

It is possible that the lack of structure gives hydrate III its instability.

TABLE III

*Surface Energy and Heat Values*

| | Heats of solution (*cal./g. hydrate*) | | | Heat of hydration (*cal./g. $H_2O$*) | Surface energy (*ergs/cm.$^2$*) |
|---|---|---|---|---|---|
| | 0.7 g. samples | 1.0 g. samples | 1.3 g. samples | | |
| Hydrate III | 455.6 ± 6.6 | 450.9 ± 6.6 | 455.3 ± 6.6 | 464.2 ± 49.5 | 418 ± 89 |
| Tobermorite | 450.9 ± 1.1 | 450.3 ± 1.1 | 451.5 ± 1.1 | 422.2 ± 9.9 | 383 ± 20 |

Just why, however, it converts to afwillite rather than to a better crystallized tobermorite, is not known at present.

### *The Kinetics of the Hydration of $Ca_3SiO_5$ in the Ball Mill*

*1.* If the reaction represented by Eq. [1] were a simple one, the rate of disappearance of $Ca_3SiO_5$ would be equal to twice the rate of appearance of afwillite, expressed in moles per unit time. The reaction, however, is complex, and there is no simple relation between the two rates. Nevertheless, it is possible to investigate the kinetics of the hydration, because hydrate III, the intermediate compound, is sufficiently stable for the determination of its amount at any stage of the reaction. Not only the amount but several important properties of the unstable intermediate could be determined quantitatively, as was shown before.

Table IV, columns 3 to 6, gives the amounts of the main constituents in the different batches, expressed in moles per mole of initial $Ca_3SiO_5$. The preparation of each batch was described earlier in this paper. The meaning of "effective grinding time" (column 2) will be explained later.

The last row of Table IV, called "theoretical maximum," gives the maximum amount of each major constituent that can be present in the reaction system (either initially or at the end), expressed in moles per mole of initial $Ca_3SiO_5$. The values follow from the stoichiometry of the reaction, Eq. [1].

*2.* The rate of disappearance of $Ca_3SiO_5$ will be first discussed. In Fig. 1, the four full circles represent the amounts of $Ca_3SiO_5$ left in Batches D-30, D-41, D-38, and D-31 after continuous grindings of 4, 4, 8, and 16 hr., respectively. D-32, another preparation ground continuously for 8

TABLE IV

*Molar Compositions of Ball-Mill Hydrates of $Ca_3SiO_5$*

| 1 Batch | 2 Effective grinding time (*hrs.*) | 3 $Ca_3SiO_5$[a] | 4 Hydrate III[a] | 5 Afwillite[a] | 6 $Ca(OH)_2$[a] |
|---|---|---|---|---|---|
| D-30 | 4 | 0.763 | 0.120 | 0.000 | 0.327 |
| D-41 | 4 | 0.626 | 0.187 | 0.000 | 0.541 |
| D-38 | 8 | 0.404 | 0.217 | 0.081 | 0.881 |
| D-29 | 9.5 | 0.339 | 0.197 | 0.134 | 0.964 |
| D-31 | 16 | 0.075 | 0.244 | 0.222 | 1.366 |
| D-33 | 48 | 0.000 | 0.193 | 0.310 | 1.488 |
| D-27 | 98 | 0.000 | 0.140 | 0.360 | 1.493 |
| D-26 | 112 | 0.000 | 0.176 | 0.324 | 1.493 |
| D-45 | 351 | 0.000 | 0.066 | 0.438 | 1.472 |
| D-57 | 617 | 0.000 | | | |
| *Theoretical Maximum* | | 1.000 | 0.500 | 0.500 | 1.500 |

[a] Moles per mole of initial $Ca_3SiO_5$.

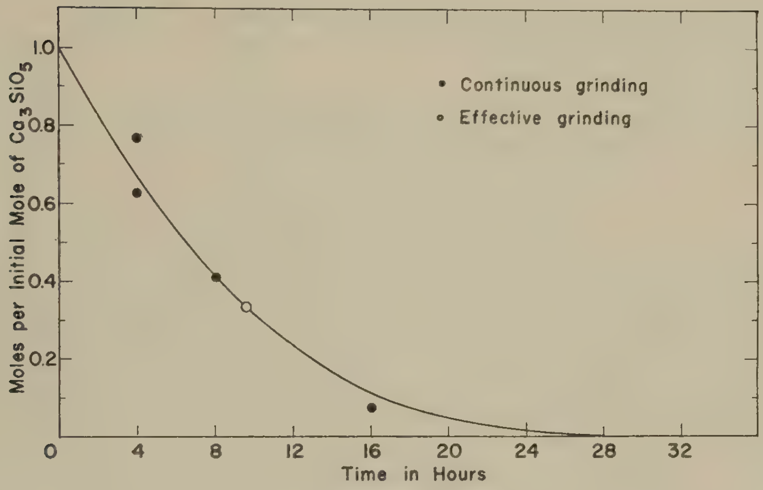

FIG. 1. Variation of $Ca_3SiO_5$ content with time.

hr., thawed during drying, as described before; consequently, it gives no useful information about rates. D-33, ground continuously for 48 hours, contained no unhydrated $Ca_3SiO_5$.

When $Ca_3SiO_5$ is hydrated at room temperature in paste form or in a bottle rotated on a wheel, months are required to achieve complete hydration (2). Hence, the rapid hydration in the ball mill is probably caused by grinding. This suggests the following mechanism. Upon contact with water, the surface of $Ca_3SiO_5$ immediately reacts, forming a hydrate which coats the $Ca_3SiO_5$ substrate. As long as this coating remains undisturbed, hydration of the substrate can occur only as the various species involved diffuse through this coating. The over-all rate of hydration would be slow because of its diffusion-controlled nature. However, if, through grinding action, the coating were continually being removed, leaving fresh $Ca_3SiO_5$ surface, hydration could proceed more rapidly.

If the rate of surface reaction were rapid relative to the surface-exposing process, then the over-all rate of disappearance of $Ca_3SiO_5$ would depend upon grinding factors and available surface area. The grinding coefficient, $c$, would include such terms as the average number of times a unit surface was struck by the steel balls in unit time, and the average amount of material removed per blow. The available area, $A$, is the area contacted by the steel balls. It does not include whatever internal area the particle may have, or even external roughness on a molecular scale. The rate of removal of the coating would then be given by

$$-\frac{d(\text{coating})}{dt} = cA. \qquad [3]$$

The variable area is taken to be proportional to $V^{2/3}$, where $V$ is the volume of $Ca_3SiO_5$. This may not be strictly true, but it is a fair approximation, as the results show.

Let ($Ca_3SiO_5$) be the amount of unreacted $Ca_3SiO_5$ in the system (expressed in moles per mole of initial $Ca_3SiO_5$). It follows that

$$-\frac{d(\mathrm{Ca_3SiO_5})}{dt} = k_1(\mathrm{Ca_3SiO_5})^{2/3} \qquad [4]$$

because the rate of disappearance of $Ca_3SiO_5$ was assumed to be equal to the rate of removal of the coating, and because the area was assumed to be proportional to the ⅔ power of the volume, hence also the weight of $Ca_3SiO_5$. The constant $k_1$ includes $c$, the grinding coefficient. Since ($Ca_3SiO_5$) = 1 when $t = 0$, the integrated form of Eq. [4] is

$$k_1 = \frac{3\,[1 - (\mathrm{Ca_3SiO_5})^{1/3}]}{t}. \qquad [5]$$

The values for $k_1$, calculated from Batches D-30, D-41, D-38, and D-31, are 0.065, 0.109, 0.098, and 0.109 hr.$^{-1}$, respectively. Thus, $k_1$ is constant within the experimental error.

Using the average value of 0.095 hr.$^{-1}$, one obtains the curve shown in Fig. 1. According to Eq. [5], the time required for complete disappearance of $Ca_3SiO_5$ is 31.5 hr. This is in agreement with the experimental observation that $Ca_3SiO_5$ disappears completely at some time between 16 and 48 hr.

*3.* The agreement between calculated and observed $Ca(OH)_2$ contents (Table I, columns 6 and 7) was discussed before. This agreement implies that the stoichiometric amounts of hydrate III (H3) and $Ca(OH)_2$ are liberated as fast as $Ca_3SiO_5$ disappears. Thus

$$\frac{d(\mathrm{H3})}{dt} = k_H(\mathrm{Ca_3SiO_5})^{2/3} \qquad [6]$$

and

$$\frac{d(\mathrm{Ca(OH)_2})}{dt} = k_C(\mathrm{Ca_3SiO_5})^{2/3}. \qquad [7]$$

It follows from Eq. [1] that $k_H = \frac{1}{2}k_1$ and $k_C = \frac{3}{2}k_1$.

*4.* Figure 2 represents the variation of hydrate III and afwillite contents with time. The time scale used is not the time spent in the ball mill (Table I, column 2) but the "effective grinding time" (Table IV, column 2). Some batches were ground continuously, others intermittently—and the latter hydrated both during the grinding period and the standing period. To bring the intermittent batches to the same time scale as the continuous

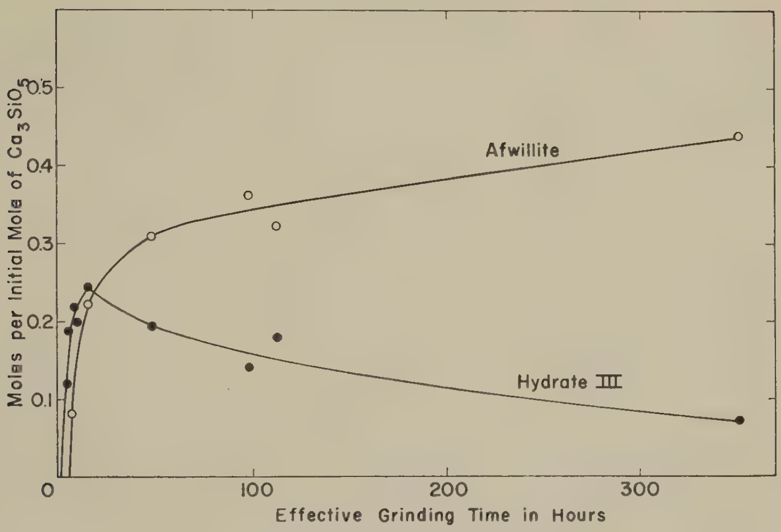

FIG. 2. Variation of afwillite and hydrate III contents with time.

batches, the effective grinding time was defined as the time of continuous grinding required to produce the same extent of reaction as was obtained by intermittent grinding. The calculation was made as follows.

It was assumed that during the standing periods the same processes occurred at slower rates but in the same ratios to one another as during the grinding periods. Batch D-29 was adopted as the standard, and its effective grinding time was taken from Fig. 1. The $Ca_3SiO_5$ content of this batch is represented by the open circle in the figure, and the time corresponding to the $Ca_3SiO_5$ content is 9.5 hr. The intermittent grinding time was 16 hours, of which 4.25 hr. were actual grinding time, and 11.75 hr. were standing time. This standing time, therefore, on the basis of $Ca_3SiO_5$ content, was equivalent to 5.25 hr. of grinding time. The equivalence of 1 hr. standing time to 0.447 hr. of grinding time was adopted for each batch.

*5.* In the initial stages, hydrate III forms faster than it disappears, but after $(Ca_3SiO_5)$ diminishes to a small value, the situation reverses itself. Thus the hydrate III curve in Fig. 2 passes through a maximum.

The conversion of hydrate III to afwillite does not begin immediately upon the appearance of the former in the reaction system. Batches D-30 and D-41, both hydrated for 4 hr., contained no afwillite. Extrapolation of the afwillite curve in Fig. 2 indicates an induction period of about 6 hr. The presence of the induction period probably indicates an autocatalytic mechanism, i.e., a rate dependent on the concentrations of both afwillite and hydrate III.

## ACKNOWLEDGMENTS

We wish to express our indebtedness to Dr. L. E. Copeland for his very helpful suggestions and discussions, to Mrs. Edith Schulz and Miss Elaine Anderson for the X-ray diffraction measurements, and to Mr. E. E. Pressler and Mr. E. LaBonde for the chemical analyses.

## REFERENCES

1. BRUNAUER, S., COPELAND, L. E., AND BRAGG, R. H., *J. Phys. Chem.* **60**, 116 (1956).
2. BRUNAUER, S., KANTRO, D. L., AND COPELAND, L. E., *J. Am. Chem. Soc.* **80**, 761, (1958).
3. BRUNAUER, S., COPELAND, L. E., AND BRAGG, R. H., *J. Phys. Chem.* **60**, 112 (1956).
4. BRUNAUER, S., KANTRO, D. L., AND WEISE, C. H., *J. Phys. Chem.* **60**, 771, (1956).
5. COPELAND, L. E., AND HAYES, J. C., *ASTM Bull.* **No. 194,** December, 1953.
6. BRUNAUER, S., HAYES, J. C., AND HASS, W. E., *J. Phys. Chem.* **58**, 279 (1954).
7. BRUNAUER, S., KANTRO, D. L., AND WEISE, C. H., *Can. J. Chem.* **37**, 714 (1959).
8. PRESSLER, E. E., BRUNAUER, S., AND KANTRO, D. L., *Anal. Chem.* **28**, 896 (1956).
9. PRESSLER, E. E., BRUNAUER, S., AND KANTRO, D. L., To be published in *Anal. Chem.*
10. COPELAND, L. E., AND BRAGG, R. H., *Anal. Chem.* **30**, 196 (1958).
11. BRUNAUER, S., KANTRO, D. L., AND WEISE, C. H., *Can. J. Chem.* **34**, 1483 (1956)
12. BRUANUER, S., KANTRO, D. L., AND WEISE, C. H., *Can. J. Chem.* **34**, 729 (1956).
13. HELLER, L., AND TAYLOR, H. F. W., "Crystallographic Data for the Calcium Silicates," Her Majesty's Stationary Office, London, 1956. p. 50.

JOURNAL OF COLLOID SCIENCE **14**, 377–384 (1959)

# ON THE VISCOELASTIC PROPERTIES OF CRYSTALLINE POLYMERS

## II. Polytrifluorochloroethylene

**Kazuo Nagamatsu and Tatsuya Yoshitomi**

*Department of Applied Science, Faculty of Engineering, Kyushu University, Fukuoka, Japan*

*Received June 11, 1958*

### ABSTRACT

The stress-relaxation of polytrifluorochloroethylene was measured by the torsional method in the temperature range between 6° and 80°C., under small values of strain (maximum 0.5%).

It was found that Ferry's reduction method is perfectly valid for the viscoelasticity of this crystalline polymer under these experimental conditions.

Although the resultant relaxation-time spectrum, extending from $10^{-3}$ to $10^{25}$ seconds, has a flat shape and high values reflecting the common features of crystalline polymers, it has a distinct maximum at about $10^{18}$ seconds.

## I. INTRODUCTION

The simple time-temperature superposition principle of viscoelasticity has been believed to be appropriate only for amorphous polymers (1). The authors, however, have shown in their previous papers its applicability also to certain kinds of crystalline polymers, namely, nylon 6 (2) and polytetrafluoroethylene (3).

In this paper, they will report on the results of stress-relaxation measurements on polytrifluorochloroethylene and discuss the possibility of applying the simple superposition method to this crystalline polymer.

## II. EXPERIMENTAL METHOD

The relaxation of torsional stresses of polytrifluorochloroethylene was measured using a small column cut from a Kel-F plate of uniform thickness. The specimen was 60.0 mm. in length and had a right square cross section of 1.4 × 1.4 mm.

The apparatus is shown schematically in Fig. 1. Here, the specimen *A* is held between two chucks *B* and *C*. The upper chuck *B* is fixed to a long metal rod *D*, which is suspended by a piano string *E*. The upper end of this piano string is connected to the fixed chuck *F*. The torsional strain is applied to the specimen *A* by rotating the lower chuck *C*. The torsional

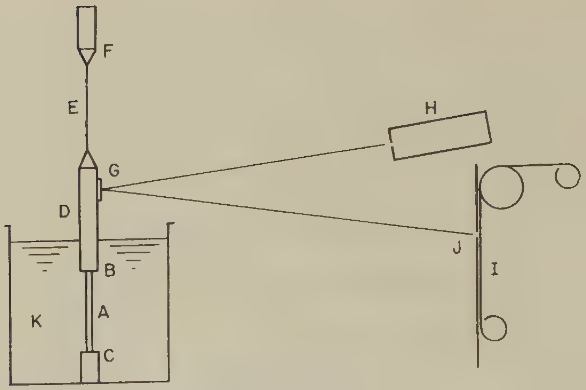

FIG. 1. Schematic diagram of the apparatus.

stress of the specimen is in equilibrium with that of the suspending piano string. The diameter and the length of the piano string $E$ are so selected as to give enough strength in comparison with that of the specimen that the torsional strain of the specimen is kept nearly constant during the course of the measurement. The relaxation of torsional stress is thus converted into the change of rotational displacement of the rod $D$, and recorded on the photographic paper $I$ running automatically behind the narrow horizontal slit $J$, by using the mirror $G$ and the lamp $H$.

The whole specimen is dipped into the thermostat $K$. The temperature fluctuation of this bath was less than 0.1°C. at an arbitrary temperature. The measurements were carried out over the temperature range between 6° and 80°C., from 6 seconds to 5 hours.

The maximum strain at the ridge of the specimen was always less than 0.5% and before each measurement the specimen was kept at constant temperature more than 18 hours in an unstrained state to insure thermal equilibrium. The procedures of measurement were nearly the same as those reported in the previous paper (3).

## III. RESULTS

To ascertain the reproducibility and linearity of the viscoelastic responses, the relaxation measurements were repeated several times with the same specimen under strains of various values. The results were quite reproducible, and the viscoelasticity was found to be perfectly linear under this range of temperature, strain, and treatments. Such reproducibility and linearity show that there occurs no irreversible change in the microscopic structure of the specimen such as change of crystallinity or molecular orientation under these experimental conditions.

The stress-relaxation curves measured at different temperatures are shown in Fig. 2. By a simple time-temperature superposition (or so-called

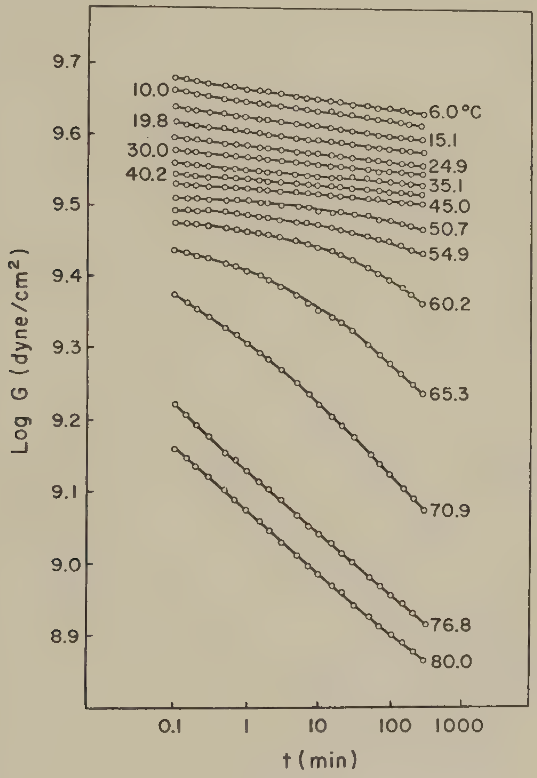

FIG. 2. Stress relaxation curves of polytrifluorochloroethylene at various temperatures.

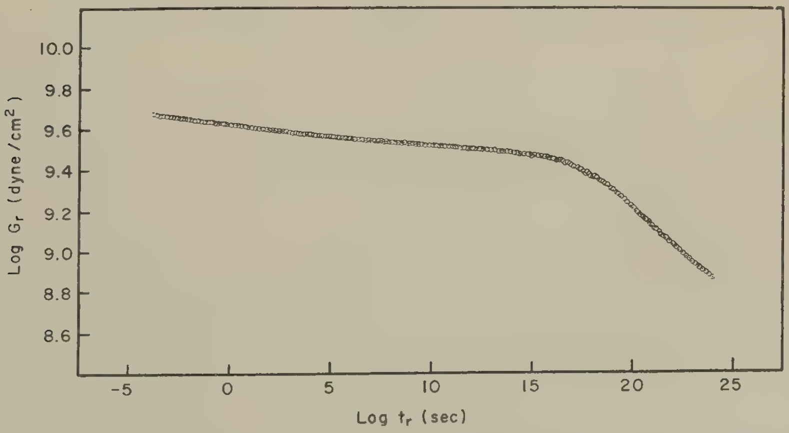

FIG. 3. Stress relaxation master curve of polytrifluorochloroethylene reduced to 20°C. Key to temperatures: upward pip, 6.0°C.; successive 45° rotation clockwise correspond to increasing temperatures at approximately 5° or 10° intervals.

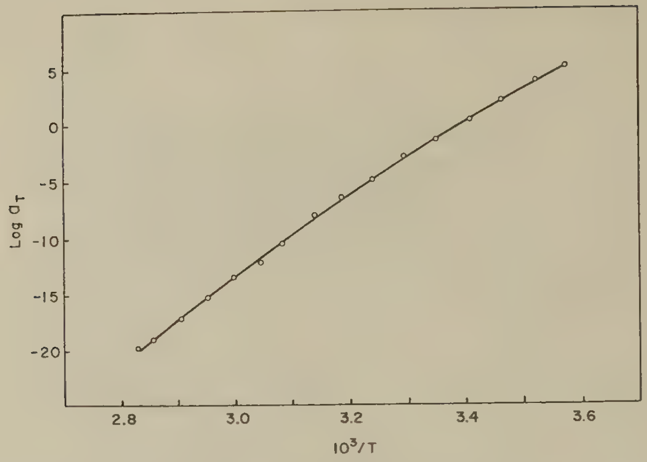

FIG. 4. Relation between Ferry's reduction factors $a_T$ and temperature.

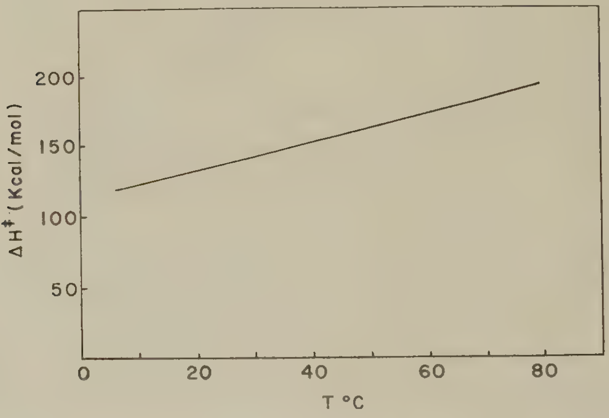

FIG. 5. Relation between the apparent activation energy $\Delta H^\ddagger$ and temperature.

Ferry's reduction method (4)), these relaxation curves can be made to overlap one another quite well, giving the so-called relaxation master curve shown in Fig. 3.

In Fig. 4, the reduction factors $a_T$ are plotted against $1/T$. Differentiation of this curve gives the relation between the so-called apparent activation energy $\Delta H^\ddagger$ and the temperature. The result of this calculation is shown in Fig. 5.

## IV. DISCUSSION

As is seen in Fig. 3, the application of Ferry's reduction method gives a fine master curve. All points lie accurately on this master curve, and almost all parts of this curve are composed of two or three componential relaxation curves. The indisputable conclusion is that Ferry's reduction method is appropriate for this crystalline polymer.

In this procedure, however, the master curve is derived without the use of the correction term of $T/T_0$ in Ferry's equation [4] (4), where $T$ is the temperature of the relaxation measurement, and $T_0$ is the reference temperature used for the reduction. It is reasonable to omit this temperature correction term in the case of crystalline polymers, because it is introduced from the entropy elasticity, which may have less contribution to the elasticity of crystalline polymers. This omission, however, matters little, for the correction is nearly equal to unity over the entire temperature range of measurements.

It is well known that Tobolsky and his co-workers paved the way in the study of rheological properties of crystalline polymers. In 1955, they reported on the measurements of the stress-relaxation of polytrifluorochloroethylene (5). They pointed out that the simple time-temperature superposition (or Ferry's reduction method) that holds properly for amorphous polymers in the transition region is not valid for polycrystalline polymers. The temperature range of their measurements was between 30° and 193°C. As is mentioned in their paper, such a range surely includes the temperature where some changes in microcrystalline structure take place, which will also cause some important vertical shift of relaxation curves along the log $E$ axis. Such vertical displacement introduced by the change of internal structure was clearly observed by the rheological properties of nylon 6 (2).

According to the measurement of the effect of heat treatment on polytrifluorochloroethylene (6), this polymer is found to show a marked irreversible increase in its crystallinity in 1 hour over 100°C. Some of Tobolsky's measurements were made in this range, and as stated by him, the time-temperature superposition principle is not applicable here. The complications introduced by a gradual change in crystallinity were even more strikingly shown for the case of natural rubber at $-25$°C. (1).

Comparison of the experimental results obtained by Tobolsky *et al.* with those of the authors, shows that the inapplicability of Ferry's method does not stem from the fact that the polymer is semicrystalline, but from the change of its crystallinity during the relaxation measurement. In this sense, it may be concluded that the rheological data for crystalline polymers under appropriate experimental conditions can be treated similarly to those for amorphous polymers. Thus it becomes an important task to seek experimental conditions where the simple time-temperature superposition method is appropriate for crystalline polymers. As is stated above, the time-temperature superposition principle can be applied to the relaxation data of polytrifluorochloroethylene, at least under the smallest values of strain and within the temperature range between 6° and 80°C. Since this temper-

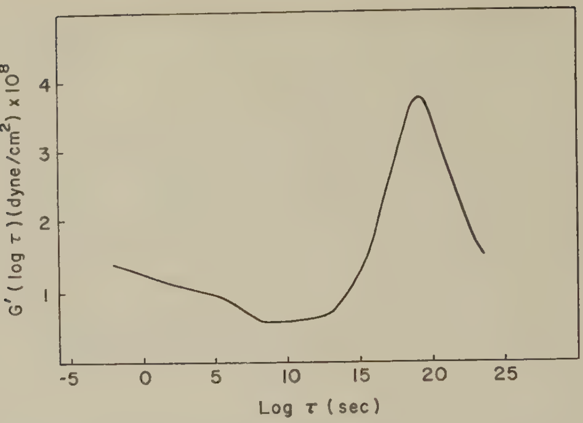

FIG. 6. Relaxation-time spectrum of polytrifluorochloroethylene at 20°C.

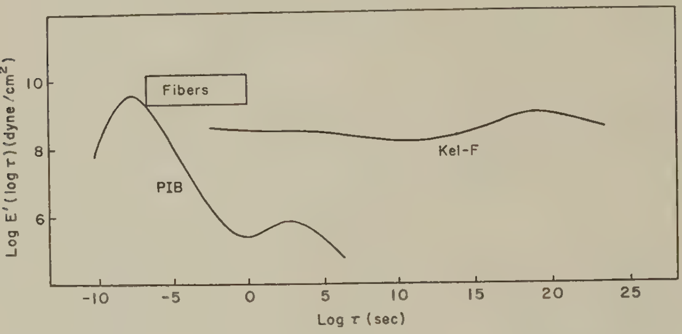

FIG. 7. Relaxation-time spectrum of polytrifluorochloroethylene, with those of several other polymers.

ature range was restricted only by the range of the thermostat, it has no definite meaning. The actual range of availability of Ferry's reduction method for this polymer may be wider.

Using the first-order approximation method (7) on the master curve shown in Fig. 3, the relaxation-time spectrum of polytrifluorochloroethylene at 20°C. is obtained. This spectrum, shown in Fig. 6, extends from $10^{-3}$ to $10^{25}$ seconds, with its distinct maximum at nearly $10^{18}$ seconds. Perhaps it will have another weak broad maximum at the shorter part of the time scale. These peaks are thought to correspond with the maxima of the temperature dispersion of the mechanical loss factor (8) at 104° and 0°C., respectively. But because of the insufficiency of related data, it is unjustified to refer to their correlation with molecular mechanisms, and the detailed discussion of this relation will be left for another occasion.

Figure 7 shows the comparison of relaxation-time spectra of several polymers in the usual scales of axes, instead of $G'$ vs. $\log \tau$ used in Fig. 6.

The square in the figure indicates the region where almost all relaxation-time spectra of filamentous (or crystalline) materials fall (9). As the torsional method was used in this experiment, the resultant data are for the relaxation of shear modulus $G$. For convenient comparison with other polymers, this is converted into the relaxation of Young's modulus $E$ using the simple assumption that $E = 3G$. As is seen in Fig. 7, the relaxation-time spectrum of polytrifluorochloroethylene is flat and has high values all over the measured range of time scale, in contrast with amorphous polymers represented by polyisobutylene (10). Such a flat shape and high values are common to other crystalline polymers (1, 2), and they must originate from the restriction of chain mobility in polycrystalline structures.

Besides these characteristic features of crystalline polymers, there are seen some differences in the character of viscoelasticity in the case of this polymer. In Fig. 5, the apparent energy of activation increases with the increase of temperature, and accordingly the temperature dependency of the reduction factor $a_T$ can not be expressed by the so-called WLF equation (11). This is a strange phenomenon, for which the authors are unable to give any reasons at present.

## V. Summary

The authors have found the simple time-temperature superposition method to be valid for the viscoelasticity of polytrifluorochloroethylene, if measured under the smallest values of strain and within the temperature range between 6° and 80°C. The resultant relaxation-time spectrum of this polymer at 20°C. has a distinct maximum at the point near $10^{18}$ seconds. It is also supposed that it has another weak broad maximum at the shorter range of time scale. Along with the relaxation-time spectra of nylon 6 and polytetrafluoroethylene reported in previous papers, it can be concluded that the flat shape and high values of the relaxation time spectrum are common features of the crystalline polymers, and are thought to arise from the restriction of chain mobility in polycrystalline systems.

In addition to this conclusion, it has been clarified that Ferry's reduction method has fairly wide applicability for crystalline polymers. The necessary conditions of such applicability are (*a*) smaller values of strain as compared with amorphous polymers, (*b*) a temperature range where no structural change occurs, and (*c*) good conditioning of the specimen.

The authors are indebted to all the members of the rheologists' group in this university for their instructive discussions throughout the course of this investigation.

## References

1. Tobolsky, A. V., *in* F. R. Eirich, ed., "Rheology, Theory and Applications," Vol. 2, p. 63. Academic Press, New York, 1958.

2. Yoshitomi, T., Nagamatsu, K., and Kosiyama, K., *J. Polymer Sci.* **27,** 335 (1958).
3. Nagamatsu, K., Yoshitomi, T., and Takemoto, T., *J. Colloid Sci.* **13,** 257 (1958).
4. Ferry, J. D., *J. Am. Chem. Soc.* **72,** 3746 (1950).
5. Tobolsky, A. V., and McLoughlin, J. R., *J. Phys. Chem.* **59,** 989 (1955).
6. Nakane, R., Meeting on Polymer Physics of Physical Society of Japan, University of Shizuoka, May, 1957.
7. Andrews, R. D., *Ind. Eng. Chem.* **44,** 707 (1952).
8. Schmieder, K., and Wolf, K., *Kolloid-Z.* **134,** 149 (1953).
   Nagamatsu, K., *Progr. Theoret. Phys., Supplement,* (1959), in press.
9. Fujino, K., Kawai, H., and Horino, T., *Textile Research J.* **25,** 722 (1955).
10. Marvin, R. S., *Proc. 2nd Intern. Congr. Rheol.*, p. 156 (1954).
11. Williams, M. L., Landel, R. F., and Ferry, J. D., *J. Am. Chem. Soc.* **77,** 3701 (1955).

JOURNAL OF COLLOID SCIENCE 14, 385–400 (1959)

# THE ELIMINATION OF ERRORS DUE TO EVAPORATION OF THE SOLUTE IN THE DETERMINATION OF SURFACE TENSIONS

**Jacques R. Hommelen**

*Université Libre de Bruxelles, Brussels, Belgium*

*Received July 15, 1958*

## I. INTRODUCTION[1]

It is well known that a correct measurement of the static surface tension of a solution, that is, the tension of a surface in thermodynamical equilibrium with the bulk, requires that:

*1*. Sufficient time be allowed for the attainment of the adsorption equilibrium.

*2*. The solution must be under conditions such that equilibrium between the gas phase and the solution is attained, so that evaporation cannot occur. Unless this condition is satisfied it is probable that with a volatile solute, surface tension values higher than the equilibrium values would be obtained.[2]

In general, the possibility of errors due to evaporation have been considered by other authors. These errors would probably be eliminated, for instance, by the use of the Harkins and Jordan apparatus (9). However, by reason of their convenience, other experimental devices have been frequently used which have allowed, as it will be shown further, more important errors than would be reasonably supposed.

The experimental data about surface tensions of the aqueous solutions of heavy alcohols seem to have been particularly influenced by these errors (1, 4–8). The present work shows how better results can be obtained by using a very simple modification of the ordinary du Noüy ring tensiometer.

On the other hand, the pendent drop method is shown to be very susceptible to these errors, and it has been used in the present work to explain the origin of the minimum observed by Ward and Ottman (1) in the time curves of the surface tension of drops and to interpret the "bag effect" of Addison (4).

---

[1] The subject has been recently treated by the author in a paper published in French in the *Bull. soc. chim. Belges* 66, 476 (1957). That paper has now been translated, revised, and completed for the present publication.

[2] A similar evaporation phenomenon creates tears on the walls of a glass containing a strongly alcoholic liquor. Merigoux (2) reminds us that this phenomenon is known by the name of "James Thomson's pearls" or by the name of "vin capiteux des Hébreux". Solomon said therefore: "Do not drink wine if it is red and if it comes up by itself in the cup" (3).

## II. PURIFICATION OF CHEMICALS USED AND PHYSICAL CONSTANTS

### *A. Alcohols*

The refractive indexes ($n_D^{20}$) of the alcohols used are given below:

| | I | II | III |
|---|---|---|---|
| Normal hexyl alcohol | 1.4180 | | 1.4179 |
| Isohexyl alcohol[3] | 1.4223 | | 1.421 |
| 1-Methyl pentanol[3] | 1.4113 | 1.411 | 1.4126 |
| 1-Dimethyl butanol | 1.4107 | | |
| Normal heptyl alcohol[3] | 1.4246 | 1.425 | 1.4241 |
| Dipropyl carbinol | 1.4201 | 1.421 | 1.4205 |
| Ethyl butyl carbinol[3] | 1.4219 | 1.4206 | |
| Normal octyl alcohol | 1.4291 | 1.430 | 1.4292 |
| Methyl hexyl carbinol[3] | 1.4259 | | 1.4260 |
| 2-Ethyl hexanol[3] | 1.4313 | | |
| Normal nonyl alcohol | 1.4339 | 1.4338 | 1.4335 |
| 3,5,5-Trimethyl hexanol[3] | 1.4322 | | |
| Normal decyl alcohol | 1.4369 | | 1.4368 |

I: Our values.
II: "International Critical Tables."
III: "Handbook of Chemistry and Physics" (C. D. Hodgman).

Although samples of some of these alcohols were obtained from different sources and had slightly different refractive indexes, the surface tensions of their aqueous solutions at any given concentration were the same.

### *B. Acids*

We used capric acid obtained from the "Institut Pasteur" in Paris, where it had been purified by distillation; a sample (m.p. 31.2°C.) of it was kindly given to us by M. Dervichian. This acid gave the same results as those obtained with another sample (m.p. 30.5°C.) obtained from Fluka.

---

[3] Alcohols obtained by fractional vacuum distillation of technically pure alcohols obtained from Fluka, B.D.H., or Kodak. This purification in general modified the refractive index, but on no occasion was the value of the static surface tensions of the aqueous solutions of these alcohols markedly altered by initial purification of the alcohol. It is unlikely therefore that any trace of impurity remaining would alter the values of the surface tension obtained.

### C. *Water*

Most of the results mentioned in this work have been obtained by preparing solutions in triple distilled water. However, similar results were always obtained when ordinary distilled water was used, the surface tension of which had been previously checked (72.6 to 72.8 dynes/cm.).

All our apparatus were frequently cleaned with a chromic-sulfuric mixture.

### D. *Temperature*

All surface tension measurements reported in this work were carried out in a room maintained at a temperature of 20° ± 0.5°C.

## III. MEASUREMENTS WITH THE RING

### A. *Experimental Technique*

We have measured the static surface tensions of a series of aqueous solutions of heavy alcohols and acids with Lecomte du Noüy's ring tensiometer. To eliminate completely the evaporation of the surface we proceeded as follows:

An empty dish, 3 cm. high, 5 cm. in diameter, designed to contain the solution to be studied, was placed under the ring of the tensiometer (the ring being ½ cm. from the bottom of the dish). The dish was then almost completely closed by laying two photographic glass plates (together 6 cm. × 6 cm.) on its level grinded edges; 10 ml. of the solution were pipetted into the dish between the two half plates which were then brought together. The platinum wire supporting the ring passed through a small aperture formed by two notches in the plates. The surface tension was then measured in the usual manner.

The uncorrected surface tension is given by:

$$\sigma_{\text{uncorr.}} = \frac{Mg}{4\pi R},$$

where $R$ is the radius of the ring and $Mg$ is the maximum force that can be applied on the ring by the torsion wire. This force equals the maximum weight of liquid that can be lifted by the ring.

The corrected surface tension ($\sigma_{\text{corr.}}$) was then calculated by multiplying $\sigma_{\text{uncorr.}}$ by the correction factor $F$ obtained from the tables of Harkins and Jordan (9, 10).

This factor is a function of $R^3/V$ for a constant value of $R/r$ ($r$ = radius of ring-wire, $V$ = maximum volume of liquid lifted by the ring):

$$\sigma_{\text{corr.}} = F\left(\frac{R^3}{V}, \frac{R}{r}\right) \times \frac{Mg}{4\pi r}.$$

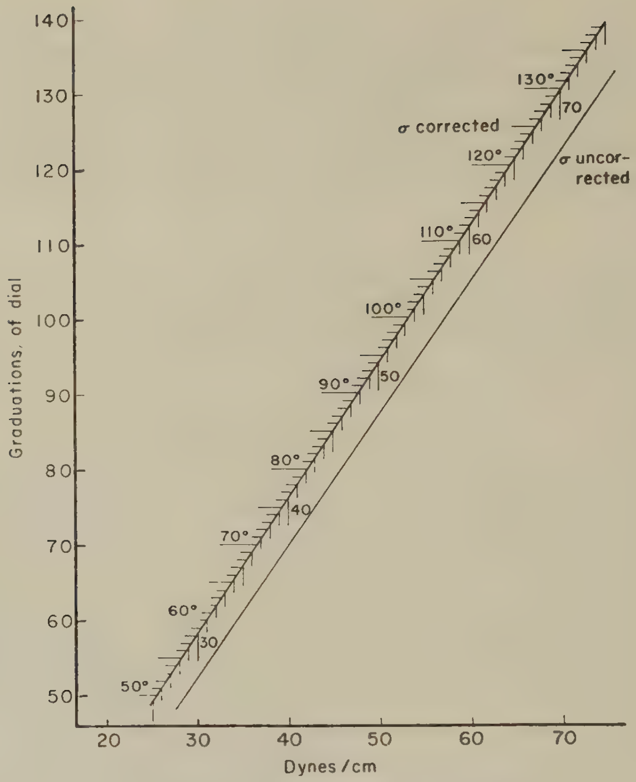

FIG. 1. Calibrating curve of the ring tensiometer.

All the solutions used were sufficiently dilute that their densities could be considered constant and equal to that of water. With dilute solutions and with the use of the same ring it follows therefore that $\sigma_{\text{corr.}}$ depends only on the maximum force applied by the torsion wire on the ring. A calibration graph can thus be drawn relating $\sigma_{\text{corr.}}$ with the dial reading of the tensiometer (Fig. 1). This curve permits the rapid use of the ring tensiometer for dilute aqueous solutions.

The dimensions of the ring used were:

$$R = 0.978 \text{ cm.}$$

$$r = 0.016 \text{ cm.}$$

The torsion wire exerts on the ring a force of 1 g. or 981 dynes for 139.5 graduations on the dial. The maximum error is ±0.2 graduation, or about 0.1 dyne/cm.

### *B. Results*

*1. Errors Caused by Evaporation.* It is proposed now to discuss details of the effect of the evaporation of the solute on the static surface tensions measured with the ring in an open dish.

The second column of Table I gives the static surface tensions measured in a closed dish, as previously described. In this case adsorption equilib-

TABLE I

*Effect of Evaporation on Measurements of Surface Tension*

| Solutions | | $\sigma_c$ | $\sigma_o$ | $\sigma_l$ |
|---|---|---|---|---|
| Normal hexyl alcohol | (0.8 g./l.) | 54.7* | 55.7* | 57 (*a, d*) |
| Isohexyl alcohol | (0.8 g./l.) | 59.9 | 60.5 | |
| Secondary hexyl alcohol (1-methyl pentanol) | (0.8 g./l.) | 59.8 | 60.3 | |
| Tertiary hexyl alcohol (1-dimethyl butanol) | (0.8 g./l.) | 62.2 | 62.8 | |
| Normal heptyl alcohol | (0.4 g./l.) | 49.5 | 50.7 | 51.3 (*g*)<br>52.2 (*a, d*) |
| Secondary heptyl alcohol (dipropyl carbinol) | (0.4 g./l.) | 58.4 | 59.0 | |
| Secondary heptyl alcohol (ethyl butyl carbinol) | (0.4 g./l.) | 58.9 | 59.4 | |
| Normal octyl alcohol | (0.2 g./l.) | 42.6 | 44.2 | 46.0 (*a*)<br>44.3 (*e*)<br>47.7 (*h*) |
| Secondary octyl alcohol (Methyl hexyl carbinol) | (0.2 g./l.) | 52.0** | 53.1** | 53.1 (*e*)<br>56 (*a, d*) |
| Branched octyl alcohol (2-ethyl hexanol) | (0.2 g./l.) | 52.4 | 53.6 | |
| Normal nonyl alcohol | (0.1 g./l.) | 33.7 | — | |
| Branched nonyl alcohol (3,5,5-Trimethyl hexanol) | (0.08 g./l. | 53.0 | 55.0 | |
| Normal decyl alcohol | (0.02 g./l.) | 39.0 | 45.0 | 44 (*c*)<br>47 (*h*)<br>47.5 (*d*) |
| Capric acid ($C_{10}$) | (0.04 g./l.) | 39.8 | 39.8 | 43 (*d*)<br>41.8 (*f*) |

$\sigma_c$: static surface tension measured with the ring in a closed dish.

$\sigma_o$: static surface tension measured with the ring in an open dish.

*: surface tension measured with the ring and the drop weight.

**: surface tension measured with the ring and the dipping plate.

$\sigma_l$: surface tension of literature: (*a*) Addison (oscillating jet) (11); (*c*) Addison (dipping plate) (4); (*d*) Addison (drop) (4, 11); (*e*) Posner and Alexander (ring) (5, 12); (*f*) Ward and Ottman (drop) (1); (*g*) Sutherland (ring) (6–8); (*h*) Harva (ring) (13).

*Note:* These results are shown graphically in Fig. 2 for $\sigma_c$ and $\sigma_l$.

rium was reached, for the concentrations used, in 10 minutes for normal nonyl alcohol, in 1 hour for normal decyl alcohol, in 30 minutes for capric acid, and in less than 1 minute for the other solutions.

When a determination in a closed dish had been carried out, the glass covering plates were removed and the surface tension was redetermined a few seconds later. The results in each case are given in Table I, column 3; agreement with the findings of other workers (column 4) is apparent in some instances. Replacement of the covering plates, however, caused a decrease in the surface tension within a few seconds to a value corresponding to that given in column 2. If, however, the dish was left uncovered, the surface tension was found to increase, but the rate of increase fell considerably after the first few seconds. For the decyl alcohol solution the increase continued until, after about 15 hours, an equilibrium value close to that of water was attained. This slow change was found to be irreversible, as the values given in Table I could not be reproduced by replacing the glass plates on the dish. A definite loss of solute would thus appear to have occurred.

In the case of capric acid there was no rapid increase of the surface tension on uncovering the dish, but a gradual increase continued for several days without attaining the water value.

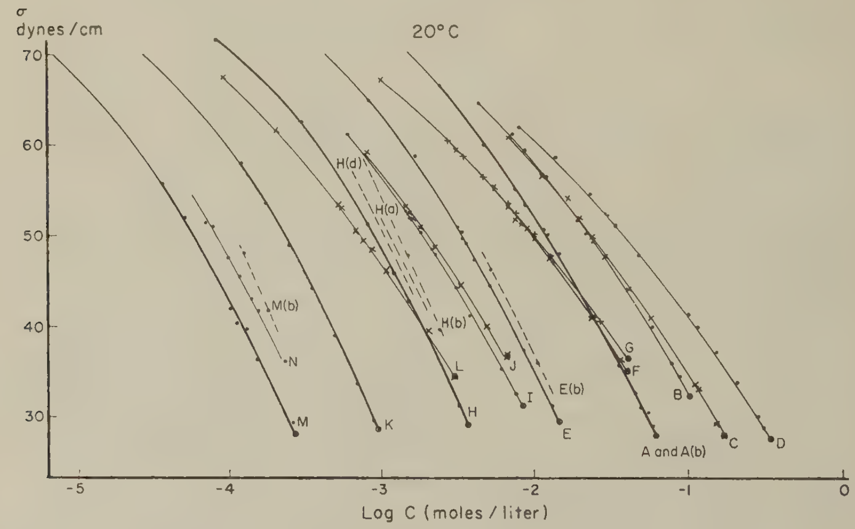

FIG. 2. Static surface tensions of aqueous solutions (20° C.). *A*. Normal hexyl alcohol; *B*. Isohexyl alcohol; *C*. 1-Methyl pentanol; *D*. 1-Dimethyl butanol; *E*. Normal heptyl alcohol; *F*. Ethyl butyl carbinol; *G*. Dipropyl carbinol; *H*. Normal octyl alcohol; *I*. Methyl hexyl carbinol; *J*. 2-Ethyl hexanol; *K*. Normal nonyl alcohol; *L*. 3,5,5-Trimethyl hexanol; *M*. Normal decyl alcohol; *N*. Capric acid ($C_{10}$), pH = 2; (*a*) Addison; (*b*) Harva; (*d*) Posner, Alexander, and Anderson.

Table I also includes surface tensions measured by the plate method (Wilhelmy) under the same conditions. The results agree with those obtained by the ring method.

Thus after the initial rapid loss has occurred, the rate of loss by evaporation becomes very slow, and this may have led other workers (column 4) to regard the values of surface tension obtained at this stage as equilibrium values.

Comparison of columns $\sigma_c$ and $\sigma_o$ of Table I shows that the most marked evaporational effects occurred with the higher and therefore less volatile alcohols. Because of their lower solubility and higher surface activity, these alcohols were used at lower concentrations, and consequently the amount which was available to diffuse to the surface was much less. Evaporation would thus have led to an impoverishment of the superficial layer to a greater extent than would occur with lower alcohols.

*2. Static Surface Tensions of the Aqueous Solutions.* The values obtained by the ring method and with the use of the glass cover plates are shown as a graph of surface tension against log concentration in Fig. 2. Comparison with the results of other workers (dotted lines) serves to emphasize again the differences caused by the evaporation effect.

The slopes of the curves in Fig. 2 give the relative Gibbs adsorptions of the solutes. Thus, at constant temperature ($T$) and pressure, this adsorption, in the case of an ideal dilute solution, is given by:

$$\Gamma = -\frac{C}{RT} \times \frac{\partial \sigma}{\partial C} = -\frac{1}{RT} \times \frac{\partial \sigma}{\partial \ln C},$$

where $C$ is the concentration of the solute and $R$ is the gas constant (ergs/mole × °C.). This gives at 20° C.

$$\Gamma = -\frac{0.4105 \times 10^{-10}}{2.303} \times \frac{\sigma}{\log_{10} C} \text{ moles/cm.}^2.$$

The values of the adsorptions when the solutions are nearly saturated are given in Table II for each alcohol. The areas occupied by the molecules are then deduced and can be compared with some published values.

The lowest point on each curve in Fig. 2 represents the saturated solution. The surface tension of each saturated solution was determined and the corresponding concentration required to plot the point was obtained in two ways: (*1*) by intrapolating the $\sigma$-log $C$ curve (already plotted for lower concentrations) to the saturated tension value; (*2*) by diluting to a known extent the saturated solution, determining its tension, and interpolating the concentration from the $\sigma$-log $C$ graph. The solubility could then be easily calculated.

Concordant results were obtained by these two methods. The solubilities are given in Table II, together with some published values.

TABLE II

*Results for Adsorption, Molecular Area, and Solubility*

| | | Γ (saturation) (*$10^{-10}$ moles/cm.$^2$*) | Molecular area ($A^2$) | | Solubility (*moles/liter*) | |
|---|---|---|---|---|---|---|
| | | | Our measurements | Literature values | Our measurements | Literature values |
| Normal hexyl alcohol | *A** | 6.0 | 28 | 26–28 (*b*)<br>28.5 (*d*) | $6.07 \times 10^{-2}$ | $6.9 \times 10^{-2}$ (*a*)<br>$6.2 \times 10^{-2}$ (*b*)<br>$6.1 \times 10^{-2}$ (*c*) |
| Normal heptyl alcohol | *E* | 6.0 | 28 | | $1.45 \times 10^{-2}$ | $1.48 \times 10^{-2}$ (*a*)<br>$1.24 \times 10^{-2}$ (*b*)<br>$1.56 \times 10^{-2}$ (*c*) |
| Normal octyl alcohol | *H* | 5.9 | 28 | | $3.68 \times 10^{-3}$ | $3.22 \times 10^{-3}$ (*a*)<br>$2.7 \times 10^{-3}$ (*b*)<br>$4.5 \times 10^{-3}$ (*c*) |
| Normal nonyl alcohol | *K* | 6.1 | 27 | | $9.34 \times 10^{-4}$ | |
| Normal decyl alcohol | *M* | 5.9 | 28 | | $2.69 \times 10^{-4}$ | $2.27 \times 10^{-4}$ (*a*)<br>$2 \times 10^{-4}$ (*b*) |
| Isohexyl alcohol | *B* | 5.2 | 32 | | $1.02 \times 10^{-1}$ | |
| 1-Methyl pentanol | *C* | 4.8 | 35 | | $1.69 \times 10^{-1}$ | |
| 1-Dimethyl butanol | *D* | 4.5 | 37 | | $3.64 \times 10^{-1}$ | |
| Ethyl butyl carbinol | *F* | 4.5 | 37 | | $4.10 \times 10^{-2}$ | |
| Dipropyl carbinol | *G* | 4.2 | 40 | | $4.09 \times 10^{-2}$ | |
| Methyl hexyl carbinol | *I* | 5.4 | 31 | | $8.6 \times 10^{-3}$ | |
| 2-Ethyl hexanol | *J* | 4.9 | 34 | | $6.76 \times 10^{-3}$ | |
| 3,5,5-Trimethyl hexanol | *L* | 4.7 | 35 | | $3.12 \times 10^{-3}$ | |
| Capric acid | | 6.1 | 27 | 31 (*e*)<br>30.5 (*d*) | — | |

(*a*) Addison (4, 11); (*b*) Harva (13); (*c*) Butler, Thomson, and Mc Lennan (14); (*d*) Taubman (15); (*e*) Harkins (16). See also reference 17.

* Capital letters in second column refer to Fig. 2.

In Fig. 3 the log of the solubility is plotted against the number of carbon atoms in the normal alcohol chains. Results obtained by Addison (4, 11) and Harva (13) (by the extrapolation procedure) are shown as well as those of Butler *et al.* (14) using a different technique. A linear relationship is obtained since the curves of Fig. 2 are equidistant for the normal alcohols, and also because the static surface tensions of the saturated solutions have nearly the same value (see reference 18).

The constant distance from one curve to the next is a manifestation of Traube's law (19, 20), which states that, provided the solution is dilute,

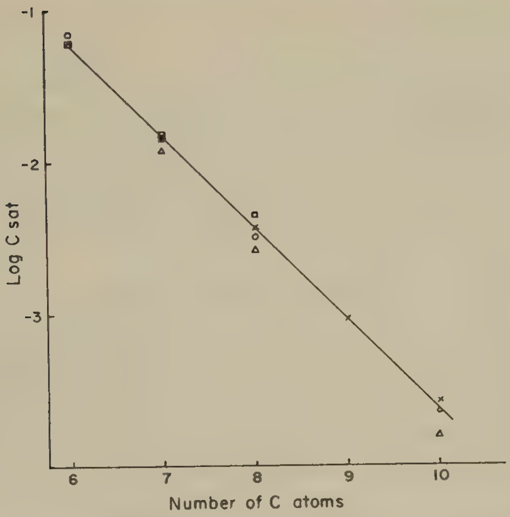

FIG. 3. Logarithm of solubility as a function of the length of the normal alcohol chains (20°C.). ○ Addison; × Hommelen; △ Harva; □ Butler *et al.*

the concentration at which equal lowering of surface tension is observed, is divided by a constant factor[4] for each additional $CH_2$ group in a homologous series of alcohols or acids. This equidistance is also a result of the identical slope of these curves, i.e., of the identical adsorption of the considered alcohols. This identical adsorption and consequently identical molecular area supports the suggestion that the alcohol molecules form a monomolecular layer on the surface, with the carbon chains extending away from the surface.

The secondary, tertiary, and branched alcohols (Fig. 2) give curves which are less steep, corresponding to lower adsorptions. This agrees with the conception of the larger cross-sectional area of these molecules.

The slope of the curve relating to the capric acid (Fig. 2) shows that the adsorption is the same as that of the normal alcohols.

## IV. MEASUREMENTS WITH DROPS

If a drop of solution is allowed to form on the lower tip of a capillary tube of known external diameter, the surface tension of this drop can be measured in different ways.

### *A. The Drop Weight Method*

This method consists in weighing the drop which falls slowly from the tip of a vertical tube, as described by Harkins for pure liquids (16, 21). The weight of the drop, the density of the liquid, and the radius of the capillary tip are sufficient to determine the surface tension of the falling drop.

---

[4] This factor had a value of about 3.8 in these experiments.

In the case of solutions which reach their adsorption equilibrium very slowly, the rapid and extensive increase in surface area of the drop at the moment of fall can increase the surface tension by lowering the amount of adsorbed solute per unit area (22). The extension of this method to include a study of solutions is therefore possible only if the solutions attain their adsorption equilibrium rapidly.

### *B. The Drop Shape Method*

Andreas, Hauser, and Tucker (23) have developed a method in which the surface tension is calculated from observations on the shape of pendent drops. Measurements necessary to determine the shape of the drop, however, usually require specialized equipment. Fordham (24) has computed a good table for the use of this method.

### *C. The Drop Length Method*

A simplification of the drop shape method due to Addison (4) is to form drops of constant volume on a capillary tip and to measure only the length of the drops. A calibration curve is initially prepared from determinations with solutions of known surface tension.

### *D. Experimental Procedure*

The apparatus (drop length method) used in the present work (Fig. 4) consisted of a micrometer screw (*A*), an insulin glass syringe (*B*, *C*), and a Pyrex capillary tube (*D*), 0.446 cm. in external diameter, attached to the syringe by a ground glass joint. A colorimeter cell (*E*) of 4 ml. capacity was attached to the capillary tube by means of a cork having a small air inlet hole. The cell contained 2 ml. of the solution under test, and the capillary tip was placed very near the surface of the solution so that a saturated atmosphere was maintained around the drop (see later).

Under these conditions a movement of the piston of 1 cm. expelled 0.1815 ml. of liquid from the capillary tip. Initial tests showed that careful greasing[5] of the ground glass joint between the syringe and capillary and also of the piston and the syringe wall, was necessary to prevent slight losses.

The syringe was filled with a solution of known surface tension (ring method), and a few drops were expelled by screwing the micrometer head. A flat meniscus was formed at the capillary tip by readjusting the micrometer head (zero reading). A drop of known volume was then formed

---

[5] Greasing had been done with vaseline to prevent pollution of the solution. It was, however, essential to minimize direct contact between vaseline and solution to prevent absorption of the solute into the vaseline.

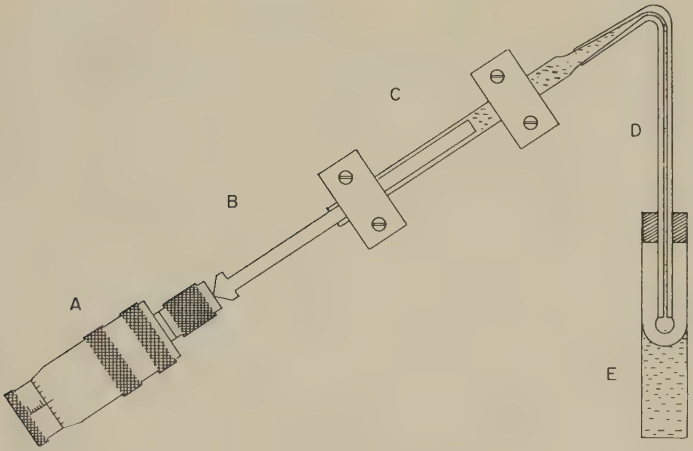

FIG. 4. Drop length apparatus.

TABLE III

*Standardization of the Drop Length Method with Normal Hexyl Alcohol Solutions*

| *C* (*g./l.*) | $\sigma_r$ | $\sigma_d$ | Length[a] of the drops for a volume in cm.$^3$ of | | | | | |
|---|---|---|---|---|---|---|---|---|
| | | | 0.0363 | 0.0454 | 0.0545 | 0.0590 | 0.0635 | 0.0726 |
| 5 | 31.4 | 31.4 | 245.5 | | | | | |
| 3.2 | 37.2 | 37.2 | 228 | 297 | | | | |
| 2.5 | 41.2 | 41.3 | 220 | 272 | | | | |
| 1.67 | 46.7 | 46.7 | 213 | 256.5 | 319 | | | |
| 1 | 52.9 | 52.9 | 209 | 248.5 | 292 | 320.5 | | |
| 0.71 | 56.8 | 56.8 | 206.5 | 243.5 | 283 | 308 | 335 | |
| 0.5 | 60.4 | 60.3 | 205 | 241 | 278 | — | 322.5 | |
| 0.25 | 66.3 | 66.3 | 203 | 237 | 270.5 | — | 307.5 | 354 |
| 0 | 72.8 | 72.6 | 202 | 234 | 265 | 282 | 299 | 336 |

$\sigma_r$: surface tension measured with the ring (dynes/cm.).

$\sigma_d$: surface tension checked by the drop weight method (dynes/cm.).

[a] The length is expressed in arbitrary units (100 units = 0.161 cm.) in terms of the reticle graduation.

on the tip and its vertical height measured with a cathetometer having a moving reticular eyepiece. This procedure was carried out for water and eight concentrations of *n*-hexyl alcohol solutions, with up to six different volumes selected in each case. The surface tension of each solution was confirmed by the drop weight method using the same apparatus (the weight of the drop being calculated from its maximum volume). Earlier tests with the oscillating jet had shown that the adsorption equilibrium of these solutions was complete within 0.005 second (25, 26). The calibration

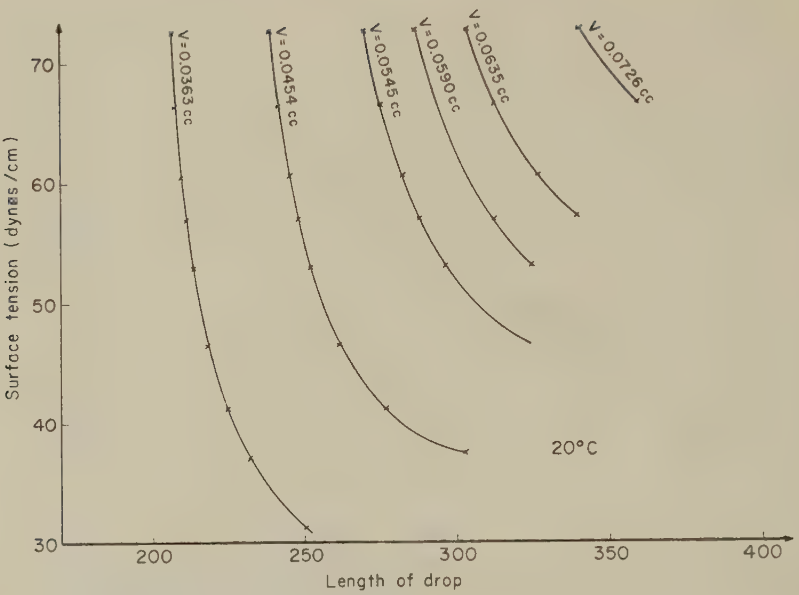

FIG. 5. Calibrating curve of the drop length tensiometer.

values are given in Table III and are plotted in Fig. 5 for each of the six drop volumes utilized.

The surface tension of any other solution can then be determined by filling the syringe, forming a drop having one of the six selected volumes on the capillary tip, and measuring its vertical height. It was clearly preferable to select the largest volume of drop, thus using the curve with the lowest gradient.

However, since the surface of the second and subsequent drops formed by this procedure is always slightly contaminated with a residual proportion of the surface of the previous drop, it is difficult to establish the age of the surface. Accordingly, the drop length method was not considered sufficiently reliable to determine dynamic surface tensions. The method has, however, proved useful to explain anomalies in the results of previous workers.

### *E. Results*

*1. Decyl Alcohol Solutions.* Addison (4) found that the surface tension of a *n*-decyl alcohol solution (0.02 g./l.) depended on the method of measurement (Fig. 6), the drop method giving higher values than were obtained by the Wilhelmy plate method. Addison attributed this behavior to a "bag effect," but for the following reasons it is suggested that evaporation may have been responsible for these differences.

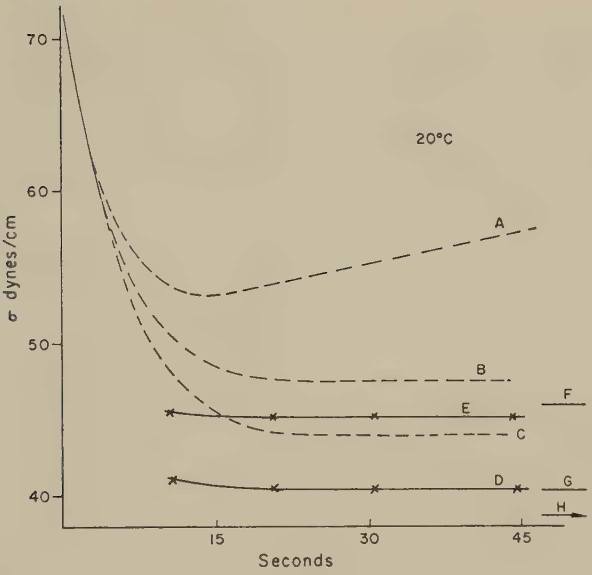

FIG. 6. Surface tensions of a normal decyl alcohol solution (0.02 g./l.):

| | | | |
|---|---|---|---|
| Drop methods | in open air | *A* | Addison |
| | in a 10-ml. cell | *B* | |
| Dipping plate method | | *C* | |
| Drop length method | with evaporation | *E* | Hommelen |
| | without evaporation | *D* | |
| Ring method | with evaporation | *F* | |
| | without evaporation | *G* | |
| Static surface tension (ring) | | *H* | |

*1.* The data in Table I show that the solute evaporates from aqueous solutions. Addison did not observe this effect with the vertical plate method; his value for the surface tension however, lies, very near that obtained with the ring method in an open dish in the present work (Fig. 6, *C*, *F*).

*2.* Since the alcohol vapor is very heavy (molecular weight 158.3), it is possible that only the region within about 2 mm. of the surface of the saturating solution will be saturated with alcohol vapor, and so a concentration gradient may exist in the vapor phase. Drops formed more than about 2 mm. above the liquid surface may therefore be subject to an evaporational error. In agreement with this suggestion, Addison's surface tension value using the drop weight method in a closed dish (curve *B*) was higher than the value obtained by the present author with the ring method in a closed (Fig. 6, *G*) or even open dish (*F*).

In support of this, very good agreement has been obtained between the

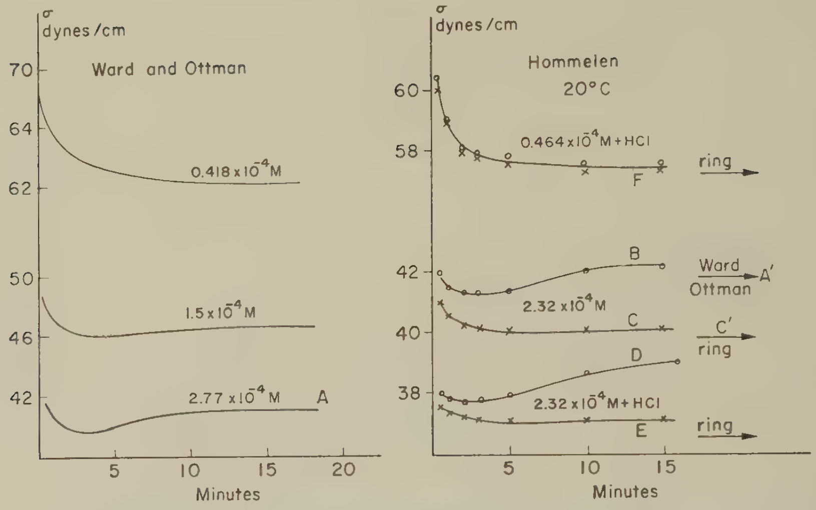

FIG. 7. Dynamic surface tensions of capric acid solutions (20°C.). O-O-O-O-O with evaporation; X-X-X-X-X without evaporation.

ring and drop methods when the drop was formed within 2 mm. of the surface of the saturating solution in the cell (Fig. 6 *D*, *G*).

However, when the drop was formed 1 cm. above this surface, the tension values obtained were much higher (curve *E*). A similar high value was observed even when an interval of an hour was allowed for saturation of the cell before the drop was formed. Curve *A* obtained by Addison with a drop in the open further supports these results.

All these experimental data are consistent with the suggestion that evaporation of solute can be prevented in the cell only by forming the drops very near the surface of the saturating solution.

It should be noted that the final equilibrium value for the *n*-decyl alcohol solution obtained by the ring method under cover after 60 minutes (Fig. 6, *H*) gave a value 1 dyne/cm. lower than *D* and *G*.

*2. Capric Acid Solutions.* Using the Andreas, Hauser and Tucker drop shape method (23), Ward and Ottman, working under conditions similar to those of Addison, found that the surface tension-time curve for a capric acid solution showed a minimum (Fig. 7, *A*). The following is an attempt to show that this effect could be due to the interplay of solute adsorption and evaporation.

In the present work, curve *B* with a minimum was obtained when the conditions of Ward and Ottman were simulated. However, when the drop was expelled near the surface of the capric acid solution saturating the cell, a curve without a minimum (curve *C*) was obtained. The static tension value from this curve after 15 minutes aging agreed with that obtained by the ring method (*C*′).

A physical interpretation of these facts would be as follows:

Curve *B*: During the first 2 to 3 minutes after the formation of the drop, the rate of adsorption of the acid exceeds its rate of evaporation. As adsorption proceeds the solution layer immediately below the surface becomes deprived of its solute, slowing down the adsorption rate. When this rate becomes slower than that of evaporation, a decrease in the net amount of acid adsorbed at the surface results. Hence the surface tension value rises and then becomes fairly constant as a balance is established between adsorption and evaporation.

Curve *C*: A minimum would not be anticipated since evaporation was prevented.

As a sequel to these experiments, the aging of a solution of the same concentration of capric acid ($2.3 \times 10^{-4}\ M$) in dilute HCl to repress acid dissociation was studied in the same apparatus. Curves *D* and *E* were obtained with and without the occurrence of evaporation.

Further, if a more dilute solution of capric acid ($0.46 \times 10^{-4}\ M$) in HCl was used, a curve without a minimum (*F*) was obtained regardless of the position of the capillary tip in the cell. It would seem likely that with this more dilute solution, the rate of evaporation of the capric acid solute was always much lower than the rate of surface adsorption.

If these explanations are accepted, they would confirm that the drop method is reliable only if the drop is formed very near the surface of the saturating solution, so that the heavy vapor mostly prevents evaporation. However, fully reliable correct values can theoretically not be obtained until the same result is obtained with the drop 1 cm. or 0.2 cm. from the surface of the liquid saturating the cell, because this is an equilibrium condition. It should yet be pointed out that results obtained in a closed dish with the ring method were practically identical to the results obtained with the drop 0.2 cm. from the surface; this means that solute evaporation was thus sufficiently prevented.

Concerning the measurement of dynamic tensions with the pendent drop method, the one limitation under these conditions would appear to be a difficulty of establishing the true zero age.

## V. Summary

The surface tensions of aqueous solutions of long-chain alcohols and acids measured by the usual techniques are shown to be high by a significant amount owing to solute evaporation during the measurement. If the ring or vertical plate method is used, only measurements in a closed vessel give equilibrium values; if the hanging drop is used, the heavy vapors do not remain near the drop, and it is therefore essential to form the drop very close to the surface of the solution which is saturating the surrounding air.

Improvements in normal procedures, designed to eliminate the evapora-

tional error, are described. Various anomalies, for example, the "bag effect" found by Addison and Hutchinson with decyl alcohol solutions, and the minimum in the time curves of surface tension observed by Ward and Ottman with capric acid solutions, are shown to be consistent with an evaporational effect.

New surface tension-concentration curves for aqueous solutions of some alcohols and acids are given in the present paper. The corresponding adsorption values have been deduced from the Gibbs equation.

## ACKNOWLEDGMENTS

An important part of the equipment necessary for the present work was obtained through the generosity of the "Centre National de Chimie-Physique Moléculaire." We should like to express our gratitude to that organization as well as to Professor Defay for his advice on numerous occasions, and to W. D. E. Thomas who helped us in the elaboration of the English text of this paper.

## REFERENCES

1. WARD, A. F. H., AND OTTMAN, M., *1er Congr. Détergence Paris* **1**, 71 (1954).
2. MERIGOUX, R., Doctor's thesis, Paris, 1938.
3. The Bible, Proverbs, Chapter XXIII, Verse 31.
4. ADDISON, C. C., *et al.*, *J. Chem. Soc.* **1949**, 3387.
5. ALEXANDER, A. E., AND POSNER, A. M., *Trans. Faraday Soc.* **45**, 651 (1949).
6. SUTHERLAND, K. L., Doctor's Thesis, London, 1950.
7. SUTHERLAND, K. L., *Rev. Pure and Appl. Chem. Australia* **1**, 35 (1951).
8. SUTHERLAND, K. L., *Australian J. Chem.* **4** (7), 319 (1954).
9. HARKINS, W. D., AND JORDAN, H. F., *J. Am. Chem. Soc.* **52**, 1751 (1930).
10. HARKINS, W. D., *in* A. Weissberger, ed., "Physical Methods of Organic Chemistry," Vol. 1, Part 1. Interscience, New York, 1949.
11. ADDISON, C. C., *et al.*, *J. Chem. Soc.* **1943**, 535; *ibid.* **1944**, 252, 477; *ibid.* **1945**, 98, 354; *Phil. Mag.* **36**, 73 (1945).
12. POSNER, A. M., ALEXANDER, A. E., AND ANDERSON, J. R., *J. Colloid Sci.* **7**, 623 (1952).
13. HARVA, O., *Rec. trav. chim.* **75**, 101 (1956).
14. BUTLER, J. A. V., THOMSON, D. W., AND MCLENNAN, W. H., *J. Chem. Soc.* **1933**, 674.
15. TAUBMAN, A. B., *Zhur. Fiz. Khim.* **26**, 389 (1952).
16. HARKINS, W. D., "Physical Chemistry of Surface Films." Reinhold Publ., New York, 1952.
17. SHOFIELD, AND RIDEAL, E. L., *Proc. Roy. Soc.* (*London*) **A109**, 57 (1925); *ibid.* **110**, 167 (1926).
18. CLARK, DEGONT, DENARD, AND DERVICHIAN, *Congr. Bordeaux*, 173 (1947).
19. TRAUBE, I., (*Liebig's*) *Ann.* **265**, 27 (1891).
20. WARD, A. F. H., AND TORDAI, L., *Trans. Faraday Soc.* **42**, 399–413 (1946).
21. HARKINS, W. D., AND BROWN, F. E., *J. Am. Chem. Soc.* **38**, 247 (1916); *ibid.* **41**, 499 (1919).
22. DEFAY, R., AND HOMMELEN, J., *J. ind. chem. Belg.* XXIII (6), 597 (1958).
23. ANDREAS, J. M., HAUSER, E. A., AND TUCKER, W. D., *J. Phys. Chem.* **42**, 1001 (1938).
24. FORDHAM, S., *Proc. Roy. Soc.* (*London*) **A194**, 1 (1948).
25. DEFAY, R., AND HOMMELEN, J., *J. Colloid Sci.* **13**, 553 (1958).
26. HOMMELEN, J., Doctor's Thesis, Brussels, 1957.

JOURNAL OF COLLOID SCIENCE **14**, 401–410 (1959)

# II. MEASUREMENT OF DYNAMIC SURFACE TENSIONS OF AQUEOUS SOLUTIONS BY THE FALLING MENISCUS METHOD

**Raymond Defay and Jacques R. Hommelen**

*Université Libre de Bruxelles, Brussels, Belgium*

*Received September 18, 1958; revised February 24, 1959*

## INTRODUCTION[1]

The falling meniscus method for the determination of surface tension is based on the fact that the height attained by a liquid in a tube is dependent only on the radius of the tube where the meniscus is situated. The method provides a rapid and convenient procedure for the measurement of both static and dynamic surface tensions.

Bigelow and Hunter (1) in 1911 used the falling meniscus method to determine static tensions, and Hiss (2) in 1913 was the first to study water surfaces within $10^{-4}$–$10^{-3}$ sec. of formation to verify the Lenard assumption (3) that such surfaces possessed values of surface tension higher than the classical equilibrium value. In 1925, Carver and Hovorka (4) showed that the height attained by a liquid in a tube was independent of the composition of the wall. Schmidt and Steyer (5) and Kleinmann (6) improved the technique, and Seits (7) studied the tensions of solutions of mineral salts by this method.

In this paper the work of some of these authors is briefly criticized, and an improved apparatus is developed and used to determine dynamic surface tensions.

## DESCRIPTION OF PROCEDURE AND METHOD OF CALCULATION OF SURFACE TENSION

A circular capillary hole formed in the closed end of a glass tube a few millimeters in internal diameter provides a convenient meniscus position. The tube is lowered vertically into the liquid under test, and when it is completely filled (Fig. 1), the liquid column height is gradually increased by lowering the vessel containing the bulk solution until, at a critical height of rise, the meniscus breaks away from the hole. The height of rise ($h_0$) of the column immediately before this occurs corresponds to the maximum pressure difference which exists between the upper and lower sides of the meniscus. The surface tension ($\sigma$) of the solution is given by:

---

[1] This is the second of a series of three papers presenting measurements of dynamic surface tensions and discussing the mechanism of adsorption of heavy alcohols and acids in dilute aqueous solutions (8). We have also recently published a detailed bibliographical study of other methods for measurement of dynamic surface tensions (9).

$$\sigma = \frac{\rho g r}{2}\left(h_0 - \frac{2r}{3}\right), \qquad [1]$$

where $h_0$ = the distance between the *highest edge* of the meniscus and the level of the liquid outside the tube, and $r$ = the radius of the capillary hole. (This equation for capillary rise when the meniscus is hemispherical,

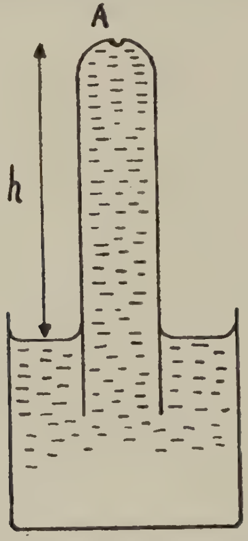

FIG. 1. Diagram of apparatus.

as well as the complementary one derived by Harkins (reference 10, p. 366), is an approximation of the Rayleigh equation.)

With sharp-edged capillary holes the tangent to the meniscus may not be vertical (as it is in a cylindrical capillary having zero contact angle). For such holes a more general equation can be derived from Sugden's treatment for the maximum bubble pressure method (11), because of the similarity between the form of the bubble as it breaks and that of the falling meniscus. This second equation has been shown with our orifices (reference 12, pp. 92–96) to give surface tension values similar to those obtained by using Eq. [1], provided the surface tension of the solution is not less than 40 dynes/cm. The radius $r$ in Eq. [1] was measured as the minimum value for the orifice and the contact angle could be neglected, if there was any.

Accordingly, Eq. [1] has been used in all work described below.

If surface tension-time effects are being investigated, the height of rise ($h_0$) is maintained constant at selected values greater than would correspond to the static surface tension. The meniscus breaks when the tension value falls below that calculated from the equation for the particular value of $h_0$ used, and the age of the solution at this tension is equal to the interval between the formation and the breaking of the meniscus.

## Critical Review of Published Work

Schmidt and Steyer (5) used a falling meniscus method to investigate the rapid aging of pure water surfaces (age: $10^{-4}$–$10^{-2}$ sec.). A continuous overflow of water from the orifice (Fig. 1) was maintained by the movement of a horizontal stream of air over it. When the air stream was interrupted, the meniscus fell until it reached the narrowest part of the capillary orifice, where it remained until the tension had fallen below the value given by Eq. [1] for the particular value of $h_0$ used. By varying $h_0$ a series of related surface tension-surface age values for pure water were obtained.

Since mechanical equilibrium of the system necessary for the application of Eq. [1] was unlikely to have been achieved in the short time intervals used by Schmidt and Steyer, it is probable that the apparent aging effects observed were spurious. The present authors have shown (9, 12) that similar results could be attributed to viscosity effects only. This would support Bohr's original findings (13) with the vibrating jet that no aging of pure water could be detected at the surface ages here considered.

Kleinmann (6) attempted to improve the method by introducing a viscosity correction, shown by the present authors to be invalid (9, 12).

In the present work a falling meniscus method has been adapted to study the aging of older surfaces, ranging in age from a few seconds to a few minutes. Some of the errors inherent in the procedures of earlier workers have thus been avoided.

## Experimental

### *A. Preparation of Orifices*

One end of a Pyrex tube 6 mm. in external diameter was heated, drawn out 1 cm., and cut at its narrowest point (Fig. 2*A*). The tip was heated to redness until the opening was only slightly larger than that finally required (Fig. 2*B*). The tube was held vertically and its end ground with carborundum on a glass plate to beyond the narrowest cross section (Fig. 2*C*), after which the tip was reheated to remove burr and to reduce the opening to the desired size (Fig. 2*D*). Finally the shoulder of the tube at the tip was ground in Pyrex dies to facilitate draining from the orifice (Fig. 2*E*). It is essential to preserve the symmetry of the end of the tube during this procedure. Prepared in this way, each orifice had its minimum radius at its outer edge, and this considerably simplified measurement of the height of rise.

Six such capillary orifices were prepared and their diameters measured with a traveling microscope (Table I, a) or with a microscope fitted with a reticular eyepiece (Table I, b). At least two such measurements were made on each orifice, and none was found to depart from the circular by more than 2%.

The orifice characteristics are given in Table I, which also includes data obtained for pure water with each orifice (see below).

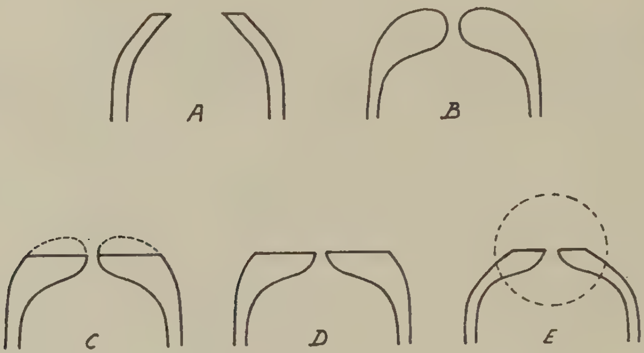

FIG. 2. Preparation of the orifices—successive stages.

TABLE I

*Orifice Characteristics and Results for Water at 20°C.*

| Capillary | $r$ (*cm.*) | $\frac{2}{3} r$ | $\frac{\rho g r}{2}$ | $h$ (*cm.*) | (*dynes/cm.*) |
|---|---|---|---|---|---|
| A | 0.0150 (b) | 0.010 | 7.35 | $9.88_3$ | 72.5 |
| B | 0.0171 (b) | 0.012 | 8.37 | $8.70_8$ | 72.7 |
| C | 0.0242 (a) (b) | 0.016 | 11.43 | $6.16_2$ | 72.6 |
| D | 0.0353 (a) (b) | 0.024 | 17.28 | $4.25_4$ | 73.0 |
| E | 0.0432 (a) (b) | 0.029 | 21.17 | $3.46_2$ | 72.6 |
| F | 0.0603 (a) | 0.040 | 29.48 | $2.51_0$ | 72.9 |
| *Mean:* | | | | | 72.7 |
| *Average variation from the mean:* | | | | | 0.2 |

### *B. Measurement of Height of Rise (Fig. 1)*

The tube prepared as above was supported vertically in a fixed clamp and the height of the column was varied by means of a movable platform supporting the vessel containing the liquid. The height of rise ($h_0$) measured by means of a cathetometer (to 0.02 mm.) involved an initial reading for the orifice tip and readings of the level of the bulk liquid surface in the vessel at different settings of the platform. In theory the height of the column should be determined immediately before the meniscus breaks (i.e., at the instant the air stream drops), but because of experimental

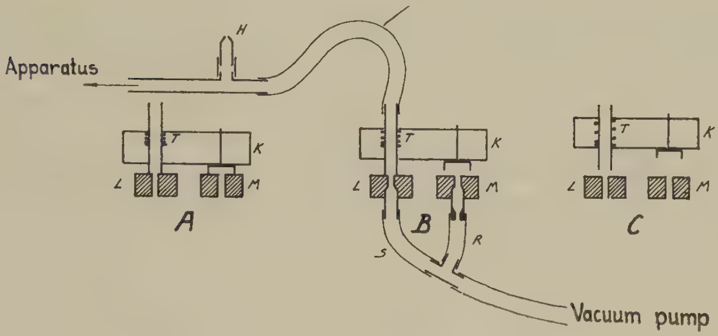

FIG. 3. Connecting device for the aspiration.

difficulties, the level of the bulk liquid was measured after the meniscus had broken in each instance, and a correction was added to allow for the liquid which had flowed from the tube.

### *C. Sources of Errors and Their Elimination*[2]

*1. Evaporation of Solute.* In the early stages of the present work a modified Schmidt and Steyer apparatus was used to investigate the aging of aqueous solutions of methyl-hexyl carbinol. An anomalous behavior was observed and shown to arise from evaporation of adsorbed solute from the surface.[3] This error was eliminated by enclosing the capillary orifice in a Pyrex cell fitted with a ground-glass cap. Slow overflow of the solution through the capillary hole was induced by pressure lowering in the cell and allowed renewing of the meniscus. A valve device (Fig. 3) was incorporated between the saturator and the water pump (*a*) to regulate the suction which controlled the overflow of solution (air inlet *H*) and (*b*) to prevent a too sudden ingress of air during the later pressure equalization. The frame *K* was vertically movable in such a way that the tubes *R* and *S* could be successively opened to the atmosphere within 0.1 sec. when position *A* was changed to position *C*. In the suction position (*A*) the spring-loaded suction tube (*T*) and the small cap (*J*) were tightly pressed against the two pieces of rubber tubing *L* and *M*. Raising of the frame (to position *B*) allowed air to enter the tube *R* while the water pump was still connected. The pressure in the system at this stage thus approached atmospheric until the suction was too weak to induce overflow of the solution but still prevented untimely breaking of the meniscus. Further raising of *K* (to position *C*) disconnected the water pump completely from the system and the pressure inside became atmospheric. A tap was incorporated to the cell for emptying it at the end of each experiment. The beaker containing the bulk solution was covered with a glass plate through which a hole was made for the rise tube.

---

[2] See detailed discussion of this part in reference 12.

[3] It has been proved by one of us that evaporation of solute in alcohol solutions very often happen and induces an important increase of the measured surface tension (14).

*2. Pollution and Surface Extension.* After elimination of the evaporation error it was observed that the residual film of solution on the external wall of the rise tube was considerably extended by draining towards the bottom of the cell (12). This surface extension occurred during the first few seconds after overflow had ceased, and as a result the effective adsorption of solute per unit area at the meniscus surface was lowered, giving a higher value for the surface tension (15, 16). This behavior has been discussed (12) in the light of similar observations by Defay and Derycker, who used the overflowing funnel (17).

It has been shown (12) that a second major effect began to operate when

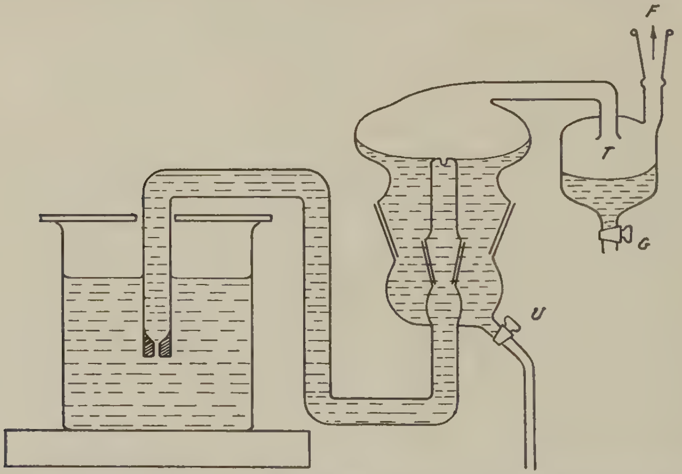

FIG. 4. Apparatus designed to eliminate pollution, extension, and evaporation errors.

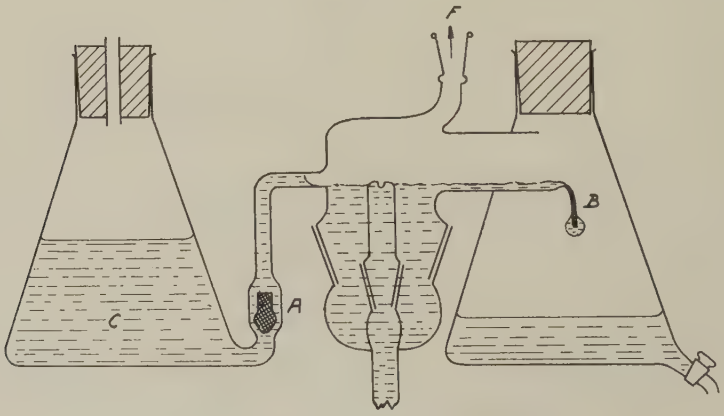

FIG. 5. Alternate design of apparatus.

the draining from the tube wall became slow enough to permit pollution of the meniscus surface by the considerably older surface existing in the bottom of the cell. Rapid equilibration between these two surfaces occurred resulting in a redistribution of the adsorbed solute, thus prematurely aging the meniscus surface.

The apparatus of Figs. 4 and 5 has been designed to eliminate these two effects (see details in reference 12) as well as the effect of evaporation.

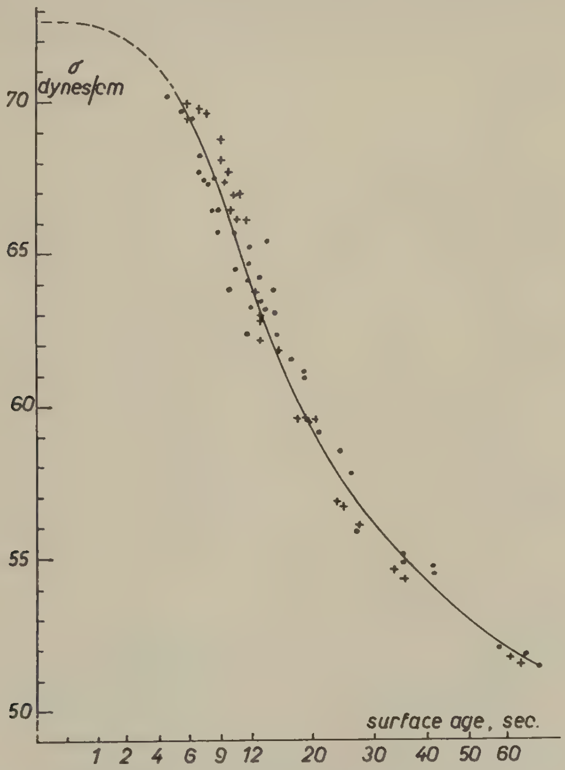

FIG. 6. Comparison between results given by apparatus of Fig. 4 (●) and Fig. 5 (+) (normal decyl alcohol 0.012 g./liter; 20°C.).

### D. *Apparatus to Eliminate Pollution and Surface Extension Effects*

The apparatus shown in Fig. 4 was designed to eliminate surface extension effects as well as those of pollution. With the use of the suction device previously described (Fig. 3) the cell was completely filled with the solution until a few drops overflowed through the tube *T*. The tap *U* was opened at the same time the suction device was adjusted to position *B*,[4] and as soon as the level of the solution had reached the orifice the tap *U* was closed and the suction device was adjusted to position *C*. At this stage the surface was considered to be 1 sec. old—the time interval during which tap *U* was open. Timing in the experiment was carried out with a stopwatch.

---

[4] In position *B* a slight negative pressure was maintained in the cell to prevent premature breaking of the meniscus.

It was considered that with this apparatus the surface of the bulk solution surrounding the rise tube was at the same age as that of the meniscus within the orifice; hence no pollution effect was possible. In addition, since the surface of both the bulk solution and the meniscus were essentially the same, no extension of surface was possible either. Any increase of meniscus surface area which did occur during aging could be neglected in comparison with the much larger surface area of the bulk solution. (The aging of the meniscus results in a change of shape.)

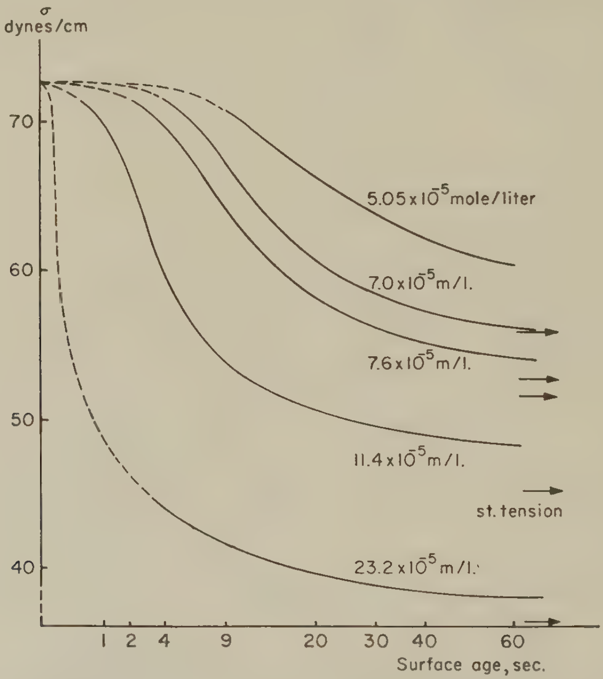

FIG. 7. Dynamic surface tensions of capric acid solutions (pH = 2; 20°C.).

An alternative design suitable for determining surface tension in the absence of pollution and extension effects is shown in Fig. 5. The effect of suction at *F* produced not only an overflow of solution through the orifice but also a movement of solution from the vessel *C*, resulting in an overflow at *B*. This ensured continual renewal of both the bulk and meniscus surfaces. When suction was discontinued a gravity-operated valve *A* stopped the movement of solution from *C* and the meniscus in the orifice was stabilized (zero time). In this apparatus as in that of Fig. 4 the freshly formed meniscus surface was connected to a larger surface having the same age.

The results obtained with *n*-decyl alcohol (0.012 g./liter) were identical with those obtained using the apparatus of Fig. 4 (see Fig. 6).

### *E. Results with Capric Acid and Decyl Alcohol*

By using sufficiently dilute solutions of capric acid or decyl alcohol in water (approx. $10^{-4}$ mole/liter) aging phenomena could be prolonged over intervals of a minute or more, and so could be investigated with the falling meniscus method. Using the apparatus of Fig. 4 surface tension-age data were obtained and the results plotted in Figs. 7 and 8.

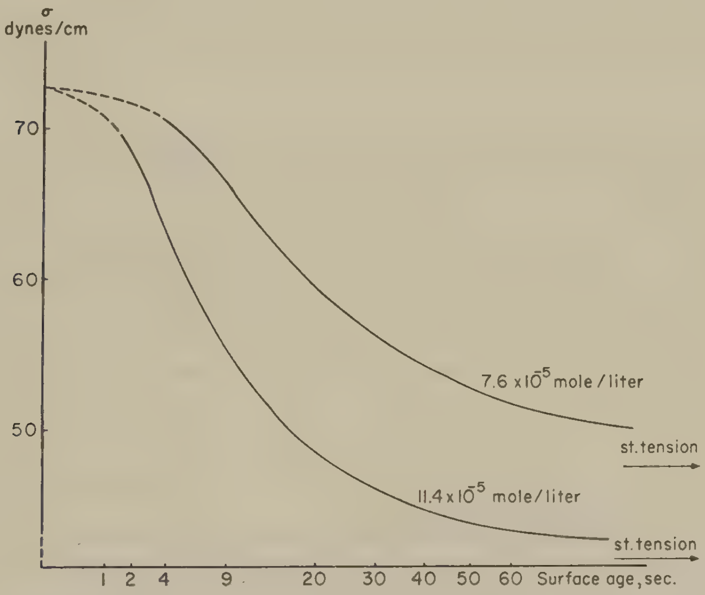

FIG. 8. Dynamic surface tensions of normal decyl alcohol solutions (20°C.).

A theoretical interpretation of these data, and of those previously reported using the oscillating jet method (8), will be published later.

### Erratum

In Part I of the present series (8) Eq. [1] should be read:

$$\sigma = \frac{4\rho D^2 \left(1 + \frac{37}{24} \frac{b^2}{a^2}\right)}{6r\lambda^2 \left(1 + \frac{5}{3} \pi^2 \frac{r^2}{\lambda^2}\right)},$$

where

$$\frac{b}{a} = \frac{r_x - r_i}{r_x + r_i}.$$

All the data in Part I have been derived from this correct formula.

## SUMMARY

The falling meniscus method (based on Rayleigh's classical capillary rise equation) is described for the determination of dynamic surface tensions. The work of several previous authors is critically reviewed. The influence of evaporation of solute, the extension of surface area, and the pollution of the surface being studied by contact with an older surface, are discussed, and an apparatus has been designed to eliminate errors caused by these effects.

Dynamic surface tensions are reported for aqueous solutions of $n$-decyl alcohol and capric acid, within the surface age range 1 sec.-1 min.

## ACKNOWLEDGMENTS

An important part of the equipment necessary for the present work was obtained through the generosity of the "Centre National de Chimie Physique Moleculaire" and the "Fonds National de la Recherche Scientifique."

We should like to express our gratitude to these two organizations, as well as to W. D. E. Thomas, who helped us in the elaboration of the English text of the present series of papers.

## REFERENCES

1. BIGELOW, S. L., AND HUNTER, F. N., *J. Phys. Chem.* **15,** 367 (1911).
2. HISS, R., Dissertation, Heidelberg, 1913.
3. LENARD, P., *Wied. Ann.* **30,** 209 (1887); *Heidelberger Akad. Wiss.* **18,** (1910).
4. CARVER, E. K., AND HOVORKA, F. J., *J. Am. Chem. Soc.* **47,** 1325 (1925).
5. SCHMIDT, F., AND STEYER, H., *Ann. Physik* **79,** 442 (1926).
6. KLEINMANN, E., *Ann. Physik* **80,** 245 (1926).
7. SEITS, E. O., *Ann. Physik*, p. 1099 (1929).
8. DEFAY, R., AND HOMMELEN, J., *J. Colloid Sci.* **13,** 553 (1958).
9. DEFAY, R., AND HOMMELEN, J., *Ind. chim. Belg.* **XXIII** (no. 6), 597 (1958).
10. HARKINS, W. D., *in* A. WEISSBERGER, ed., "Physical Methods of Organic Chemistry," Vol. 1, Part 1. Interscience Publishers, New York, 1949.
11. SUGDEN, S., *J. Chem. Soc.* **121,** 858 (1922); *ibid.* **125,** 27 (1924).
12. HOMMELEN, J., Doctor's thesis, Brussels, 1957.
13. BOHR, N., *Phil. Trans.* **A209,** 281 (1908).
14. HOMMELEN, J., *Bull. soc. chim. Belges* **66,** 476 (1957); *J. Colloid Sci.*, **14,** 385 (1959).
15. DEFAY, R., AND ROBA-THILLY, J., *J. Colloid Sci. Supplement* **I,** 36 (1954).
16. DEFAY, R., *Mém. services chim. état (Paris)* **41** (no. 3), 253 (1956–1957).
17. DEFAY, R., AND DERYCKER, M., *Bull. soc. chim. Belges* **65,** 794 (1956).

JOURNAL OF COLLOID SCIENCE **14**: 411–418 (1959)

# III. THE IMPORTANCE OF DIFFUSION IN THE ADSORPTION PROCESS OF SOME ALCOHOLS AND ACIDS IN DILUTE AQUEOUS SOLUTIONS

**Raymond Defay and Jacques R. Hommelen**

*Université Libre de Bruxelles, Brussels, Belgium*

*Received October 22, 1958; revised February 24, 1959*

## ABSTRACT

With the use of accurately obtained values of static and dynamic surface tensions, the procedure of Ward and Tordai has been followed to investigate the nature of the adsorption mechanism. It was found that with the dilute aqueous solutions of mono-alcohols and mono-acids studied, adsorption at the air-solution interface occurred in each instance at a rate governed by a diffusion process. Some results obtained by other workers are also shown to be consistent with a diffusion mechanism.

For the dicarboxylic acid studied (azelaic acid) it is necessary to postulate an activation energy barrier for the latter part of the aging process.

## I. INTRODUCTION[1]

It has been shown since the work of Dupré (1) in 1869 and Rayleigh (2) in 1879 that the surface tension of a freshly formed surface is higher than its equilibrium value.

Milner (3) and Lecomte du Nouy (4) observed slow time effects of the tensions of soap solutions and of complex systems (e.g., blood serum), and these observations together with the Gibbs adsorption theory have given rise to the conception that such time effects are due to the rate at which the solute molecules adsorb at the surface.

The adsorption process may be assumed to occur in two stages:

*1*. movement of solute molecules from the bulk to the subsurface (which is the layer immediately below the surface layer);

*2*. movement of the solute molecules from the subsurface into the surface layer.

These stages occur at different rates, and for convenience the time interval required for (*1*) is referred to as the diffusion time, and for (*2*) as the real adsorption time. It will be seen that in most of the systems studied the real adsorption time can be neglected compared with the diffusion time, and for such systems surface aging is dependent only on the diffusion of solute molecules towards the subsurface. This assumption, however, cannot be regarded as a generalization, and for at least one of the systems we have studied it has been shown to be invalid.

---

[1] This is the last of a series of three papers presenting measurements of dynamic surface tensions and discussing the mechanism of adsorption of heavy alcohols and acids in dilute aqueous solutions (6, 7).

The experimental results obtained by us (5–9) are compared with those of previous workers (3, 10–14) and have led to more acceptable values of diffusion coefficients than have been deduced by other authors (15).

## II. Earlier Work

Various hypotheses have been proposed to explain stage (*2*) of the adsorption process (16–29), but these are not further discussed here as it will be shown that considerations of diffusion alone are adequate to explain the adsorption in most of our systems.

On this assumption it is possible, if the diffusion coefficient of the solute is known, to calculate the number of molecules which arrive at the surface in a given time after its formation. Such calculations have been made by Bond and Puls (11), Langmuir and Schaefer (12), Ross (13), Doss (14), Addison (30–32), Blair (33), and in more detail by Ward and Tordai (15), who have considered the influence of increasing concentration in the subsurface (which they regard as having a thickness of a few molecular diameters) on the diffusion rate. The surface layer is regarded as being approximately monomolecular. Ward and Tordai assume that thermodynamical equilibrium is instantaneously established between the subsurface and the surface layer, and they further consider that the concentration of the subsurface decreases from the initial bulk concentration ($C_0$) to nearly zero immediately after the surface is formed, owing to the migration of solute to the surface. The concentration gradient thus formed between the subsurface and the bulk promotes diffusion transport of the solute in the solution bulk towards the subsurface. These authors then emphasize that as the surface concentration increases, there is an increased probability that a solute molecule will not find a "site" on the surface and will thus remain in the subsurface. As soon as the concentration in the subsurface becomes finite, a back diffusion process from the subsurface into the bulk solution must be considered. As the concentration in the subsurface approaches that in the bulk, so the rate of diffusion away from the surface approaches the rate towards the surface.

Ward and Tordai have shown that if the subsurface concentrations were known at each instant, the diffusion of the solute towards the subsurface could be treated by applying the classical diffusion equations. By considering very short ages only, so that the concentration in the subsurface was negligible, they showed that the surface concentration Γ, (moles/cm.²) at time $t$ after surface formation, is given by:

$$\Gamma = 2C_0(Dt/\pi)^{1/2}, \qquad [1]$$

where $D$ is the Fick's diffusion coefficient, and $C_0$ is the bulk concentration in moles/cm.$^3$.

Furthermore they have shown that when the subsurface concentration can no longer be neglected, Eq. [1] can be extended to include an expression for back diffusion:

$$\Gamma = 2\left(\frac{D}{\pi}\right)^{1/2}\left\{C_0\, t^{1/2} - \int_0^{t^{1/2}} \phi(z)\, d[(t-z)^{1/2}]\right\}, \qquad [2]$$

where $z$ varies from zero to $t$ and where $\phi(z)$ is the subsurface concentration at time $z$ after surface formation.

From Eq. [2] it is clear that in theory either $\Gamma$ or $D$ may be calculated if one of them is known. The evaluation of the function $\phi(z)$, however, presents a difficulty. If instantaneous subsurface surface layer equilibrium is assumed, i.e., absence of an activation barrier between these two layers, a particular value of the tension (static or dynamic) corresponds to a unique value of the subsurface concentration. The relationship between surface tension and subsurface concentration $\phi(z)$ can therefore be obtained from observations under equilibrium conditions and hence a plot of the equilibrium surface tension against concentration together with the time curve of the dynamic surface tensions of a given solution gives the variation of $\phi(z)$ with time in this solution, without the necessity of making arbitrary assumptions regarding the surface concentrations.

Ward and Tordai (15) have employed a physical artifice which makes possible a graphical integration of the second part of Eq. [2]. From the curve giving the variation of $\phi(z)$ with time, another graph may be drawn showing the relation between $\phi(z)$ and $(t - z)^{1/2}$, the area under which is equal to the integral

$$\int_0^{t^{1/2}} \phi(z)\, d[(t-z)^{1/2}]. \qquad [3]$$

If the assumption made above is true, then the surface adsorption $\Gamma$ is a function of the surface tension—whether it be static or not[2]—and the instantaneous values of $\Gamma$ under dynamic conditions may be calculated by means of the Gibbs equation using the experimental values of static surface tensions. From eq. [2], the diffusion coefficient $D_{\text{calc.}}$ may be obtained (since $C_0$ and the integral [3] are known) and compared with the classical values.

The value of this calculation depends essentially on the accuracy with which $\phi(z)$ and $\Gamma$ are known. The function $\phi(z)$ can be determined to within 5% and $\Gamma$ can be evaluated to within $0.5 \times 10^{-10}$ mole/cm.$^2$, which leads to an error of less than 10% in $D_{\text{calc.}}^{1/2}$. The maximum error in $D_{\text{calc.}}$ is therefore about 20% or $10^{-6}$ cm.$^2$/sec.

---

[2] The surface tension depends only on both subsurface and surface concentration and not on bulk concentration.

Values of $D_{\text{calc.}}$ which are lower than accepted diffusion coefficients would indicate the existence of an energy barrier at the surface.

Ward and Tordai used this procedure to calculate diffusion coefficients of some normal alcohols using the experimental data of Addison (30–32, 34–38). The values obtained (Fig. 1) deviated considerably from those generally accepted, and it is thought that these discrepancies were due to the experimental procedure developed by Addison. Sutherland (39), using the vibrating jet method, and Posner and Alexander (40), using a technique based on surface potential measurements, failed to reproduce Addison's data for the dynamic surface tensions of aqueous solutions of some aliphatic alcohols. The surface potential method as used by Posner and Alexander was, however, shown by Addison to be invalid, since the potential still varied after surface adsorption was complete.

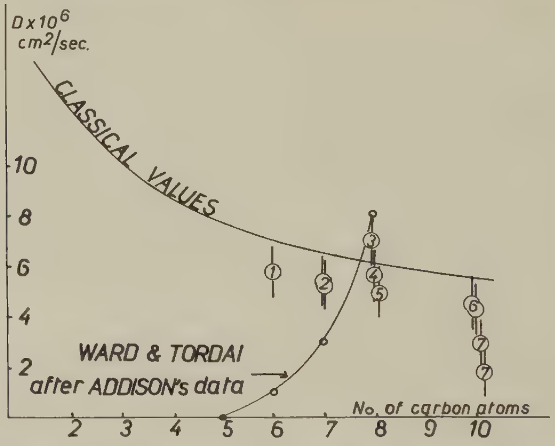

FIG. 1. Diffusion coefficients at 20°C. (*1*) Normal hexyl alcohol; (*2*) normal heptyl alcohol; (*3*) methyl hexyl carbinol; (*4*) 2-ethyl hexanol; (*5*) normal octyl acohol; (*6*) capric acid; (*7*) normal decyl alcohol.

## III. Review of Results in Present Investigations

It is suggested that the disagreement between our experimental values of static surface tensions (5–8), and those previously published are due to the lack of sufficient precautions by other workers to exclude solute evaporational errors. Using our static surface tension data together with the dynamic tension values determined in this work (5–7, 9) diffusion coefficients for some aliphatic alcohols were calculated from Eq. [2] (see Table I).

These values and their limits of error are plotted in Fig. 1, and it is seen that except for decyl alcohol they lie near to the classical curve extrapolated to include alcohols containing more than 5 carbon atoms. With decyl al-

TABLE I

*Calculation of Diffusion Coefficients (20°C.)*

| | $t$ | $C_0$ | * | ** | $\Gamma$ | $D$ |
|---|---|---|---|---|---|---|
| Normal hexyl alcohol | $10^{-2}$ | $3.44 \times 10^{-6}$ | 3.88 | 2.3 | 3.6 | 5.7 |
| Normal heptyl alcohol | $10^{-2}$ | $3.44 \times 10^{-6}$ | 3.88 | 1.8 | 4.9 | 5.2 |
| Normal heptyl alcohol | $10^{-2}$ | $2.43 \times 10^{-6}$ | 2.74 | 1.1 | 3.8 | 5.3 |
| Normal octyl alcohol | $10^{-2}$ | $3.44 \times 10^{-6}$ | 3.88 | 1.3 | 5.8 | 4.9 |
| Methylhexyl carbinol | $10^{-2}$ | $1.96 \times 10^{-6}$ | 2.21 | $0.4_3$ | 4.7 | 7.0 |
| 2-Ethyl hexanol | $10^{-2}$ | $2.10 \times 10^{-6}$ | 2.38 | $0.6_1$ | 4.2 | 5.6 |
| Normal decyl alcohol | 60 | $7.6 \times 10^{-8}$ | 6.6 | 2.9 | 4.9 | 1.7 |
| Normal decyl alcohol | 60 | $1.14 \times 10^{-7}$ | 10.0 | 6.5 | 5.7 | 2.7 |
| Capric acid | 60 | $7.6 \times 10^{-8}$ | 6.6 | 4.3 | 4.9 | 4.5 |
| Capric acid | 60 | $1.14 \times 10^{-7}$ | 10.0 | 7.2 | 5.7 | 4.2 |
| Azelaïc acid | $10^{-2}$ | $10^{-5}$ | 11.3 | 0.6 | 2.3 | 0.05 |
| Azelaïc acid | 60 | $10^{-5}$ | 870 | 300 | 2.4 | $1.7 \times 10^{-5}$ |

$t$: seconds

$C_0$: concentration (moles/cm.$^3$)

$\Gamma$: adsorption (moles/cm.$^2 \times 10^{-10}$)

$D$: diffusion coefficient (cm.$^2$/sec. $\times 10^{-6}$)

*: $2\, C_0(t/\pi)^{1/2} \times 10^{-7}$

**: $\dfrac{2}{\pi^{1/2}} \displaystyle\int_0^{t^{1/2}} \phi(z)\, d[(t - z)^{1/2}] \times 10^7$

cohol the dilution used was so great that evaporation effects may not have been completely prevented.

In the light of these findings it is suggested that the mono alcohols and mono acids studied follow a mechanism of adsorption which is governed mostly by diffusion.

When calculations of the diffusion coefficient for a $10^{-2}$ $M$ solution of a dicarboxylic acid (azelaïc acid) were carried out it was found that whereas the earlier part of the aging process (up to 14 millisec., investigated by the vibrating jet (6)) seemed to be governed mostly by a similar diffusion mechanism, the data for subsequent aging (up to 1 min.), investigated by the falling meniscus (7) would be consistent with the existence of an energy barrier at the surface. The fact that Hotta and Isemura (41) had found in 1951 that adsorption of dicarboxylic acids occurred in two stages—the first at a faster rate than the second—would lend support to this mechanism. Defay and Roba-Thilly (42) suggested the same mechanism in 1954.

## IV. ASSESSMENT OF THE ROLE OF DIFFUSION IN SURFACE ADSORPTION

In order to examine published surface tension data in systems for which reliable $\phi(z)$ values could not be assumed, it is proposed to restrict the analyses to surface ages where the tensions have not decreased appreciably

TABLE II

*Values of Parameters for Aliphatic Alcohols and Acids*

| | $t_1$ (*seconds*) | $C_0$ (*moles/cm.*$^3$) | $\log t_1$ | $\log \frac{\Gamma}{C_0\sqrt{D}}$ |
|---|---|---|---|---|
| Normal hexyl alcohol | $2.5 \times 10^{-3}$ | $3.44 \times 10^{-6}$ | −2.6 | −1.6 |
| Normal heptyl alcohol | $4 \times 10^{-3}$ | $2.43 \times 10^{-6}$ | −2.4 | −1.4 |
| Normal heptyl alcohol | $2 \times 10^{-3}$ | $3.44 \times 10^{-6}$ | −2.7 | −1.6 |
| Normal octyl alcohol | $2 \times 10^{-3}$ | $3.44 \times 10^{-6}$ | −2.7 | −1.6 |
| Normal decyl alcohol | 4 | $7.6 \times 10^{-8}$ | 0.6 | 0.1 |
| Normal decyl alcohol | 1.5 | $11.4 \times 10^{-8}$ | 0.2 | −0.1 |
| Capric acid | 7 | $5.05 \times 10^{-8}$ | 0.85 | 0.3 |
| Capric acid | 1.5 | $11.4 \times 10^{-8}$ | 0.2 | −0.1 |
| Undecylic acid (Dervichian) | 480 | $6.8 \times 10^{-9}$ | 2.7 | 1.1 |
| Eosine/mercury (Kalousek) | 1400 | $7.5 \times 10^{-10}$ | 3.0 | 1.3 |
| Lauric acid (Saraga) | 2100 | $1.4 \times 10^{-9}$ | 3.3 | 1.8 |
| Lauric acid (Frumkin) | 6000 | $1.4 \times 10^{-9}$ | 3.8 | 1.8 |

from the water value. Under these conditions the back diffusion term in Eq. [2] can be neglected.

It can be seen on our curves (reference 6, Figs. 4, 5, 8, reference 7, Figs. 6–8) that the surface tension does not decrease appreciably before a particular surface age has been attained[3] ($t_1$) which can be approximately measured on the curves by extrapolation of the steep part of the curves to the value of 72 dynes/cm. Equation [2] becomes

$$\Gamma = 2(D/\pi)^{1/2}C_0t_1^{1/2} \qquad [4]$$

and rearranging

$$\log t_1 = 2 \log (\Gamma/C_0\sqrt{D}) + \log \pi/4. \qquad [5]$$

Taking $D = 5 \times 10^{-6}$ cm.$^2$/sec. and $\Gamma = 2 \times 10^{-10}$ moles/cm.$^2$,[4] values of $\log \Gamma/C_0\sqrt{D}$ are calculated for some aliphatic alcohols and acids in Table II and are plotted in Fig. 2. (The $t_1$ values are taken from our curves.)

The data lie on a straight line with an intercept only slightly different from the calculated value. This slight displacement could be due to the neglect of the back diffusion term.

[3] The surface tension starts decreasing appreciably when diffusion has driven sufficient solute into the surface to form a compact layer.

[4] These values should be slightly different with the different chemicals used. Mean values have been taken to simplify calculation. The $\Gamma$ value has been deduced from the Gibbs equation using revised values of static tensions (reference 8, Fig. 2).

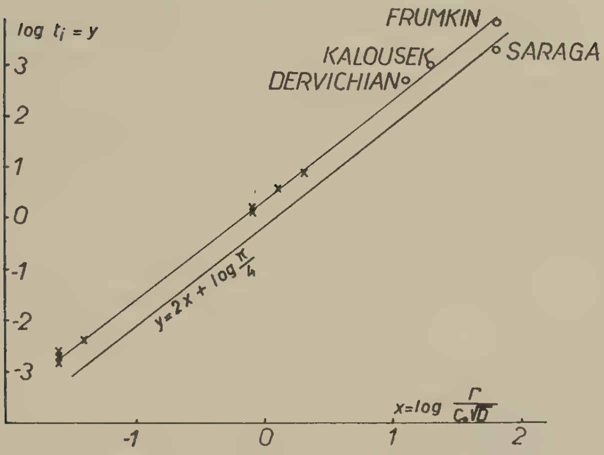

FIG. 2. Results plotted according to Eq. [5].

Table II and Fig. 2 also include the results of the following workers; these conform to the same pattern and so lend support to the diffusion mechanism:

| | |
|---|---|
| Dervichian (1956) (43) | Undecyl acid aqueous solution |
| Kalousek and Blahnik (1955) (44) | Eosine solution at water-mercury interface ($\Gamma = 3 \times 10^{-11}$ mole/cm.$^2$) |
| Saraga (1956) (45) | Lauric acid aqueous solution |
| Frumkin (45) | Lauric acid aqueous solution |

These last results were obtained on much older surfaces than our own. In addition, as acid solutions are here concerned (or a water-mercury interface), the solute evaporation was not supposed to induce the same experimental difficulties as those concerning the measurements at the air-water interface with alcohol solutions (8).

## ACKNOWLEDGMENTS

An important part of the equipment necessary for the present work was obtained through the generosity of the "Centre National Belge de Chimie Physique Moléculaire" and the "Fonds National de la Recherche Scientifique."

We should like to express our gratitude to these two organizations as well as to W. D. E. Thomas, who helped us in the elaboration of the English text of this series of papers.

## REFERENCES

1. DUPRÉ, A., "Théorie mécanique de la Chaleur." Paris, 1869.
2. RAYLEIGH, Lord, *Proc. Roy. Soc.* (*London*) **29**, 71 (1879).
3. MILNER, S. R., *Phil. Mag.* **13**, 96 (1907).
4. LECOMTE DU NOUY, P., *J. Exptl. Med.* **35**, 575 (1922).
5. HOMMELEN, J. R., Doctor's Thesis, Brussels, 1957.

6. Defay, R., and Hommelen, J. R., *J. Colloid Sci.* **13,** 553 (1958).
7. Defay, R., and Hommelen, J. R., *J. Colloid Sci.* **14,** 401 (1959).
8. Hommelen, J. R., *J. Colloid Sci.* **14,** 385 (1959) *Bull. soc. chim. Belges* **66,** 476 (1957).
9. Hommelen, J. R., *Mém. services chim. état (Paris)* **41**(No. 3), 267 (1956–1957).
10. Ghosh, J. C., and Nath, M. C., *J. Phys. Chem.* **36,** 1916 (1932).
11. Bond, W. N. and Puls, H. O., *Phil. Mag.* **24**(7), 864 (1937).
12. Langmuir, J., and Schaefer, R. V. J., *J. Am. Chem. Soc.* **59,** 2400 (1937).
13. Ross, S., *J. Am. Chem. Soc.* **67,** 990 (1945).
14. Doss, K. S. G., *Kolloid-Z.* **86,** 205 (1939).
15. Ward, A. F. H., and Tordai, L., *J. Chem. Phys.* **14,** 453 (1946).
16. Nutting, G. C., and Long, F. A., *J. Am. Chem. Soc.* **63,** 84 (1941).
17. Lottermoser, A., *et al., Kolloid-Z.* **73,** 155, 276 (1935).
18. Lottermoser, A., *et al., Kolloid-Beih.* **41,** 73 (1935).
19. Lottermoser, A., *et. al., Trans. Faraday Soc.* **31,** 200 (1935).
20. Ross, S., *J. Phys. Chem.* **49,** 377 (1945).
21. Haydon, D. A., and Phillips, J. N., *Nature* **178,** 813 (1956).
22. Hutchinson, E., *J. Colloid Sci.* **3,** 413 (1948).
23. Miles, G. D., and Shedlovsky, L., *J. Phys. Chem.* **48,** 57 (1944).
24. Mitchell, J. S., Rideal, E. K., and Schulman, J. H., *Nature* **139,** 625 (1937).
25. Myers, R. J., and Harkins, W. D., *Nature* **139,** 367 (1937).
26. Palmer, R. C., and Cassie, A. B. D., *Trans. Faraday Soc.* **37,** 156 (1941).
27. Reichenberg, D., *Trans. Faraday Soc.* **43,** 467 (1947).
28. Robinson, C., *Nature* **139,** 626 (1937).
29. Sutherland, K. L., *Revs. Pure and Appl. Chem. (Australia)* **1,** 35 (1951).
30. Addison, C. C., *et al., J. Chem. Soc.* **1944,** p. 252.
31. Addison, C. C., *et al., J. Chem. Soc.* **1944,** 477.
32. Addison, C. C., *et al., J. Chem. Soc.* **1945,** 98.
33. Blair, C. M., *J. Chem. Phys.* **16,** 113 (1948).
34. Addison, C. C., *et al., J. Chem. Soc,* **1943,** 535.
35. Addison, C. C., *et al., Phil. Mag,* **36,** 73 (1945).
36. Addison, C. C., *et al., J. Chem. Soc,* **1945,** 354.
37. Addison, C. C., *et al., J. Chem. Soc,* **1953,** 1143, 1151, 1155.
38. Addison, C. C., *et al., Nature* **171,** 393 (1953).
39. Sutherland, K. L., Thesis, London, 1950.
40. Alexander, A. E., and Posner, A. M., *Trans. Faraday Soc.* **45,** 651 (1949).
41. Hotta, H., and Isemura, T., *Bull. soc. chim. Japan* **25,** 101 (1952).
42. Defay, R., and Roba-Thilly, J., *J. Colloid Sci. Supplement* **I,** 36 (1954).
43. Dervichian, D. G., *Kolloid-Z.* **146,** 96 (1956).
44. Kalousek, M., and Blahnik, R., *Trav. Chim. Tchécosl.* **20,** 782 (1955).
45. Ter Minassian-Saraga, L., Thesis, Paris (1956).

JOURNAL OF COLLOID SCIENCE **14**, 419–429 (1959)

# THE VISCOSITY OF SODIUM HUMATE SOLUTIONS FROM COAL

**N. Rajalakshmi, S. R. Sivarajan[1], and R. D. Vold[2]**

*Department of Inorganic and Physical Chemistry, Indian Institute of Science,*
*Bangalore 3, India*

*Received August 19, 1958, revised January 6, 1959*

## Abstract

Preparations of sodium humate made by different extractive procedures all showed a similar dependence of reduced viscosity on concentration and on added salt despite the fact that lignins were present in some preparations and absent in others. The results obtained are characteristic of the behavior of flexible polyelectrolytes, and suggest that the sodium humate molecule or aggregate must have many single bonds in its structure so as to permit the indicated configurational changes. In the case of the purest sodium humate studied the apparent degree of dissociation is only about 50%.

## Introduction

Recently Mukherjee and Lahiri (1) have shown that the viscosity-concentration curves of sodium humate prepared from coal have the same form as those given by typical linear polyelectrolytes. This is rather unexpected in view of the presumption (2) that humic acid has a highly condensed ring structure which would be expected to result in a relatively rigid molecule incapable of undergoing sufficient configurational change with changing counter-ion concentration to account for the observed increase in reduced viscosity ($\eta_{sp}/C$) with dilution (3, 4). Moreover, humic acid as ordinarily obtained is known (5) to contain other materials such as polysaccharides, sterols, proteins, and lignins. The last named would certainly be expected to behave like a polyelectrolyte on the basis of its presumed structure (6, 7), and in fact, lignin sulfonates have actually been shown to be flexible polyelectrolytes (8). Hence viscosity measurements were carried out on a series of sodium humates obtained from the original humic acid complex as well as from humic acids remaining after extraction of resins, fats, and lignin-type bodies by solvents such as benzene, alcohol, and dioxane. The results obtained confirm the conclusion that humic acid itself behaves as a flexible polyelectrolyte, and thus support Thiele's concept (9) of its structure.

---

[1] Present address: Physics Division, Ahmedabad Textile Industry's Research Association, Ahmedabad 9, India.

[2] Department of Chemistry, University of Southern California, Los Angeles 7, California. Correspondence concerning this paper should be sent to this address.

## EXPERIMENTAL

### *Materials*

The humic acids used in the present work were prepared from a sample of oxidized coal (1) kindly furnished us by Dr. Lahiri. Humic acid I, the acid-insoluble portion of the alkali extract of oxidized coal, was prepared as follows: Five grams of oxidized coal was refluxed for 2½ hours with 375 ml. of 1 *N* NaOH, the mixture cooled, diluted fourfold with water, and filtered through a sintered glass funnel. The filtrate was neutralized with 2 *N* HCl, and further addition continued dropwise until a precipitate was clearly visible, requiring about 180 ml. of acid. After settling 2½ hours the supernatant solution was decanted. The precipitate was suspended in five successive portions of 1 liter of water, which were decanted after settling. Since the fifth such suspension did not settle, it was filtered on a Büchner funnel using #42 Whatman paper. The residue was then suspended in a Visking casing and dialyzed until there was no test for chloride in the external water (4 days in running water and 3 days in still water with daily changes). It was then filtered under mild suction, dried under vacuum at 50°C., and finally to constant weight at room temperature over $P_2O_5$. This product should be identical with that used by Mukherjee and Lahiri (1).

Humic acid II was prepared from humic acid I by solvent extraction to remove resins, waxes, etc., and mild acid hydrolysis to decompose and remove carbohydrates (10). Eight grams of humic acid I was extracted 6 hours in a Soxhlet extractor with boiling 1/1 alcohol-benzene, finally giving a colorless solution on replacement of the solvent, filtered on #1 Whatman paper, washed with alcohol-benzene and then alcohol, and dried to constant weight under vacuum at room temperature. Six grams of this residue was then kept at 50°C. for 2 hours in 1 *N* HCl, cooled, filtered, and washed thoroughly first with water and then with 20 ml. portions of alcohol. Finally it was dried to constant weight under vacuum at room temperature.

Humic acid III was prepared from humic acid II by extraction with dioxane to remove lignin and lignin complexes (11). Two grams of humic acid II was refluxed for 2 hours with 60 ml. of dioxane containing 0.12% HCl, the first extract being colored black. After two further extractions the extract was clear. The residue was filtered, washed with water, and dried to constant weight under vacuum at room temperature.

Humic acid IV was prepared exactly the same as humic acid I, starting with oxidized coal, except that the final product was not heated to 50°C. but was dried directly at room temperature. Thus any decomposition or further condensation possibly resulting from heating the dry humic acid at 50°C. is avoided in this preparation.

In order to prepare sodium humate from these acids it was first necessary to determine the total acidic groups since variable results have been reported (9) for the end point in a titration depending on the speed of addition of the base. A 0.2 g. sample of humic acid dried over $P_2O_5$ was refluxed for an hour with 20 ml. of alcoholic KOH (2.5 g. KOH, 2 ml. $CO_2$-free water, 200 ml. 99% ethanol, centrifuged to remove turbidity), protected from entry of carbon dioxide by a soda lime tube on the condenser. After cooling and filtering, the residue was washed with 90% alcohol until it was free of alkali (tested with phenolphthalein), and the filtrate and washings were combined and titrated with *N*/10 HCl. By combining these data with the results of direct titration of the alcoholic KOH and correcting with a blank (virtually negligible) the amount of KOH required to neutralize 1 g. of the humic acid was determined. The equivalent weights calculated from these data are given in Table II.

Sodium humate was prepared from the humic acid by the following method. A 1.5 g. sample of humic acid was allowed to stand for a day with the stoichiometric amount of aqueous, $CO_2$-free NaOH until it was completely dissolved. The solution was then diluted to a liter with 95% alcohol to precipitate the sodium humate. After separation by a combination of decantation and vacuum filtration the precipitate was washed with eight successive portions of 75 ml. each of 90% alcohol. It was then dried almost to constant weight in a vacuum desiccator at 50°C., and finally to constant weight over $P_2O_5$ at room temperature. Samples were kept over $P_2O_5$ until use since all were very hygroscopic.

In this way the following preparations were obtained.

Sodium humate I—from humic acid I, dried at 50°C.

Sodium humate II—from humic acid II, resins and polysaccharides extracted.

Sodium humate III—from humic acid III, resins, polysaccharides, and lignins extracted.

Sodium humate IV—from humic acid IV, dried at room temperature.

### *Apparatus and Methods*

The viscosities were determined at a temperature of $30.00° \pm 0.01°$C. in an Ubbelohde viscometer (12) with a flow time for 5.00 ml. of water of 167.6 sec., and time intervals were determined to 0.05 sec. Flow times for benzene and toluene were used to determine and check the constants $A$ and $B$ in the equation $\eta = \rho AT - \rho B/T$, the the values being, respectively, $4.78723 \times 10^{-5}$ and $2.08714 \times 10^{-3}$. Since the specific gravity of a 1% sodium humate solution was found to be 1.0004, $\rho$, the density, was taken as unity throughout. With the viscometer used the kinetic energy correction resulting from the second term of the equation was never more than 0.25%. The average velocity gradient, calculated as $\beta = (8V/3\pi r^3 t)$, where $V$ is the volume of liquid flowing through a capillary of radius $r$ in time $t$ (13, 14), was 1222 sec.$^{-1}$. All solutions were freshly prepared and carefully filtered before use.

In the case of polyelectrolytes values of specific viscosity $[\eta_{sp.} = (\eta - \eta_0/\eta_0)]$ determined at high rates of shear (1000–5000 sec.$^{-1}$ for capillary viscometers) are generally lower than values obtained at low rates of shear (0.3–40 sec.$^{-1}$ in Couette-type instruments) (15), and may even give rise to a different dependence of the reduced viscosity on the concentration of polymer. Moreover, it is not possible to extrapolate the data adequately to zero rate of shear unless values are available at velocity gradients much lower than those attainable in capillary viscometers (16). These defects are not too serious in the present case, however, where the primary interest is in the properties of a similar series of samples, in which case direct comparison of the reduced viscosity of each under the same high-velocity gradient suffices to demonstrate any gross differences between the preparations. Moreover, in the case of solutions with added salt where the reduced viscosity varies linearly with the concentration of polyelectrolyte, it has been shown (17) that meaningful extrapolation to zero concentration is possible even from relatively high concentrations and with data obtained at high-velocity gradients.

## RESULTS AND DISCUSSIONS

The data obtained are shown in Figs. 1–4, where the reduced viscosity, $\eta_{sp}/C$, is plotted as a function of the concentration of sodium humate. These

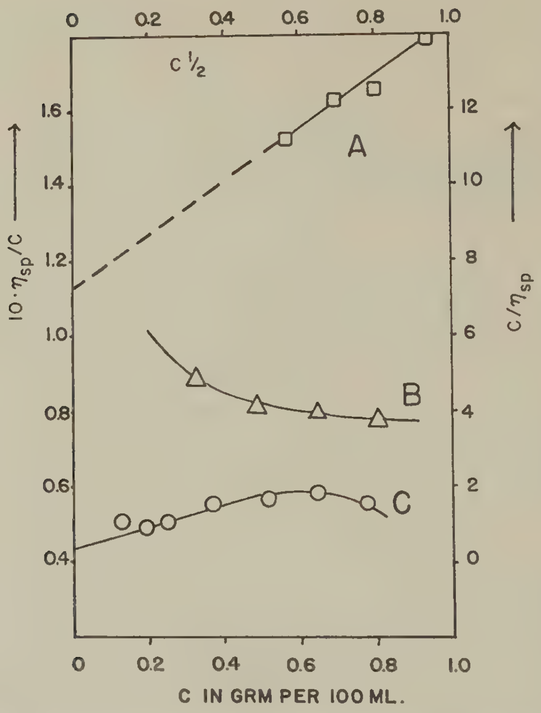

FIG. 1. Reduced viscosity of solutions of sodium humate I. *A*, Reciprocal of reduced viscosity vs. $C^{1/2}$; *B*, reduced viscosity vs. concentration; *C*, reduced viscosity vs. concentration in 0.02077 *M* NaCl.

figures also show plots of $C/\eta_{sp}$ vs. $C^{1/2}$ to test the conformity of the data to the empirical equation, $\eta_{sp}/C = A/(1 + BC^{1/2})$, found to hold in the case of many polyelectrolytes (3, 18). The effect of progressively increasing the salt concentration while holding the concentration of sodium humate constant is shown in Table I.

Perhaps the most significant result of these observations is the demonstration that all four preparations behave in a manner characteristic of typical polyelectrolytes. Particularly, the reduced viscosity increases on dilution—an effect attributed (3) primarily to extension of the molecular coil of a flexible polymer due to increasing dissociation of the ionizing groups with dilution, although it has recently been pointed out (15) that at the relatively high concentrations here involved concentration-dependent interactions between the solute molecules are also important. The effect of added salts is likewise similar to that found with typical polyelectrolytes, the reduced viscosity being greatly diminished in all cases, curves of reduced viscosity vs. humate concentration passing through a maximum at lower concentrations of added salt and becoming linear at higher salt concentra-

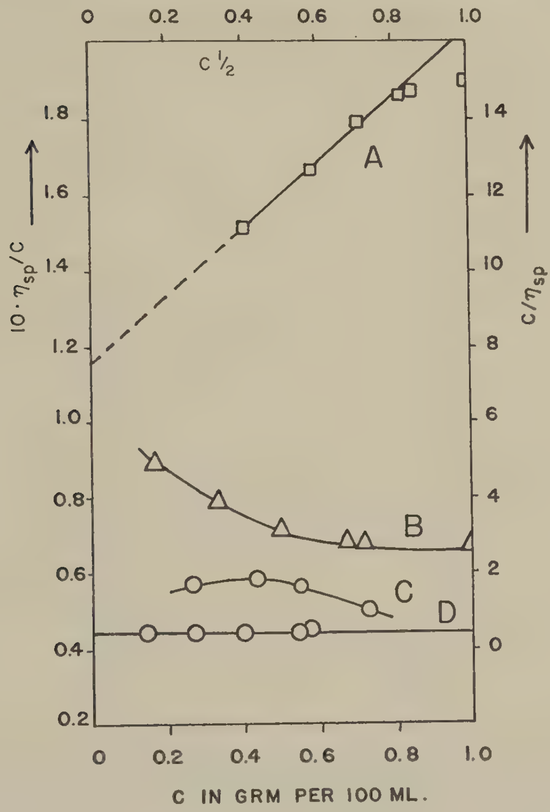

FIG. 2. Reduced viscosity of solutions of sodium humate II. *A*, Reciprocal of reduced viscosity vs. $C^{1/2}$; *B*, reduced viscosity vs. concentration; *C* and *D*, reduced viscosity vs. concentration in 0.02077 and 0.2077 *M* NaCl, respectively.

tions. The added salt acts principally (19) to reduce the electrostatic interaction by lowering the zeta potential around the charged polymer molecule, thus reducing the intermolecular interactions and the viscosity, although there is also a small effect on the molecular configuration.

That the polyelectrolyte behavior is maintained in all preparations confirms the earlier presumption that this is an intrinsic property of the sodium humate itself, and shows that it can not be attributed to lignins or other bodies associated with the humic acids. The absolute values of the reduced viscosity of sodium humate I solutions are in good agreement with those of the previous investigators (20), *ca.* 0.09–0.07 dl./g. They are lower than values reported for typical polyelectrolytes (5–56 dl./g. for polyvinylbutylpyridinium bromide (21) from a polyvinylpyridine parent (22) of molecular weight around $10^5$) but of the same order of magnitude as those of the polysoaps (intrinsic viscosity 0.1–0.04 dl./g. for the dodecyl

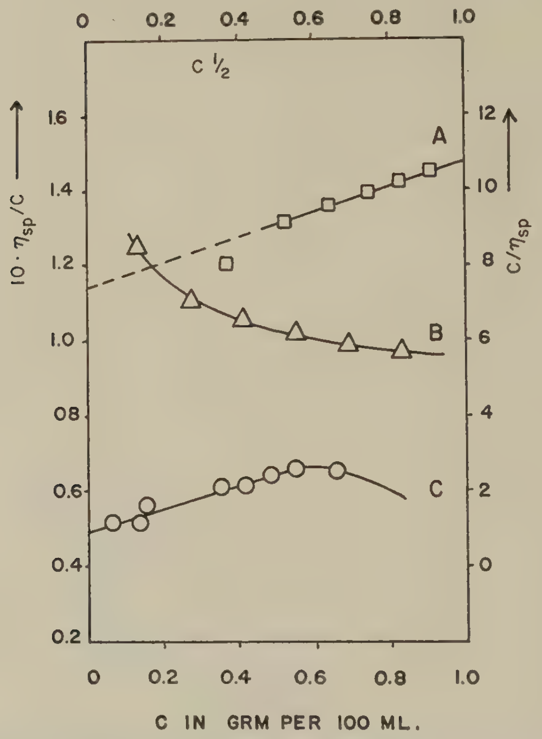

FIG. 3. Reduced viscosity of solutions of sodium humate III. *A*, Reciprocal of reduced viscosity vs. $C^{1/2}$; *B*, reduced viscosity vs. concentration; *C*, reduced viscosity vs. concentration in 0.02077 *M* NaCl.

bromide and ethyl bromide quarternization product of polyvinylpyridine (23) the intrinsic viscosity of which is 5 dl./g.).

Extraction of lignin (about 50% of the present humic acid II dissolved in acidified dioxane, as might be expected from the fact that peats commonly contain 30%–60% lignin) raises the value of the reduced viscosity. This is unexpected since lignins supposedly have molecular weights around 1000, lignin sulfonates 3500–100,000 (7, 8), and humic acids 300–1200 (1), and it would be expected that the higher molecular weight material would show the greater viscosity. The seeming anomaly may be due to error in the reported values of the molecular weights, to use of different methods of molecular weight determination on these presumably heterodisperse materials, to preferential extraction of low rather than high molecular weight lignins by dioxane, or to association of simple molecules of humic acid to larger kinetic units in solution, analogous to the micellization of soap solutions.

In view of the good straight lines obtained on plotting $C/\eta_{sp}$ vs. $C^{1/2}$ it is tempting to extrapolate to zero concentration to obtain the intrinsic

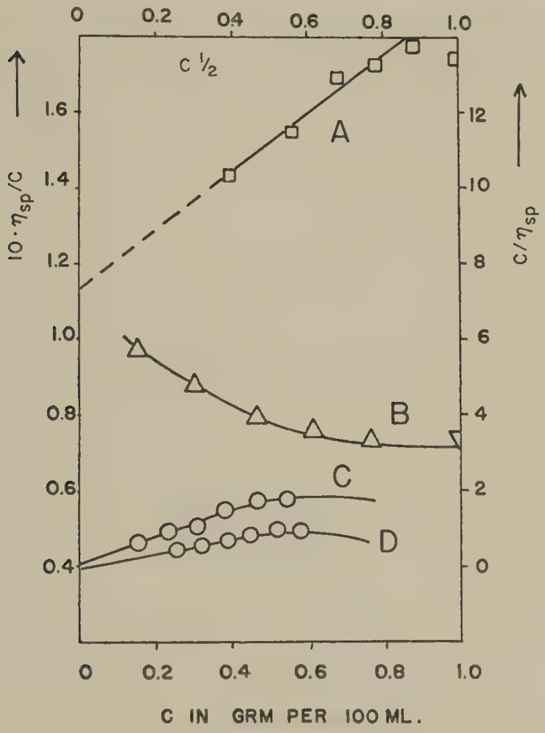

FIG. 4. Reduced viscosity of solutions of sodium humate IV. *A*, Reciprocal of reduced viscocity vs. $C^{1/2}$; *B*, reduced viscosity vs. concentration; *C* and *D*, reduced viscosity vs. concentration in 0.02077 and 0.03505 *M* NaCl, respectively.

TABLE I

*Reduced Viscosity of 0.3% Sodium Humate IV in Salt Solutions*

| NaCl con. (*g./100 ml.*) | $\eta_{sp}/C \times 10$ (*dl./g.*) |
|---|---|
| 0.00 | 0.8780 |
| 0.10 | 0.5187 |
| 0.20 | 0.4989 |
| 0.40 | 0.4775 |
| 0.60 | 0.4766 |
| 0.80 | 0.4760 |

viscosity, which is proportional to the molecular weight and is a measure of the volume occupied by the molecule in solution. On this basis sodium humates I, II, III, and IV give, respectively, 0.133, 0.132, 0.135, and 0.138 dl./g., again indicative of no great difference between the different preparations. The slopes of the lines, which are related to the interaction energy between solute and solvent, are nearly the same for preparations I and IV, as might be expected. On a unit weight basis preparation II interacts more strongly with the solvent and preparation III less strongly than the original composite sample (I and IV). However, it must be emphasized (16, 25) that intrinsic viscosities obtained in this fashion by extrapolation from results on relatively concentrated solutions can not be attributed to individual molecular characteristics. For such an extrapolation is based on a curve which is rising with decreasing concentration, whereas it is now known that with most polyelectrolytes at sufficient dilution the curve reverses itself, and the reduced viscosity decreases with dilution as the concentration approaches zero. For this same reason Fuoss' viscosity function (26), although it fits the present data very well and arranges all the values on a common curve, can not be given any physical significance.

This limitation does not apply to extrapolation of the viscosity results obtained in salt solutions in cases where the reduced viscosity varies linearly with the concentration, since here the excess salt has swamped the effect of electrostatic interactions. In 0.02077 $M$ NaCl solution the extrapolated intrinsic viscosities are found to be 0.0434, 0.0448, 0.0490, and 0.0410 dl./g. for sodium humates I, II, III, and IV, respectively. In 0.03505 $M$ NaCl the intrinsic viscosity of sodium humate IV is 0.0400 dl./g. These results can also be represented very well by Huggins equation (27), $\eta_{sp}/C = [\eta] + k'[\eta]^2C$, where $k'$, which is a measure of relative polymer-solvent interaction, has the values 0.162, 0.146, 0.133, and 0.208 for preparations I, II, III, and IV, respectively. Both the intrinsic viscosities and values of $k'$ are substantially lower than values reported for typical polyelectrolytes although the intrinsic viscosities are not greatly different from results obtained with polysoaps (23). The absolute values of intrinsic viscosity are less than twice the Einstein value of 0.025 for spheres, indicating that in salt solution these molecules must be tightly coiled to give a highly compact structure. This would be expected for an initially extended polyelectrolyte molecule which would coil up and contract because of a suppression of its dissociation, and consequent reduction in the intramolecular coulombic repulsion, due to the presence of excess positive ions from the added electrolyte.

The effect of salt on the viscosity can be used to deduce still more information concerning the geometrical structure of the sodium humate molecule and its ion-binding power and configuration in solution. The results in Table I, together with the data of Figs. 1–4, show that small amounts of salt greatly decrease the reduced viscosity whereas larger amounts have only a slight effect, the value rapidly approaching a limit independent of salt concentration. The marked effect of the first additions of salt suggests that intermolecular electrostatic interaction is probably the most important factor determining the reduced viscosity in the range investigated (15, 16, 19, 25), with the smaller changes in value with increasing salt concentration attributable to configurational changes resulting from the effect of added salt on the intramolecular interaction of the ionizable groups.

Further support for the view that sodium humate is a flexible polyelectrolyte rather than a more rigid structure is the existence of a maximum in the reduced viscosity-humate concentration curve at low salt concentrations, as well as the small but nevertheless appreciable change with increasing salt concentration at constant humate concentration. Apparently this behavior, characteristic of flexible, linear polyelectrolytes, is not shown by more rigid, noncontractile molecules such as sodium deoxyribonucleate (19), where there is no maximum in the reduced viscosity-concentration curve and the intrinsic viscosity is constant independent of the salt concentration. Sodium alginate, which is also more rigid than the usual polyelectrolytes (17), also behaves in such a way as to suggest that coil contraction is less important and intermolecular attraction more important in determining the rheological behavior, although here the increasing values of reduced viscosity with decreasing concentration indicate some molecular flexibility. Since the behavior of sodium humate so closely resembles that of the typical synthetic polyelectrolytes, it must be concluded that the structure is not exclusively composed of massive condensed rings, but that there must be numerous linkages about which relatively free rotation can occur, such as the "bridges" postulated by Thiele (9) as an integral part of the structure.

The concentration of sodium humate where the maximum occurs in the reduced viscosity-concentration curve in dilute salt solutions can be used to derive some information about the extent of binding of sodium ions by the humate radical. At concentrations of sodium humate giving a sodium ion concentration greater than that from the added salt, as humate concentration decreases the degree of dissociation increases, resulting in an expansion of the molecular coil and increasing value of reduced viscosity on dilution. However, when the humate concentration reaches a value such that sodium ion from the added salt is in excess, this tends to suppress the dissociation of the former, with the result that the sodium humate becomes more tightly coiled and the reduced viscosity decreases with further decrease in concentration. Hence there is a maximum in the curve where the concentration of sodium ion from the added electrolyte is just equal to that furnished by dissociation of the sodium humate.

That polyelectrolytes are only partially dissociated has long been known (28), and more recently it has been shown (18) that if polyelectrolytes are diluted with a salt solution in which the concentration of counter-ion is equal to that resulting from dissociation of the polyelectrolyte, the resultant curve of reduced viscosity vs. concentration is linear as in the case of un-

TABLE II

*Apparent Degree of Dissociation of Sodium Humate in 0.02077 M NaCl Solutions*

| Preparation | Eq. Wt. of humic acid (*g./equiv.*) | Conc. of Na humate at max. (*g./100 ml.*) | Fractional Dissociation $\alpha$ |
|---|---|---|---|
| I | 242 | 0.55 | 0.997 |
| II | 146 | 0.39 | 0.895 |
| III | 140 | 0.60 | 0.561 |
| IV | 155 | 0.52 | 0.707 |

charged polymers. The present work shows that sodium humate also is not fully dissociated. Taking the sodium ion concentration from dissociation of sodium humate at the maximum in the reduced viscosity-concentration curve as equal to the stoichiometric concentration of the added sodium chloride, and determining the number of equivalents of sodium humate present from its concentration and the analytical values of equivalent weight, the values of the apparent degree of dissociation, $\alpha$, shown in Table II, were calculated. It is evident that in the case of sodium humate the charge field around the humate ion is sufficient to bind a substantial fraction of the sodium ion in contradistinction to the behavior of simple electrolytes, where sodium salts are usually completely dissociated.

## ACKNOWLEDGMENT

The authors wish to express their appreciation to Professor K. R. Krishnaswami, Head of the Department of Inorganic and Physical Chemistry, Indian Institute of Science, for his keen interest during the course of this work.

## REFERENCES

1. MUKHERJEE, P. N., AND LAHIRI, A., *J. Colloid Sci.* **11,** 240 (1956); *Fuel* **37,** 220 (1958).
2. WAKSMAN, S. A., "Humus," p. 56. Williams & Wilkins, Baltimore, 1938.
3. FUOSS, R. M., AND STRAUSS, U. P., *J. Polymer Sci.* **3,** 246 (1948); *Ann. N. Y. Acad. Sci.* **51,** 836 (1949).
4. FLORY, P. J., "Principles of Polymer Chemistry," pp. 629–637. Cornell University Press, Ithaca, New York, 1953.
5. WAKSMAN, S. A., "Humus," p. 154. Williams & Wilkins, Baltimore, 1938.
6. WAKSMAN, S. A., "Humus," p. 113. Williams & Wilkins, Baltimore, 1938.
7. *Chem. Eng.* News **34,** 4776 (1956).
8. GORDON, J. L., AND MASON, S. G., Abstracts of Papers at the 130th American Chemical Society Meeting, p. 13E. 1956.
9. VON THIELE, H., AND KETTNER, H., *Kolloid-Z.* **130,** 131 (1953).
10. BONE, W. A., AND HIMUS, G. W., "Coal; Its Constitution and Uses," p. 46. Longmans, Green and Co., London, 1936.
11. KONDRATLEV, E. V., *Fuel Abstr.* **10,** Abstr. No. 4909 (1951).
12. UBBELOHDE, L., *Ind. Eng. Chem, Anal. Ed.* **9,** 85 (1937).

13. Kroepelin, H., *Kolloid-Z.* **47,** 294 (1929).
14. Strauss, U. P., and Fuoss, R. M., *J. Polymer Sci.* **8,** 593 (1952).
15. Mathieson, A. R., and Porter, M. R., *J. Polymer Sci.* **21,** 495 (1956).
16. Eisenberg, H., *J. Polymer Sci.* **23,** 579 (1957).
17. Mathieson, A. R., and Porter, M. R., *J. Polymer Sci.* **21,** 483 (1956).
18. Tereyama, H., and Wall, F. T., *J. Polymer Sci.* **16,** 357 (1955).
19. Conway, B. E., *J. Polymer Sci.* **18,** 257 (1955).
20. Mukherjee, P. N., and Lahiri, A., *J. Colloid Sci.* **11,** 240 (1956). In Fig. 1 of this paper the reduced viscosity is given in dl./g.; even though the concentration scale is in mg./dl. Personal communication from the authors, July 17, 1958.
21. Jordan, D. O., Mathieson, A. R., and Porter, M. R., *J. Polymer Sci.* **21,** 463 (1956).
22. Jordan, D. O., Mathieson, A. R., and Porter, M. R., *J. Polymer Sci.* **21,** 473 (1956).
23. Strauss, U. R., Gershfeld, N. L., and Crook, E. H., *J. Phys. Chem.* **60,** 577 (1956).
24. Waksman, S. A., "Humus," p. 154, Williams & Wilkins, Baltimore, 1938.
25. Eisenberg, H., and Pouyet, J., *J. Polymer Sci.* **13,** 85 (1954).
26. Fuoss, R. M., *J. Polymer Sci.* **3,** 603 (1948).
27. Huggins, M. L., *J. Am. Chem. Soc.* **64,** 2716 (1942).
28. Fuoss, R. M., and Cathers, G. I., *J. Polymer Sci.* **4,** 121 (1949).

JOURNAL OF COLLOID SCIENCE **14**, 430–440 (1959)

# EQUILIBRIUM AND KINETICS OF WATER EXCHANGE BETWEEN RAYON AND DETERGENT MICELLES IN A HYDROCARBON MEDIUM[1]

**E. Hirschhorn and M. B. Mathews**

*R. R. Street & Co. Inc., Chicago, Illinois*

*Received February 5, 1959*

## Abstract

Equilibrium conditions and exchange rates of water were determined in systems containing rayon, micelles of 2% OT in a hydrocarbon solvent, and solubilized water. Above 5.5% regain, the water regain of rayon is linearly dependent on the micellar water content. At 25°C., the water regain of rayon in 2% OT solutions is the same as in air. This relationship does not hold at other temperatures and at relative humidities over 80%. The vapor pressure-temperature relations for micellar water and water in rayon are comparable to those for water in concentrated electrolyte solutions, with the heats of vaporization comparable to those of pure water. A modified Raoult's law holds for the activity of solubilized water. The water may be conceived as forming a very concentrated electrolyte solution of the polar ends of the detergent molecules. The kinetics of water exchange between micelles and viscose rayon fabric were followed by $D_2O$ tracer in the micellar water. A simple rate equation applies in the limited range of water contents studied. Every minute approximately 0.005 g. water exchanged per square meter of rayon surface. The water exchange between micelle and fabric may occur directly or may be mediated by water which is in true solution in the solvent.

## Introduction

Comparatively little is known about solubilization phenomena in nonaqueous systems. Further, it is important in the dry cleaning process to understand the nature of water exchange between fabrics and water solubilized in nonpolar solvents.

Singleterry (1) has reviewed the evidence that solubilized water is contained within micelles of oil-soluble detergents. Fulton *et al.* (2) established that a dynamic water exchange exists between the detergent solution, fabric, and air phase. In earlier work (3), we presented evidence that similar nonaqueous systems contain solubilized water in micellar state. This lipophilic micelle consists of a spherical or near-spherical water core surrounded by a monolayer of detergent molecules. The size of the micelle depends upon the ratio of detergent to water in the system.

---

[1] Presented in part at the 132nd National Meeting of The American Chemical Society, New York, New York, September 8–13, 1957.

It was the aim of our present studies to gain an insight into the thermodynamics of the type of system used by Fulton *et al.* (2) with micellar structures of a chemically defined detergent containing solubilized water and at an extended range of temperatures. Micellar systems of 2% di-(2-ethylhexyl) sodium sulfosuccinate, viscose rayon, and varying small amounts of added water in a hydrocarbon solvent were investigated. Equilibrium water vapor pressures were determined at several temperatures for varying amounts of water in the detergent micelles and in the viscose rayon. The other part of our investigation was the determination of the exchange rate of water in equilibrium between detergent micelles and viscose rayon.

## WATER EQUILIBRIUM

When fabrics are immersed in a nonpolar medium containing solubilized water an equilibrium will be established between the water content of the solution and the water in the fabric.

### *1. Materials*

The di-(2-ethylhexyl) sodium sulfosuccinate (Aerosol OT) and *n*-dodecane used have been described (3). The hydrocarbon solvent was Shell Sol 140, an aliphatic hydrocarbon fraction of boiling range 185°–208°C. from the Shell Oil Company, New York. The textile fabric used in all experiments was white filament viscose rayon purchased from A. S. Heineman, Inc., New York, counting 30 by 40 threads per square centimeter. The water used in all experiments was triple distilled. Deuterium oxide was obtained from the Stuart Oxygen Co., San Francisco, California, in 99.5% strength and was diluted 1:10 with water before use.

### *2. Method*

Water equilibrium between detergent solution, rayon fabric, and vapor phase was established in an apparatus similar to Fulton's (2), consisting of a 1-liter three-neck round-bottomed flask containing 500 ml. of a solution of 2% Aerosol OT in Shell Sol 140, two suspended fabric swatches about 4 × 4 cm. in size each weighing 0.20 ± 0.03 g. and varying amounts of water. For experiments at low water content the rayon swatches were predried at 50°C. in order to approach water equilibrium uniformly under conditions of adsorption. A constant rapid stream of air was recirculated through the liquid and, after trapping the liquid spray in glass beads, over the sensing element of an electric hygrometer. This hygrometer was an American Instrument Company type in which all plastic parts had been replaced by Kel-F and Nylon, making it resistant to the action of solvent vapors. The relative humidity readings were accurate to ±1.5%. Water vapor pressures were calculated from the relative humidity readings at each temperature. Flask, sensing element, and solvent trap were enclosed in a constant-temperature cabinet and the vapor phase was recirculated through the system until no further change of relative humidity or temperature was observed, but at least for 30 minutes to attain complete water equilibrium in the three phases.

After the end of each run the fabrics were removed and freed from adhering detergent solution by rinsing in pure solvent. The water content was determined in the solvent and in the fabric swatches. Karl Fischer reagent in an automatic Beckman Aquameter was used for the water determination. The dry weight of the rayon was determined after drying overnight in an oven of 100°–105°C.

### 3. *Equilibrium Data*

For convenient reference Fig. 1 shows the vapor pressure data plotted as a function of the water which is solubilized in the 2 % Aerosol OT micelles for six temperatures in the range of 13°–46°C.

The data represented in Fig. 2 show that the water regain of rayon is linearly dependent on the quantity of water which is solubilized and independent of the temperature in the range 13°–35°C., considering only the water above 5.5 % regain. The positive intercept on the regain axis suggests that the first 5.5 % water of regain are more strongly bound than subsequently sorbed water. A similar phenomenon is shown by viscose rayon which is in equilibrium with atmospheric moisture.

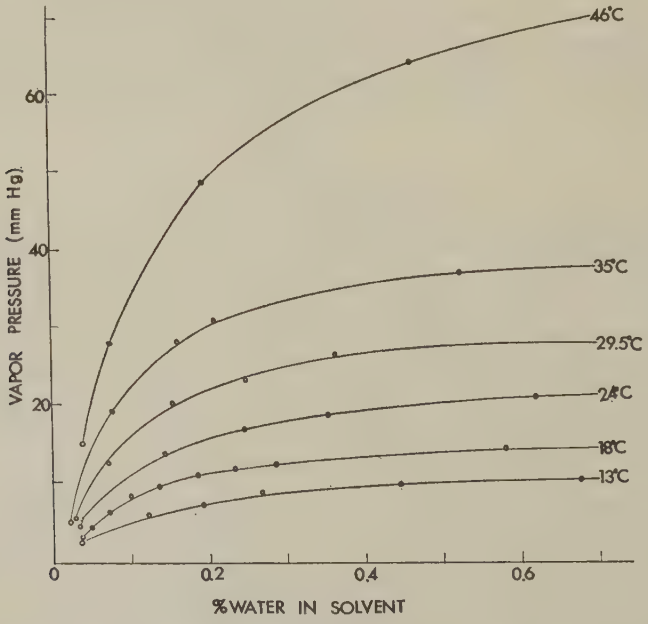

FIG. 1. Water vapor pressure in mm. Hg versus % water content in 2% Aerosol OT solutions (wt./vol.).

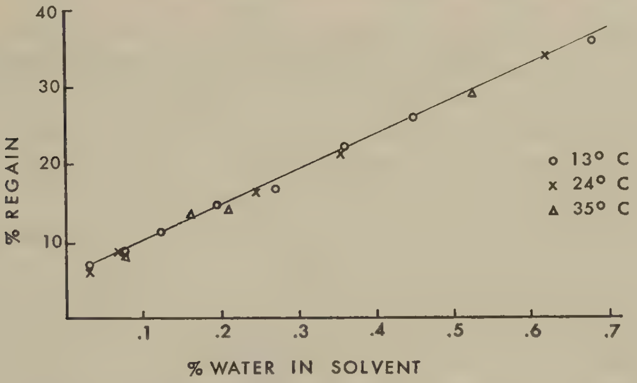

FIG. 2. Per cent water regain in viscose rayon versus per cent water in solvent (wt./vol.) in 2% Aerosol OT solutions (wt./vol.).

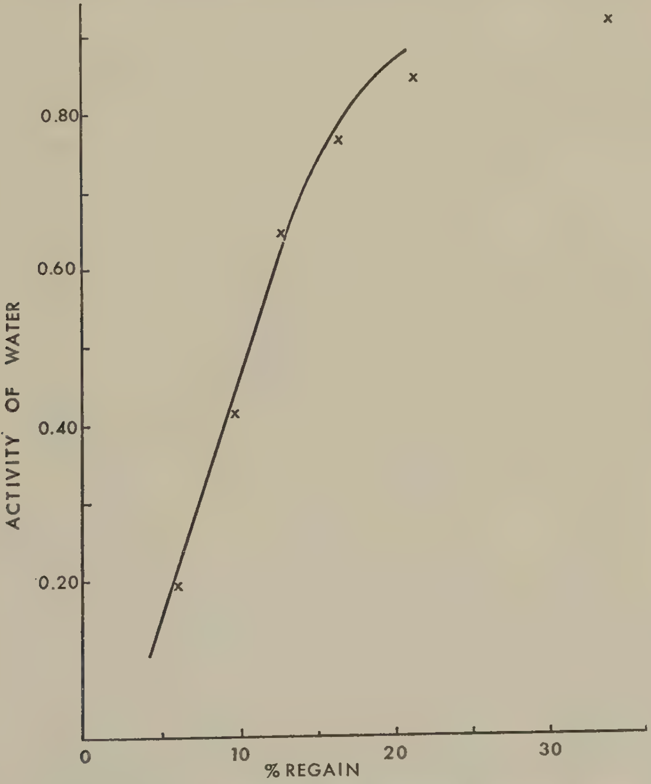

FIG. 3. Activity of water (determined as relative humidity in air) versus per cent regain of viscose rayon in air (*solid line*), and in 2% OT solution at 24°C. (×).

A comparison of the water regain of rayon in air, which is known (4), and that determined in 2% OT solutions of varying water content and corresponding water vapor pressures is shown in Fig. 3. For room temperatures (24°–25°C.) and in the range of micelle formation the regain of rayon in solvent is practically identical to that in air. At extremely high relative humidities (over 80%), where the micellar range merges with that of emulsions, some discrepancies are noted. Although not shown in Fig. 3, the same results are obtained for 13°C., 18°C., 30°C., and 46°C.

As has been established for aqueous systems (5–7) solubilization reduces the vapor pressure of the solubilizate. The vapor pressure of water which is micellarly solubilized in a hydrocarbon solvent is likewise less than that of pure water at the same temperature.

In Fig. 4 the logarithm of the vapor pressure is plotted versus the reciprocal absolute temperature for various micellar water contents. The top line A represents pure water. The solid lines below it represent 0.6%–0.05% of solubilized water in 2% OT solution. Similar linear vapor pressure-temperature relationships exist for water in rayon at different regains.

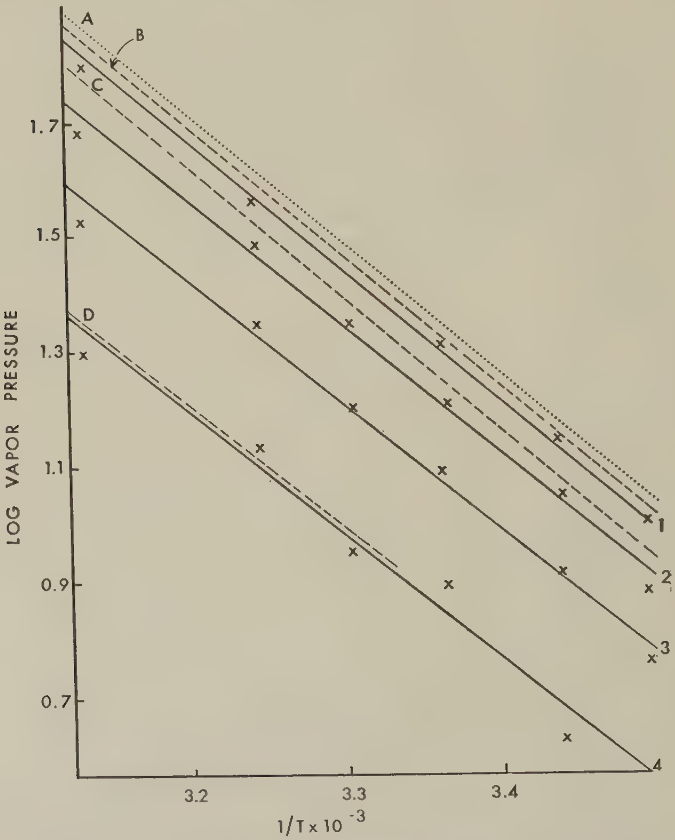

FIG. 4. Relation of the log of the water vapor pressure (in mm. Hg) to the reciprocal of the absolute temperature for 0.6% (*1*), 0.2% (*2*), 0.1% (*3*), 0.05% (*4*) solubilized water in 2% OT micelles; pure water (*A*), 10 g. NaCl in 100 g. $H_2O$ (*B*), 35 g. NaCl in 100 g. $H_2O$ (*C*), 85 g. $NaClO_3$ in 100 g. $H_2O$ (*D*).

The vapor pressure-temperature relations for micellar water as well as those for water in rayon are comparable to those for water in concentrated inorganic electrolyte solutions as shown in lines *B*, *C*, and *D* of Fig. 4. Calculated heats of vaporization of water are close to that of pure water.

## KINETICS OF WATER EXCHANGE

The second part of our investigation was concerned with the kinetics of the water exchange after water balance has been reached between fabric and micelles in dodecane. All the water incorporated into the detergent micelles is tagged with 10% deuterium oxide. Starting with a certain water vapor pressure, for which the amount of $H_2O$-$D_2O$ added to the solution is known to be in equilibrium with the water in the fabrics, the total water content of each phase, i.e., detergent solution and fabric, will remain unchanged. The $D_2O$ content in the solution, however, will be reduced from its original value at the start of the run according to the speed of the water exchange. The solubility of water in pure dodecane has been estimated at less than 0.001% and is therefore considered negligible in these experiments.

### *1. Method*

The exchange rate of $D_2O$ between micelles and fabric was determined in a Lucite container holding 500 ml. solution of 2% Aerosol OT and a $H_2O$-$D_2O$ mixture in dodecane. Into this was quickly immersed (and sealed) a Monel rack on which were hung 20 viscose rayon swatches, $6 \times 3$ inches in size. Prior to the experiment the fabrics had been conditioned overnight at constant temperature and predetermined equilibrium relative humidity. Magnetic stirring at a constant speed of 500 r.p.m. was provided. At the end of each experiment the fabrics were quickly removed from the detergent solution. The $H_2O$-$D_2O$ mixture was quantitatively separated from the dodecane solution by refluxing over a water trap. The isolated water mixture was freed from traces of impurities in a specially designed micro-still. In this apparatus from 0.4 ml. to 1.0 ml. water was frozen in dry ice and completely recovered after evacuating and subsequent regaining of room temperature. The $D_2O$ content of the mixture was determined in a LaMotte falling-drop densiometer. The dropping time of the sample of unknown $D_2O$ concentration was compared with that of water samples of known $D_2O$ concentrations (8, 9).

### *2. Rate Equation*

The exchange reaction at equilibrium may be written as follows

$$(H_2O + D_2O)_{\text{in solvent}} \rightleftarrows (H_2O + D_2O)_{\text{in fabric}} \qquad [1]$$

The following quantities are defined:

$a$ is grams $H_2O + D_2O$ in solvent;

$b$ is grams $H_2O + D_2O$ in fabric;

$c$ is grams $D_2O$, total;

$x$ is fraction $\frac{D_2O}{H_2O + D_2O}$ in solvent at time $t$;

$y$ is fraction $\frac{D_2O}{H_2O + D_2O}$ in fabric at time $t$;

$k$ is rate of transfer from solvent to fabric in grams water per minute per gram water in solvent.

From these definitions follows:

$$ax + by = c. \qquad [2]$$

Neglecting isotope fractionation effects in this system the rate equation may be written as

$$\frac{dx}{dt} = -kx + ky. \qquad [3]$$

Substitution and integration yields

$$x = \left(x_0 - \frac{c}{a + b}\right) e^{-[(a+b)/b]kt} + \frac{c}{a + b} \qquad [4]$$

Calculations of $k$ in Eq. [4] were carried out from data in Table I:

$a$ was calculated from column 3 and a solvent volume of 500 ml.
$b$ was calculated from column 4 and dry weight of fabric of 20 g.
$c$ is 10% of $a$.
$x_0 = 0.1$.
$x$ is determined experimentally for time $t$.

### *3. Results*

Several preliminary experiments conducted with fabrics which had been conditioned at 75% relative humidity to attain a regain of 15%, (in equilibrium with 0.24% water solubilized in the 2% Aerosol OT solution) showed that exchange of water was taking place at a rate too rapid for accurate determination by this method.

At regains of 12%–13%, obtained by conditioning rayon near 65% relative humidity, which is in equilibrium with 0.15%–0.16% water in the solvent and at a temperature of 30°C., the rate constant was calculated from Eq. [4] to be 0.13–0.14 as shown in Table I, column 7. Calculations of the rate constant for 6-, 7.5-, and 11-minute runs lead to constant values for $k$ and give confidence in the validity of Eq. [4]. Small temperature and regain variations did not change the rate constant significantly.

TABLE I

*Exchange Rate of $D_2O$ between Rayon and 2% OT in Dodecane*

| 1 Temp. (°C.) | 2 % Rel. humidity | 3 % $H_2O + D_2O$ in solvent (*wt./vol.*) | 4 % Regain (*wt./wt.*) | 5 Time of run (*min.*) | 6 % $D_2O$ in water after run (*wt./vol.*) | 7 Rate constant *k* |
|---|---|---|---|---|---|---|
| 30 | 63 | 0.164 | 12.3 | 6 | 5.1 | 0.14 |
| 30 | 61 | 0.152 | 12.0 | 7.5 | 4.7 | 0.13 |
| 30 | 63 | 0.162 | 13.0 | 11 | 3.5 | 0.13 |
| 20 | 59 | 0.150 | 11.1 | 6 | 4.8 | 0.14 |

According to Rowen and Blaine (10) 1 gram of rayon has an adsorptive surface of 0.98 m.². On this basis, every minute approximately 0.005 g. of water exchange per square meter of the viscose rayon surface.

## DISCUSSION

Fulton *et al.* (2) concluded that at equilibrium, fabric immersed in solvent containing solubilized water has the same water regain as fabric in the vapor phase. Our results confirm this conclusion with experiments carried out at 24°C. and below 80% relative humidity. However, above 80% relative humidity, as may be seen from Fig. 3, fabric immersed in solvent regains more water than fabric in air at the same relative humidity. This difference becomes greater with increase of temperature to 46°C.

It should be pointed out that there is no thermodynamic requirement for equality of regain by fabric in the two phases. It is of interest that the regain of rayon immersed in the solvent phase at constant relative humidity was found to be independent of temperature in the range 13°–46°C. Hess (11) reports similar results between 20° and 40°C. In contrast, regain of rayon in air at constant relative humidity is markedly decreased with increase in temperature (4).

The plot of solubilized water versus water vapor pressure fits a modified form of Raoult's law as given by Dole (12). Figure 5 shows a plot of $p_2{}^0/p_2$ versus $n_1/n_2$, where $p_2{}^0$ is vapor pressure of pure water, where $p_2$ is the vapor pressure of micellar water, and where $n_1$ and $n_2$ refer, respectively, to moles OT and moles water. This plot, a reciprocal form of the plot given by Dole, was recently used by Brady and Huff (7) in treatment of vapor pressure data of solubilized benzene in aqueous detergent solutions. The solubility of water in the hydrocarbon solvent is very small and has therefore been neglected.

To facilitate comparison of the analogous micellar systems the results are expressed in the form

$$\frac{p_2}{p_2{}^0} = \frac{n_2 k_{12}}{n_2 + f n_1}. \quad [5]$$

Values of $k_{12}$ (Table II) are close to ideal (Raoult's law requires $f = k_{12} = 1$) and are unlike those for the aqueous system which lie between 1.7 and 2.0. The quantity $f$ increases in general with temperature and lies between 1.20 and 1.81. Brady and Huff have interpreted their values of $f$, which average at 0.75, as indicating that only ¾ of the detergent molecules are available for solubilization of benzene in the hydrocarbon portion of the molecule. Water in the core of the lipophilic micelle, however, may be thought of as forming a very concentrated solution with the electrolyte represented by the polar end of the detergent molecule.

Each molecule of detergent contributes a maximum of two ions toward interaction with solubilized water. Values of $f$ less than 2 may possibly be regarded as indicating a reduced availability of detergent ions.

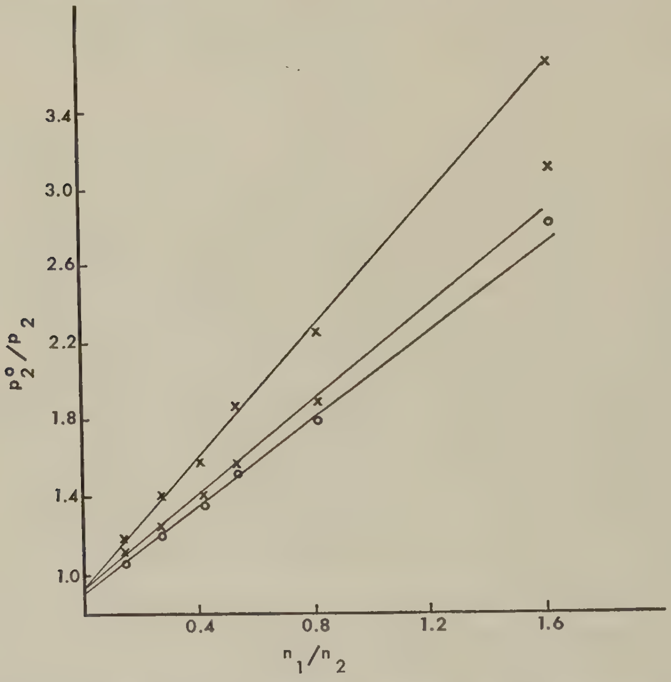

FIG. 5. Reciprocal plot for solubilized water in 2% OT solution at: 24°C. (O), 35°C. (+), 46°C. (X).

TABLE II

*Constants of Equation [5]*

| Temperature (°*F.*) | 55 | 65 | 75 | 85 | 95 | 115 |
|---|---|---|---|---|---|---|
| $k_{12}$ | 1.09 | 1.09 | 1.09 | 1.11 | 1.08 | 1.08 |
| $f$ | 1.20 | 1.20 | 1.25 | 1.38 | 1.30 | 1.81 |

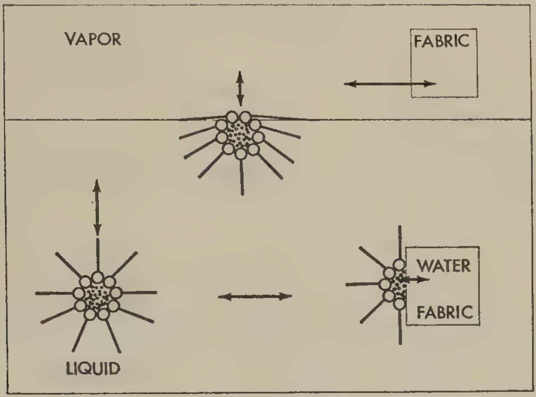

FIG. 6. Schematic representation of mechanism of direct exchange of micellar water.

Stokes and Robinson (13) have interpreted vapor pressure data for electrolytes in the concentration range of 7 molal to 20 molal as an adsorption phenomenon. Values for the heat of adsorption of water in the first hydration layer are in the range of 1 to 3 kilocalories in excess of the heat of liquefaction of pure water. This excess heat of adsorption is largely eliminated in subsequent layers of hydration. The heat of sorption of water into the micelle, however, is very nearly the same as the heat of liquefaction of pure water. This suggests a reduced availability of hydration sites on detergent ions in the micelle, a possible consequence of the special "lattice" form of the lipophilic micelle.

Two suggestions for the mechanism of exchange of water in nonaqueous micellar solutions may be considered. First, exchange of micellar water with water in the vapor phase or the fabric phase may be mediated by water in true solution in the hydrocarbon solvent. Second, direct exchange of micellar water may occur without passage of water through a solution state. This latter mechanism is illustrated schematically in Fig. 6.

The absence of significant surface tension alteration by detergent and water in this system, however, implies that only a very small portion of the solvent surface may contain detergent micelles in highly dynamic interchange of molecular components. Calculations of diffusion rates for micelles and for dissolved water indicate that diffusion is not a rate-limiting step in the exchange of water between phases.

## ACKNOWLEDGMENT

We are grateful to Mr. P. V. Warren and Mr. C. E. Stauffer for their assistance and permission to publish this work.

## REFERENCES

1. SINGLETERRY, C. R., *J. Am. Oil Chemists Soc.* **32,** 466 (1955).
2. FULTON, G. P., ALEXANDER, J. C., LLOYD, A. C., AND SCHWARTZ, M., *ASTM Bull.* **No. 192,** 63 (Sept. 1953).
3. MATHEWS, M. B., AND HIRSCHHORN, E., *J. Colloid Sci.* **8,** 86 (1953).
4. MATTHEWS, J. M., "Textile Fibers," 5th ed., pp. 768–770. Wiley, New York, New York, 1947.
5. KLEVENS, H. B., *Chem. Revs.* **47,** 1 (1950).
6. MCBAIN, J. W., AND O'CONNOR, J. J., *J. Am. Chem. Soc.* **62,** 2855 (1940).
7. BRADY, A. P., AND HUFF, H., *J. Phys. Chem.* **62,** 644 (1958).
8. BARBOUR, H. G., AND HAMILTON, W. F., *J. Biol. Chem.* **69,** 625 (1926).
9. COHN, M., "Preparation and Measurement of Isotopic Tracers," p. 51. J. W. Edwards, Ann Arbor, Michigan, 1948.
10. ROWEN, J. W., AND BLAINE, R. L., *Ind. Eng. Chem.* **39,** 1659 (1947).
11. HESS, R., *Melliand Textilber.* **39,** 404 (1958).
12. DOLE, M., *Ann. N. Y. Acad. Sci.* **51,** 705 (1949).
13. STOKES, R. H., AND ROBINSON, R. A., *J. Am. Chem. Soc.* **70,** 1870 (1948).

JOURNAL OF COLLOID SCIENCE **14**, 441–451 (1959)

# DETERMINATION OF SURFACE-AVERAGE PARTICLE DIAMETER OF COLORED EMULSIONS BY REFLECTANCE, AND APPLICATION TO EMULSION STABILITY STUDIES

**Norman E. Lloyd**

*George M. Moffett Research Laboratory, Corn Products Co., Argo, Illinois*

*Received November 19, 1958; revised March 23, 1959*

## Abstract

The relationship between the reflectances of colored emulsions (oil-in-water) and the surface-average diameter of their dispersed phases was investigated. The dispersed oil phases of the emulsions contained a red azo dye (1-xylyl, azo-2-naphthol) so that reflectance at 450 m$\mu$ was a function of both scattering and absorption by the emulsions. Reflectances at wavelengths at which the colored internal phase partially absorbed the incident light were found to be inversely proportional to the surface-average particle diameter raised to some power, $k$. The relationship between reflectance and surface-average particle diameter was independent of particle size distribution. Examples are given to show the applicability of the technique to evaluation of different emulsion stabilizers and to studies of the kinetics of emulsion coalescence. Some of the emulsions studied displayed limited coalescence. The mode of coalescence up to the point of limiting particle size followed first-order kinetics in which the rate of decrease in specific interfacial area at any given time was proportional to the specific interfacial area at that time.

## Introduction

Several methods have been used to evaluate stabilities of emulsions, ranging from simple estimates of shelf-life to complex and time-consuming determinations of particle size distribution of the dispersed phase (1, 2). Application of optical methods to determination of emulsion particle size, with reference to emulsion stability studies, has received little attention. Langlois *et al.* (3) investigated the relationship between the specific interfacial area of emulsions composed of nonabsorbing components, and the transmission of light by the emulsions relative to the continuous phase. An optical probe which could be dipped into the emulsions was used for the transmission measurements. The relative light transmission $I_0/I$ was related to interfacial area $A$ by the following equation:

$$I_0/I = 1 + \beta A$$

The term $\beta$ was a constant found to be a function of the ratio $n_d/n_c$ of the refractive indices of the disperse and continuous phases, respectively.

Schulman and Friend (4) investigated light scattering in emulsions composed of oleic acid, potassium hydroxide, *p*-methylcyclohexanol, and water. Particle sizes of the dispersed phases of the emulsions were extremely small, ranging from 100 to 400 A. in diameter. None of the emulsion components was light absorbing. The emulsions were studied at relatively high concentrations of the dispersed phase so that secondary scattering effects were observed.

This paper describes a reflectance technique for determining surface-average particle diameters in oil-in-water emulsions containing 50 volume per cent of dispersed phase. The technique is applied to studies of the stabilities of paraffin oil emulsions containing different starches, starch derivatives, water-soluble gums, and surfactants.

## Materials and Methods

Sufficient amounts of a red dye, FDC Scarlet B (1-xylyl, azo-2-naphthol, H. Kohnstamm and Co., Chicago, Illinois), were dissolved in the different oils used in the following studies to bring them to a uniform absorbancy of 0.710 at 450 mμ.[1] Absorbancy was checked in a Beckman DU spectrophotometer using 1-cm. cuvettes with inserts which reduced the absorbing path to 0.099 cm. Water was used as a reference liquid. Paraffin oil and kerosene each required 0.1735 g. of Scarlet B per liter of solution; corn oil required only 0.1685 g. of dye per liter to give absorbancy of 0.710 since its absorbancy at 450 mμ was 0.021 before addition of the dye.

The different emulsion stabilizers were dissolved or dispersed in water at a concentration of 1 g. per 100 ml. before adding the oil. The following stabilizers were used: 80-fluidity corn starch; hypochlorite-oxidized corn starch; corn starch methyl ether (0.1-degree of substitution); corn starch sulfate (0.016-degree of substitution); gum tragacanth, purified; "Methocel HG" (methyl cellulose, Hercules Powder Co.); "Pluronic F68" (polyoxyethylene polyoxypropylene, Wyandotte Chemical Co.); "Kelcoloid HV" (Kelco Corp.); "Arquad 18" (*N*,*N*-dimethyl,*N*-octadecyl quaternary ammonium chloride, Armour and Co.); and "Duponol ME" (sodium lauryl sulfate, du Pont). Degree of substitution represents the number of substituent groups introduced per glucose unit of starch. "Fluidity" is a measure of the reduction in the viscosity of acid-modified starches. These terms, as well as descriptions of the various commercial modified

---

[1] Absorbancy, $A_s$, is defined as follows:

$$A_s = \log_{10} T_w/T_0$$

Here $T_w$ is the overall transmittance of a cell of specified absorbing path containing water as reference liquid, and $T_o$ is the overall transmittance of a duplicate cell containing the oil solution of dye.

starches, are more fully described by Kerr (5). The method for dispersing the starches or starch derivatives was as follows:

> The requisite amount of starch (calculated to dry basis) was added to 300 ml. of distilled water in an 800-ml. beaker fitted with a cover and stirring device. After the starch was uniformly suspended, the mixture was heated in a boiling water bath for 15 minutes with continuous stirring. It was then cooled in a water bath at room temperature for 15 minutes and a few drops of phenyl mercuric acetate solution (10% in formamide) was added to prevent spoilage. The cooled dispersion was then adjusted to pH 6.0 with 0.1 *N* NaOH or HCl solution.

### *Preparation of Emulsions*

Equal volumes of oil and aqueous phase (prepared as described above) were combined and stirred manually to form a coarse emulsion. The latter was then passed four times through a motor-driven, valve-type homogenizer (Logeman Mfg. Co.) to obtain a fine dispersion. All emulsions were oil-in-water.

### *Reflectance Determinations*

Cylindrical glass cups 26 mm. in diameter and 12 mm. deep with flat ground rims were used as sample holders in the determination of reflectances of colored emulsions. The cups were filled to overflowing with the emulsions, and 1-inch square microscope coverglasses were placed over the top and pressed down to squeeze out any excess. Reflectances of duplicate samples were then determined immediately at 450 m$\mu$ (slit width = 0.53 mm.) in a Beckman Model B spectrophotometer fitted with reflectance attachment, using as reference a vitrolite block calibrated against a freshly prepared magnesium oxide surface (6). The thicknesses of the emulsion samples were such that any increase in thickness did not change their reflectances so that, for practical purposes, the values reported here are equivalent to reflectance at infinite sample thickness. Precision of the technique was ±0.1% reflectance.

### *Determination of Emulsion Particle Size Distribution by Microscopy*

Particle size distributions of the different emulsions were determined in duplicate. Samples of emulsion were diluted with about 50 volumes of a 2% solution of Pluronic F68 and mounted on microscope slides with coverglasses. Photomicrographs were then made on 5 × 7 inch cut film using a Bausch and Lomb microscope equipped with camera and calibrated eyepiece. An image of the calibrated scale of the micrometer eyepiece was recorded on the film thereby allowing accurate determination of the magnification factor. An exposure time of 0.02 second was used so that motion of the suspended emulsion particles due to Brownian movement was effectively "stopped." The finished negatives were placed on a milk glass plate illuminated from the bottom, and the diameters of 200 to 500 droplets determined. The results were then classified according to particle diameter to obtain the particle size distribution. "Surface-average particle diameter" ($D$) is defined and calculated as follows:

$$D = \frac{\sum n_i d_i^3}{\sum n_i d_i^2} \qquad [1]$$

where $n_i$ is the number of particles with diameter $d_i$. Average precision of the mean of duplicate determinations was ±2% of the reported values.

## RESULTS AND DISCUSSION

In the course of experiments on emulsion stability, it was noted that the intensity of the color imparted to corn oil emulsions (oil-in-water) by the yellow pigments normally present in corn oil was diminished considerably by reducing the average particle size of the emulsion. For example, a corn oil emulsion with an average particle size of 3 microns was lighter in shade than a similar emulsion with an average particle size of 30 microns. Experiments were run to determine the specific relationship between the reflectance of colored emulsions and the average particle size of the dispersed phase.

Five different emulsions were prepared, each containing 50 volume per cent of corn oil containing the red dye Scarlet B as previously described. The emulsions were made using aqueous solutions of different stabilizers known from previous experience to yield emulsions of widely different average particle diameters. Reflectances of the emulsions were determined at 450 mμ. Surface-average particle diameters of the internal phases were then determined by microscopy. Table I shows compositions of the emulsions with results typical of the reflectance and particle diameter determinations. When reflectance was plotted against surface-average particle diameter on logarithmic paper, a straight line was obtained as shown in Fig. 1. Figure 1 also shows the results of similar experiments wherein the reflectances of emulsions containing 50 volume per cent of colored kerosene or paraffin oil were determined and plotted as a function of surface-average

TABLE I

*Reflectance and Surface-Average Particle Diameter of Corn Oil Emulsions*

| Emulsion Stabilizer | Per cent reflectance at 450 mμ | Surface-average particle diameter (*microns*) |
|---|---|---|
| Gum tragacanth | 13.4 | 23.5 |
| Gum tragacanth | 14.6 | 19.3 |
| Gum arabic | 20.3 | 10.3 |
| "Kelcoloid HV" | 37.8 | 2.96 |
| "Pluronic F68" | 41.8 | 2.52 |

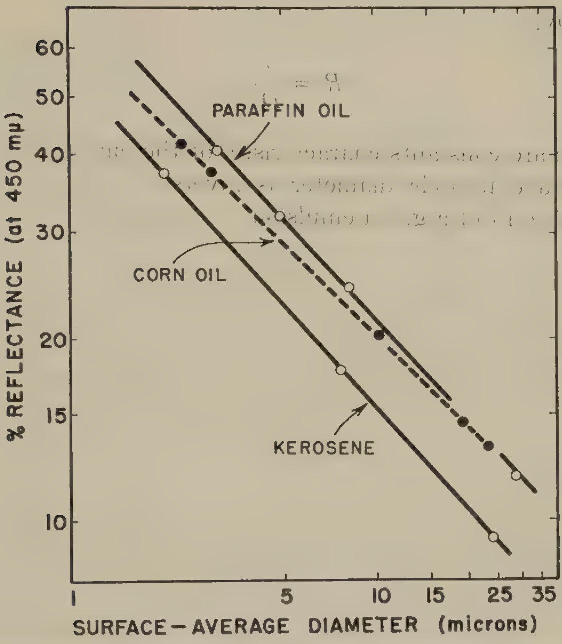

FIG. 1. Reflectance of various emulsion systems versus surface-average particle diameter.

particle diameter. The data for the kerosene emulsions were obtained by a slightly different technique. Two emulsions (A and B) were prepared, each containing 50 volume per cent of kerosene colored with Scarlet B. The surface-average particle diameters of the emulsions were then determined microscopically. A third emulsion (M) was prepared by mixing four parts (by volume) of emulsion A with one part of emulsion B. The surface-average particle diameter of the mixture ($D_m$) was then calculated as follows,

$$D_m = \frac{D_a D_b(P_a + P_b)}{(D_a P_b + D_b P_a)} \qquad [2]$$

where $P_a$ is the proportion (in the mixed emulsion) of emulsion A having particle diameter $D_a$, and $P_b$ is the proportion of emulsion B of particle diameter $D_b$. The fact that the particle size distribution of the mixed emulsion M was radically different than that of either of its component emulsions A and B, establishes conclusively that the logarithmic relationship between reflectance and surface-average particle diameter indicated by Fig. 1 is independent of particle size distribution.

The relationship between per cent reflectance ($R$) and surface-average particle diameter ($D$) can be expressed by the following equation:

$$\log R = -k \log D + \log c \qquad [3]$$

or alternatively,

$$R = \frac{c}{D^k}, \tag{4}$$

where $k$ and $c$ are constants characteristic of the emulsion system.

Surface-average particle diameter is inversely related to the specific interfacial area ($A$) of a given emulsion as follows,

$$D = \frac{6f}{A}, \tag{5}$$

where $f$ is the volume fraction of dispersed phase. Thus, the reflectance is proportional to the specific interfacial area of the emulsion raised to the $k$ power,

$$R = c'A^k \tag{6}$$

where $c' = c/(6f)^k$.

Values of the constants $k$ and $c$ for the emulsion systems shown in Fig. 1 are given in Table II. The values shown in Table II for these constants are valid only for the emulsion systems described, i.e., for systems containing 50 volume per cent of internal phase with the absorbancy of the dispersed phase equal to 0.710 as stated previously. Also, the ratio of the refractive

TABLE II

*Values of the Constants k and c for Three Different Emulsions Containing 50 Volume Per Cent of Colored Oil Phase*

| Disperse phase | $k$ | $c$ |
|---|---|---|
| Kerosene | 0.558 | 55.8 |
| Corn oil | 0.500 | 64.0 |
| Paraffin oil | 0.548 | 76.4 |

TABLE III

*Absorbancies of Paraffin Oil Containing 0.1735 Gram of Scarlet B Per Liter of Solution*

| Wavelength ($m\mu$) | Absorbancy[a] |
|---|---|
| 450 | 0.710 |
| 525 | 0.596 |
| 530 | 0.469 |
| 535 | 0.300 |
| 540 | 0.172 |
| 545 | 0.095 |
| 550 | 0.052 |

[a] Determined in Beckman Model B spectrophotometer at slit width of 0.20 mm. using cuvettes of 0.099 cm. absorbing path.

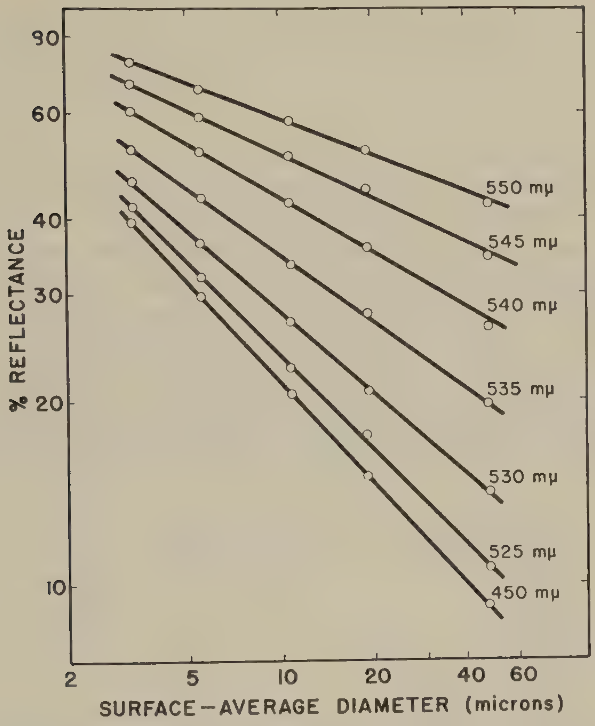

FIG. 2. Reflectance of paraffin oil emulsions at different wavelengths of incident light versus surface-average particle diameter.

indices of the continuous to the dispersed phase affects the values of the constants $k$ and $c$. No specific data on the influence of refractive index ratio was collected other than the observation that the greater the ratio, the greater the value of the constant $c$. This is to be expected since the light scattering ability of a dispersion increases with an increase in the relative refractive index ratio of its components.

It is of interest that the numerical value of the constant $k$ can be determined solely from reflectance data without recourse to particle size distribution determinations. Two emulsions A and B are made up having widely different particle sizes (e.g., kerosene emulsions A and B described above), and a third emulsion M is prepared by mixing emulsions A and B in known proportions. Reflectances of the emulsions are then determined. The following equation, derived from Eqs. [2] and [4], may be used to calculate the numerical value of $k$ by the process of iteration (7),

$$k = \frac{\log\left(\dfrac{R_a}{R_m}\right)}{\log\left[\dfrac{1}{P_a} - \dfrac{P_b}{P_a}\left(\dfrac{R_b}{R_m}\right)^{1/k}\right]} \qquad [7]$$

where $R_a$, $R_b$, and $R_m$ are the reflectances of emulsions A, B, and M, respectively, and $P_a$ and $P_b$ are the volume fractions of A and B in the mixture. Also, the values of the factors in Eq. [7] are assigned so that $R_a > R_m > R_b$, and $P_a + P_b = 1$.

An experiment was run to determine whether the logarithmic relationship between reflectance and surface-average particle diameter was valid at different wavelengths of incident light. Several emulsions of different particle size were prepared containing 50 volume per cent of colored paraffin oil. Reflectances of the emulsions were determined at 450 m$\mu$ and particle diameters determined by reference to the plot in Fig. 1. Reflectances of the emulsions were again determined at several other wavelengths over a range where the absorbancies of the colored paraffin oil differed considerably, as shown in Table III. Figure 2 shows graphs of per cent reflectance of the paraffin oil emulsions (plotted on logarithmic scales)

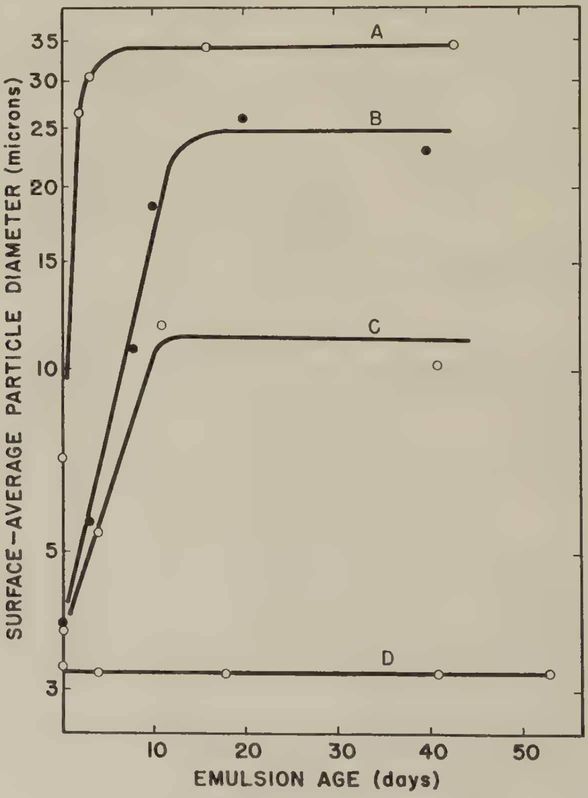

FIG. 3. Stability of paraffin oil emulsions containing various starches and starch derivatives: (*A*) 80-fluidity corn starch, (*B*) hypochlorite-oxidized corn starch, (*C*) 0.1-D.S. corn starch methyl ether, (*D*) 0.016-D.S. corn starch sulfate.

against surface-average particle size. The results show that the relationship described by Eq. [3] holds at the different wavelengths.

*Stability of Paraffin Oil Emulsions*

A method for evaluating emulsion stability was devised, based on the reflectance experiments above. Emulsions containing 50 volume per cent of paraffin oil colored with Scarlet B were prepared as previously described, using 1 % solutions of several different stabilizers. Reflectances of the emulsions at 450 mμ were determined immediately after homogenizing, and initial surface-average diameters were calculated by reference to the plot in Fig. 1. Several 100-ml. samples of each emulsion were placed in 4-oz. jars, tightly capped, and stored at room temperature (28 ± 5°C.). In order to determine the change in average particle diameter as a function of storage time, reflectances of samples of the different emulsions were measured at progressive intervals during the storage period. A different sample of each

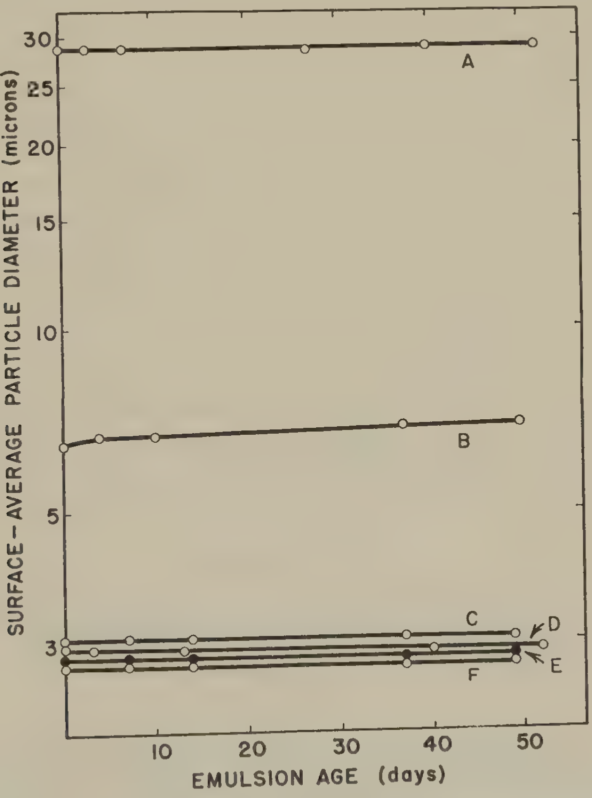

FIG. 4. Stability of paraffin oil emulsions containing various water-soluble gums and surfactants: (*A*) gum tragacanth, (*B*) "Methocel HG," (*C*) "Pluronics F68," (*D*) "Kelcoloid HV," (*E*) "Arquad 18," (*F*) "Duponol ME."

emulsion was used for each reflectance determination. The emulsions "creamed" in some instances, so that the emulsions were shaken gently just before determination of reflectance in order to redistribute the partially creamed oil phase.

Figures 3 and 4 show the results of stability studies on emulsions containing several different starches, starch derivatives, and surfactants. Surface-average particle diameter is plotted on a logarithmic scale, and emulsion age is plotted on a linear scale. The emulsions shown in Fig. 3 were unstable, with the exception of the preparation stabilized by the starch sulfate derivative. The emulsions stabilized by 80-fluidity corn starch, hypochlorite-oxidized corn starch, and corn starch methyl ether displayed limited coalescence, i.e., coalescence of oil droplets progressed until a limited particle diameter was reached, whereupon coalescence stopped. Figure 4 shows the results of stability determinations on emulsions containing different water-soluble gums and surface-active agents. The surfactants gave highly disperse stable emulsions, as likewise did the "Kelcoloid HV." Gum tragacanth gave an emulsion which was stable but relatively coarse.

The portions of the curves shown in Fig. 3 during the periods of active coalescence (i.e., up to the points of limited coalescence) approximate straight lines. Thus, the rate of decrease in specific interfacial area at a given time was proportional to the specific interfacial area at that time. Since specific interfacial area simulates a concentration factor (interfacial area per unit volume of oil), the coalescence behavior of the emulsions shown in Fig. 3 simulated a first-order reaction. First-order kinetics in emulsion coalescence has been suggested by Lotzkar and Maclay (8), who studied coalescence rates (rates of decrease in specific interfacial area) of emulsions containing 25, 40, and 60 volume per cent of olive oil, cottonseed oil, and mineral oil stabilized with pectin, tragacanth, karaya, and acacia gums. They determined interfacial areas microscopically by means of size-frequency analyses. However, the precision of their analyses was such that no definite statement as to first-order dependence was made.

## Acknowledgment

The author expresses his gratitude to Dr. Thomas J. Schoch, George M. Moffett Research Laboratory, Corn Products Company, for his many helpful suggestions and for his aid in preparation of the manuscript.

## References

1. Becher, Paul, "Emulsions, Theory and Practice." New York, 1957.
2. Merrill, R. C., Jr., *Ind. Eng. Chem., Anal. Ed.* **15**, 743 (1943).
3. Langlois, G. E., Gulberg, J. E., and Vermeulen, T., *Rev. Sci. Instr.* **25**, 360 (1954).

4. Schulman, J. H., and Friend, J. A., *J. Colloid Sci.* **4,** 497 (1949).
5. Kerr, R. W., "Chemistry and Industry of Starch," 2nd ed. Academic Press, New York, 1950.
6. NBS Letter Circular LC547, National Bureau of Standards, Washington 25, D. C.
7. Scarborough, James B., "Numerical Mathematical Analysis," 2nd ed., p. 197. Johns Hopkins Press, Baltimore, 1950.
8. Lotzkar, Harry, and Maclay, W. Dayton, *Ind. Eng. Chem.* **35,** 1294 (1943).

JOURNAL OF COLLOID SCIENCE **14**, 452–454 (1959)

## LETTER TO THE EDITORS

# MEASUREMENT OF THE MAGNETIZATION OF THIN FILM

An electron beam is deflected by a magnetic field (Lorentz effect). This effect is observable in a diffraction pattern obtained from a ferromagnetic substance. Since a thin film gives rise to a distinct diffraction pattern, it is convenient to study the magnetization of it by the electron diffraction process.

A film of nickel was deposited electrolytically onto a brass film. The deposited film (thickness: about 5 microns, size: 5 × 5 mm.) was isolated by dissolving the brass film in a dilute nitric acid. One piece of permanent magnet (size about 0.5 mm.) was attracted to the edge of the nickel film thus prepared, as illustrated in Fig. 1. An incident beam passed through a pin hole (about 0.05 mm.) found in the film. Such a pin hole is frequently produced in an electrodeposited film.

A process of double exposure with a nonferromagnetic gold foil was employed in order to measure the deflection of the incident beam caused by the magnetic field of the specimen. A diffraction pattern of the gold foil was photographed beforehand and then that of the specimen was superposed upon it. During this process, the wavelength of the incident electrons and the position of the photographic plate were kept fixed. The double diagram obtained in this way is shown in Fig. 2. Here the diffraction rings are eccentric as the result of the Lorentz effect. The deflection $\Delta Z$ of the incident beam caused by the specimen is calculable from the ring eccentricity, as is illustrated in Fig. 3. That is

$$\Delta Z = \frac{Z_1 - Z_2}{2} = 0.142 \text{ cm.}$$

Under the experimental arrangement we have a relation between $\Delta Z$ and the magnetization $B$ of the specimen:

$$\Delta Z = \frac{eL}{mv} \int_0^l B dl = \frac{eL\lambda}{h} \int_0^l B dl, \qquad [1]$$

where $e$ means the electron charge ($1.6 \times 10^{-20}$ e.m.u.), $L$ means the camera length (495 mm.), $m$ means the electron mass, $v$ means the velocity of the electrons, $\lambda$ means the wavelength of the incident electrons (0.0327 A.), $h$ means Planck's constant ($6.6 \times 10^{-27}$ erg. sec.) and $l$ means the distance traveled by the electrons in the region of magnetic field. It is plausible under the conditions of Fig. 1 and Fig. 2 that this $l$ is approximately equal to the film thickness of the specimen (5 microns) and that the $B$ is homogeneous. According to Eq. [1] we obtain $B \simeq 7000$ gausses for Fig. 2. This value is reasonable as the saturation induction of nickel.

The magnetic state of an amorphous film of iron was studied by the present process. Iron was electrodeposited onto a thin foil of gold. A composite film thus prepared, consisting of the iron and the gold layer (thickness: about 1 and 0.1 micron, respectively) was readily investigated by the same process as in Fig. 1. Figure 4 is a double diagram containing the diffraction pattern of this composite film and that of a gold foil. In Fig. 4 the diffraction rings from the amorphous layer of iron are not

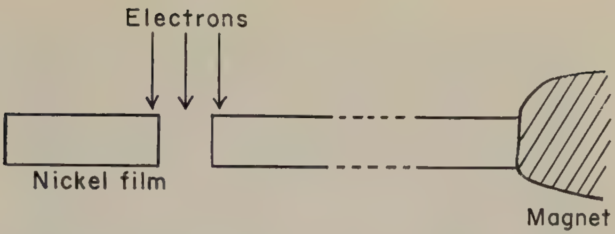

FIG. 1. Arrangement of the magnetized film of nickel for the incident electrons.

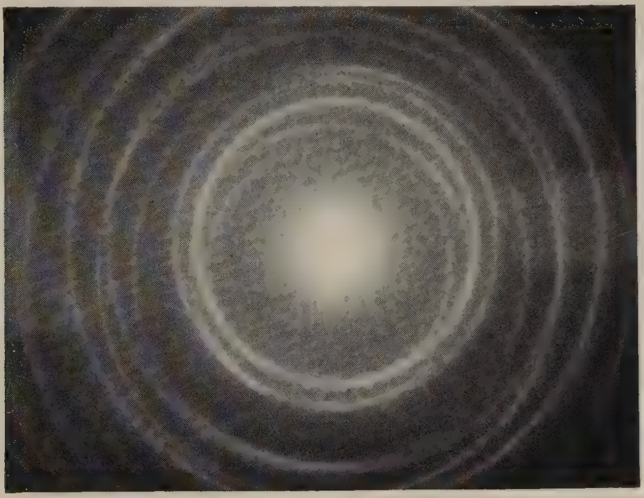

FIG. 2. Double diagram consisting of the diffraction pattern of nickel and that of gold.
Wavelength: 0.0327 A.; camera length: 495 mm. Positive is enlarged 2.3 times

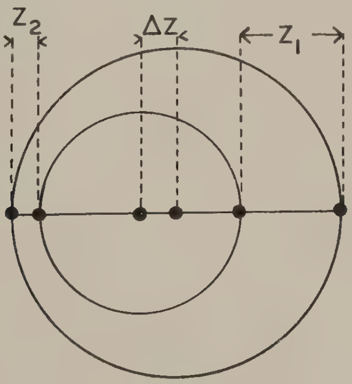

FIG. 3. Illustration for the calculation of $\Delta Z$.

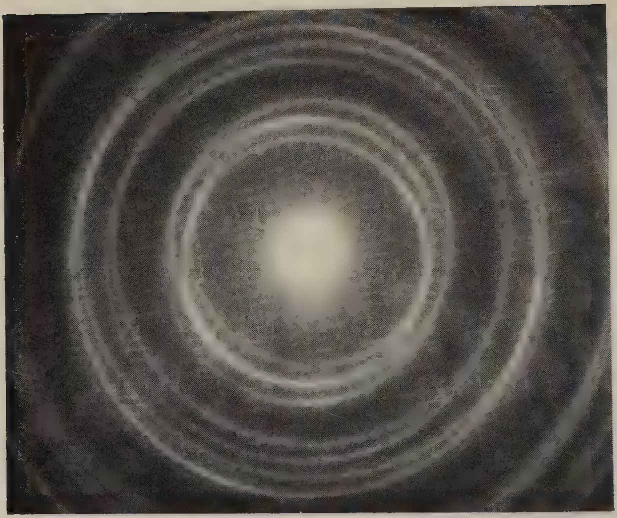

FIG. 4. Double diagram obtained with the Fe-Au composite film and with a gold foil.
Wavelength: 0.0332 A.

discernible, but those of the gold layer in the composite film and those of the single film of gold are eccentric as the result of the Lorentz effect. In this way the ferromagnetism of the amorphous layer was indirectly observable through the diffraction rings of gold. As the thickness of iron layer in Fig. 4 is presumably about 1 micron, we obtain $B \simeq 30{,}000$ gausses according to Eq. [1] ($\lambda$: 0.0332 A. and $\Delta Z$: 0.109 cm.). This value is approximately in accordance with the known saturation induction of iron.

The iron film here prepared appears to be "amorphous," insofar as the electron diffraction experiment is concerned. Our magnetic analysis reveals that the crystallites constructing this film are larger than about 20 A. This is because the iron crystallite whose grain size is larger than this value is ferromagnetic (1). Our process therefore makes it possible to estimate the grain size of a ferromagnetic substance. It is also possible to estimate the film thickness with Eq. [1] if we measure $\Delta Z$ for a film with the known magnetization ($B$).

## REFERENCE

1. KÖNIG, H., *Naturwiss.* **33**, 71 (1946).

*The Institute of Physical & Chemical Research,*
*31 Kamifuji (Hongo),*
*Tokyo, Japan.*
S. YAMAGUCHI

*Received April 27, 1959.*

JOURNAL OF COLLOID SCIENCE **14,** 455–456 (1959)

# BOOK REVIEWS

**Electrophoresis: Theory, Methods and Applications.** Edited by Milan Bier. Academic Press New York and London, 1959. xx, + 563 pp. Price $15.00.

The term "electrophoresis" was originally defined to mean the movement of charged colloidal particles and macromolecular ions, such as proteins, polysaccharides, and nucleic acids, under the influence of an electric field; the term "ionophoresis" being reserved for the electromigration of low molecular weight materials, e.g., amino acids, sugars, purines, pyrimidines, and simple, inorganic ions. However, with the rapid advances in the application of the various electrophoretic methods to the whole spectrum of charged substances, the term "electrophoresis" has become an all-inclusive one. Differences in migration velocities in an electric field provide a powerful means for the analysis and separation of substances which are difficult to fractionate by other methods. In fact, electrophoresis is often the only method available for the quantitative analysis of such systems. In addition, the characterization of biologically important macromolecules with respect to size, shape, and electrical charge, is important for a molecular understanding of their reactions and physiological activities. For these reasons, the abundant results obtained with the Tiselius moving-boundary electrophoresis apparatus, as modified by Longsworth, have contributed significantly to the rapid progress made in the past two decades in the various branches of biochemistry and medicine; and there is every reason to believe that the more recently developed methods of preparative- and zone-electrophoresis will likewise become indispensable to both the biologist and chemist. These generalities are amply substantiated by the book under review, which is the first extensive treatment of electrophoresis to appear in the English language since 1942.

The first chapter, written by J. Th. Overbeek and J. Lijklema, is a theoretical treatment of the electrical double layer surrounding charged particles in solution and its relationship to electrophoresis. In conjunction with the article by Overbeek on the quantitative interpretation of electrophoretic mobilities which appeared in *Advances in Colloid Science* **3,** 97 (1950), this treatment gives the reader the theoretical background required for the interpretation of electrophoretic mobilities in terms of molecular parameters, such as net charge and frictional coefficient, and composition of the supporting medium. Having established the theoretical relationship between electrophoretic mobility and net charge, the book proceeds to a discussion of the quantitative interpretation of the acid-base titration curves of proteins (K. Linderstrøm-Lang and S. O. Nielsen). The theory and methods of moving-boundary electrophoresis are then discussed in detail by L. G. Longsworth. One is now prepared for a discussion of the applications of moving-boundary electrophoresis to biocolloidal systems; this, however, does not appear until four chapters later. In the opinion of the reviewer, avoidance of this break in continuity of thought would have been a great aid to the expert as well as to the novice in the field. In any event, the chapter by R. A. Brown and S. N. Timasheff clearly shows what a variety of information can be obtained by the application of moving-boundary electrophoresis to biological problems.

Likewise, the principles and applications of preparative electrophoresis without supporting media and preparative and analytical zone-electrophoresis, are discussed in detail in four chapters written by M. Bier, Ch. Wunderly, H. G. Kunkel and R. Trautman, and T. Willand. One is impressed by the important analyses and separations which these relatively new methods have made possible. But, here again, the reader would probably have gained from some reorganization of the book. For example, the chapter on the applications of zone-electrophoresis is reserved for the end of the book, separated by four chapters from the other two chapters dealing with electrophoresis on paper and other supporting media.

The clinical and physiological applications of electrophoresis are discussed by D. Moore; and C. C. Brinton, Jr., and M. A. Lauffer treat microscopic electrophoresis.

The reviewer objects to the use of the term "anomalies" when referring to non-ideal electrophoretic behaviors (e.g., p. 324 and p. 440) which are understood at least qualitatively. It should also be pointed out that the statement on page 494 to the effect that electrophoretic separations of low molecular weight substances can be accomplished only by methods utilizing supporting media, does not take cognizance of the fact that moving-boundary electrophoresis has been used for the quantitative analysis of mixtures of adenosinephosphates and glutamic and aspartic acids. Finally, the book is a bit repetitious, but this is difficult to avoid with a large number of contributors. In any case, this is an important book which brings the reader up to date in a rapidly expanding field and should be an invaluable aid to the researcher who wishes to apply electrophoresis to his problems, whether biochemical, biophysical, clinical, or industrial in nature.

JOHN R. CANN, Denver, Colorado

**Fast Reactions in Solids.** By F. P. BOWDEN AND A. D. YOFFE, Academic Press, New York and London, 1959. x + 164 pp. Price $7.00

The authors of this monograph and their colleagues at the Physics and Chemistry Laboratory, Department of Physics, Cambridge University, are well known for their investigations into solid state decompositions. An earlier work by the same authors (1952) described experimental studies on mechanisms of initiating explosions in liquids and solids. Here they describe more recent researches in this field. In particular they are concerned with the mechanisms by which an explosive crystal can be decomposed when subjected to heat, light, shock, or nuclear radiation. High-resolution electron microscopy combined with electron diffraction is used to investigate the early stages of decomposition. High-speed photography and electronic methods are employed to follow the fast reactions.

This book is certainly of first importance to the relatively few workers in this field. Its appeal, however, is much wider. Experimental problems of studying reactions which are complete in the millisecond-microsecond range and are often initiated in minute "hot spots" have been met in ingenious and fascinating ways. An example of the approach is the study of the electron diffraction pattern of a crystal of silver azide in the process of decomposition, clearly showing that the silver azide lattice is converted to a special silver lattice based on the silver azide structure and then this lattice collapses to the normal silver lattice. At the same time, normal silver crystals are formed on surface defects and grow down into the crystal.

The photographs are particularly striking. One set demonstrates the initiation of explosions in the nitroglycerin by the intersection of three (but not two or one) shock waves. Another remarkable series shows the decomposition of silver crystals of various substances when exposed to hot wires.

Implicit in the entire discussion is a slight air of excitement because of the violent nature of most of the compounds.

This book is recommended to scientists of all sorts for browsing, to physical chemists for the unique experimental techniques, and to specialists in solid-state kinetics as an authoritative report on recent progress in this field.

BENSON R. SUNDHEIM, New York, New York

Electrophoresis

*Theory, Methods, and Applications*

*Edited by* MILAN BIER *Fordham University and Institute of Applied Biology, Inc., New York*

*1959, 563 pp., illus., $15.00*

Introduction
By Arne Tiselius, University of Uppsala

Electric Potentials in Colloidal Systems
By J. Th. G. Overbeek and J. Lijklema, University of Utrecht

Acid-Base Equilibria of Proteins
By K. Linderstrøm-Lang and Sigurd O. Nielsen, Carlsberg Laboratory, Copenhagen

Moving Boundary Electrophoresis—Theory
By L. G. Longsworth, The Rockefeller Institute, New York

Moving Boundary Electrophoresis—Practice
By L. G. Longsworth, The Rockefeller Institute, New York

Paper Electrophoresis
By Ch. Wunderly, Kanton Hospital, University School of Medicine, Zurich

Zone Electrophoresis in Various Types of Supporting Media
By Henry G. Kunkel and Rodes Trautman, The Rockefeller Institute, New York

Preparative Electrophoresis without Supporting Media
By Milan Bier, Fordham University, New York, and Institute of Applied Biology, Inc., New York

Applications of Moving Boundary Electrophoresis to Protein Systems
By R. A. Brown, The Wistar Institute for Anatomy and Biology, Philadelphia, and S. N. Timasheff, Eastern Regional Research Laboratory, U. S. Department of Agriculture, Philadelphia

Clinical and Physiological Applications of Electrophoresis
By Dan H. Moore, The Rockefeller Institute, New York

The Electrophoresis of Viruses, Bacteria, and Cells and the Microscope Method of Electrophoresis
By Charles C. Brinton, Jr. and Max A. Lauffer, University of Pittsburgh

Applications of Zone Electrophoresis
By Theodor Wieland, Institut für Organische Chemie der Johann-Wolfgang-Goethe Universität, Frankfurt

AUTHOR INDEX—SUBJECT INDEX.

ACADEMIC PRESS, New York and London
111 Fifth Avenue, New York 3, New York
40 Pall Mall, London S. W. 1

## Announcing METHODS O

## Volume 6 SOLID STATE

*Edited by* K. LARK-HOROVITZ and VIVIAN A. JOHNSO

**PART A—Preparation, Structure, Mechanical and Thermal Properti**

*August 1959, 466 pp., illus., approx. $10.00*

### Introduction

Evaluation of Measurement
  by Sidney Reed
Solid State Physics
  by K. Lark-Horovitz and V. A. Johnson

### Preparation and Purification of Materials

Purification
  by P. H. Egli, L. R. Johnson, and W. Zimmerman, III
Detection of Impurities
  by Mark G. Inghram
The Control of Impurities in Solids
  by C. D. Thurmond
Single Crystal Growing
  by M. Tanenbaum
Preparation of Thin Films
  by Georg Hass and A. F. Turner
Agglomeration
  by S. S. Flaschen and J. C. Williams
Preparation of Laboratory Glass Samples
  by C. L. Babcock
Surface Preparation
  by J. W. Faust, Jr.
Electron Microscopy of Surfaces
  by H. J. Yearian and J. F. Radavich

### Crystal Structure Determination

The Diffraction of Short-Wavelength Radiation by Matter
  by David Harker
X-Ray Diffraction
  by W. P. Binnie and I. G. Geib
Electron Diffraction Methods
  by H. J. Yearian
Neutron Diffraction Methods
  by C. G. Shull

### Mechanical Properties

High-Precision Density Determination of Solids
  by Alexander Smakula
Elastic, Anelastic, and Plastic Properties
  by T. A. Read, C. A. Wert, and Marvin Metzger
Line Imperfections or Dislocations
  by S. Amelinckx
Radiation Damage
  by J. W. MacKay
Diffusion
  by Carl T. Tomizuka

### Thermal Properties

Heat Capacity
  by P. H. Keesom and N. Pearlman
Thermal Conductivity
  by N. Pearlman

### Solid State Studies under High Pressure

  by John C. Jamieson and A. W. Lawson
Introduction
The Generation of Static High Pressure
The Measurement of Pressure
The Measurement of Temperature at High Pressure
Dilatometric Measurements
Determination of Elastic Constants under Pressure
The Study of Phase Changes
Thermal Measurements
Dielectric Measurements
The Measurement of Electrical Resistance
Magnetic Measurements
Optical Measurements
Mechanical Properties of Solids under High Hydrostatic Pressure
Shock Wave Techniques
Miscellaneous
AUTHOR INDEX—SUBJECT INDEX

**ACADEMIC PRESS,** **New York and London**
**111 Fifth Avenue, New York 3, New York**
**40 Pall Mall, London, S.W. 1**

# XPERIMENTAL PHYSICS

# HYSICS

epartment of Physics, Purdue University

## PART B—Electrical, Magnetic and Optical Properties

*August 1959, about 430 pp., illus., approx. $10.00*

### Electrical Properties

Dielectric Measurement Procedures
by A. H. Sharbaugh and S. Roberts
Conductivity Measurements on Solids
by W. Crawford Dunlap, Jr.
Superconductivity
by A. L. Schawlow
Nonequilibrium Semiconductor Phenomena
by R. Bray and A. Many
High Frequency Effects in Semiconductors
by T. S. Benedict
Thermoelectric Effects
by H. P. R. Frederikse, V. A. Johnson, and W. W. Scanlon
Thermionic Emission
by E. Coomes
Surface States
by W. H. Brattain and C. G. B. Garrett

### Galvanomagnetic and Thermomagnetic Effects

The Hall Effect
by Hellmut Fritzsche
Magnetoresistance
by G. L. Pearson
Other Transverse Galvanomagnetic and Thermomagnetic Effects
by Wayne W. Scanlon

### Magnetic Properties

The Measurement of Magnetic Susceptibility
by Thomas R. McGuire
Ferromagnetism and Ferrimagnetism
by Louis R. Maxwell
Permeability and Losses of Ferro- and Ferrimagnets
by C. P. Bean and J. J. Becker
Resonance Phenomena
by A. F. Kip
Magnetic Anisotropy
by H. Shenker

### Optical Properties

Introduction
General Experimental Equipment
Optically Isotropic Materials
Crystal Optics
Induced Double Refraction and Rotation
by H. Y. Fan
Optical Measurements on Thin Films
by G. Hass and A. F. Turner
Electronic Band Structure of Solids by X-Ray Spectroscopy
by L. G. Parratt

### Luminescence

Fundamental Concepts
Preparation of Phosphors
Photoluminescence and Cathodoluminescence (General Luminescence Measurements)
Thermoluminescence—Glow Curves
Electroluminescence
by F. Matossi and S. Nudelman
Production and Detection of Recombination Radiation
by J. R. Haynes
Color Centers
by James H. Schulman and Howard W. Etzel

### Photoelectric Phenomena

Photoconductivity
by R. H. Bube
Photoelectromagnetic Effect
by H. S. Sommers, Jr.
Photovoltaic Effect
by J. J. Loferski and P. Rappaport
Photoelectric Emission
by A. H. Sommer and W. E. Spicer

AUTHOR INDEX—SUBJECT INDEX

**Previously Published: Volume 1: CLASSICAL METHODS**
**Edited by I. Estermann, Office of Naval Research, 1959, 596 pp., illus., $12.80**

**Detailed literature available upon request**

*Volume III Ready August 1959*

# Rheology

## THEORY AND APPLICATIONS

*Edited by* Frederick R. Eirich
*Polytechnic Institute of Brooklyn*

**Volume III**

*August 1959, about 670 pp., illus., approx. $20.00*

The Normal-Coordinate Method for Polymer Chains in Dilute Solution, by B. H. Zimm
The Principles of Rheometry, by S. Oka
Viscosity of Suspensions of Electrically Charged Particles and Solutions of Polymeric Electrolytes, by B. E. Conway and A. Dobry-Duclaux
The Rheology of Latex, by Samuel H. Maron and Irvin M. Krieger
The Rheology of Printing Inks, by A. C. Zettlemoyer and Raymond R. Myers
Rheology of Pastes and Paints, by Ruth N. Weltmann
Atomistic Approach to the Rheology of Sand-Water and of Clay-Water Mixtures, by W. A. Weyl and W. C. Ormsby
The Rheology of Inorganic Glasses, by W. A. Weyl
The Rheology of Concrete, by M. Reiner
The Deformation of Crystalline and Cross-Linked Polymers, by I. L. Hopkins and W. O. Baker
The Viscosity and Elasticity of Interfaces, by Dean W. Criddle
Rheology of Lubrication and Lubricants, by A. Bondi
The Rheology of Adhesion, by J. J. Bikerman
Rheology in Molding, by C. E. Beyer and R. S. Spencer
Rheology of Spinning, by Bruno R. Roberts
Theory of Screw Extruders, by W. L. Gore and James M. McKelvey
AUTHOR INDEX—SUBJECT INDEX.

**Volume I,** *1956, 761 pp., illus., $20.00*
**Volume II,** *1958, 591 pp., illus., $18.00*

*Review of Volume I:*

"Some of the theories which are discussed may in time be extended, but will hardly be substituted by new developments. Therefore in spite of the present rapid growth of rheology, this volume will be used for a long time to come as a textbook by the research worker who wants to penetrate into the field of rheology and as a reference book for those who are already actively engaged in the field. In conclusion it is to be strongly recommended to all those whose scientific activities lead to problems of rheology."

—*Applied Mechanics Review*

*Literature describing all volumes available upon request*

ACADEMIC PRESS, New York and London
111 Fifth Avenue, New York 3, New York
40 Pall Mall, London, S.W. 1

JOURNAL OF COLLOID SCIENCE **14**, 457–472 (1959)

# PARTICLE MOTIONS IN SHEARED SUSPENSIONS

## IX. SPIN AND DEFORMATION OF THREADLIKE PARTICLES

**O. L. Forgacs[1] and S. G. Mason**

*Physical Chemistry Division, Pulp and Paper Research Institute of Canada, and Department of Chemistry, McGill University, Montreal, Canada*

*Received December 12, 1958*

### *List of Symbols*

$a', b'$ = semi-length and semi-diameter of a cylindrical particle.
$C$ = spherical elliptical orbit constant.
$E, E_b$ = tensile and bending moduli of elasticity.
$F$ = axial force acting on the central cross section of a rod.
$G$ = velocity gradient.
$I$ = transverse moment of inertia.
$l$ = coordinate measured along the length of a rod.
$M$ = orientation factor.
$n$ = number of axial spins per rotation.
$t$ = time.
$u, v, w$ = velocity components along the $X$-, $Y$-, and $Z$-axes of the shear field.
$X, Y, Z$ = Cartesian co-ordinates.
$\zeta$ = a co-ordinate in the theory of deformation.
$\eta$ = viscosity of suspending medium.
$\theta, \phi$ = colatitudinal and azimuthal polar coordinates, $Z$ = polar axis.
$\lambda$ = azimuthal angle, $Y$ = polar axis.
$\psi, k$ = parameters in the theory of axial spin.
$\Omega$ = angle of axial spin.
$\omega_s$ = angular velocity of axial spin.

### INTRODUCTION

When a viscous liquid containing suspended particles is subjected to laminar shear, the particles rotate and experience deforming stresses. Jeffery (1) predicted theoretically that the major axis of a prolate spheroid of axis ratio $r_e$ rotates in a spherical elliptical orbit described by the equations:

$$\tan \theta = \frac{C r_e}{(r_e^2 \cos^2 \phi + \sin^2 \phi)^{1/2}} \qquad [1]$$

and

$$\tan \phi = r_e \tan (2\pi t/T) \qquad [2]$$

---

[1] Holder of a Studentship from the National Research Council of Canada, 1957–58.

in a field of fluid shear defined by $u = Gy$, and $v, w = 0$ where $u$, $v$, and $w$ are, respectively, the components of velocity of the undisturbed liquid along the $X$-, $Y$-, and $Z$-axes of the co-ordinate system shown in Fig. 1; $\theta$ and $\phi$ are the spherical polar co-ordinates of the major axis of the spheroid, and $C$ is the orbit constant which is related to the eccentricity of the spherical elliptical path described by the ends of the particle axis. Here $T$ is the period of rotation about the $Z$-axis and is given by

$$T = 2\pi\left(r_e + \frac{1}{r_e}\right)\Big/ G; \qquad [3]$$

$$= 2\pi r_e/G \quad \text{for} \quad r_e \gg 1.$$

In addition, it was predicted that the particle undergoes spin about its major axis at an angular velocity $\omega_s$ given by

$$\omega_s = d\Omega/dt = \frac{G}{2}\cos\theta, \qquad [4]$$

where $\Omega$ is the angle of rotation (spin) about the main axis.

Various experimental studies (2–4) of the rotations of straight rigid rods have shown excellent agreement with the details of the orbits defined by Eqs. [1] and [2] provided that the "equivalent ellipsoidal axis ratio" ($r_e$) calculated from the measured period of rotation using Eq. [3], was used instead of the true axis ratio $r$ in the orbital equations. Values of the ratio $r_e/r$ varying from 0.7 to 0.5 were found experimentally over the range of $r$ between 20 and 115 (3). Observations of the spin of wood-pulp fibers were made which showed qualitatively agreement with Eq. [4] (5).

In earlier studies of the rotations of wood-pulp fibers it was found that under certain conditions the fibers were deformed by the action of the liquid and that this deformation resulted in orbits which were different from those of rigid particles (6). In this paper a simple theory of the onset of bending and corroborative experimental data obtained by means of uniform filaments are presented. In addition experiments are described which were designed to provide for the first time a quantitative test of the spin predicted from Eq. [4].

## THEORETICAL PART

### *1. The Spin of Rigid Rods*

The simplest test of Eq. [4] is to calculate the number of complete axial spins executed in the course of a complete rotation about the $Z$-axes, and to compare this with the observed value. This calculation is made below.

The variation of $\theta$ with time can be determned by eliminating $\phi$ from Eqs. [1] and [2] to yield:

$$\cos\theta = \frac{A}{B}\left[\frac{1 + \tan^2(2\pi t/T)}{1 + \Gamma^2\tan^2(2\pi t/T)}\right]^{1/2} = F(t) \qquad [5]$$

where

$$A^2 = \frac{r_e^{\,2}}{r_e^2 - 1}, \qquad B^2 = \frac{r_e^{\,2}(C^2 + 1)}{r_e^2 - 1}, \quad \text{and} \quad \Gamma^2 = \frac{C^2 r_e^{\,2} + 1}{C^2 + 1}.$$

The theoretical number of complete spins through $\Omega = 2\pi$ which a particle undergoes in time $T$ is therefore given by integrating Eq. [4]:

$$n = \Delta\Omega/2\pi = \frac{G}{2}\int_0^{T/4} F(t)\,dt.$$

By making the substitutions into the above equation:

$$\psi = 2\pi t/T, \qquad k = \Gamma^2 - 1$$

it may readily be shown that

$$n = \left(\frac{TG}{2\pi^2}\right)\left(\frac{A}{B}\right) f(k), \tag{6a}$$

where

$$f(k) = \int_0^{\pi/2} \frac{d\psi}{(1 + k^2 \sin^2 \psi)^{1/2}}. \tag{6b}$$

The function $f(k)$ was evaluated by graphical integration for a series of values of $k$, with the results shown in Fig. 2. Equation [6*a*] was tested by viewing individual particles along the $Y$-axis, so that the $XZ$-projection of the particles was observed. The particle rotations may also be described by the variation of the azimuthal angle $\lambda$ formed by the $Z$-axis and the projection of the particle on the $XZ$-plane (Fig. 1). By combining Eqs. [1] and [2] it has been shown (2) that

$$\tan\lambda = Cr_e \sin(2\pi t/T). \tag{7a}$$

According to Eq. [7*a*], the $XZ$-projection rocks back and forth between $\pm\lambda_{\text{max.}}$ given by

$$\tan\lambda_{\text{max.}} = Cr_e, \tag{7b}$$

from which the orbit constant $C$, a parameter in Eq. [6*a*], can be evaluated if $\lambda_{\text{max.}}$ and $r_e$ are known.

### *2. The Forces Causing Deformation*

*a. Burgers' Theory.* In this section we consider briefly an approximate theory of the forces acting on a thin rod in laminar shear, developed by Burgers (7) to explain certain anomalies in the streaming birefringence of macromolecules in solution. The theory assumes the particles to be rigid, nonsedimenting, without Brownian motion, and to be so thin that the disturbance of the flow pattern of the suspending medium is negligible; inertial effects are neglected and it is assumed that there is no slip at the interface.

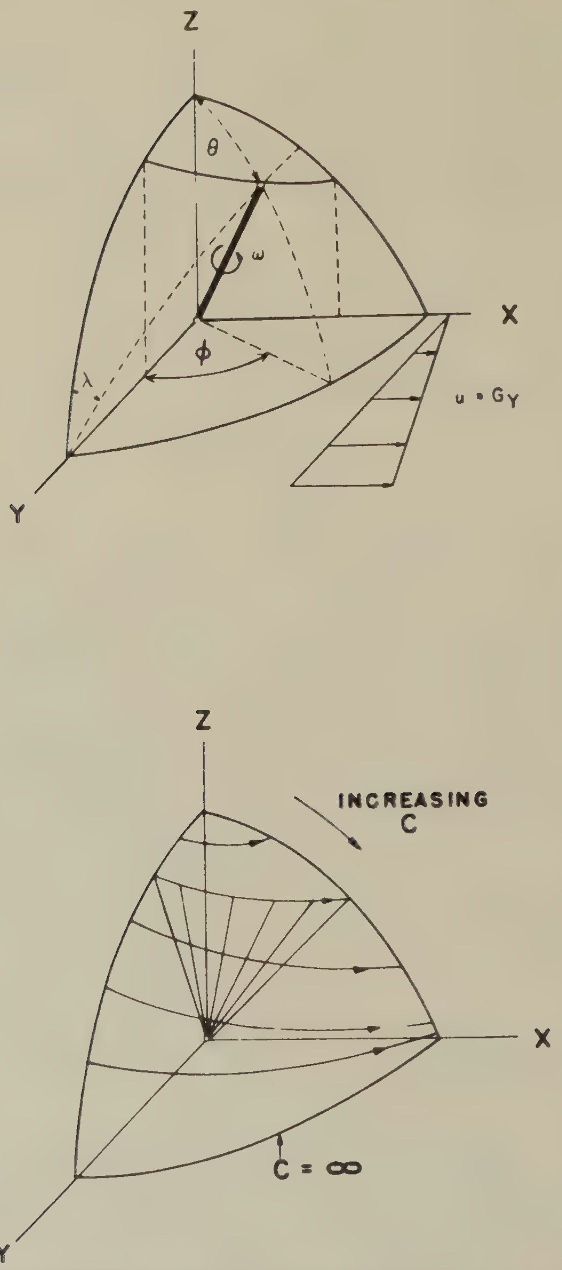

FIG. 1. The spherical elliptical orbit of a rotating cylinder. The co-ordinate system is shown in relation to the shear field (upper diagram). In studying the particle orbits, the angle λ is conveniently measured by viewing along the $Y$-axis. The lower diagram shows a series of orbits corresponding to various values of the orbit constant $C$.

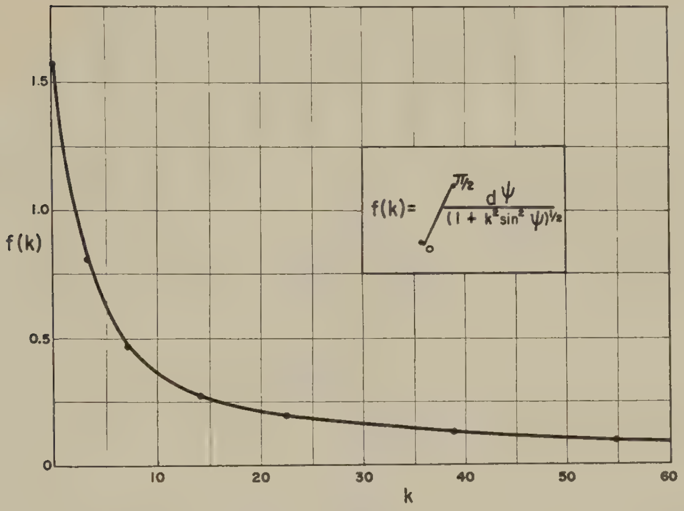

FIG. 2. The variation of $f(k)$ with $k$. Values of $f(k)$ were obtained by graphical integration of Eq. [6*b*].

Let $l$ be the distance from the center along the rod of total length $2a'$,* so that $l = 0$ at the origin of the co-ordinate system shown in Fig. 1. We may now write

$$u = Gl \sin \theta \cos \phi.$$

The velocity $u$ in the $X$-direction may be resolved into three perpendicular components. Two of the components act at right angles to the axis of the rod, one tending to increase $\phi$ and the other $\theta$. Since inertial effects are assumed to be negligible, these components will cause rotation of the rod about the $Z$-axis but will not create stresses along the axis of the rod. The third velocity component given by

$$u' = Gl \sin^2 \theta \sin \phi \cos \phi = GlM \qquad [8]$$

acts along the axis of the rod. Here $M = \sin^2 \theta \sin \phi \cos \phi$ is an orientation factor. To satisfy the condition that there be no slippage at the rod-fluid interface, $u'$ must set up a system of forces $f(l)\, dl$ ($=$ the increment of force over length $dl$) to produce a velocity $-u'$ at the surface of the rod.

The total axial force $F$ acting on the central cross section of the rod (at $l = 0$) is obtained from the integral

$$F = -\int_{a'}^{0} f(l)\, dl,$$

---

* In previous publications in this series $a$ and $b$ have been used to designate the length and diameter, respectively, of a rod. In the analysis given here it is convenient to use the semi-length and semi-diameter. To avoid confusion with the earlier symbols, $a'$ and $b'$ are employed.

which Burgers has shown to have the approximate form

$$F \simeq \frac{\pi G\eta a'^2 M}{\log_e (2a'/b') - 1.75}, \qquad [9]$$

where $\eta$ is the viscosity of the suspending medium. The sign of $F$ depends upon whether $\phi$ is negative or positive, and determines whether the rod is under compression or tension, respectively.

*b. Effect of Orientation on Axial Forces.* Equation [9] shows that $F$ depends on the dimensions of the particles, the product $G\eta$, and the orientation factor $M$. To find how $F$ varies with $M$ we write:

$$M = \frac{\tan^2 \theta \sin \phi \cos \phi}{\tan^2 \theta + 1}. \qquad [10]$$

Substituting for tan $\theta$ by means of Eq. [1] yields

$$M = \frac{C^2 r_e^2 \sin \phi \cos \phi}{C^2 r_e^2 + r_e^2 \cos^2 \phi + \sin^2 \phi}$$

or [11]

$$2M \simeq \frac{C^2 \sin^2 \phi}{C^2 + 1 - \sin^2 \phi} \quad \text{for} \quad r_e^2 \gg 1.$$

Figure 3 shows $2M$ as a function of $\phi$ at orbit constants $C = \infty$, 1, 0.5, and 0.1. It will be seen that when $C = \infty$, the magnitude of $2M$ (and hence $F$) is a maximum at $\phi = \mp 45°$. As $C$ decreases, the values $2M_{\text{max.}}$ (corresponding, respectively, to maximum compression and tension) decrease and occur at angles $\phi$ which approach $\mp 90°$. Calculated values of $2M_{\text{max.}}$ are given in Table I.

*c. Shear-Induced Buckling.* We now assume that under the system of axial forces predicted from Burgers' theory, $a'$ remains constant, and the rod remains straight until the critical condition for buckling under compression is exceeded. This represents the onset of bending of the particle by the action of the liquid.

From Fig. 3 it may be seen that the greatest stresses are exerted on a particle which rotates wholly in the $XY$-plane ($C = \infty$), and that compression reaches a maximum when $\phi = -45°$. In this position, Eq. [9] gives

$$F \simeq \frac{\pi G\eta a'^2}{2 (\log_e (2a'/b') - 1.75)}. \qquad [12]$$

We wish to calculate the least force required to buckle a rod in the orbit $C = \infty$. To do this we must know the distribution of compressive forces along the axis of the rod.

Let us assume that the increment of axial force per unit length along

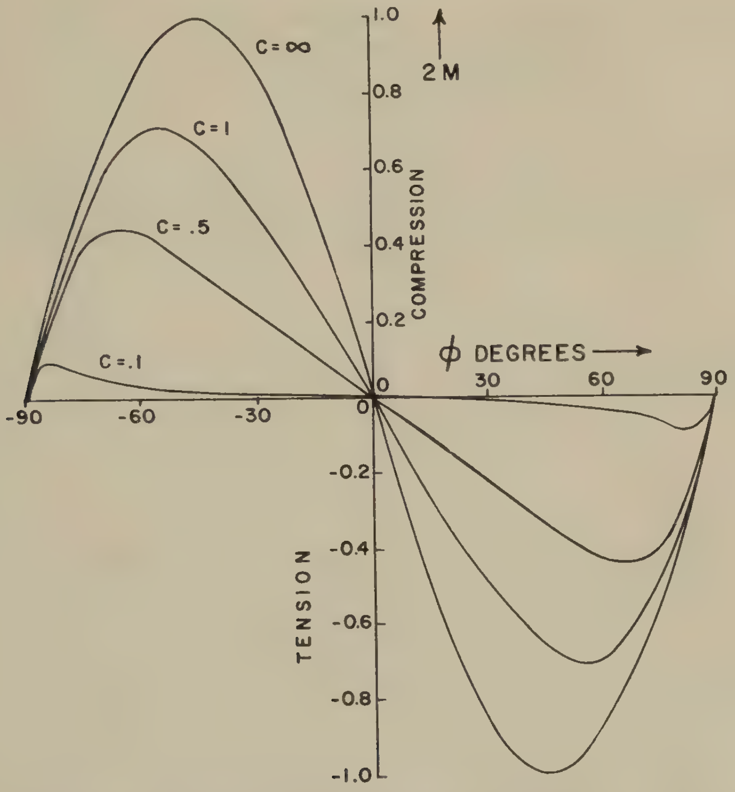

FIG. 3. Calculated variation with $\phi$ of the orientation factor $2M$ of the axial force on a thin rod. As $C$ decreases the peak values of $2M$ decrease and approach $\phi = \mp 90°$.

the rod is proportional to the axial component of fluid velocity $u'$ given by Eq. [8], i.e.,

$$f(l) = pl,$$

where $p$ is a proportionality constant which depends on the particle orientation and on $G\eta$. Corresponding to the position of maximum compression ($\phi = -45°$, $\theta = 0$) we have

$$F_{\text{max.}} = -\int_{a'}^{0} p_{\text{max.}}\, l\, dl = \frac{p_{\text{max.}}\, a'^2}{2}. \qquad [13]$$

Eliminating $F_{\text{max.}}$ from Eqs. [12] and [13], we obtain

$$p_{\text{max.}} \simeq \frac{\pi G \eta}{\log_e (2a'/b') - 1.75}. \qquad [14]$$

Let us consider the rod to be hinged at the ends, as shown in Fig. 4, and to be subjected to a system of axial forces given by $pl\, dl$ acting on an

TABLE I

$2M_{\max.}$ *at Different Values of C*

| C | $\phi$ at $M_{\max.}$ | $2M_{\max.}$ |
|---|---|---|
| $\infty$ | 45.0 | 1.000 |
| 5 | 45.2 | 0.982 |
| 3 | 45.5 | 0.950 |
| 2 | 46.4 | 0.894 |
| 1 | 54.8 | 0.707 |
| 0.5 | 64.6 | 0.447 |
| 0.3 | 74.0 | 0.258 |
| 0.1 | 84.3 | 0.099 |
| 0 | 90.0 | 0 |

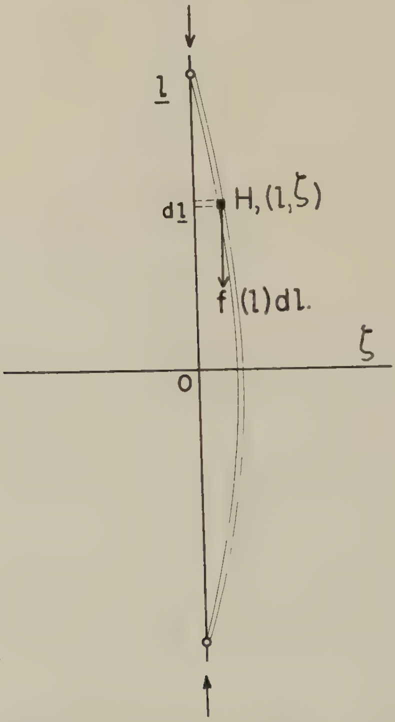

FIG. 4. A rod, hinged at both ends, used as a model in the theory of shear-induced buckling. Euler's equation [Eq. 16] for critical buckling is derived by assuming that the rod is slightly bent under axial compression.

element *dl*. The total compressive force at any point *H* with co-ordinates $(\zeta, l)$ acting on a cross section of the rod is given by

$$F_H = -\int_l^{a'} pl\, dl = \frac{p(a'^2 - l^2)}{2}. \qquad [15]$$

The equation for the shape of the rod suffering small deformations under compressive forces (8) is given by Euler's classical equation

$$E_b I \frac{d^2\zeta}{dl^2} = -F_H \zeta, \qquad [16]$$

where $E_b$ is the bending modulus of the rod, $I$ is the moment of inertia of the smallest cross section, and $\zeta$ is the displacement of the rod at $l$ (Fig. 4). By eliminating $F_H$ from Eqs. [15] and [16] we have

$$\frac{d^2\zeta}{dl^2} + c(a'^2 - l^2)\zeta = 0, \qquad [17]$$

where $c = p/2EI$. We require the solution to Eq. [17] for the least permissible value of $c$.

Substituting $z = c^{1/4}l$ into Eq. [17] yields

$$\frac{d^2\zeta}{dz^2} + (c^{1/2}a'^2 - z^2)\zeta = 0; \qquad [18]$$

by making the further substitution $\zeta = ye^{-z^2/2}$ Eq. [18] becomes

$$\frac{d^2y}{dz^2} - 2z\frac{dy}{dz} + (c^{1/2}a'^2 - 1)y = 0. \qquad [19]$$

Provided that $c^{1/2}a'^2$ is of the form $2n + 1$, Eq. [19] has the solution

$$y = He_n(z),$$

where $He_n$ denotes the Hermite function of order $n$ (9).

The smallest even value of $n$ is zero, and corresponds to the first mode of buckling of the rod, so that

$$ca'^4 = 1$$

or

$$p_{\text{max.}} = 2E_bI/a'^4. \qquad [20]$$

By combining Eqs. [14] and [20] for the position of maximum compression and writing

$$I = \frac{\pi b'^4}{4}$$

$$(G\eta)_{\text{crit.}} \simeq \frac{E_b(\log_e 2r - 1.75)}{2r^4}, \qquad [21]$$

where $(G\eta)_{\text{crit.}}$ is the minimum value at which rodlike particles of axis ratio $r = a'/b'$ may be expected to buckle under shear-induced compression. It follows that for any given value of $G\eta$ and $E_b$ there also exists a critical value $r = r_{\text{crit.}}$ which will satisfy Eq. [21]. It should be noted that Eq. [21] depends solely on $r$ and not on the absolute dimension of the particle.

In the experiments described below, the validity of Eq. [21] was tested.

## EXPERIMENTAL METHODS

The experiments were conducted by means of two Couette devices (2, 4) in which the suspension was placed between two concentric cylinders which were rotated in opposite directions. In one of these (Apparatus No. 1) particles were observed through a microscope aligned along the $Y$-axis (Fig. 1), and in the other apparatus (No. 2) observations were made along the $Z$-axis.

The following materials were used:

*1.* Rayon continuous filament, highly stretched, of circular cross section 3.5 $\mu$ diameter, supplied by the Research Department, American Viscose Corporation, Marcus Hook, Pennsylvania.

*2.* Nylon continuous filament, of circular cross section 12.2 $\mu$, supplied by the Textile Fibers Division, Du Pont of Canada Limited, Kingston, Ontario.

*3.* Dacron continuous filament, of circular cross section 7.8 $\mu$ diameter, from the Pioneering Research Laboratory, Experimental Station, E. I. du Pont de Nemours and Co., Wilmington, Delaware.

Particles of known length were prepared from the filaments by mounting the strands in embedding wax and cutting them in a sliding microtome.

Most of the work was conducted in a medium of household corn syrup (made by the Canada Starch Co.) of viscosity 91.2 poises at 20°C., having an equilibrium relative water-vapor pressure of 70%. Castor oil (No. 300 Oil, Baker Castor Oil Co., New York) of viscosity 40.5 poises at 20°C. was used to provide a nonswelling medium in the experiments with rayon. Both liquids exhibited Newtonian flow properties up to velocity gradients of 100 $\text{sec.}^{-1}$ as determined by viscosity measurements in a Couette type viscometer. Since the viscosities of these liquids were highly temperature dependent, the experiments were conducted in a room conditioned to $20° \pm 1°$C. The temperature of the suspension was measured after each experiment and the viscosity of the medium read to $\pm 0.5$ poise from previously determined viscosity-temperature calibration curves.

Particle concentrations of about $10^{-4}\%$ by weight were used. At these low concentrations interaction effects were negligible.

The Young's (tensile) modulus of elasticity $E$ of each material was determined from the linear portion of the tensile load-extension curve of samples of thread. The curves were obtained using an Instron Tensile Testing Instrument, Model TT-B, operating at a low constant rate of strain in a room conditioned to 50% relative humidity and 22.8°C. In calculating $E$ from the curves, the stress was calculated from the total load and the total cross-sectional area calculated from the mean optically measured cross-sectional area per filament and the number of filaments per strand. The cross-sectional area agreed well with the value calculated from the density and the measured denier per strand.

## RESULTS AND DISCUSSION

### *1. The Spin of Rigid Rods*

In the experiments to test the validity of Eq. [6*a*] for axial spin, rayon filaments cut to lengths between 100 and 150 $\mu$ were suspended in corn syrup and the suspension was sheared in Apparatus No. 1.

The following measurements were made for each of twelve particles:

*1.* The angle $\lambda_{\text{max.}}$ by means of a goniometric ocular.

*2.* The average period of rotation $T$ in the spherical elliptical orbit over ten successive rotations.

*3.* The average number of spins per rotation $n$ over the same ten rotations as for (*2*) above.

*4.* The shear rate $G$ from the speeds and diameters of the cylinders (2).

The $r_e$ of each particle was calculated from Eq. [3] using measured values of $T$ and $G$, and the orbit constant $C$ from Eq. [7] using the measured $\lambda_{\text{max.}}$. The $f(k)$ for the appropriate value of $k$ was found from Fig. 2. The theoretical numbers of spins calculated from Eq. [5] are compared with observed values in Table II.

The observed values were generally low. Possible reasons for this difference were the deviation of the shapes of the particles from those of prolate spheroids, and the errors introduced by counting $n_{\text{obs.}}$ only to the nearest ½ and in measuring the $\lambda_{\text{max.}}$ of curved particles. In view of these sources of error, the agreement between theory and experiment is considered to be good.

TABLE II

*Predicted and Observed Axial Spin for Slightly Curved Rayon Filaments*

| Mean $T$ (*sec.*) | $G$ (*sec.*$^{-1}$) | $r_e$ | $\lambda_{\text{max.}}$ | $f(k)$ | Calculated $n$ | Observed $n$ | $n_{\text{obs.}}/n_{\text{calc.}}$ |
|---|---|---|---|---|---|---|---|
| 145.0 | 1.65 | 38.1 | 12.0 | 1.45 | 17.6 | 18.0 | 1.02 |
| 113.0 | 1.80 | 32.4 | 52.0 | 1.24 | 12.8 | 11.5 | 0.90 |
| 135.4 | 1.60 | 34.5 | 57.5 | 1.11 | 12.2 | 10.0 | 0.78 |
| 145.0 | 1.34 | 30.9 | 49.0 | 1.23 | 12.1 | 11.5 | 0.94 |
| 410.0 | 0.37 | 24.5 | 28.0 | 1.38 | 10.8 | 11.5 | 1.06 |
| 120.0 | 1.69 | 31.5 | 60.0 | 1.07 | 10.7 | 8.0 | 0.75 |
| 86.0 | 1.49 | 25.8 | 57.0 | 1.13 | 9.3 | 9.0 | 0.97 |
| 92.4 | 1.82 | 28.6 | 69.5 | 0.92 | 8.3 | 7.0 | 0.84 |
| 126.0 | 1.42 | 20.4 | 45.5 | 1.25 | 8.1 | 6.5 | 0.80 |
| 105.0 | 1.11 | 19.2 | 43.0 | 1.19 | 7.3 | 6.5 | 0.80 |
| 82.0 | 1.85 | 24.1 | 69.0 | 0.90 | 6.9 | 5.5 | 0.80 |
| 62.0 | 1.83 | 18.0 | 80.0 | 0.59 | 3.4 | 2.5 | 0.74 |

*Mean* $n_{\text{obs.}}/n_{\text{calc.}} = 0.87$

TABLE III

*The Effect of Viscosity on Critical Bending*

| Dacron filament ($r = 310$) in corn syrup | | |
|---|---|---|
| $\eta$ (*poises*) | $G_{\text{crit.}}$ (*sec.*$^{-1}$) | $(G\eta)_{\text{crit.}}$ (*gm. cm.*$^{-1}$ *sec.*$^{-2}$) |
| 11.5 | 7.24 (2.15) | 83.7 |
| 17.9 | 3.95 (.70) | 70.6 |
| 41.8 | 2.10 (.50) | 88.5 |
| 91.2 | 0.72 (.30) | 65.8 |

Mean $(G\eta)_{\text{crit.}} = 77.1$ c.g.s. units
$(G\eta)_{\text{crit.}} \cdot F(r) = 29.2 \times 10^{10}$ dynes. cm.$^{-2}$

Values in brackets are standard deviations of associated means of 10 samples.

### 2. *The Onset of Bending*

The validity of Eq. [21] was tested by measuring $(G\eta)_{\text{crit.}}$ at various values of $\eta$ and $r$, and using materials of different elastic constants. The experiments were performed in Apparatus No. 2, using filaments with orbits in the $XY$-plane ($C = \infty$) and without visible permanent deformation.

*a. Variation of $\eta$.* Samples of Dacron filament of $r = 310$, suspended in corn syrup diluted with water to yield viscosities ranging from 11.5 to 91.2 poises, were used. The critical values of $G$ at which bending during rotation was just detectable were measured for ten filaments at each viscosity.

The results given in Table III support the theory which predicts that $G_{\text{crit.}}$ varies inversely with $\eta$.

The high standard deviations from the mean in $G_{\text{crit.}}$ may be caused by small variations in $r$ which can have a profound effect since, according to Eq. [21], $G_{\text{crit.}}$ is roughly proportional to $r^{-4}$. Small permanent deformation in the $XZ$-plane of some of the particles which are not apparent in the $XY$-projection seen in Apparatus No. 2 could be an additional cause. Such a deformation might be expected to cause a particle to bend at a lower $G_{\text{crit.}}$ than if its unstressed shape were perfectly straight.

*b. Variation of $r$.* These experiments were performed with Dacron particles having axis ratios ranging from 180 to 310 using undiluted corn syrup as the medium. The mean values of $(G\eta)_{\text{crit.}}$ are summarized in Table IV. The table includes the product $G\eta_{\text{crit.}} \times F(r)$ where

$$F(r) = \frac{2r^4}{(\log_e 2r - 1.75)}. \qquad [22]$$

If Eq. [21] applies, the product should be constant for a given series of particles; for the Dacron particles it was constant within 30%, yielding

TABLE IV

*Comparison of $E_b$ at Various Axis Ratios with E for Dacron, Rayon, and Nylon Filaments*

| Material | Medium | $r$ | Mean $G_{\text{crit.}}$ ($sec.^{-1}$) (10 specimens) | Mean $(G\eta)_{\text{crit.}}$ ($gm.\ cm.^{-1}\ sec.^{-2}$) | $F(r) \times 10^{-8}$ | $(G\eta)_{\text{crit.}} \cdot F(r) = E_b \times 10^{-10}$ ($dynes.\ cm.^{-2}$) | Tensile modulus $E \times 10^{-10}$ ($dynes.\ cm.^{-2}$) |
|---|---|---|---|---|---|---|---|
| Dacron | Corn syrup | 180 | 6.93 (1.54) | 632 | 5.08 | 32.2 | 7.26 |
| | | 228 | 3.12 (0.57) | 260 | 12.2 | 31.8 | |
| | | 268 | 1.32 (0.26) | 112 | 22.6 | 25.4 | |
| | | 310 | 0.72 (0.30) | 66 | 39.6 | 26.2 | |
| Rayon | Corn syrup | 190 | 2.67 (0.55) | 248 | 6.28 | 15.6 | 26.4 |
| | | 281 | 0.38 (0.11) | 34.7 | 26.8 | 9.32 | |
| | Castor oil | 241 | 10.30 (2.35) | 386 | 15.3 | 59.2 | |
| Nylon | Corn syrup | 170 | 3.84 (1.02) | 350 | 4.48 | 15.6 | 6.30 |
| | | 194 | 2.32 (0.75) | 209 | 6.90 | 14.4 | |

Bracketed values are standard deviations of associated means.

a mean value of $28.9 \times 10^{10}$ dynes/cm.$^2$. This value agreed well with the mean value of $29.2 \times 10^{10}$ dynes/cm.$^2$ calculated from the data of Table II.

Similar results for less extensive experiments using rayon and Nylon were obtained and are included in Table IV.

*c. The Elastic Constants.* According to Eq. [21]

$$E_b = (G\eta)_{\text{crit.}} F(r). \qquad [23]$$

Values of the tensile modulus $E$ are included in Table IV and compared to corresponding values of $E_b$ calculated from Eq. [23]. Since Dacron does not absorb appreciable quantities of water and hence is not plasticized by contact with water, the comparison would appear to be most valid for this material; in this case $E_b/E = 4$ *approx.*

Closer agreement was obtained for Nylon. However, it has been shown (10) that the (dynamic) tensile modulus of Nylon increases by about 20% for a decrease in relative humidity from 70% to 50%. If the value of $E_b$ for Nylon shown in Table IV is increased by 20% for direct comparison with $E$, the ratio $E_b/E$ corrected to 50% relative humidity is approximately 3.2.

With rayon, the decrease in $E_b$ between castor oil and corn syrup clearly shows the plasticizing effect due to water absorbed from the corn syrup.

It will be noted that with each material, the values of $E_b$ obtained tended to decrease slightly with increasing $r$. This deviation from Eq. [21] may have been due to the approximations made in developing the theory. It could also have resulted from a greater incidence of slight permanent deformations in the longer samples.

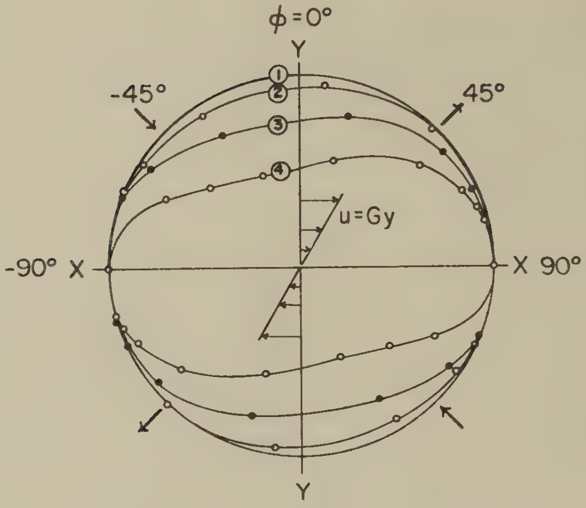

FIG. 5. Polar plot of the loci of the ends of a Nylon filament ($r = 170$) during rotation in the $XY$-plane. Curve 1 represents rigid rotation at $G < G_{crit}$. Curves 2, 3, and 4, for which $G_{crit.}$ has been exceeded, correspond to $G = 3.20, 3.54$, and $4.25$ sec.$^{-1}$, respectively. The theory predicts that as $G$ approaches $G_{crit.}$, deviation from curve 1 will commence at $\phi = -45°$.

Whereas values of $E_b$ obtained were of the same order of magnitude as the corresponding values of $E$, they were nevertheless 2 to 4 times greater. It should be noted that $E_b = E$ only if the filaments are homogeneous, but that the two moduli frequently differ owing to "skin" effects (11). It is improbable that skin effects can account entirely for the differences between $E_b$ and $E$ in the above results. However, in view of the assumptions and approximations made in Burgers' treatment and in the present extension of the theory, exact numerical agreement could hardly be expected.

It has been shown that the experimentally determined relationships between $G$, $\eta$, and $r$ were in general agreement with those predicted by Eq. [21]. The results indicate that the theory of deformation presented above is correct in principle, if not in detail.

*d. Orbits of Bent Particles.* Attempts were also made to determine if critical bending of a particle rotating in the $XY$-plane ($C = \infty$) commences at $\phi = -45°$, as implied in Eq. [12]. The experiments proved difficult to perform.

Photomicrographs were taken at short time intervals during the rotations of Nylon filaments close to $G_{crit.}$, again using Apparatus No. 2. The loci of the ends of the filament images were plotted as a function of $\phi$. Figure 5 clearly shows the assymmetry of the loci about the $Y$-axis due to the compression and the tension forces. It also shows the increase in deformation occurring above $G_{\text{crit.}}$; this will be discussed further (12). The results suggest but do not definitely show that initial bending occurred at $\phi = -45°$. The main experimental difficulty is to obtain a particle which not only appears free from permanent deformation, but also rotates wholly in the $XY$-plane, since even slight displacements from $C = \infty$ would result in foreshortening of the $XY$-projection due to the spherical elliptical orbit.

It should be noted that the above theory of bending as the result of axial forces does not apply once the particles are deformed. Evidence is to be presented (12) that the disturbance to the flow field caused by curved particles is much greater than that due to straight ones: this indicates that the system of forces acting on a curved particle is more complicated and cannot be analyzed even approximately by a treatment which assumes the disturbance to the flow field to be negligible.

The phenomena considered here are of interest in connection with the viscosity (13) and other flow properties of suspensions of threadlike particles. In addition they form an important background to the study of the more complex orbits of flexible particles above $(G\eta)_{\text{crit.}}$ which are considered in the succeeding paper (12).

## Summary

The axial spin of slightly curved but rigid cylindrical particles rotating in a velocity gradient have been shown to be in good accord with Jeffery's theoretical equation for ellipsoids of revolution provided that the equivalent ellipsoidal axis ratio is substituted for the true axis ratio in the equation.

A theory of deformation of cylindrical particles rotating in a velocity gradient is presented. Equations are developed to calculate the critical value of (gradient × viscosity) at which the shear-induced axial compression causes the particle to buckle. Experiments conducted with Dacron, Nylon, and rayon filaments cut to various axis ratios and dispersed in various liquid media showed reasonably good agreement with the theory. Some observations of the increase of particle deformation beyond the critical gradient for bending are presented.

## References

1. Jeffery, G. B., *Proc. Roy. Soc.* (*London*) **A102**, 161 (1922).
2. Trevelyan, B. J., and Mason, S. G., *J. Colloid Sci.* **6**, 354 (1951).
3. Mason, S. G. and Manley, R. St. J., *Proc. Roy. Soc.* (*London*) **A238**, 117 (1956).
4. Bartok, W., and Mason, S. G., *J. Colloid Sci.* **12** (No. 3), 243 (1957).
5. Mason, S. G., *Tappi* **37** (No. 11), 494 (1954).
6. Arlov, A. P., Forgacs, O. L., and Mason, S. G., *Svensk Papperstidn.* **61** (No. 3), 61 (1958).

7. BURGERS, J. M., "Second Report on Viscosity and Plasticity," Ch. 3, pp. 19 and 10. North Holland Publishing Co., Amsterdam, 1938.
8. PRESCOTT, J., "Applied Elasticity," Ch. 4, p. 76. Dover Publications, New York, 1946.
9. MARGENAU, H., AND MURPHY, G. M., "The Mathematics of Physics and Chemistry," Ch. 3, p. 10. Van Nostrand, New York, 1943.
10. QUISTWATER, J. M. R., AND DUNELL, B. A., *J. Polymer Sci.* **28,** 309 (1958).
11. MEREDITH, R., "The Mechanical Properties of Textile Fibres," Ch. 4, p. 8. North Holland Publishing Co., Amsterdam, 1956.
12. FORGACS, O. L., AND MASON, S. G., *J. Colloid Sci.*, **14,** 457 (1959).
13. NAWAB, M. A., AND MASON, S. G., *J. Phys. Chem.* **62,** 1248 (1958).

JOURNAL OF COLLOID SCIENCE **14**, 473–491 (1959)

# PARTICLE MOTIONS IN SHEARED SUSPENSIONS

## X. ORBITS OF FLEXIBLE THREADLIKE PARTICLES

**O. L. Forgacs[1] and S. G. Mason**

*Physical Chemistry Division, Pulp and Paper Research Institute of Canada, and Department of Chemistry, McGill University, Montreal, Canada*

*Received December 12, 1958*

## INTRODUCTION

Particles in liquid suspensions subjected to velocity gradients undergo rotational and translational motions. In addition, the shear field exerts stresses on the particles which under certain conditions are capable of causing deformation. The forces exerted in a field of laminar shear on cylindrical particles were considered in the preceding paper (1), where it was shown that there exist critical conditions beyond which a particle will bend in the course of rotation. In this paper, the effects of shear-induced deformation on the rotational motions of threadlike particles are described.

Previous work in this laboratory has dealt with the rotations, orientations, and interactions of simple particles such as rigid spheres (2–4), fluid drops (5, 6), and smooth rigid rods (2, 4, 7). Most of the phenomena observed could be explained theoretically. There exists, however, no comparable theory for the phenomena described in the present work.

A recent paper (8) described the motions of wood-pulp fibers. It was found that rigid fibers executed the same types of rotation as rigid cylinders. When the fibers were flexible, their orbits and periods of rotation differed appreciably from those of rigid cylinders. However, a quantitative study using pulp fibers was limited in scope because of irregular shapes of the individual particles. A classification of orbit types has nevertheless been used to determine the flexibility spectrum of samples of wood fibers (9, 10). In the present investigation, a more systematic study of orbits was possible with uniform particles prepared from synthetic filaments.

Rigid rods in suspensions subjected to laminar shear rotate in spherical elliptical orbits (2, 4) and spin about their major axes (1) according to the predicted equations of motion for prolate spheroids (8), provided the "equivalent ellipsoidal axis ratio" $r_e$ is used in place of the true axis ratio $r$ of the particles. The $r_e$ is calculated from Jeffery's equation (11):

---

[1] Holder of a Studentship from the National Research Council of Canada, 1957–1958.

$$\begin{aligned} TG &= 2\pi(r_e + 1/r_e) \\ &= 2\pi r_e \quad \text{for} \quad r_e \gg 1. \end{aligned} \qquad [1]$$

Here $T$ is the measured periodic time of rotation of the particle axis through $\phi = 360°$ where $\phi$ is the azimuthal polar co-ordinate ($Z$ = polar axis) as shown in Fig. 1 of reference (1), and $G$ is the velocity gradient.

It follows from Eq. [1] that for a particle which has two perpendicular axes of symmetry (so that its shape relative to the field of flow will remain unchanged by axial spin), e.g., prolate spheroids and straight cylindrical rods, the product $TG$ will depend solely on the particle shape and will be independent of $G$.

If, however, a particle undergoes shear-induced deformation, its shape, and hence the flow pattern around it, will depend at any instant on the deforming forces. Since these were shown (1) to be a function of the product $G\eta$, where $\eta$ is the viscosity of the suspending medium, we may expect that for deformable particles, Eq. [1] will take the form

$$TG = S(G\eta), \qquad [2]$$

where $S(G\eta)$ is a particle shape factor which varies with $G\eta$. If $\eta$ is constant we should expect that if a particle is deformable, $\Delta TG/\Delta G$ will be related to the deformation undergone by the particle as the result of an increment $\Delta G$. Experiments with deformable pulp fibers (8) have shown that $TG$ increases with $G$. Similarly, measurements of the period of circulation $T$ of the interface of a deformed fluid drop (6) have shown that $TG$ increases with $G$. The product $TG$ therefore becomes a useful parameter in studying the effects of deformation on particle rotations.

The experimental results of the present investigation are presented in two sections. The first describes the motions of deformable threadlike particles over a wide range of flexibility; the second deals principally with the effects of deformation on the product $TG$.

## Experimental Part

### 1. *Apparatus and Materials*

The technique using the two twin-cylinder Couette devices for viewing along the $Y$- and $Z$-axes, respectively, was similar to that used previously (1, 2, 4).

In addition to the 3.5 $\mu$ diameter rayon and 7.8 $\mu$ Dacron filaments previously used (1) which were microtomed to required lengths, the following materials were also used:

*a.* Spruce sulfite-pulp fibers, screened to yield a mean length of 1.6 mm. with a standard deviation from the mean of about 20%. These were used in preliminary experiments.

*b.* Elastomer continuous filament, approximately elliptical in cross section, width of largest cross section = 12 $\mu$, supplied by the Pioneering Research Laboratory, E. I. du Pont de Nemours and Company, Wilmington, Delaware. This material was highly flexible in comparison to the other materials. Because of its extensibility, it could not be embedded and microtomed; instead, single filaments were cut to lengths ranging from 1 to 20 mm., using a sharp razor.

The suspending media used were household corn syrup and castor oil (No. 300 oil, Baker Castor Oil Co., New York). The castor oil, which was also used in associated studies of the viscosity of suspensions (12), provided a nonswelling medium for rayon.

Concentrations by weight of about $10^{-4}$% were used in experiments with pulp fibers, rayon, and Dacron, since at these low concentrations individual particles could be studied in the absence of interactions over extended periods of time. With the elastomer, observations were made of single filaments which were introduced into the medium by means of a fine needle.

Observations were made visually or with the aid of photomicrography.

### *2. Method of Varying Particle Flexibility*

The ability of a threadlike particle to bend could be increased by swelling the material, by increasing the deforming forces exerted by the shear field, or by increasing the particle length (1).

Since swelling tended to be nonuniform along the length of a filament, this method of increasing flexibility was rejected. The deforming forces could be increased in a particular suspending medium by increasing $G\eta$. However, $G$ was limited by practical considerations to a maximum of 10 sec.$^{-1}$. The viscosity $\eta$ could be varied by diluting the suspending medium, but the range of $\eta$ that could be used was limited, since at low viscosities sedimentation effects became significant. The flexibility was therefore varied principally by varying the particle length, while small changes in the particle orbits were studied by varying $G$ and $\eta$.

The orbits of rayon filaments were studied up to $r$ = 780, corresponding to a length of over 3 mm. At greater lengths, the thin filaments could no longer be resolved in the microscope at the low magnifications required to obtain a sufficiently wide field. Studies of very long and flexible filaments were therefore made using the thicker but much more flexible elastomer.

## RESULTS AND DISCUSSION

### *1. The Orbits of Deformable Threads*

In this section are described the motions of threadlike particles under conditions at which the values of $(G\eta)_{\text{crit.}}$ or $(r)_{\text{crit.}}$ (defined in reference (1)) for the onset of deformation were exceeded.

*a. Springy and Snake Orbits.* The orbits exhibited by filaments when the critical conditions for bending were only slightly exceeded were termed "springy." This type of rotation is illustrated by the Dacron filament rotating in the $XY$-plane in Fig. 1. The particle in frame 1 was aligned in the $X$-direction. Frames 2 to 7 were taken at intervals during a rotation through 180° (from $\phi = -90°$ to $+90°$). As the particle approached $\phi = -45°$, it bent like a leaf-spring, and then flicked straight as it rotated into the quadrant $0 < \phi < 90°$.

The loci of the ends of a filament undergoing springy orbits in the $XY$-plane are shown in Fig. 5 of the preceding paper (1): curves 2, 3, and 4 show that as $G$ was increased, deformation became more pronounced, and the onset of bending during rotation tended towards $\phi = -90°$.

When the flexibility of a filament was increased further, by increasing either $G\eta$ or $r$, a stage was reached at which the two ends of the filament appeared capable of independent movement; however, the particle continued to straighten in the positions $\phi = \mp 90°$. This type of orbit was termed "snake turn" (8) and is identical with the orbit designated as

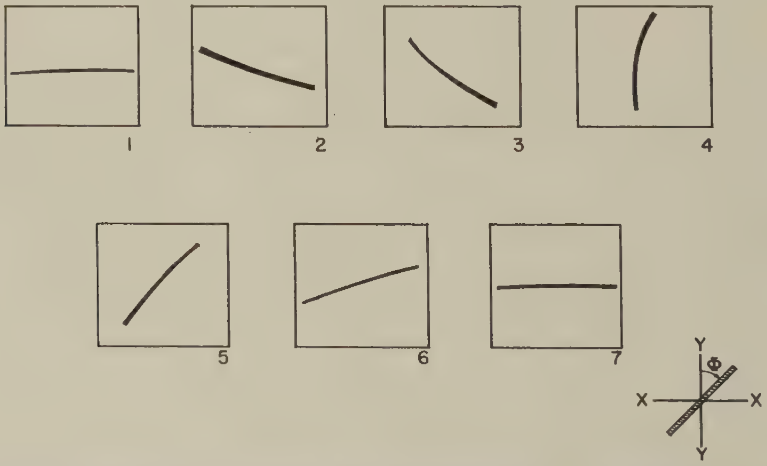

FIG. 1. Springy rotation. Tracings of photomicrographs of a 7.8$\mu$ diameter Dacron filament rotating in the $XY$-plane. In frame 1, the filament is aligned along the direction of flow. In the first quadrant ($-90° < \phi < 0°$), frames 1 to 4, the filament bends under compression. In the second quadrant, ($0 < \phi < 90°$), frames 4 to 7, it relaxes rapidly under tension. Axis ratio = 180. $G\eta$ = 640 gm. cm.$^{-1}$sec.$^{-2}$.

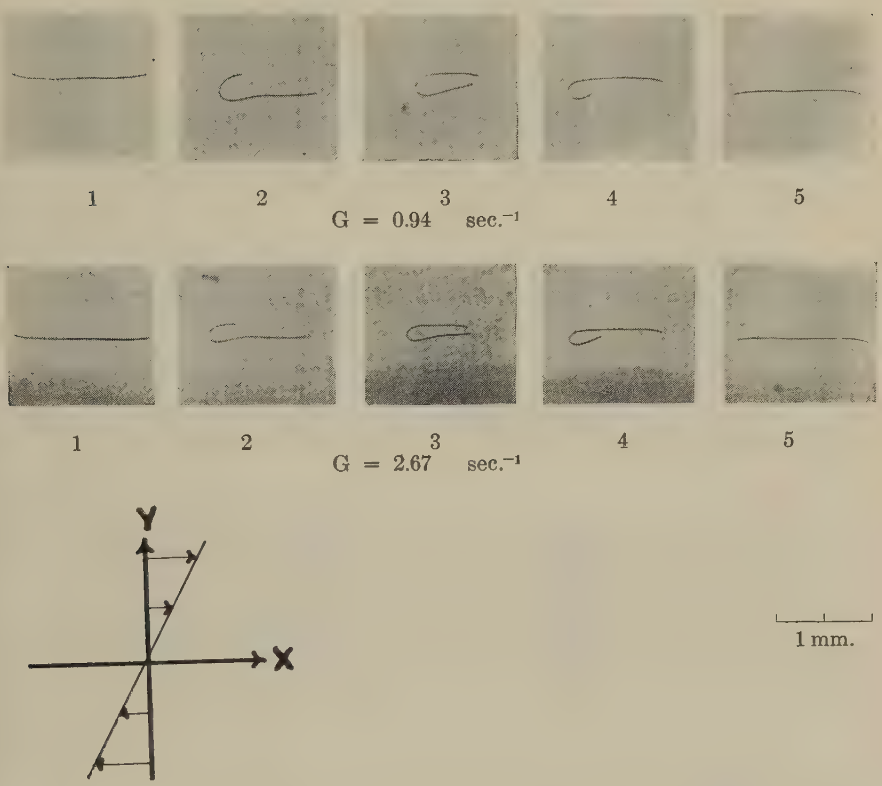

FIG. 2. Snake rotation. Photomicrographs of an elastomer filament undergoing snake turns through $\phi = 180°$, at $G = 0.94$ sec.$^{-1}$ (upper series) and $G = 2.57$ sec.$^{-1}$ (lower series). By comparing corresponding pictures of the two series it will be seen that deformation increases as $G$ increases.

"flexible rotation" in papers dealing with the flexibility of pulp fibers (9, 10). It is illustrated by photomicrographs of an elastomer filament in Fig. 2. The filament was aligned in the $X$-direction in frame 1. After an interval during which little motion could be observed, one end bent abruptly in the $XY$-plane. The bend ran along the particle until it once again lay in the $X$-direction, but pointing the opposite way (frame 5). After another interval during which little motion was apparent, the process was repeated, the particle thereby completing a rotation through $\phi = 360°$. By comparing the two series of pictures in Fig. 2 it may be seen that, as with the springy rotation, the extent of deformation of the particle during rotation was increased by increasing $G$.

The period of rotation was found to be constant for successive rotations of the particle at constant $G$; the abrupt bending of one end occurred at definite and reproducible time intervals in the course of each rotation.

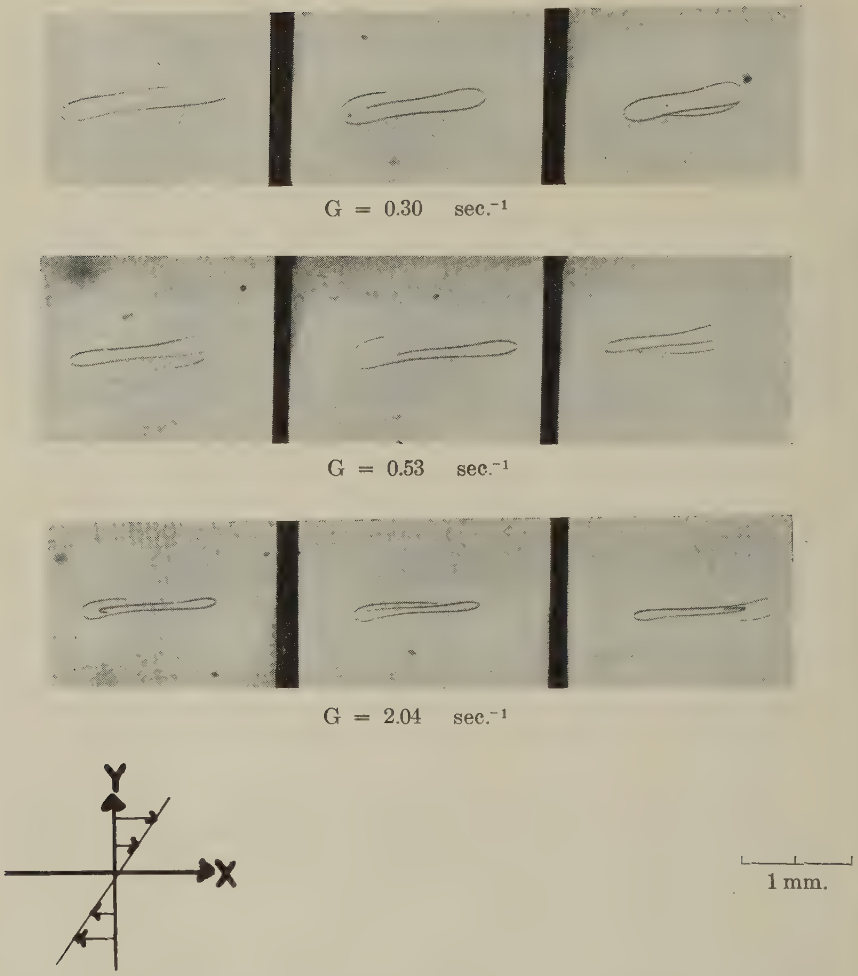

FIG. 3. Helix rotation viewed along the $Z$-axis. Photomicrographs of an elastomer filament. As $G$ increases, the amount of deformation increases and the major axis of the configuration tends toward the direction of flow (the $X$-axis).

When the particles were highly symmetrical, that is, entirely free of any permanent deformations, both ends bent simultaneously in opposite directions, so that the particles formed an S-shape and then straightened again (8). This orbit proved to be the exception rather than the rule with the filaments used in this work.

Particles undergoing snake turns showed a preference for orbits lying close to the $XY$-plane. Previous work on rigid rods (5) failed to establish any definite drift in the orbital constant $C$ with time. However, it was observed that flexible pulp fibers either drifted so that they rotated in the $XY$-plane or so that their axes were aligned in the $Z$-direction (8). When the filaments used in the present work underwent sufficient deformation to describe snake turns, they invariably drifted so as to rotate wholly in or very close to the $XY$-plane. The drift occurred in the course of two or three half-rotations whatever the orientation of the filaments was at the onset of shear. Further work on this phenomenon is required before an explanation of it can be attempted.

The orbits of rayon filaments and Dacron filaments of various axis ratios in corn syrup and at constant $G$ are given in Table III. These results indicated that the snake orbits commenced at values of $r = 1.5(r_{\text{crit.}})$ approximately.

*b. Coiled Orbits without Entanglement.* Experiments with rayon filaments showed that at values of $r > 3$ $(r_{\text{crit.}})$ approximately, the filaments no longer straightened between half-rotations but assumed coiled configurations. A particle which was initially orientated at random relative to the Couette cylinders became on setting the apparatus in motion fully extended close to the $X$-direction. After a time, one end started to bend as described for snake-turns. The bend ran along the length of the filament, but before it had reached the tail end, the head began a second bend so that the particle never straightened completely. This type of orbit was also observed in corn syrup at $G > 3$ sec.$^{-1}$ with long, highly delignified pulp fibers (9), and elastomer filaments over 2.5 mm. in length.

If sufficiently long and flexible, filaments rotated so that the $XY$-projection of their configurations appeared as closed loops, as illustrated with an elastomer filament in Fig. 3. The leading end was usually displaced slightly in the $Z$-direction, presumably as the result of hydrodynamic interaction with the tail, so that the filament rotated in a helix about the $Z$-axis. The greatest cross section of the $XY$-projection of the orbit was inclined at an angle to the direction of flow as the result of the compressive and tensile forces of the kind described previously (1, 6). Figure 3 also shows that as $G$ was increased, this angle of inclination approached the $X$-direction $(\phi = 90°)$ in a manner similar to that observed with fluid drops (6). As with springy and snake orbits, deformation was increased by increasing $G$. At $G = 0.30$ and $0.53$ sec.$^{-1}$ the filament in Fig. 3 had two bends along its length. At $G = 2.04$ sec.$^{-1}$, three bends were present during certain stages of the orbit: this indicates that the number of "turns" of the helix tended to increase with increasing flexibility. Further evidence of this is given below.

Elastomer filaments between 3 and 10 mm. in length frequently assumed these helical configurations, although with the longer samples, the orbits passed through a number of intermediate phases. Once the helix was formed, however, a filament rotated like a corkscrew about the $Z$-axis

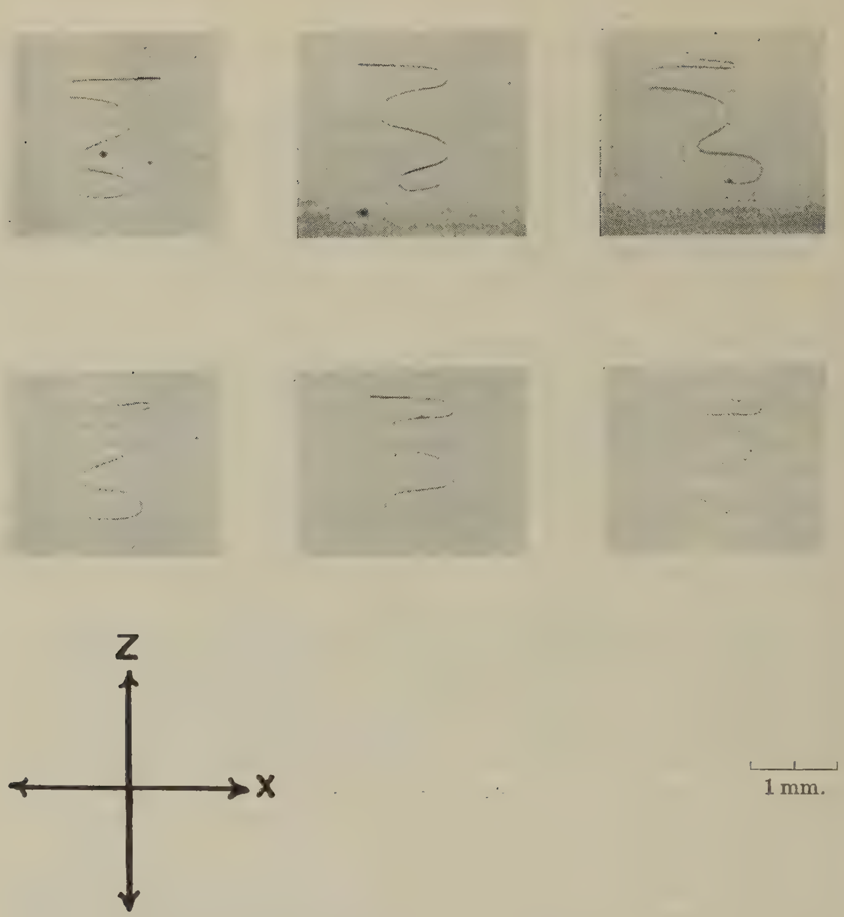

FIG. 4. Helix rotation viewed along the $Y$-axis. Photomicrographs of an elastomer filament. The filament rotates about the $Z$-axis like a corkscrew unless disturbed by another particle.

TABLE I

*Helix Formation of Elastomer Filaments*

$G = 3 \pm 1$ sec.$^{-1}$

| Particle no. | Filament length (*mm.*) | Time observed (*min.*) | Time to form stable helix (*min.*) | No. of turns in helix |
|---|---|---|---|---|
| 1 | 3.25 | 30 | 2 | 1½ |
| 2 | 4.00 | 55 | 18 | 2½ |
| 3[a] | 4.50 | 40 | — | — |
| 4[a] | 4.50 | 38 | 5[b] | 3 |
| 5 | 5.00 | 50 | 24 | 3 |
| 6 | 5.75 | 45 | 32 | 3½ |
| 7 | 6.50 | 72 | 70 | 4 |
| 8 | 7.00 | 60 | — | — |

[a] Permanently deformed.

[b] Unstable helix formed at intervals.

for many hundreds of rotations, unless disturbed by another particle. It will be seen from Table I that of eight samples observed, six formed helices. The time to form the helix increased with the filament length. The width of the helices in the $X$-direction varied little with the filament length, and in each case was between 1 and 2 mm.; the number of turns of the coil, however, increased with the filament length. Figure 4 shows photomicrographs taken along the $Y$-axis of a helix of 3 turns, similar to that formed by particle no. 5 (Table I). Particles no. 3 and 4 did not form stable helices; it was noticed that both these filaments had permanent deformations which appeared to inhibit their rotation in a smooth spiral.

A tentative reason for the stability of the helical configuration is that it is the only way in which a long filament can rotate without axial spin, and thus without setting up torsional stresses along its axis.

The mode of formation and the stability of these configurations require further investigation.

*c. Coiled Orbits with Entanglement.* Elastomer filaments over 10 mm. in length were never observed to form helices. It appeared that the complicated entanglement during initial coiling prevented the formation of the spiral configuration, even after prolonged shearing. The coiling of a very long filament may be considered in five consecutive stages, illustrated in Fig. 5. These may be described as follows:

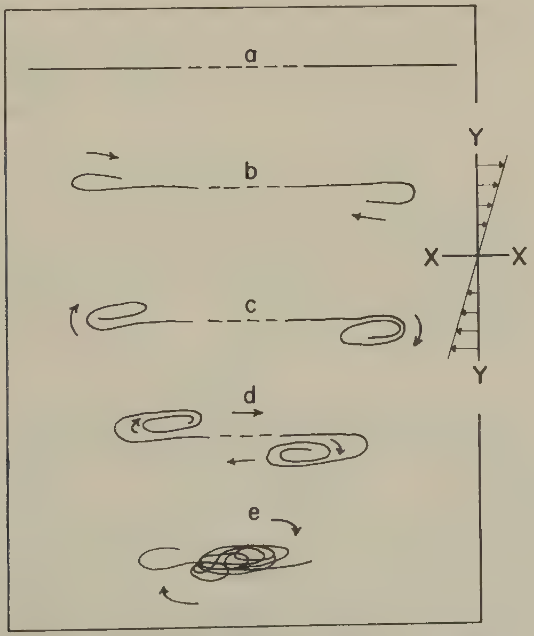

Fig. 5. Coil formation. Schematic diagram showing the stages of coiling of a very long flexible filament.

*a*. Whatever its initial orientation, the filament always aligned itself close to the $X$-axis on the commencement of shear, either fully extended or, occasionally, folded double.

*b*. After a time in the extended position, the ends started to bend as though commencing independent snake orbits.

*c*. After the ends had traveled towards each other for some distance, they once more turned to form closed loops. After traveling away from each other, the ends eventually turned again, until coils of two or three loops had formed at the extremities of the otherwise extended filament.

*d*. As the coils at the ends grew, they began to rotate bodily and to move towards each other, slowly winding up the extended part of the filament.

*e*. After passing each other a few times, the coiled ends, which were continuously growing in complexity, entangled with one another to form a complex writhing bundle. Sometimes the ends worked themselves free and moved away from the main coil, only to bend again and re-enter the coil, thereby adding to the entanglement.

These stages represent a simplification of the process. Often the two ends did not reach the first four stages simultaneously. Sometimes one end had coiled considerably before the other had even started to bend.

The projection on the $XY$-plane of the coiled bundle was always longer in the $X$-direction than in the $Y$-direction. As with the helical configurations, this asymmetry was increased by increasing $G$. The projection on the $XZ$-plane of a coil was usually longer in the $Z$-direction than in the $X$-direction. The bundle usually rotated about the $Z$-axis at a more or less constant angular velocity, though the individual elements continued to move relative to each other.

### *2. The Effect of Deformation on TG*

To avoid the complicating effect of axial spin mentioned in the Introduction, measurements of the periods of rotation $T$ of filaments were made exclusively in or very close to the $XY$-plane, where it has been shown that there is no axial spin (1).

TABLE II

*The Effect of Flexibility on TG of Pulp Fibers*

| Orbit | No. of fibers | Mean $TG$ |
|---|---|---|
| Rigid | 19 | 124.0 (32.8) |
| Springy | 20 | 92.8 (21.0) |
| Snake | 61 | 45.4 (12.7) |

Bracketed values are standard deviations of associated means.
Mean length of fibers = 1.6 mm.

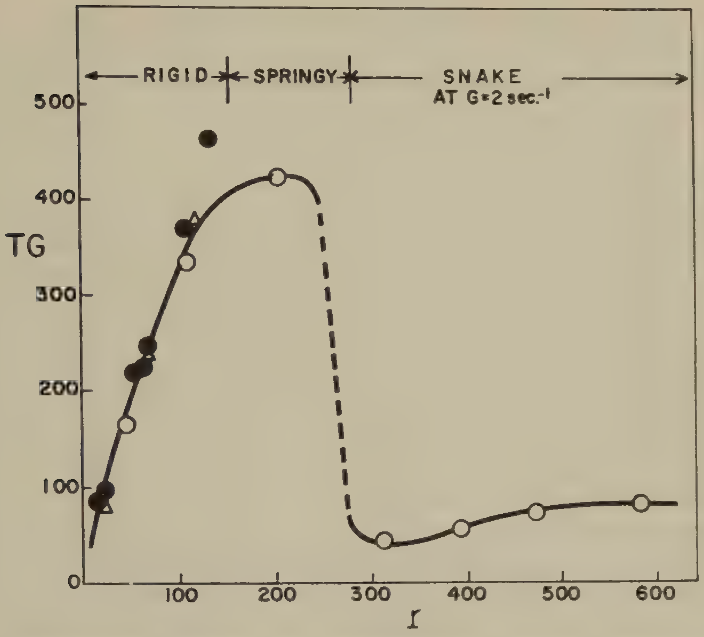

Fig. 6. Preliminary measurements of *TG* of flexible particles. *Open circles:* 4.5$\mu$ diameter. Rayon filaments in corn sorn syrup. *Closed circles:* 9.5$\mu$ diameter glass fiber (2). *Triangles:* 12.4$\mu$ Dacron filaments (7).

*TG* decreases appreciably at the axis ratio corresponding to the onset of snake rotations. Subsequent experiments showed this effect to be the result of permanent deformation.

*a. Preliminary.* Preliminary experiments were conducted in the Couette Apparatus No. 1 (viewing along the $Y$-axis), using pulp fibers 1.6 mm. in length suspended in corn syrup. The periods of rotation of 100 fibers were measured at $G = 3 \pm 1$ sec.$^{-1}$. The results (Table II) show that the mean *TG* was lower for fibers describing springy orbits than for those that were rigid, and lower still for fibers describing snake orbits.

Figure 6 shows the variation of *TG* with $r$ for rayon filaments (diameter in corn syrup = 4.5 $\mu$). Each point represents the mean *TG* of about five filaments at each axis ratio. Over the rigid range, the results were in good agreement with earlier values (2, 5). The sharp fall in *TG*, which coincided with the beginning of the snake-orbit region, was first considered to be a characteristic of the orbit resulting from flexibility (10). This conclusion was, however, based on the incomplete information obtained by viewing the particles along the $Y$-axis. Experiments with pulp fibers and rayon filaments in the Apparatus No. 2 (viewing along the $Z$-axis) revealed that after shearing for prolonged periods, the particles frequently remained curved in the $XY$-plane when motion was stopped. In the experiments on rayon filaments, summarized in Fig. 6, the suspensions had been sheared for several hours before making observations to ensure good dispersion. This caused the particles to have permanent deformations which could not be seen by viewing along the $Y$-axis.

It was therefore considered to be important to study as a next step the effect of permanent deformations on the period of rotation.

*b. The Effect of Permanent Deformation.* Rayon filaments 3.5 $\mu$ diameter, $r = 173$, which had been permanently bent into circular arcs were used for these measurements. These particles were from one of a number of samples having various axis ratios the viscosities of which in dilute castor oil suspensions were measured by Nawab and Mason (12) in a rotational viscometer at $G = 93$ sec.$^{-1}$. Using the data from the preceding paper (1), it is estimated that at this gradient, $r_{\text{crit.}} = 140$. Filaments having axis ratios greater than this were found to be permanently bent into circular arcs after the viscosity measurement.

The previously sheared suspension was diluted and placed in Apparatus No. 2 (viewing along the $Z$-axis). The periods of rotation of 24 filaments the $XY$-projections of which showed various degrees of permanent deformation were timed at known shear rates between 9 and 10 sec.$^{-1}$. The particles described rigid rotations at these reduced gradients. After the period of rotation of each particle had been measured, the apparatus was stopped and a photograph of the corresponding filament was taken through the microscope aligned along the $Z$-axis.

The negatives were projected on a screen and the angle $\alpha$ subtended by the tangents at the ends of each filament image (see inset Fig. 7) was measured. This angle served as an inverse measure of the extent of permanent curvature of the filaments in the $XY$-plane.

The $r_e$ for each particle was calculated from measured values of $T$ and $G$ using the exact version of Eq. [1].

The experimental points in Fig. 7 show that $r_e$ (or more correctly $TG$) was extremely sensitive to small deformations. As $\alpha$ fell from 180° for a straight particle to 160° for a bent one, $r_e$ decreased by a factor of about 9.

For comparison, the axis ratio $r_v$ of the figure formed by rotating the $XY$-projection of each filament about the chord joining its ends was calculated from the equation

$$r_v = \frac{\cos(\alpha/2)}{1 - \sin(\alpha/2)}, \qquad [3]$$

which is based on the approximation that the configurations formed arcs of a circle.

The change in $r_v$ with $\alpha$ is shown as the solid line in Fig. 7. The trends of $r_e$ and $r_v$ with $\alpha$ showed remarkable agreement except at $\alpha = 180°$,

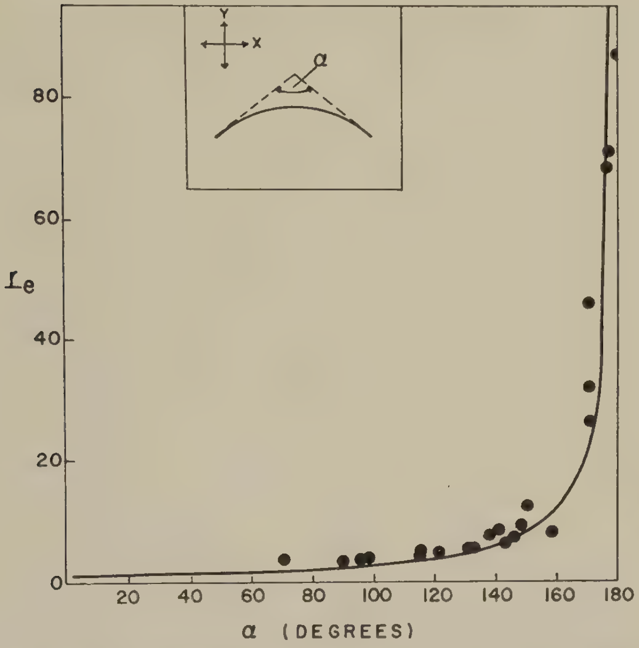

FIG. 7. The effect of permanent deformation on $r_e$ for rigid rotation in the $XY$-plane. The angle $\alpha$ (inset) is an inverse measure of the curvature of a particle in the $XY$-plane. The experimental points show that $r_e$ is highly sensitive to small deformations. The line represents calculated values of the axis ratio $r_v$, of the solid formed by revolution of the $XY$ projection of the filament about the chord joining the ends.

where $r_v$ tends to infinity since Eq. [3] neglects the finite thickness of the particles.

The above experiment demonstrated the sensitivity of *TG* to small permanent deformations. The fall in *TG* found previously (Fig. 6) in the region of $r$ where pronounced shear-induced bending of the particles occurred was therefore explainable as the result of permanent deformation of the particles in the $XY$-plane. To determine the variation of *TG* with $r$ up to values of $r$ at which the particles described springy and snake orbits, it was therefore necessary to use particles which were free of permanent deformations. Such experiments are described below.

It is interesting to note that the intrinsic viscosity of the 3.5 $\mu$ diameter rayon suspensions in castor oil increased linearly with $r$ up to $r_{\text{crit.}}$, after which it increased much more rapidly, presumably because of permanent deformation of the filaments by the action of the gradients (12). This is illustrated in Fig. 8.

*c. The Variation of TG with r.* Experiments on *TG* vs. $r$ were repeated, using the Apparatus No. 2, taking great care to use only those particles which were initially straight.

Rayon and Dacron filaments were each cut to a series of lengths corre-

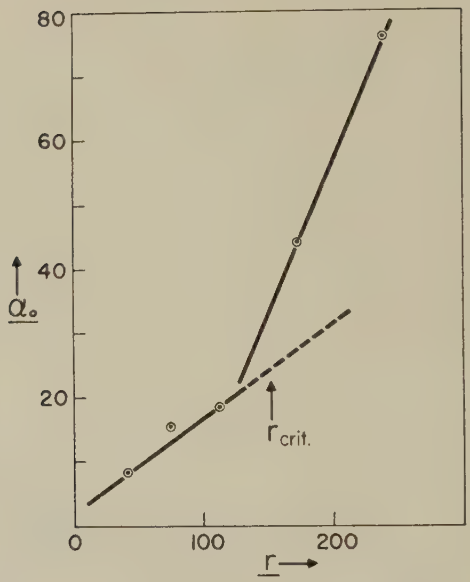

FIG. 8. Intrinsic viscosity $\alpha_0$ of 3.5 $\mu$ diameter rayon filaments in castor oil at various axis ratios below and above the calculated critical values corresponding to $G$ = 93 sec.$^{-1}$. From the data of Nawab and Mason (12).

TABLE III

*Variation of TG with r*

| Material and suspending medium | $r$ | No. in sample | Mean $G\eta$ (*g./cm. sec.*$^2$) | Mean $TG$ | Orbit |
|---|---|---|---|---|---|
| 3.5$\mu$ rayon filament in castor oil $\eta$ = 40.5 poises | 43 | 10 | 319 | 172 (13) | Rigid |
| | 100 | 10 | 249 | 347 (23) | Rigid |
| | 173 | 10 | 338 | 513 (40) | Rigid |
| | 241 | 10 | 311 | 549 (48) | Springy |
| | 357 | 10 | 308 | 622 (51) | Springy-snake |
| 7.8$\mu$ Dacron filament in corn syrup $\eta$ = 91.2 poises | 102 | 12 | 541 | 321 (36) | Rigid |
| | 139 | 10 | 542 | 397 (44) | Rigid |
| | 180 | 10 | 469 | 477 (59) | Rigid |
| | 228 | 10 | 544 | 580 (58) | Just springy |
| | 310 | 10 | 445 | 631 (43) | Springy |
| | 414 | 5 | 440 | 648 (53) | Snake |
| 7.8$\mu$ Dacron filament in diluted corn syrup $\eta$ = 11.4 poises | 228 | 10 | 44.7 | 537 (65) | Rigid |
| | 310 | 10 | 54.3 | 610 (68) | Rigid |
| | 414 | 5 | 54.3 | 616 (78) | Just springy |

Bracketed values are standard deviations of associated means.

sponding to axis ratios from 50 to 400. The Dacron samples were suspended in corn syrup and the rayon in castor oil. The periods of rotation of ten filaments, of each length and material, were timed at known shear rates.

Table III and Fig. 9 show that the results for rayon and Dacron were in good agreement despite the high standard deviations of *TG* from the mean. With the precautions taken in these experiments *TG* was found to increase with *r* over the entire range of *r*, even at values at which springy and snake orbits were observed. As *r* increased, the value of *TG* deviated at an increasing rate from the predicted value for rigid prolate spheroids of corresponding axis ratios.

It was previously shown (1) that the deforming forces exerted by the shear field and hence the extent of shear-induced deformation were a function of $G\eta$. It was therefore of interest to repeat the experiments with Dacron samples of $r = 228$, 310, and 414 at similar shear rates, this time in corn syrup diluted with water to reduce the viscosity (and therefore $G\eta$) by a factor of about 10. In the diluted medium, the $r = 228$ and 310 samples described rigid orbits (compared to springy in the undiluted medium) and the $r = 414$ sample appeared springy (compared to snake

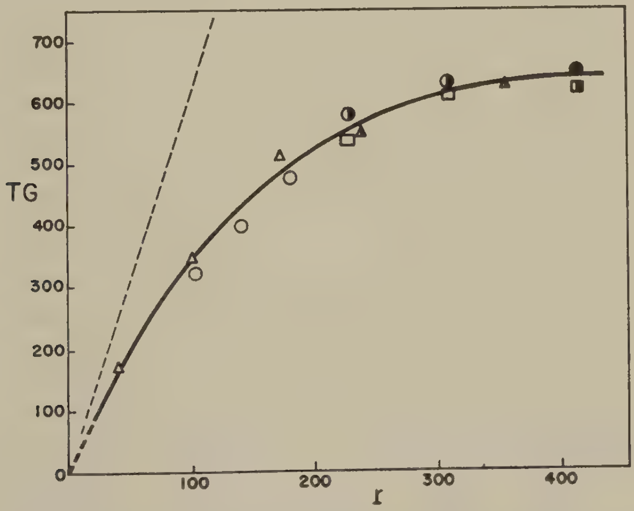

FIG. 9. *TG* vs. *r*. for particles having no permanent deformation. *Triangles:* 3.5$\mu$ diameter rayon in castor oil, $\eta = 40.5$ poises. *Circles:* 7.8$\mu$ diameter. Dacron in corn syrup, $\eta = 91.2$ poises. *Squares:* 7.8$\mu$ diameter. Dacron in corn syrup, $\eta = 11.4$ poises. *Open points:* rigid rotations. *Half-closed points:* springy rotations. *Closed points:* snake rotations.

The thin broken line represents the relationship for prolate spheroids as calculated from Eq. [1].

orbits). It seemed that a small drop in *TG* resulted from the reduced flexibility, as is evident in Table III; however, the scatter in *TG* for the individual specimens in each sample was too high to draw quantitative conclusions from this set of experiments. The results nevertheless indicated that with filaments of high *r* which are straight when at rest, any change in *TG* resulting from changes in recoverable deformation is small when compared to the changes caused by permanent deformation.

In this work, the relationship between *TG* and *r* was determined up to values of *r* at which snake orbits occurred. A further extension to filament lengths at which coiled orbits occur would be of interest.

*d. The Variation of TG with G.* The change in *TG* with *G* was investigated for a series of rayon filaments undergoing flexible orbits. Slightly curved particles were used, since the lower periods of rotation (compared with straight particles) greatly facilitated accurate timing, without altering the nature of the experiments.

Figure 10 shows the *TG* vs. *G* curves for filaments of axis ratios 311,

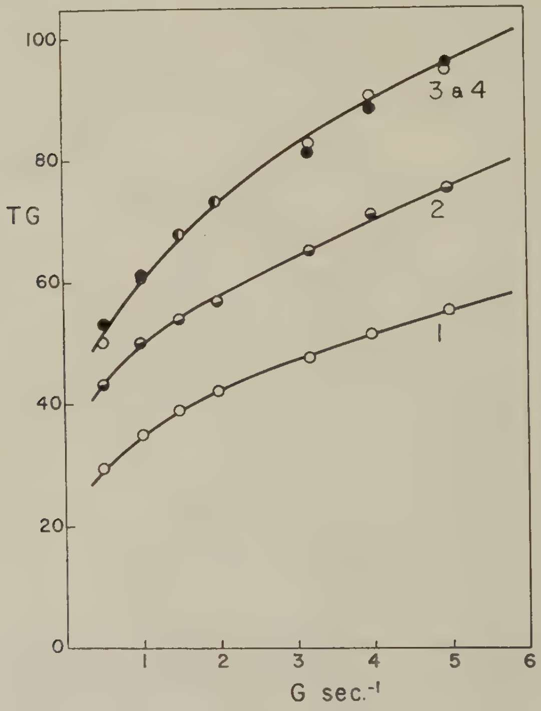

FIG. 10. *TG* vs. *G* for rayon filaments undergoing snake rotations. *Curve 1:* $r = 311$. *Curve 2:* $r = 386$. *Curve 3* (open points): $r = 491$. *Cvrve 4* (closed points): $r = 583$. The increase of *TG* with *G* is more pronounced, the longer (and hence more flexible) the filaments.

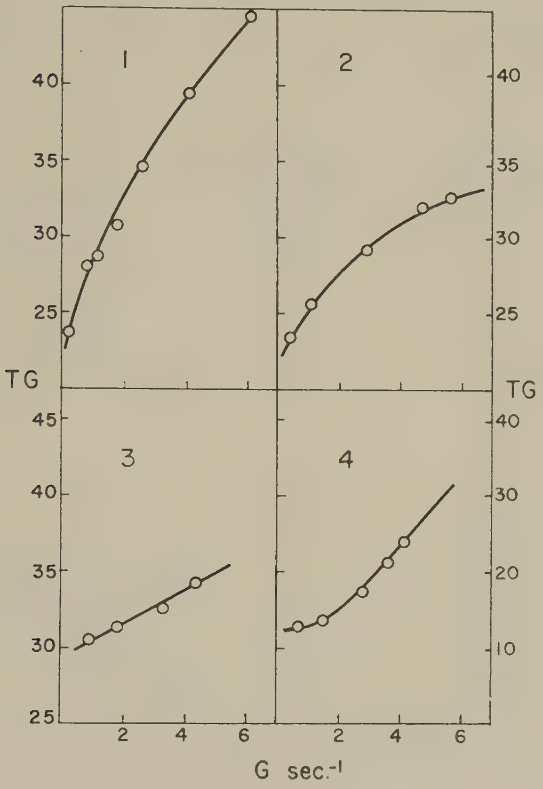

FIG. 11. *TG* vs. *G* for various deformable particles. (*1*) Rayon filament (snake rotation), $r = 311$. (*2*) Rayon "bundle." (*3*) Elastomer helix. (*4*) CHP drop. In each case, *TG* increases with *G*.

386, 491, and 583. Each curve represents the average of separate measurements on three single filaments of the same $r$. The value of $TG$ increased with $G$, following the same pattern as for pulp fibers (8). The rate of increase $d(TG)/dG$ was greater the longer the filaments, though no further change between the two samples of highest $r$ was apparent. Since the ability of filaments to deform under given shear stresses increases with $r$, the results support the previous evidence (8) that $\Delta(TG)/\Delta G$ is determined by the amount of shear-induced deformation.

It is reasonable to assume that the change in $TG$ with $G$ would be less pronounced for filaments which are perfectly straight when relaxed, since permanently curved particles not only bend under compression but also straighten visibly in the quadrants of the rotation during which the filaments are under tension, thereby enhancing the over-all shear-induced deformation.

The increase of $TG$ with $G$ is not limited to threadlike particles. Several bundles of rayon filament ($r = 311$) were prepared by joining about 20 filaments at their centers by means of droplets of wax, and their periods of rotation over a range of $G$ were measured. The periods of rotation of elastomer helices at various velocity gradients were also measured, as were the periods of circulation of deformed cyclohexanol phthalate drops ($\eta$ = 238 poises at 20°C.), using small particles of dust at the drop interface as markers. Figure 11 shows the $TG$ vs. $G$ curves for a flexible rayon filament, a bundle, a helix, and a drop, all of which underwent increasing deformation with increasing $G$. In each case, $TG$ increased with $G$, in contrast with rigid particles such as rods and spheres (2) where $TG$ was independent of $G$. These results generally support the hypothesis presented in the Introduction.

## SUMMARY

The behavior of deformable threadlike particles in suspensions subjected to velocity gradients has been studied.

For a given value of (shear rate) × (viscosity of suspending medium), there exists a critical length at which threadlike particles in suspension will bend during rotation under the stresses imposed by the shear field. Over a limited range of particle lengths above the critical length, the deformation increased as the length was increased. However, the particles straightened twice during each rotation, during that part of the orbit in which they lay parallel to the planes of shear. When the particle length was increased further, the particles formed rotating helices or coils. As the shear rate was increased, the change in shape of the projection of the coils on the plane parallel to the velocity gradient resembled the change in shape of deformed fluid drops.

The periods of rotation of permanently bent particles were shown to be appreciably lower than those of straight particles. Whereas the product (period of rotation) × (velocity gradient) was constant for rigid spheres, ellipsoids, and rods, it increased with deformable particles at a rate which was related to the amount of deformation resulting from shear.

The work is of interest in connection with the viscosity and other flow properties of suspensions and the streaming birefringence of solutions of macromolecules. It also forms the basis of a method of measuring the flexibility of wood-pulp fibers.

## REFERENCES

1. FORGACS, O. L., AND MASON, S. G., *J. Colloid Sci.* **14** (No. 5), 457 (1959).
2. TREVELYAN, B. J., AND MASON, S. G., *J. Colloid Sci.* **6** (No. 4), 354 (1951).
3. MANLEY, R. ST. J., AND MASON, S. G., *J. Colloid Sci.* **7** (No. 4), 354 (1952).

4. Bartok, W., and Mason, S. G., *J. Colloid Sci.* **12** (No. 3), 243 (1957).
5. Manley, R. St. J., and Mason, S. G., *Can. J. Chem.* **33**, 763 (1955).
6. Bartok, W., and Mason, S. G., *J. Colloid Sci.* **14** (No. 1), 13 (1959).
7. Mason, S. G., and Manley, R. St. J., *Proc. Roy. Soc.* (*London*) **A238**, 117 (1956).
8. Arlov, A. P., Forgacs, O. L., and Mason, S. G., *Svensk Papperstidn.* **61**, (No. 3), 61 (1958).
9. Forgacs, O. L., and Mason, S. G., *Tappi* **41** (No. 11), 695 (1958).
10. Forgacs, O. L., Robertson, A. A., and Mason, S. G., *Pulp & Paper Mag. Can.* **59** (No. 5) (1958).
11. Jeffery, G. B., *Proc. Roy. Soc.* (*London*) **A102**, 117 (1922).
12. Nawab, M. A., and Mason, S. G., *J. Phys. Chem.* **62**, 1248 (1958).

JOURNAL OF COLLOID SCIENCE **14**, 492–500 (1959)

# INTERPRETATION OF FLOW CURVES IN TERMS OF MOLECULAR PROPERTIES

J. Schurz

*Institut fur physikalische Chemie der Universitat Graz, Graz, Austria*

*Received October 10, 1958; revised February 5, 1959*

## Introduction

In the interpretation of flow curves, little progress has been made since the extensive work of Philippoff (1). Only in the last few years have several investigators undertaken the task of analyzing flow curves with the intention of obtaining more information on the solute molecules. In our view, most noteworthy is the observation by Umstätter (2) that there exists a relation between the inflection point of a flow curve (on a log-log plot) and the molecular weight of the solute in that the former is found at smaller shear gradients when the molecular weight is increased. Edelmann (3) has presented some experimental evidence for that finding. Umstätter, it is true, has also put forward a theory to explain this behavior along with many other rheological phenomena, namely, his "Strukturmechanik," but since quite a number of serious objections have been raised against these ideas we shall dispense with a discussion of the theory. Furthermore, Philippoff (1) himself gave the clue that useful information about the polydispersity of a given sample might be contained in the flow curves, and in this regard Meskat (4) was the first one to show experimentally that there exists a connection between polydispersity and the shape of the flow curve; by means of an approximation method he was even able to derive a relation between these two properties. Edelmann (3) too has contributed to this question following Umstätter's theoretical ideas. Finally, it has to be mentioned that Umstätter (5) also claims to be able to calculate molecular weights from the flow curve on an absolute scale. His results, however, are somewhat dubious and in any case open to critical reconsideration.

Our earlier work (6) has been concerned with attempts to draw information from flow curves, and with many experiments we have confirmed the statements that (*1*) a relationship exists between the molecular weight and the inflection point of the flow curve, and (*2*) the shape of the flow curve reflects the polydisperity of the solute. With these two points in mind, we felt that a thorough experimental analysis of flow curves would be worth while. A short account of our latest results is presented.

## THE FLOW CURVE

By "flow curve" we understand a plot of log $D$ versus log $\tau$ (Philippoff), where the mean shear gradient $D$ and the maximum shearing stress $\tau$ are given as:

$$D = \frac{4Q}{\pi r^3}$$

$$\tau = \frac{pr}{2l}$$

where $Q$ is the flow volume per second, $r$ is the radius of the capillary, $l$ is the length of the capillary, and $p$ is the driving pressure. The complete flow curve starts out as a straight line with a 45° slope (range of constant initial viscosity $\eta_0$), then assumes an S-shape, and finally ends up again as a 45° straight line ($\eta_\infty$). The slope of the flow curve will be designated as $\sigma$, it has a maximum value at the inflection point. Obviously, only flow curves extending from $\eta_0$ up to $\eta_\infty$ can be regarded as complete. Since the range of $\eta_\infty$ is sometimes rather difficult to attain experimentally, it is not always feasible to obtain complete flow curves. More detailed information on this subject is given elsewhere (7, 8).

## EXPERIMENTAL INTERPRETATION OF FLOW CURVES

On the basis of experimental results, we have developed a certain formalism regarding flow curves of high polymer solutions, which we find valid for all systems investigated so far. Quantities referring to the inflection point of the flow curve will be denoted with a ^-sign (e.g., $\hat{D}$, $\hat{\eta}$, $\hat{\sigma}$). The value of $D$ at the inflection point (the "critical" mean shear gradient $\hat{D}$) is related to the molecular weight by the equation:

$$\hat{D} = a \cdot M^{-b} \qquad [1]$$

where $a$ and $b$ are constants for a given system. Primarily, $\hat{D}$ seems to be related to the particle weight in general. By observing $\hat{D}$ as a function of the concentration $c$, we should be able to detect eventual variations of the particle weight. If, however, $\hat{D}$ turns out to be independent of concentration, we are dealing with very stable particles—very likely with macromolecules. What we actually observe is, that when beginning with higher concentrations, $\hat{D}$ becomes first larger as the concentration goes down; until, from a certain concentration $c^+$ on, no more change of $\hat{D}$ with $c$ is found. We suggest that $c^+$ may be regarded as that concentration at which molecular dispersion takes place. Naturally, only values of $\hat{D}$ independent of concentration should be used for determining the constants of Eq. [1]. Also, it must be considered that Eq. [1] allows determination of molecular weights only after calibration, and thus the nature of the molecular weight average depends also on the method of calibration.

The slope of the flow curve $\sigma$ is connected with the concentration $c$ of the solute by the equation:

$$\sigma = 1 + \beta(M) \cdot c \qquad [2]$$

$\beta(M)$ is a function of the molecular weight, the nature of which is not known in general. For several systems, we found that—at least as an approximation—:

$$\beta(M) = \beta' \cdot M$$

so Eq. [2] would read:

$$\sigma = 1 + \beta' \cdot M \cdot c. \qquad [3]$$

Finally, we approach the polydispersity problem by the outlined formalism. In general, we assume that the shape of the flow curve is shaped by four effects, namely, the response of the single, isolated particle (flow curve of the isolated particle), the statistics of the chain molecule, interaction effects, and the polydispersity of the sample. Only if the last effect—namely, polydispersity—plays a role much larger than the other three can we hope to derive polydispersity from flow curves. This assumption seems to be supported by several findings. In order to arrive at a formula for polydispersity, we may argue as follows. Every point on the flow curve corresponds to a certain molecular weight, the relationship given by Eq. [1]. The slope in each point, corrected for the influence of molecular weight and interaction (the latter is kept small by working with dilute solutions), gives us the relative concentration, in which the respective molecular weight is present. By plotting $\sigma - 1/\beta(M)$ vs. $M$ ($M$ calculated from $\hat{D}$ by means of Eq. [1]), we should obtain curves resembling the polydispersity curves. Of course, we have to regard these curves as an approximate expression for polydispersity; they may well be distorted by other effects (*cf.* reference 7), but in general they should correspond to the molecular weight distribution. We have named these $\sigma - 1/\beta(M)$ vs. $M$ curves "PD-Kennkurven" to stress the approximate character of the relation.

## RESULTS

We distinguish between the rheological behavior of macromolecules known as more or less freely draining ($a$ in the Mark-Houwink equation close to 1) and those with a pronounced immobilization of solvent ($a$ close

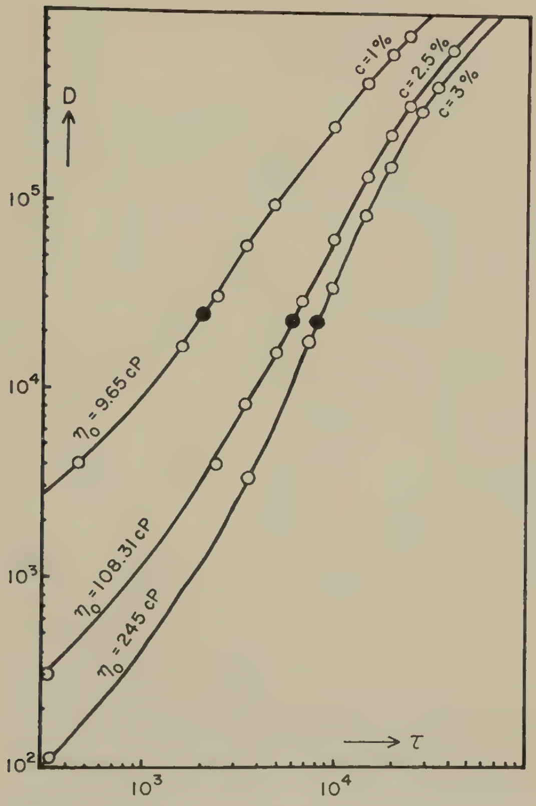

FIG. 1. Flow curves of Na-carboxymethylcellulose ($P$ = 510) in 6% NaOH.

to 0.5). In the first case, structural viscosity is very significant, and even with rather small concentration and molecular weight we obtain well-pronounced flow curves. Also, in this case the inflection point is constant up to considerable concentrations. In Fig. 1 such flow curves are shown for Na-carboxymethylcellulose in 6% NaOH. With such systems (including viscose, cellulose nitrate, carboxymethylcellulose, etc.) all our empirical equations are valid, and, for example, molecular weight determinations are possible with great accuracy. Figure 2 gives the plot according to Eq. [1] for a number of systems.

With the second type of polymers, which include polystyrene, polyisobutylene, polyvinylpyrrolidone, etc., things are somewhat different. Structural viscosity is not so pronounced (it becomes sometimes difficult exactly to locate the inflection point!) and in order to obtain good flow curves, we have to use relatively high concentrations and molecular weights.

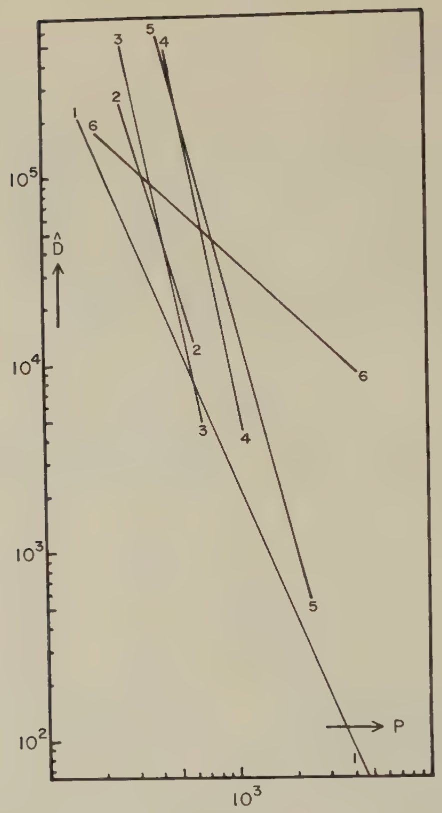

FIG. 2. Relation between $\hat{D}$ and $P$. *1:* Cellulose nitrate/butyl acetate. *2:* Na-carboxymethylcellulose/6% NaOH. *3:* Viscose 8% Cell., 8% NaOH. *4:* Viscose 4% Cell., 15% NaOH. *5:* Cellulose/cupriethylenediamine ($c = 1\%$). *6:* Cellulose/Fe-Na-tartrat-NaOH ($c = 1\%$).

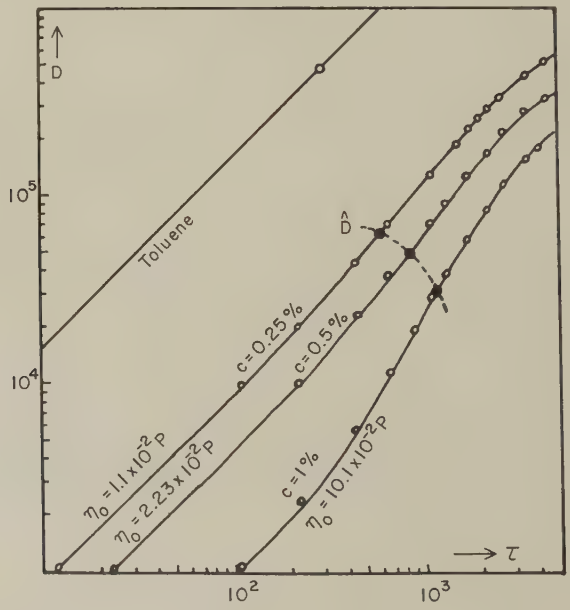

FIG. 3. Flow curves of polystyrene in toluene (mol. wt. = $9 \times 10^5$).

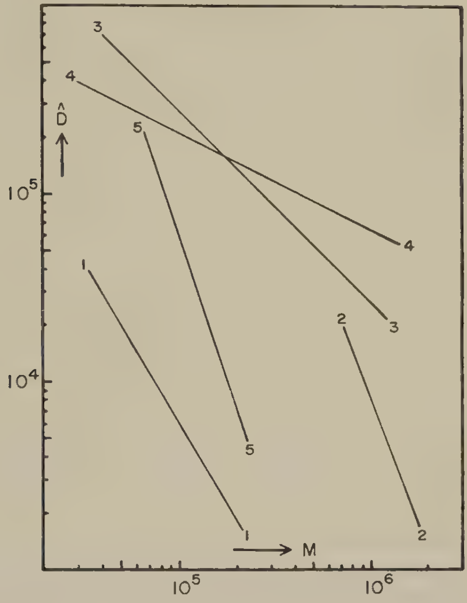

FIG. 4. Relation beteen $\hat{D}$ and $M$. *1:* Polyacrylonitrile/dimethylformamide. *2:* Natural rubber/toluene. *3:* Polystyrene/toluene ($c = 1\%$). *4:* Polyvinylpyrrolidone/water ($c = 1\%$). *5:* Polyisobutylene/toluene ($c = 1\%$).

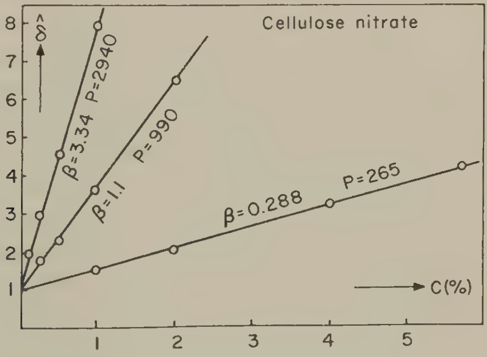

FIG. 5. Slope $\sigma$ vs. concentration $c$ for cellulose nitrate/butyl acetate.

The inflection point becomes constant only for rather small concentrations, and in some cases structural viscosity vanishes before the concentration $c^+$ (i.e., inflection point independent of concentration) is reached. In such cases, since an extrapolation of the inflection point to zero concentration is not satisfying, it turned out best to use flow curves of one single, possibly lowest concentration in order to set up curves corresponding to

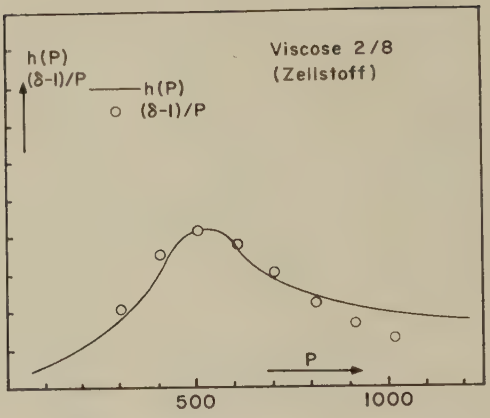

Fig. 6. Differential mass distribution curve $h(P)$ and PD-Kennkurve of a cellulose sample.

Eq. [1]. Figure 3 shows some flow curves of polystyrene in toluene; the inconstancy of the inflection point is readily observed. Finally, in Fig. 4 the plots according to Eq. [1] for several systems with hindered flow are shown. As we see, Eq. [1] is still valid, but the accuracy is less owing to possible errors in the determination of $\hat{D}$, and the relations are valid only for one concentration. Interestingly enough, cellulose, dissolved in cupriethylenediamine or in Fe-Na-tartrat-NaOH, shows no constant inflection point and so seems rather to belong to the second group.

In order to present some support also for our further equations, we have plotted in Fig. 5 the slopes of a series of flow curves for cellulose nitrate; we recognize easily all features of Eq. [2]. Finally, in Fig. 6 we have compared our method of the "PD-Kennkurven" with classical polydispersity determination. For a sample of cellulose we have plotted the differential mass distribution curve, as obtained from a usual fractionation with the nitrate, and the PD-Kennkurve derived from a flow curve of viscose made of this sample. The agreement is astonishingly good, if we consider the approximate character of the method. Of course, the PD-Kennkurven are reliable only so long as the molecules in solution show structural viscosity. So, with lower molecular weight, the reliability decreases and finally the curves become meaningless as soon as the molecular weight is so low that no more structural viscosity is exhibited under given conditions. That is why most of our PD-Kennkurven suddenly become useless at degrees of polymerization below 200. Furthermore, PD-Kennkurven are meaningful only if derived from very low concentrations, since obviously with higher concentrations mutual interactions of solute molecules distort the flow curve in such a way that polydispersity effects are completely masked.

## Discussion

It is our conviction that flow curves yield much information. Unfortunately we do not yet know how to derive them. Fundamentally, we recognize that experimental flow curves are complicated. First, the macromolecule in solution has no definite shape; being a chain molecule its shape is changing continuously in a statistical sense and is characterized by a "change of constellation time." This, however, should not be very important since we can describe adequately the shape of the molecule by an average value. So the single, isolated molecule will respond to the shearing force applied in a way given by its characteristics; namely, molecular weight, shape, and stiffness. This shear dependent response, summed over all molecules present in the investigated sample, will lead to a certain relationship between shear gradient and shearing stress (or, more exactly, between the respective tensors): this relationship we may call the friction law of the single molecule. Actually things are still more complicated. We never deal with uniform molecules, but our samples are more or less polydisperse, that is, they contain molecules of varying size. Since the molecular weight is an important factor in determining the rheological behavior of a molecule, this polymolecularity will be also reflected in the friction law. Finally, in the finite concentrations we are working with, interactions ranging from pure hydrodynamical hindrance to actual associations will modify the flow pattern. All these effects will cooperate to define the friction law of the sample investigated; thus, it should be possible to derive information on these points once the friction law is known, provided the different effects can be separated.

Now the friction law is not identical with the flow curve we measure (*cf.* reference 9). The friction law gives a relationship (for the volume element) between actual shear gradient and shearing stress. Measurements, however, are carried out not on a volume element but on a macromolecular scale, that is, for example, in a capillary, in which the hydrodynamical forces are varying across the diameter. What we measure here are average or extreme values; for the capillary, for example, it has become customary to measure a "mean shear gradient" (which actually represents a reduced mean flow velocity) as a function of the "maximal shearing stress" (at the capillary wall). This function is called the flow curve. In addition to these instrumental particularities, a further modification (mathemathical) is brought in by the way of plotting (variables or their log). Methods have been suggested of rendering actual measurements more or less independent of instrument dimensions by appropriate choice of variables; in any event, however, the flow curves we obtain in our experiments are not identical with the friction law, though they contain it. It has been shown for several cases (capillary, couette-gap) how the friction law can be derived from experimental flow curves by solving an integral equation. Such a calculation has, for example, been carried out for the capillary by Weissenberg (among others), and his formula allows the graphical construction of the friction law when the experimental flow curve is known.

In order to establish relations between flow curves and molecular properties, several points have to be considered. If a physical interpretation is attempted, following the ideas of any theory, we must try to establish the friction law first. Only figures given in this may be interpreted as actual molecular properties. Such a procedure is lengthy and troublesome and has not been tried out too frequently in the past. Another possibility would be to look for connections between experimental flow curves and molecular properties in an empirical way. We have employed this method and useful relations can be found. These relations are obtained after an empirical calibration, and so all those factors mentioned in the foregoing are put into the empirical constants. Our equations are readily open to experimental tests on an extensive scale, but it has to be remembered that their constants have no longer a straightforward physical meaning: they will not allow absolute calculation of molecular parameters, and their physical interpretation must be carried out with the utmost care.

This method of flow curve interpretation is only a first step. The final aim must be the absolute calculation of molecular parameters from data taken from the friction law via flow curves. Much work will be necessary to reach this goal. Concerning instruments, we prefer those with a rather translucent theory in order to keep the apparatus influence small. As to materials, most promising appear investigations on free-draining macromolecules of approximate monodispersity in very dilute solutions; these conditions would help to give us, approximately, the flow curves of single molecules free from interaction and polydispersity effects. It would be most important to measure flow curves of strictly monomolecular materials free from interaction effects, "ideal flow curves," as we have called them. Finally, there remains a pressing need for a theory which can describe complete flow curves in sufficient agreement with experimental findings.

## References

1. Philippoff, W., "Viskosität der Kolloide." Steinkopff, Dresden and Leipzig, 1942.
2. Umstätter, H., "Strukturmechanik." Steinkopff, Dresden and Leipzig, 1948.
3. Edelmann, K., *Faserfarsch. u. Textiltech.* **3,** 341, 412 (1952); *ibid.* **5,** 59, 139, 325 (1954).
4. Meskat, W., *Chem. Ing. Tech.* **14,** 333 (1952).
5. Umstätter, H., *Kolloid. Z.* **139,** 120 (1952).
6. Schurz, J., *Kolloid-Z.* **147,** 57 (1956).
7. Schurz, J., *Kolloid. Z.* **154,** 97 (1957); *ibid.* **155,** 45, 55 (1957).
8. Schurz, J., *Kolloid Z.* **148,** 76 (1956).
9. Meskat, W., "Viskosimetrie," *in* "Messen und Regeln in der chemischen Technik." Springer, Berlin-Göttingen-Heidelberg, 1957.

JOURNAL OF COLLOID SCIENCE **14,** 501–509 (1959)

# STABILITY OF EMULSIONS OF WATER IN OIL

## I. THE CORRELATION BETWEEN ELECTROKINETIC POTENTIAL AND STABILITY

**W. Albers[1] and J. Th. G. Overbeek**

*van 't Hoff Laboratory, University of Utrecht, Netherlands*

*Received January 21, 1959*

### Abstract

Experiments on W/O emulsions of moderate concentration, stabilized with oil-soluble, ionizing stabilizers, show that in these emulsions no correlation exists between stability against flocculation and electrokinetic potential. Although, according to theoretical calculations, energy barriers of over 15 $kT$ are present, if the radius of the dispersed globules is about 1 $\mu$ and the electrokinetic potential exceeds 25 mv., they apparently do not prevent lasting contact between particles. All our emulsions flocculate rapidly, even in the presence of a surface potential considerably higher than 25 mv.

A rather pronounced anticorrelation exists between the zeta potential and coalescence. It is explained as a consequence of the free mobility of the stabilizing molecules in the interface.

The good stabilization against coalescence caused by some oleates of polyvalent metals is due to the formation of a thick film of partial hydrolyzates in the interface.

### Introduction

As early as 1914 Newman (1, 2) reported that the oleates of barium, magnesium, zinc, and cadmium stabilize W/O emulsions. Shortly afterwards Briggs and Schmidt (3) used Mg-oleate to stabilize W/O emulsions containing up to 90% of water. They were the first to notice that the stabilized water globules were of irregular shape—a fact observed afterwards many times by other investigators. In 1940 Schulman and Cockbain (4) attributed this irregularity to the stiffness of the interfacial film. From their experiments they concluded that W/O emulsions are formed only when the film of stabilizer molecules in the interface is uncharged and stiff as a result of complex formation. In the discussion of their experimental results they argued that a W/O emulsion can not be stabilized against flocculation by charge on the water droplets because, oil being a nonionizing medium, an electrical diffuse layer or ionic atmosphere can not be built up. Further, according to them a charged film is not able to prevent coalescence because owing to repulsion between the stabilizer molecules in the interface, no interlinked solid condensed film can be formed. In 1951 Moilliet and Collie (5) endorsed this view.

---

[1] Present address: Philips' Research Laboratories, Eindhoven, Netherlands.

In 1933, however, Fuoss and Kraus (6) had already shown that even in apolar oils a distinct though very small ionization may occur. An ion-forming compound, such as a polyvalent metal salt of an organic acid, dissolved in benzene (for convenience we refer to this liquid) in a concentration of about 10 mmoles per liter possesses a degree of ionization in the order of $10^{-8}$. Consequently the ionic concentration is in the order of $10^{-10}$ $N$, so that, in spite of the low dielectric constant of the medium, the electrical double layer is very diffuse, i.e., the corresponding Debye length $1/\kappa$ is several microns. Therefore, as Koelmans and Overbeek (7) remark, the capacity of the double layer in such apolar systems is very low and only very little charge is needed to obtain appreciable surface potentials. The repulsion at the low ionic concentrations involved, is described in good approximation by Coulomb's law

$$V_R = \psi_0^2 \, \epsilon \, a^2/R,$$

in which $V_R$ = energy of interaction, $\psi_0$ = surface potential, $\epsilon$ = dielectric constant, $a$ = radius of the droplet, and $R$ = distance between the centers of the particles. When the Coulomb repulsion is combined with the van der Waals attraction (van der Waals' constant $A = 10^{-12}$ erg, cf. Hamaker (8)) an energy barrier of 15 $kT$ is obtained in the case of a radius $a = 1$ $\mu$ and a surface potential $\psi_0 = 25$ mv. (see Fig. 1). This surprisingly high maximum of about 15 $kT$, which value as a rule is sufficiently high to stabilize against flocculation, is due to the very slow decay of the electrical repulsion between the particles with the distance.

On the one hand, these calculations are supported by experiments of van der Minne and Hermanie (9). They observed a carbon suspension of concentration 0.1% in mineral oil and found that stabilization against flocculation is obtained when the electrokinetic potential, $\zeta$, exceeds 20–25 mv. The carbon suspension was stabilized with the calcium salt of diisopropylsalicylic acid, an oil-soluble soap. Similar facts were found by Koelmans (7) for suspensions in xylene.

On the other hand, the above calculation seems to be contradicted by the general experience that W/O emulsions of moderate concentration always flocculate, or as Pink (10) expressed it, that the fundamental difference in the two types of emulsions is reflected in the more rapid creaming which is so characteristic of the oil-continuous type.

In order to try to solve the contradiction pointed out above, we determined the electrokinetic potential and the stability against flocculation and against coalescence of a number of water-in-oil emulsions, stabilized with stabilizers, which ionize to some extent in the oil phase.

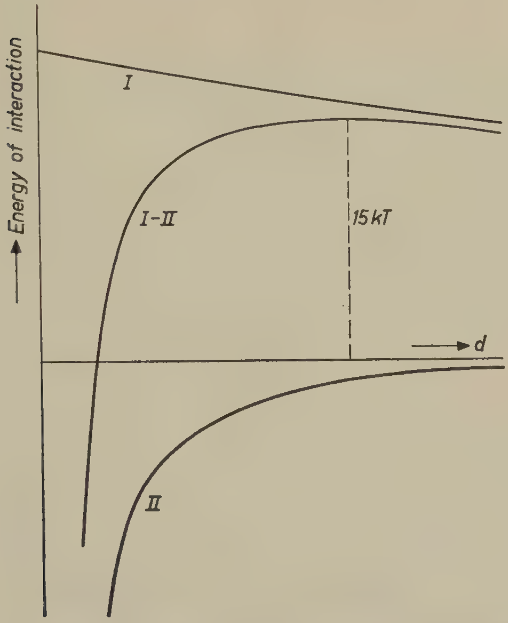

FIG. 1. Potential energy of interaction between two globules with radius $a = 1\ \mu$ in oil as a function of the distance $d$ between the surfaces. The surface potential $\psi_0 = 25$ mv.; dielectric constant of the oil $\epsilon = 2.3$. I = Coulomb repulsion; II = van der Waals' attraction.

## MATERIALS AND EXPERIMENTAL METHODS

Oleates of polyvalent metals were prepared by double decomposition between inorganic salts of the bi- and trivalent metals and the calculated equivalent amount of sodium oleate, dissolved in water of about 90°C. to prevent enclosure of impurities (11). The precipitated oleates were washed with water, dried first over $CaCl_2$ in a desiccator, next in a hot air oven during 45 minutes at 105°C.

Ca-didodecylsalicylate and petroleum sulfonates of some bivalent metals were obtained from Koninklijke Shell Laboratorium, Amsterdam. The sulfonates were liberated from mineral oils by dissolving in a hot mixture of 50% ethanol in water, subsequent extraction of the mineral oil with a low-boiling petrol fraction, followed by evaporation of the solvent.

Benzene was thoroughly dried by distillation over sodium to prevent the precipitation of any possible hydrated modification of the soap (12).

Electric conductivity, down to about $10^{-14}\ \Omega^{-1}$ cm.$^{-1}$, was measured by a simple d.-c. method following Koelmans (7). The conductivity cell (see Fig. 2) was treated on the outside with silicons to repel moisture. The distance between the platinum electrodes is small compared with the

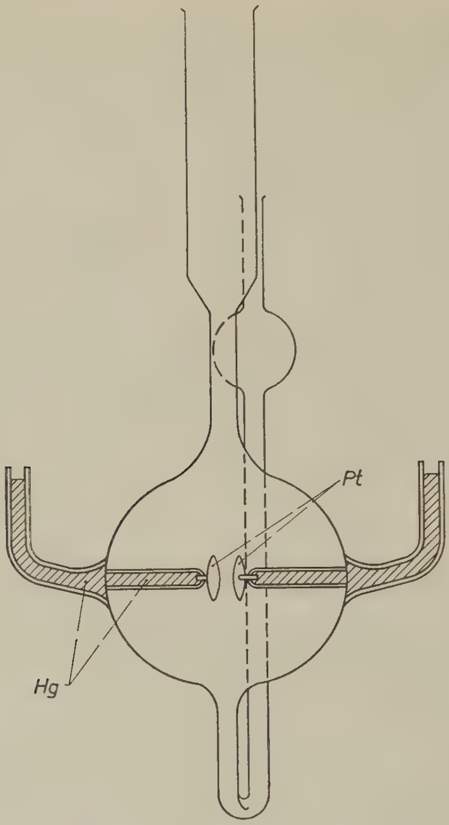

Fig. 2. Conductivity cell for media with low dielectric constant.

distance between the inner wall of the bulb and the electrodes. Thus trouble by conduction of the electric current alongside the glass walls of the cell is diminished. This has been proved to be effective because by measurements on pure benzene a specific conductivity lower than $10^{-14}$ $\Omega^{-1}$ cm.$^{-1}$ was obtained. This is small as compared with the specific conductivities of the solutions of soaps of polyvalent metals and other ionic stabilizers in benzene, which are in the order of $10^{-10}$ $\Omega^{-1}$ cm.$^{-1}$.

A Philips d.-c.-electronic Voltmeter-pH meter G.M. 4491 was used to determine the potential in the circuit.

The electrophoresis measurements were carried out in the cylindrical cell as described by van der Minne and Hermanie (13). During these measurements the applied voltage never exceeded 100 v./cm. to prevent electrostatic induction effects that would otherwise disturb the electrophoresis measurements.

The emulsions were prepared by adding water slowly to the solution of stabilizer in benzene under the influence of the vigorous stirring of a centrifugal emulsifier, the IKA Ultra Turrax (type TV 45, Janke and Kunkel, KG, Staufen i. Br.). The concentration of the soap in the oil in most cases amounted to 10 mmoles/l. The W/O emulsions used in the sedimentation or breaking experiments contained 15 volume per cent of water. The percentage of water used in the electrophoresis measurements was about 0.005. This low percentage was obtained from an emulsion containing 15 volume per cent of water by diluting with the oil phase of an identical emulsion. The radii of the water droplets ranged mostly between 1 and 4 $\mu$. Measurements of sedimentation and breaking were carried out in glass-stoppered graduated cylinders.

## MEASUREMENTS AND RESULTS

Emulsions of water in benzene have been prepared in the presence of oleates of the metals Al, Ba, Ca, Cd, $Cu^{II}$, $Fe^{III}$, $Hg^{II}$, Mg, Mn, Ni, Pb, Sr, and Zn, petroleumsulfonates of Ba, Mg, and Zn and Ca-didodecylsalicylate. The soaps are soluble in benzene except the oleate of $Hg^{II}$. They are insoluble in water. When they are dissolved in benzene in concentrations of 10 mmoles/l. their specific conductivity appears to be in the order of $10^{-10}$ $\Omega^{-1}$ cm.$^{-1}$. These soaps of polyvalent metals promote water in oil emulsions which, however, all flocculate, as observed by sedimentation velocity and microscopic examination. Some of these flocculated emulsions are stable against coalescence, others are not. In column 1 of Table I a series of oleates has been given, from the top downwards increasing in ability to stabilize emulsions of water in benzene against coalescence. The time interval between the preparation and the breaking of the emulsion is adopted as a measure for stability against coalescence. From Ba-oleate up to and including Sr-oleate the time of coalescence increases from a quarter of an hour to about 20 days. The oleates of $Fe^{III}$, Mg, Pb, and $Cu^{II}$ stabilize against coalescence for several months and even longer.

Determination of the interfacial tension by stalagmometer showed that the oleate molecules are strongly adsorbed at the interface between water and benzene. The polar head will dip in the water phase; the hydrophobic hydrocarbon chains will point into the oil phase. By ionization of one negative oleate ion from the oleate molecule a positive metal-mono-oleate ion will remain in the interface. It is observed actually from electrophoresis measurements that the water droplets of the water in benzene emulsions are positively charged. Zeta potentials have been calculated from the observed electrophoretic velocities using the equation:

$$v_e = \frac{\epsilon E \zeta}{6\pi\eta},$$

in which $v_e$ = electrophoretic velocity, $\epsilon$ = dielectric constant, $E$ = ap-

TABLE I

*Correlation between the Electrokinetic Potential $\zeta$ and the Stability against Coalescence in Water-in-Benzene Emulsions Stabilized by the Oleates of Polyvalent Metals and Some Other Stabilizers*

| 1 Sequence of increasing stability against coalescence | 2 $\zeta$-potential $= \psi_0$ potential (*mv.*) | 3 Time interval between preparation and beginning of breaking of the emulsion |
|---|---|---|
| Ca-didodecylsalicylate | 130 | A few hours |
| Ba-oleate | 0 | |
| Mn-oleate | 70 | Some days |
| Ca-oleate | 20 | |
| Zn-oleate | 50 | |
| Al-oleate | 45 | |
| Mg-petroleum sulfonate | 80 | |
| Ba-petroleum sulfonate | | |
| Zn-petroleum sulfonate | | |
| Ni-oleate | 32 | 10–20 days |
| Cd-oleate | 22 | |
| Sr-oleate | 10 | |
| Fe$^{III}$-oleate | 15 | Several months |
| Mg-oleate | | |
| Pb-oleate | | |
| Cu$^{II}$-oleate | | |

plied field strength, $\zeta$ = electrokinetic potential, and $\eta$ = viscosity of the oil phase.

As the double layer in oil is extremely diffuse and therefore the decay of the potential with the distance from the interface slow, the surface potential $\psi_0$ may be identified with $\zeta$.

Electrophoresis measurements on water in benzene emulsions stabilized with Ca-didodecylsalicylate gave a surface potential of 130 mv. These emulsions broke immediately after preparation. When stabilized with Mg-, Zn-, Ba-petroleum sulfonates a $\psi_0$ of about 80 mv. was obtained. These emulsions break within a week.

### Stability against Flocculation

It is obvious from the experiments described above that a surface potential considerably higher than 25 mv. is not sufficient to stabilize dispersed droplets with a radius equal to or larger than 1 $\mu$ against flocculation. This is shown on the one side by the high sedimentation velocities, on the other side more spectacularly by the rapid breaking of some such W/O emulsions. For, evidently, coalescence can take place only after introductory flocculation. These observations seem to be in contradiction with the calculations of Koelmans (7) mentioned above, from which it followed that in nonpolar media surface potentials of 25 mv. provide a sufficiently high energy barrier to prevent flocculation of two particles with radii above 1 $\mu$. In a subsequent paper in this journal we shall show that although Koelmans's conception is correct for very dilute suspensions and emulsions it is not applicable to more concentrated emulsions and certainly not to the cream layer. In this paper we direct our attention to stabilization against coalescence.

## STABILITY AGAINST COALESCENCE

The specific conductivities of the solutions of the different oleates in benzene have almost the same value, indicating equal degrees of ionization. Nevertheless as shown in Table I surface potentials differ appreciably. The low value observed in water in benzene emulsions stabilized by $Cu^{II}$—and some other oleates might be due to partial hydrolysis of the soap. The products of hydrolysis are insoluble both in water and in benzene, accumulate at the interface, and interfere with the formation of an electrical double layer in the oil phase.

To test this point of view interfacial films of emulsions with low surface potentials, stabilized by $Cu^{II}$, $Fe^{III}$, or Mg-oleate were collected and analyzed. After breaking the emulsions by centrifuging the films were filtered, dried first over $CaCl_2$ in a desiccator, next in a hot air oven during 45 minutes at 105°C.

The results of the analysis are shown in Table II, together with the calculated compositions of the pure oleates and the calculated compositions of possible products of hydrolysis.

The data for Cu, Fe, C, and H in column 2 of Table II are obtained by polarography, by colorimetry, and via combustion in the conventional gravimetric way, respectively. The percentage of O is acquired by subtraction from 100%.

Comparison of column 2 and column 3 makes it plausible that these emulsions are stabilized by hydrolysis products.

The notion that soaps which do not stabilize water in benzene emulsions against coalescence do not hydrolyze either is supported by the experiments of Pink (12). He studied the effect of water on benzene solutions of Mg-, Ca-, Sr-, Ni-, and Zn-oleates. Two per cent solutions of the soaps in benzene were shaken with an equal volume of water. After breaking of the resulting emulsions the concentration of soaps remaining in the benzene layer was estimated. It appeared that almost the whole quantity of Mg-oleate had been removed from the benzene phase. Ca- and Sr-oleate had disappeared for the greater part but the oleates of Ni and Zn were found back nearly completely in the benzene phases, indicating that the poor stabilizers, viz., Ni- and Zn-oleate, scarcely hydrolyze.

The stabilizing action of the hydrolysis products may be explained in two ways. They may be considered as small particles, insoluble in both

TABLE II

*The Composition of the Hydrolysis Products of the Oleates in the Interfacial Film with Low Potential*

| 1 | 2 | 3 | |
|---|---|---|---|
| Theoretical oleates | Hydrolysis products | Possible composition of the hydrolysis products | |
| Mg-oleate: | | | |
| Mg 4.14 | | 7.45 | |
| C 73.68 | 67.06 | 67.02 | |
| H 11.26 | 10.41 | 10.55 | |
| O 10.92 | | 14.98 | |
| | | Mg-OlOH or $Mg(OH)_2MgOl_2$ complex | |
| $Cu^{II}$-oleate: | | | |
| Cu 10.16 | 24.25 ± 0.25 | 23.96 | |
| C 69.06 | 46.87 | 45.28 | |
| H 10.55 | 6.35 | 6.41 | |
| O 10.23 | 22.53 | 24.35 | |
| | | $Cu\text{-}OlHCO_3 \cdot CuCO_3$ or $(CuCO_3)_2 \cdot HOl$ complex | |
| $Fe^{III}$-oleate: | | a or b | |
| Fe 6.21 | 10.08 ± 0.17 | 10.75 | 9.86 |
| C 72.08 | 53.26 | 48.37 | 53.06 |
| H 11.01 | 7.33 | 7.10 | 7.89 |
| O 10.70 | 29.33 | 33.78 | 29.19 |
| | | (a) $Fe(HCO_3)_3 \cdot HOl$ complex or<br>(*b*) $(Fe(HCO_3)_3)_7 \cdot (HOl)_8$ complex in which<br>Ol = oleate HOl = oleic acid | |

phases and therefore accumulating at the interface. By virtue of their largely hydrocarbon character (see analysis) they will be more easily wetted by benzene than by water, stick out at the oil side, and stabilize the emulsion of water in oil mechanically (14). Alternatively they may be considered as forming a continuous, multimolecular, rather rigid layer separating the two phases by a layer impermeable to water and preventing coalescence of the water droplets.

Table I shows the unexpected fact that an increase in surface potential is roughly correlated with a decrease in stability against coalescence. High charge indicates little hydrolysis. Oleates that give a high charge will probably be present in the interface as a monolayer as contrasted to the multilayer formed by hydrolysis products. The molecules in the monolayer are expected to be quite mobile, because the van der Waals attraction between the hydrocarbon chains, dissolved in the oil side of the interface, will be quite small. After coagulation, the nonhydrolyzed soap molecules may be easily pushed away by the attraction forces between the water droplets and coalescence will follow.

In Table I the position of the oleates of the alkaline earth metals is exceptional. The low electrokinetic potential suggests a pronounced hydrolysis though rapid coalescence is observed. However, the formed hydroxides and hydrocarbonates of these metals are soluble in the water phase of the emulsion globule. Consequently the ability of the interfacial film to stabilize against coalescence is strongly diminished.

## REFERENCES

1. NEWMAN, F. R., *J. Phys. Chem.* **18,** 45 (1914).
2. See for review: CLAYTON, W., "The Theory of Emulsions and Their Technical Treatment," 5th ed. Churchill, London, 1954.
3. BRIGGS, T. R., AND SCHMIDT, H. F., *J. Phys. Chem.* **19,** 491 (1915).
4. SCHULMAN, J. H., AND COCKBAIN, E. G., *Trans. Faraday Soc.* **36,** 661 (1940). See also the review: BOWCOTT, J. E., AND SCHULMAN, J. H., *Z. Elektrochem.* **59,** 283 (1955).
5. MOILLIET, J. L., AND COLLIE, B., "Surface Activity." Spon, London, 1951.
6. FUOSS, R. M., AND KRAUS, C. A., *J. Am. Chem. Soc.* **55,** 3614 (1933).
7. KOELMANS, H., Thesis, Utrecht, 1955. KOELMANS, H., AND OVERBEEK, J. TH. G., *Discussions Faraday Soc.* **18,** 52 (1954).
8. HAMAKER, H. C., *Physica* **4,** 1058 (1937).
9. VAN DER MINNE, J. L., AND HERMANIE, P. H. J., *J. Colloid Sci.* **8,** 38 (1953).
10. PINK, R. C., *Trans. Faraday Soc.* **37,** 180 (1941).
11. REILLY, J., AND RAE, W. N., "Physico-chemical Methods," Vol. 3 (supplementary). Methuen, London, 1948.
12. PINK, R. C., *J. Chem. Soc.* **1938,** 1252.
13. VAN DER MINNE, J. L., AND HERMANIE, P. H. J., *J. Colloid Sci.* **7,** 600 (1952).
14. PICKERING, S. U., *J. Chem. Soc.* (*Trans.*) **91,** 2001 (1907). SCHULMAN, J. H., AND LEJA, J., *Trans. Faraday Soc.* **50,** 598 (1954).

JOURNAL OF COLLOID SCIENCE **14**, 510–518 (1959)

# STABILITY OF EMULSIONS OF WATER IN OIL

## II. CHARGE AS A FACTOR OF STABILIZATION AGAINST FLOCCULATION

**W. Albers[1] and J. Th. G. Overbeek**

*Van't Hoff Laboratory, University of Utrecht, Netherlands*

*Received January 21, 1959*

### Abstract

It is shown by theoretical calculations that the energy barrier between charged droplets in water-in-oil emulsions is strongly diminished when the concentration of the emulsion is not extremely low. This is a consequence of the great extension of the diffuse electrical double layer in oil. The high concentration in the sediment (or cream) therefore strongly promotes flocculation. Gravity also promotes flocculation directly in all but the most dilute W/O emulsions because the weight of the particles in higher layers transmitted by the extended double layers presses on those in the lower layers and forces them together.

### Introduction

It has been pointed out in a preceding paper (1) that water-in-oil emulsions flocculate rapidly, notwithstanding the presence of a rather high potential on the water droplets. Calculating the energy barrier in the approach of two water droplets with a radius of 1 $\mu$ and a surface potential of 25 mv. a value of 15 $kT$ is found, which ought to retard flocculation quite considerably. It will be shown in this paper that because of the long range of the electrical repulsion the two particle calculations have to be abandoned. By taking interactions between large numbers of particles into account the observed behavior of W/O emulsions with respect to flocculation can be understood.

### Effect of the Concentration of the Disperse Phase on the Stability Against Flocculation in Media of Low Dielectric Constant

In systems in which water is the continuous phase the thickness of the double layer generally equals about $10^{-3}$–$10^{-2}\mu$ so that electrical interaction takes place only at very short distances. The potential energy of the charged particles at a mutual distance of a few times $10^{-2}\mu$ thus equals zero with regard to infinite distance. Consequently the total energy barrier has to be crossed before flocculation can occur.

---

[1] Present address, Philips Research Laboratories, Eindhoven, Netherlands.

In an oil-continuous system, however, the thickness of the diffuse double layer is several microns. The thickness is of the same order as the distance between the dispersed globules in a moderately concentrated emulsion. The globules therefore possess a potential energy with regard to separation at an infinite distance. Consequently the energy barrier is lowered and the stability against flocculation is diminished. This effect has already been mentioned by Verwey (2). A further lowering of the energy barrier occurs as a consequence of the combined interaction of more than two particles, as has been illustrated schematically in Fig. 1 for a globule *b* under the influence of two neighboring globules *a* and *c*.

The influence, however, of all the globules must be taken into account. The charged globules of the disperse phase are distributed more or less homogeneously in the continuous medium. Very short distances between the globules will rarely occur owing to the double layer repulsion.

To calculate the influence of all the surrounding globules on a particular globule *b* a model for the arrangement of the globules has to be assumed. In this model we consider twelve nearest neighbor globules to be situated on a spherical shell $R_{\mathrm{I}}$ with radius $R_1$, and all the other globules to be homogeneously distributed in the space outside a sphere $R_{\mathrm{II}}$ with radius

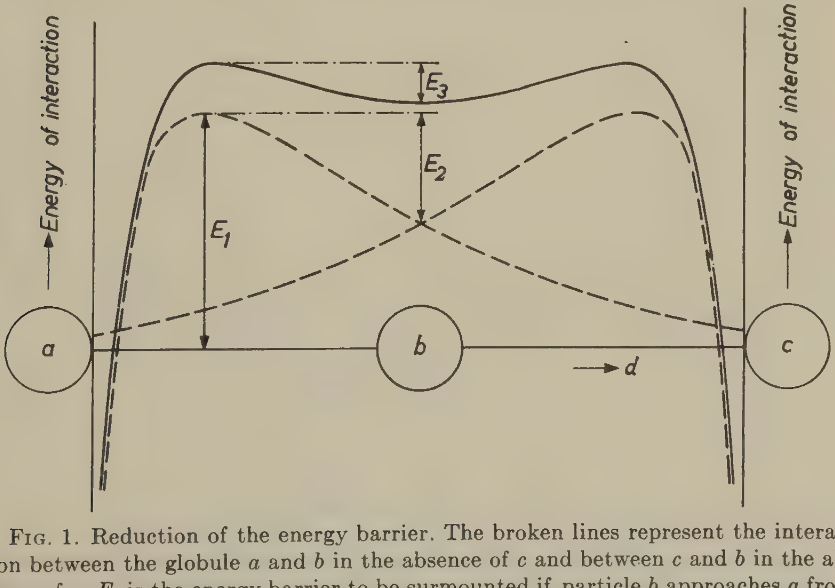

FIG. 1. Reduction of the energy barrier. The broken lines represent the interaction between the globule *a* and *b* in the absence of *c* and between *c* and *b* in the absence of *a*. $E_1$ is the energy barrier to be surmounted if particle *b* approaches *a* from infinity. It is reduced to $E_2$ if *b* is assumed to start from the position in the drawing. It is still further reduced to $E_3$ if the simultaneous interaction with *c* is taken into account. The drawn line is the sum of the two broken lines.

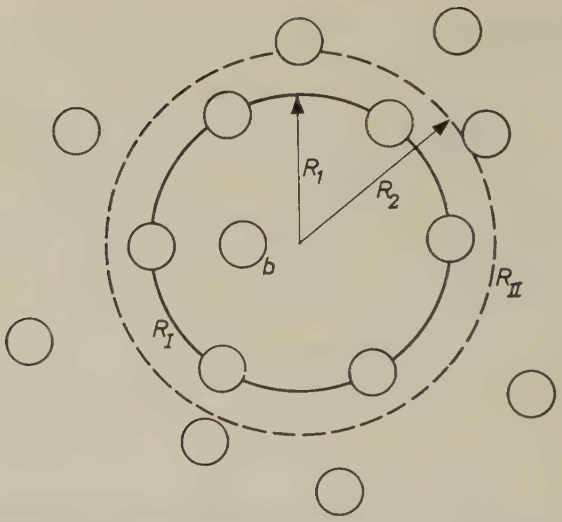

FIG. 2. Distribution of droplets interacting with droplet $b$. Twelve droplets on sphere $R_{\text{I}}$, all other droplets outside sphere $R_{\text{II}}$.

$R_2$ as shown in Fig. 2. The radius $R_1$ is chosen equal to the average distance between the droplets or to the distance they would have in a regular 12 coordinated lattice.

So if $\varphi$ is the volume fraction of spheres with radius $a$

$$\varphi = 0.74 \frac{a^3}{\left(\frac{R_1}{2}\right)^3}$$

or

$$R_1 = \frac{1.81a}{\sqrt[3]{\varphi}}; \qquad [1]$$

and $R_2$ is chosen in such a way that the volume within $R_{\text{II}}$ just corresponds to the volume available to thirteen particles.

$$\frac{4\pi}{3} R_2^3 = \frac{13}{0.74} \frac{4\pi}{3} \left(\frac{R_1}{2}\right)^3$$

or

$$R_2 = 1.3\, R_1 = \frac{2.36a}{\sqrt[3]{\varphi}}. \qquad [2]$$

The energy of interaction between a pair of globules at a distance $x$ between the centers is, according to Verwey and Overbeek (3):

$$V_R = \beta\epsilon a^2 \psi_0^2 \, e^{2ka} \frac{e^{-kx}}{x}, \qquad [3]$$

in which $\psi_0$ is the surface potential, $\epsilon$ is the dielectric constant of the medium, and $\kappa$ is the reciprocal thickness of the double layer. Here, $\beta$ is a factor varying between 0.60 and 1.00 which for simplicity will be put equal to 1.

If the twelve nearest neighbors can occupy any arbitrary position on the sphere $R_{\mathrm{I}}$ the probability of finding one on unit area of the surface is $12/4\pi R_1^2$. Assuming that the droplet $b$ is situated at a distance $q$ from the center of the sphere $R_{\mathrm{I}}$ and using coordinates as given in Fig. 3, the interaction energy of droplet $b$ with the droplets in the surface element $P$ is given by

$$\mathrm{d}V_R = \frac{12}{4\pi R_1^2} R_1 \sin\alpha\,\mathrm{d}\theta \cdot R_1\,\mathrm{d}\alpha \cdot \epsilon\psi_0^2 a^2 \mathrm{e}^{2\kappa a} \frac{\mathrm{e}^{-\kappa x}}{x}. \qquad [4]$$

Observing that $x = \sqrt{R_1^2 + q^2 - 2qR_1\cos\alpha}$ and integrating over $\alpha$ and $\theta$ we find:

$$V_R = 6\epsilon\psi_0^2 a^2 \mathrm{e}^{2ka} \frac{\mathrm{e}^{-\kappa R_1}}{\kappa R_1} \frac{\mathrm{e}^{\kappa q} - \mathrm{e}^{-\kappa q}}{q}. \qquad [5]$$

The assumption incorporated in Eq. [5] that the twelve nearest neighbors can occupy any position on the sphere $R_{\mathrm{I}}$ is not correct for one of the twelve neighbors, viz., for the one with which the droplet $b$ possibly flocculates.

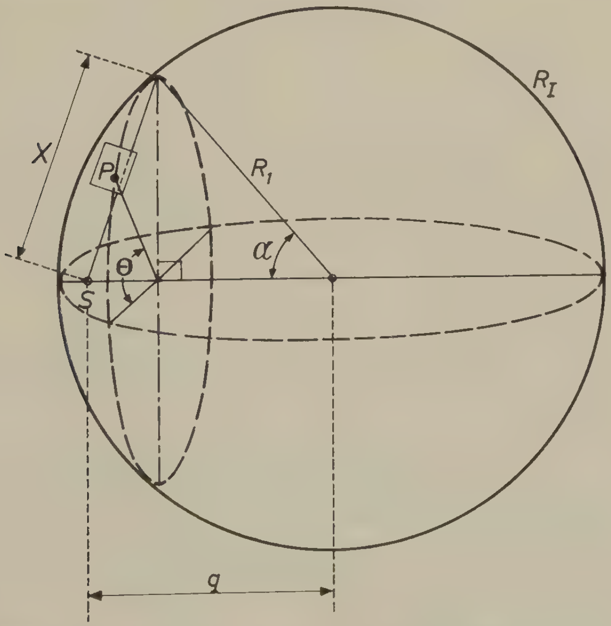

FIG. 3. Interaction of the surface element of the sphere $R_{\mathrm{I}}$ and globule $b$ situated in $S$. Here $x$ and $q$ represent the distances between $S$ and the element $P$ and between $S$ and the center of the sphere, respectively.

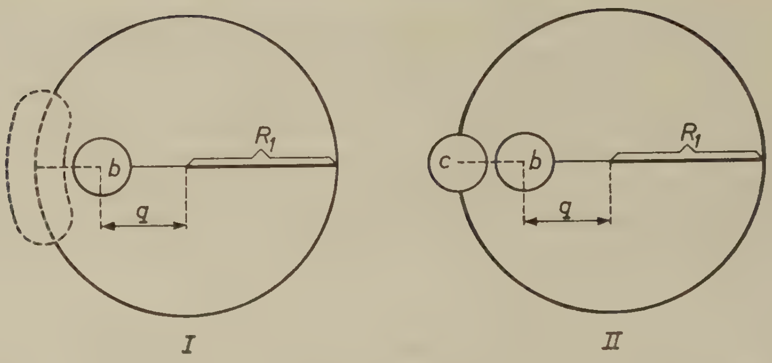

FIG. 4. I. Interaction between globule $b$ and globule $c$ spread over the spherical shell. II. Interaction between globule $b$ and globule $c$ in fixed position.

If we consider, for simplicity, only head-on collisions, this droplet, which we call $c$, has a fixed position as shown in Fig. 4, instead of being spread out over one-twelfth of the surface of the sphere. The interaction with particle $c$ spread out on one-twelfth of the shell has to be subtracted from Eq. [5] and the interaction with $c$ in this fixed position to be added.

An expression for the first effect is easily found by integrating Eq. [4] over $\theta$ from 0 to 2 $\pi$ and over $\alpha$ from 0 to arc cos 5/6.

The final expression for the interaction with the first twelve neighbors is:

$$V_R = \epsilon\psi_0^2 a^2 e^{2\kappa a}\left[\frac{e^{-\kappa(R_1-q)}}{R_1-q} + \frac{6}{\kappa R_1 q}\left\{e^{-\kappa\sqrt{R_1^2+q^2-5/3R_1q}} - e^{-\kappa(R_1+q)}\right\}\right]. \qquad [6]$$

The calculation of the interaction with all nonnearest neighbors is carried out in a similar way by integrating an expression like [4] but now integrating also over the radius of the shell between 1.3 $R_1$ and $\infty$. The proportionality constant has now to be equal to the number of droplets per unit volume. Consequently

$V_R$(nonnearest neighbors) =

$$\frac{0.74}{\frac{4\pi}{3}(R_1)^3}\,\epsilon\psi_0^2 a^2 e^{2\kappa a}\int_{R=1.3R_1}^{\infty}\int_{\alpha=0}^{\pi}\int_{\theta=0}^{2\pi}\frac{e^{-\kappa x}}{x}\,R^2\,dR\,\sin\alpha\,d\alpha\,d\theta\,, \qquad [7]$$

in which $x = \sqrt{R^2+q^2-2Rq\cos\alpha}$. After carrying out the integration and adding the result to Eq. [6] the final expression for the interaction energy of droplet $b$ with all other droplets becomes:

$$V_R(\text{total}) = \epsilon\psi_0^2 a^2 e^{2\kappa a}\left[8.88\,\frac{1.3\kappa R_1+1}{\kappa^3R_1^3}\,e^{-1.3\kappa R_1}\,\frac{e^{\kappa q}-e^{-\kappa q}}{q}\right.$$
$$\left.+\frac{e^{-\kappa(R_1-q)}}{\underline{\underline{R_1-q}}} - \frac{6}{\kappa R_1 q}\left\{e^{-\kappa(R_1+q)} - e^{-\kappa\sqrt{R_1^2+q^2-5/3Rq}}\right\}\right]. \qquad [8]$$

In most cases the underlined term representing the interaction between droplets $b$ and $c$ (see Fig. 4) gives the major effect, but the other terms are by no means negligible. The lowering of the energy barrier in per cent of the value for the simple interaction of two particles is given by:

lowering =

$$\frac{\lim\limits_{R_1\to\infty} V_R\,\mathrm{total}\,(q = R_1 - 2a) - \{V_R\,\mathrm{total}\,(q = R_1 - 2a) - V_R\,\mathrm{total}\,(q = 0)\}}{\lim\limits_{R_1\to\infty} V_R\,\mathrm{total}\,(q = R_1 - 2a)}$$

$$\times\, 100\% = \frac{1200a\,\mathrm{e}^{2\kappa a}}{\kappa R_1(R_1 - 2a}\Bigg\{1.48\,\frac{1.3\kappa R_1 + 1}{\kappa^2 R_1^2}\,\mathrm{e}^{-1.3\kappa R_1} \qquad [9]$$

$$(2\kappa(R_1 - 2a) - \mathrm{e}^{\kappa(R_1-2a)} + \mathrm{e}^{-\kappa(R_1-2a)}) + 2\kappa(R_1 - 2a)\mathrm{e}^{-\kappa R_1}$$

$$+\, \mathrm{e}^{-2\kappa(R_1-a)} - \mathrm{e}^{-\kappa\sqrt{1/3R_1^2-2/3R_1a+4a^2}}\Bigg\}\,\%\,.$$

This lowering is represented in Fig. 5 for different values of the volume fraction $\varphi$ and the reciprocal thickness of the double layer $\kappa$.

Although the calculation is admittedly quite rough, the order of magni-

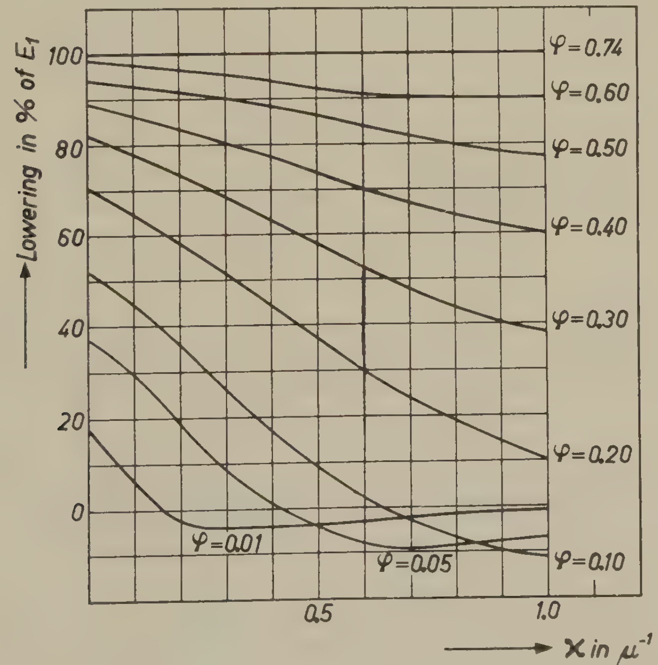

FIG. 5. Lowering of the energy barrier for flocculation in concentrated emulsions expressed in per cent of the energy barrier in an infinitely dilute emulsion. Drop radius $a = 1\mu$.

tude of the effect is quite obvious. A more refined calculation, taking account of the van der Waals attraction, would make the lowering of the barrier more pronounced.

It is evident from Fig. 5 that the concentration influence of the dispersed phase diminishes the stability against flocculation already at low concentration of water in oil, when the reciprocal thickness of the double layer is in the order of 0.1 $\mu^{-1}$. In the cream layer, where the concentration may come close to 74 %, the effect is enormous.

## INFLUENCE OF GRAVITY ON THE STABILITY AGAINST FLOCCULATION

In an emulsion the droplets settle under the influence of a force $f_g$, which equals

$$f_g = \tfrac{4}{3}\pi a^3 g(\rho_i - \rho_e), \qquad [10]$$

where $g$ = acceleration of gravity and $\rho_i$ and $\rho_e$ are the densities of the droplets and the continuous phase, respectively.

This force should be compared to the maximal repulsive force between two particles in order to see whether gravity can accelerate flocculation.

An upper limit for the repulsive force, $f_r$, can be found by differentiation of Eq. [3].

$$f_r = -\frac{dV_R}{dx} = \epsilon a^2 \psi_0^2 e^{2\kappa a} \frac{e^{-\kappa x}}{x}\left(\kappa + \frac{1}{x}\right),$$

in which the factor $\beta$ has been put equal to 1. The maximum value of $f_r$ is obtained for $x = 2a$, the minimum possible value of $x$:

$$(f_r)_{\text{max.}} = \frac{\epsilon \psi_0^2}{4}(1 + 2\kappa a). \qquad [11]$$

TABLE I

*Correlation between the Radius a, the Gravitational Force $f_g$ Acting on the Globules, and the Maximum Slope of the Energy Function between Two Globules as Represented in Column 3*

| 1<br>$a(\mu)$ | 2<br>$\kappa(\mu^{-1})$ | 3<br>$(f_r)_{\text{max.}}$ (*dynes* × $10^{10}$) | 4<br>$f_g$ (*dynes* × $10^{10}$) |
|---|---|---|---|
| 1 | 0.1 | 480 | 5 |
| 1 | 0.3 | 640 | 5 |
| 1 | 1.0 | 1200 | 5 |
| 10 | 0.1 | 1200 | 5000 |
| 10 | 0.3 | 2800 | 5000 |
| 10 | 1.0 | 8400 | 5000 |

In Table I $(f_r)_{\max.}$ and $f_g$ are compared for a number of relevant cases, $f_g$ being calculated for water globules of density = 1.00 in benzene of density = 0.88 and $\epsilon = 2.3$ with $\psi_0 = 80$ mv.

It is obvious from Table I that in the case of water-in-benzene emulsions flocculation occurs as soon as a few to a few hundred droplets of water are situated above each other. For the cumulative weight of a vertical row of droplets acts on the lowest one as soon as the condition

$$\left(\frac{\mathrm{d}V_R}{\mathrm{d}x}\right)_{x=2a+d} \geqq f_g, \tag{12}$$

where $d$ is the distance between the surfaces of the droplets, is satisfied. It usually is if the concentration of the disperse phase is not very low. The globules on the bottom of the vessel must therefore flocculate, even if the disperse phase is homogeneously distributed over the continuous phase.

The figures of column 3 are too high. On the one hand, the van der Waals attraction and the factor $\beta$ (see Eq. [3]) in the formula according to Verwey and Overbeek have not been taken into account. On the other hand, according to Eq. [8] the decay of the energy barrier as a result of the contribution of all the surrounding globules is less steep than in the case of interaction between two globules, for which Eq. [11] has been derived.

## RATE OF FLOCCULATION IN MEDIA OF LOW DIELECTRIC CONSTANT

Since the distance between the globules is generally not very large compared with the thickness of the double layer in oil continuous systems, every globule possesses a higher potential energy than if it were at infinite distance from all other globules. For this reason after flocculation of a number of globules on the bottom of the vessel, the remaining globules act like an expanding spring which accelerates their migration to the bottom of the vessel.

Moreover, every globule is forced downwards under the action of the cumulative weight of all globules lying above, as has already been pointed out. So the velocity with which the globules sink is some orders higher than the velocity of a globule that settles out under the influence of its own weight alone.

Consequently a very rapid flocculation occurs until the remaining bulk concentration of the disperse phase is very small; i.e., until the distance between the globules has become large with regard to the thickness of the double layer.

## Conclusion

Flocculation by Brownian motion as well as under the influence of gravity is strongly promoted and proceeds very rapidly in oil continuous systems, if the concentration of the dispersed charged globules is not very low.

## References

1. Albers, W., and Overbeek, J. Th. G., *J. Colloid Sci.* **14,** 501 (1959).
2. Verwey, E. W. J., *Trans. Faraday Soc.* **36,** 192 (1940).
3. Verwey, E. W. J., and Overbeek, J. Th. G., "Theory of the Stability of Lyophobic Colloids," p. 84. Elsevier, New York, Amsterdam, 1948.

JOURNAL OF COLLOID SCIENCE **14**, 519–523 (1959)

# NONIONIC SURFACE-ACTIVE AGENTS

## II.[1] Time Dependence of Micellar Breakdown

**Paul Becher and Nancy K. Clifton**

*Chemical Research Department, Atlas Powder Co., Wilmington, Delaware*

*Received March 30, 1959; revised May 25, 1959*

### Abstract

The existence of nonequilibrium states in micellar solutions, described by Nash, has been confirmed in aqueous and nonaqueous solutions of nonionic surface-active agents by a light-scattering method.

### Introduction

Recently, Nash (1–3) has shown that nonequilibrium states may exist in micellar solutions of cationic detergents. The existence of such nonequilibrium states was established by observations on foam viscosity and by means of fluorometry. In the course of an extensive study on the light-scattering properties of solutions of nonionic surface-active agents, we have confirmed this finding with respect to this class of materials, both in aqueous and in nonaqueous solvents.

### Methods and Materials

The light-scattering determinations were carried out in a conventional Brice-Phoenix Light-Scattering Photometer[2] using the standard 40 × 40 × 120 mm. semioctagonal cell. Measurements were carried out at 436 m$\mu$. Solutions, or in the dilution experiments, solvent, were clarified by pressure filtration under dry nitrogen through a Corning UF (ultrafine) sintered glass disc. The usual precautions to exclude dust and other extraneous matter were taken.

The materials the light-scattering characteristics of which are reported herein were a commercial polyoxyethylene (23) lauryl alcohol[3] and a commercial sorbitan monostearate.[4] The latter material was purified to the extent that most of the free polyol was removed by extraction, rendering the sorbitan monostearate completely benzene-soluble. Solvents employed were distilled water and freshly distilled reagent grade benzene.

---

[1] Paper I in this series: P. Becher, *J. Phys. Chem.*, to be published.

[2] Phoenix Precision Instrument Co., Philadelphia, Pennsylvania.

[3] Brij 35, Atlas Powder Co.

[4] Span 60, Atlas Powder Co.

## RESULTS AND DISCUSSION

In general, there are two principal procedures whereby light-scattering measurements may be carried out. These may be conveniently designated the "dilution" and the "solution" methods. In the first, a filtered concentrated solution is introduced into the scattering cell, and subsequent concentrations are obtained by dilution in the cell with filtered solvent. In the second method, a series of solutions are made up (possibly by step-wise dilution of a more concentrated solution) and each solution is filtered directly into the cell.

The principal difference, of course, is in the fact that if equilibration of the solutions is required only the second method is appropriate. On the other hand, it appears likely that many light-scattering investigations have been in fact carried out by the "dilution" method.

Light-scattering measurements were carried out on a water-soluble and an oil-soluble nonionic agent by both techniques. The solutions prepared by the "solution" technique were allowed to equilibrate for 18–24 hours.

The results of the measurements on the water-soluble polyoxyethylene (23) lauryl alcohol are shown in Fig. 1. The data obtained by the solution method (circles) give a classic type of turbidity-concentration curve for surface-active agents, with a well-defined break corresponding to a CMC of 0.014 g./dl. and extrapolating to the solvent turbidity in a perfectly normal

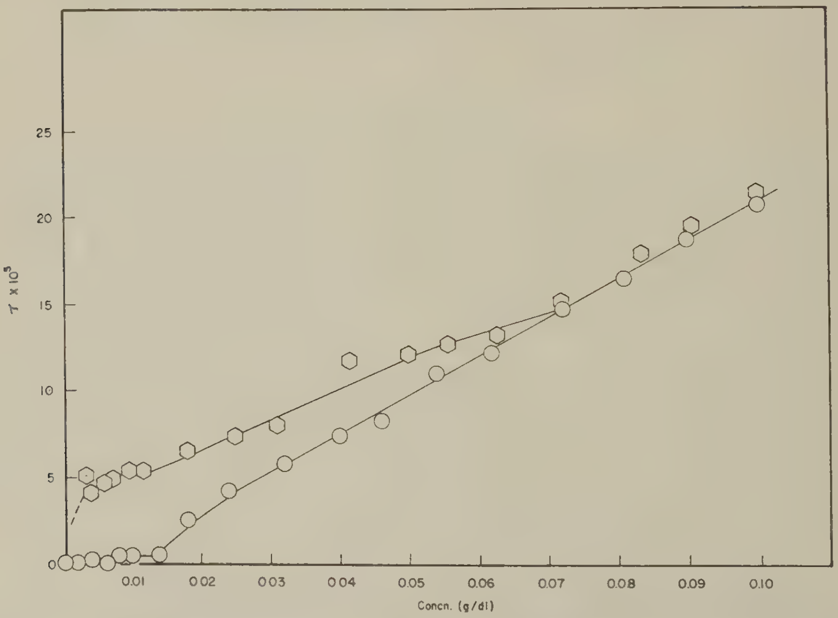

FIG. 1. Turbidity-concentration curve for polyoxyethylene (23) lauryl alcohol in aqueous solution. ○—"Solution" method. ⬡—"Dilution" method.

manner. On the other hand, the data obtained by the "dilution" method (hexagons), although coinciding at the higher concentrations, show a progressive deviation in the direction of higher turbidities as the CMC is approached.

Less extensive data were obtained for the oil-soluble agent, presented in Fig. 2. However, it is clear in this case also that different turbidity-concentration curves are obtained by the two methods. The slight upward slope at concentrations below the CMC for the "solution" method curve may possibly indicate that even 24 hours was insufficient time for complete equilibration, although alternate explanations suggest themselves.

These data are consistent with the existence of a time-dependent demicellization process, as proposed by Nash. Quite evidently, nonequilibrium solutions containing an appreciable concentration of micelles may exist at concentrations below the CMC.

The wide divergence in turbidity obtained in the nonaqueous system on dilution (Fig. 2) probably indicates that the demicellization rate is even slower in nonaqueous solvents than in aqueous. On the other hand, Nash (3) has suggested that if a large dilution is made, i.e., from appreciably above the CMC to appreciably below, equilibrium ought to be established quickly. In one rough experiment, this was done for the aqueous system, and it was found that a minimum of 3 hours was required in order to get an equilibrium value for the 90° light scattering.

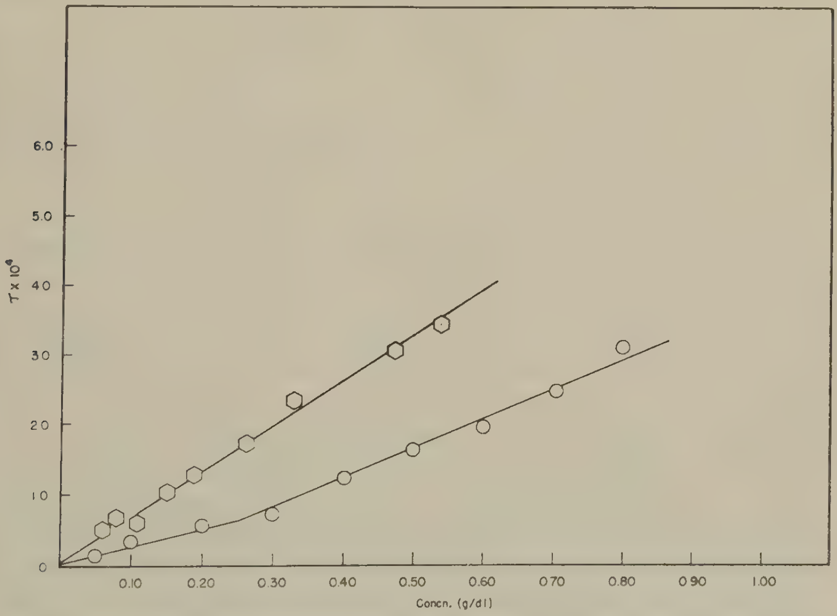

FIG. 2. Turbidity-concentration curve for sorbitan monostearate in benzene solution. ○—"Solution" method. ⬡—"Dilution" method.

It is interesting to note that the systems reported herein are characterized by a rather slow development of *surface* equilibrium, as measured by surface tension lowering. This effect has been interpreted as representing a combination of diffusion and orientation processes (4). However, it would appear that when these effects are of more than a matter of seconds duration, it is the latter process which is governing. It would be interesting to examine solutions of agents which are known to reach surface equilibrium quickly in order to see if a relation exists between the two phenomena.

Aside from the purely theoretical interest of this phenomenon, it should be pointed out that these observations raise questions about the validity of some micellar molecular weights reported in the literature. To be sure, most of these data relate to anionic compounds, and this phenomenon may be absent or very small in that case. However, if it does exist, the result of such measurements would be to give micellar molecular weights which are too low, since $\tau_0$, the turbidity at the CMC, would be too high, and the net (solute) turbidity too low.

For example, the "solution" data of Fig. 1 yield a micellar molecular weight of 48,800, whereas the "dilution" data give a value of 37,000. This is, of course, a considerable discrepancy. More complete data on these, and other, compounds will be given in a subsequent publication.

In addition, it is possible that the "monomer saturation concentration" observed to exist above the CMC by Kushner and Hubbard (5) in a light-scattering investigation of a polyoxyethylene octyl phenol is an artifact arising from examination of nonequilibrium solutions.

*Note:* The referees have suggested two alternate explanations of the phenomena reported. These are: (*1*) that the phenomena are attributable to incipient crystallization, the degree of incipiency differing with the mode of preparation of the solution; and (*2*) that the phenomena are attributable to solubilization of "impurities" in the micelle, and that this, too, depends somewhat on the mode of preparation of the solutions.

The first of these may be readily disposed of. Incipient crystallization is possible only in a poor solvent. All the observations on the polyoxyethylene (23) lauryl alcohol were made at concentrations of less than 0.10 g./dl. However, this material is completely soluble in water at 25°C. at concentrations above 10 g./dl. Ordinarily, sorbitan monostearate contains a polyol component which is not benzene-soluble. However, this is readily removed by extraction with ethyl acetate, and the thus-purified material is soluble up to concentrations much higher than the minimum of 1.0 g./dl. used.

The second alternate explanation is not so readily disregarded, because of the semantic haze surrounding the word "impurity" when used with reference to compounds of this nature. Nonionic surface-active compounds are, by their nature, heterogeneous mixtures of compounds of differing surface activities. But, and this is most important, our investigations have shown that if they are heterogeneous, they are reproducibly so. In other words, the surface properties (including light scattering by micellar solutions) exhibited by one sample of Brij 35 are exhibited by another sample to within very narrow limits. Thus, from one point of view, they may be regarded as "pure," even if heterogeneous, compounds.

Obviously, however, mixed micelles are formed (although again here the distinction between a mixed micelle and a micelle containing solubilizate remains somewhat hazy). That it is the existence of these mixed micelles which is the cause of the nonequilibrium states is a possibility which it would be impossible to deny, but this is not the same thing as regarding our observations as an artifact arising in *some* way from the existence of these micelles.

A proper method of clarifying this point would be a study of a *homogeneous* nonionic compound of the type examined here. This we propose to do in the near future.

## REFERENCES

1. NASH, T., *J. Appl. Chem.* **8,** 440 (1958).
2. NASH, T., *Nature* **182,** 1536 (1958).
3. NASH, T., *J. Colloid Sci.* **14,** 59 (1959).
4. ADDISON, C. C., *Nature* **156,** 600 (1945).
5. KUSHNER, L. M., AND HUBBARD, W. D., *J. Phys. Chem.* **58,** 1163 (1954).

JOURNAL OF COLLOID SCIENCE **14**, 524–532 (1959)

# BLOCK AND GRAFT COPOLYMERS[1]

## III. APPARENT DISSOCIATION CONSTANTS OF COPOLYMERS OF ACRYLIC ACID AND ACRYLAMIDE

**M. L. Miller and C. E. Rauhut**

*Polymer Research Department, Research Division Stamford Laboratories, American Cyanamid Company*

*Received February 17, 1959; revised May 21, 1959*

### Abstract

The apparent dissociation constant of block, graft, and random copolymers of acrylamide and acrylic acid and of branched and linear polyacrylic acid has been measured by electrometric titrations in 0.1 $N$ sodium chloride solution. Block copolymers have the same acid strength as linear homopolymers. Random copolymers are stronger acids than linear homopolymers, and graft and branched polymers are weaker acids. Reasons for the difference in apparent acid strength between branched and linear polyacrylic acids have been considered.

### Introduction

This work is part of a study of block and graft copolymers of acrylamide and acrylonitrile and acrylamide and acrylic acid. The study attempts to relate changes in the arrangement of the monomer units in the molecule to changes in representative physical chemical properties. Previous papers in the series described the preparation of block and graft polymers and reported on their softening points and intrinsic viscosities (1, 2). This paper presents a study of the effect of changes in the number and arrangement of the carboxyl groups on the acid dissociation constant of polyacrylic acid in copolymers with acrylamide. Measurements of the apparent dissociation constant of linear and branched polyacrylic acid are included because the behavior of copolymers cannot be interpreted without knowledge of the behavior of the component homopolymers. Studies on branched and linear polyacrylamide have been reported (3).

### Experimental

#### *Preliminary Tests*

Luttinger (4) and Gregor, Luttinger, and Loebl (5) found that in the titration of polyacrylic acid the pH, especially near half neutralization, does not reach equilibrium immediately but requires hours to become constant. Before starting our work preliminary experiments to look into this "time effect" were carried out.

---

[1] Presented at the 134th meeting of the American Chemical Society, Chicago, Illinois, September 7–12, 1958.

The first preliminary test was a titration of polyacrylic acid of molecular weight 140,000 in a nitrogen atmosphere with a Beckman pH meter reading to 0.02 pH unit. Measurements of pH were taken at intervals of 0.4 to 0.6 pH unit. At each of these points the pH was followed for periods of 18 to 65 hours. At the end of the test the calibration of the electrodes, which remained in the solution during the entire titration, was found to be unchanged. To prevent evaporation, the vessel containing the solution was sealed with Parafilm during the waiting period. The results of this test showed that, as previously reported (4), the pH does require time to reach a constant value and that the largest fall in pH with time, 0.12 pH unit, occurred between pH 4 and 6. The data showed that, with the technique used here, a time lapse of 4 hours was sufficient to attain a constant pH reading (i.e., one that remained unchanged for at least 60 hours).

To rule out the possibility that the "time effect" was a result of adsorption of gas or polymer on the electrodes (6), a second preliminary experiment was carried out. In this experiment a North American Phillips Universal pH Meter, Model G, reading to 0.002 pH unit was used. This apparatus was equipped with a glass electrode, a saturated calomel electrode, and a saturated KCl salt bridge. The junction between the salt bridge and the solution to be titrated was made through a porous stone plug which was bathed, during the course of the measurements, by a minute flow of saturated KCl solution. The entire test was run in a nitrogen-filled chamber under a slight positive pressure of nitrogen. Nitrogen was not bubbled through the sample. Varying amounts of 0.1 *N* sodium hydroxide were added to beakers containing identical solutions of polyacrylic acid (molecular weight 140,000) dissolved in water. The solutions were vigorously stirred, the stirring was stopped, and the pH readings were taken. The electrodes (both glass and calomel) were removed, thoroughly washed, and stored in distilled water. The beakers containing the solutions were covered tightly with Parafilm and set aside. At the end of 5 hours the pH was read again. As in the first preliminary test, the pH dropped on standing, and the maximum change, 0.115 pH unit, occurred between pH 4 and 6.

The results of this experiment showed that the fall in pH with time was not a result of adsorption of polymer or bubbles on the electrodes. The rate of fall in pH between the initial and final reading depended on the size of the increments of base added. When the sodium hydroxide was added in small increments as in the first preliminary test the drop in pH at each point was complete in 3 to 4 hours. When all the sodium hydroxide required to reach a given pH was added at once as in the second preliminary experiment, at least 24 hours were required to attain a constant pH reading.

An additional experiment on a branched sample of polyacrylic acid showed that with the first technique 4 hours was also sufficient to attain a constant pH reading with branched polyacrylic acid.

### *Titrations*

Titrations were carried out in a "dry box" under nitrogen. A North American Phillips pH meter reading to 0.002 pH unit was used in all except one of the titrations. As an additional check against the possibility of instrumental error, a pH meter made by the Cambridge Instrument Company, and also reading to 0.002 unit, was used in one titration. The results of this titration differed in no way from results with the Phillips pH meter. Solutions were stirred vigorously with a glass rod before all readings. Over the pH range 4 to 6 or 6½, readings were taken immediately after adding sodium hydroxide solution and again 4 to 5 hours later. Usually four of these "timed" pH measurements were made at approximately equal pH intervals. In going from one "timed" pH to another, sodium hydroxide solution was added in small increments and readings were taken at once as in ordinary titration.[2]

During the waiting period the vessel containing the solution was covered with Parafilm to prevent evaporation. The calibration of the apparatus (meter plus electrodes) was checked at the beginning and at the end of each titration to be sure that the calibration remained constant throughout the titration which lasted 2 to 4 days. There was no difference between titrations run in a constant-temperature room at 24° ± 1°C. and at room temperature.

Since it was desired to work at approximately constant ionic strength, solutions of polyacrylic acid were made up in 0.1 *N* sodium chloride solution. For each titration 0.3 g. of polyacrylic acid was dissolved in 150 ml. of 0.1 *N* sodium chloride solution (copolymer solutions were made up on the basis of the acid content, i.e., 0.6 g. of a 50/50 copolymer was dissolved in 150 ml.). Titration was with 0.1000 ± 0.0002 *N* carbonate-free sodium hydroxide.

---

[2] It was found that over a small pH interval "untimed" readings could be corrected for the time effect as follows: Given timed pH readings, $\text{pH}_1$ and $\text{pH}_2$, and an untimed reading, $\text{pH}_x$, such that $\text{pH}_1 < \text{pH}_x < \text{pH}_2$ and given $\Delta\text{pH}_1$ and $\Delta\text{pH}_2$, the differences between the initial and 4-hour readings at $\text{pH}_1$ and $\text{pH}_2$, respectively. A linear interpolation between $\Delta\text{pH}_1$ and $\Delta\text{pH}_2$ gives $\Delta\text{pH}_x$, which is the difference between the initial and 4-hour reading which would have been observed if a timed reading had happened to fall at $\text{pH}_x$. Since the time effect depends on the size of the interval between timed readings, the correction to be applied to the untimed reading $\text{pH}_x$ is not $\Delta\text{pH}_x$ but $\Delta X$ where

$$\Delta X = \frac{\text{pH}_x - \text{pH}_1}{\text{pH}_2 - \text{pH}_1}\,\Delta\text{pH}_x\,.$$

### *Preparation and Characterization of Polymers*

Block and graft polymers were prepared as described in references 1 and 2. The block polymers consisted of two or three long blocks and the graft polymers had polyacrylamide backbones and polyacrylic acid branches. Linear polyacrylic acids and linear random copolymers were made by polymerization in water at 30°C. with a persulfate-bisulfite catalyst. Conversion in these copolymers was to 20% or less. The composition of the copolymers was determined by infrared examination. Branched polyacrylic acid was made by first polymerizing acrylic acid in the presence of a small amount of $N,N'$-methylenebisacrylamide to form a gel. The gel was later broken to soluble polymer by treatment with ultrasonics. A typical polymerization used:

5 g. of glacial acrylic acid
125 ml. of oxygen-free water
10 ml. of catalyst A (0.30 g. ammonium persulfate in 50 ml. water)
10 ml. of catalyst B (0.06 g. sodium metabisulfite in 50 ml. water)
13 mg. $N,N'$-methylenebisacrylamide.

The above ingredients were cooled to 0 to 2°C., mixed and left at 7°C. overnight. The supernatant liquid was decanted from the gel that formed in the flask. The gel was dispersed in twice its volume of water, broken up by a laboratory blendor, and after settling, the supernatant solution was decanted. The gel was washed three times with water and then dispersed in an equal volume of water. The dispersion was treated with a Raytheon ultrasonic generating unit at 30°C. The setting was 9 kc. at 80 v. and 0.6 of the maximum power. After 2 hours, approximately 90% of the gel was broken to soluble polymer. The product was filtered twice through two thicknesses of Whatman #1 filter paper to give a clear solution which was freeze-dried. To be sure that this clear filtered solution did not contain finely dispersed gel or microgel, one preparation was spun in a Model L, Spinco Preparative Ultracentrifuge at an average of 90,000 times gravity for 1 hour. This treatment gave no sediment. The polymer had an intrinsic viscosity of 0.38 dl./g. in dioxane at 30°C. The weight-average molecular weight, determined by light scattering, was 470,000. A linear polyacrylic acid of molecular weight 490,000 would have an intrinsic viscosity of 0.65 (7). On the basis of the theory of Zimm and Stockmayer (8), this acid may be estimated to have, on the average, 3.5 trifunctional branches per molecule. The theory of Zimm and Stockmayer has been found to give reasonable values for the number of branches in polyacrylamide (3) but low values for branching in polyethylene (9).

The molecular weights of the linear polyacrylic acids were estimated from intrinsic viscosities in dioxane at 30°C. by use of the data of Newman *et al.* (7). The molecular weights of random copolymers were estimated from

TABLE I

*Polymers Studied*

| Type polymer | Mol. % acrylic acid | Weight-average molecular weight × $10^{-3}$ |
|---|---|---|
| Linear | 100 | 140 |
| Linear | 100 | 22 |
| Random 4 | 26.5 | 46 |
| Random 5 | 59 | 195 |
| Graft B | 62 | 270 |
| Graft A | 15 | 90 |
| Block | 10 | 2000 |
| Branched 7 | 100 | >165 |
| Branched 8 | 100 | 470 |

intrinsic viscosities in 1 $N$ sodium nitrate at 30°C. by use of plots, prepared by Dr. W. A. Barber,[3] which relate the intrinsic viscosity of partly hydrolyzed samples of polyacrylamide in sodium nitrate solution to molecular weight.

Table I summarized the polymers used in this study. All polymers were freeze-dried from water under vacuum for 2 days and further dried in a vacuum oven at 50°C. for 2 to 3 hours. The samples were rapidly weighed in air.

## RESULTS

### *Titration Data*

Table II summarizes the titration data. The table gives values of pH + log $(1 - \alpha)/\alpha$ (where $\alpha$ is the fraction of the acid neutralized) at rounded values of $\alpha$. These figures were taken from smooth plots that fitted the data, over the range of $\alpha$ values from 0.15 to 0.85, with the average deviations shown in the last column of the table. A straight line could not be fitted to the measurements except over the narrower range between $\alpha = 0.3$ and $\alpha = 0.7$. The curvature in the plots of pH + log $(1 - \alpha)/\alpha$ for polymeric acids has been pointed out by Arnold (10). Table II shows that random copolymers of acrylamide and acrylic acid are stronger acids than homopolymers of acrylic acid and that the acid strength increases as the per cent of acrylamide in the copolymer increases. This is to be expected. The acid strength of polyacrylic acid is independent of molecular weight and is the same for block copolymers and homopolymers. Therefore, a single curve has been drawn through the data for the block copolymer and the homopolymers. This is referred to in the table as "composite."

[3] We are indebted to Dr. W. A. Barber for permission to use these data prior to publication.

TABLE II

*Summary of Titration Data*

| $\alpha$ | 0.2 | 0.3 | 0.4 | 0.5 | 0.6 | 0.7 | 0.8 | Average deviation |
|---|---|---|---|---|---|---|---|---|
| | Values of pH + log $[(1 - \alpha)/\alpha]$ | | | | | | | |
| *Sample* | | | | | | | | |
| Composite[a] | 4.66 | 4.77 | 4.87 | 4.99 | 5.13 | 5.28 | 5.45 | 0.04 |
| Random 5 | 4.65 | 4.73 | 4.83 | 4.93 | 5.04 | 5.15 | 5.28 | 0.01 |
| Random 4 | 4.51 | 4.53 | 4.55 | 4.58 | 4.60 | 4.63 | 4.68 | 0.02 |
| Graft 15% | 4.64 | 4.81 | 4.98 | 5.16 | 5.36 | 5.58 | 5.81 | 0.01 |
| Graft 60% | 4.88 | 5.04 | 5.23 | 5.41 | 5.60 | 5.81 | 6.04 | 0.02 |
| Branched 8 | 4.76 | 4.89 | 5.02 | 5.15 | 5.27 | 5.39 | 5.52 | 0.03 |
| Branched 7 | 4.75 | 4.92 | 5.08 | 5.26 | 5.45 | 5.64 | 5.83 | 0.02 |

[a] Single curve drawn through the data on the block copolymer and the homopolymers of molecular weight 22,000 and 140,000.

Table II shows that graft polymers are weaker acids than block polymers or homopolymers and that acid strength decreases as the number of grafts increases. This result is unexpected and must be associated with the branched structure of the graft polymer. This interpretation is supported by the data in the last two lines of Table II, which gives titration data for branched samples of polyacrylic acid. These data show that branched polyacrylic acid is weaker than linear polyacrylic acid and that the difference increases as the extent of branching increases.

This observation is reminiscent of the decrease in acid strength with increased number of cross links which Fisher and Kunin (11) observed in studies on gels of polyacrylic acid and of polymethacrylic acid.

The values in Table II are not pK values because there is as yet no completely satisfactory way to compute the dissociation constants of polymeric acids. The average dissociation constant at a given value of $\alpha$ cannot be computed by the equation used for computing the dissociation constant of monomeric acids, i.e.,

$$\text{pK} = \text{pH} + \log \frac{1 - \alpha}{\alpha}. \qquad [1]$$

Equation [1] is not correct because (*a*) it neglects the statistical effect (12) and (*b*) it neglects cation binding. The statistical effect is absent at $\alpha = 0.5$ and relatively small over the range $\alpha = 0.2$ to 0.8. Workers in the field of polyelectrolytes disagree as to whether any or all of the ion binding is binding at a site or a diffuse trapping of the ions in the coils of the polymer molecule; nevertheless experiments on osmotic pressure (13), transference (14), and diffusion (15) show that approximately 60% of the sodium ions in sodium polyacrylate *act as if* they are bound to the polymeric anion. If pK values are to be compared with theoretical predictions, Rice and Harris (16) point out, ion binding must not be neglected.

When values of pH + log $(1 - \alpha)/\alpha$ for homopolymers and copolymers of acrylic acid are plotted against $\alpha$, the lines converge to a common value, $4.45 \pm 0.05$, at $\alpha = 0$. This value is the dissociation constant, in 0.1 *N* sodium chloride, of a single carboxyl group in polyacrylic acid when it is removed from the influence of neighboring ionized carboxyls. This value of $pK_{\alpha=0}$ is 0.1 of a pK unit lower than the $pK_{\alpha=0}$ of propanoic acid in 0.1 *N* sodium chloride solution. This difference could be due to the presence of a liquid junction in the titration or it could, more likely, represent a real difference between the intrinsic dissociation constants of a carboxyl in polyacrylic and in propanoic acid.

### *The "Time Effect"*

Before considering possible reasons for the difference in apparent acid strength between linear and branched polyacrylic acid, let us examine the time effect. The preliminary experiments showed that the time effect depends on the way in which the experiment is carried out. If the increments of base between timed readings are small, a constant pH reading is attained more rapidly than when large increments of base are added. When a series of titrations uses the same technique it is possible to compare the magnitude of the fall in pH between the zero and 4-hour readings, ΔpH, for different polyacids. Examination of the titration data shows that ΔpH depends on molecular weight. The maximum value of ΔpH, i.e., ΔpH (max.) for a sample of polyacrylic acid of molecular weight 140,000 titrated in 0.1 *N* NaCl was 0.1 pH unit, whereas for a sample of molecular weight 22,000 ΔpH (max.) was only 0.02 unit. For branched polymers ΔpH (max.) was approximately one-half as large as ΔpH (max.) for linear polymers of the same molecular weight. No time effect was observed when HCl was added to a solution of sodium polyacrylate. In a back titration in which the end point occurred in 0.1 *N* sodium chloride the pH increased 0.002 unit in 4 hours; in the forward titration of this same acid the pH dropped 0.060 of a pH unit between the zero and the 4-hour reading.

## DISCUSSION

Any explanation for the difference in apparent acid strength between branched and linear polyacids must be consistent with the "time effect" and should, if possible, explain both phenomena. The first explanation that comes to mind is as follows.

When polyacrylic acid is neutralized the molecule expands. If the expansion were not instantaneous the increased distance between the carboxyls could account for the "time effect." Since branched molecules are more compact than linear molecules the closer packing of carboxyls in branched molecules might, similarly, explain the difference in pK between branched and linear polyacrylic acids. However, this explanation for the time effect is untenable because there is no change in viscosity during the time when the pH is changing most rapidly. This explanation is also untenable for the effect of branches because experiments show that with homopolymers the pK is independent of molecular weight. This means that the dissociation of a given carboxyl is influenced by carboxyls which are neighbors, or near neighbors, in the polymer chain but not by carboxyls on nearby loops of the molecules.

A second explanation of the apparent difference in acid strength between branched and linear polyacids is based on the fact that the more compact structure of the branched molecule results in a greater density of paraffinic units around the dissociating carboxyl. Therefore the internal dielectric constant of the branched acid is lower than the internal dielectric constant of a linear acid. This explanation for the effect of branching on apparent acid strength is acceptable but it contributes nothing to the theory of the "time effect."

It seems likely that neither of the above explanations is correct. When alkali is added to a solution of a linear polyacid the molecules of which are random coils the carboxyls on the outside of the coil are neutralized first. The carboxyls in the interior of the coil may, on the other hand, be very slow to react.

In a linear molecule segmental diffusion would, *in time*, bring carboxyls originally in the interior to the surface of the molecule. This could explain the "time effect." In branched molecules, some of the interior carboxyls cannot diffuse to the surface of the molecule because the branched structure is tied together by chemical bonds. Therefore some of the carboxyls could be, in effect, buried in the interior of the molecule. This could account for the apparently lower acid strength of branched polyacids.

Recently Dux and Steigman (17) advanced a somewhat similar idea to explain their observations on the molecular weight dependence of diffusion in polymer solutions.

## ACKNOWLEDGMENTS

The authors wish to express their appreciation to Dr. G. F. Sheats and Miss R. Lewis for the light-scattering measurements on the branched polymers and to Dr. L. B. Luttinger for helpful discussion.

## REFERENCES

1. MILLER, M. L., *Can. J. Chem.* **36**, 303 (1958).
2. MILLER, M. L., *Can. J. Chem.* **36**, 309 (1958).
3. GLEASON, E., MILLER, M. L., AND SHEATS, G. F., Paper presented at the 137th meeting of the American Chemical Society, San Francisco, California, April 17, 1958.
4. LUTTINGER, L. B., Dissertation, Brooklyn Polytechnic Institute, 1954.

5. Gregor, H. P., Luttinger, L. B., and Loebl, E. M., *J. Phys. Chem.* **59,** 34 (1955).
6. Gregor, H. P., and Frederick, M., *J. Polymer Sci.* **23,** 451 (1957).
7. Newman, S., Krigbaum, W. R., Laugier, C., and Flory, P. J., *J. Polymer Sci.* **14,** 451 (1954).
8. Zimm, B. H., and Stockmayer, W. H., *J. Chem. Phys.* **17,** 1301 (1949).
9. Billmeyer, F. W., Jr., *J. Am. Chem. Soc.* **75,** 6118 (1953).
10. Arnold, R., *J. Colloid Sci.* **12,** 549 (1957).
11. Fisher, S., and Kunin, R., *J. Phys. Chem.* **60,** 1030 (1956).
12. Gregor, H. P., *Trans. N. Y. Acad. Sci.* [11] **18,** 667 (1956).
13. Kern, W., *Z. physik. Chem.* **A181,** 249, 283 (1938); *ibid.* **A184,** 197, 302 (1939).
14. Huizenga, J. R., Grieger, P. F., and Wall, F. T., *J. Am. Chem. Soc.* **72,** 2636 (1950).
15. Huizenga, J. R., Grieger, P. F., and Wall, F. T., *J. Am. Chem. Soc.* **72,** 4228 (1950).
16. Rice, S. A., and Harris, F. E., *J. Phys. Chem.* **58,** 725 (1954).
17. Dux, J. P., and Steigman, J., *J. Phys. Chem.* **62,** 288 (1958).

JOURNAL OF COLLOID SCIENCE **14**, 533–542 (1959)

# DIFFUSION OF STRONTIUM IN ION-EXCHANGE MEMBRANES

**J. de Lopez-Gonzalez[1] and Hans Jenny**

*University of California, Berkeley, California*

*Received August 15, 1958; revised June 12, 1959*

## Abstract

Cation-exchange membranes containing various proportions of $Sr^{++}$ and $H^+$ were permitted to interact. If the membranes are brought into direct contact, transfer of radioactive strontium is rapid, but if the membranes are kept separated so that migration of ions must proceed via solution, Sr transfer is exceedingly slow.

The rate of diffusion of Sr inside the membranes depends on the degree of Sr saturation. In membranes fully saturated with Sr the self-diffusion coefficient is $1.3 \times 10^{-8}$ cm.$^2$/sec. The activation energy is 6600 cal./mole.

## Introduction

Amberplex-C-1 is a cation-exchange membrane manufactured by Rohm and Haas Co., Philadelphia, Pennsylvania. The negative charges are incorporated in the rigid framework, mainly as sulfonic acid groups. They are neutralized by cations which are exchangeable and which possess considerable mobility, even in the absence of electric fields. The cation-exchange component is cross linked with approximately 8%–9% divinylbenzene.

Since these artificial membranes resemble natural membranes (e.g., cell walls of roots) in certain diffusion properties we have determined diffusion coefficients of Sr and their dependency on temperature.

## Preparation of Membranes

*H-membranes.* Commercial Na-membranes were converted to H-membranes by leaching with normal HCl. They were then rinsed in distilled water until free from chlorides.

In the wet, swollen stage, H-amberplex is 0.80 mm. thick. If quickly "dried" between filter paper and immediately placed on a balance, 1 cm.$^2$ of moist membrane (counting one exposed surface only) weighs 0.0746 g. Its weight after oven-drying at 110° C. is 0.0493 g.

With neutral salts the H ions can be readily replaced in accordance with ion-exchange principles. The maximum quantity of H liberated amounts to 0.127 meq. per 1 cm.$^2$, or 2.57 meq. per gram of oven-dry membrane.

---

[1] Universidad de Granada y Junta de Energia Nuclear, Spain.

It represents the exchange capacity of the membrane. The equivalent volume of an exchange site in a wet H-membrane is 1040 A.$^3$ The mean distance between two exchange sites is therefore 10 A. If the exchangeable cations are considered dissolved in the liquid phase (33% of moist membrane) their concentration would amount to 4.7 normal. The mean distance between two ions would be 7 A. Pressing a glass electrode assembly upon a wet H-membrane yields pH readings of 1.4–2.4. As explained elsewhere (1), these measurements may be strongly affected by junction potentials.

The acidity of the membranes is reduced by adding bases. The percentage fraction of H ions neutralized is designated as *degree of saturation* (D.S.).

*Sr-membranes.* To H-membranes was added $Sr(OH)_2$ in desired amounts. The base had been prepared by electrodialysis of $SrCl_2$, and it was stored in absence of $CO_2$. The stock solution of $Sr(OH)_2$ was tagged with carrier-free $Sr^{85}$ ($\gamma$-radiation). After a reaction time of 24 hours the supernatant liquid contained but a very small fraction of the Sr added. Specifically, a disc having a diameter ($\phi$) of 2.08 cm., suspended in 100 ml. of solution containing 390 $\mu$eq. of Sr sorbed all but 0.36 $\mu$eq. Sr. The degree of saturation was then 90%. The same disc at a D.S. of 5% (23.5 $\mu$eq. Sr) left only 0.015 $\mu$eq. in the 100 ml. of solution.

All Sr determinations to be reported are based on radioactive counting. However, asterisks will be assigned to Sr in self-diffusion experiments only.

## TRANSFER OF STRONTIUM FROM ONE MEMBRANE TO ANOTHER VIA SOLUTION AND BY CONTACT

An H-membrane placed in a solution which is in equilibrium with an Sr-membrane will sorb the dissolved Sr and become a H-Sr-membrane. If vigorous agitation is provided—but care is taken that the H-membrane never touches the Sr-membrane—the rate of Sr transfer from one membrane to another via solution can be measured by removing the H-membrane at suitable intervals and counting its radioactivity.

In Table I are given the quantities of Sr transferred from a highly saturated (D.S. = 90%) Sr-H-membrane disc containing initially ($q_i$) 390 $\mu$eq. Sr and 42 $\mu$eq. H to a pure H-membrane disc. The volume of solution was 150 ml., and initially it contained 0.54 $\mu$eq. Sr. Also included is the transfer from a 45% Sr-H-disc with $q_i$ values of 195 $\mu$eq. Sr and 237 $\mu$eq. H. Initially Sr in solution was less than 0.059 $\mu$eq. in 150 ml. Regardless of degree of saturation, the rate of solution transfer is exceedingly slow.

Transfer of Sr may also be accomplished by placing Sr- and H-membrane discs in intimate contact with each other. Sr and H may then switch positions by direct interaction, designated as contact exchange (2). This mode of migration is readily achieved by placing the two touching membranes

TABLE I

*Transfer of Strontium from Sr-H-Membranes to H-Membranes via Solution and by Contact*

(μeq. = microequivalents; D.S. = degree of saturation)

| Initial concentration ($q_i$) of Sr in Sr-H-membrane (*μeq./disc*) | Time (*hours*) | Transfer of Sr to H-membrane |  | Ratio $\frac{\text{contact}}{\text{solution}}$ |
|---|---|---|---|---|
|  |  | Via solution (*μeq./disc*) | By contact (*μeq./disc*) |  |
| 390 (D.S. = 90%) | 24 | — | 130 | — |
|  | 48 | 0.090 | 170 | 1888 |
|  | 170 | 0.126 | 192 | 1524 |
|  | 555 | 0.140 | — | — |
|  | 1558 | 0.175 | — | — |
|  | 1966 | 0.180 | — | — |
|  | ∞ (equil.) | 195 | 195 | — |
| 195 (D.S. = 45%) | 24 | — | 50 | — |
|  | 48 | — | 82 | — |
|  | 172 | 0.022 | 90 | 4091 |
|  | 560 | 0.072 | — | — |
|  | 1011 | 0.102 | — | — |
|  | 2090 | 0.104 | — | — |
|  | ∞ (equil.) | 97.5 | 97.5 | — |

between two lucite plates, under water and in horizontal position, and putting a 5 kg. weight on the assembly.

According to Table I contact exchange is very rapid and efficient. Within 48 hours 84%–87% of the equilibrium distribution is reached. It would require many years to accomplish the same transfer by means of the solution process. The superiority of contact exchange increases as the degree of saturation decreases.

The velocity of transfer of Sr depends on the nature of the *complementary ion*. Discs of Sr*-H-amberplex ($\phi$ = 2.08 cm., D.S. = 90%, $q_i$ = 390 μeq. Sr) were put in contact with equivalent Sr-H-discs, and with H-discs ($q_i$ = 432 μeq. H) and with Na-discs ($q_i$ = 432 μeq. Na). According to Table II, Sr* migrated much faster into the H-membrane than into the Sr-H-membrane or Na-membrane.

The *degree of saturation* also plays a role. Standard Sr-discs having D.S. values of 2%, 5%, 20%, 40%, 60%, 80%, and 90% were placed in contact with H-discs of equal sizes. The relative amounts of Sr transferred, that is, microequivalents Sr which migrated into H-amberplex divided by microequivalents Sr initially in the Sr-H-membrane, is lowest at low D.S. and highest at high D.S. Between D.S. 5% and 90% the relative transfer ($y$ in %) in any given time interval closely follows a straight line

$$y = ax + b, \qquad [1]$$

TABLE II

*Contact Transfer of Strontium from Sr*-H-Membranes ($q_i$ = 390 μeq. Sr*) to H-,Sr-,Na-Membranes*

(Diam. of discs = 2.08 cm.)

| Time period of contact (*hours*) | Microequivalents(μeq.) Sr* transferred to | | |
|---|---|---|---|
| | H-membrane ($q_i$ = 432 μeq. H) | Na-membrane ($q_i$ = 432 μeq. Na) | Sr-H-membrane ($q_i$ 390 μeq. Sr 42 μeq. H) |
| 4 | 51 | 23 | 19.5 |
| 24 | 130 | 75 | 74 |
| 48 | 170 | 123 | 115 |
| 72 | 191 | 159 | 138 |
| 170 | 192 | 188 | 176 |
| ∞ (equil.) | 195 | 195 | 195 |

where $x$ denotes D.S. For contact periods of 4, 24, 48, and 72 hours, the corresponding values of $a$ are 0.058, 0.083, 0.082, 0.089, and those of $b$ are 7.78, 26.8, 37.7, 41.0. The correlation coefficients $r$ are 0.89, 0.94, 0.86, 0.91.

We interpret the dependency of the rate of Sr-transfer upon D.S. in the following way. Each Sr ion may be considered attracted to two adjacent negative charges, viz., two sulfonic groups. Within the membrane the spatial distribution of the negative loci is, presumably, randomized, and the distance between adjacent loci is thus variable. If small amounts of $Sr(OH)_2$ are added to a H-membrane, producing a low D.S., the Sr ions will seek those pairs of loci which are the smallest distance apart, for they will attract Sr most strongly. As D.S. increases the additional Sr ions will be held less tightly because they are confined to those pairs of $SO_3^-$ radicals which are spatially farther apart. Hence, these Sr ions are more mobile and they will diffuse more readily into the adjoining H-membrane.

## Diffusion Coefficients in Membrane Piles

A pile of five identical membranes (Subpile I) was placed in contact with a pile (Subpile II) of five membranes different from I, but equal among themselves. The ten discs, each having a diameter of 2.08 cm. and a volume of 0.272 cm.$^3$, were assembled as one pile, under water between lucite plates. They were pressed together with a 5 kg. weight (Fig. 1). After a contact period of 20 hours the pile was dismantled and the individual membranes were analyzed. Thirty piles were set up, with variations in Sr content and in temperatures.

Since the two end members of the total pile never were affected by the diffusion process the disc assemblies correspond to diffusion cylinders of infinite extent in both $-x$ and $+x$ directions. Mathematical interpretation

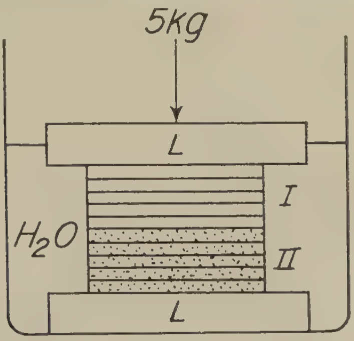

FIG. 1. Membrane pile for determination of diffusion coefficients ($L$ = lucite plate).

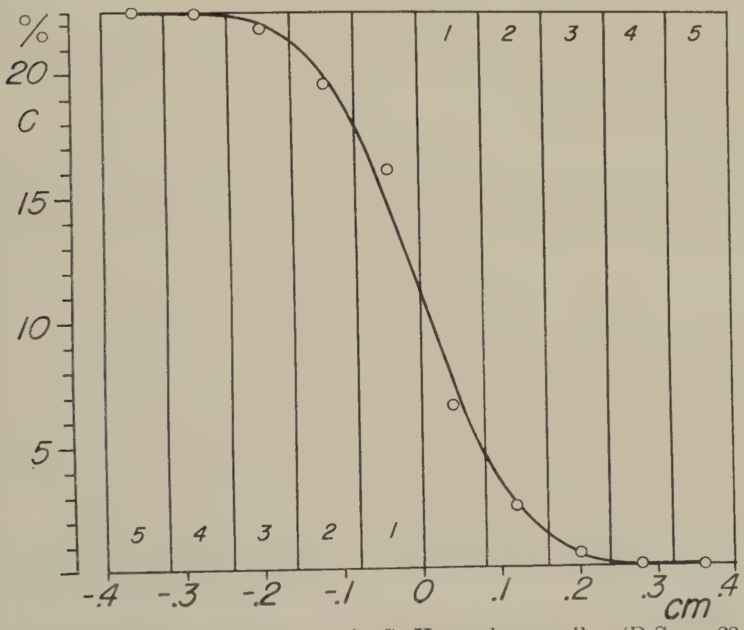

FIG. 2. Self-diffusion of strontium in Sr-H-membrane piles (D.S. = 22.5%) at 64°C.

is thereby facilitated. To give an example, Fig. 2 illustrates the diffusion curve obtained for the self-diffusion system:

$$\text{Sr}^*\text{-H-membranes/Sr-H-membranes}$$

at a temperature of 64° ± 0.5° C. All these membranes had a D.S. of 22.5% strontium. Since a D.S. of 100% corresponds to 0.432 meq. cation per membrane, each disc contained 0.0972 meq. strontium. In Fig. 2 the quantities of tagged strontium in each disc at $t$ = 20 hours are plotted at the midpoints of the membranes. The magnitudes are shown on the ordinates as D.S.

The curve was calculated from the standard equation (3)

$$C_{(x,t)} = \frac{C_0}{2}\left(1 = \operatorname{erf}\frac{x}{2\sqrt{DT}}\right), \qquad [2]$$

in which $C$ is the Sr concentration in a membrane disc at the distance $\pm x$ cm. from the boundary, $C_0$ the initial concentration in the discs at the left in Fig. 2, $t$ the time in seconds, erf the error integral, and $D$ the diffusion coefficient, considered to be independent of concentration.

A mean diffusion coefficient of $D = 6.7 \times 10^{-8}$ cm.$^2$/sec. was used. The observed points deviate systematically from the curve, especially the amounts of Sr in the first membrane on either side of the mid-point boundary. Their $D$ is smaller, namely, $3.4 \times 10^{-8}$ cm.$^2$/sec. At lower temperatures the systematic deviations from Eq. [1] disappear and mean $D$ values have real significance. The case illustrated in Fig. 2 is an extreme one, even for the 64° C. sets.

In Table III are listed the diffusion coefficients of six different kinds of membrane piles kept at five different temperatures. The diffusion coefficients were computed graphically with the aid of the Matano-Boltzmann procedure as described by Crank (3), using the equation

$$D_{c_1} = -\frac{1}{2t}\frac{dx}{dc}\int_0^{c_1} x\,dc.$$

Each $D$ is an average of three computations from a given experimental diffusion curve.

The effect of the *degree of saturation* is again very marked. Strontium

TABLE III

*Diffusion Coefficients ($D \times 10^8$ cm.$^2$ sec.$^{-1}$) of Sr in Amberplex Membranes*

| Membrane piles (initial conditions) | | | Temperature (°C.) | | | | |
|---|---|---|---|---|---|---|---|
| No. | Subpile I | Subpile II | 4 | 8 | 16 | 32 | 64 |
| 1 | 22.5% Sr, 77.5% H | ⇌ 100% H | 0.88 | 1.01 | 1.60 | 4.08 | 7.17 |
| 2 | 45% Sr, 55% H | ⇌ 100% H | 0.86 | 1.28 | 2.37 | 2.80 | 9.59 |
| 3 | 90% Sr, 10% H | ⇌ 100% H | 1.81 | 2.17 | 2.63 | 3.47 | 7.97 |
| | Self-diffusion of Sr: | | | | | | |
| 4 | 22.5% Sr*, 77.5% H | ⇌ 22.5% Sr, 77.5% H | 1.00 | 1.10 | 1.50 | 3.49 | 7.71 |
| 5 | 45% Sr*, 55% H | ⇌ 45% Sr, 55% H | 0.98 | 0.96 | 1.50 | 2.33 | 6.77 |
| 6 | 90% Sr*, 10% H | ⇌ 90% Sr, 10% H | 0.58 | 0.60 | 0.97 | 1.85 | 4.56 |
| 7 | 100% Sr*, 0% H<br>(extrapolated) | ⇌ 100% Sr, 0% H | 0.50 | 0.60 | 0.85 | 1.75 | 4.08 |

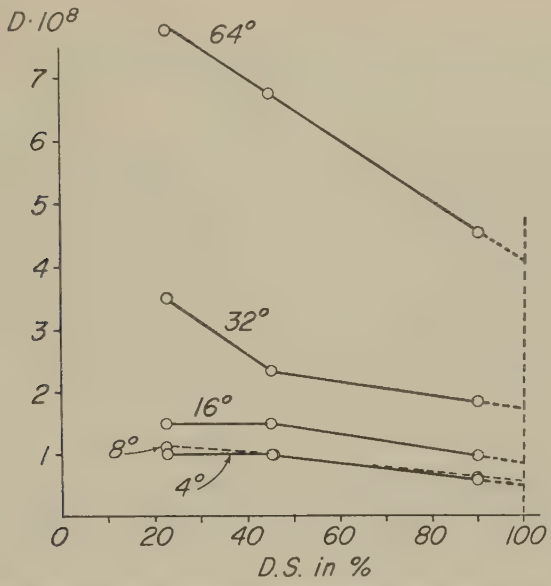

FIG. 3. Coefficients of self-diffusion of strontium (ordinate) in relation to degree of saturation (abscissa) of Sr-H-membranes at various temperatures (°C.).

diffusion against hydrogen ions tends to increase as D.S. of Sr increases, in accord with the observations made on membrane pairs in Table I. However, for self-diffusion of Sr* the value of the diffusion coefficient decreases consistently as D.S. increases (Fig. 3). A similar trend was observed by Soldano and Boyd (4) for self-diffusion of $Zn^{++}$ in Na-Zn-resins.

Extrapolating the self-diffusion curves to a D.S. of strontium equal to 100% gives the self-diffusion constants for pure strontium membranes. They are recorded in the bottom row of Table III. Interpolating for 25° C., the self-diffusion coefficient for Sr is $1.3 \times 10^{-8}$ cm.$^2$/sec. Boyd and Soldano's values (5) range from 0.3 to $23 \times 10^{-8}$ cm.$^2$/sec., depending on cross-linking in their Dowex resins.

In aqueous solution at room temperature the differential diffusion coefficient of $SrCl_2$ at infinite dilution is $1.34 \times 10^{-5}$ cm.$^2$/sec., according to Harned and Polestra (6). It decreases slightly with increasing concentration. Accordingly, $D$ for self-diffusion of Sr in amberplex is about 1000 times lower.

## OBSERVED ACTIVATION ENERGIES OF DIFFUSION

Plotting the logarithms of the diffusion constants $D$ against the reciprocals of the absolute temperatures $T$ permits calculation of the experimental activation energies ($E$) according to the related equations

$$D = A \exp(-E/RT) \qquad [3]$$

$$\log D = \log A - \frac{E}{2.303 \cdot 1.987} \cdot \frac{1}{T} \qquad [4]$$

The parameter $A$, which varies relatively little with temperature, is often designated "frequency factor."

Straight lines were fitted according to the method of least squares. Correlation is high, though not perfect. The computed $E$ values are listed in Table IV. They are many times smaller than $E$ values of diffusion of metal atoms in alloys (7), or of Na in solid NaCl (8), or of Na in analcite (9), but they are substantially larger than the activation energies of tracer diffusion of monovalent cations in water (10) or of the viscosity of water (11). Boyd and Soldano's values for self-diffusion of Sr in resins range from 5640 to 10980 cal./mole, depending on cross linkage (5).

## ENTROPY FACTOR OF DIFFUSION

Following the procedures of Boyd and Soldano (5) we have interpreted the parameter $A$ of Eq. [3] according to the theory of absolute reaction rates (12)which yields the expression

$$A = e\frac{kT}{h} d^2 \exp\left(\frac{\Delta S\ddagger}{R}\right), \qquad [5]$$

where $e$ = base of nat. log., $k$ = the Boltzmann constant, $T$ = absolute temperature, $h$ = Planck's constant, $d$ = the average distance between equilibrium positions during diffusion, $\Delta S\ddagger$ = entropy of activation, $R$ = the gas constant. At 25° C., $ekT/h = 1.685 \times 10^{13}$. In Table IV are listed the values for $d[\exp(\Delta S\ddagger/R)]^{1/2}$, designated as $\sigma$, which has the magnitude of length.

Boyd and Soldano's comparable values for self-diffusion of Sr in resins vary between 1.6 and 16.1 (5). Those for Zn in Na resins range from 1.4

TABLE IV

*Derived Values from Tabte III*

| Membrane pile (see Table III) | Activation energy $E$ (*cal./mole*) | Correlation coeff. $r$ | $A \times 10^4$ (Eq. [3]) | $\sigma = d\exp\left(\frac{\Delta S\ddagger}{R}\right)^{\frac{1}{2}}$; $\sigma \times 10^8$ cm |
|---|---|---|---|---|
| No. 1, Sr → H | 6804 | −0.977 | 22.4 | 1.2 |
| No. 2, Sr → H | 6883 | −0.977 | 28.4 | 1.3 |
| No. 3, Sr → H | 4418 | −0.994 | 0.57 | 0.2 |
| Self-diffusion | | | | |
| No. 4, Sr* → Sr | 6616 | −0.993 | 16.4 | 1.0 |
| No. 5, Sr* → Sr | 6160 | −0.996 | 6.6 | 0.6 |
| No. 6, Sr* → Sr | 6625 | −0.996 | 9.7 | 0.7 |
| No. 7, Sr* → Sr (extrapolated) | 6590 | −0.995 | 8.5 | 0.7 |

to 18.5; those for self-diffusion of Zn are 2.5–8.0. The values in Table IV are all smaller. We shall interpret them in the ensuing section.

## DISCUSSION

The simplest picture of the diffusion process is provided by the self-diffusion of Sr in fully saturated strontium membranes (homoionic systems). Two equal diffusion currents flow in opposite directions. There is no mass flow if we neglect the very small differences in mass between isotopes. Two equal concentration gradients of opposite sign are operating or, better, two chemical-potential gradients which arise from the entropy of mixing, as pointed out by Crank (13). No volume changes take place.

Since the fraction of strontium that is dissolved in the pore space—as $Sr(OH)_2$ or $Sr(HCO_3)_2$—is very small, we conclude that strontium migrates mainly along the internal surfaces or walls of the gel channels and pores. Interstitial or pore diffusion probably plays a minor role in our systems. In this respect our experiments differ significantly from the resin studies of Despić and Hills (14), of Boyd and Soldano (5), and of Soldano and Boyd (4). Schlögl (15) has given a good description of gel diffusion in the absence and presence of free electrolytes in the pore space. His ideas parallel those expressed by Jenny and Overstreet (2) many years ago.

The magnitude of the diffusion coefficient is conditioned by the strength of attraction between Sr and the negative gel spots and by the labyrinth paths of the gel structure. For molecules and ions which are not adsorbed we may define a labyrinth factor $l$ as "$D$ in gel/$D$ in infinitely dilute gel." The measurements of urea diffusion in cation-resins by Gregor *et al.* (16) give $l$-values of 0.06–0.09; from self-diffusion of $Br^-$ in systems $NH_4$-resin + $NH_4Br$ observed by Boyd and Soldano (17) $l$ varies between 0.02 and 0.3. For ions which exist exclusively in the adsorbed state, $l$ may be considerably smaller.

The mechanism of transport may be visualized as ion-exchange diffusion (2, 18). The Sr ions oscillate in the vicinity of a pair of exchange sites. The oscillation space is conditioned, among other factors, by the Coulomb attraction exerted by the constellation of the sulfonic groups. If the oscillation spaces of two neighboring Sr ions become large enough to overlap the two ions may exchange places in a statistical manner. The magnitude of the effective oscillation volume determines the energy barrier of exchange which finds expression in the activation energy.

One might also say, in different words, that a radioactive Sr* ion jumps from one pair of negative sites of the gel framework to an adjoining pair, and that an ordinary Sr ion simultaneously hops in the opposite direction. The mean distance $d$ between two sites was computed to be 10 A. for the gel and 7 A. for the solution phase. It calls for rather large jumps, but if migration proceeds along the threads of the network or in narrow channels the jumping distance might be substantially shorter.

According to the reaction-rate factor $\sigma$ (Table IV) the equilibrium distance $d$ is about 1 A. only, provided that $\Delta S\ddagger$ is assumed to be zero. However, the pertinent parameter $A$ in Eq. [3] also contains the labyrinth factor $l$ which may be largely temperature-independent. If a proper correction could be applied, $d$ would become substantially greater. Furthermore, larger values of $d$ become possible by making $\Delta S\ddagger$ positive, which implies that bonds are broken—probably those of water—to get Sr in condition for jumping.

In hetero-ionic systems containing the three ions Sr*, Sr, H, radioactive Sr may change place with nonradioactive Sr directly, or via $H^+$ as an intermediate step. Since the presence of $H^+$ increases the self-diffusion of Sr (Fig. 3) the latter alternative is apparently the preferred one. In the diionic (Sr, H) membrane piles higher degrees of Sr-saturation accelerate migration of Sr, especially at lower temperatures. As pointed out above, this behavior is attributable to the variable distances between sulfonic groups.

Applications of these observations and ideas to problems of mineral nutrition of plants have been reported in *Science* (19).

## REFERENCES

1. JENNY, H., *et al.*, *Science* **112,** 164 (1950).
2. JENNY, H., AND OVERSTREET, R., *J. Phys. Chem.* **43,** 1185 (1939).
3. CRANK, J., "The Mathematics of Diffusion." Oxford, 1956.
4. SOLDANO, B. A., AND BOYD, G. E., *J. Am. Chem. Soc.* **75,** 6107 (1953).
5. BOYD, G. E., AND SOLDANO, B. A., *J. Am. Chem. Soc.* **75,** 6091 (1953).
6. HARNED, H. S., AND POLESTRA, F. M., *J. Am. Chem. Soc.* **75,** 4168 (1953).
7. SEITZ, F., *Phys. Rev.* **74,** 1513 (1948).
8. JOST, W., "Diffusion in Solids, Liquids, Gases." Academic Press, New York, 1952.
9. BEATTY, M. T., *Trans. Faraday Soc.* **53,** 61 (1957).
10. WANG, J. H., *J. Am. Chem. Soc.* **74,** 1612 (1952).
11. EWELL, R. E., AND EYRING, H., *J. Chem. Phys.* **5,** 726 (1937).
12. GLASSTONE, S., LAIDLER, J. K., AND EYRING, H., "The Theory of Rate Processes." McGraw-Hill, New York, 1941.
13. CRANK, J., *Discussions Faraday Soc.* **23,** 99 (1957).
14. DESPIĆ, A., AND HILLS, G. J., *Trans. Faraday Soc.* **53,** 1262 (1957).
15. SCHLÖGL, R., *Z. Elektrochem.* **57,** 195 (1953).
16. GREGOR, H. P., COLLINS, F. C., AND POPE, M., *J. Colloid Sci.* **6,** 304 (1951).
17. BOYD, G. E., AND SOLDANO, B. A., *J. Am. Chem. Soc.* **75,** 6105 (1953).
18. JENNY, H., *in* E. Truog, ed., "Mineral Nutrition of Plants," Chapter 5, "Contact phenomena between adsorbents and their significance in plant nutrition." University of Wisconsin Press, Madison, Wisconsin, 1951.
19. LOPEZ-GONZALEZ, J. DE D., AND JENNY, H., *Science* **128,** 90 (1958).

JOURNAL OF COLLOID SCIENCE **14,** 543-561 (1959)

# THE PARTICLE DIAMETER DETERMINATION OF FILM-FORMING LATEXES BY ELECTRON MICROSCOPY[1]

**E. B. Bradford and J. W. Vanderhoff**

*Physical Research Laboratory, The Dow Chemical Company, Midland, Michigan*

*Received April 10, 1959*

## ABSTRACT

The specimen preparation of film-forming or "soft" particle latexes is complicated by the tendency of these particles to deform and coalesce upon drying; these deformed particles appear indistinct in the electron microscope. Soft particles of butadiene-containing polymers can be hardened by bromination prior to deposition. The particular diameter increase of brominated styrene-butadiene copolymers is dependent upon their butadiene content and varies from about 0.2% for polystyrene to 24.8% for polybutadiene.

Exposure of these particles to high-energy irradiation, e.g., from a van de Graaff accelerator, also hardens them owing to cross-linking reactions between adjacent polymer molecules. Particles hardened by this technique appear as well-defined spheres in the electron microscope. High-energy irradiation also hardens certain latex systems which do not respond to bromination, e.g., polyethyl acrylate and polyvinyl acetate.

## INTRODUCTION

The increasing importance of synthetic polymer latexes has intensified interest in determining their average particle sizes and particle size distributions. The average size can be determined by light scattering (1), ultracentrifugation (2), soap titration (3), low-angle X-ray scattering (4), and electron microscopy (5). Of these, electron microscopy is the only technique by which the particle size distribution can be determined directly. The purpose of this paper is to describe electron microscopic techniques for film-forming latexes.

All latexes may be separated into two arbitrary clasifications: the "hard" particle (non-film-forming) latexes and the "soft" particle (film-forming) latexes. This distinction depends upon the composition of the polymer and its degree of plasticization. The particle diameter determination of hard particle latexes has been extensively investigated (5-8); however, measurements of soft particles are complicated by their indistinct images. Figure 1 is a chromium-shadowed electron micrograph showing both hard and soft

---

[1] Presented, in part, at the 131st Meeting of the American Chemical Society, Miami, Florida, April 12, 1957.

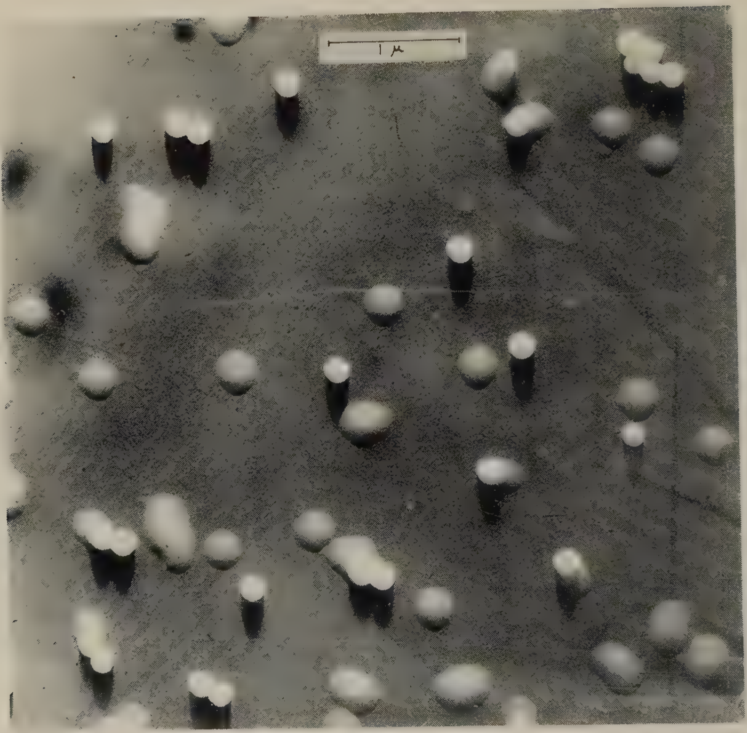

Fig. 1. Hard and soft latex particles as observed in the electron microscope.

particles in the same field. The soft particles are elastic spheres of a 60–40 styrene-butadiene copolymer (in all cases the proportions stated represent the monomer charge in the polymerization); the discrete spheres are bromine-hardened particles of the same latex. The length of the shadows cast by the particles is indicative of their height above the substrate. The soft particles have been deformed and flattened during the drying process while the brominated or hard particles are unaffected. In several cases, two soft particles have partially coalesced; this coalescence is a prerequisite to film formation. These soft particles can be hardened for electron microscopy by two techniques: bromination and high-energy irradiation.

## Experimental Results

### *A. Bromination Technique*

The hardening of soft particles with bromine prevents their coalescence to the substrate upon deposition and increases their opacity in the electron beam. Either a solution of bromine is added to the diluted latex (9, 10) or the diluted latex is exposed to bromine vapors (11). These treatments usually increase the degree of aggregation of the latex particles; this flocculation may be reduced by the addition of surface-active agents (11–13).

Although this technique has been widely used, the effect of bromine on the latex particle diameter has not been reported other than by Brown (9), who found a 9% diameter increase on bromination for GR-S and Hycar OR 15 latexes, and Willson, Miller, and Rowe (10), who reported a 9.6% increase for a 40–60 styrene-butadiene copolymer. Therefore, the extension of this technique to a wider range of polymer compositions is of interest.

The reported diameter increase of styrene-butadiene copolymer particles on bromination implies that the particle volume increase due to the addition of bromine exceeds the particle volume decrease due to the increased density of the brominated copolymer. If this is the case, the particle diameter might be expected to vary with increasing bromine concentration at least in a certain range. Latex I, comprised of 60–40 styrene-butadiene copolymer particles with a relatively narrow particle size distribution (from electron microscopy), was diluted to 13 p.p.m. and treated with increments of saturated aqueous bromine. The brominated samples were then dried on collodion membranes supported by stainless steel grids. Monodisperse polystyrene particles (6), 3650 A. in diameter, had been dried on each membrane previously to calibrate each photographic exposure. An R.C.A. Model EML electron microscope was used for all experiments. The particle diameter measurements are shown in Table I. From these data, bromine concentrations of 0.002*M* and above are necessary to harden all the particles. Moreover once all the particles are hardened, additional bromine has no observable effect on the average particle diameter.

TABLE I

*Effect of Bromine Concentration on the Particle Diameter of Latex I*

| Approximate bromine concentration (*M*) | Average particle diameter (*A.*) | Standard deviation (*A.*) | Number of particles measured |
|---|---|---|---|
| 0.0008[a] | 2400 | 120 | 18 |
| 0.001[b] | 1990 | 92 | 25 |
| 0.002 | 1820 | 120 | 40 |
| 0.003 | 1810 | 85 | 20 |
| 0.004 | 1840 | 80 | 42 |
| 0.006 | 1840 | 66 | 17 |
| 0.009 | 1840 | 57 | 29 |
| 0.011 | 1820 | 81 | 23 |
| Average (0.002 to 0.011 *M* bromine) | 1830 | 87 | 171 |

[a] All particles are soft.

[b] Only hard particles are included; the soft particle measurements range from 2000 to 2400 A. in diameter.

TABLE II

*Analyses of 60-40 Styrene-Butadiene Copolymers*

| Latex | Density (*g./ml.*) | Per cent bromine | $V_f/V_0$ |
|---|---|---|---|
| I—control | 1.003 | None | — |
| I—brominated (1) | 1.549 | 41.9 | 1.11 |
| I—brominated (2) | 1.624 | 46.2 | 1.15 |
| II—control | 1.004 | None | — |
| II—brominated | 1.590 | 45.3 | 1.16 |

In order to determine the density of the brominated particles, samples of Latex I and Latex II (512K,[2] a commercial 60–40 styrene-butadiene copolymer latex; average particle diameter ≈ 2000 A., standard deviation ≈200 A.) were diluted to about 6% solids and stabilized with additional surface-active agents. Liquid bromine was then added dropwise with agitation; this addition was repeated whenever bromine droplets could no longer be observed in the latex. When the periodic electron microscope samples indicated that all the particles were hardened, the bromine addition was discontinued. The latexes, discolored by bromine, were coagulated by freezing and the filtered polymer was washed with deionized water and methanol to remove the unreacted bromine. After drying *in vacuo*, the polymer was compression-molded into circular buttons (½ inch diameter, ⅛ inch thick); these moldings were rigid, opaque, and black. For both latexes, unbrominated control moldings were prepared; these were flexible, translucent, and pale yellow in color. The densities and bromine contents of both the brominated and unbrominated specimens are listed in Table II.

Assuming that $X$ grams bromine are combined with one gram polymer and $Y$ is the fraction of bromine in the final product, then

$$X = Y(1 + X).$$

If the polymer densities before and after bromination are $d_0$ and $d_f$, respectively, and the respective particle volumes and diameters are $V_0$ and $V_f$, and $D_0$ and $D_f$, then

$$D_f/D_0 = (V_f/V_0)^{1/3} = [d_0(1 + X)/d_f]^{1/3}.$$

The value of $V_f/V_0$ is unity if the particle volume does not change on bromination. The experimental values shown in Table II range from 1.11 to 1.16, i.e., the particle volume increase on bromination ranges from 11% to 16%. This corresponds to a particle diameter increase ranging from 3.7% to 4.9%.

Another technique was employed to determine the bromine content of

---

[2] The Dow Chemical Company, Midland, Michigan.

TABLE III

*Analyses of Brominated Latex II*

| Polymer concentration (*ppm.*) | Approximate bromine conc. (*M*) | Per cent bromine in sample | Per cent bromine in polymer | Appearance of particles in E.M. |
|---|---|---|---|---|
| 58 | 0.0009 | 0.004 | $3_4$ | Most soft, some hard |
| 0 | 0.0009 | 0.001 | — | |
| 58 | 0.004 | 0.008 | $5_1$ | Hard |
| 0 | 0.004 | 0.002 | — | |
| 58 | 0.006 | 0.012 | $5_1$ | Hard |
| 0 | 0.006 | 0.005 | — | |
| 385 | 0.027 | 0.059 | 53 | Hard |
| 0 | 0.027 | 0.014 | — | |

latexes brominated at concentrations approaching those used for electron microscopy. A sample of Latex II was diluted and brominated with saturated aqueous bromine; the excess was removed by nitrogen-sparging. The bromine contents were determined by X-ray fluorescence; the results shown in Table III are reproducible to within ±0.001%. The values for the bromine content in the first three cases have only one significant figure with the uncertain figure as the subscript. All particles are hardened at a bromine concentration somewhere between 0.0009 and 0.004$M$. This is in agreement with the 0.001 to 0.002$M$ range found in Table I. Experimentally the bromine content must approach 40% to 50% before the particles appear hard in the electron microscope, and additional bromine does not result in a higher bromine content in the copolymer.

The theoretical maximum bromine content of a brominated 60–40 styrene-butadiene copolymer is 54.2% assuming that: (*1*) one molecule of bromine adds quantitatively to each residual double bond; (*2*) substitution of bromine for either ring or side-chain hydrogens does not occur; and (*3*) each butadiene unit in the copolymer chain contains one residual double bond, i.e., no appreciable reaction of these double bonds by cross-linking or oxidation occurs. In view of these assumptions, the experimental results are in fair agreement with this calculated value, e.g., 42% to 46% bromine is found where the bromination was carried out at 6% solids and approximately 51% to 53% at very low solids. Moreover the previously reported 9.6% increase (10) was determined for a 40–60 styrene-butadiene copolymer which has a theoretical maximum bromine content of 63.9%. If the variation of $D_f/D_0$ with bromine content (from Table II) is extrapolated to 63.9% bromine, the value, $D_f/D_0 = 1.09$ to 1.13, is in reasonable agreement with the 1.096 value reported. Therefore the point at which these particles first appear hard in the electron microscope coincides with the point at which almost all residual double bonds are reacted with bromine.

TABLE IV

*Analyses of Brominated Styrene-Butadiene Copolymers*

(Including polystyrene and polybutadiene)

| Latex | 4.0% to 1.2% Polymer | | | 380 (*ppm.*) Polymer |
|---|---|---|---|---|
| | Per cent bromine | $d_f$ (*g./ml.*) | $d_0$ (*g./ml.*) | Per cent bromine |
| III | 12.4 | 1.204 | 1.077 | $1_7$ |
| IV | 39.4 | 1.514 | 1.042 | $50._4$ |
| V | 51.4 | 1.717 | 0.999 | $61._9$ |
| VI | 56.8 | 1.658 | 0.870 | $68._0$ |
| VII | 65.1 | 1.650 | 0.906 | 72.4 |
| VIII | 68.9 | 1.794 | 0.916 | 75.0 |

To test this hypothesis further, Latexes III (polystyrene), IV (80–20 styrene-butadiene copolymer), V (60–40), VI (40–60), VII (20–80), and VIII (polybutadiene), were prepared and brominated. Saturated aqueous bromine was added with agitation to the original latex (~35% solids) in varying amounts assuring an excess for each composition. After addition of the bromine the unbrominated polymer content ranged from 4.0% (Latex III) to 1.2% (Latex VIII). The brominated polymer was recovered by evaporating the latexes to dryness at room temperature and washing with deionized water and methanol. The densities and bromine contents were determined on the dried polymer. Unbrominated control specimens were treated and analyzed identically. The results are shown in Table IV.

Since bromination at very low concentrations is more quantitative, the same latexes diluted to 400 p.p.m. polymer were treated with saturated aqueous bromine until the bromine concentration was about $0.010M$. The bromine contents as determined by X-ray fluorescence are also shown in Table IV.

From these data, polystyrene particles also absorb bromine, e.g., the polymer from Latex III (4% solids) contained 12.4% bromine. To determine whether the washing technique was effective in removing the unreacted bromine, this sample was dissolved in methyl ethyl ketone and precipitated in methanol three times. After drying *in vacuo*, this sample contained 12.5% bromine, indicating that the washing technique was effective and that the bromine is chemically bound to the polystyrene. Thus the assumption that bromine substitution reactions do not occur is incorrect.

The variation of bromine content with butadiene content is shown in Fig. 2. In all cases, the data are corrected for the bromination of styrene units assuming that these units in each composition brominate in the same proportion as in the polystyrene sample. The curve shown represents the

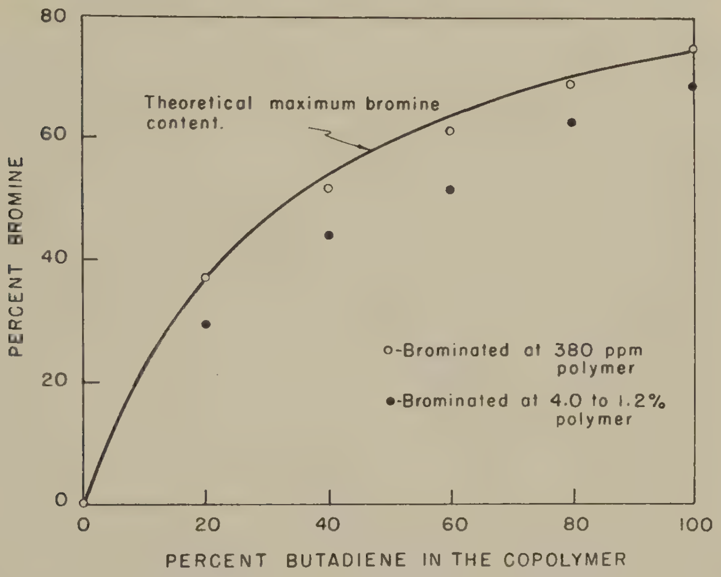

FIG. 2. Variation of bromine content with butadiene content (corrected for the bromination of styrene units).

maximum theoretical bromine content according to the foregoing assumptions. In all cases, the points for samples brominated at 380 p.p.m. polymer agree very well with this theoretical curve, whereas those at 1.2% to 4.0% polymer are consistently lower. In view of the assumptions made this agreement offers convincing evidence for the validity of this hypothesis.

In order to calculate the particle diameter increase on bromination, $d_0$ and $d_f$ as well as the bromine content must be known. Unfortunately values of $d_f$ are available only for the relatively incomplete brominations at the higher concentrations, since the samples brominated at 380 p.p.m. polymer contained insufficient polymer for these determinations. However, from all available data, the density increase on bromination $(d_f - d_0)$ increases approximately linearly with increasing bromine content as shown in Fig. 3. The least-squares equation calculated from this data is:

$$(d_f - d_0) = 0.0130\ (100\ Y) - 0.0079.$$

The standard deviation of the slope 0.0130 is 0.00109. The standard deviation of the intercept $-0.0079$ is 0.054 (the bar in Fig. 3 represents $\bar{X} \pm 1\sigma$). This line almost certainly passes through the origin since the calculated statistical $t$-value of 0.15 is much smaller than the critical value (50% probability) of 0.71.

By means of this relationship approximate values of $(d_f - d_0)$ were calculated from the bromine contents of the samples brominated at 380 p.p.m.

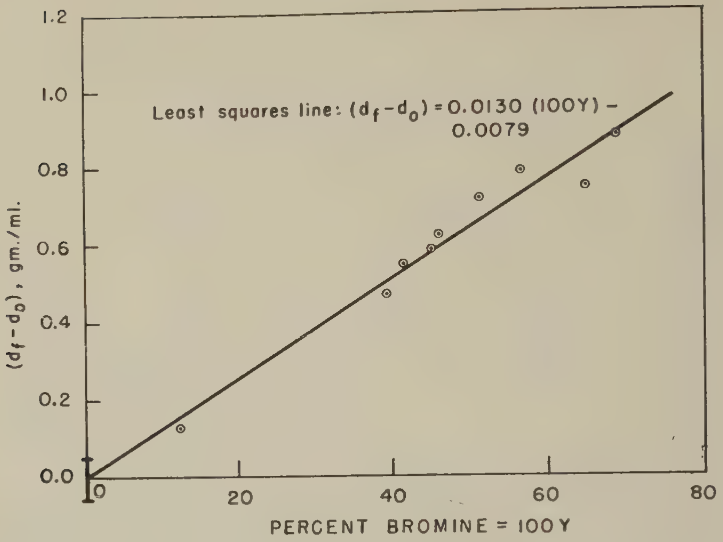

FIG. 3. Variation of density increase on bromination with bromine content.

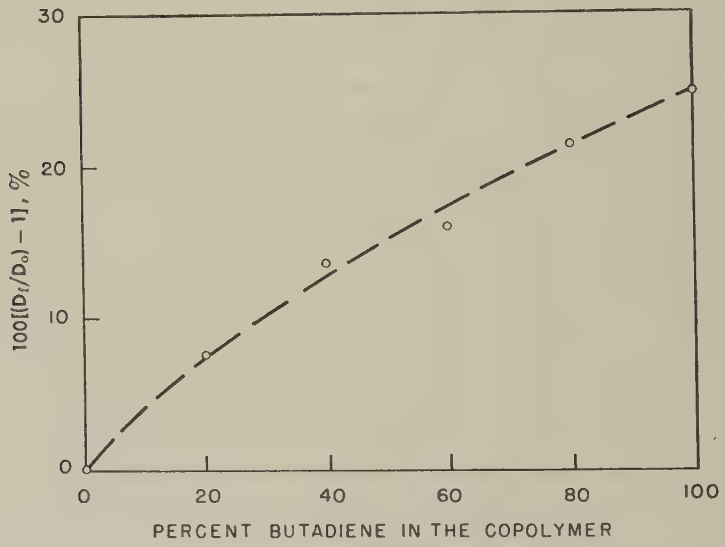

FIG. 4. Variation of diameter calibration factor with butadiene content.

The variation of the diameter calibration factor, i.e., 100 $(D_f/D_0 - 1)$, with butadiene content of the copolymer is shown in Fig. 4. These values, ranging from 0.2% for polystyrene to 24.8% for polybutadiene, are offered as approximate calibration constants which take into account the variation in copolymer composition as well as concentration during bromination.

### *B. High-Energy Irradiation Technique*

In this technique (8), recently developed in this laboratory, the diluted latex is subjected to electrons from a 2-m.e.v. (million-electron-volt) van de Graaff accelerator. High-energy irradiation initiates simultaneous cross-linking and degradation in high polymers. The relative importance or predominance of these two reactions depends upon the particular polymer irradiated. For instance, with polyethylene (14), the cross-linking reaction is predominant although some degradation occurs. However, for polymethyl methacrylate (15) degradation is predominant and the average molecular weight of the polymer decreases on irradiation. For polybutadiene and various styrene-butadiene copolymers, cross-linking is predominant; hence, exposing these latexes to high-energy irradiation transforms each particle into a rigid three-dimensional network which is much more resistant to mechanical deformation.

Latex I was irradiated with electrons from the van de Graaff accelerator for various lengths of time. Figure 5*a* is a micrograph of the latex particles before irradiation; their outlines are indistinct and considerable deformation has occurred on drying. At a 9.3 mrad dosage (1 mrad = 1,000,000 rads; a rad is a measure of absorbed radiation equivalent to 100 ergs/gm.) the particles are partially hardened; their images are much more distinct than those of the nonirradiated sample. At 23 mrads this hardening is more apparent; the images of some particles are more distinct than others in the same micrograph. From this it might be inferred that the cross-linking or hardening depends upon the capture of free radicals from the aqueous phase. In the statistical distribution of available free radicals among the particles, some may capture radicals at a rate considerably greater than the average. At 47 mrads all particles are hardened and their images are distinct as shown in Fig. 5*b*. Additional irradiation, e.g., 93 mrads, slightly increases the electron density of the particles; however, more extraneous matter is observed at this dosage than at lower levels. At 186 mrads even more extraneous matter is observed; the particle images are quite distinct but the particles appear spheroidal.

Since about 47 mrads irradiation hardens the particles to about the same extent as bromination, this technique was adapted to particle diameter determinations. Measurements of Latex I irradiated at various dosages were carried out using the technique described in the foregoing section; the results are shown in Table V. The average particle diameters of the irradiated samples agree with that of the brominated sample. This agreement is surprising since the particle diameter increases about 13% on bromination whereas an identical increase on irradiation seems improbable. The particles irradiated at 47 mrads (as well as the brominated particles) possess the narrowest particle size distributions of the series. This is an

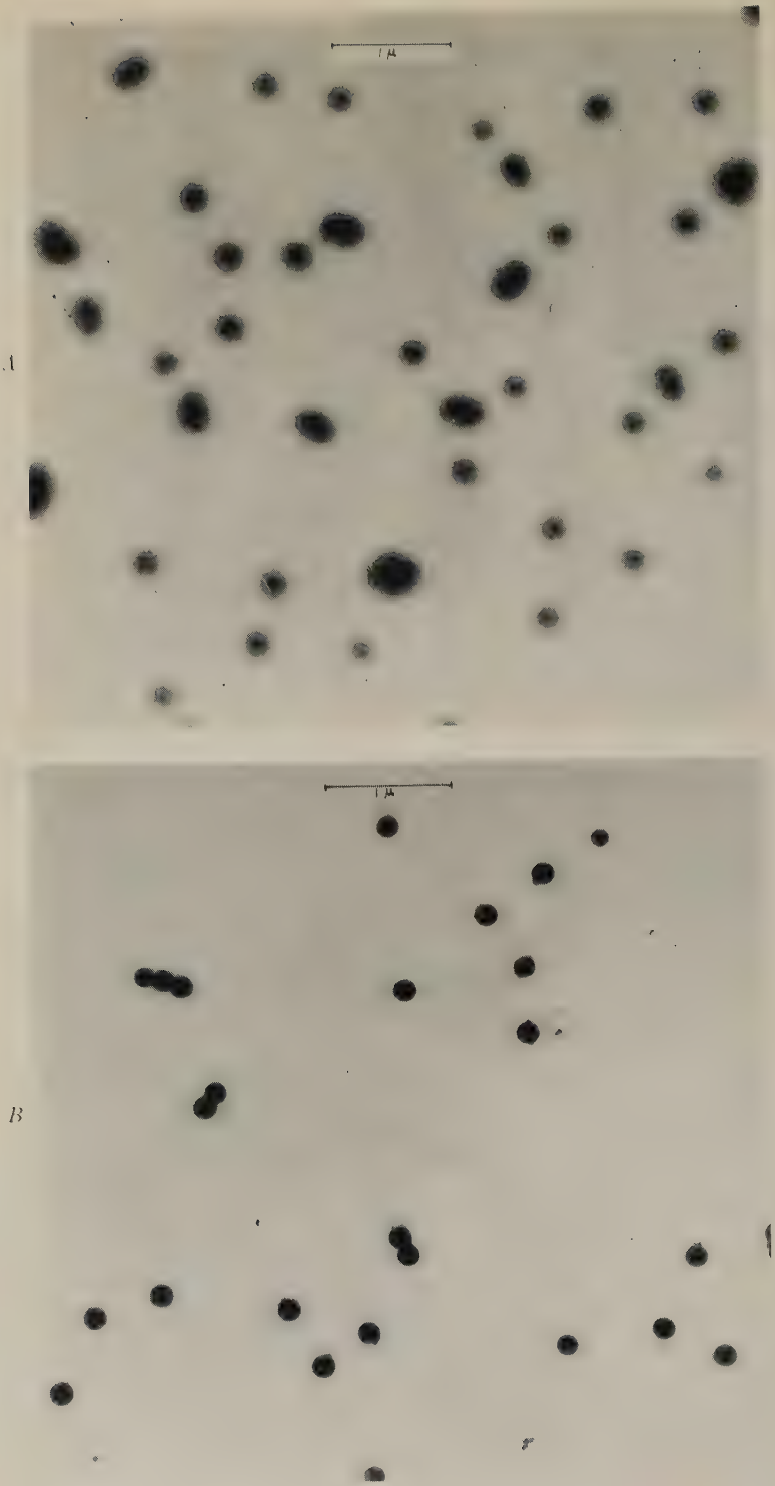

FIG. 5. The effect of high-energy irradiation on particles of Latex I: (*a*) untreated; (*b*) 47 mrads.

TABLE V

*Particle Diameter of Latex I*

| Treatment | Average particle diameter (*A*.) | Standard deviation (A.) | Number of particles measured |
|---|---|---|---|
| Brominated | 1830 | 90 | 188 |
| 47 mrad | 1820 | 87 | 111 |
| 93 mrad | 1830 | 170 | 147 |
| 186 mrad | 1880 | 210 | 23 |

TABLE VI

*Particle Diameters of Polybutadiene and Styrene-Butadiene Copolymer Latexes*

| Latex | Treatment | Average particle-diameter (*A*.) | Standard deviation (*A*.) | Number of particles measured |
|---|---|---|---|---|
| IX | Brominated | 1900 | 220 | 17 |
| | 47 mrad | 1890 | 170 | 59 |
| | 93 mrad | 1930[a] | 200 | 52 |
| X | Brominated | 1640 | 200 | 51 |
| | 47 mrad | 1700[b] | 200 | 60 |
| | 93 mrad | 1690[a] | 190 | 49 |
| XI | Brominated | 2590 | 180 | 87 |
| | 47 mrad | 2620 | 180 | 105 |
| | 93 mrad | 2550[b] | 190 | 81 |
| XII | Brominated | 2060 | 69 | 44 |
| | 23 mrad | 2080 | 100 | 64 |
| | 47 mrad | 2020[b] | 120 | 52 |

[a] The particle surfaces are roughened; the particles appear spheroidal.

[b] These particles display a surface shell; the particle surfaces are slightly roughened.

optimum level under these conditions because not all particles are hardened at lower levels while the particle surfaces become roughened and more extraneous matter is observed at higher levels.

Similar experiments were carried out using Latexes IX (polybutadiene), X (25–75 styrene-butadiene copolymer), XI (60–40), and XII (80–20). The results are shown in Table VI. From these data, the agreement between the brominated and irradiated samples is generally quite good. Further increases in irradiation dosage over the optimum level (47 mrads for Latexes IX, X, and XI, 23 mrads for Latex XII) do not appreciably affect the measured particle diameter. This agreement is, at present, inexplicable, since the particle diameter increase on bromination varies with polymer composition and an equivalent increase on irradiation seems improbable. This is the subject of a current investigation.

In some cases, the electron micrographs show a pronounced "shell"

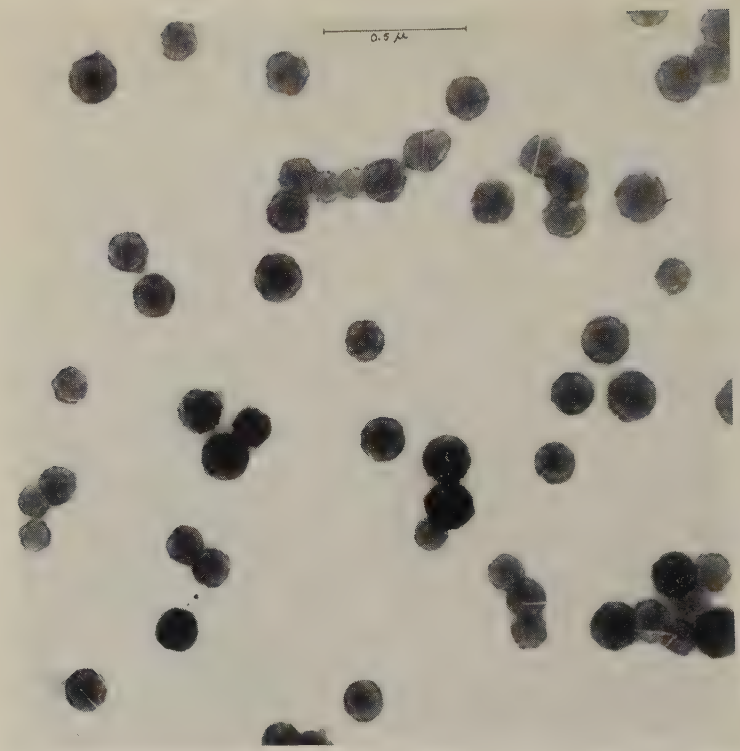

Fig. 6. Particles illustrating a shell effect resulting from 47 mrads irradiation of a styrene-butadiene copolymer latex.

around particles exposed to high-energy electrons; an example is shown in Fig. 6. The latexes were diluted to ~20 p.p.m. before irradiation; hence, the primary absorption of energy is in the aqueous phase. The shell might be caused by free radicals which are initiated in the aqueous phase and are subsequently captured by the polymer particles; this would result in a higher degree of cross-linking at the surface than near the particle center where only the free radicals initiated inside the particle, or diffusing from the surface, can cause cross-linking.

In order to determine the effect of copolymer molecular weight on the optimum irradiation level, three 60–40 styrene-butadiene copolymers of varying molecular weights were prepared. The recipes used were identical to that of Latex I except for varying increments of *t*-dodecyl mercaptan, a well-known chain-regulator. Thus these three latexes were comprised of uniform particles of approximately equal particle diameters but with varying copolymer molecular weights. The molecular weights vary in an inverse order with mercaptan concentration, the higher the mercaptan concentration, the lower the molecular weight.

Samples of these latexes were irradiated at dosage levels ranging from 25 to 200 mrads. With the copolymer of highest molecular weight, 50 mrads hardens some of the particles leaving others still soft, and 75 mrads are necessary to harden all the particles completely. With the copolymer of intermediate molecular weight, the particles appear soft at 50 mrads but all are hardened at 75 mrads. With the copolymer of lowest molecular weight, the particles all appear soft at 50 mrads, some appear soft while others appear hardened at 75 and 100 mrads, and 150 mrads are necessary to harden all the particles. Thus, at least qualitatively, the optimum irradiation dosage level is dependent upon the molecular weight of the copolymer; this optimum dosage level may be determined for each system to be studied.

This high-energy irradiation technique is applicable to other systems, e.g., polyethyl acrylate, polyvinyl acetate, and natural rubber. The untreated polyethyl acrylate particles shown in Fig. 7*a* appear hazy and indistinct. Bromination does not harden these particles; indistinct images as well as an increased degree of aggregation are observed as shown in Fig. 7*b*. Polyethyl acrylate contains few residual double bonds available for the bromine addition reaction; the particle densities and contrast of the brominated and unbrominated specimens are not appreciably different. The effect of high-energy irradiation is shown in Fig. 7*c* (93 mrads, the optimum level); here the particles appear hard and discrete with little aggregation. The average particle diameter can be readily determined from this exposure, whereas measurements of the untreated and brominated specimens are obviously inaccurate.

In electron micrographs, polyvinyl acetate particles appear as hard as 80–20 styrene-butadiene copolymer particles, i.e., harder than polyethyl acrylate or 60–40 styrene-butadiene copolymer particles, but not as hard as polystyrene particles. Bromination tends to aggregate these particles and does not harden them. High-energy irradiation partially hardens the particles at the 9.3 mrad level, but 23 mrads (optimum) are necessary to yield hard, discrete spheres. Higher dosages (47 and 93 mrads) aggregate the particles to a greater extent without appreciably increasing their contrast on the photographic plate.

The effect of high-energy irradiation on particles of natural rubber (Hevea) was also studied. These particles appear very soft and amorphous. Bromination hardens them but there is considerable aggregation and coalescence; many of the particles appear as spheroids. High-energy irradiation (47 mrads, the optimum level) hardens these particles, producing discrete spheres with little aggregation. A higher dosage (93 mrads) results in uneven particle surfaces and pronounced aggregation.

Some polymers are predominantly degraded rather than cross-linked by high-energy electrons; polymethyl methacrylate is an example of this type. Figure 8*a* shows these particles before irradiation; Figs. 8*b* and 8*c* show par-

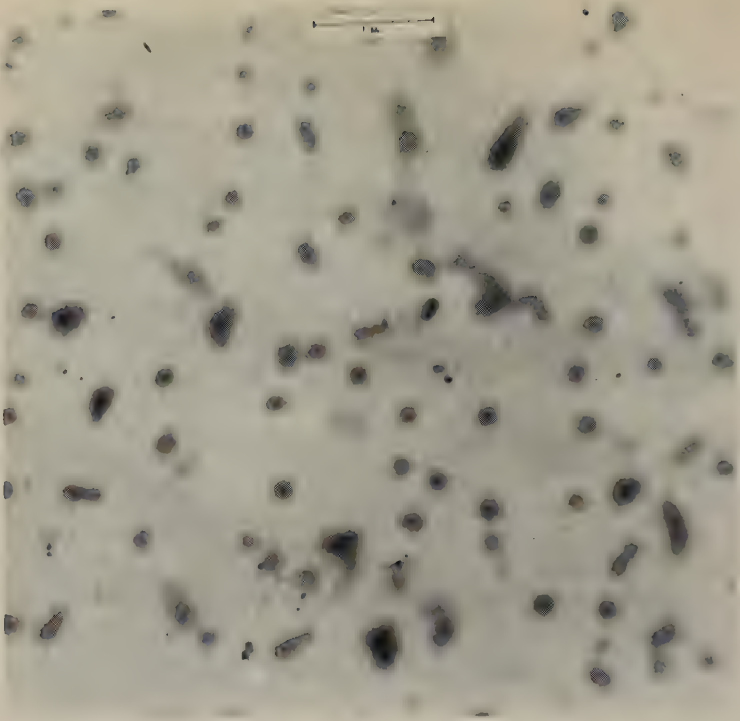

Fig. 7a

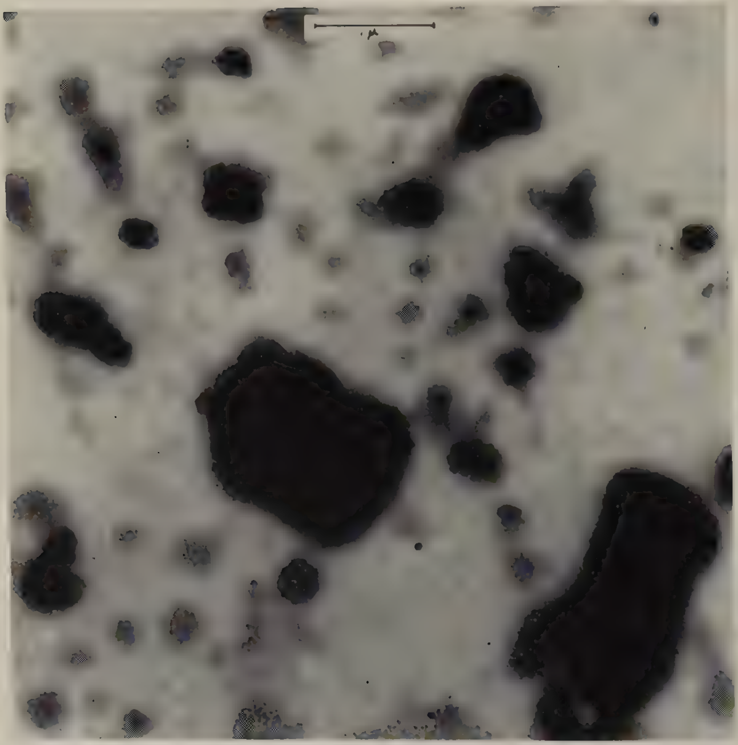

Fig. 7b

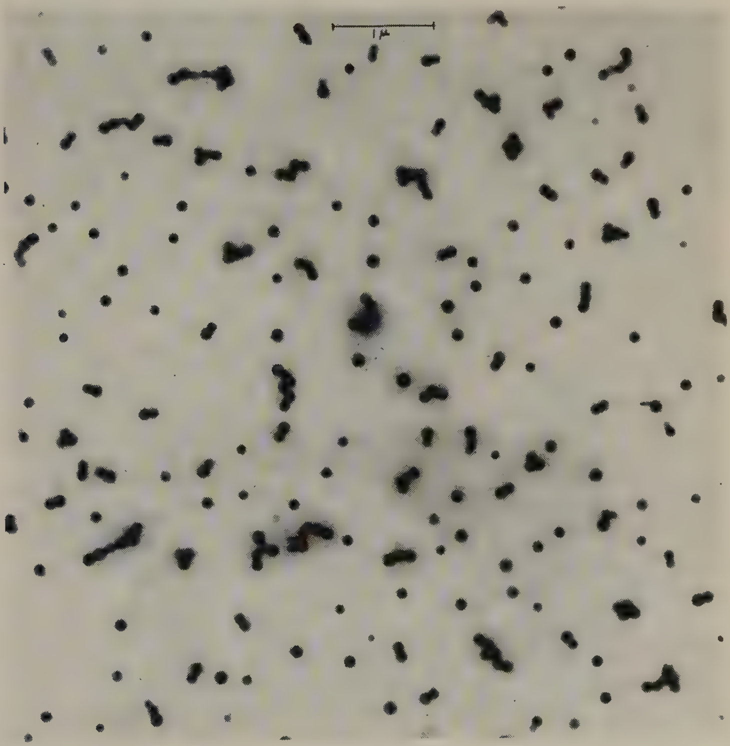

Fig. 7c

Fig. 7. The effect of bromination and irradiation on latex particles of polyethyl acrylate: (*a*) untreated; (*b*) brominated; (*c*) 93 mrads.

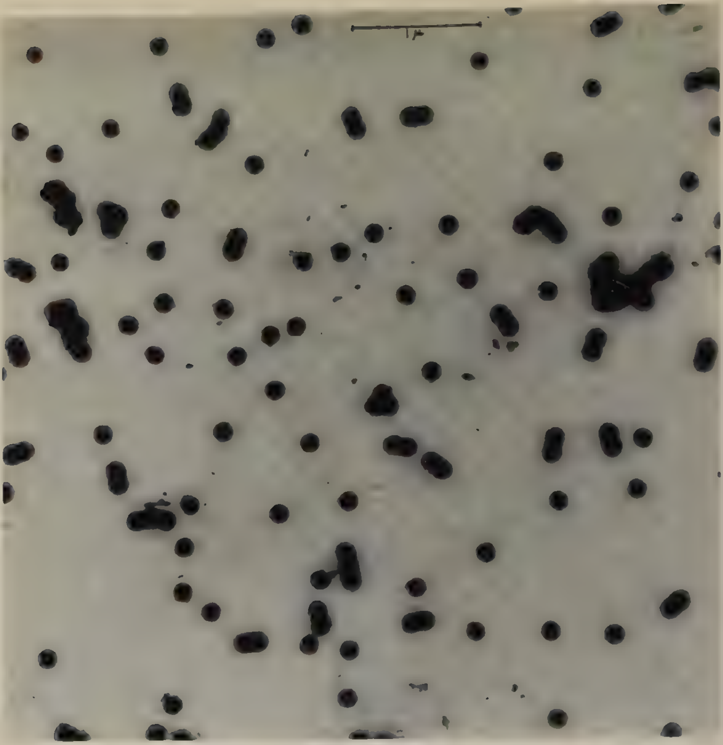

Fig. 8a

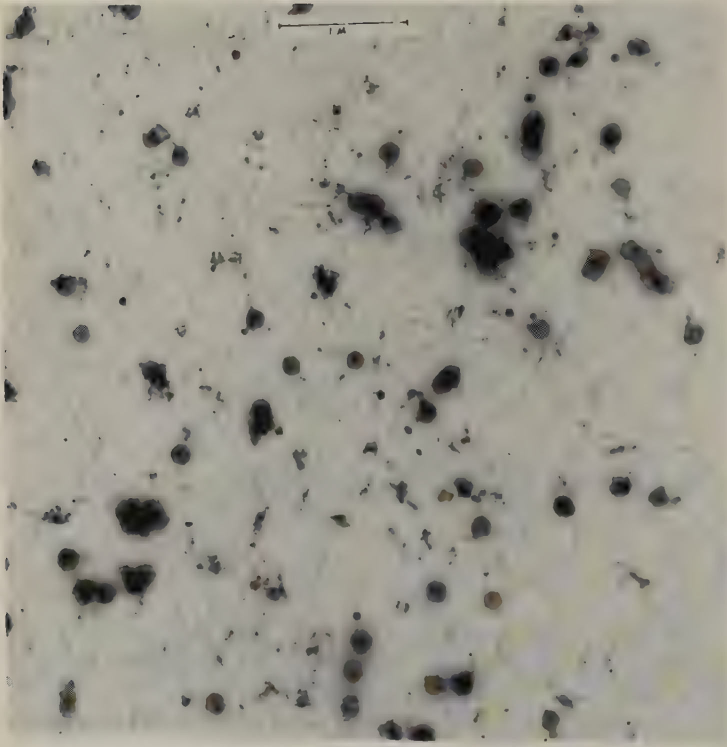

Fig. 8b

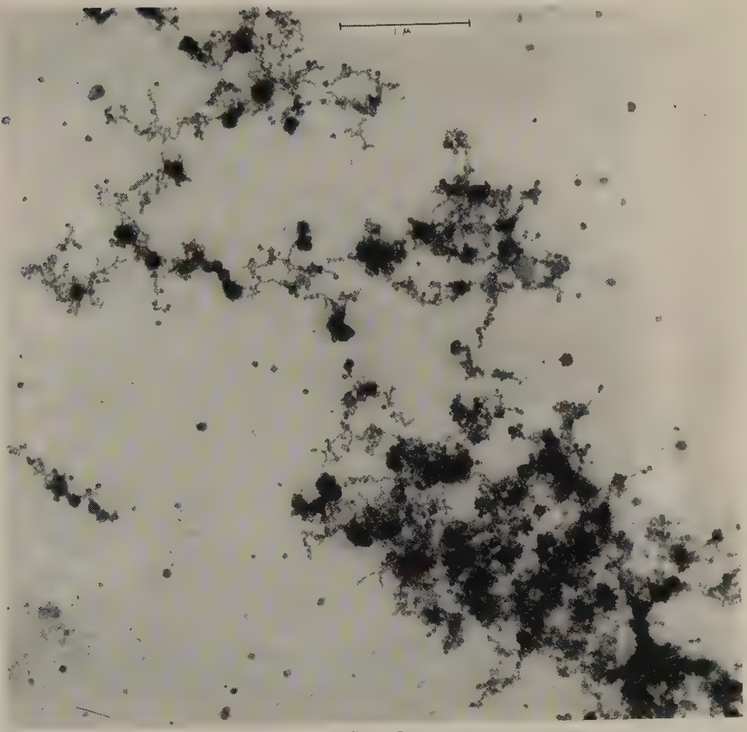

FIG. 8c

FIG. 8. The effect of irradiation on latex particles of polymethyl methacrylate: (*a*) untreated; (*b*) 23 mrads; (*c*) 186 mrads.

ticles after irradiation dosages of 23 and 186 mrads, respectively. Few of the original particles are observed after irradiation; much extraneous matter may be seen, however. This extraneous matter may arise from the disintegration of latex particles owing to excessive degradation of the polymer molecules.

## SUMMARY

Styrene-butadiene copolymer particles are hardened for electron microscopy by the addition of bromine to the residual double bonds. The amount of bromine required depends upon the butadiene content of the copolymer. The particle diameter increase on bromination ranges from 0.2% for polystyrene to 24.8% for polybutadiene.

High-energy electrons also harden these particles owing to the cross-linking of polymer molecules. The irradiation dosage required depends upon the composition and molecular weight of the copolymer. This technique is applicable to natural rubber and also to polymers which are unaffected by bromination, e.g., polyethyl acrylate and polyvinyl acetate. The degradation of polymethyl methacrylate particles on irradiation is evidenced by their apparent disintegration.

## ACKNOWLEDGMENTS

The authors gratefully acknowledge the assistance of W. D. Keiser, L. E. Morford, H. E. Campbell, and H. L. Tarkowski of the Physical Research Laboratory, and G. J. Atchison of the Radiochemistry Laboratory.

## REFERENCES

1. DANDLIKER, W. B., *J. Am. Chem. Soc.* **72,** 5110 (1950); ALFREY, T., JR., BRADFORD, E. B., VANDERHOFF, J. W., AND OSTER, G., *J. Opt. Soc. Amer.* **44,** 603 (1954); SCOTT, P. H., CLARK, G. C., AND SLIEPCEVICH, C. M., *J. Phys. Chem.* **59,** 849 (1955); TABIBIAN, R. M., HELLER, W., AND EPEL, J. N., *J. Colloid Sci.* **11,** 195 (1956); LAMER, V. K., AND PLESNER, I. W., *J. Polymer Sci.* **24,** 147 (1957).
2. SHARP, D. G., *J. Appl. Phys.* **21,** 71 (1950); CHENG, P. Y., AND SCHACHMAN, H. K., *J. Polymer Sci.* **16,** 19 (1955).
3. MARON, S. H., ELDER, M. E., AND ULEVITCH, I. N., *J. Colloid Sci.* **9,** 89 (1954); MARON, S. H., ELDER, M. E., AND MOORE, C., *ibid.* **9,** 104 (1954); MARON, S. H., AND ELDER, M. E., *ibid.* **9,** 263 (1954); *ibid.* **9,** 347 (1954); *ibid.* **9,** 353 (1954); KLEVENS, H. B., *J. Colloid Sci.* **2,** 365 (1947).
4. YUDOWITCH, K. L., *J. Appl. Phys.* **22,** 214 (1951); LEONARD, B. R., ANDEREGG, J. W., KAESBERG, P., AND BEEMAN, W. W., *ibid.* **23,** 152 (1952); DANIELSON, W. E., SHENFIL, L., AND DUMOND, J. W. M., *ibid.* **23,** 860 (1952).
5. BACKUS, R. C., AND WILLIAMS, R. C., *J. Appl. Phys.* **20,** 224 (1949); *ibid.* **21,** 11 (1950); SCOTT, G. D., *ibid.* **20,** 417 (1949); KERN, S. F., AND KERN, R. A., *ibid.* **21,** 705 (1950); MING FENG, I., *ibid.* **22,** 820 (1951); ELLIS, S. G., *ibid.* **23,** 728 (1952); BRADFORD, E. B., *ibid.* **23,** 609 (1952); WATSON, J. H. L., AND GRUBE, W., *ibid.* **23,** 793 (1952); MARON, S. H., MOORE, C., AND POWELL, A. S., *J. Appl. Phys.* **23,** 900 (1952); BRADFORD, E. B., AND VANDERHOFF, J. W., *ibid.* **26,** 864 (1955).

6. Bradford, E. B., and Vanderhoff, J. W., *J. Appl. Phys.* **26,** 864 (1955).
7. Bradford, E. B., Vanderhoff, J. W., and Alfrey, T., Jr., *J. Colloid Sci.* **11,** 135 (1956).
8. Bradford, E. B., and Vanderhoff, J. W., Presented at the Fourteenth Annual Meeting of the Electron Microscope Society of America, Madison, Wisconsin, September 10, 1956.
9. Brown, W. E., *J. Appl. Phys.* **18,** 273 (1947).
10. Willson, E. A., Miller, J. R., and Rowe, E. H., *J. Phys. & Colloid Chem.* **53,** 357 (1949).
11. Maron, S. H., Moore, C., and Powell, A. S., *J. Appl. Phys.* **23,** 900 (1952).
12. Schmidt, E., and Kelsey, R. H., *Ind. Eng. Chem.* **43,** 406 (1951).
13. Stromberg, R. R., Swerdlow, M., and Mandel, J., *J. Research Natl. Bur. Standards* **50,** 299 (1953).
14. Charlesby, A., *Proc. Roy. Soc.* (*London*) **A215,** 187 (1952).
15. Wall, L. A., and Brown, D. W., *J. Phys. Chem.* **61,** 129 (1957).

JOURNAL OF COLLOID SCIENCE **14** (1959)

LETTER TO THE EDITOR

# CALCULATION OF SURFACE TENSIONS OF LIQUIDS FROM LIQUID DENSITY AND VAPOR PRESSURE

It is well known that there is a relationship between the total surface energy and the heat of vaporization of a liquid. The approximation is often made that the total surface energy per mole of surface molecules is a fixed fraction of the molar heat of vaporization, since a surface molecule has a smaller number of near neighbors than a molecule in the interior.

The writer has found that, by somewhat analogous reasoning, it is possible to derive an expression for the free surface energy of a liquid as a function of its density, vapor pressure, and molecular weight. When a vapor is condensed to a liquid at the vapor pressure of that liquid, there is no change in free energy. However, if the vapor were not condensible and behaved like an ideal gas, there would be an increase in free energy equal to $RT \ln V_v/V_1$, where $V_v$ is the initial volume of the vapor and $V_1$ is the final volume. We can assume that the surface molecules of a liquid have a free energy content greater than the vapor molecules because some of their near neighbors are missing, so that they resemble to some extent a compressed perfect gas. As about ¼ of the neighbors are missing, this excess free energy should be ¼ $RT \ln V_v/V_1$. Since 1 mole of molecules at the surface occupy an area of $N^{1/3}\ (M/D)^{2/3}$, the excess free energy per unit area is

$$\gamma = \frac{RT \ln V_v/V_1}{4N^{1/3}(M/D)^{2/3}}, \qquad [1]$$

where $R$ is the gas constant, $T$ is the temperature, $V_v$ and $V_1$ are the molar volumes of vapor and liquid, $N$ is Avogadro's number, $M$ is the molecular weight, and $D$ is the density of the liquid. Assuming the ideal gas law, we may replace $V_v$ by $RT/P$. Making the proper numerical substitutions, we then obtain

$$\gamma = \frac{0.567\ T(4.795 + \log\ (TD/PM))}{(M/D)^{2/3}}, \qquad [2]$$

where $T$ is temperature in degrees K., $D$ is liquid density in grams per cubic centimeter, $P$ is vapor pressure in millimeters of mercury, and $M$ is molecular weight.

The assumption made in deriving these equations is simply that the surface molecules, which have only ¾ as many neighbors as the interior

TABLE I

| Substance | Temp. (°*K.*) | Liquid density (*g./c.c.*) | Mol. wt. | Vapor pressure (*mm.*) | Surface tension (*dynes/cm.*) | |
|---|---|---|---|---|---|---|
| | | | | | Calculated by Eq. [2] | Literature |
| | | | *Group 1* | | | |
| Hydrogen | 14.7 | 0.07 | 2.02 | 100 | 2.50 | 2.88 |
| Neon | 25.0 | 1.2 | 20.2 | 400 | 5.1 | 5.5 |
| Nitrogen | 70.0 | 0.80 | 28.0 | 330 | 9.6 | 10.6 |
| Bromine | 293 | 3.12 | 159.8 | 200 | 39.1 | 41.5 |
| Phosphorus trichloride | 293 | 1.574 | 137.4 | 95 | 28.2 | 29.1 |
| Carbon monoxide | 70.0 | 0.814 | 28.0 | 155 | 11.0 | 12.1 |
| Ethane | 143 | 0.597 | 30.0 | 38 | 21.9 | 22.9 |
| Propane | 173 | 0.646 | 44.0 | 22 | 22.7 | 23.4 |
| *n*-Butane | 203 | 0.670 | 58.1 | 19 | 22.9 | 23.4 |
| *n*-Hexane | 293 | 0.659 | 86.1 | 125 | 19.7 | 18.4 |
| *n*-Octane | 293 | 0.702 | 114.1 | 10.5 | 22.5 | 21.8 |
| *n*-Dodecane | 373 | 0.690 | 170.2 | 15 | 20.5 | 18.5 |
| *n*-Pentadecane | 423 | 0.676 | 212.2 | 19 | 18.9 | 16.9 |
| 2,2,3-Trimethylbutane | 293 | 0.690 | 100.1 | 82 | 19.2 | 18.8 |
| Benzene | 293 | 0.879 | 78.0 | 75 | 28.7 | 28.9 |
| Toluene | 293 | 0.867 | 92.0 | 22 | 28.9 | 28.5 |
| *o*-Xylene | 333 | 0.846 | 106.0 | 40 | 27.3 | 28.7 |
| Perfluoro *n*-heptane | 293 | 1.733 | 388.0 | 63 | 13.9 | 13.6 |
| Perfluoro methylcyclohexane | 293 | 1.799 | 350.0 | 90 | 14.9 | 15.4 |
| Perfluoro *p*-dimethylcyclohexane | 293 | 1.850 | 400.0 | 29 | 16.0 | 16.3 |
| Carbon tetrachloride | 293 | 1.595 | 153.8 | 85 | 26.4 | 26.9 |
| Chlorobenzene | 293 | 1.107 | 112.5 | 8.8 | 32.4 | 33.2 |
| Benzophenone | 305 | 1.10 | 182.2 | 0.0014 | 45.4 | 44.0 |
| Carbon disulfide | 293 | 1.26 | 76.0 | 325 | 32.1 | 32.3 |
| Water | 353 | 0.97 | 18.0 | 355 | 103.0 | 62.6 |
| Acetic acid | 293 | 1.05 | 60.0 | 11.7 | 48.5 | 27.6 |
| | | | *Group 2* | | | |
| Helium | 4.0 | 0.122 | 4.00 | 760 | 0.21 | 0.12 |
| Argon | 90.0 | 1.41 | 39.94 | 760 | 13.3 | 13.2 |
| Chlorine | 233 | 1.56 | 70.9 | 570 | 28.5 | 27.3 |
| Chlorine | 293 | 1.41 | 70.9 | 4990 | 22.8 | 18.4 |
| 2-Methylbutane | 293 | 0.620 | 72.0 | 575 | 17.0 | 15.0 |
| Propane | 233 | 0.578 | 44.0 | 830 | 17.3 | 15.2 |
| Benzene | 353 | 0.813 | 78.0 | 760 | 23.7 | 21.2 |
| Carbon dioxide | 248 | 1.00 | 44.0 | 12,630 | 16.2 | 9.1 |
| Ammonia | 332 | 0.54 | 17.0 | 19,000 | 22.0 | 13.0 |

molecules, have total free energy equal to $\frac{3}{4}F_1 + \frac{1}{4}F_{ig}$, where $F_1$ is the free energy of the bulk liquid (and the equilibrium vapor) and $F_{ig}$ is the free energy of an ideal gas compressed to the density of the liquid. This application of the concept of local interaction to free energy has theoretical objections, since the entropy term of the free energy cannot be localized in the same manner as the energy term. Nevertheless Eq. [2] appears to be quite useful.

Group 1 in Table I shows calculated and actual surface tensions of various liquids at fairly low temperatures (vapor pressure well under 1 atmosphere). Agreement of calculated with observed values is good. In most cases the calculated value agrees with the observed more closely than that obtained from the familiar Ramsay-Shields modification of the Eötvös equation. Equations [1] and [2] have the further advantage over the Ramsay-Shields equation of not including any arbitrary constant and of being based on variables which are more readily determined than the critical temperature. As would be expected, the equations do not hold for highly associated liquids such as water and acetic acid.

In another way, however, the equation is more limited than the Ramsay-Shields equation. It sometimes gives calculated surface tensions which are 10%–15% high when the temperature is high enough for the vapor pressure to approach 1 atmosphere, while at still higher vapor pressures, the calculated values become much too high (Group 2). Equation [2] can, however, be applied indirectly to calculate the surface tensions of liquids at higher temperatures. From the vapor pressure of the liquid at a lower temperature, an accurate calculation of surface tension can be made. This can be substituted into the Ramsay-Shields equation to obtain a calculated critical temperature. The Ramsay-Shields equation can then be applied, using this calculated critical temperature, to calculate surface tension at temperatures where the vapor pressure exceeds one atmosphere.

The data in the table are taken from the *Handbook of Chemistry and Physics*, *International Critical Tables*, and *Landolt-Börnstein, Physikalisch-Chemische Tabellen.*

*Lever Brothers Research Center* IRVING REICH
*Edgewater, New Jersey*
*Received March 11, 1959;*
*revised July 8, 1959*

JOURNAL OF COLLOID SCIENCE **14**, 565 (1959)

# BOOK REVIEW

**Brief Course in Organic Chemistry,** 2nd edition. By L. C. Behr, R. C. Fuson, and H. R. Snyder. John Wiley & Sons, Inc., New York 16, New York, 1959. 289 pp. Price $5.75.

This brief textbook of organic chemistry includes a large amount of basic information, and appears to be well designed for students whose primary interests are in areas requiring some knowledge of organic chemistry. The use of pictures of molecular models throughout the text, together with the structural formulas, is a particularly good feature of this book. The subject matter is intelligently condensed and clearly stated. Aromatic compounds are introduced early, and the integration of this material with the aliphatic compounds throughout the remaining chapters is well suited to a short course in organic chemistry. The reviewer feels that it would perhaps be more desirable to include the subject matter in the final chapter on "Mechanisms" throughout the text where it is pertinent to the reactions under discussion. On the whole, the selection of information included in the discussion of mechanisms is unusually good for the amount of space allotted to the subject. However, the illustration for the displacement reaction on page 271 is poorly drawn and does not show the inversion of the carbon atom in a clear way. The book appears to be quite free of errors; the one noted involves an incorrect structure of insulin on page 200. It is well known that insulin contains two chains, and not four, as given in the text.

The faults of the book are relatively minor, and this appears to be a good text indeed for a short course intended for students of agriculture, home economics, medical technology and related fields.

R. R. Becker, New York, New York

JOURNAL OF COLLOID SCIENCE **14**, 567–571 (1959)

# LIGHT SCATTERING OF COLLOIDAL SILICA[1]

**Byrg E. Bonnelycke and W. B. Dandliker**

*Department of Biochemistry, University of Washington, Seattle, Washington*

*Received July 13, 1959*

## INTRODUCTION

In the calibration of light-scattering instruments by the transmission method, the turbidities of a set of solutions are obtained in a spectrophotometer and are compared with the scattering at 90° to obtain the instrument constant.

A colloidal solution of silica (Ludox) has been used in this method for a number of years (1–9), on the assumption that it does not absorb at the wavelengths used. This assumption was based on the constancy of $\lambda_0^4\tau/(\eta_0\partial n/\partial c)^2$ with varying $\lambda_0$ as shown, for example, by Goring (10). Goring and co-workers, however, recently pointed out (9) that this constancy might still obtain approximately despite absorption and suggested that Ludox solutions develop absorption on aging.

We have employed a sensitive method to prove the absence of absorption by showing that for a set of solutions of the same silica concentration but increasing solvent refractive index, the turbidity and scattering due to the silica go to zero concomitantly.

## EXPERIMENTAL METHODS

Light-scattering measurements were made with a Brice-Halwer instrument employing the conical cell and cell container of Dandliker and Kraut (11). Photocurrents were read as voltage drops across a 20-megohm resistor by means of a Cambridge potentiometer. The instrument reading for solutions or blanks was taken as photocurrent at 90° with the cell in place divided by the photocurrent at 0° with the cell removed.

To measure the lowest turbidities encountered, a spectrophotometer with a 50-cm. cell was constructed on an optical bench. The instrument is shown diagrammatically in Fig. 1. A Bausch and Lomb grating monochromator (*A*) with mercury arc serves as the light source and illuminates the circular aperture (*1*) which is 1 mm. in diameter. Achromatic lens (*B*) with

---

[1] This work was supported by Grant No. H2217 of the National Heart Institute.

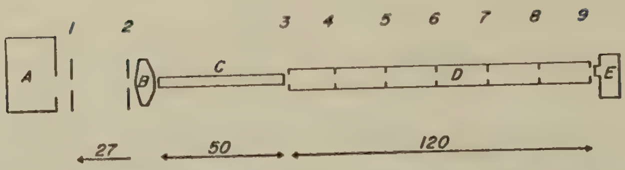

FIG. 1. Diagram of spectrophotometer using a 50 cm. cell. See text for description.

its aperture stop (*2*) focuses an image of (*1*) onto a diffusor plate in the photomultiplier tube housing (*E*). Two cells (*C*) were made of 25 mm. Pyrex tubing ground accurately to 50 cm. in length. End windows were made of microscope slides sealed on with an epoxy resin. Reproducible positioning of the cells is insured by two glass legs (near one end of the cell) terminating in more or less spherical glass feet resting in V-grooves 120° apart. The other end of the cell rests directly in a V-shaped support with sharp edges. Initial alignment of the cells was accomplished by heating the glass legs of the cell with a burner and by moving the cell into proper position while on the optical bench. The contribution of forward scattering to the emerging beam is minimized by a 1.2-m. blackened tube (*D*) having seven circular apertures just outside the main beam. The solid angle defined by aperture (*9*) and a point at the exit window of the cell (*C*) is about $10^{-4}$ steradians. In Fig. 1, the upper numbers (*1* through *9*) indicate circular apertures and the lower numbers (*27*, *50*, and *120*) indicate dimensions in centimeters. Photocurrents from a 1P21 photomultiplier tube housed in (*E*) were measured by a 10-turn Helipot shunted by a galvanometer which was used at constant deflection. The accuracy of the instrument was checked with potassium chromate using the data of Haupt (12), and also by comparison with the Beckman DU spectrophotometer when the turbidities were sufficiently high. The instrument is described in a thesis (13).

The stock 30% silica sol obtained from the E. I. DuPont de Nemours Company was from a special batch (G. C. −3413-85) selected during manufacture for its particle size (10–15 mμ) and particle weight ($10^6$). To vary the solvent refractive index, 25 ml. portions of the 30% stock Ludox were diluted with 0, 70, 110, 150, 200 ml. of reagent grade glycerol and each mixture was brought to 250 ml. with water. The blanks used in both the light-scattering instrument and the spectrophotometer were made from the appropriate amounts of water and glycerol. No attempt was made to remove the few large aggregates present in the stock Ludox solution, since it was felt that their elimination would not alter any absorption appreciably. The ratio of the vertical component in the scattered light at 25.8° divided by that at 90° was of the order of 1.29 for a 1/100 dilution of the stock 30% Ludox.

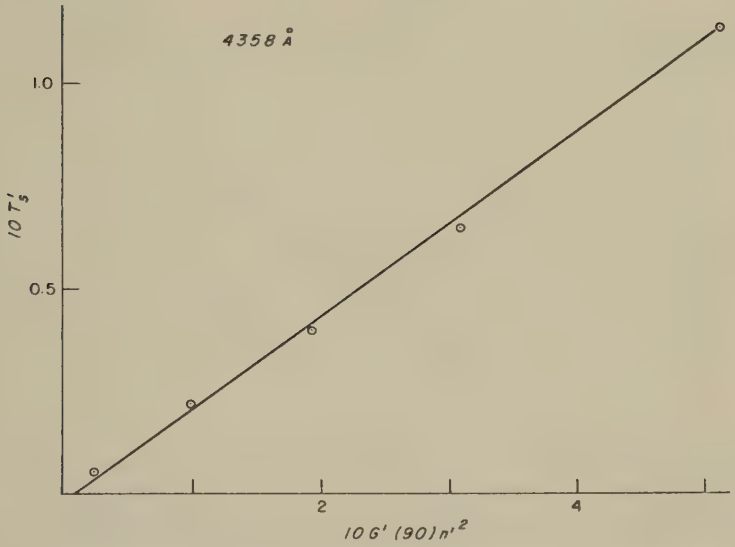

FIG. 2. Excess turbidity versus excess scattering at 4358 A for silica at constant concentration but varying solvent refractive index.

## RESULTS AND DISCUSSION

The excess turbidity is plotted versus excess scattering in Figs. 2 and 3 for two wavelengths. The values for excess scattering, $G'(90)$, have in each case been multiplied by $n'^2$, where $n'$ is the ratio of the refractive index of the solution to that of water. Literature data (14) on the refractivity of glycerol-water solutions were used to compute $n'$, which was assumed to be the same at 4358 A. and 5461 A. For the points in Fig. 2 and 3 beginning at the origin and proceeding to the upper right-hand corner the values of $n'^2$ applied are 1.18, 1.13, 1.10, 1.06, and 1.00, respectively. Figures 2 and 3 show that the 90° scattering and the turbidity measured by transmission are proportional to one another, indicating the absence of specific absorption in our Ludox silica sol. This method can also be used to ascertain whether the changes resulting from the aging of Ludox are due to absorption, as suggested by Goring *et al.* (9), or to the altered scattering accompanying aggregation.

The validity of the refractive index correction applied to Figs. 2 and 3 warrants some comment. Carr and Zimm (15) considering a point scatterer and Hermans and Levinson (16) a finite scattering volume have derived refractive index corrections for cells with plane or cylindrical surfaces. In our instrument the photometer never sees all the illuminated volume in the horizontal direction but sees past it in the vertical direction. This should give rise to a correction factor of $n$ in the horizontal direction (16).

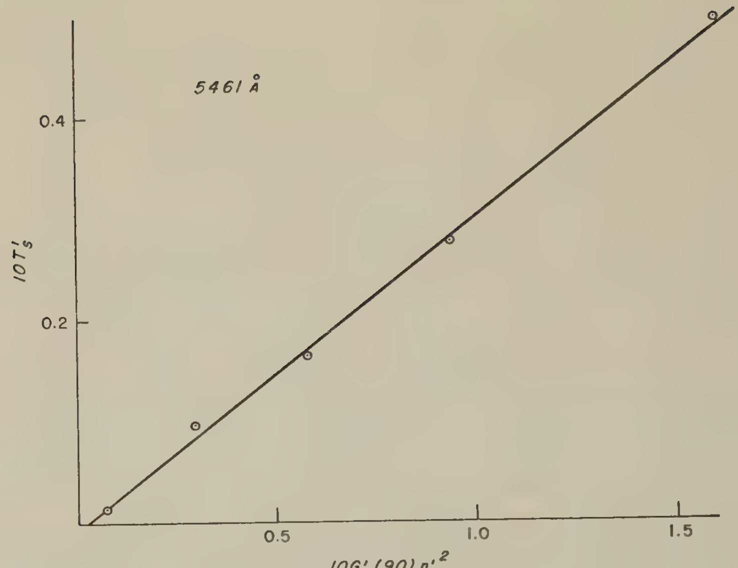

FIG. 3. Scattering at 5461 A, otherwise similar to Fig. 2.

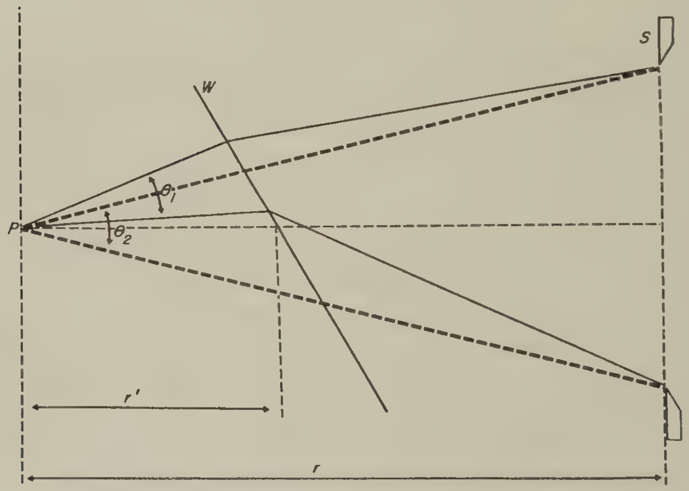

FIG. 4. Refractive index correction for a point scatterer inside a conical cell.

Following Carr and Zimm (15) the correction can be calculated for a point scatterer situated at $P$ (Fig. 4) on the axis of a conical cell. The cell wall $W$ makes an angle $i$ with the vertical direction (axis of revolution of the cone). The scattered light entering the photometer is defined by the slit $S$. The dotted lines indicate the path in the absence of refractive effects, and the solid lines the path when the ratio $n'$ of refractive index inside to that outside is greater than 1. The ratio $\theta_2/\theta_1$ can be found by approximation from the relationships:

$$\theta_1 = \gamma - \alpha$$

$$\theta_2 = 2\phi$$

$$\cos \alpha = \frac{r' \cos i \cos \phi \sin (\beta - \alpha)}{r \sin (\beta + \phi - i)}$$

$$\cos \gamma = \frac{r' \cos i \cos \phi \sin (\delta - \gamma)}{r \sin (\delta - \phi - i)}$$

$$\sin \beta = n' \sin \alpha$$

$$\sin \delta = n' \sin \gamma$$

The above equations reduce to those of Carr and Zimm (15) when $i$ is made sufficiently small. Under the circumstances of the present work $\theta_2/\theta_1$ reduces to approximately $n'$ leading to the total correction factor of $n'^2$.

## Summary

The absence of absorption in colloidal silica was demonstrated by varying the solvent refractive index of a set of solutions of the same silica concentration and by showing that the excess turbidity and scattering go to zero concomitantly. A spectrophotometer with a 50-cm. cell was used.

## References

1. Tietze, F., and Neurath, H., *J. Biol. Chem.* **194,** 1 (1952).
2. Oster, G., *J. Polymer Sci.* **9,** 525 (1952).
3. Mommaerts, W. F. H. M., *J. Colloid Sci.* **7,** 71 (1952).
4. Edelhoch, H., Katchalski, E., Maybury, R. H., Hughes, W. L., and Edsall, J. T., *J. Am. Chem. Soc.* **75,** 5058 (1953).
5. Oth, A., Oth, J., and Desreux, V., *J. Polymer Sci.* **10,** 551 (1953).
6. Maron, S. H., and Lou, R. L. H., *J. Polymer Sci.* **14,** 29 (1954).
7. Kraut, J., and Dandliker, W. B., *J. Polymer Sci.* **18,** 563 (1955).
8. Hughes, W. J., Johnson, P., and Ottewill, R. H., *J. Colloid Sci.* **11,** 340 (1956).
9. Goring, D. A. I., Senez, M., Melanson, B., and Huque, M. M., *J. Colloid Sci.* **12,** 412 (1957).
10. Goring, D. A. I., *Can. J. Chem.* **31,** 1078 (1953).
11. Dandliker, W. B., and Kraut, J., *J. Am. Chem. Soc.* **78,** 2380 (1956).
12. Haupt, G. W., *J. Research Natl. Bur. Standards* **48,** 414 (1952).
13. Bonnelycke, B. E., M.S. Thesis, University of Washington, 1958.
14. "International Critical Tables," ed. by E. W. Washburn. McGraw-Hill, New York, 1930.
15. Carr, C. I., and Zimm, B. H., *J. Chem. Phys.* **18,** 1616 (1950).
16. Hermans, J. J., and Levinson, S., *J. Opt. Soc. Amer.* **41,** 460 (1951).

JOURNAL OF COLLOID SCIENCE 14, 572–583 (1959)

# A SIMPLIFIED THERMODYNAMIC APPROACH TO CAPILLARITY

## I. APPLICATION TO FLOW IN CAPILLARY CHANNELS[1]

**Anthony M. Schwartz and Francis W. Minor**

*Harris Research Laboratories, Inc., Washington, D. C.*

*Received November 21, 1958; revised April 14, 1959*

### INTRODUCTION

The term "capillarity" as used in this discussion will refer primarily to the relative motion between a solid and a liquid, caused by the particular group of mechanical and hydrodynamic forces generally termed capillary forces. The fundamental mechanical system involved in capillarity consists of a liquid phase ($L$) in contact with a second fluid phase ($A$) which may be vapor or liquid, both fluid phases being in contact with a single solid phase ($S$). Capillary movement may be defined more precisely as the movement of the $L$-$A$-$S$ line boundary along the solid surface under the influence of the capillary forces. These are forces which arise from intermolecular attractions within condensed phases. They are responsible for the surface tension of liquids and for the characteristic contact angle at the boundary line between a solid and two fluids.

The classical treatments of capillarity and the procedures for solving familiar problems in capillarity are based most frequently on Laplace's equation for the pressure difference across a curved phase boundary between two fluids. This pressure difference is proportional to the curvature of the surface and can be expressed by the equation

$$p_1 - p_2 = \gamma[(1/R_1) + (1/R_2)], \qquad [1]$$

where $p_1$ and $p_2$ are the pressures within the two phases near the interface and $\gamma$ is the interfacial tension. The greater of the two pressures exists on the concave side of the interface. Equation [1] is valid for all cases where the thickness of the interface itself is small compared with the absolute values of $R_1$ and $R_2$, the principal radii of curvature of the interface (1).

The curvature of the fluid ($L$-$A$) interface is determined by the geometry of the solid surfaces with which it is in contact and by the contact angle at the $L$-$A$-$S$ boundary line. This classical treatment of capillarity is readily applied to systems in which the solid surfaces form closed cylindrical channels, or to systems having a single moving liquid front and a total volume of liquid which is large compared to the volume of the capillary spaces. In many such capillary systems the pressure difference due to curvature may be balanced against the hydrostatic pressure due to gravity, or against other mechanical pressures, to determine the movement of the liquid front.

---

[1] This work was performed in partial fulfillment of a research contract with the Chemical Warfare Laboratories, Army Chemical Center, Maryland.

Some time ago an extensive study was started in our laboratory of the movement of liquids in textile fabrics, particularly the wicking and penetration of single drops and small splashes. In systems of this type the liquid moves almost entirely by capillarity and the effect of gravity is negligibly small. Another characteristic of these textile fabric systems is the presence of two or more liquid fronts, fed from the same reservoir, moving simultaneously in different directions. For these reasons, and because the geometry of the solid surfaces is relatively complex, the conventional treatment based on curvature calculations was found impractically difficult to apply.

The treatment described below is based on the energy changes which take place during capillary motion. The energy approach is not new, although it has been largely neglected, and there are surprisingly few illustrations of its use in the literature of capillarity. It has proved very useful in explaining and calculating capillary motion in textile-liquid systems, and we believe it should be equally applicable to a wide range of other capillary systems.

## FUNDAMENTAL EQUATIONS FOR CAPILLARITY

Consider the system of Fig. 1, which shows in profile a flat-surfaced solid plate of fixed total surface area = $S$, upon which is placed a drop of liquid $AOHB$ having a fixed volume $V$. At any instant of time the free energy of the system, $F$, is expressed as:

$$F = \text{Area } LA \cdot \gamma_{LA} + \text{Area } SL \cdot \gamma_{SL} + \text{Area } SA \cdot \gamma_{SA} ,$$

where areas $LA$ and $SL$ refer to the liquid-vapor and solid-liquid interfacial areas, respectively, and the gammas refer to the free energy per unit area of the interfaces indicated in the subscripts. But Area $SA$ = Area $S$ − Area $SL$; therefore

$$F = \text{Area } LA \cdot \gamma_{LA} + \text{Area } SL \cdot \gamma_{SL} + \text{Area } S \cdot \gamma_{SA} - \text{Area } SL \cdot \gamma_{SA} ;$$

$$F = \text{Area } LA \cdot \gamma_{LA} + \text{Area } SL \cdot (\gamma_{SL} - \gamma_{SA}) + \text{Area } S \cdot \gamma_{SA} .$$

The term Area $S \cdot \gamma_{SA}$ is a constant for any specified system. Provided Area $S$ always remains larger than Area $SL$, so that a line boundary of three phases exists:

$$F = \text{Area } LA \cdot \gamma_{LA} + \text{Area } SL \cdot (\gamma_{SL} - \gamma_{SA}) + K. \qquad [2]$$

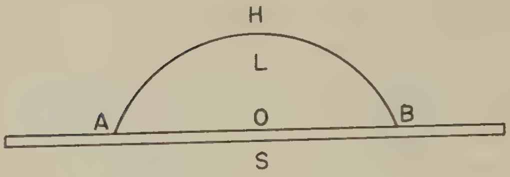

FIG. 1. Fundamental liquid-fluid-solid system.

In the region near the $L$-$A$-$S$ boundary line in any specified capillary system $\gamma_{LA}$, $\gamma_{SL}$, and $\gamma_{SA}$ all have fixed values, i.e., they are constants. For convenience in discussion we shall refer to $\gamma_{LA}$ as $k_1$, and to the quantity $(\gamma_{SL} - \gamma_{SA})$ as $k_2$.

Equation [2] can be considered the fundamental equation used in calculating the driving forces in capillary systems.

A system corresponding to the mathematical description of Eq. [2] can be considered as a representative capillary system in which gravitational forces (and any other forces tending to cause motion) are negligible when compared to the capillary forces associated with the interfacial free energies. A wide range of practical textile-liquid systems are of this simple type, to which the present discussion shall be limited.

Movement of the liquid relative to the solid in such a system corresponds to a change in the magnitude of Area $LA$ and/or Area $SL$. In order for such movement to occur spontaneously it must take place with a decrease in the free energy of the system. Thus, capillary movement will occur when and only when the time derivative of Eq. [2] is negative.

Differentiating Eq. [2] with respect to time, we obtain

$$\frac{dF}{dt} = k_1 \frac{d(\text{Area } LA)}{dt} + k_2 \frac{d(\text{Area } SL)}{dt}. \qquad [3]$$

On a qualitative basis it is frequently possible to determine the signs of $k_1[d(\text{Area } LA)/dt]$ and $k_2[d(\text{Area } SL)/dt]$ by simply inspecting the geometry of the system, provided that values for $k_1$ and $k_2$ are available. The value of $k_1$ is, of course, the free surface energy at the $L$-$A$-$S$ boundary line. In systems having a one-component liquid phase, the free energy at the line boundary is the same as at all other places on the liquid surface. With two or more components in the liquid phase, there is the possibility of variation in the free energy over the surface. The value of $k_2$ can be calculated from the equilibrium contact angle $\theta$ of the $L$-$A$-$S$ system using the relationship $\cos\theta = -k_2/k_1$. It can also be determined experimentally, using any suitable variation of the Wilhelmy plate technique, as described later in this paper. The value of $k_2$ is negative where $\theta$ is less than 90° and positive where $\theta$ is greater than 90°.

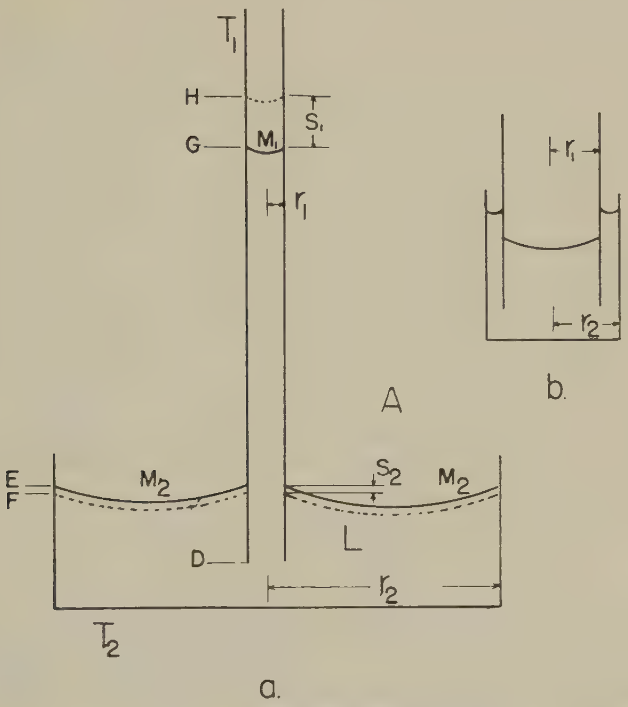

FIG. 2. Capillary tubes dipping into cylindrical reservoirs. *a.* Liquid rising in center tube. *b.* Liquid rising in annular space between tubes.

## DIRECTION OF CAPILLARY MOTION

A simple illustration of the use of Eq. [3] is provided by the familiar system of Fig. 2, in which a relatively small-bore cylindrical capillary tube $T_1$ dips into a reservoir of liquid $L$ contained in a cylindrical vessel $T_2$ of larger bore. Let us assume that the effect of gravity is negligible, and indeed it can be made negligible by using Plateau's technique (2). This consists in replacing air by a fluid $A$ which is immiscible with $L$ but has the same density as $L$.

In this system the total Area $S$ of Eq. [2] can be taken to be the internal wall area of $T_2$ plus the internal and external wall area of $T_1$. Area $LA$ is equal to the sum of the two meniscus areas $M_1 + M_2$. Area $SL$ is equal to the internal area of $T_2$ covered by liquid $L$, plus the internal area of $T_1$ from $D$ to $G$, plus the external area of $T_1$ from $D$ to $E$. For simplicity in calculation we may assume that the wall thickness of $T_1$ is negligible. When the liquid moves upward or downward in $T_1$, Area $LA$ remains constant but Area $SL$ changes.

When surface $M_1$ moves from $G$ to $H$, a distance $s_1$, the change in Area $SL$ is equal to

$$\Delta \text{ Area } SL = 2\pi r_1 s_1 - (2\pi r_2 s_2 + 2\pi r_1 s_2).$$

Since $s_1$ Area $M_1 = s_2$ Area $M_2$, $\Delta$ Area $SL$ is zero when $r_2 = 2r_1$. Thus, if $r_2 > 2r_1$ as in Fig. 2*a*, $\Delta$ Area $SL$ is positive when the liquid front $M_1$ moves from $G$ toward $H$. If $r_2 < 2r_1$ as in Fig. 2*b* $\Delta$ Area $SL$ is positive when the front $M_1$ moves from $G$ toward $E$.

Applying Eq. [3] to this system, the manner in which the signs of $\Delta$ Area $SL$ and of $k_2$ control the direction of liquid movement becomes evident. The liquid will move spontaneously in the direction which makes $\Delta$ Area $SL$ positive, provided $k_2$ is negative. If $k_2$ is positive the liquid will move in the opposite direction. If $k_2$ is zero (corresponding to an equilibrium contact angle of 90°), the liquid has no tendency to move. Thus the direction of liquid movement can be predicted without reference to the curvatures of the surfaces $M_1$ and $M_2$ and without direct or explicit reference to the contact angle, $\theta$, of the system.

## Calculation of Driving Force and Pressure

To calculate quantitatively the driving force or pressure associated with capillary movement it is necessary to express Area $LA$ and Area $SL$ in terms of some common convenient geometrical parameter of the system, $x$. Equation [2] can then be rewritten as

$$F = f(x) \cdot k_1 + g(x) \cdot k_2 + K, \qquad [4]$$

where $f(x) = $ Area $LA$ and $g(x) = $ Area $SL$.

This equation can now be differentiated with respect to $x$ to give

$$dF/dx = f'(x) \cdot k_1 + g'(x) \cdot k_2 . \qquad [5]$$

Equation [5] can be used to calculate numerically the change in $F$, corresponding to the change in $x$. From the geometry of the system $\Delta s$, the change in location of the liquid front in the desired direction, can be expressed as a function of $\Delta x$ and can therefore be calculated and expressed as a function of $\Delta F$.

The average force $Q$ driving the liquid front through the distance $\Delta s$ is given by the equation

$$\Delta F = Q \cdot \Delta s. \qquad [6]$$

If the liquid front is moving in a thermodynamically reversible manner, the pressure is constant from point to point over the $L$-$A$ interface. We can then write

$$P = Q/(\text{Area } LA).$$

Thus the pressure causing the liquid front to move is calculable with no reference to the curvature of the front.

It should be noted that the value of $k_2$ may vary from point to point over a contaminated surface or a nonhomogeneous surface. It is the equilibrium value of $k_2$ *at the locus of action on the L-A-S line boundary* which determines $\Delta F$ and $Q$ at that point.

As an illustration this treatment may be applied to the system of Fig. 2*a*. In this system it is convenient to choose $s_1$, the distance moved by the liquid front $M_1$ in the direction from $G$ toward $H$, as the independent variable $x$ in terms of which Area $LA$ and Area $SL$ are expressed.

For purposes of illustration, let $k_2 = -30$ and $k_1 = 40$; let $r_1 =$ unit distance and $r_2 = 10$ units of distance.

$$\frac{dF}{ds_1} = 40\,\frac{d(\text{Area } LA)}{ds_1} - 30\,\frac{d(\text{Area } SL)}{ds_1}\,.$$

Since Area $LA$ remains constant as $s_1$ changes,

$$\frac{dF}{ds_1} = -30\,\frac{d(\text{Area } SL)}{ds_1}\,.$$

As the liquid rises 10 units of distance in the tube of $r_1$, Area $SL$ is increased by $20\pi$ in the tube of $r_1$, and decreased by $2.2\pi$ in the tube of $r_2$, a net gain of $17.8\pi$ units of solid-liquid area, i.e.,

$$\frac{d(\text{Area } SL)}{ds_1} = 1.78\pi$$

and $dF/ds_1 = -53.4\pi$ energy units per unit distance rise in the small tube. This is equal to the *force* driving the liquid up the tube, since the tube is uniform in diameter. Since this force is distributed over $\pi r_1^2$ or $\pi$ units of area, the *pressure* exerted by the liquid front is 53.4 pressure units. When $r_1 = 1$ cm., the pressure is 53.4 dynes/cm.$^2$. Note that the pressure on the surface of liquid in the reservoir can be calculated in the same manner. In this case there is a net gain of $17.8\pi$ units in Area $SL$ for a decrease of 0.101 distance unit in $s_2$, i.e., $[d(\text{Area } SL)/ds_2] = 176\pi$ and $dF/ds_2 = -5280\pi$ force units. This force is distributed over $\pi(r_2^2 - r_1^2)$ or $99\pi$ units of area. The pressure, therefore, is equal to 53.4 dynes/cm.$^2$.

It is noteworthy that in this system a portion of the net driving pressure (the portion due to the liquid front $M_1$ at $G$) can easily be calculated from Laplace's equation [1]. Since the tube is cylindrical, the surface $M_1$ is spherical and

$$\Delta P_{M_1} = \frac{2\gamma\cos\theta}{r_1} = \frac{-k_2}{k_1}\cdot\frac{2\gamma}{r_1}\,.$$

Using the above values for $k_1$ and $k_2$, $\Delta P_{M_1} = 60$ dynes/cm.$^2$.

The opposing portion of the net driving pressure due to $M_2$ at $E$ cannot easily be calculated by the classical method, however, because the curvature of the nonspherical surface $M_2$ is not readily evaluated.

## MODEL CAPILLARY SYSTEMS

There are several relatively simple capillary systems which serve as excellent models for the systems encountered in textile fabrics. These systems can, in general, be resolved more satisfactorily by the above method, using Eqs. [2] to [6], than by the conventional methods based on Eq. [1]. Four such systems are illustrated below.

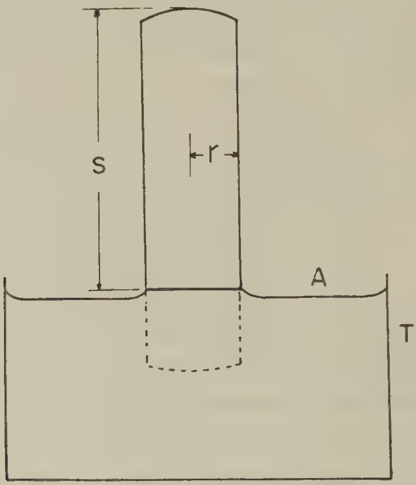

FIG. 3. Pull of a liquid on a cylindrical Wilhelmy plate.

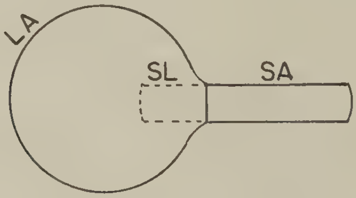

FIG. 3*a*. Pull of liquid on cylinder when gravity is negligible.

## PULL OF A LIQUID ON A WILHELMY PLATE IN THE FORM OF A CYLINDER

Figure 3 represents a large reservoir of liquid into which is dipping a solid cylindrical rod. It is known that the liquid exerts a positive pull on the rod when the contact angle is less than 90°, i.e., when $k_2$ is negative. To calculate the pull from the basic equation [2] the procedure is as follows: As the rod moves in and out of the liquid, Area $LA$ remains constant ($A$ in the diagram): Area $SL$ increases as $s$ decreases. Assuming that the cross-sectional area of the rod ($\pi r^2$) is very small compared with Area $LA$, the changes in Area $SL$ on the walls of the container $T$ become negligible, and

$$-d(\text{Area } SL) = 2\pi r\, ds.$$

Therefore,

$$dF/ds = Q = -k_2 \cdot 2\pi r. \qquad [7]$$

When $k_2$ has a negative value, $dF/ds$ is positive and $F$ decreases as $s$ decreases, i.e., the liquid exerts a pull on the rod.

The classical expression for pull on the rod in this system is

$$Q = 2r\gamma_{LA} \cos \theta.$$

It can be shown that $\cos \theta = -k_2/\gamma_{LA}$.
Thus, the classical expression and Eq. [7] are identical.

It is noteworthy that the *physical* pull on the rod cannot exceed $2\pi r k_1$ even though $k_1$ can be less than $-k_2$. When $k_1$ is less than $-k_2$, and a withdrawing force greater than $2\pi r \cdot k_1$ is applied to the rod, the liquid surface yields to this force and allows itself to be broken (extended). The break occurs at the solid-liquid boundary, so that the liquid surface maintains its shape according to Laplace's formula.

It should also be noted that in the absence of gravity the system described would in general not have the appearance of Fig. 3, but rather that of Fig. 3*a*. The liquid would require no container and it would be substantially spherical in shape. As the solid rod moved into or out of the liquid, Area $LA$ would change and this change would have to be accounted for in a rigorous calculation. This system frequently occurs in practice when single fiber ends encounter small droplets of liquid.

## Capillary Motion of Liquid between Two Parallel Rods

It is an experimental fact that when two parallel fibers are dipped into a liquid, or when a large drop of liquid is placed across the two fibers, capillary motion can occur. The motion occurs, however, only when the distance separating the fibers is less than a fixed calculable critical value. The problem is to calculate this critical separation and to evaluate the capillary forces.

Consider the system illustrated in Figs. 4 to 6. Assume for simplicity in calculation that the sides of the rods ($AB$ and $A'B'$) are flat and that the air surfaces of the advancing liquid column are flat. In practice the liquid-air surfaces have curved boundaries and the calculations are thus more complicated. The results, however, are completely analogous to those outlined below. Assume also that the reservoir $L$ is very large, so

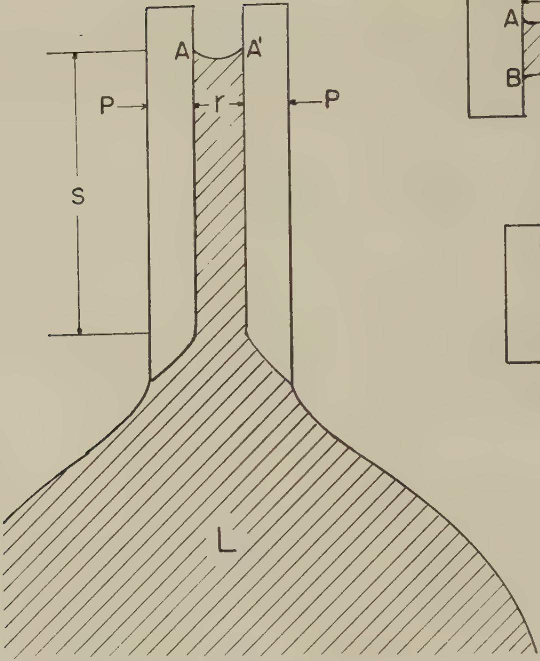

FIG. 4

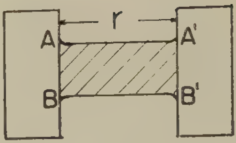

FIG. 5

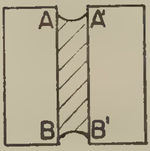

FIG. 6

FIG. 4. Parallel rods surrounded by large drop of liquid.
FIG. 5. Top view. Rods far apart.
FIG. 6. Top view. Rods close together.

that we may neglect the new solid-air interface exposed on the reservoir walls as liquid moves out of the reservoir.

Considering the liquid front to advance a distance $s$ between the rods

$$\frac{dF}{ds} = \frac{d}{ds}\,(\text{Area } LA)\cdot k_1 + \frac{d}{ds}\,(\text{Area } SL)\cdot k_2\,; \qquad [8]$$

$$\frac{d}{ds}\,(\text{Area } LA) = \text{the linear distance } AA' + BB';$$

$$\frac{d}{ds}\,(\text{Area } SL) = \text{the linear distance } AB + A'B'.$$

Substituting in Eq. [8]

$$\frac{dF}{ds} = 2k_1\cdot AA' + 2k_2\,AB.$$

Thus for $dF/ds$ to be negative, and for the liquid to start advancing $AB$ must be greater than $k_1/-k_2\cdot AA'$.

It is evident that as the rods are moved closer, $AA'$ decreases and $AB$ increases. The value of $dF/ds$, equal to the force against the liquid front, decreases (i.e., becomes greater in the negative direction). It is also evident that if $k_1 = -k_2$, $AB$ need only exceed $AA'$ for wicking to proceed.

As in the case of the Wilhelmy plate, $-k_2$ may in fact be greater than $k_1$, but for purposes of calculating the capillary movement of the liquid it cannot exceed the value of $k_1$. This expresses the fact that any stress greater than $k_1$ applied to the liquid simply causes the liquid surface to yield.

When $dF/ds$ is negative and wicking is proceeding there exists a pressure $P$ (shown at $P$ in Fig. 4) tending to push the two rods together. This can be calculated by differentiating the free energy $F$ with respect to $r$, the distance $AA'$. It is evident that we may consider either $s$ to remain constant while $AB$ and $r$ change, or $AB$ to remain constant while $s$ and $r$ change. In this case let $s$ remain constant while $r$ and $AB$ change. The quantity $r \cdot AB$ is also a constant which we shall call $C$.

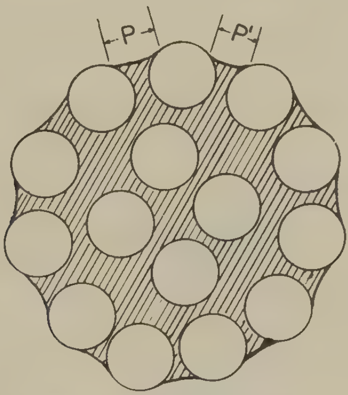

FIG. 7. Liquid moving in yarn. Yarn and liquid viewed (schematic) in cross section.

$$\frac{dF}{dr} = 2k_1 s + 2k_2 s \cdot \frac{d}{dr}(C/r);$$

$$\frac{dF}{dr} = Q = 2k_1 s - \frac{2k_2 s \cdot AB}{r}.$$

The value of $dF/dr$ is positive because $F$ decreases as $r$ decreases. The total force pushing the rods together is the quantity $Q$ above. The pressure pushing the rods together, $P$, is given by the expression

$$P = \frac{Q}{ABs} = \frac{Qr}{Cs}.$$

## CAPILLARY MOTION OF LIQUID IN A YARN

A cross section of a model yarn with liquid moving parallel to the yarn axis is pictured schematically in Fig. 7. Direct examination and measurement of this system shows that it consists of 15 similar filaments of circular cross section. If we call the radius of each cross section 1 unit of length, the total length wet filament perimeter is found to measure about 84 units. The total liquid-air boundary along the cross section $(P + P' \cdots)$ measures about 11 units. The liquid-air front (shaded area) which remains constant as the liquid advances is approximately 31 square units in area.

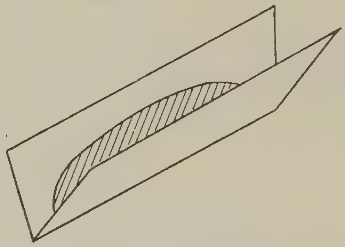

FIG. 8. Liquid in a notch.

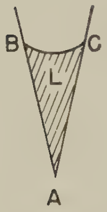

FIG. 9

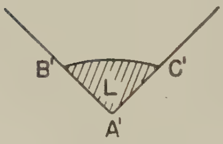

FIG. 10

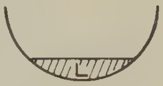

FIG. 11

FIG. 9. Narrow notch.
FIG. 10. Wide notch.
FIG. 11. Semicylindrical trough.

Let the liquid advance a distance $s$ toward the reader, perpendicular to the plane of the page. Differentiate the free energy with respect to $s$, as in Eq. [8].

$$\frac{d(\text{Area } LA)}{ds} = (P + P' \cdots) = 11;$$

$$\frac{d(\text{Area } SL)}{ds} = 84;$$

$$\frac{dF}{ds} = 11 \cdot k_1 + 84 k_2 .$$

In a typical liquid-fiber system, $k_1$ may have a value of 40 ergs per cm.$^2$ and $k_2$ a value of $-30$ ergs per cm.$^2$. In this case the total force normal to the liquid front would be 2080 dynes and the pressure would be 67 dynes per cm.$^2$.

## CAPILLARY MOTION OF LIQUID IN A V-SHAPED NOTCH OR TROUGH

A form which may be assumed by liquid in a **V**-shaped notch is shown in Fig. 8. The problem is to predict the motion of the liquid based on the geometry of the system and the constants $k_1$ and $k_2$.

Assume that $k_2$ is negative but that $k_1$ is greater than $-k_2$. This corresponds to a contact angle between zero and 90°.

The system is governed by Eq. [8] where $s$ is distance lengthwise along the notch.

Figures 9 and 10 show two notches of differing angle. In the two notches

$$\frac{d(\text{Area } LA)}{ds} = BC \text{ and } B'C', \text{ respectively.}$$

Similarly

$$\frac{d(\text{Area } SL)}{ds} = 2AB \text{ and } 2A'B', \text{ respectively.}$$

The ratio $BC/BA$ is small, whereas the ratio $B'C'/B'A'$ is relatively greater. It is evident that there is a value of $k_2/k_1$ for which the liquid will move lengthwise in $ABC$ but not in $A'B'C'$. Furthermore, it is evident that if the liquid does move (i.e., if $dF/ds$ is negative) it will keep moving indefinitely until the liquid surface coincides with $A$. Note that this will happen even though the contact angle is greater than zero, provided it is less than 90°.

For any value of $k_2$ less than zero but greater than $-k_1$, there is a critical vertex angle $BAC$ of the notch. If the vertex angle is greater than the critical, the liquid will not keep spreading but will eventually stop in some such position as illustrated in Fig. 8.

A semicylindrical trough is shown in Fig. 11. Here the "vertex angle" may be regarded as 180°. The liquid will keep spreading in this trough only if $-k_2$ is equal to or greater than $k_1$, i.e., if the contact angle is zero.

## REFERENCES

1. Authoritative discussions of the basic theory of capillarity are contained in POYNTING AND THOMSON: "Text Book of Physics," Vol. 1, "Properties of Matter," Griffin & Co., London, 1903; in ADAM, N. K., "The Physics and Chemistry of Surfaces," 3rd ed., Oxford University Press, London, 1941; and in BOUASSE, H., "Capillarité phenomenes superficiels," Delagrave, Paris, 1924.
2. PLATEAU, Smithsonian Institution Annual Reports, 1863, 1864, 1865, and 1866.

JOURNAL OF COLLOID SCIENCE 14, 584–597 (1959)

# A SIMPLIFIED THERMODYNAMIC APPROACH TO CAPILLARITY

## II. APPLICATIONS TO CONTACT ANGLE AND SPREADING PHENOMENA[1]

**Anthony M. Schwartz and Francis W. Minor**

*Harris Research Laboratories, Washington 11, D. C.*

*Received April 14, 1959*

### Introduction

In the previous publication of this series, a fundamental capillary system was defined as consisting of a solid phase $S$, a liquid phase $L$, and a second fluid phase $A$, in mutual contact. It was shown that free energy of the system can be expressed by the equation

$$F = \text{Area } LA \cdot k_1 + \text{Area } SL \cdot k_2 + K, \tag{1}$$

and that the free energy change associated with the capillary motion in this system can be expressed by the equation

$$dF = d(\text{Area } LA) \cdot k_1 + d(\text{Area } SL) \cdot k_2 , \tag{2}$$

where the areas relate to the indicated interphase boundary areas, $k_1$ is the free surface energy per unit area of the $LA$ interface at the $L$-$A$-$S$ boundary $= \gamma_{LA}$, and $k_2 = (\gamma_{SL} - \gamma_{SA})$.

Certain aspects of capillarity, particularly the spreading of a drop of liquid over an open solid surface, are not easily described in conventional terms without referring to the contact angle $\theta$ at the $LAS$ boundary. Most modern expositions of surface chemistry and physics use either of two methods in deriving the expression for the solid-liquid-vapor contact angle in terms of the free surface energies of the three phases. The first and by far the most common method is to use the familiar vector construction, attributed to Young and Dupré, shown in Fig. 1*a*. This is frequently criticized for lack of rigor. In particular, the substituting of hypothetical forces for the free surface energy values of the solid-vapor ($SA$) and solid-liquid ($SL$) interfaces is open to criticism. The second method is usually referred to as the thermodynamic derivation of Young's equation. It is

---

[1] This work was performed in partial fulfillment of a research contract with the Chemical Warfare Laboratories, Army Chemical Center, Md.

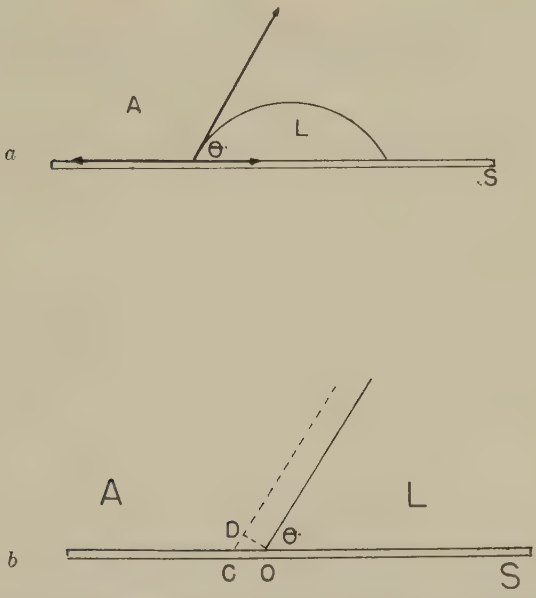

FIG. 1. Conventional representation of forces involved in determining the contact angle. (*a*) Dupré-Young diagram. (*b*) Classical thermodynamic interpretation.

ascribed to Quincke and has been presented in modern terms by Poynting and Thomson, Baxter and Cassie, Moilliet and Collie, and others (1). It is illustrated in the diagram of Fig. 1*b*. While the $LA$ interface stands at the equilibrium angle $\theta$ to the $SA$ interface, the line boundary is moved a distance along the solid surface from $O$ to $C$. The liquid front is assumed to move parallel to itself since the system is at equilibrium. Thus, if a small displacement of $O$ toward $C$ causes $\theta$ to decrease, a similar displacement of $O$ away from $C$ would cause $\theta$ to increase. If the distance $OC$ is called $dx$, the energy changes associated with the area changes are $\gamma_{SA} \cdot dx$, $\gamma_{SL} \cdot dx$, and $\gamma_{LA} \cos \theta \cdot dx$. At equilibrium, the algebraic sum of the energy changes is equal to zero, and the Young equation is thereby established. Neither of the above methods can provide any information on the configurations the system might assume while in the process of reaching equilibrium. Thus they cannot describe the changes in the phase boundary areas, nor in the angle between the $LA$ interface and the $SL$ interface as this quantity approaches its equilibrium value $\theta$.

The purpose of this paper is to show how Eq. [2] may be used advantageously in the treatment of contact angle phenomena. Particular emphasis is placed on the relationship of contact angle to the geometry of the total $LAS$ system, on apparent vs. real contact angles, and on certain aspects of contact angle hysteresis.

In all the systems which are discussed below it is assumed that gravitational forces and other mechanical forces are negligible, unless otherwise specified. It is also assumed that the liquid phase consists of a single component and is substantially nonvolatile. Under these conditions the Laplace equation for pressure difference across a curved phase boundary between two fluids may be written

$$P_1 - P_2 = \gamma\left(\frac{1}{R_1} + \frac{1}{R_2}\right) = C, \qquad [2a]$$

where $C$ is constant from point to point over the whole interface; $R_1$ and $R_2$ are the principal radii of curvature of the interface.

## DERIVATION OF EQUILIBRIUM CONTACT ANGLES IN SYSTEMS OF VARIOUS SHAPES

### *A. Droplet on a Flat Plate or a Sphere*

The system of Fig. 2 consists of a flat, solid plate *AOB*, in contact with which is placed a drop of liquid *AOBH* having a fixed volume *V*. The flat, solid surface is represented by *AOB*, which also represents the profile of Area *SL*. The profile of the liquid-vapor surface, Area *LA*, is represented by *AHB*. The contact angle *OAP* is represented by $\theta$ and is equal to angles *OCA* and *OCB*. Laplace's law of constant curvature governs the equilibrium form of the *LA* interface which maintains the form of a spherical

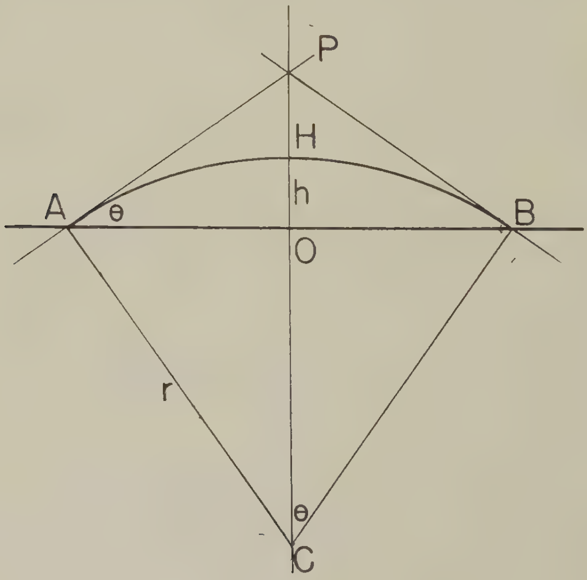

FIG. 2. Drop of liquid on a flat plate.

zone of height $OH = h$. The $LAS$ boundary of $AOB$ will move along the solid surface until equilibrium is established, i.e., until

$$dF = 0. \qquad [3]$$

Starting with Eq. [2], it is necessary only to set up expressions for Area $LA$ and Area $SL$ and solve Eq. [3].

As in previous discussions, we shall call $\gamma_{LA} = k_1$, $(\gamma_{SL} - \gamma_{SA}) = k_2$, and $S \cdot \gamma_{SA} = K$. It should be noted that $k_2$ is negative if $\gamma_{SA} > \gamma_{SL}$. In most practical cases, $k_2$ is, indeed, negative. As we shall see later, a negative value of $k_2$ corresponds to a contact angle of less than 90°.

In this case it is expedient to express Area $LA$ and Area $SL$ in terms of $h$ as the variable parameter for the areas; $V$ is, of course, also a necessary parameter.

The equations are as follows:

$$V = \pi r h^2 - \frac{\pi}{3} h^3;$$
$$r = \frac{V}{\pi h^2} + \frac{h}{3}. \qquad [4]$$

$$\text{Area } LA = 2\pi r h;$$
$$= \frac{2V}{h} + \frac{2\pi h^2}{3}. \qquad [5]$$

$$\text{Area } SL = \pi \overline{AO}^2 = 2\pi r h - \pi h^2; = \text{Area } LA - \pi h^2 = \frac{2V}{h} - \frac{\pi h^2}{3}. \qquad [5a]$$

$$F = k_1 \left( \frac{2V}{h} + \frac{2\pi h^2}{3} \right) + k_2 \left( \frac{2V}{h} - \frac{\pi h^2}{3} \right) + K.$$
$$\frac{dF}{dh} = \frac{2\pi}{3} (2k_1 - k_2) h - \frac{2V(k_1 + k_2)}{h^2} \qquad [5b]$$

Equating to zero and solving:

$$h^3 = \frac{3V(k_1 + k_2)}{\pi(2k_1 - k^2)};$$
$$h = \frac{[3V(k_1 + k_2)]^{1/3}}{[\pi(2k_1 - k_2)]^{1/3}}. \qquad [6]$$

Equation [4] is a formula for the volume of a spherical segment. Equation [5] is a formula for the area of the spherical zone. The expression for $F$ is simply a substitution in Eq. [1]. When $dF/dh$ is zero, the surface free energy of the system is minimum and $h$ assumes the value shown in Eq. [6].

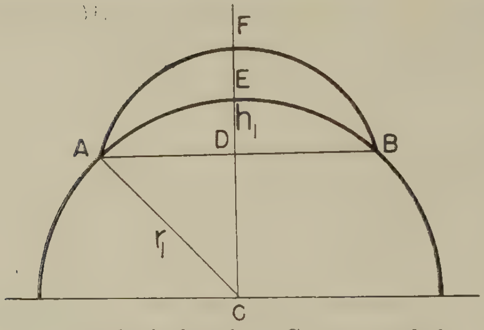

FIG. 3. Drop on a spherical surface. Contact angle less than 90°.

Using Eq. [6], it is evident that we can (by assigning numerical values to $V$, $k_1$, and $k_2$) calculate the equilibrium values for Area $LA$, Area $SL$, $r$, the contact angle $\theta$, or any other parameter of the system in which we are interested.

The calculation for contact angle is as follows:

$$\cos\theta = \frac{r-h}{r};$$

$$r = \frac{V}{h^2} + \frac{h}{3}.$$

Substituting:

$$\cos\theta = \frac{3V - 2h^3}{3V + h^3}.$$

Substituting the value for $h^3$ (Eq. [5$c$]) and simplifying:

$$\cos\theta = -\frac{k_2}{k_1}. \qquad [7]$$

By means of the simple expression shown as Eq. [7], we can calculate $\theta$ if we know the values for $k_1$ and $k_2$.

If $\gamma_{SL} = \gamma_{SA}$, then $k_2 = 0$ and $\theta$ becomes 90°. In this case the drop has a hemispherical shape.

Expressions for $F$ and $\theta$ in the system of Fig. 3, where the drop of liquid $AEBF$ rests on a sphere of radius $= r_1$, have also been worked out. This was done by assuming an arbitrary fixed value for $V$, the volume of the drop, as a fraction of $r_1$. The numerical values of Area $LA$ ($AFB$) and Area $SL$ ($AEB$) were calculated in terms of a series of assumed values for $ED$ ($h_1$). Arbitrary values were then assigned to $k_1$ and $k_2$. The function

$$F = \text{Area } LA \cdot k_1 + \text{Area } SL \cdot k_2$$

was then plotted graphically against $h_1$ and the minimum point in this curve was taken as the equilibrium value of $h_1$. The contact angle was calculated from this equilibrium value of $h_1$. Regardless of the values assigned to $V$, $k_1$, and $k_2$, the value for $\cos \theta$ was equal to $-k_2/k_1$ just as in the system of Fig. 2.

In any system involving a given volume of liquid $V$ disposed against a solid surface of fixed, geometrically describable configuration, we may apply the above procedure to calculate the equilibrium values for Area $SL$, Area $LA$, and the contact angle.

The procedure may be summarized as follows:

*1.* Using Laplace's relationship (Eq. [2$a$]) find the geometrical form of the liquid-air surface (Area $LA$). This may be spherical or cylindrical or may have any of a variety of other forms which have been worked out and are known to satisfy the Laplace's relationship. Write the algebraic expression for this form in terms of a satisfactory parameter. It is noteworthy that the choice of a suitable parameter may involve considerable trial and error.

*2.* Similarly, write the algebraic expression for the form of the solid-liquid interface (Area $SL$) in terms of the same parameter. Note that the expressions for Area $LA$ and Area $SL$, which we shall call $f(x)$ and $g(x)$, respectively, both contain $V$, the fixed volume of the liquid.

*3.* Calling the chosen parameter $x$, write Eq. [1] as follows:

$$F = f(x) \cdot k_1 + g(x) \cdot k_2 + K. \tag{1b}$$

*4.* If possible, differentiate with respect to $x$, obtaining

$$\frac{dF}{dx} = f'(x) \cdot k_1 + g'(x) \cdot k_2.$$

*5.* Equate the above expression to zero and solve for $x$. This gives the equilibrium value for $x$, from which the equilibrium values for Area $LA$ and Area $SL$ can be calculated.

*6.* The value of $\theta$, the contact angle, can be calculated from the values for Area $LA$ and Area $SL$ and the geometry of the system. The only calculations which we have made to date have been on systems where $LA$ is spherical in form. In all these systems, the value of $\theta$ has been found equal to $-k_2/k_1$. This is completely in accord with the classical theory, even though the classical derivation differs quite widely in detail from the present derivation and does not use the constant $k_2$.

*7.* Where it is not possible to differentiate Eq. [1$b$], use form [1] neglecting $K$, and plot $F$ graphically. This is conveniently done by assigning a series of arbitrary values to $x$ and calculating the corresponding values for $f(x)$ and $g(x)$. Using known or reasonably chosen values for $k_1$ and $k_2$, $F$ can then be plotted as a function of $x$. The minimum value of this function can be attained with any desired degree of accuracy by choosing values of $x$ close together in the region of the minimum and using a computer to calculate the values of $f(x)$ and $g(x)$.

### *B. Droplet on Hemispherical End of a Cylindrical Rod*

It is evident in the system of Fig. 3 that the ratio of $r_1$ to $r_2$, as well as the contact angle, has a great effect on the location of the *LAS* line of contact. The importance which this may assume in practical systems is illustrated in Fig. 4, where the solid surface has the form of a cylindrical rod with a hemispherical end. This can be regarded as an idealized form of a single fiber protruding from a yarn or fabric structure.

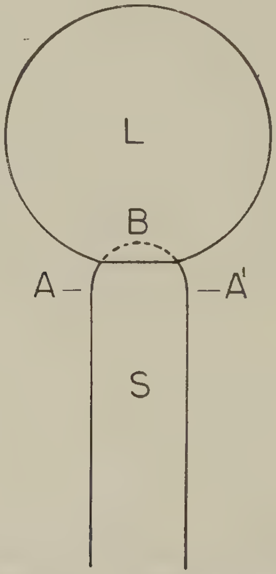

FIG. 4. Drop on hemispherical end of a cylindrical rod. Contact angle greater than 90°.

If the liquid drop $L$ has a zero contact angle, $\theta$, it can cover the hemispherical cap $ABA'$ completely, and can even extend down over the cylindrical portion of $S$, regardless of how small the volume $V$ may be. If $\theta$ is between zero and 90°, there is a critical drop volume $V$ which must be exceeded for the *LAS* boundary to extend past the line $AA'$ which separates the cylindrical and spherical portions of the surface. If $\theta$ is 90° or over, it is impossible for the liquid front spontaneously to move past the $AA'$ line, regardless of how large the drop may be. As $\theta$ increases from zero to 90°, the critical drop size (critical ratio of $r_1$ to $r_2$ in Fig. 3) necessary for the *LAS* boundary to reach the $AA'$ line at equilibrium increases greatly. Thus, the tip of a pointed fiber can tend to prevent a relatively large drop

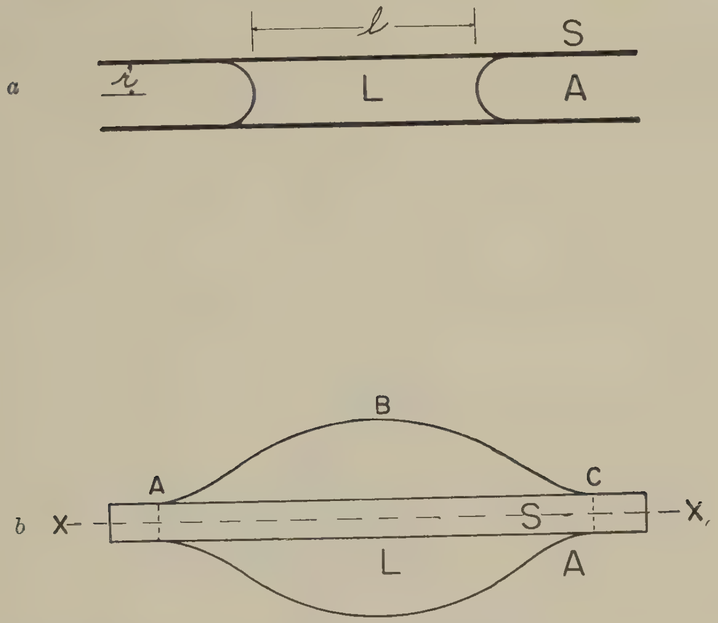

FIG. 5. Nonspreading systems of zero contact angle. (*a*) Drop of liquid in a tube. (*b*) Drop of liquid on a cylindrical fiber.

from engulfing it even if the equilibrium contact angle is somewhat less than 90°.

### *C. Drop of Liquid in a Cylindrical Tube*

Figure 5*a* shows a drop of liquid $L$ of volume $V$ in a cylindrical tube of radius $r$. According to the Laplace law, the $LA$ surfaces are spherical in form. For any given values of $k_1$ and $k_2$, the equilibrium value of $\theta$ can be calculated by exactly the same procedure used above for the drop on a flat plate. Each of the $LA$ menisci in this case can vary in area from a minimum of $\pi r^2$ to a maximum of $2\pi r^2$ (when $\theta$ is zero and the meniscus is a hemisphere). It is noteworthy that in the example of Fig. 5*a* the liquid will not spread over the solid surface indefinitely even though $\theta$ is zero. If the volume $V$ is so small that the length $l$ becomes zero, the drop will, of course, break at the center and form a figure of revolution on the interior wall of the tube.

### *D. Drop of Liquid Surrounding a Cylinder*

When a liquid drop of sufficient volume is placed on a cylindrical fiber and the equilibrium value for the contact angle of the system is low, the liquid assumes the shape shown in Fig. 5*b*. This figure of revolution, called an unduloid, is obtained geometrically by revolving curve $ABC$, an elliptical cycloid, about the axis $X$–$X$ (2). The curvature of this surface is constant from point to point. As in the case of Fig. 5$a$, the liquid does not spread over the solid surface even when the contact angle is zero.

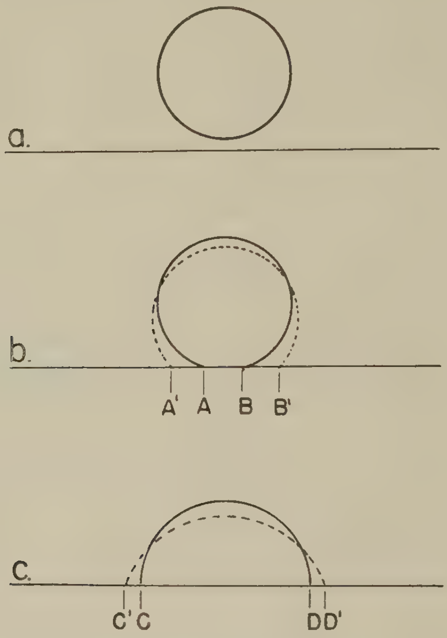

FIG. 6. Drop contacting a solid plate, illustrating driving force toward equilibrium contact angle.

## THE DRIVING FORCE CAUSING THE SYSTEM TO ASSUME EQUILIBRIUM CONTACT ANGLE

When a spherical drop of liquid contacts a planar solid surface (Fig. 6$a$–6$c$), the area of contact (Area $SL$) grows from a geometrical point to the final equilibrium area represented by the profile $C'D'$ in Fig. 6$c$. This spontaneous movement of the liquid is a true example of capillarity and is associated at every stage with a definite driving force and pressure. For this system (which is the same as the system of Fig. 2), Eq. [5$b$] gives the *force* in the direction of the parameter $h$ as the drop changes shape and moves out over the solid surface. Using Eq. [5$a$], which relates Area $SL$ to $h$, the radial force in the $SL$ plane pushing the perimeter $AB$ toward $A'B'$ or $CD$ toward $C'D'$ (Figs. 6$b$ and 6$c$) can be calculated. Similarly, the energy decrease $\Delta F$ involved in this movement can be calculated as a definite integral of Eq. [5$b$].

## SURFACE ROUGHNESS AND CONTACT ANGLE HYSTERESIS

The fact has long been recognized that the *SA* interface and the *SL* interface are seldom planar in real systems, and that this roughness has an effect on contact angle measurements (3). Wenzel's discussion of this effect (4) is particularly well known and widely referred to. There is, of course, no doubt that the apparent interfacial energy on a rough surface differs from the true interfacial energy in the same proportion as the apparent area differs from the true area. Whether or not this discrepancy in energy is related to change in *observed contact angle*, however, depends largely on the geometry of the system and on the dynamics of contact between the liquid and the solid surface, as described below.

It is necessary first of all to define "surface roughness" and "observed contact angle" from an operational point of view. The "apparent" or observed contact angle can be defined as the angle between the *LA* profile (known to be smooth to molecular dimensions) and the observed *SL* profile *at the LAS boundary*. The observation must always be made against an *SL* profile which *appears* smooth, i.e., where precise outlines of roughness are not optically resolved by the instrument and the observer. The observed profile is accordingly dependent on the resolving power of the system, and roughnesses of less than about 200 millimicrons are not ordinarily observable. There is, however, good reason to believe that most normal nonpolymeric pure liquids have macroscopic flow properties in layers as thin as 2 to 5 millimicrons. Thus, a range of dimensions exists within which the roughnesses are not observable in conventional microscopic goniometers. The liquid "sees" these roughnesses and behaves in the normal manner toward them.

Figure 7*a* shows a drop of liquid on a roughened solid surface. The solid ridges shown in profile are concentric. If viewed from above, the *SL* surface would look rippled, as when a pebble falls into a still pond. The distance from hilltop to valley is less than 200 millimicrons, but more than 20 millimicrons, and the angle of the slopes, as shown, is 135° or 45°. The *SL* and *SA* profile under the microscope looks flat and can be represented by the line $X$–$X'$. In the following discussion "equilibrium contact angle" will refer to the energy quantity $\cos^{-1}[-(k_2/k_1)]$. "True contact angle" will refer to an *angle*, conceptually measurable with perfect resolution, between the *SL* and *LA* interfaces. Let us assume that the equilibrium contact angle of this system is 90°. In the diagram the drop $BB'$ stands at its true contact angle on the *SL* surface. The apparent contact angle (the grossly observed angle between the *LA* profile and the $X$–$X'$ plane) is also 90°, but this is purely a matter of chance. The $BB'$ front can, for example, be moved inward one corrugation, coming to rest at $RR'$. Since the volume $V$ of liquid is constant, the apparent contact angle would now be very slightly greater than 90° (probably not observable, since the horizontal distance $BR$ is

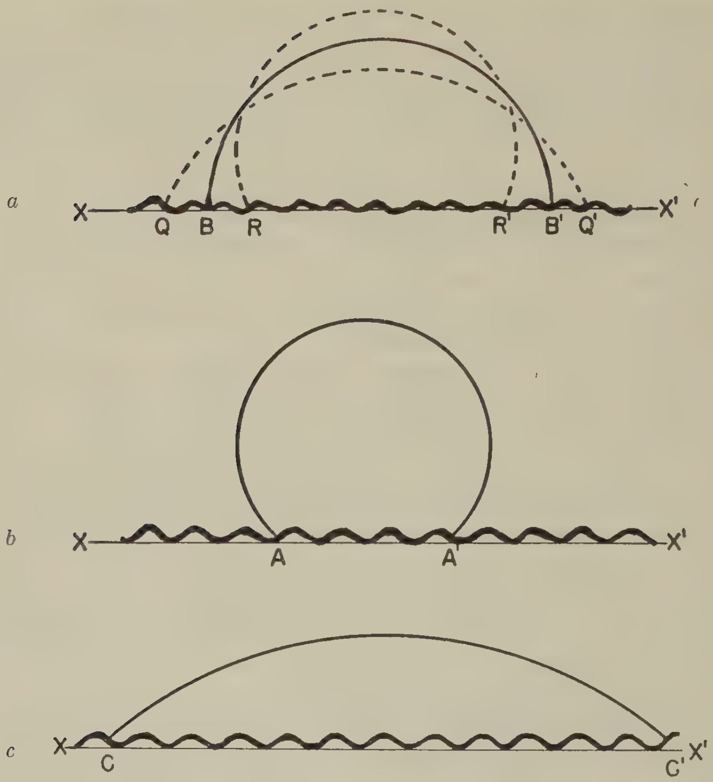

FIG. 7. Apparent versus real contact angles. Effect of surface roughness and hysteresis. (*a*) Real $\theta = 90°$. Apparent $\theta = 90°$. (*b*) Real $\theta = 90°$. Apparent $\theta = 135°$. (*c*) Real $\theta = 90°$. Apparent $\theta = 45°$.

approximately equal to the depth of the corrugation and is therefore not resolvable). The true contact angle is still 90°. Similarly, the front $BB'$ can be moved to $QQ'$ where the apparent contact angle is less than 90° but the true contact angle is still 90°. Figures 7*b* and 7*c* show the cases where the apparent contact angles are 135° and 45°, respectively. It is evident from the diagram that the true contact angle is still 90° in both instances.

Every one of the positions illustrated in Figs. 7*a*–7*c* is energetically stable. Each diagram represents a position of the system in a potential energy trough. It requires an initial input of energy to push the liquid front from $BB'$ over a potential barrier to the point where it will move spontaneously into the next energy trough at $RR'$ (or $QQ'$). The necessary input of energy *can be calculated quantitatively* by the procedure illustrated above.

At least one type of contact angle hysteresis can thus be accounted for quantitatively. If we start with a droplet barely contacting the rough surface at point $O$ in Fig. 7*a* (analogous to Fig. 6*b*), the initial outward thrust, together with outside forces, can give the front $BB'$ sufficient momentum to carry it in and out of many of the potential troughs associated with the physical ridges. As it nears the ultimate position of minimum free energy, the momentum will be insufficient to carry the front over the energy humps and the front will come to rest in one of the potential troughs at a position where the *apparent* contact angle is still obtuse.

Similarly, if a drop is pressed out mechanically over the solid surface to a position flatter than the one represented in Fig. 7*c*, it will tend to retract. The momentum of retraction may take the front over several ridges, but eventually the front will come to rest at a position corresponding to one of the potential troughs where the *apparent* contact angle is still acute.

The position of *absolute minimum free energy* in the system of Fig. 7 can be calculated, starting with Eq. [2] and following the indicated mathematical steps. In this case, it would be necessary to have an algebraic expression for the undulating form of the $SL$ profile as well as for the (sphercal) form of the $LA$ interface. The best parameter in which to express these functions might not be $h$ (the distance $OH$), but might be some monotonically changing quantity, such as the distance $BB'$ measured parallel to the $X$ axis. The form of $F$ as a function of increasing distance $BB'$ might have to be obtained graphically rather than algebraically (depending on the form of the expression for Area $SL$). In any event, $F$ would have an undulating form with each of the valleys corresponding to a physically stable state of the system. One of these regularly occurring valleys in the plot of the $F$ function would be lower than all the others and would correspond to the position of least total free energy. The *apparent* contact angle at this physical position of absolute minimum $F$ would depend largely on the geometrical form of the $SL$ interface and on the ratio of drop volume $V$ to the height of the corrugations. It would not necessarily be equal to the equilibrium contact angle. The *true* contact angle (as defined above) would equal the equilibrium contact angle at all physical positions corresponding to the bottoms of dips in the plot of the $F$ function (i.e., at the bottom of each potential trough).

It should be noted that the above discussion does not suggest surface roughness to be the only cause for contact angle hysteresis. It is intended only to show the detailed mechanisms by which surface roughness in the range greater than molecular but less than visibly resolvable can alter the apparent contact angle.

Another type of surface roughness is exemplified by the system of Fig. 8, in which a drop of liquid $L$ is in contact with an array of vertical hemispherically tipped cylinders $S$, separated by air gaps $A$. This system has been

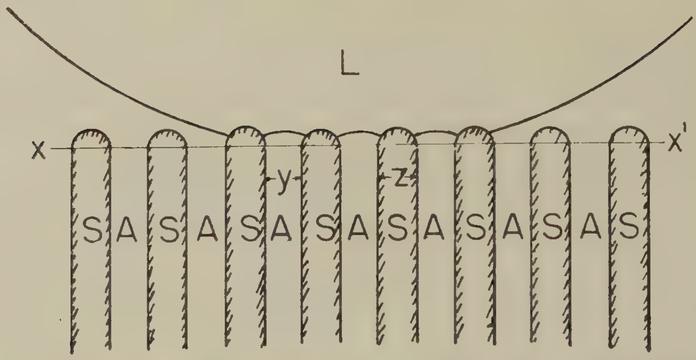

FIG. 8. Apparent versus real contact angles. Drop on a set of parallel cylindrical fibers with hemispherical ends. Gravity—zero. Real contact angle slightly greater than 90°. Apparent contact angle almost 180°.

discussed in great detail by Baxter and Cassie (5), particularly for the case where the equilibrium contact angle is greater than 90°, and where external forces (such as gravity and mechanical pressures) are not negligible. In the context of the present discussion, this system may be treated as an extension of the system of Fig. 4. At equilibrium, the true contact angle will be equal to the equilibrium contact angle, $\cos^{-1}[-(k_2/k_1)]$. If the true contact angle is 90° or greater, and if the distances $z$ and $y$ are unresolvably small but substantially greater than molecular dimensions, the apparent contact angle will be close to 180°. The exact position of the $LS$ and $LA$ profiles along the array of rods $S$ will depend on the volume of liquid $V$ relative to the $y$ and $z$ spacings, as well as on the equilibrium contact angle. It is noteworthy that if the equilibrium contact angle is *less* than 90° and the $LS$ front is forced onto the cylindrical portion of $S$, the $LS$ front will tend to move spontaneously into the $A$ spaces. If the equilibrium contact angle is greater than 90° the $LS$ front will always tend to stay on the hemispherical caps, and even if the $LS$ front is forced into the $A$ spaces it will tend to retreat to its original position on the caps. In this case each rod $S$ is acting as a cylindrical Wilhelmy plate (6), and it will tend to be expelled from the drop when the equilibrium contact angle is greater than 90°. This system is amenable to the same mathematical treatment used in the other illustrations of this paper. The mathematical expressions for areas $SL$ and $LA$ will obviously be quite complicated. They will have irregularities and may have discontinuities corresponding to points where the liquid contacts a new rod $S$. In this case, a configuration of *absolute minimum F* can be calculated as in the case of Fig. 7. The *apparent* contact angle for this configuration will depend on a set of factors similar to those noted in the discussion of Fig. 7, namely, the volume of liquid, the $y$ and $z$ spacings, and the numerical value of the equilibrium contact angle.

## REFERENCES

1. POYNTING, J. H., AND THOMSON, J. J., "Text Book of Physics." Vol. I, Properties of Matter. Griffin & Co., London, 1903.
   BAXTER, S., AND CASSIE, A. B. D., *J. Textile Inst.* **36,** T67–90 (1945); MOILLIET, J. L., AND COLLIE, B., "Surface Activity." Van Nostrand, New York, 1951.
2. BOUASSE, H., "Capillarité phenomenes superficiels." Delagrave, Paris, 1924.
3. BIKERMAN, J. J., "Surface Chemistry." Academic Press, New York, 1958.
4. WENZEL, R., *Ind. Eng. Chem.* **28,** 988 (1936).
5. BAXTER, S., AND CASSIE, A. B. D., *J. Textile Inst.* **36,** T67–90 (1945).
6. Paper I of this series, *J. Colloid Sci.* **14,** 572–583 (1959).

JOURNAL OF COLLOID SCIENCE 14, 598–618 (1959)

# THE ABSORPTION OF CATIONIC SURFACTANTS BY CELLULOSIC MATERIALS

## I. THE UPTAKE OF CATION AND ANION BY A VARIETY OF SUBSTRATES[1, 2]

**Frederick H. Sexsmith[3] and Howard J. White, Jr.**

*Frick Chemical Laboratory, Princeton University, Princeton, New Jersey, and Textile Research Institute, Princeton, New Jersey*

*Received May 6, 1959; revised July 14, 1959*

### Abstract

The interaction between cationic surfactants and cellulosic fibers has been studied. Most of the work involves cetyltrimethylammonium bromide (CTAB) and four substrates: kiered cotton, a medium-high-tenacity viscose rayon, a viscose rayon monofil, and oxycellulose. Absorption isotherms for the cation and anion of the surfactant were measured and some attention was given to rates of absorption and to the effects of temperature, added electrolyte, and solubilized dyes.

Two major absorption processes occur in the concentration range studied: cation exchange and ion-pair absorption. The cation exchange is dependent on the exchange capacity of the substrate. The ion-pair absorption begins to become important in the vicinity of the critical micelle concentration of the surfactant and also seems to depend on the cation-exchange capacity of the substrate. If the ion-pair absorption is assumed to consist of a clustering of ions on exchanged long-chain cations, the results for all but very high ionic strengths can be explained. In the presence of large amounts of added electrolyte an additional ion-pair absorption seems to occur.

### Introduction

Although surface-active agents are used extensively in the textile field for several purposes, relatively few studies of the physical chemistry of their interactions with fibers have been reported. Most of these studies have been concerned with anionic agents; in fact, about the only extensive work involving cationics is that of Weatherburn, Bayley and Rose (1–3).

The experiments reported here were primarily concerned with the interaction of one cationic surfactant, cetyltrimethylammonium bromide

---

[1] Taken from a thesis submitted by F. H. Sexsmith to the Department of Chemistry, Princeton University, in partial fulfillment of the requirements for the degree of Doctor of Philosophy.

[2] Presented in part before the Polymer Division at the 130th National Meeting of the American Chemical Society, Atlantic City, New Jersey, September, 1956.

[3] Present address: Chicopee Manufacturing Co., Milltown, New Jersey.

(CTAB), with various fibrous cellulosic substrates. Attention was focused on the equilibrium absorption of the cation and anion of the surfactant from solution at room temperature. Some attention was paid to the effects of temperature and added salt and acid. Some observations on the kinetics of the absorption process were also made, and a few experiments were carried out using other surfactants.

It soon developed that there were two absorption processes: an absorption of long-chain cations by ion exchange, and an absorption of ion pairs. The cellulosic substrates were chosen so as to differ in cation-exchange capacity, accessibility, and fiber size in order to show the effects of these factors on the absorption.

## Experimental Methods

Fiber samples were equilibrated with surfactant solutions and the change in concentration of $Q^+$ or $Br^-$ in the treating bath as a function of final concentration was measured by potentiometric titration. The surfactants used were CTAB, stearyltrimethylammonium bromide (STAB), and Emcol E-607-L. The fibers used were cotton, a medium-high-tenacity viscose (Cordura), a viscose monofil, and oxycellulose. The fiber samples were thoroughly washed, treated with acid to remove cations other than hydrogen, and neutralized. Bath concentrations are expressed in terms of molarity, and the amount absorbed is expressed in terms of milligram-ions per gram of dry fiber.

Complete experimental details are given in Appendix 1 and may be of importance, since, as will become apparent, experimental difficulties, apparently resulting from incomplete purification of the fiber samples, were met. Also in Appendix 1 are tables of the water absorptivities (a measure of accessibility) and the alkali numbers (a measure of cation-exchange capacity) of the fiber samples.

## Experimental Results

### *Absorption Isotherms*

*Preliminary Measurements Involving Ion Exchange.* The ion-exchange process was studied using several substrates having different alkali numbers. These included, in addition to the four primary substrates described above, a bright textile viscose rayon supplied by the American Viscose Corp., Fortisan, a saponified cellulose acetate supplied by the Celanese Corp. of America, and several samples of Cordura which were oxidized with alkaline hypobromite according to the method of Davidson (4). This treatment supposedly causes preferential oxidation of the primary alcohol groups in the 6 position of the glucose anhydride residue in cellulose to carboxylic acid groups. These additional samples were purified in the usual way.

Each of these substrates was equilibrated with a CTAB solution of initial

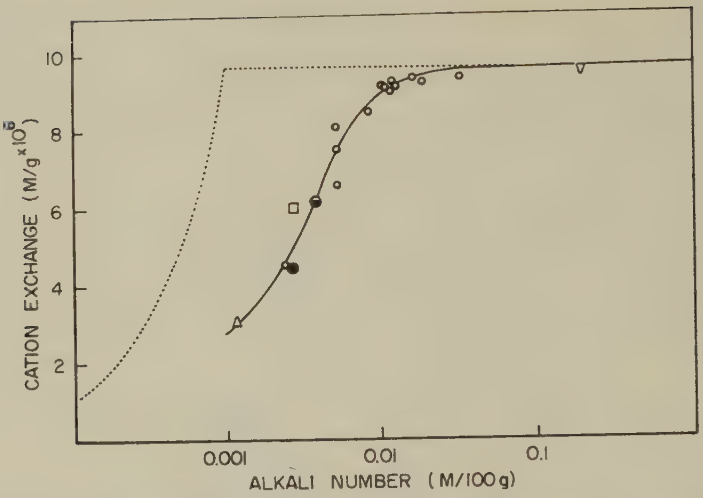

Fig. 1. Cation exchange of oxidized celluloses with a 0.00049 $M$ CTAB solution as a function of the alkali number of the substrate. ▽ Oxycellulose; ◒ Viscose monofil; □ Fortisan; ● Textile rayon; ○ Cordura; △ Cotton.

concentration $4.8 \times 10^{-4}$ $M$. This concentration is below the critical micelle concentration (CMC) of CTAB, which is $10^{-3}$ $M$ (5, 6). For the final cation concentrations obtained from this initial concentration, cation exchange is the predominant interaction with the substrate. The amounts exchanged are shown in Fig. 1 plotted against the alkali numbers of the substrates. The dotted curve shows hypothetical results which would be obtained if the exchange was complete and the alkali number was an accurate measure of the cation-exchange capacity. The upper limit on this curve is the total amount of cation present in the solution initially.

*Cotton.* The equilibrium uptakes of cation ($Q^+$) and $Br^-$ at room temperature (~25°C.) for cotton are shown in Fig. 2, where they are plotted against the concentration of $Q^+$ in the treating bath at equilibrium. It is evident that, at very low concentrations, cation exchange alone occurs. As the concentration of the bath increases, there is an abrupt increase in the absorption of $Q^+$ and an accompanying absorption of $Br^-$. We have chosen to call this second type of absorption, ion-pair absorption.

In addition to measurements made using 5 g. of fiber to 100 ml. of bath some measurements were made using 10 g. of fiber to 100 ml. of bath. The use of this fiber-to-bath ratio made examination of a higher range of concentrations possible, and the results are included in Fig. 2. However, it should be understood that the results at the two ratios are not strictly comparable, since the capacity for cation exchange differs in the two cases, or, in other words, the pH and $Br^-$ concentrations of the equilibrium baths may differ at the same $Q^+$ concentration.

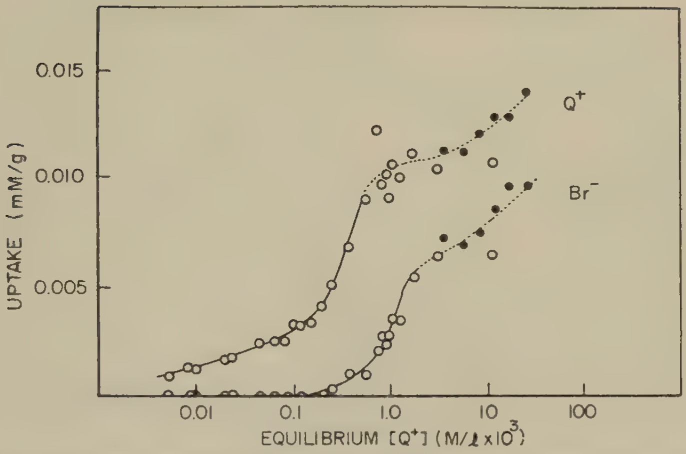

FIG. 2. Equilibrium absorption from CTAB solutions by purified cotton at room temperature. ○ 5 g. fiber/100 ml. solution; ● 10 g. fiber/100 ml. solution.

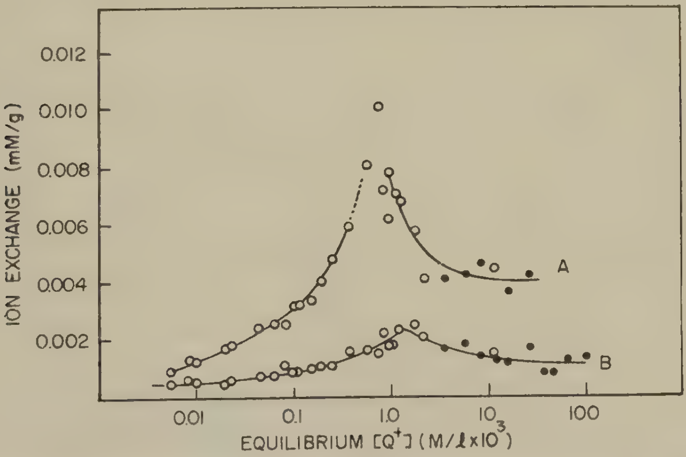

FIG. 3. Equilibrium cation exchange between purified cotton and CTAB solution at room temperature. *A*, determined by change of titer; *B*, determined by pH change; ○ 5 g. fiber/100 ml. solution; ● 10 g. fiber/100 ml. solution.

In Fig. 3 the cation exchange is plotted as a function of the equilibrium concentration of $Q^+$. The exchange has been calculated from the results shown in Fig. 2 and from direct measurement of the pH changes of the solutions. It is evident that the two methods are not in agreement. Experiments, which will be discussed later in this paper, showed incomplete removal of cations other than $H^+$ in the purification process to be the most probable source of this discrepancy, which occurred to some degree with most of the substrates. The cation exchange determined as $Q^+ - Br^-$ is

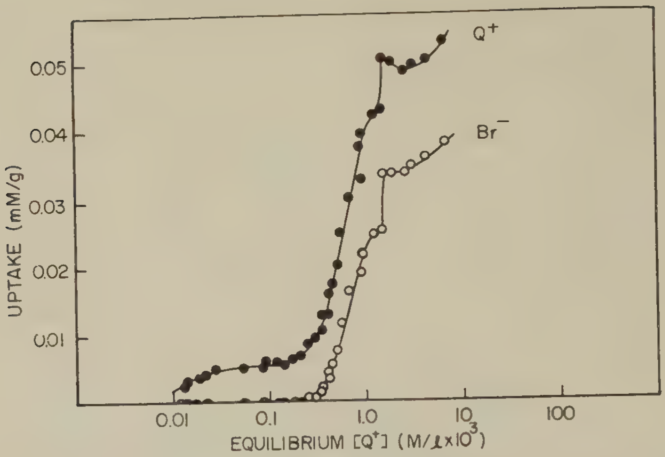

FIG. 4. Equilibrium absorption from CTAB solutions by Cordura at room temperature.

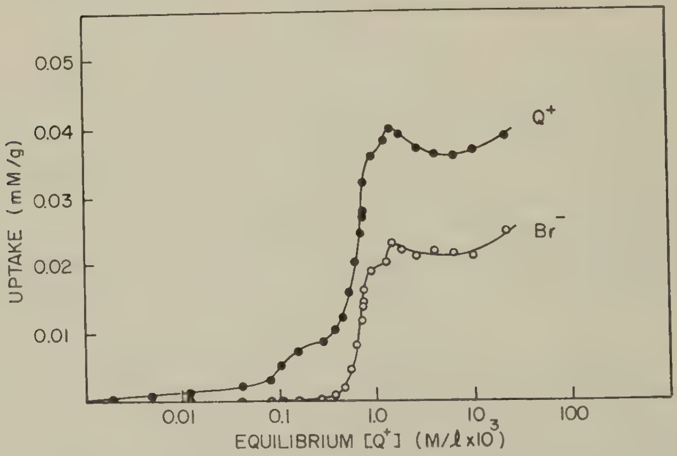

FIG. 5. Equilibrium absorption from CTAB solutions by Cordura at 35°C.

presumably the better value, although, since it is the difference between two experimental measurements, there is considerably more uncertainty in the results. It should be noted that there is a maximum in the cation-exchange curve.

*Cordura.* Equilibrium isotherms for Cordura rayon at room temperature and at 35°C. are shown in Fig. 4 and Fig. 5, respectively. In Figs. 6 and 7 are shown the cation-exchange isotherms. Again there are discrepancies between the cation exchange as measured by $Q^+ - Br^-$ and the apparent exchange indicated by the changes in pH of the solutions. In every case

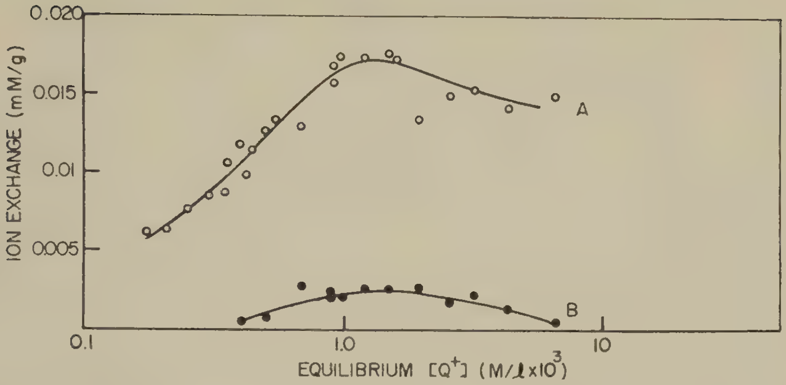

FIG. 6. Equilibrium cation exchange between Cordura and CTAB solutions at room temperature. *A*, determined by change of titer; *B*, determined by pH change.

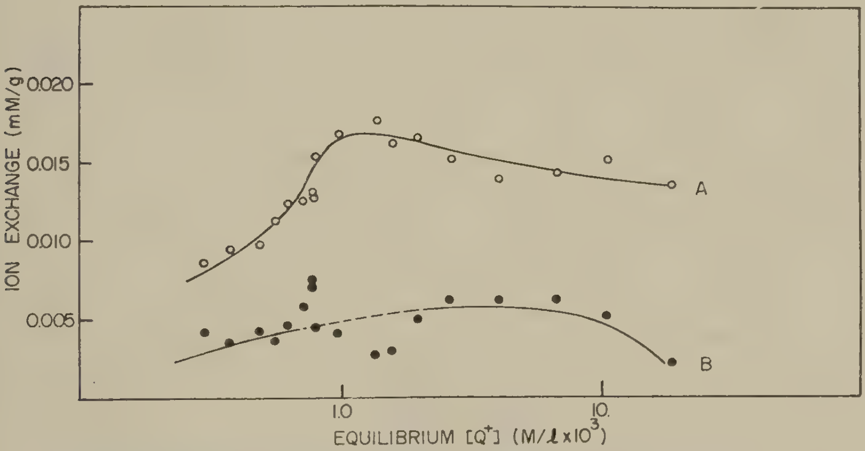

FIG. 7. Equilibrium cation exchange between Cordura and CTAB solutions at 35°C. *A*, determined by change of titer; *B*, determined by pH change.

there is a maximum in the plot showing cation exchange and some indications of maxima in the overall absorption curves in some cases.

Another set of equilibrium results at room temperature was obtained in preliminary experiments. These were very similar to the set shown with respect to the shape of curve and relationship to the $Q^+$ concentration axis. However, the amounts of $Q^+$ and $Br^-$ absorbed were considerably less and the $H^+$ generated more. The difference undoubtedly arises from the fact that the samples used in the respective runs were taken from different batches of pretreated fiber.

Another study of the effect of temperature was made in which samples of the same size were equilibrated with aliquots of the same solution at differ-

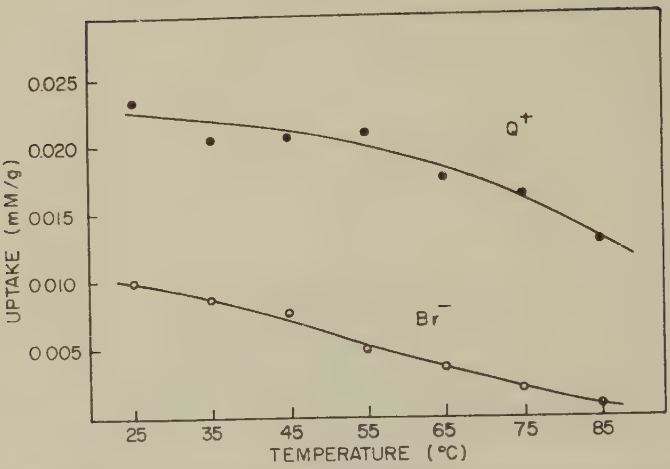

FIG. 8. Equilibrium absorption from 0.00156 *M* CTAB solution as a function of temperature.

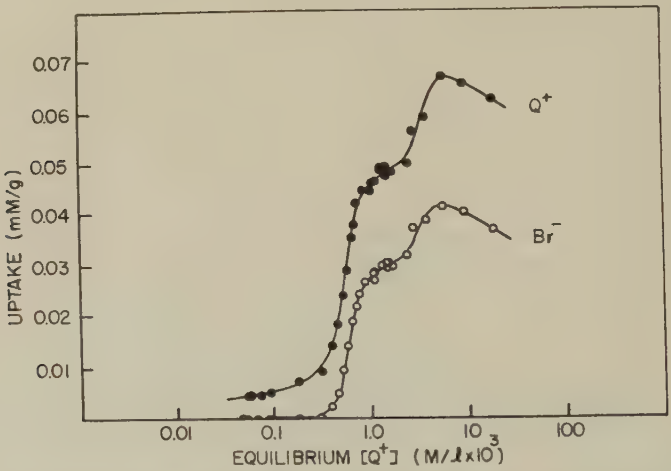

FIG. 9. Equilibrium absorption from CTAB solutions by viscose monofil at room temperature.

ent temperatures and the amount absorbed was measured. The initial concentration of the bath was 0.00156 *M*. The results are shown in Fig. 8. It is evident that the absorption of ion pairs decreases as the temperature increases. The effect of temperature on the cation exchange is definite but small under these experimental conditions.

*Monofil.* The equilibrium absorption isotherms at room temperature are given in Fig. 9; the cation exchange is shown in Fig. 10. Maxima are observed in all curves except for the cation absorption as measured by $Q^+ - Br^-$, which behaves in an unique manner at higher concentrations. Attempts

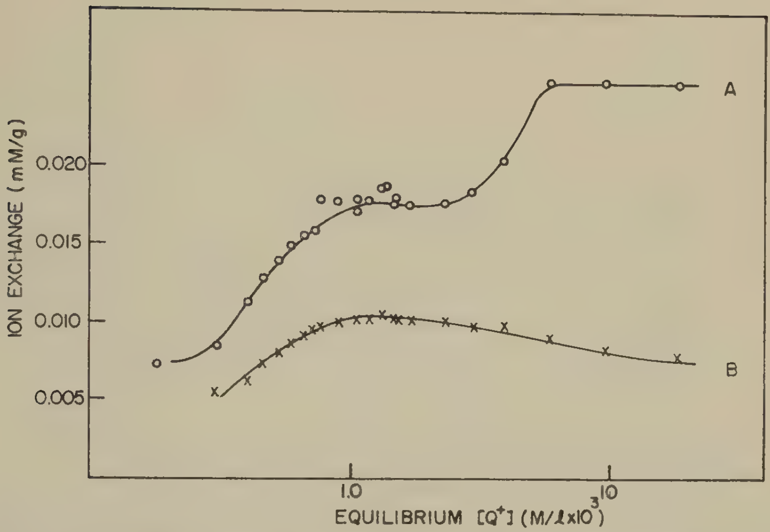

FIG. 10. Equilibrium cation exchange between viscose monofil and CTAB solutions at room temperature. *A*, determined by change of titer; *B*, determined by pH change.

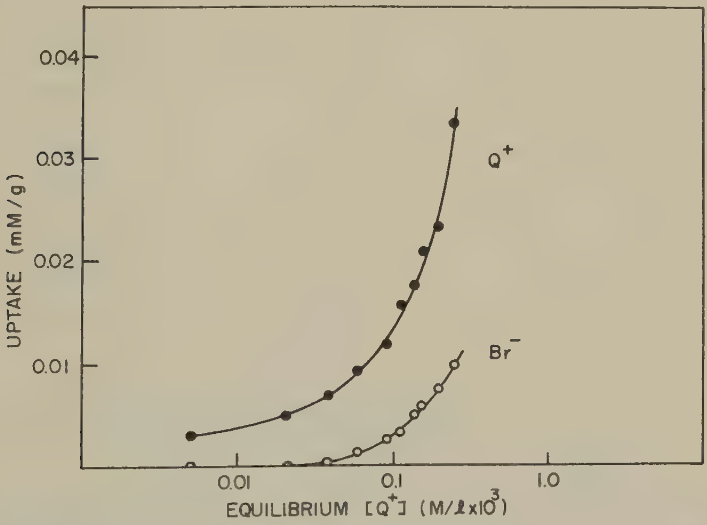

FIG. 11. Equilibrium absorption from STAB solutions by viscose monofil at room temperature.

to restudy part of the absorption isotherm with a different batch showed a lack of reproducibility once again.

The absorption isotherm for STAB at room temperature is shown in Fig. 11. STAB is not soluble above 0.0004 *M*. These results are important

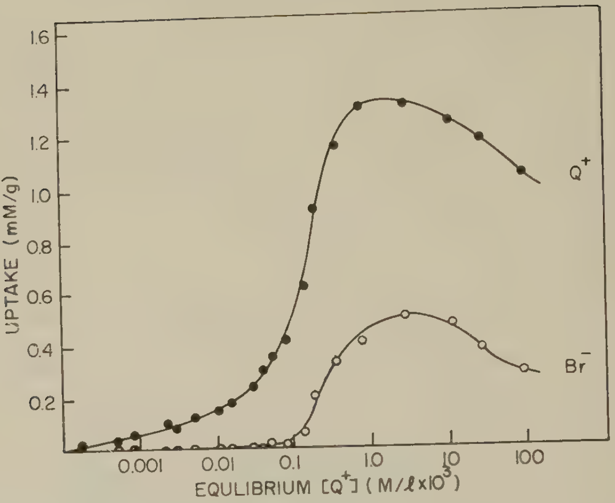

FIG. 12. Equilibrium absorption from CTAB solutions by oxycellulose at room temperature (1.00 g. fiber/100 ml. solution).

primarily because they show that the rapid increase in ion-pair absorption starts at a considerably lower concentration for STAB. The CMC for STAB has been estimated to be 0.00032 *M* by an extrapolation of Debye's results for other homologous *n*-alkyltrimethylammonium bromides (7). Thus the rapid increase in ion-pair absorption seems to occur in the vicinity of the CMC for each surface-active agent.

*Oxycellulose.* The equilibrium uptakes of $Q^+$ and $Br^-$ by oxycellulose are shown in Fig. 12; the cation exchange as measured by $Q^+ - Br^-$ and by pH change are shown in Fig. 13. Although a fiber-to-bath ratio of 1/100 was used for the oxycellulose, it absorbed roughly 100 times as much quaternary ion as did the cotton. All the isotherms show pronounced maxima, and there is no large systematic difference between the cation-exchange values as measured by $Q^+ - Br^-$ and from pH change.

The large amount of material absorbed made it possible to check the analytical techniques by comparing predicted and measured weight increases for the samples. As is shown in Fig. 14, the agreement between the two methods is good.

The absorption of Emcol E-607-L by oxycellulose was also studied. This material has a high molecular weight and is quite soluble, but was not purified and proved to be difficult to titrate by the methods used in this work, especially at higher concentrations. The isotherm for the weight increase is shown in Fig. 15. The CMC, which is apparently not available in the literature, was found to be in the vicinity of 0.001–0.002 *M* by capillary rise measurements. The isotherm for the change of pH also showed a maxi-

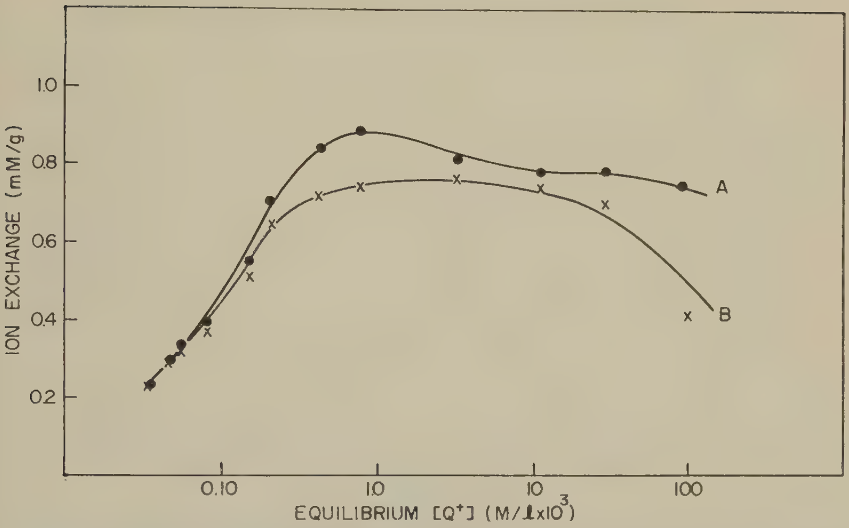

FIG. 13. Equilibrium cation exchange between oxycellulose and CTAB solutions at room temperature. *A*, determined by change of titer; *B*, determined by pH change.

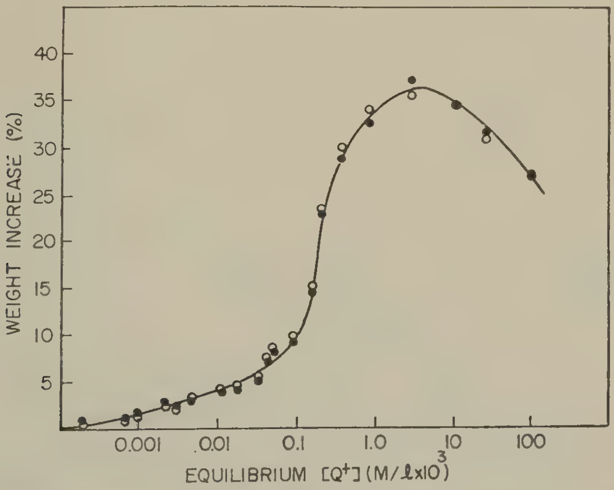

FIG. 14. Increase in weight of oxycellulose from absorption from CTAB solutions. ● direct observation; ○ calculated from change of titer.

mum near the CMC. The halide-ion uptake was studied by both absorption and desorption (samples treated with concentrated solutions equilibrated with water). In the region of overlap there was good agreement between the two. The desorption measurements, which in principle can be extended to much higher concentrations, showed no maximum; however, at high

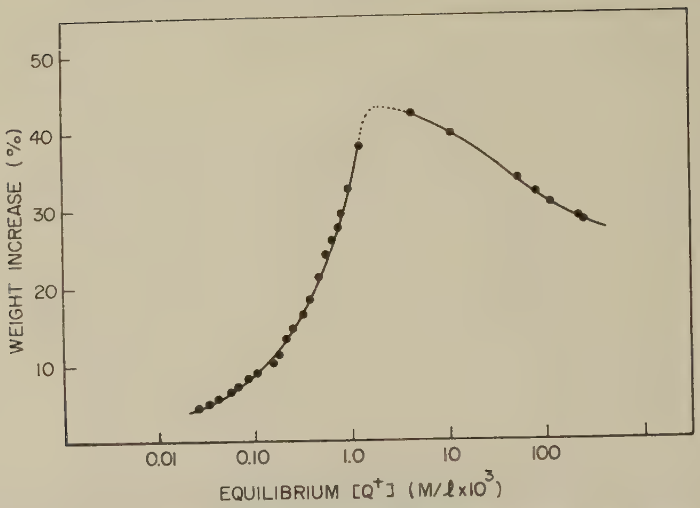

FIG. 15. Increase in weight of oxycellulose from absorption from Emcol E-607-L solutions.

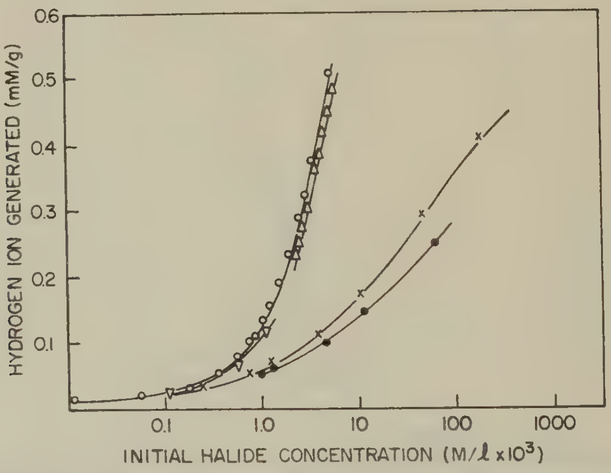

FIG. 16. Hydrogen ion generated from equilibration of oxycellulose with various halides. ○ CTAB; △ Emcol E-607-L; ▽ $C_{12}H_{25}(CH_3)_3$ N Br; × K Br; ● NaBr.

concentrations, small amounts of surfactant solution entrained by the sample in its initial treatment can become the source of a large error.

Finally, in Fig. 16 are some results showing the relative powers of a variety of quaternary ions to replace $H^+$ in oxycellulose. It is clear that the long-chain ions are considerably more effective than are the simpler cations. Less extensive measurements showed $NH_4Br$, LiBr, $Me_4NBr$, $Et_4NBr$, and $BzMe_3NBr$ to be similar in behavior to the simpler cations shown.

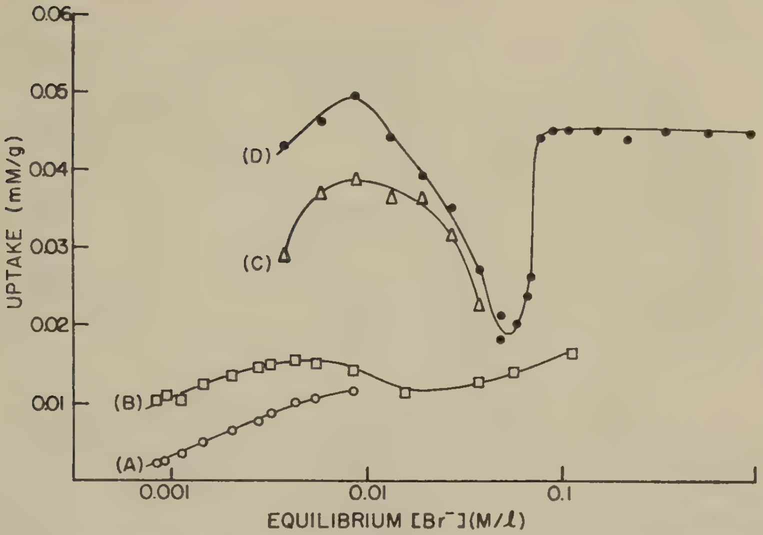

FIG. 17. Absorption by Cordura from CTAB solutions to which KBr was added. Initial CTAB concentration 0.000942 *M*. *A*, Br absorbed; *B*, Q absorbed. Initial CTAB concentration 0.00500 *M*. *C*, Br absorbed; *D*, Q absorbed.

*Effects of Added Salt or Acid.* Samples of Cordura were equilibrated with CTAB solutions of initial concentration 0.00094 *M* (slightly below the CMC) with various amounts of KBr added. The results are shown in Fig. 17. As the concentration of $Br^-$ increases the uptake of ion pairs increases and the ion exchange, as measured by $Q^+ - Br^-$, decreases. The curve for $Q^+$ goes through a minimum and finally rises again (the $Br^-$ curve could not be measured to such high concentrations).

A similar study involving initial concentrations of CTAB of 0.005 *M* (well above the CMC) was also made. The results are also shown in Fig. 17. The initial increase in ion-pair absorption is smaller and the subsequent decrease is greater, but the same general effects are noted.

The effect of HBr was also noted using Cordura as substrate again. The absorption from solutions of various pH values and 0.002 *M* in CTAB was followed and is shown in Fig. 18. A decrease of $Q^+$ uptake followed by an increase was noted. Subsidiary experiments showed that cation exchange involving the $Q^+$ ion was decreasing, as would be expected, so that the final rise in absorption must involve ion pairs.

*Rates.* The rates of the absorption processes were studied primarily in order to assure that equilibrium was reached; however, certain general features were noted. Figure 19 shows the rates of change of pH and of $Q^+$ concentration in the bath for Cordura. The final concentration of $Q^+$ in the bath is well below the CMC so that the measurements refer to ion exchange Although the system was agitated sporadically rather than continuously,

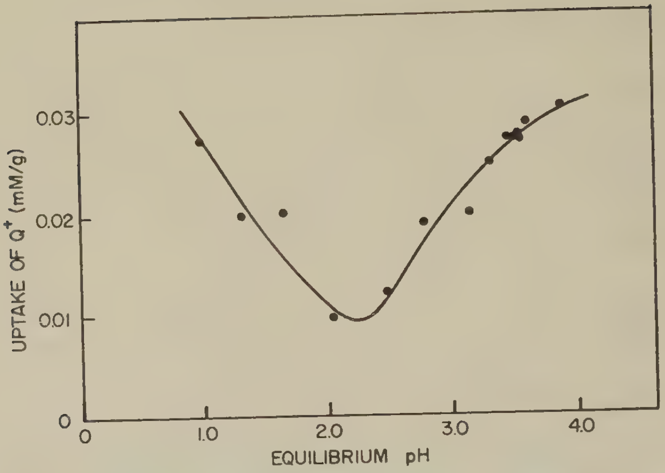

FIG. 18. Absorption by Cordura from 0.00200 *M* CTAB solutions to which HBr was added.

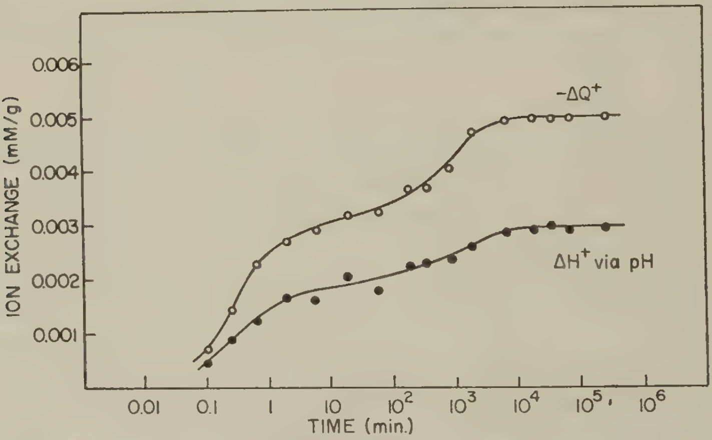

FIG. 19. Rate of exchange of cation for Cordura immersed in 0.000367 *M* CTAB solution (fiber-to-bath ratio, 4 g./100 ml.).

some collateral experiments involving continuous agitation make it seem likely that no serious error has been introduced by the use of sporadic agitation.

The shapes of the curves are consistent with the existence of two different types of sites for exchange; however, no further effort has been made to confirm their existence. The curve for cotton was similar; those for the monofil and oxycellulose showed no inflection. Measurements made on Cordura well above the CMC showed that cation and anion were absorbed at the same rate with no inflection in either curve. Results, especially with oxycellulose, show that equilibrium is reached more slowly when high con-

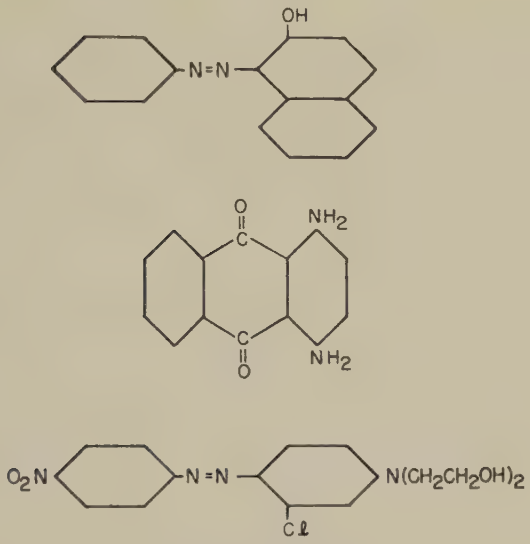

FIG. 20. Structures of dyes used.

centrations of CTAB are used. About 50,000 minutes were allowed for equilibrium at the highest concentrations.

### *Properties of Treated Fibers*

One of the well-known properties of detergent solutions at concentrations above the CMC is the ability to solubilize dyes which are soluble in hydrocarbon-like solvents but relatively insoluble in water. If fibers were equilibrated with solutions containing solubilized dye, it was found that, when concentrations were chosen so that the equilibrium concentration of surfactant was above the CMC, dye was taken up by the fiber sample. The amount of dye taken up varied with the amount of ion-pair absorption of the surfactant and with the size and characteristics of the dye molecule, oxycellulose taking up the most dye and cotton the least. The dyeings were quite fast to washing with water or with solutions of sodium lauryl sulfate at room temperature. Furthermore, dye solubilized in a sodium lauryl sulfate solution would not color the fibers to anywhere near the same extent; the dyeing is apparently a property of cationic surfactants. Cross sections of dyed fibers showed that the dyes had penetrated throughout. Dyes with the structures shown in Fig. 20 could be used to obtain good coloration; some of the larger vat dyes in their oxidized forms could not.

### *Difficulties Encountered in Preparing Fiber Samples*

All the fiber samples except for the oxycellulose samples were treated with acid in an attempt to remove foreign cations before use. In spite of the treatment the $H^+$ generated, as determined from the pH change, was less than the amount of $Q^+$ taken up by cation exchange. This result could be caused by the presence of another cation in the cellulose, by the presence of a proton-accepting impurity in the CTAB solution, or possibly by an unforeseen effect of CTAB on the functioning of the pH meter. The second possibility was eliminated by trial titrations with known quantities of acid. With respect to the third, CTAB was indeed found to raise the apparent pH of acid solutions in high concentrations, but the effect was not sufficient to account for the observed results.

One set of Cordura samples gave positive tests for ammonium ion when treating solutions were tested with Nessler's reagent. The presence of ammonium ion in ostensibly purified celluloses has also been noted by Davidson (8). However, the samples of monofil gave no evidence of ammonium ion although discrepancies in the cation-exchange results were noted.

Duplicate experiments with samples from a given batch agreed well, but experiments involving samples from different batches of treated material did not agree. This result again points to an incomplete purification procedure. Apparently cations, such as $Zn^{++}$, which are present in the formation of viscose rayon, are not completely removed by the treatment used and contamination with ammonium ions is an ever-present threat. Only in the case of oxycellulose was the presence of foreign cations of minor importance.

Although the uptake values cannot be accepted without reservation, it should be emphasized that there is no reason to suppose that the general features of the absorption isotherms are incorrect. The influence of the bath concentration on the shape of the curves was reproducible, and the differences between fiber types were maintained.

## Discussion

The absorption isotherm results from two processes: cation exchange and ion-pair absorption. The ion-pair absorption first becomes important in the vicinity of the CMC; the cation exchange becomes appreciable at much lower concentrations. Because of the ion-exchange process, the composition of the bath at equilibrium is different for each substrate, the greater the ion exchange the more HBr in the bath. Since the CMC is lowered by the presence of electrolyte, the CMC of a bath at equilibrium with an oxycellulose sample could be considerably lower than that of a solution of pure CTAB (0.001 $M$). If this factor is taken into account, the coincidence between the onset of micelle formation in the solution and ion-pair absorption in the fiber is quite marked, especially since the fine structures of the substrates might be expected to have an influence on the absorption too. The results for the other surfactants, although less extensive, seem to show similar behavior.

### *The Cation-Exchange Process*

As would be expected, there is a general correlation between the amount of cation exchange and the alkali number of the substrate, which has been taken as a measure of the carboxyl content. Perhaps this is shown most directly by Fig. 1. The results in Fig. 1 cannot be rationalized by simple considerations involving one type of ion-exchange site. However, this is not surprising; complications arising from electrostatic interactions, swelling, and varying degrees of accessibility are to be expected with polymeric solids. Furthermore there seems to be some evidence from the rate curves for cotton and Cordura for the existence of two types of cation-exchange site.

The long-chain cations have a special affinity for cellulosic fibers, as is shown graphically in Fig. 16. In this respect the cationic surfactants are similar to certain cationic dyes, for example, methylene blue (see Davidson (9)). Davidson found that the smaller cations such as $K^+$, $NH_4^+$, $Na^+$ have roughly similar affinities with the larger ions in this group having the smaller affinities, probably because of decreased electrostatic binding. However, the very large dye cations had much greater affinities because of specific structural affinity effects. Apparently, as the size of cations capable of existing in rodlike configurations increases, interactions resulting in increased affinities predominate. Both cationic dyes and surfactants fall in this class. One result is the logical expectation that the quaternary cation will replace any small cation other than $H^+$ present in the substrate as an impurity.

Finally it should be noted that, in the great majority of cases, the cation-exchange process showed a maximum in the amount of cation exchanged as a function of the concentration of cation in the bath, whether the amount exchanged was measured by pH change or directly.

### *Ion-Pair Absorption*

As has been noted, ion-pair absorption begins to become important for concentrations in the vicinity of the CMC. It might be inferred that what has been called ion-pair absorption is, in reality, a concentrating of surfactant at the interface between the fibrous substrate and the bath. If the interface is defined by the gross visible surface of the fibers, the monofil, with its small specific surface, should show the least absorption, and hence the inference is not tenable. If the surface is taken to include internal surfaces such as the surfaces of micelles and those caused by differential swelling along defects in the amorphous regions, then the measurement of surface is more difficult and the amount of surface depends on the conditions prevailing at the time of measurement. Such measurements are usually classed as accessibility measurements. Moisture regain has been chosen as a measure of relative accessibility in this paper. For the purposes at hand, it should be crude but qualitatively sufficient. From Table I it can be seen that ion-pair absorption does increase as the moisture regain increases. However, the results show that the ion-pair absorption also increases with the alkali number (a measure of cation-exchange capacity) or the cation exchange itself. The correlation with the alkali number is more striking than that with moisture regain because oxycellulose is more markedly set apart from the other substrates by its alkali number. Thus, although accessibility undoubtedly has an effect on the amount of ion-pair absorption, the effect seems less marked than that of the amount of cation exchanged or the cation-exchange capacity. Further work would be needed to separate these two effects more completely (see the next paper in this series (10)).

The ion-pair-absorption isotherms show distinct maxima in the case of oxycellulose and monofil and a levelling off in the case of Cordura. This behavior again parallels the behavior of the cation-exchange process.

If it is assumed that the ion-pair absorption is a process related to micelle formation which occurs with a cation absorbed by cation exchange serving as a nucleus, then the results discussed so far can be rationalized. Ion-pair absorption will not occur until appreciable cation exchange has taken place and the free energy of the surfactant has been raised to the point that micelle formation is to be expected. Clusters forming within the fibrous substrate would not need to be identical in size, shape or free energy with micelles forming in solution.[4] However, since cellulosic substrates are highly swollen by water (25%–100%+ depending on the fiber), it is reasonable to expect the onset of cluster formation in the vicinity of the CMC of the solution as a first approximation. The dependence of the ion-pair absorption on the amount of cation exchanged or on the cation-exchange capacity is given a reasonable basis, and the correlation of maxima in the ion-pair absorption with maxima in the cation exchange is also understandable. It will be shown in a later paper (11) that a rough theoretical treatment can be given for all the above results including the maxima.

It is interesting to examine the results for absorption in the presence of KBr and HBr in terms of the above hypothesis. Added KBr or HBr will increase the free energy of the quaternary bromide by a common-ion effect and decrease the CMC and, as a result, tend to lead to increased ion-pair absorption. At the same time a cation will be introduced to compete in the cation-exchange process and hence reduce the number of sites for ion-pair absorption. If the quaternary solution is just below the CMC and the cation introduced does not compete strongly with the $Q^+$ ion, then an increase in ion-pair absorption with an increase in added salt would be expected. As more salt is added a decrease resulting from the competition between cations and the consequent loss of sites for ion-pair absorption would be expected. If the quaternary solution is above the CMC and hence is not so sensitive to added electrolyte, and if the cation of the added electrolyte has a marked affinity for carboxyl groups, then a decrease in ion-pair absorption with added electrolyte would be expected. Behavior of the first type and of intermediate type is shown in Fig. 17, and that of the second type in Fig. 18.

---

[4] In fact, as one referee has pointed out, there are somewhat similar cases where the "cluster" consists of one surfactant ion with counter ion (not necessarily in the cluster). See H. Lundgren, *Textile Research J.* **15**, 335 (1945), for example.

An increase in ion-pair absorption is noted at high electrolyte concentrations and sometimes at very high surfactant concentrations. This increase presumably occurs by a different process, possibly by the absorption of unionized surfactant or by a process similar to the absorption of dyes. In any event it is probably independent of the cation-exchange process. Since it occurs at the limit of sensitivity of the experimental methods used, it has not been studied further.

The uptake of solubilized dyes also tends to confirm a clustering process within the fiber. It is particularly interesting that an anionic surfactant, which could not take part in cation exchange, was not nearly as effective in producing dyeing even though the dye was solubilized by the surfactant. The fact that the dyeing occurs throughout the fiber is further proof of penetration of the cationic surfactant.

## APPENDIX

### *Preparation of Materials*

*Surface-Active Agents.* A technical grade of CTAB supplied by Eastman Organic Chemicals was used as received. Analyses for cation and anion showed the sample to be pure within the accuracy of the analytical method.

Stearyltrimethylammonium bromide (STAB) was prepared from a sample of Arquad 18 (Armour and Co., Chemical Division). The commercial product, a mixture of hexadecyl, octodecyl (stearyl), and octodecenyl chlorides in isopropyl alcohol, was precipitated by addition of acetone. The solid material was then dissolved in hydrobromic acid and taken to dryness four times to produce the bromides, and the bromides were separated by seven recrystallizations. Analysis of the final product for bromide ion indicated 98% purity.

Encol E-607-L (Emulsol Corp.) was used as obtained. It has the formula

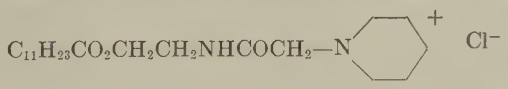

Analyses of the solutions showed the halide-ion content to be 5% greater than the apparent quaternary ion content, possibly because of the presence of a cation insensitive to the titration method.

*Cellulosic Fibers.* The fiber samples used were the following:

*1.* A roving of a commercial American Upland cotton of 82% maturity by the USDA array method.

*2.* A medium-high-tenacity 300 denier/120 filament, Cordura viscose rayon yarn supplied by E. I. DuPont de Nemours & Co. The fibers had a serrated cross section and probably a relatively high skin-to-core ratio.

*3.* A 16-denier viscose rayon monofil from the American Viscose Corporation. These fibers were round and had a small skin-to-core ratio.

*4.* An oxycellulose gauze from Tennessee Eastman Corp. This material was cotton which had been oxidized with $NO_2$ so that about one-half of the primary alcohol groups in the 6-position were converted to carboxyl groups.

All the fiber samples were dried and conditioned at 65% relative humidity and 70°F. The oxycellulose was not otherwise conditioned. The viscose rayon samples were refluxed for several hours with carbon tetrachloride and either acetone or methanol. The samples were then soaked in hydrochloric acid at pH 3.5–4.0 for 24 hours and washed with distilled water until the washing gave no turbidity with silver nitrate and finally soaked in successive portions of distilled water with intermittent heating (50°–80°C.) for one week. In addition, the high-denier monofils were heated in water at 90°C. for 1 hour—a process which had previously been found to stabilize the fibers for long-term absorption experiments. Early samples were dried in air, later ones *in vacuo* or in a forced-draft oven at 90°C.

The cotton samples were extracted with solvents in the same way as the viscose samples. They were then refluxed with 2% sodium hydroxide solution under nitrogen in an autoclave for 5 hours and left under nitrogen in the autoclave another 16 hours at room temperature. The samples were then washed with acid, water, and dried in the same way as the viscose rayons.

The moisture contents at 65% relative humidity and 70°C. for the samples are given in Table I. These give a measure of relative accessibility.

The alkali number was determined by reacting samples with an excess of 0.1 $N$ sodium hydroxide solution and back-titrating the excess alkali. The values are given in Table II. The alkali number is known not to be an accurate measure of carboxyl content but it gives an adequate approximate measure.

### *Analytical Methods*

*Cation Analysis.* The surfactant cations in the baths were determined by potentiometric titration with potassium triiodide (12) using platinum electrodes and a Beckman Model G pH meter. The quaternary ammonium triiodides precipitate from solution and occasionally adhere to the electrodes; however, this problem is not serious. An error of about 3% for the cation determinations has been estimated.

*Anion Analysis.* The halide contents of the baths were determined by potentiometric titration using silver nitrate as titrant and silver and copper electrodes, with a moderate concentration of copper sulfate present (13).

TABLE I

*Water Absorbed at 65% R.H. and 70°C. by Cellulose Samples*

| Sample | Water absorbed |
|---|---|
| | *(% dry weight)* |
| Cotton | 7.9 |
| Cordura | 12.5 |
| Monofil | 12.6 |
| Oxycellulose | 15.4 |

TABLE II

*Alkali Numbers of Cellulose Samples*

| Sample | Alkali number |
|---|---|
| | *(moles absorbed/100 g.)* |
| Cotton | 0.0012 |
| Cordura | 0.0024 |
| Monofil | 0.0038 |
| Oxycellulose | 0.19 |

The error in the halide determination was less than that in the cation determination but was not estimated directly.

*Hydrogen Ion Analysis.* The cation exchange in the cellulosic substrate produced a decrease in pH of the bath. The pH changes were measured with a Beckman Model G pH meter.

### *Absorption Procedure*

A constant fiber-to-bath ratio of 5.00 g. conditioned fiber to 100 ml. solution was used for all samples except for the oxycellulose samples, where a ratio of 1 to 100 was used. Loosely tied fiber bundles were put in glass-stoppered Erlenmeyer flasks containing the surface-active agent. Concentrations ranged from $10^{-5}$ $M$ to 0.3 $M$, being limited by the sensitivity of the analytical method and the solubility of the surface-active agent. Most of the experiments were run at room temperature without special temperature control. The maximum range in temperature observed was 5°C. Experiments at higher temperatures were done in thermostats. The temperature effects observed were not so large that serious error from minor variations in temperature would be expected.

Kinetic studies indicated that most of the fiber types came to equilibrium at room temperature within 10,000 minutes. Samples intended to go to equilibrium were left for 3 to 4 weeks with periodic shaking. When rates were evaluated agitation was made as nearly continuous as feasible. Particular efforts to achieve continuous shaking were made for short-time runs.

## ACKNOWLEDGMENTS

One of us (F.H.S.) wishes to thank Textile Research Institute for a fellowship held during the course of this work. We also wish to acknowledge the part played by Dr. R. O. Steele in the early stages of the work.

## REFERENCES

1. ROSE, G. R. F., WEATHERBURN, A. S., AND BAYLEY, C. H., *Textile Research J.* **21,** 427 (1951).
2. WEATHERBURN, A. S., AND BAYLEY, C. H., *Textile Research J.* **22,** 797 (1952).
3. WEATHERBURN, A. S., *Textile J. Australia* **28,** 826 (1953).
4. DAVIDSON, G. F., *J. Textile Inst.* **43,** T291 (1952).
5. COLLIE, B., HARTLEY, G. S., AND SAMIS, C. S., *Trans. Faraday Soc.* **32,** 795 (1936).
6. SCOTT, A. B., AND TARTAR, H. V., *J. Am. Chem. Soc.* **65,** 692 (1943).
7. DEBYE, P., *J. Phys. & Colloid Chem.* **53,** 1 (1949).
8. DAVIDSON, G. F., *Shirley Inst. Mem.* **21,** 47 (1947).
9. DAVIDSON, G. F., *Shirley Inst. Mem.* **21,** 69 (1947).
10. GOTSCHAL, Y., REBENFELD, L., AND WHITE, H. J., JR., *J. Colloid Sci.* **14,** 619 (1959).
11. SEXSMITH, F. H., AND WHITE, H. J., JR., *J. Colloid Sci.* **14,** 630 (1959).
12. HAGER, O. B., YOUNG, E. M., FLANAGAN, T. L., AND WALKER, H. B., *Ind. Eng. Chem., Anal. Ed.* **19,** 885 (1947).
13. DEAN, R. B., AND HAWLEY, R. L., *Ind. Eng. Chem., Anal. Ed.* **19,** 841 (1947).

JOURNAL OF COLLOID SCIENCE 14, 619–629 (1959)

# THE ABSORPTION OF CATIONIC SURFACTANTS BY CELLULOSIC MATERIALS

## II. THE EFFECTS OF ESTERIFICATION OF THE CARBOXYL GROUPS IN THE CELLULOSIC SUBSTRATES

**Yehezkiel Gotshal,[1] Ludwig Rebenfeld, and Howard J. White, Jr.[2]**

*Textile Research Institute, Princeton, New Jersey*

*Received May 6, 1959; revised July 14, 1959*

### ABSTRACT

Viscose rayon and oxycellulose containing a high concentration of carboxyl groups have been esterified at the carboxyl group using ethylene oxide. This reagent was chosen to minimize changes in accessibility caused by the esterification reaction. Measurements were made of the carboxyl contents, of the capacities of the samples to absorb water, and of their capacities to absorb the cation and anion from solutions of cetyltrimethylammonium bromide. These last measurements were made to test the hypothesis advanced by Sexsmith and White (1) that absorption of ion pairs from the surfactant solution was a clustering process dependent on the presence of exchanged cations which served as nuclei. The marked decrease in ion-pair absorption found after esterification was in agreement with this hypothesis.

Some other properties of the esterified oxycellulose samples are also discussed.

### INTRODUCTION

In a previous paper, Sexsmith and White (1) studied the interaction of various cellulosic substrates with solutions of cetyltrimethylammonium bromide (CTAB). They concluded that the primary interactions, over the concentration range covered, were a cation-exchange process and an absorption of ion pairs which involved the clustering of neutral groups of ions about a cation absorbed through ion exchange. One of the primary reasons for the conclusion was a marked correlation between ion-pair absorption and cation-exchange capacity of the substrate. However, all the cellulosic substrates differed in fine structure and in accessibility. The extent to which differences in accessibility influenced the ion-pair absorption process could not be determined.

To separate the effects of cation-exchange capacity from those of accessibility it was necessary to vary one while keeping the other constant. Esterification of the carboxyl groups in viscose rayon with ethylene oxide at room temperature would appear to change the cation-exchange capacity without altering accessibility. Since only about 1 in 100 residues contains a carboxyl group, the swelling caused by introduction of the glycoester should not change the overall accessibility greatly, and the conditions of the reaction are so mild that no changes resulting from the method of treatment are to be expected. Appropriate conditions to carry out the esterification were determined and some properties of the esterified product were examined.

---

[1] Present address: 4 Saadya Gaon, Jerusalem, Israel.

[2] To whom correspondence should be addressed.

A similar procedure was carried out using oxycellulose (primarily oxidized to carboxylic acid at the 6 position) as substrate. In this case the carboxyl groups occur so frequently that substantial esterification alters the properties of the material appreciably, and presumably the accessibility is among those changed. However, since in some respects the highly esterified oxycellulose is a new derivative of cellulose, it was prepared and some of its properties were determined.

Particular attention was given to the interactions of the substrates with CTAB solutions; however, some observations on dyeing, swelling, x-ray diffraction, and water absorption were also made.

## EXPERIMENTAL

### *Preparation of Materials*

*Viscose Rayon.* A 16-denier viscose rayon monofil obtained from the American Viscose Corp. was used. The samples were extracted in a Soxhlet apparatus for 8 hours with carbon tetrachloride and for 7 hours with methanol. They were soaked for 30 minutes at room temperature in dilute HCl solution (pH 3.5) and then washed until the washings gave no test for chloride with silver nitrate. They were dried at 60°C. and conditioned at 70°F. and 65% R.H. before use.

*Oxycellulose.* Oxycellulose prepared by nitrogen dioxide oxidation of cotton was obtained in the form of gauze from the Tennessee Eastman Co. It was stated to have 10%–12% carboxyl content. The samples were treated with acid, washed, dried, and conditioned as above.

*Ethylene Oxide.* Commercial ethylene oxide was used. Solutions of about 30% ethylene oxide in water can be obtained at room temperature. Below the boiling point of ethylene oxide (10.7°C.) the liquids are miscible.

*Glycoester of Viscose Rayon.* Deuel (2) has reacted ethylene oxide with pectic acid to form the glycoester; Farrar and Neale (3) have reported complete esterification of cellophane using a 1% solution of ethylene oxide. A 1% solution of ethylene oxide produced no apparent reaction with the viscose rayon sample used, after 2 days at room temperature; however, solutions of higher concentration did bring about a reaction.

Two samples were prepared. The first sample was prepared by treating 50 g. of washed viscose rayon with 2 l. of 29% solution at room temperature for 5 days. The samples were then washed, dried, and conditioned as above.

The second sample was prepared by treating 30 g. of the first sample with 1 l. of 52% solution at 5°C. for 6 days. The reaction system was then allowed to stand at room temperature overnight, and the ethylene oxide gas coming out of solution was permitted to escape through a mercury trap. The sample was then washed, dried, and conditioned.

*Glycoester of Oxycellulose.* No reaction was observed with a 1% solution, but reaction occurred with more concentrated solutions. Again two samples were prepared, the first by treating 30 g. of sample with 2 l. of 30% solution for 7 days at room temperature. The second was prepared by treating 15 g. of the first sample with 1 l. of 68% solution at 5°C. for 6 days and then allowing the reaction system to stand at room temperature overnight with a mercury trap to allow excess ethylene oxide to escape. The samples were washed, dried, and conditioned.

### *Characterization of Materials*

*Carboxyl Analysis.* The accurate measurement of the carboxyl content of cellulosic materials is a difficult and painstaking operation. Classical methods have been reviewed by Davidson and Nevelle (4) and Geiger and Kunzler (5). In addition to the classical methods, methods using radioactive tracers (6, 7) which have been recently developed show great promise and are, perhaps, the most accurate available at the present time.

Since changes in carboxyl content were of primary importance for the work at hand, a quicker and less refined method than would be used for a precise absolute measurement could be tolerated. The method chosen involved cation exchange with the cationic dye, methylene blue. The procedure followed was that established by Davidson (8) except that the $KH_2PO_4$-NaOH buffer system described by Skinkle (9) was used. This method has the advantage that the pH is controlled and remains close to pH 7. The rayon samples were equilibrated with a solution containing 0.2 m$M$/l. of methylene blue hydrochloride; the oxycellulose samples were equilibrated with one containing 2.2 m$M$/l. The change in concentration of the dye solution was measured spectrophotometrically.

Some measurements were made on untreated viscose rayon using a neutralization technique. Samples were treated with excesses of sodium hydroxide solutions ranging in concentration from 0.0423 $N$ to 0.00644 $N$ at 5°C. for 26 hours, and the excess sodium hydroxide was back titrated. Good agreement between samples and between concentration ranges was obtained; however, the method was not used for the esterified samples for fear of error resulting from hydrolysis.

Samples of the same viscose rayon which had been given a somewhat different initial preparation were analyzed for carboxyl content by Moncrieff-Yeates and White (7) using measurements of the uptake of sodium ion and sulfate ion from sodium sulfate solutions.

*Uptake of Cetyltrimethylammonium Bromide.* Samples of the viscose-rayon substrates weighing 1 g. were treated with 40-ml. portions of CTAB solutions at room temperature for at least 4 days, to assure attainment of equilibrium. Samples of oxycellulose substrates weighing 0.200 g. were treated with 20-ml. portions of CTAB solutions for at least 7 days. Commercial CTAB was used in water purified by distillation and ion exchange.

The analytical procedures were those described by Sexsmith and White (1).

*Absorption of Water and Dyes.* Samples were dried *in vacuo* over magnesium perchlorate at room temperature for three weeks and conditioned at 70°F. and 65% R.H. in a conditioned room.

Three types of dyes were used: anionic dyes, cationic dyes, and a disperse dye. For the anionic dyes, 0.12 g. of fiber sample was treated for 1 hour at 90°C. with 20 ml. of a solution containing 0.5 g. of dye and 3.2 g. of $Na_2SO_4 \cdot 10H_2O$ per liter.

The same procedure for treating the fibers used to determine the carboxyl content with methylene blue was used for the cationic dyeing.

In the case of the disperse dye, 50 ml. of 0.055 $M$ CTAB solution saturated with dye (the dye is solubilized in micelles of the surfactant) were used for dyeing 0.12 g. of the viscose substrates. Only 25 ml. of 0.009 $M$ CTAB saturated with dye were used to dye 0.50 g. of oxycellulose and 0.56 g. of its glycoester. The 0.56 g. of glycoester is equivalent to the 0.50 g. of oxycellulose in oxycellulose content. In all cases dyeings were carried out at room temperature overnight. The smaller amount of dye was used with oxycellulose because the dye was taken up so strongly that ready differentiation between samples was impossible with greater amounts.

## Results

### *Properties of Viscose Rayon and Its Glycoester*

No change in appearance on esterification was noted with the viscose monofil. Cross sections showed no change under the microscope and the x-ray diffraction pattern was unchanged. As is evident from Table I esterification of the carboxyl groups did not alter the amount of water absorbed at 70°F. and 65% R.H.

The carboxyl contents of the viscose samples are given in Table II. For the untreated samples results obtained using two other methods are also shown. The results for the method using methylene blue appear to be low. Since the method involves cation exchange, it is necessary to have sufficient dye to insure complete exchange. However, at high dye concentrations, the dye is also absorbed as ion pairs so that for accurate measurements it is necessary to measure anion uptake as well. As can be seen from Table II, the reproducibility of the method as used is good, and it is highly unlikely that errors of the magnitude of the differences between the various types

TABLE I

*The Absorption of Water by Cellulosic Fibers and Their Glycoesters at 70°F. and 65% R. H.*

| Material | Water absorbed (*g./100 g. sample*) | |
|---|---|---|
| | Duplicate samples | |
| Oxycellulose | 13.6 | 13.4 |
| Glycoester of oxycellulose (1st sample) | 12.7 | 12.8 |
| Glycoester of oxycellulose (2nd sample) | 12.8 | 12.8 |
| Viscose rayon monofil | 11.9 | 11.9 |
| Glycoester of viscose monofil (1st sample) | 11.8 | 11.8 |
| Glycoester of viscose monofil (2nd sample) | 12.0 | 11.9 |

TABLE II

*Carboxyl Contents of Cellulosic Substrates*

| Material | Method | Carboxyl content (*mM COOH/g. sample*) | |
|---|---|---|---|
| | | Duplicate measurements | |
| Oxycellulose | Methylene blue | 3.45 | 3.45 |
| Glycoester of oxycellulose (1st sample) | | 1.40 | 1.38 |
| Glycoester of oxycellulose (2nd sample) | | 0.11 | 0.11 |
| Glycoester of viscose monofil (1st sample) | | 0.0089 | 0.0085 |
| Glycoester of viscose monofil (2nd sample) | | 0.0072 | 0.0072 |
| Viscose monofil | | 0.024 | 0.024 |
| | Direct neutralization | 0.044 | |
| | $Na_2SO_4$ method (7) | 0.039 | |

of samples can be expected; thus the method is suitable for relative ranking of the substrates.

No quantitative measurements were made in the case of the dyeing experiments; the dyed samples were characterized as to depth of dyeing visually. The results are shown in Table III.

The absorption isotherms at room temperature for the cation and anion from a CTAB solution are plotted in Figs. 1 and 2 as functions of the cation concentration in the bath at equilibrium. Figure 1 shows results for the absorption of the cation, and Fig. 2 shows results for the absorption of the

TABLE III

*Qualitative Estimates of Dye Uptake for the Various Cellulosic Substrates and Different Types of Dyes*

| Dye ("Colour Index," 2nd ed. designation) | Type | Viscose monofil | Esterified monofil | Oxycellulose | Esterified oxycellulose |
|---|---|---|---|---|---|
| Basic Blue 9 (methylene blue) | Cationic | Dark | Medium | Has a tanning effect[a] | Very dark |
| Janus Green B (C.I. Part II #11050) | Cationic | Very dark | Dark | — | — |
| Direct Red 81 | Anionic | Medium | Medium | Light | Dark |
| Acid Orange 7 | Anionic | Medium | Medium | Very light | Dark |
| Direct Red 2 | Anionic | Medium | Medium | — | — |
| Disperse Red 1 | Disperse | Medium | Light | Dark | Medium |

[a] Heavily dyed and made hard and harsh by the dyeing.

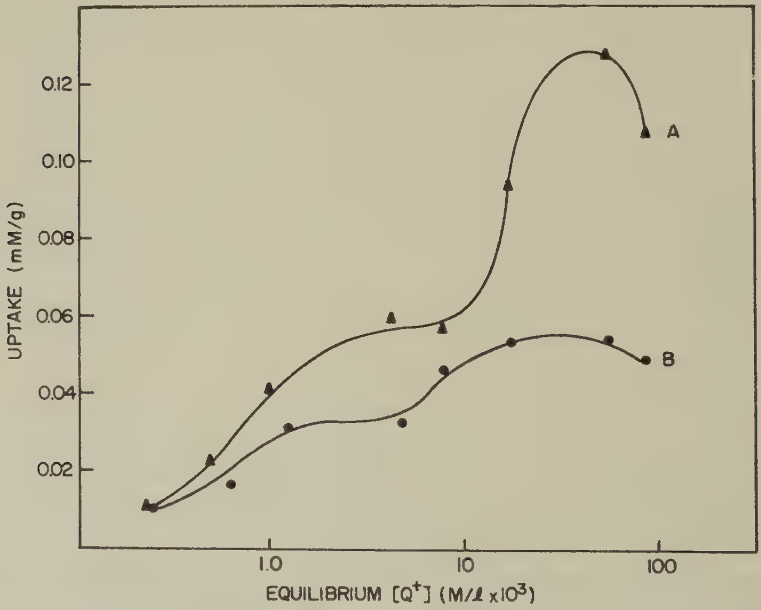

FIG. 1. Equilibrium absorption of cation from CTAB solutions by esterified and unesterified viscose rayon at room temperature. (*A*) viscose rayon; (*B*) esterified viscose rayon.

anion. Each point on a curve represents the average result of two duplicate experiments using the same master batch of fibers and the same master solution of CTAB. (Sexsmith and White (1) found difficulty in obtaining reproducible behavior in the purification process.) The error at the lower

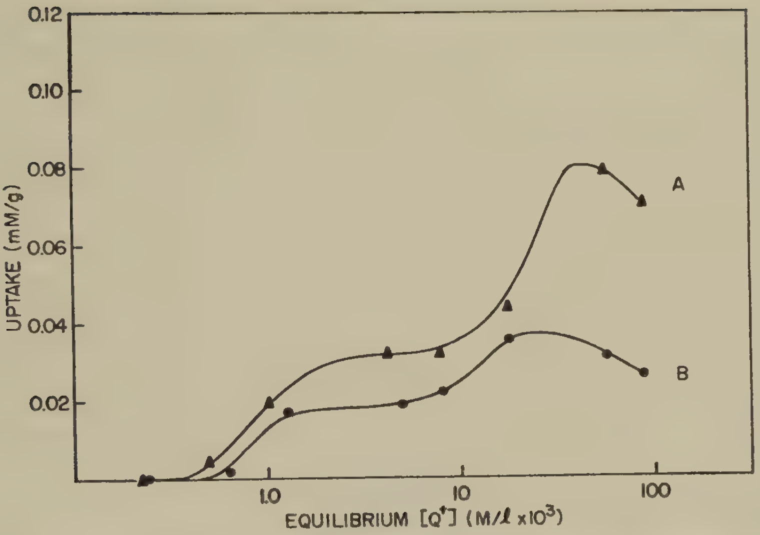

FIG. 2. Equilibrium absorption of anion from CTAB solutions by esterified and unesterified viscose rayon at room temperature. (*A*) viscose rayon; (*B*) esterified viscose rayon.

concentration of CTAB is relatively small, but at the higher concentrations, where only small changes in concentration are measured, a confidence limit of ±6% is estimated.

### *Properties of Oxycellulose and Its Glycoester*

Esterification causes no color change. The esterified material is more elastic when wet and retains a greater elasticity if dried at a low temperature or by a solvent-replacement technique. However, drying at or above 80°C. causes the material to darken and become hard and brittle. The esterified material has a lower tensile strength than the oxycellulose.

It seemed possible that the glycoester of oxycellulose might be soluble in some simple solvent. Although the esterified material was almost gelatinized by 0.25*M* CTAB solution, no solvent was found. Water and dimethylformamide at 100°C. cause appreciable swelling; pyridine, methanol, diethyl ether, acetone, and dioxane either cause no swelling or slight swelling at elevated temperatures.

Cross sections of the esterified material (sample 2) showed the cross-sectional area to be roughly four times that of the unesterified material and twice that of sample 1. The lumen, visible in the unesterified material and in sample 1, had disappeared.

The x-ray diffraction patterns of the two oxycellulose materials were similar to those for extremely amorphous cellulose.

The absorption of water by the oxycellulose samples is given in Table I

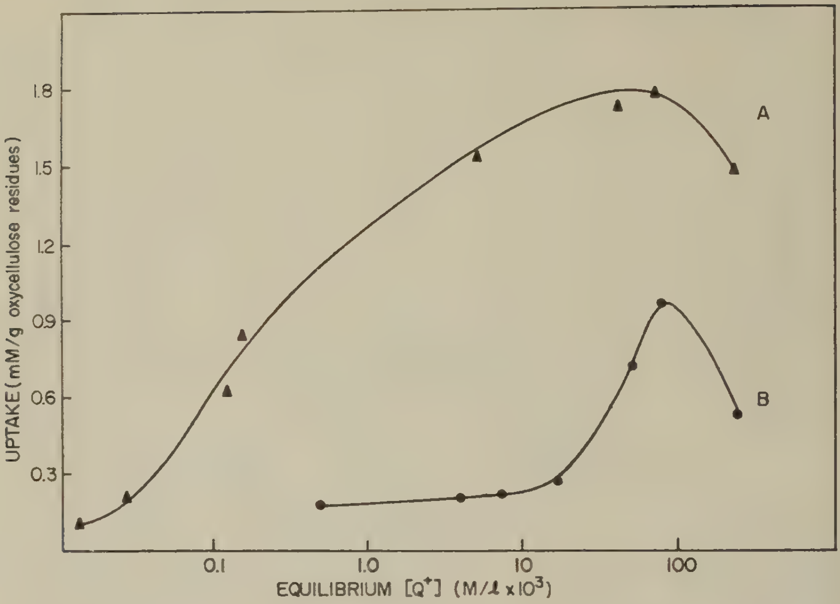

FIG. 3. Equilibrium absorption of cation from CTAB solutions by esterified and unesterified oxycellulose at room temperature. (*A*) oxycellulose; (*B*) esterified oxycellulose.

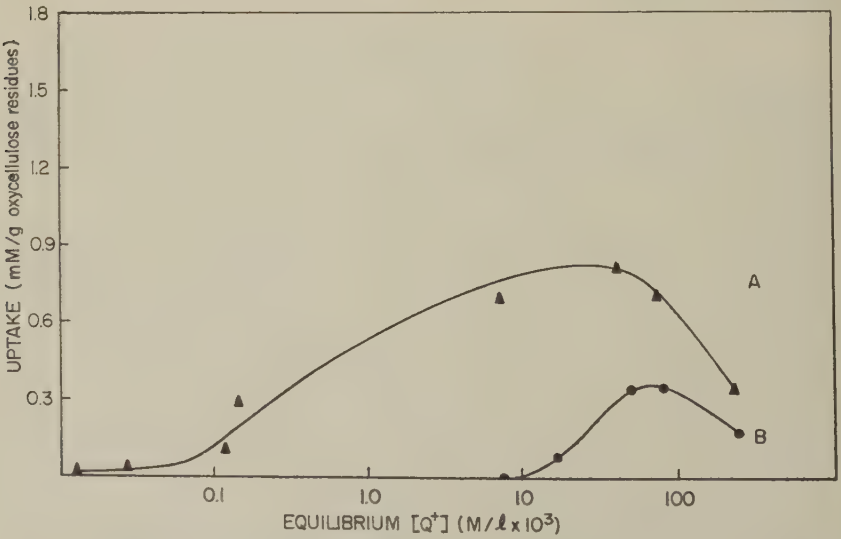

FIG. 4

FIG. 4. Equilibrium absorption of anion from CTAB solutions by esterified and unesterified oxycellulose at room temperature. (*A*) oxycellulose; (*B*) esterified oxycellulose.

and the carboxyl content in Table II. Table III shows the dyeing behavior.

The uptake of bromide ion from a CTAB solution by esterified sample 1 was found to be almost identical with that of untreated oxycellulose. An analysis of the sorption bath revealed the presence of ethylene glycol, indicating that hydrolysis of the ester groups had occurred. A test for the presence of ethylene glycol in the baths used with sample 2 was negative. All results pertaining to the uptake of CTAB refer to sample 2.

The absorption isotherms for the cation and anion from CTAB solutions at room temperature are shown in Figs. 3 and 4, respectively. The values for the glycoester have been corrected so that the results refer to the same number of monomer units in each case. Each point on the curve represents the average of two measurements using samples from the same batch of substrate and the same CTAB solution. The error was less than with the viscose monofil because larger changes were measured.

## Discussion

### *Viscose Fibers*

As has been mentioned, the relative infrequency of carboxyl groups in viscose rayon and the very mild conditions of treatment make it unlikely that the accessibility of the viscose rayon has been changed by the esterification. No changes were noted in dimensions, x-ray diffraction pattern, or absorption of water at 70°F. and 65% R.H. Actually it might be anticipated that esterification would alter the amount of water absorption somewhat. However, there are many sites for water absorption in viscose rayon, and esterification without change in accessibility affects only a relatively small number. It may be that slight changes in capacity to absorb water would be noticed at very high relative humidities.

Properties directly dependent on the carboxylic acid content of the viscose rayon have, of course, been markedly affected by the esterification. These include both the absorption of cation and of anion from CTAB solutions. It was hypothesized by Sexsmith and White (1) that absorption from CTAB solutions consisted of cation exchange followed by clustering of ion pairs on the absorbed long-chain cations which served as nuclei. Since the anion absorption is a measure of the absorption of ion pairs, the decrease in anion absorption with esterification is further support for the validity of the hypothesis.

If the ion-pair absorption is dependent on the number of cations exchanged, then both types of absorption depend on the number of sites. The amounts of cation or anion absorbed by two substrates of equal accessibility in equilibrium with identical solutions would bear the same ratio as the numbers of sites for cation exchange in the two substrates. However, the actual substrates will not be in equilibrium with identical solutions; for a given long-chain cation concentration the hydrogen-ion concentration, and hence the anion concentration, will increase with the capacity for cation exchange of the substrate. Thus the ion product for the ion pairs and hence the tendency for an ion pair to be absorbed on an absorbed cation will increase. As a result the ratio for anion absorption at a given long-chain cation concentration in the solution should be smaller than the ratio for cation absorption. The ratios for esterified monofil and monofil are roughly 0.55 and 0.70, respectively.

The CTAB absorption isotherms for the monofil are quite similar to those determined previously except at the higher concentrations, where a larger maximum at a higher concentration is found with these measurements. Presumably this results from the different fiber-to-bath ratio used, and possibly from difficulties in completely removing foreign cations from the viscose monofil.

The maximum difference between cation and anion absorption for the monofil is 0.048 m$M$/g.; this agrees well with the cation-exchange capacity as determined by direct neutralization.

### *Oxycellulose Fibers*

The ester linkage in sample 1 of the esterified oxycellulose was found to be hydrolyzed by treatment with CTAB solutions. Probably the low pH of the treating bath resulting from cation exchange with the partially esterified oxycellulose was a major factor in the hydrolysis. Another factor may have been the presence of the quaternary ammonium ion, which has been reported to have a catalytic effect on the hydrolysis of esters (10).

The second and more completely esterified sample of esterified oxycellulose showed the expected large decrease in both cation and anion absorption. The results again agree qualitatively with the hypothesis that the ion-pair absorption is directly linked to the cation-exchange process. The swelling and other structural alterations brought about by the esterification clearly indicate that changes in accessibility as well as changes in cation-exchange capacity have resulted, so that no simple relationship between the absorption of CTAB by the treated and untreated samples, such as exists for the viscose samples, is to be expected.

Although the decrease in cation absorption on esterification is large, it is not as large as would be predicted from the change in carboxyl content as determined with methylene blue. This may result in part from hydrolysis of the ester as occurred with sample 1, although no positive test for ethylene glycol was obtained from the treating bath. However, the maximum cation exchange as determined from the results for absorption of cation and anion by the untreated oxycellulose is considerably less than that determined by the methylene-blue method; apparently the absorption processes for CTAB and methylene blue are appreciably different.

### *Dyeing Experiments*

The absorption of basic dyes, which is primarily an ion-exchange process, is reduced by esterification. The absorption of the disperse dye which is solubilized within micelles in the solution is also reduced. Presumably the absorption of ion pairs within the fiber assists in the absorption of the dye. A decrease in the number of anionic groups within the fiber would be expected to increase the absorption of anionic dyes. However, the change in electrostatic repulsive energy does not seem large enough under the conditions of dyeing to make an appreciable effect with the viscose monofils. However, there is an observable effect in the case of the oxycellulose substrates.

## ACKNOWLEDGMENT

One of us, Y. G., wishes to express his appreciation to Textile Research Institute for a Special Research Fellowship held during the course of this work.

## REFERENCES

1. SEXSMITH, F. H., AND WHITE, H. J., JR., *J. Colloid Sci.* **14**, 598 (1959).
2. DEUEL, H., *Helv. Chim. Acta* **30**, 1523 (1947).
3. FARRAR, J., AND NEALE, S. M., *J. Colloid Sci.* **1**, 186 (1952).
4. DAVIDSON, G. F., AND NEVELLE, T. P., *Shirley Inst. Mem.* **21**, 41 (1947).
5. GEIGER, E., AND KUNZLER, P., *Helv. Chim. Acta* **28**, 283 (1945).
6. VALLS, P., VENET, A. M., AND POURADIER, J., *Bull. soc. chim. France* **1953**, 106.
7. MONCRIEFF-YEATES, M., AND WHITE, H. J., JR., *Am. Dyestuff Reptr.* **46**, P87 (1957).
8. DAVIDSON, G. F., *Shirley Inst. Mem.* **21**, 47 (1947).
9. SKINKLE, J. H., "Textile Testing." Chemical Publ. Co., New York, 1949.
10. RIESZ, P., AND HAMMETT, P., *J. Am. Chem. Soc.* **76**, 992 (1954).

JOURNAL OF COLLOID SCIENCE **14**, 630–639 (1959)

# THE ABSORPTION OF CATIONIC SURFACTANTS BY CELLULOSIC MATERIALS

## III. A THEORETICAL MODEL FOR THE ABSORPTION PROCESS AND A DISCUSSION OF MAXIMA IN ABSORPTION ISOTHERMS FOR SURFACTANTS[1, 2]

**Frederick H. Sexsmith[3] and Howard J. White, Jr.**

*Frick Chemical Laboratory, Princeton University, Princeton, New Jersey, and Textile Research Institute, Princeton, New Jersey*

*Received May 6, 1959; revised July 14, 1959*

### Abstract

A theoretical model is proposed to account for the results observed when cationic surfactants are absorbed by cellulosic substrates. The model consists of the absorption of cations by an exchange process followed by a clustering of ion pairs on the exchanged cations. When this model is combined with a mass-action treatment of the surfactant solution, absorption isotherms, similar to those found experimentally, are obtained. In particular, there are maxima in the absorption isotherms. A discussion of the factors which lead to maxima is given, and a model to account for the maxima observed with anionic surfactants is proposed.

### Introduction

In two previous papers (1, 2) experimental results on the absorption of cationic surfactants by cellulosic substrates have been reported. Two absorption processes took place, a cation exchange and an ion-pair absorption. The ion-pair absorption was shown to be dependent on the cation exchange, and the hypothesis was advanced that the ion-pair absorption involved the formation of neutral clusters of ions about an exchanged cation which served as a nucleus. The ion-pair absorption started to become important when the concentration of the treating solution neared the critical micelle concentration (CMC), and, hence, was presumably related to the processes which caused micelle formation in the treating bath.

The absorption isotherms for both the cation exchange and the ion-pair absorption showed maxima in amount absorbed as a function of cation

---

[1] Taken from a thesis submitted by F. H. Sexsmith to the Department of Chemistry, Princeton University, in partial fulfillment of the requirements for the degree of Doctor of Philosophy.

[2] Presented in part before the Polymer Division at the 130th National Meeting of the American Chemical Society, Atlantic City, New Jersey, September, 1956.

[3] Present address: Chicopee Manufacturing Co., Milltown, New Jersey.

concentration in the treating solution in many cases. The maxima occurred at concentrations somewhat higher than the CMC.

Although there do not appear to be any results directly comparable with those presented in the previous papers, some closely related experiments have been done, with analogous results. The interactions of soluble proteins with anionic surfactants have been studied extensively (see, for example, Gibbs, Timasheff, and Nord (3)). Few, Ottewill, and Parreira (4) and Foster and Yang (5) have studied the interactions of cationic surfactants with soluble proteins. For both cationic and anionic surfactants the results were interpreted as showing binding of amounts of surfactant ion electrostatically equivalent to the (opposite) charge on the protein, followed by further uptake involving surfactant-surfactant interaction.

Maxima in absorption isotherms involving surfactants and insoluble polymeric substrates have been found by Aicken (6), who found maxima at the CMC followed by minima for sodium alkyl sulfates absorbed by cotton and wool; by Corrin *et al.* (7) for anionic surfactants on graphite and polystyrene; by Meader and Fries (8) for an alkylarylsulfonate on cotton; by Vold and Phansalkar (9) for sodium dodecylsulfate on carbon black and cotton; by Evans (10) for sodium alkyl sulfates and sodium oleate on various textile fibers; by Fava and Eyring (11) for sodium dodecylbenzene sulfonate on cotton; and by Flett, Hoyt, and Walter (12) using detergents on cotton under processing conditions. In the last example some question may be raised as to whether or not equilibrium was attained. In every case the concentration of the long-chain anion alone was followed so that it is impossible to separate the absorption processes into ion exchange and ion-pair absorption.

The cause of maximum formation was discussed in each of the first five papers and, very recently, by Vold and Sivaramakrishnan (13). However, no entirely satisfactory explanation has been given.

In this paper a discussion of the factors leading to the presence of maxima will be given, and a theory which rationalizes the qualitative features of the results found for cationic surfactants on cellulosic substrates will be developed. The theory is a first approximation but appears to contain certain essential features which should not change in more detailed and sophisticated treatments. A discussion of possible mechanisms for the maxima found using anionic surfactants is also given.

### *Conditions for the Formation of Maxima in Ion Exchange*

The underlying cause of a maximum in ion exchange seems to be the maximum in the concentration of single long-chain ions, first noted by Murray and by Hartley (14–16). Hartley found the maximum on applying the mass-action principle to micelle formation. In the example worked out by Hartley, the maximum is not very pronounced, and it is often stated that only a slight maximum can be obtained with this approach. This is not so.

At the time that the work reported here was done no more extensive examination of the application of the principle of mass action to micelle formation was available to us. After the work was completed, a more extensive treatment was published by Mysels (17). Our treatment will be outlined here because it includes some results not covered by Mysels, and because it forms the basis for the considerations about absorption maxima that follow.

It will be assumed that a cationic surfactant, which exists in the pure form as $QX$, can form a micelle, $Q_nX_m$, where $n > m$. It will also be assumed that the activities of ions are directly proportional to their concentrations. Then, from the principle of mass action,

$$K_\mu = \frac{C_M}{C_Q{}^n C_x{}^m}; \qquad [1]$$

where $K_\mu$ is a constant and the $C$'s represent molar concentrations with $C_M$ referring to the concentration of micelles. For conservation of total solute, $C$, present

$$C = nC_M + C_Q = mC_M + C_x. \qquad [2]$$

Equations [1] and [2] can be solved for $C_Q$ as a function of $C$. An examination of $dC_Q/dC$ and $d^2C_Q/dC^2$ shows that a maximum in $C_Q$ will occur if $n > m \geqq 2$ with the maximum occurring at the point,

$$C_Q = \left[\frac{(m-1)^{m-1}}{m^m(n-m)K_\mu}\right]^{\frac{1}{n+m-1}}. \qquad [3]$$

Similar considerations for $C_M$ show that there is no maximum in micelle concentration.

The changes of $C_Q$ with respect to $C$ for various values of $m$ and $n$ and $K_\mu = 10$ are shown in Figs. 1 and 2. Whether or not a pronounced maximum in $C_Q$ is obtained is seen to be dependent on the ratio of $m$ to $n$ and on the value of $n$. Using a maximum in $dC_M/dC$ as a criterion for the CMC, the variation in CMC with $K_\mu$ for fixed values of $m$ and $n$ is shown in Fig. 3. It is noticeable that very large values of $K_\mu$ are needed to bring the CMC into the concentration range found experimentally. The nearness of the maximum to the CMC depends on the value of $n$.

Values of the various concentrations in terms of the total concentration of surfactant are shown in Fig. 4 for $n = 100$, $m = 90$, and $\log K_\mu = 563$. These values were picked to give behavior similar to that of cetyltrimethylammonium bromide, the surfactant used in the previous experimen-

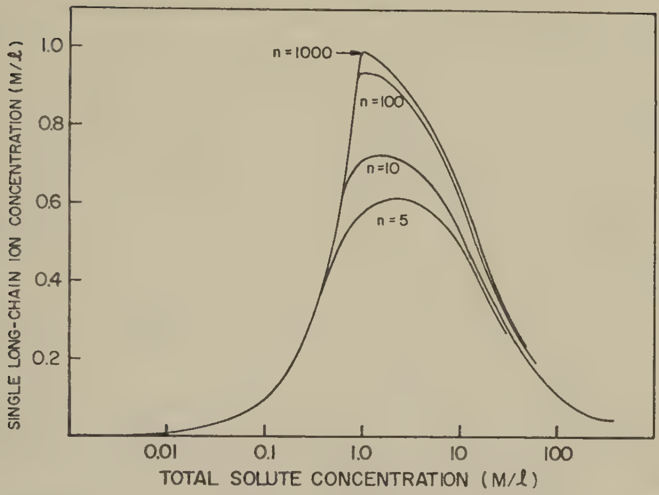

FIG. 1. Variation in single long-chain ion concentration with total solute concentration—effect of $n$ ($K_\mu$ = 10; $m/n$ = 0.9).

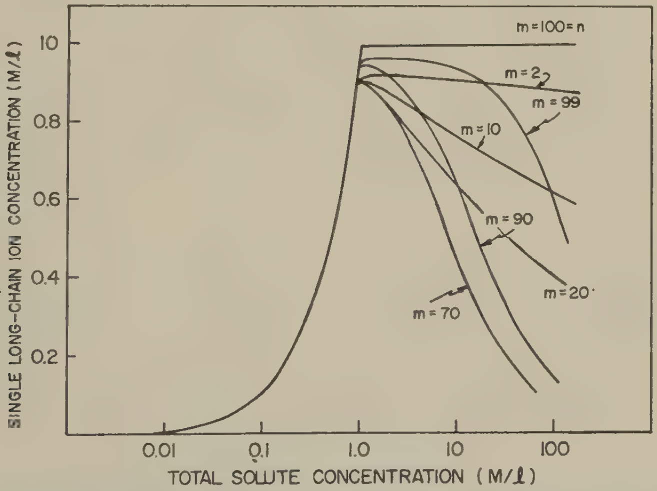

FIG. 2. Variation in single long-chain ion concentration with total solute concention—effect of $m/n$ ($K_\mu$ = 10; $n$ = 100).

tal work (1, 2). The values of $m$ and $n$ were based on the osmotic results of Vold (18) and on the light-scattering results of Debye and Anacker (19). The value of $K_\mu$ was chosen to give an appropriate CMC ($10^{-3}M$). A pronounced maximum in $C_Q$ is evident, as is the fact that the mean ion product is always increasing as would be expected from general thermodynamic reasoning.

The formation of the maximum in $C_Q$ does not result because of any

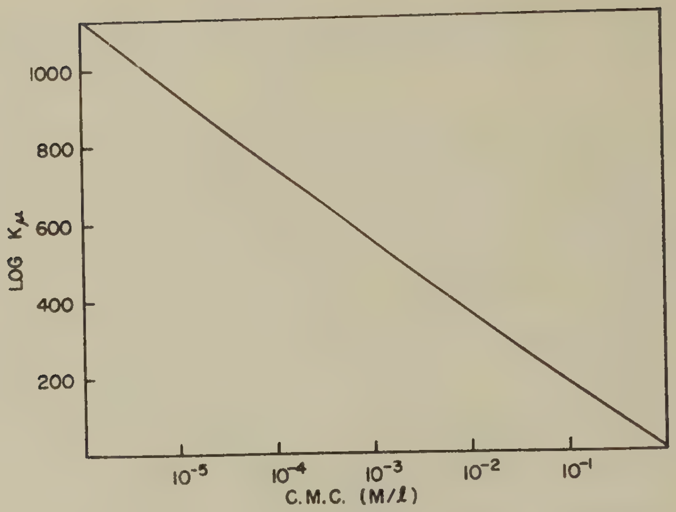

FIG. 3. Variation of critical micelle concentration with $K_\mu$ ($n = 100$; $m = 90$).

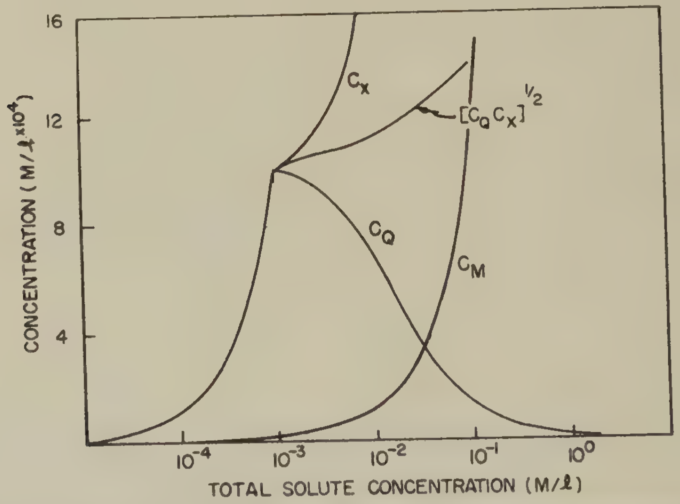

FIG. 4. Variation in mean ion product, single long-chain ion concentration, free-counter-ion concentration, and micelle concentration with total solute concentration (log $K_\mu = 563$; $n = 100$; $m = 90$).

ionic or electrostatic reasons. If two organic compounds, $Q$ and $X$, which would combine to form $Q_nX_m$ were to be fed into a reaction vessel in equimolar quantities, a maximum in $C_Q$ would result if $n > m \geqq 2$. Some workers (see, for example, Hutchinson, Inaba, and Bailey (20)) prefer to think of micelle formation as a form of phase change. Although it is difficult to speak categorically without suitable equations for a phase-change theory of micelle formation, it seems intuitively evident that the maximum results from the different ratio of $Q$ to $X$ in the micelle, $Q_nX_m$, as compared with the material fed into the system, $QX$, and not from any factor involved with the exact mechanism for micelle formation.

Entirely analogous equations will, of course, apply to an anionic surfactant. For either a cationic or an anionic surfactant a maximum in long-chain ion exchange can result directly from the maximum in concentration of the long-chain ion.

### *Maxima in Ion-Pair Absorption*

As has been mentioned, the experimental results for the absorption of cetyltrimethylammonium bromide by cellulosic substrates showed that ion-pair absorption occurred to a considerable extent, that maxima occurred in ion-pair absorption, and that the extent of ion-pair absorption could be correlated directly with the extent of ion exchange. It was proposed that the absorption of ion pairs resulted from a clustering about exchanged cations which served as nuclei.

A mechanism for the maximum in ion-pair absorption can now be proposed. The amount of cation exchanged will go through a maximum with increasing concentration of surfactant, reflecting the maximum in concentration of the cation in solution. If the ion-pair absorption depends directly on the cation exchange, it, too, will show a maximum.

A simplified quantitative theory can be developed to give concreteness to the ideas expressed above. Let the ion-exchange process be represented schematically by

$$\mathrm{Q^+ + CellCOOH \rightleftharpoons H^+ + CellCOOQ}$$

and let $B$ represent the cation-exchange capacity of the substrate and $K_e$ the equilibrium constant for cation exchange. Assume that the equilibrium for ion exchange can be represented by the equation,

$$\frac{C_Q}{C_H} = K_e \frac{\theta}{1 - \theta - \alpha}, \tag{4}$$

where $C_Q$ and $C_H$ are concentrations and

$$\theta = \frac{\mathrm{CellCOOQ}}{B} \quad \text{and} \quad 1 - \theta - \alpha = \frac{\mathrm{CellCOOH}}{B}.$$

The assumption of Eq. [4] requires that the solutions be adequately dilute so that activities are proportional to concentrations and that there are no interactions between absorbed cations on the substrate. It is not required that no micelles be formed since $C_Q$ refers to single cations only. Assuming the substrate to be, initially, in the hydrogen form, it is possible to write

$$\frac{C_H V}{B} = \theta + \alpha, \tag{5}$$

where $V$ is the volume of the solution. Then Eq. [4] can be written

$$C_Q = \frac{BK_e}{V} \frac{\theta(\theta + \alpha)}{1 - \theta - \alpha}. \tag{6}$$

Assume that ion-pair clustering on exchanged cations occurs according to the scheme

$$pQ^+ + pX^- + \text{CellCOOQ} \rightleftharpoons \text{CellCOOQ}(QX)_p$$

The equilibrium constant for this process, $K_a$, can be assumed to be

$$K_a = \frac{\alpha}{\theta(C_Q C_X)^p}, \tag{7}$$

where $\alpha = \text{CellCOOQ}(QX)_p/B$.

For conservation of the total amount of solute in the system (expressed as a concentration, $C_0$, in the solution)

$$C_Q + nC_M + \frac{\text{CellCOOQ}}{V} + \frac{(p+1)\,\text{CellCOOQ}(QX)_p}{V} = C_0, \tag{8}$$

$$C_X + mC_M + \frac{p\,\text{CellCOOQ}(QX)_p}{V} = C_0. \tag{9}$$

The total amounts of $Q$ and $X$ absorbed can be written

$$A_Q \equiv B\theta + (p+1)B\alpha, \tag{10}$$

$$A_X \equiv pB\alpha, \tag{11}$$

and Eqs. [8] and [9] can be written

$$C_Q + nC_M + \frac{B\theta}{V} + (p+1)\frac{B\alpha}{V} = C_0, \tag{8$'$}$$

$$C_X + mC_M + p\frac{B\alpha}{V} = C_0. \tag{9$'$}$$

Using Eqs. [8′], [9′], [6], and [7], $C_M$ can be written

$$C_M = \frac{1}{n - m} \cdot \left[ \frac{(x/K_a)^{1/p}}{\dfrac{BK_e}{V} \dfrac{\theta^2(1+x)}{1 - \theta(1+x)}} - \frac{BK_e}{V} \frac{\theta^2(1+x)}{1 - \theta(1+x)} - \frac{B\theta(1+x)}{V} \right], \tag{12}$$

where $x = \alpha/\theta$. Using Eqs. [1], [6], and [7], $C_M$ can be expressed as

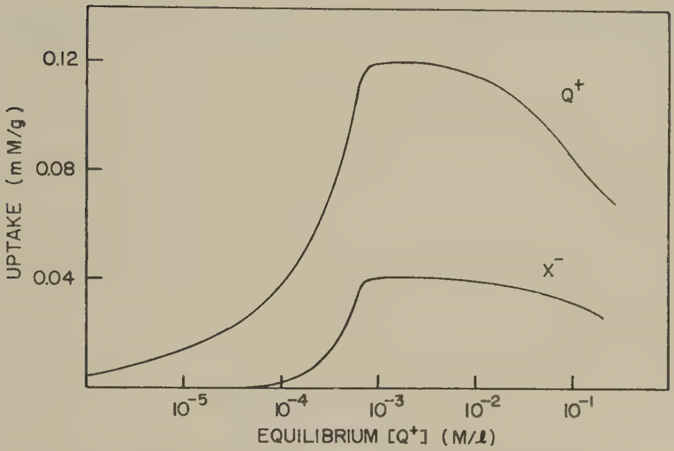

FIG. 5. Hypothetical isotherms for the absorption of the ions of $QX$ by a cellulose-like substrate.

$$C_M = K_\mu \left(\frac{x}{K_a}\right)^{m/p} \left(\frac{BK_e}{V} \frac{\theta^2(1+x)}{1-\theta(1+x)}\right)^{n-m}. \qquad [13]$$

By assigning values to the constants and choosing a value of $x$, $C_M$ can be plotted against $\theta$ and the point of intersection of Eqs. [12] and [13] determined. Enough information is then available to determine all the other variables, in particular $A_Q$ and $A_X$.

Since the computations required are lengthy, no attempt has been made to fit the equations to experimental results. However, a numerical example has been calculated using constants chosen to be reasonable for cetyltrimethylammonium bromide and to provide absorption curves similar to those found for cellulosic substrates. The constants chosen were:

$K_\mu = 10^{563}$ $\qquad n = 100$

$K_a = 10^6$ $\qquad m = 90$

$K_e = 0.5$ $\qquad p = 1$

$B = 0.1$ (m$M$/g.) $\qquad V = 100$ ml.

The results of the calculations are shown in Fig. 5. The similarity in character between the theoretical and experimental curves shows that the model is capable of providing behavior of the type found experimentally.

## DISCUSSION

Aicken and Corrin, Lind, Roginsky, and Harkins cite the work of Hartley in explanation of the observed maxima. However, it is unlikely that anion exchange can account for all the absorption by substrates such as cotton, carbon black, graphite, or polystyrene. Meader and Fries postulate an independent micellar absorption which reaches a limiting value so that the maximum in single anion absorption resulting from the maximum in the concentration of the single anion in the solution leads to the observed maximum in absorption. A solid polymeric substrate can be separated from the aqueous phase, and only ion-pair absorption and ion exchange can make any appreciable contribution to the observed absorption, since the gross phases must remain essentially neutral electrically. (It is true that charge separations can conceivably occur in a microlayer along the internal and external surfaces of the polymer, but such a separation cannot be recognized by thermodynamic measurements such as are under discussion here, and the overall absorption determined experimentally would involve ion pairs.) However, anion exchange does not occur with cotton, which was the substrate used by Meader and Fries, and their model provides no mechanism for a maximum in ion-pair absorption.

The chemical potential for ion pairs depends on the ion product for the surfactant in the solution and must increase steadily with concentration for basic thermodynamic reasons. Thus no model producing a maximum in the absorption isotherm can be devised without the introduction of some additional factor such as was done in the previous section of this paper. In particular a tendency to micelle formation, in itself, cannot produce a maximum. Vold and Sivaramakrishnan, from kinetic considerations, have devised a set of equations which seems to provide for a maximum in this way, but their derivation appears to violate the principle of microscopic reversibility. Statistical thermodynamic derivations using models similar to theirs produce no equations showing maxima for ion-pair absorption. Evans attributes the maxima to alterations in the surface available for adsorption within the polymer. The reasons for the changes in the surface are not clear.

Two mechanisms can be advanced to explain maxima in cases involving anionic surfactants. If anion exchange can occur, a model entirely analogous to that given above for cationic surfactants suffices. Also, if hydrolysis should occur and the buffering action of the water and of dissolved carbon dioxide should keep the concentration of hydrogen ion from changing to as great an extent as does the concentration of single anion, then the concentration of the undissociated acid form of the surfactant could go through a maximum. This unionized form might be expected to be strongly absorbed by the polymeric substrate. Once absorbed, molecules of the acid form of the surfactant could serve as nuclei for the clustering of ion pairs. Thus it would not be necessary for all (or even a major part) of the adsorbed material to be in the acid form. In connection with this second proposal, it may be pointed out that Meader and Fries found their results to be very sensitive to pH and the hardness of the water used and postulated that hydrolysis played an important role.

As was shown in the first paper of this series (1), the clustering of ion pairs on exchanged cations provides qualitative explanations for the effects of added acid and salt on the uptake of cationic surfactants at least until very high concentrations are reached. The studies of Meader and Fries and of Evans using anionics also seem to be in qualitative agreement.

Finally a reviewer has pointed out that some or all of the counter ions need not be in a cluster but could be free in the fiber phase. It is clear that such an occurrence would change the form of the activity of the counter ion in Eq. [7], but would not interfere with the occurrence of a maximum.

## Acknowledgment

One of us (F.H.S.) wishes to thank textile Research Institute for a fellowship held during the course of this work.

## References

1. Sexsmith, F. H., and White, H. J., Jr., *J. Colloid Sci.* **14,** 598 (1959).
2. Gotshal, Y., Rebenfeld, L., and White, H. J., Jr., *J. Colloid Sci.* **14,** 619 (1959).
3. Gibbs, R. J., Timasheff, S. N., and Nord, F. F., *Arch. Biochem. Biophys.* **40,** 85 (1952).
4. Few, A. V., Ottewill, R. H., and Parreira, H. C., *Biochim. et Biophys. Acta* **18,** 136 (1955).
5. Foster, J. F., and Yang, J. T., *J. Am. Chem. Soc.* **76,** 1015 (1954).
6. Aicken, R. G., *J. Soc. Dyers Colourists* **60,** 60 (1944).
7. Corrin, M. L., Lind, E. L., Roginsky, A., and Harkins, W. D., *J. Colloid Sci.* **4,** 485 (1959).
8. Meader, A. L., and Fries, B. A., *Ind. Eng. Chem.* **44,** 1636 (1952).
9. Vold, R. D., and Phansalkar, A. K., *Rec. trav. chim.* **74,** 41 (1955).
10. Evans, H. C., *J. Colloid Sci.* **13,** 537 (1958).
11. Fava, A., and Eyring, H., *J. Phys. Chem.* **60,** 890 (1956).
12. Flett, L. H., Hoyt, L. F., and Walter, J., *Am. Dyestuff Reptr.* **41,** 139 (1952).
13. Vold, R. D., and Sivaramakrishnan, N. H., *J. Phys. Chem.* **62,** 984 (1958).
14. Murray, R. C., and Hartley, G. S., *Trans. Faraday Soc.* **31,** 183 (1935).
15. Murray, R. C., *Trans. Faraday Soc.* **31,** 206 (1935).
16. Hartley, G. S., "Aqueous Solutions of Paraffin Chain Salts." Hermann et Cie, Paris, 1936.
17. Mysels, K. J., *J. Colloid Sci.* **10,** 507 (1955).
18. Vold, M. D., *J. Colloid Sci.* **5,** 506 (1950).
19. Debye, P., and Anacker, E. W., *J. Phys. & Colloid Chem.* **55,** 644 (1951).
20. Hutchinson, E., Inaba, A., and Bailey, L. G., *Z. physik. Chem.* **5,** 344 (1955).

JOURNAL OF COLLOID SCIENCE **14**, 640–645 (1959)

# THE EFFECT OF pH ON SOLUBILIZATION OF WEAK ACIDS AND BASES

**Denzel L. Dyer** *

*Biochemical Research Laboratory, The Dow Chemical Company, Midland, Michigan*

*Received June 8, 1959*

## Abstract

Recent studies of the nature of surface-active agents in solution indicate that micelles formed in such solutions behave somewhat as a separate phase. Solubility measurements were made on *o*-phenylphenol, pentachlorophenol, and *p*-dimethylaminoazobenzene in solutions with and without surfactant over a wide pH range. The ratio of solubility in a surfactant solution to solubility in a similar solution without surfactant is defined as relative solubilization. This varies with solution pH and solute pK, being at a maximum for nonionized solute and at half-maximum when pH is equal to pK. The variation of relative solubilization with pH is that which is predicted from treatment of micelles as a separate phase.

## Introduction

Aqueous solutions of surface-active agents are able to dissolve appreciable quantities of materials which are only slightly soluble in water. This is the well-known phenomenon of solubilization, which has been reviewed fairly recently (1–3). It is now widely accepted that solubilization requires the presence of micelles of the surface-active agent (4–6). Such micelles are aggregates of surfactant in which many of the hydrophobic groups of the surfactant have associated to form very small oil-like "droplets," the surfaces of which are covered by the surfactant hydrophilic groups (7, 8). Although solutions of surfactants are homogeneous when considered on a macroscopic scale, it appears that many of the properties of such solutions may be explained fairly well by treatment of the micelles as a separate phase (3, 9).

According to the phase treatment, solubilization amounts to solution of material in the hydrocarbon-like interiors of the micelles. If this is the case, the distribution of solute between aqueous and micelle phases should depend on the nature of the solute. For an ionizable solute one would expect the ionic form to be soluble in water and the nonionic form to be soluble in micelles. The effect of pH on water-micelle distribution should be basically the same as its effect on the partition coefficient for bulk phases (10–12). At a pH such that essentially all the solute is ionized, the solute would occur mostly in the aqueous phase, so that the effect of surfactant would be small. On the other hand, with a pH at which the solute is nonionized, the solute would occur primarily in the micelles and the surfactant would be an effective solubilizer.

---

* Present address: Space Medicine Section, The Martin Company, Denver, Colorado.

The effect of pH on solubilization was measured for two weak acids in an anionic surfactant and for a weak base in a cationic surfactant.

## Experimental Methods

For each system studied a series of solutions was made up to cover a wide pH range with and without surfactant. Excess solute was added to all solutions, which were then sealed and shaken continuously for 10 or more days. The room temperature was maintained at very nearly 23°C. After shaking, the final pH of each solution was measured. Suspended solute was removed by settling or low-speed centrifugation. Solute concentrations were determined with a Beckman Model DU spectrophotometer.

Since solubilization is affected by electrolyte concentration, a swamping electrolyte was used in all solutions. In some cases, it was a buffer, but buffering was unnecessary when the solute did not ionize and ineffective when it did. In each case results were plotted with respect to the final pH.

The systems considered were:

*a.* *o*-Phenylphenol in 0.05 *M* sodium lauryl sulfate with 0.25 *N* disodium phosphate; pH adjusted with phosphoric acid and sodium hydroxide.

*b.* Pentachlorophenol in 0.0104 *M* sodium lauryl sulfate with 0.1 *M* sodium chloride; pH adjusted with hydrochloric acid and sodium hydroxide.

*c.* *p*-Dimethylaminoazobenzene (DMAB) in 0.01 *M* dimethyl dodecylphenacylammonium bromide with 0.1 *M* sodium chloride; pH adjusted with hydrochloric acid and sodium hydroxide.

The *o*-phenylphenol (m.p. 58°C.) and pentachlorophenol (m.p. 188°–191°C.) were purified products of The Dow Chemical Company. The DMAB (m.p. 116°–118°C.) was used as obtained from Eastman Kodak. Sodium lauryl sulfate was Fisher USP grade. The quaternary ammonium compound was prepared by the author from phenacyl bromide and specially distilled dimethyldodecylamine.

Solutions of *o*-phenylphenol were diluted into weak acid for measurement of optical density at 243 m$\mu$. Pentachlorophenol was determined in dilute base at 320 m$\mu$. DMAB was measured at 420 m$\mu$ in pH 7 buffer.

## Results and Discussion

Results of solubility measurements for the *o*-phenylphenol system are shown in Fig. 1. Both curves are flat in the region where *o*-phenylphenol is not appreciably ionized. With higher pH and increasing ionization both curves climb, but the ratio of their heights decreases. The latter is the effect which would be expected from solubilization by a separate oil-like phase.

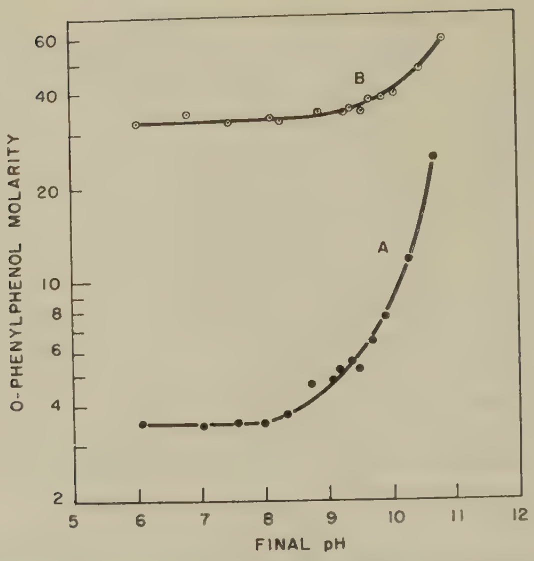

FIG. 1. The effect of pH on solubility of *o*-phenylphenol in presence (*B*) and absence (*A*) of sodium lauryl sulfate.

When a surfactant solution is saturated with the poorly soluble weak acid HA, the acid will occur in several forms:

$$\begin{tikzcd} HA_{(\text{excess})} \arrow[r, shift left] & HA_{(\text{water})} \arrow[l, shift left] \arrow[r, shift left] \arrow[d, shift left] & H^+ + A^- \arrow[l, shift left] \\ & HA_{(\text{micelles})} \arrow[u, shift left] & \end{tikzcd}$$

It is assumed that $A^-$ occurs only in the aqueous phase. The total concentration is then:

$$[HA] = [HA_{(\text{micelles})}] + [HA_{(\text{water})}] + [A^-] \qquad [1]$$

All the terms refer to concentration in moles per liter of surfactant solution.

In strongly acidic solutions HA will be essentially nonionized, so that the concentration of $A^-$ will be negligible. The micelles might then dissolve much more of HA than would the aqueous phase. Under these conditions the surfactant would seem to be a good solubilizing agent. In alkaline solutions, however, ionization would be extensive, with $[A^-]$ becoming the dominant term in Eq. [1]. The micelles, still saturated with HA, would no longer make a significant contribution and the surfactant would seem ineffective as a solubilizer.

The contribution of $A^-$ to the total solubility depends on the pH of the solution and on the ionization constant, *Ka*, of the acid:

$$[A^-] = [HA_{(\text{water})}]\ (Ka/[H^+]) = [HA_{(\text{water})}] \cdot 10^{(\text{pH}-\text{pKa})} \qquad [2]$$

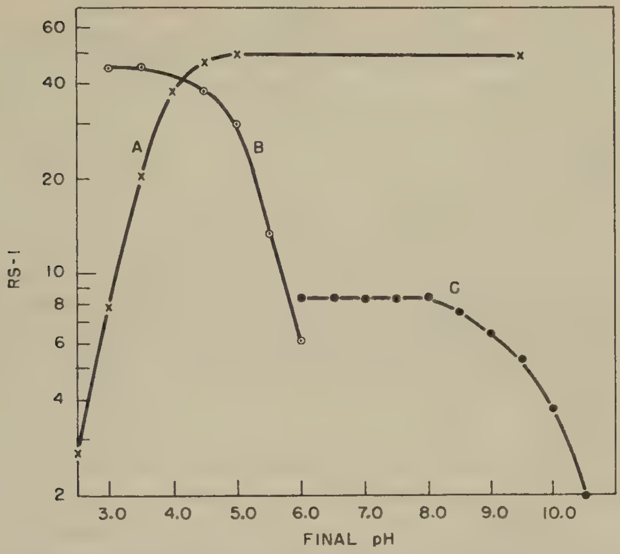

FIG. 2. The effect of pH on Relative Solubilization of DMAB (*A*), pentachlorophenol (*B*), and *o*-phenylphenol (*C*).

Let the term "relative solubilization" (RS) be defined as the ratio of the solubility of a material in a surfactant solution to its solubility in a similar solution without surfactant. Then:

$$\mathrm{RS} = \frac{[\mathrm{HA}_{(\mathrm{micelles})}] + [\mathrm{HA}_{(\mathrm{water})}] + [\mathrm{A}^-]}{[\mathrm{HA}_{(\mathrm{water})}] + [\mathrm{A}^-]} . \qquad [3]$$

From Eqs. [2] and [3] it follows that:

$$\mathrm{RS} = 1 + \frac{[\mathrm{HA}_{(\mathrm{micelles})}]}{[\mathrm{HA}_{(\mathrm{water})}](1 + 10^{(\mathrm{pH}-\mathrm{pK}_a)})} . \qquad [4]$$

When: $\mathrm{pH} \ll \mathrm{pK}_a,\ \mathrm{RS} = 1 + \dfrac{[\mathrm{HA}_{(\mathrm{micelles})}]}{[\mathrm{HA}_{(\mathrm{water})}]}$ ;

$$\mathrm{pH} = \mathrm{pK}_a,\ \mathrm{RS} = 1 + \frac{[\mathrm{HA}_{(\mathrm{micelles})}]}{2\,[\mathrm{HA}_{(\mathrm{water})}]} ;$$

$$\mathrm{pH} \gg \mathrm{pK}_a,\ \mathrm{RS} = 1 .$$

Thus, for HA the relative solubilization (less one) is at a maximum when $\mathrm{pH} \ll \mathrm{pK}_a$ and at half-maximum when $\mathrm{pH} = \mathrm{pK}_a$. For weak bases the pH and pK terms are reversed.

Experimentally, the final pH values did not coincide exactly in solutions with and without surfactant. Relative solubilization, therefore, was determined from the ratio of heights of solubilization curves (Fig. 1) at arbitrary

TABLE I

*Comparison of Experimental and Literature pK Values*

| Solute | Calc. pK | Lit. pK |
|---|---|---|
| *o*-Phenylphenol | 9.85 | 9.97 (13) |
| Pentachlorophenol | 5.2 | 5.3 (14) |
| DMAB | 3.6 | 3.5 (15) |

pH values. In Fig. 2, relative solubilization is plotted vs. final pH for each of the three systems reported. In each case the pH at which (RS − 1) was half its maximum was taken as the solute pK. In Table I these pK values are compared with those reported in the literature. For the control solutes naphthalene and *o*-dichlorobenzene, relative solubilization varied only slightly with pH.

The pK values derived from the assumption that micelles act as a separate phase are in close agreement with values determined by other methods. These observations tend to substantiate the suggestions (3, 9) that micelles behave in many ways as a separate phase. This, to be sure, cannot be a complete explanation. Hutchinson, Inaba, and Bailey (9), while suggesting the phase treatment, pointed out that the concept of phase breaks down at the microscopic size of micelles. McBain and McHan (16) reported that the solubility of dimethyl phthalate in potassium laurate micelles was greater than in dodecane, and measurements by the author have shown that *o*-phenylphenol is more soluble, mole for mole, in sodium lauryl sulfate micelles than in decane. In spite of these difficulties the phase concept of micelles appears to be fruitful. Among other things, it explains the repeated observations that the biological activity of phenols is decreased in the presence of micelles. Such an explanation was presented as early as 1942 (17) and has been suggested several times by Alexander and co-workers (18–20), but has apparently not been accepted entirely.

## REFERENCES

1. KLEVENS, H. B., *Chem. Revs.* **47,** 1 (1950).
2. WINSOR, P. A., "Solvent Properties of Amphiphilic Compounds." Butterworth, London, 1954.
3. MCBAIN, M. E. L., AND HUTCHINSON, E., "Solubilization and Related Phenomena." Academic Press, New York, 1955.
4. RIGG, M. W., AND LIU, F. W. J., *J. Am. Oil Chemists' Soc.* **30,** 14 (1953).
5. STRAUSS, U. P., AND JACKSON, E. G., *J. Polymer Sci.* **6,** 649 (1951).
6. HARRIS, J. C., *J. Am. Oil Chemists' Soc.* **35,** 428 (1958).
7. REICH, I., *J. Phys. Chem.* **60,** 257 (1956).
8. HARRIS, J. C., *Soap Chem. Specialties* **34** (6), 50 (1958).
9. HUTCHINSON, E., INABA, A., AND BAILEY, L. G., *Z. physik. Chem.* [N. F.] **5,** 344 (1955).
10. CRAIG, L. C., *J. Biol. Chem.* **150,** 33 (1943).

11. Golumbic, C., Orchin, M., and Weller, S., *J. Am. Chem. Soc.* **71,** 2624 (1949).
12. Cymerman-Craig, J., and Diamantis, A. A., *J. Chem. Soc.* **1953,** 1619.
13. Kieffer, F., and Rumpf, P., *Compt. rend.* **238,** 360 (1954).
14. Griffith, R. O., McKeown, A., and Shutt, W. J., "Annual Tables of Constants and Numerical Data," No. 22, Vol. 13. Hermann, Paris, 1938.
15. Klotz, I. M., Fiess, H. A., Chen Ho, J. Y., and Mellody, M., *J. Am. Chem. Soc.* **76,** 5136 (1954).
16. McBain, J. W., and McHan, H., *J. Am. Chem. Soc.* **70,** 3838 (1948).
17. Hueter, R., and Engelbrecht, H. J., *Die Chemie* **8,** 55, 329 (1942); *Record Chem. Progr.* (*Kresge-Hooker Sci. Lib.*) **4,** 58 (1943).
18. Trim, A. R., and Alexander, A. E., *Nature* **154,** 177 (1944).
19. Alexander, A. E., and Trim, A. R., *Proc. Roy. Soc.* (*London*) **B133,** 220 (1946).
20. Alexander, A. E., and Tomlinson, M. A., p. 317 in "Surface Chemistry", supplement to Research, (London) 1949.

JOURNAL OF COLLOID SCIENCE **14**, 646 (1959)

# BOOK REVIEWS

**Light Scattering by Small Particles.** By H. C. VAN DE HULST. John Wiley & Sons, Inc., New York, Chapman & Hall, Ltd., London, 1957. 470 pp. Price $12.00.

The central theme of this book is a detailed physical and mathematical presentation of light scattering by independent particles. This means that the particles are separated from each other in such a manner that there is sufficient room for each to form its own scattering pattern, undisturbed by the presence of others. It thus treats dilute colloidal dispersions, polymer latices, gold and sulfur hydrosols, aerosols of all types, but specifically excepts the fine dispersions of high polymeric macromolecules which require special treatments as dependent particles. (See text by Stacey.) It is the most authoritative, comprehensive, and useful book on this subject that has appeared. The author, a distinguished astronomer, has made significant discoveries in the study of the polarization patterns of interstellar matter. His studies coincided with the renaissance of interest in the quantitative applications of the Mie theory to military problems of aerosols and of colloidal dispersions in general, initiated notably in this country during World War II.

Anyone interested in colloids will find this monograph useful if he wishes to understand the phenomena of light scattering. Colloid Science is fortunate indeed that such an eminent mathematical physicist has taken the time to present this very difficult and complicated subject in such a clear and practically useful way. The treatment is not easy, but the subject is presented in as simple a way as is possible, considering its inherent difficulties and complexities.

VICTOR K. LA MER, New York, New York

**Handbook of Physics.** Edited by E. U. CONDON AND HIGH ODISHAW. McGraw-Hill Book Company, Inc., New York, 1958. 1504 pp. Price $25.

Two distinguished editors, one a former Director and the second a former Assistant to the Director of the National Bureau of Standards, working with a competent group of scientists, present a comprehensive and authoritative guide to basic physics. This handbook will be very useful to chemists as well. It concentrates on principles, ideas, concepts, and mathematical methods of all branches of classical and modern physics, and, we add, physical chemistry and chemical physics.

The treatise starts with several hundred pages of mathematics, followed by mechanics of particles and rigid bodies, mechanics of deformable bodies, electricity and magnetism, heat and thermodynamics, including mechanical kinetics, optics, atomic physics, solid state, nuclear physics, etc.

Readers of this Journal will be interested in Chapter 7 of Part V entitled: Surface Tension, Adsorption by Stephen Brunauer and L. E. Copeland. The price of $25 is high, but there is much valuable material in one volume. The handbook can be recommended to anyone in the physical sciences.

VICTOR K. LA MER, New York, New York

# AUTHOR INDEX

A

Aebi, Claude M., 161
Ahlbeck, Richard A., 354
Albers, W. 501, 510
Alexander, A. E., 91, 101, 190
Allan, A. J. G., 206
Arnaki, Margarita, 281

B

Barnes, G. T., 91, 101
Bartok, W., 13
Bateman, J. B., 308
Becker, Paul, 519
Berge, John W., 135
Blei, Ira, 358
Bonnelycke, Burg E., 567
Bradford, E. B., 543
Brown, A. M., 1, 343
Brunauer, Stephen, 363

C

Clifton, Nancy K., 519
Comer, Joseph J., 175

D

Dandliker, W. B., 567
Defay, Raymond, 401, 411
Demeny, Margaret, 281
De Smet, M., 330
Drozin, Vadim G., 74
Dyer, Denzel L., 640

E

Eshler, D. C., 308

F

Farlow, Neil H., 356
Ferry, John D., 36, 147
Forgacs, O. L., 457, 473
Fort, Tomlinson, Jr., 190
Frost, Arthur A., 247

G

Gabor, Joseph, 354
Ghosh, Ashim Kumar, 338
Gillespie, Thomas, 123
Gotshal, Yehezkiel, 619

H

Harrap, B. S., 300
Hermans, J. J., 252
Hirschhorn, E., 430
Hommelen, Jacques R., 385, 401, 411

J

Jellinek, H. H. G., 268
Jenny, Hans, 533

K

Kantro, D. L., 363
Kurath, Sheldon F., 222

L

La Mer, Victor K., 74
Lloyd, Norman E., 441
Lopez-Gonzalez, J. de, 533

M

Mankowich, A. M., 131
Mason, S. G., 13, 457, 473
Mathews, M. B., 430
Miller, John C., 287
Miller, M. L., 524
Minor, Francis W., 572, 584
Moore, W. R., 1, 343
Myers, Raymond R., 287

N

Nagamatsu, Kazuo, 377
Napjus, P. J., 252
Nash, T., 59
Ninomiya, Kazuhiko, 36, 49

O

Overbeek, J. Th. G., 501

P

Perry, Ernest J., 27
Phillips, J. N., 111
Prakash, Satya, 338

R

Rajalakshmi, N., 419
Rauhut, C. E., 524
Rebenfeld, Ludwig, 619
Reich, Irving, 562
Ries, Herman E., Jr., 354
Rigole, W., 330
Rutgers, A. J., 330

S

Sakoonkim, Charoen, 222
Saunders, P. R., 222
Schurz, J., 492
Schwartz, Anthony M., 572, 584
Sexsmith, Frederick H., 598, 630
Sivarajan, S. R., 419
Sobotka, Harry, 281
Stern, Donald M., 222

T

Tartar, H. V., 115

V

Vanderhoff, J. W., 543
Vold, Marjorie J., 168
Vold, R. D., 419

W

Weise, C. H., 363
Weneck, E. J., 308
White, Howard J., Jr., 598, 619, 630
White, Malcolm L., 247
Wiebush, Joseph, R. 161

Y

Yamaguchi, S., 452
Yin, Theodore P., 147
Yoshitomi, Tatsuya, 377

Z

Zettlemoyer, A. C., 287

# SUBJECT INDEX

A

Acrylic acid copolymers, Miller and Rauhut, 524
Aerosols, particle size distribution, Drozin and La Mer, 74

C

Capillarity, rise of liquid in filter paper, Gillespie, 123; thermodynamic approach, Schwartz and Minor, 572, 584
Carboxymethylcellulose, characteristics, Napjus and Hermans, 252
Cellulose, viscosity-temperature relation of derivatives, Moore and Brown, 1, 343
Cellulosic fibers, and cationic surfactants, Sexsmith and White, 598, 630; Gotshal *et al.*, 619
Cetyl trimethyl ammonium salts, micelle formation, Nash, 59
Crystals, habit-modified phosphates and arsenates, Comer, 175

D

Diffusion, in the adsorption process, Defay and Hommelen, 411
Dyes, binding by wool keratin derivatives, Harrap, 300

E

Emulsions, surface-average particle diameter, Lloyd, 441; emulsions of water in oil, Albers and Overbeek, 501, 510

F

Films, splitting, Myers *et al.*, 287
Flow curves, and molecular properties, Schurz, 492

I

Ice, adhesive properties, Jellinek, 268

L

Latexes, particle diameter determination, Bradford and Vanderhoff, 543

M

Magnetization, of thin film, Yamaguchi, 452
Monolayers, ionized, Phillips, 111

P

Paraffin chain salts, micellar molecular weights, Tartar, 115
Polyethylene film, surface properties, Allan, 206
Poly-*n*-butyl methacrylate, properties, Saunders *et al.*, 222
Poly-*n*-docosyl methacrylate, properties, Saunders and Ferry, 239
Poly-*n*-dodecyl methacrylate, properties, Kurath *et al.*, 147
Poly-*n*-octyl methacrylate, properties, Berge *et al.*, 135
Polyvinyl acetate, stress-relaxation, Ninomiya, 49; mixed monolayers, Ries *et al.*, 354
Polyvinyl alcohol, aerosol particles, Farlow, 356
Potassium nitrate, nucleation, White and Frost, 247
Protein, detergent complex, Blei, 358

R

Rayon, water exchange between rayon and detergent micelles, Hirschhorn and Mathews, 430

S

Sediment volume, Vold, 168
Silica, light scattering of collodial silica, Bonnelycke and Dandliker, 567
Silver halide, crystal growth, Perry, 27
Silver hydrosol, and ultrasonic waves, Prakash and Ghosh, 338

Sodium chloride, and Aerosol OT, Aebi and Wiebush, 161
Sodium humate, viscosity, Rajalakshmi *et al.*, 419
Solubilization, micellar, Mankowich, 131; solubilization of weak acids and bases, Dyer, 640
Spectrophotometry, and particle size, Bateman *et al.*, 308
Streaming currents, with nonaqueous solutions, Rutgers *et al.*, 330
Strontium, diffusion in ion-exchange membranes, de Lopez-Gonzalez and Jenny, 533
Surface-active agents, Becher and Clifton, 519
Surface tension, determination, Hommelen, 385; Defay and Hommelen, 401; calculation, Reich, 562
Suspensions, aggregation of colloidal suspensions, Barnes and Alexander, 91, 101; particle motions in sheared suspensions, Bartok and Mason, 13; Forgacs and Mason, 457, 473

T

Tricalcium silicate, hydration, Kantro *et al.*, 363
Triiodostearic acid, multimolecular films, Sobotka *et al.*, 281

V

Vinyl compounds, surface films, Fort and Alexander, 190
Viscoelastic data, Ninomiya and Ferry, 36
Viscoelastic properties, of polymers, Nagamatsu and Yoshitomi, 377

## INDEX OF BOOK REVIEWS

Behr, L. C., *et al.*, Brief Course in Organic Chemistry, 2nd ed. (Becker, R. R.), 565
Bier, M., (ed.), Electrophoresis: Theory, Methods and Applications (Cann, J. R.), 455
Bowden, F. P., and Yoffe, A. D., Fast Reactions in Solids (Sundheim, B. R.), 456
Condon, E. U., and Odishaw, H. (eds.), Handbook of Physics (La Mer, V. K.), 646
Gordon, L., *et al.*, Precipitation from Homogeneous Solution (Weiss, G. R.), 362
Gunstone, F. D., An Introduction to the Chemistry of Fats and Fatty Acids (Barnes, G. T.), 362
Klyne, W., and de la Mare, P. B. D. (eds.), Progress in Stereochemistry, Vol. II (Curtin, D. Y.), 113
van de Hulst, H. C., Light Scattering by Small Particles (La Mer, V. K.), 646

# JOURNAL OF COLLOID SCIENCE

*Editor-in-Chief*

Victor K. La Mer, Columbia University, New York

*Advisory Board*

A. E. Alexander
Stephen Brunauer
J. A. Christiansen
P. J. W. Debye
B. Derjaguin
D. G. Dervichian
John T. Edsall
I. Fankuchen
John D. Ferry
J. J. Hermans
John G. Kirkwood
L. G. Longsworth
S. G. Mason
Karol J. Mysels
J. Th. G. Overbeek
J. H. Schulman
Leo Shedlovsky
Theodore Shedlovsky
Robert Simha
R. H. Smellie
Harry Sobotka
Jacinto Steinhardt
Torsten Teorell
A. C. Zettlemoyer
Bruno H. Zimm
W. A. Zisman

VOLUME 14

1959

ACADEMIC PRESS,
New York and London

COPYRIGHT ©, 1959, BY ACADEMIC PRESS INC.

ALL RIGHTS RESERVED

NO PART OF THIS VOLUME MAY BE REPRODUCED IN ANY FORM, BY PHOTOSTAT, MICROFILM, OR ANY OTHER MEANS, WITHOUT WRITTEN PERMISSION FROM THE PUBLISHERS.

*Made in the United States of America*

## Contents of Volume 14

### Number 1, February 1959

W. R. Moore and A. M. Brown. Viscosity-Temperature Relationships for Dilute Solutions of Cellulose Derivatives. I. Temperature Dependence of Solution Viscosities of Ethyl Cellulose.............. 1

W. Bartok and S. G. Mason. Particle Motions in Sheared Suspensions. VIII. Singlets and Doublets of Fluid Spheres............ 13

Ernest J. Perry. Effect of Adsorbed Substances of High Molecular Weight on the Growth of Silver Halide Crystals.............. 27

Kazuhiko Ninomiya and John D. Ferry. Some Approximate Equations Useful in the Phenomenological Treatment on Linear Viscoelastic Data.......................................... 36

Kazuhiko Ninomiya. Effects of Blending on the Stress-Relaxation Behavior of Polyvinyl Acetate in the Rubbery Region......... 49

T. Nash. Thermodynamic Barrier to Micelle Formation and Breakdown. I. Cetyl Trimethyl Ammonium Salts.................. 59

Vadim G. Drozin and Victor K. La Mer. The Determination of the Particle Size Distribution of Aerosols by Precipitation of Charged Particles............................................ 74

G. T. Barnes and A. E. Alexander. Aggregation of Colloidal Suspensions by Fibrous Surfaces. I. The Influence of the Fiber Surface.. 91

G. T. Barnes and A. E. Alexander. Aggregation of Colloidal Suspensions by Fibrous Surfaces. II. The Effects of Added Salts and Soaps............................................. 101

LETTER TO THE EDITOR

J. N. Phillips. Equations of State for Ideal Ionized Monolayers. 111

BOOK REVIEW

David Y. Curtin. Progress in Stereochemistry, Volume II...... 113

### Number 2, April 1959

H. V. Tartar. On the Micellar Molecular Weights of Normal Paraffin Chain Salts in Dilute Aqueous Solutions...................... 115

Thomas Gillespie. The Capillary Rise of a Liquid in a Vertical Strip of Filter Paper............................................ 123

A. M. Mankowich. The Linearity of the Log Solubilization-Log Concentration Function in Micellar Solubilization................ 131

JOHN W. BERGE, P. R. SAUNDERS, AND JOHN D. FERRY. Mechanical Properties of Poly-*n*-Octyl Methacrylate at Low Frequencies and in Creep; Entanglements in Methacrylate Polymers . . . . . . . . . . . 135

SHELDON F. KURATH, THEODORE P. YIN, JOHN W. BERGE, AND JOHN D. FERRY. Dynamic Mechanical Properties and Creep of Poly-*n*-Dodecyl Methacrylate . . . . . . . . . . . . . . . . . . . . . . . . . . . . . . . . . . . 147

CLAUDE M. AEBI AND JOSEPH R. WIEBUSH. Solubility of Sodium Chloride in Organic Solvents with Aerosol OT in the Presence of Moisture . . . . . . . . . . . . . . . . . . . . . . . . . . . . . . . . . . . . . . . . . . 161

MARJORIE J. VOLD. A Numerical Approach to the Problem of Sediment Volume . . . . . . . . . . . . . . . . . . . . . . . . . . . . . . . . . . . . . . . . . . . 168

JOSEPH J. COMER. Replica Studies of Habit-Modified Ammonium Dihydrogen Phosphate and Ammonium Dihydrogen Arsenate Crystals . . . . . . . . . . . . . . . . . . . . . . . . . . . . . . . . . . . . . . . . . . 175

TOMLINSON FORT, JR. AND A. E. ALEXANDER. Surface Films of Vinyl Stearate, Cetyl-Vinyl Ether, and their Polymers . . . . . . . . . . . . . . . . 190

A. J. G. ALLAN. Surface Properties of Polyethylene: Effect of an Amphipathic Additive . . . . . . . . . . . . . . . . . . . . . . . . . . . . . . . . . . . 206

P. R. SAUNDERS, DONALD M. STERN, SHELDON F. KURATH, CHAROEN SAKOONKIM, AND JOHN D. FERRY. Dynamic Mechanical Properties of Concentrated Solutions of Poly-*n*-Butyl Methacrylate in Diethyl Phthalate . . . . . . . . . . . . . . . . . . . . . . . . . . . . . . . . . . . . 222

P. R. SAUNDERS AND JOHN D. FERRY. Dynamic Mechanical Properties of Poly-*n*-Docosyl Methacrylate . . . . . . . . . . . . . . . . . . . . . . . . . . . . . 239

Papers Accepted for Publication . . . . . . . . . . . . . . . . . . . . . . . . . . . . . 244

Books Received for Review . . . . . . . . . . . . . . . . . . . . . . . . . . . . . . . . . 245

NUMBER 3, JUNE 1959

MALCOLM L. WHITE AND ARTHUR A. FROST. The Rate of Nucleation of Supersaturated Potassium Nitrate Solutions . . . . . . . . . . . . . . . . . . . 247

P. J. NAPJUS AND J. J. HERMANS. Electrophoresis, Conductance, and Viscosity of Aqueous Solutions of Carboxymethylcellulose in the Presence of Sodium Chloride . . . . . . . . . . . . . . . . . . . . . . . . . . . . . 252

H. H. G. JELLINEK. Adhesive Properties of Ice . . . . . . . . . . . . . . . . . . . 268

HARRY SOBOTKA, MARGARET DEMENY, AND MARGARITA ARNAKI. Multimolecular Films of Triiodostearic Acid . . . . . . . . . . . . . . . . . 281

RAYMOND R. MYERS, JOHN C. MILLER, AND A. C. ZETTLEMOYER. The Splitting of Thin Liquid Films. Kinematics . . . . . . . . . . . . . . . . . . 287

B. S. HARRAP. The Binding of Dyes by Soluble Wool Keratin Derivatives . . . . . . . . . . . . . . . . . . . . . . . . . . . . . . . . . . . . . . . . . . . . . 300

J. B. BATEMAN, E. J. WENECK, AND D. C. ESHLER. Determination of Particle Size and Concentration from Spectrophotometric Transmission . . . . . . . . . . . . . . . . . . . . . . . . . . . . . . . . . . . . . . . . . . . . 308

A. J. RUTGERS, M. De Smet, and W. RIGOLE. Streaming Currents with Nonaqueous Solutions . . . . . 330
SATYA PRAKASH AND ASHIM KUMAR GHOSH. The Influence of Ultrasonic Waves on Silver Hydrosol . . . . . 338
W. R. MOORE AND A. M. BROWN. Viscosity-Temperature Relationships for Dilute Solutions of Cellulose Derivatives II. Intrinsic Viscosities of Ethyl Cellulose . . . . . 343

LETTERS TO THE EDITOR

HERMAN E. RIES, JR., RICHARD A. AHLBECK, AND JOSEPH GABOR. Mixed Monolayers with Polyvinyl Acetate . . . . . 354
NEIL H. FARLOW. Impingement of Aerosol Particles on Polyvinyl Alcohol Film . . . . . 356
IRA BLEI. The Solubilizing Properties of the Protein-Detergent Complex . . . . . 358

BOOK REVIEWS

GEORGE R. WEISS. Precipitation from Homogeneous Solution . . . 362
G. T. BARNES. An Introduction to the Chemistry of Fats and Fatty Acids . . . . . 362

NUMBER 4, AUGUST 1959

D. L. KANTRO, STEPHEN BRUNAUER, AND C. H. WEISE. The Ball-Mill Hydration of Tricalcium Silicate at Room Temperature . . . . 363
KAZUO NAGAMATSU AND TATSUYA YOSHITOMI. On the Viscoelastic Properties of Crystalline Polymers II. Polytrifluorochloroethylene . . . . . 377
JACQUES R. HOMMELEN. The Elimination of Errors Due to Evaporation of the Solute in the Determination of Surface Tensions . . . . . 385
RAYMOND DEFAY AND JACQUES R. HOMMELEN. II. Measurement of Dynamic Surface Tensions of Aqueous Solutions by the Falling Meniscus Method . . . . . 401
RAYMOND DEFAY AND JACQUES R. HOMMELEN. III. The Importance of Diffusion in the Adsorption Process of Some Alcohols and Acids in Dilute Aqueous Solutions . . . . . 411
N. RAJALAKSHMI, S. R., SIVARAJAN, AND R. D. VOLD. The Viscosity of Sodium Humate Solutions from Coal . . . . . 419
E. HIRSCHHORN AND M. B. MATHEWS. Equilibrium and Kinetics of Water Exchange Between Rayon and Detergent Micelles in a Hydrocarbon Medium . . . . . 430
NORMAN E. LLOYD. Determination of Surface-Average Particle Diameter of Colored Emulsions by Reflectance, and Application to Emulsion Stability Studies . . . . . 441

LETTER TO THE EDITOR

S. Yamaguchi. Measurement of the Magnetization of Thin Film . 452

BOOK REVIEWS

John R. Cann. Electrophoresis: Theory, Methods and Applications . . . 455
Benson R. Sundheim. Fast Reactions in Solids . . . 456

Number 5, October 1959

O. L. Forgacs and S. G. Mason. Particle Motions in Sheared Suspensions. IX. Spin and Deformation of Threadlike Particles . . . 457
O. L. Forgacs and S. G. Mason. Particle Motions in Sheared Suspensions. X. Orbits of Flexible Threadlike Particles . . . 473
J. Schurz. Interpretation of Flow Curves in Terms of Molecular Properties . . . 492
W. Albers and J. Th. G. Overbeek. Stability of Emulsions of Water in Oil. I. The Correlation between Electrokinetic Potential and Stability . . . 501
W. Albers and J. Th. G. Overbeek. Stability of Emulsions of Water in Oil. II. Charge as a Factor of Stabilization against Flocculation . . . 510
Paul Becher and Nancy K. Clifton. Nonionic Surface-Active Agents. II. Time Dependence of Micellar Breakdown . . . 519
M. L. Miller and C. E. Rauhut. Block and Graft Copolymers. III. Apparent Dissociation Constants of Copolymers of Acrylic Acid and Acrylamide . . . 524
J. de Lopez-Gonzalez and Hans Jenny. Diffusion of Strontium in Ion-Exchange Membranes . . . 533
E. B. Bradford and J. W. Vanderhoff. The Particle Diameter Determination of Film-Forming Latexes by Electron Microscopy . . . 543

LETTER TO THE EDITOR

Irving Reich. Calculation of Surface Tensions of Liquids from Liquid Density and Vapor Pressure . . . 562

BOOK REVIEWS

R. R. Becker. Brief Course in Organic Chemistry . . . 565

Number 6, December 1959

Byrg E. Bonnelycke and W. B. Dandliker. Light Scattering of Colloidal Silica . . . 567
Anthony M. Schwartz and Francis W. Minor. A Simplified Ther-

modynamic Approach to Capillarity. I. Application to Flow in Capillary Channels........ 572
ANTHONY M. SCHWARTZ AND FRANCIS W. MINOR. A Simplified Thermodynamic Approach to Capillarity. II. Applications to Contact Angle and Spreading Phenomena........ 584
FREDERICK H. SEXSMITH AND HOWARD J. WHITE, JR. The Absorption of Cationic Surfactants by Cellulosic Materials. I. The Uptake of Cation and Anion by a Variety of Substrates........ 598
YEHEZKIEL GOTSHAL, LUDWIG REBENFELD, AND HOWARD J. WHITE, JR. The Absorption of Cationic Surfactants by Cellulosic Materials. II. The Effects of Esterification of the Carboxyl Groups in the Cellulosic Substrates........ 619
FREDERICK H. SEXSMITH AND HOWARD J. WHITE, JR. The Absorption of Cationic Surfactants by Cellulosic Materials. III. A Theoretical Model for the Absorption Process and a Discussion of Maxima in Absorption Isotherms for Surfactants........ 630
DENZEL L. DYER. The Effect of pH on Solubilization of Weak Acids and Bases........ 640

BOOK REVIEWS

VICTOR K. LA MER. Light Scattering by Small Particles........ 646
VICTOR K. LA MER. Handbook of Physics........ 646

Author Index........ 647
Subject Index........ 649
Index of Book Reviews........ 650

# Ultracentrifugation

## in Biochemistry

**By HOWARD K. SCHACHMAN**

*Biochemistry and Virus Laboratory, University of California, Berkeley*

*1959, 272 pp., illus., $8.80*

***From the Foreword by* JOHN T. EDSALL:**

"Over the past decade the use of the ultracentrifuge as a tool in biochemical research has developed in a dramatic fashion. Problems scarcely imagined ten years ago can now be investigated with brilliant success and with techniques only recently developed. There remains a need for a moderately extended discussion of these more recent developments, combined with a statement of the basic and indispensable theory and a general description of the old and new experimental techniques. I believe that these needs are admirably met by the present book.

"It is likely to become an indispensable companion to the laboratory worker who is planning and conducting an ultracentrifuge run for almost any purpose. It should also be of fundamental value to the thoughtful student or investigator who wants to know the present state of our knowledge in the field, both experimental and theoretical.

"Dr. Schachman has, I believe, performed a major service by portraying the broad range of experimental techniques in sedimentation experiments and by providing a rigorous discussion of the underlying principles."

***CONTENTS:***

Introduction
General Considerations
Experimental Aspects
Sedimentation Velocity
The Transient States during the Approach to Sedimentation Equilibrium
Sedimentation Equilibrium
Interpretation of Sedimentation Data
References
Glossary
AUTHOR INDEX—SUBJECT INDEX.

ACADEMIC PRESS, NEW YORK and LONDON
111 Fifth Avenue, New York 3, New York
40 Pall Mall, London, S. W. 1

# Electrophoresis

## *Theory, Methods, and Applications*

*Edited by* MILAN BIER *Fordham University and Institute of Applied Biology, Inc., New York*

*1959, 563 pp., illus., $15.00*

Introduction
By Arne Tiselius, Institute of Biochemistry, Uppsala

Electric Potentials in Colloidal Systems
By J. Th. G. Overbeek and J. Lijklema, University of Utrecht

Acid-Base Equilibria of Proteins
By K. Linderstrøm-Lang and Sigurd O. Nielsen, Carlsberg Laboratory, Copenhagen

Moving Boundary Electrophoresis—Theory
By L. G. Longsworth, The Rockefeller Institute, New York

Moving Boundary Electrophoresis—Practice
By L. G. Longsworth, The Rockefeller Institute, New York

Paper Electrophoresis
By Ch. Wunderly, Kantonsspital, Zürich Mediznische Universitatsklinik, Zürich

Zone Electrophoresis in Various Types of Supporting Media
By Henry G. Kunkel and Rodes Trautman, The Rockefeller Institute, New York

Preparative Electrophoresis without Supporting Media
By Milan Bier, Fordham University, New York, and Institute of Applied Biology, Inc., New York

Applications of Moving Boundary Electrophoresis to Protein Systems
By R. A. Brown, The Wistar Institute for Anatomy and Biology, Philadelphia, and S. N. Timasheff, Eastern Regional Research Laboratory, U. S. Department of Agriculture, Philadelphia

Clinical and Physiological Applications of Electrophoresis
By Dan H. Moore, The Rockefeller Institute, New York

The Electrophoresis of Viruses, Bacteria, and Cells, and the Microscope Method of Electrophoresis
By Charles C. Brinton, Jr. and Max A. Lauffer, University of Pittsburgh

Applications of Zone Electrophoresis
By Theodor Wieland, Institut für Organische Chemie der Universität, Frankfurt

AUTHOR INDEX—SUBJECT INDEX.

**ACADEMIC PRESS, New York and London**
111 Fifth Avenue, New York 3, New York
40 Pall Mall, London, S. W. 1

*International Review of*
**CYTOLOGY**

**VOLUME VIII**

*Edited by*
G. H. BOURNE, *Emory University*
J. F. DANIELLI, *King's College, London*

*August 1959, 541 pp., illus., $13.00*

**CONTENTS**

**The Structure of Cytoplasm**
By Charles Oberling, Institut de Recherches sur le Cancer, Villejuif, France
**Wall Organization in Plant Cells**
By R. D. Preston, University of Leeds, England
**Submicroscopic Morphology of the Synapse**
By Eduardo de Robertis, Facultad de Ciencias Médicas, Buenos Aires
**The Cell Surface of *Paramecium***
By C. F. Ehret and E. L. Powers, Argonne National Laboratory, Lemont, Illinois
**The Mammalian Reticulocyte**
By Leah Miriam Lowenstein, Oxford University
**The Physiology of Chromatophores**
By Milton Fingerman, Tulane University, New Orleans
**The Fibrous Components of Connective Tissue with Special Reference to the Elastic Fiber**
By David A. Hall, School of Medicine, Leeds, England
**Experimental Heterotopic Ossification**
By J. B. Bridges, Queen's University, Belfast, Ireland
**A Survey of Metabolic Studies on Isolated Mammalian Nuclei**
By D. B. Roodyn, Medical Research Council, Radiobiological Research Unit, Harwell, England
**Trace Elements in Cellular Function**
By Bert L. Vallee and Frederic L. Hoch, Harvard Medical School and The Peter Bent Brigham Hospital, Boston
**Osmotic Properties of Living Cells**
By D. A. T. Dick, Oxford University
**Sodium and Potassium Movements in Nerve, Muscle, and Red Cells**
By I. M. Glynn, Cambridge University
**Pinocytosis**
By H. Holter, Carlsberg Laboratory, Copenhagen
AUTHOR INDEX—SUBJECT INDEX.

***Previously published:***

Volume 1, 1952, 368 pp., illus., $10.00
Volume 2, 1953, 545 pp., illus., $11.00
Volume 3, 1954, 530 pp., illus., $10.00
Volume 4, 1955, 419 pp., illus., $10.00
Volume 5, 1956, 570 pp., illus., $11.50
Volume 6, 1957, 566 pp., illus., $12.00
Volume 7, 1958, 684 pp., illus., $16.00

AP
**ACADEMIC PRESS, New York and London**
111 Fifth Avenue, New York 3, New York
40 Pall Mall, London, S. W. 1

*Volume III Ready January 1960*

# Rheology

## THEORY AND APPLICATIONS

*Edited by* FREDERICK R. EIRICH
*Polytechnic Institute of Brooklyn*

**Volume III**

*January 1960, 680 pp., illus., approx. $20.00*

The Normal-Coordinate Method for Polymer Chains in Dilute Solution, by B. H. ZIMM
The Principles of Rheometry, by S. OKA
Viscosity of Suspensions of Electrically Charged Particles and Solutions of Polymeric Electrolytes, by B. E. CONWAY AND A. DOBRY-DUCLAUX
The Rheology of Latex, by SAMUEL H. MARON AND IRVIN M. KRIEGER
The Rheology of Printing Inks, by A. C. ZETTLEMOYER AND RAYMOND R. MYERS
Rheology of Pastes and Paints, by RUTH N. WELTMANN
Atomistic Approach to the Rheology of Sand-Water and of Clay-Water Mixtures, by W. A. WEYL AND W. C. ORMSBY
The Rheology of Inorganic Glasses, by W. A. WEYL
The Rheology of Concrete, by M. REINER
The Deformation of Crystalline and Cross-Linked Polymers, by I. L. HOPKINS AND W. O. BAKER
The Viscosity and Elasticity of Interfaces, by DEAN W. CRIDDLE
Rheology of Lubrication and Lubricants, by A. BONDI
The Rheology of Adhesion, by J. J. BIKERMAN
Rheology in Molding, by C. E. BEYER AND R. S. SPENCER
Rheology of Spinning, by BRUNO R. ROBERTS
Theory of Screw Extruders, by W. L. GORE AND JAMES M. MCKELVEY
AUTHOR INDEX—SUBJECT INDEX.

**Volume I,** *1956, 761 pp., illus., $20.00*
**Volume II,** *1958, 591 pp., illus., $18.00*

*Review of Volume I:*

"Some of the theories which are discussed may in time be extended, but will hardly be substituted by new developments. Therefore in spite of the present rapid growth of rheology, this volume will be used for a long time to come as a textbook by the research worker who wants to penetrate into the field of rheology and as a reference book for those who are already actively engaged in the field. In conclusion it is to be strongly recommended to all those whose scientific activities lead to problems of rheology."

—*Applied Mechanics Review*

*Literature describing all volumes available upon request*

ACADEMIC PRESS, New York and London
111 Fifth Avenue, New York 3, New York
40 Pall Mall, London, S.W. 1